Architectural fabric properties: determination, representation & prediction

A thesis submitted for the degree

Doctor of Philosophy

in the School of Civil Engineering & Geosciences

at the University of Newcastle-upon-Tyne

by

Benjamin Nathan Bridgens

October 2005

Abstract

Coated woven fabrics are used in state-of-the-art structures and yet broad assumptions are made in both material testing and behaviour. Current design practice makes little reference to the complex non-linear behaviour of architectural fabrics. A better understanding of fabric response should enable reduction of safety factors, use of more economic materials and allow more architectural freedom in the forms that can be achieved.

With limited availability of test equipment and no European standards on biaxial testing, a biaxial test rig has been designed and built for this work and a new test protocol has been developed. Application of prestress followed by cyclic loading conditions the fabric and enables medium to long term properties to be measured which are appropriate for structural design. Thorough sampling of all feasible design stress states fully quantifies the fabric response. Testing has been carried out on a wide range of PVC coated polyester and PTFE coated glass-fibre fabrics.

Fabric test data is commonly manipulated to fit within a plane stress framework. It is shown in this work that plane stress theory is inappropriate for representing the complex deformation mechanisms of coated woven fabrics. It is proposed that the test data is used directly in finite element structural analysis by interpolation between values in a database of test results, with no limiting plane stress assumptions. 'Feasible strain plots' provide a new tool for quantifying fabric behaviour.

A predictive fabric model based on force equilibrium in the fabric 'unit cell' has been developed. The model aims to be easily accessible to the design engineer, with all parameters derived from standard tests. Whilst avoiding unnecessary complexity, the model realistically models key fabric deformation mechanisms. The model provides a more accurate representation of fabric behaviour than current industry best practice (i.e. use of elastic constants based on biaxial test data), but without the need for specialist testing.

Acknowledgements

I would like to thank my supervisor, Peter Gosling, for his enthusiasm, patience & humour, and William Cragie for fabricating the test rig and for endless help in the lab. I would also like to thank Brian Forster, Tristan Simmonds, Clare Perkins, Thomas Li, Jim Burridge, Matthew Birchall & Stephen Hendry (Arup), Alex Heslop (Architen-Landrell), Rainer Blum & Heidrun Boegner (Laboratorium Blum), David Wakefield (Tensys), Francoise Fournier & Jean-Luc Perignon (Ferrari S.A.) and Sean Seary (Taconic). Finally I would like to thank the Engineering and Physical Sciences Research Council and Arup (London & Newcastle offices) for providing financial support for this research, and Architen-Landrell, Ferrari S.A. & Taconic for material contributions.

Outline contents

Detailed tables of contents and tables of figures & tables are included at the start of each chapter.

Chapter 1

Introduction

Contents

Figures

1.1 CONTEXT

1.1.1 Background

Fabric canopies are one of the earliest forms of roofing, and have been used for traditional forms of construction for thousands of years. However, modern fabric structures using synthetic materials have only been in use for about thirty years. A fabric membrane acts as both structure and cladding, thereby reducing the weight, cost and environmental impact of the construction. Fabric structures enable striking forms to be realised, which are unique to this type of construction (Figure 1-1, Figure 1-2, Figure 1-3 & Figure 1-4).

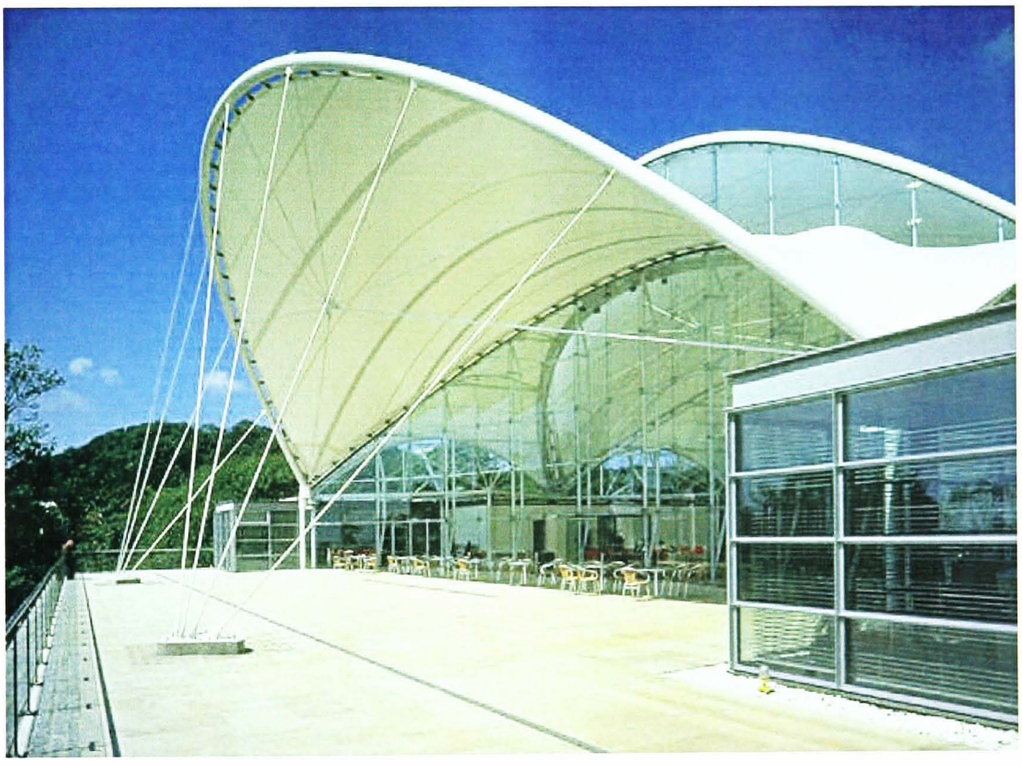

Figure 1-1. Saga headquarters, UK (Arup)

Figure 1-2. Marsyas, sculpture at the Tate Modern, London (Arup)

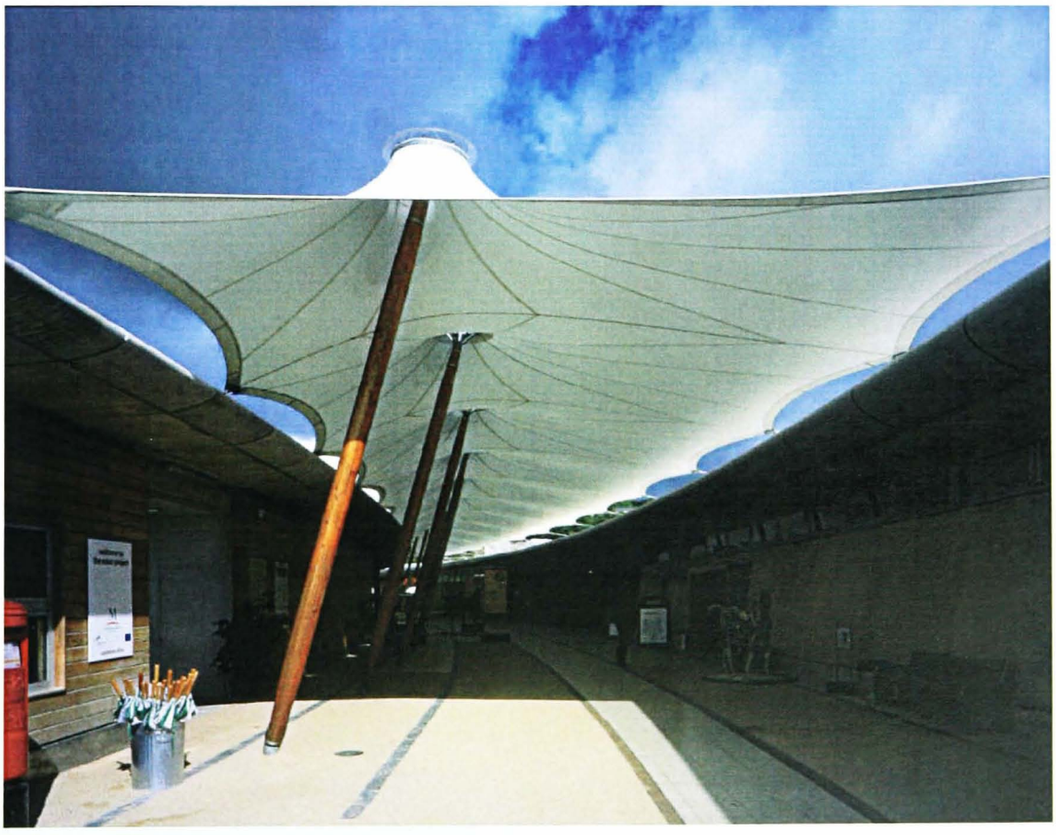

Figure 1-3. Eden project entrance, Cornwall, UK (Arup)

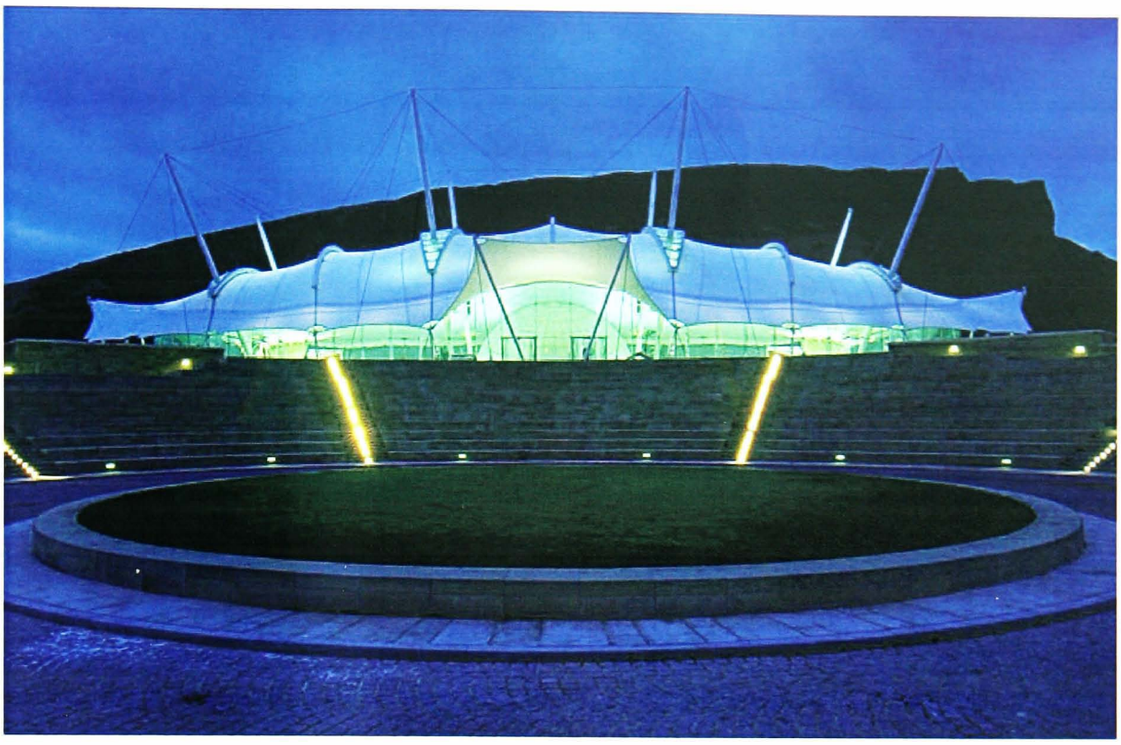

Figure 1-4. Dynamic Earth Centre, Edinburgh, UK (Arup)

Architectural fabrics consist of woven yarns with a water resistant coating. They have negligible bending and compression stiffnesses. Hence fabric structures are designed with sufficient curvature to enable environmental loads to be resisted as tensile forces in the plane of the fabric. This contrasts with conventional roofs in which loads are typically resisted by arch action or by stiffness in bending. The shape of the fabric canopy is vital to its ability to resist all applied loads in tension. To resist both uplift and down-forces (typically due to wind and snow respectively) the surface of the canopy must be *double-curved*. Conic or saddle shapes are frequently used to achieve this, taking advantage of their inherent double-curvature (Figure 1-5). For a flat panel to form a surface with double curvature the membrane must undergo shear deformation. Fabric structures are prestressed to ensure that the fabric remains in tension under all load conditions and to reduce deflections. The low weight of the fabric means that gravity or 'self weight' loading is often negligible. Consequently, tensile fabric is frequently more structurally efficient and cost-effective for large span roofs than conventional construction methods.

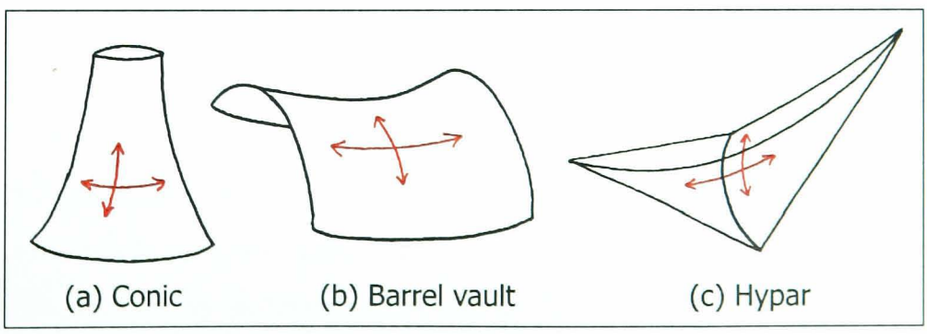

Figure 1-5. Shapes for double-curvature

Boundary conditions play an important role in determining the fabric shape and stress distribution; ideally a uniform prestress is applied to the fabric. To achieve a uniform prestress the fabric must take the form of a minimal surface. Early work on fabric structures (Otto, 1967) used soap films to determine this form, in a process known as *form finding*. Models using stretch fabrics (e.g. lycra) are commonly used for conceptual design (Figure 1-6).

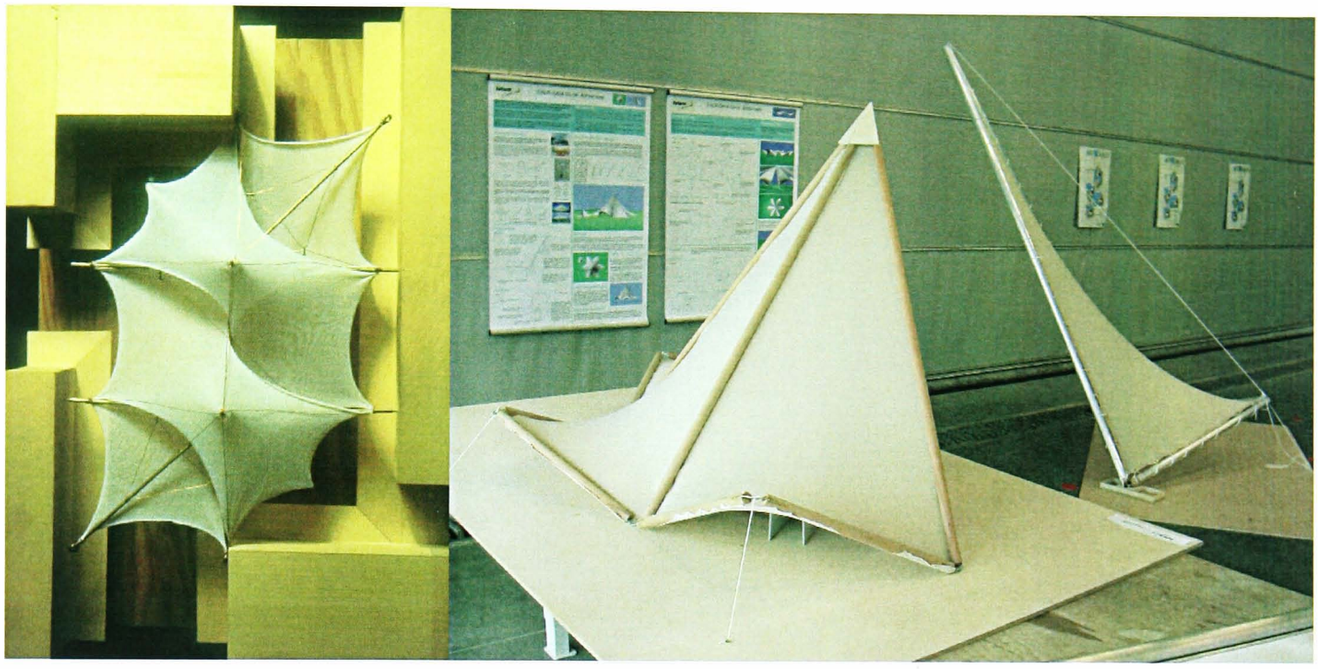

Figure 1-6. Form finding with physical models (images: (a) Arup, (b) the author)

A minimal surface joins a set of boundary points with the smallest possible membrane area and has uniform in-plane tensile stresses throughout. However, true minimal surfaces cannot be formed between all boundary conditions. For example, two rings of different diameters are typically used to form a conic (Figure 1-5a). As the distance between the rings is increased the minimal surface will 'neck': a point is reached where a soap film/minimal surface cannot be formed between the rings. A pseudo-minimal surface can be developed for a fabric membrane by accepting increased stresses in the region where the soap bubble would have failed. This reduces the limitations on the forms that can be created. However, as the desired shape moves away from the minimal surface form, the stress variations increase and the structure becomes less efficient.

An alternative to prestressed fabric is the use of air-supported structures. The negligible weight of the fabric enables an internal pressure that is slightly higher than ambient to support the roof, providing an extremely efficient roofing solution with no supporting structure required. The small pressure difference is imperceptible to the inhabitants and relatively easy to maintain. This type of structure is not discussed directly in this thesis, but a better understanding of fabric material behaviour is equally applicable to air-supported structures.

The distinctive forms that are typically achieved with fabric structures ensure their popularity for making bold architectural statements. There must always be a close relationship between Architect and Engineer

as the possible shapes are limited by the boundary conditions of the fabric. Form-finding must go hand-in-hand with architectural design. It is important to be aware of the architectural considerations that can conflict, but hopefully coincide, with the structural requirements. For example, the shape of a smooth, white fabric structure is visually defined primarily by the seam lines (Rice, 1994, p.97). This leads to definite architectural requirements for the shape and orientation of the cutting patterns, which in turn are fundamental to the structural analysis and choice of fabric.

1.1.2 Current design practice

The design of fabric structures is complicated by the response of coated woven fabrics to biaxial loads in the plane of the fabric. Non-linear material behaviour, large displacements and the use of membrane action to resist loads require a fundamentally different approach to structural design compared to traditional roof structures.

"Too often, however, the design of fabric roof structures is considered an art form rather than a design science"

Mott, Huber & Leewood (1985)

Determination of the minimal surface shape (*form finding*) and analysis of large displacement behaviour under load requires non-linear analysis. Typically the non-linear finite element analysis utilizes the *Dynamic Relaxation* algorithm and a constant strain triangle formulation (Barnes, 1999; Lewis & Gosling, 1993). The analysis of wind and snow loading on the structure – together with the experience of the designer - determines the level of prestress required to maintain tension in the membrane. For flatter areas of the structure it is vital to ensure that the fabric shape is maintained and ponding of rainwater or snow-melt cannot occur. The collapse in 1999 of the new fabric roof covering Montreal's Olympic Stadium (New Civil Engineer, 28th January 1999) highlights the importance of accurately predicting fabric strain levels, and hence the fabric form under extreme loading, to prevent ponding. Snow and meltwater loading resulted in excessive deflections of the fabric surface, which led to an increase in load and consequently to failure. The actual cause of failure has been identified as design based and not due to accidental damage. This event, which is not unique, serves as a timely reminder of the need for further research in the design of fabric structures.

The tensile and shear stresses in the fabric due to prestress are combined with those arising from the effect of appropriate combinations of snow and wind loading (Figure 1-7) to check fabric strength and provide loads for the design of the supporting cables and steelwork. The true behaviour of coated woven fabrics is highly nonlinear, and can only be determined by extensive biaxial testing. The only biaxial fabric testing carried out routinely for most projects is at prestress to determine values for *compensation* (§1.1.3). However, this is generally inappropriate for structural design as the stresses arising from environmental loads are substantially higher than prestress. Consequently, assumed equivalent linear

elastic material properties are generally adopted for analysis and design. The actual fabric stress-strain behaviour is considerably more complex than these linear approximations (§2.1).

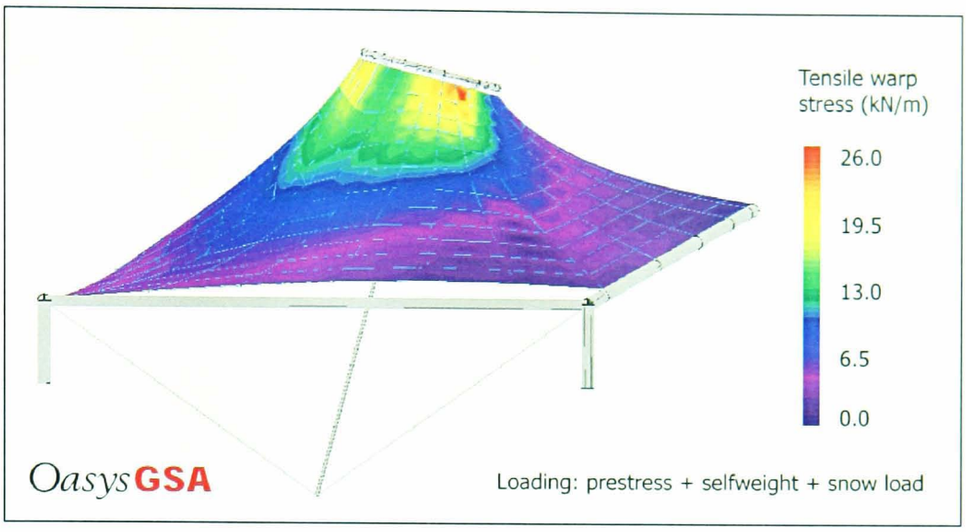

Figure 1-7. Stress distribution in fabric canopy

There are currently no standard British or European codes for the design of fabric structures; although the European collaborative group *TensiNet* (www) has recently published a design guide which collates current good practice and recommendations (Mollaert & Forster, 2004). Most structural design codes for other materials are based on a limit state approach with partial safety factors being applied to loads and material strengths. In structures that exhibit strong geometric non-linearity a limit state approach is not appropriate as the deformed geometry of the structure under load is dependent on the magnitude as well as the distribution of the loading. It is therefore standard practice to use a permissible stress approach for the design of fabric structures.

The maximum design stress is compared to the fabric strength reduced by a composite safety factor. In the design of fabric membranes high safety factors are used; typically between five and ten for the fabric, with lower factors (2.3 to 3) used to calculate the stresses in the supporting cables, rods and webbing. Factors such as material variation, accuracy of material properties, load variation, environmental degradation (including ultraviolet, cyclic loading, high temperatures, creep, humidity and pollution), loading uncertainty and tear propagation are combined to give these high safety factors.

Tear propagation is the dominant factor. Fabric structures are designed such that a tear does not propagate even when subjected to wind and snow loading. A maximum tear length of 40mm is commonly chosen on the grounds that a tear of this length is just visible to the naked eye at a distance of 15m - although this seems to be a fairly arbitrary choice. Smaller tears may not be visually apparent and so the fabric must be strong enough not to fail with this potentially undetected damage. Tear tests on 400mm wide PVC-polyester fabric samples indicate that a 40mm long tear in the membrane has a tear propagation stress of 25% of fabric tensile strength (Happold et al, 1987), suggesting a factor of safety of four is prudent in case of damage. The increase in safety factor to between five and ten is commonly based on experience and rules of thumb rather than a detailed assessment of the many contributory factors. Several design

guides have been developed in Europe, North America and Japan and their recommendations are summarised in the *European Design Guide for Tensile Surface Structures* (Mollaert & Forster, 2004). Composite safety factors are proposed based on tear propagation, material variability, test reliability, calculation accuracy, future material degradation and 'other factors'. However, too little information is currently available to make an informed decision on the appropriate value for many of these factors.

1.1.3 Fabrication & installation

Fabric membrane surfaces must be subdivided into panels that can be cut from a flat roll of fabric. The panels are subsequently welded together in a controlled environment to produce the complete canopy ready for delivery to site and installation (Figure 1-8). The membrane behaves in a highly non-linear fashion during prestressing, with a complex interaction occurring between the warp and fill yarns. The fabric panels must therefore be *compensated* such that after prestressing they have the correct dimensions for the roof geometry.

The accurate determination of material properties is essential for the successful installation of fabric membranes. The importance of this material data is reflected in the industry acceptance of biaxial testing of samples from each roll of fabric. This testing is carried out at prestress loading to accurately determine the percentage length reduction (or increase) required in warp and fill directions. If the fabric will not be subjected to a constant prestress throughout, then varying levels of compensation should be applied to different parts of the canopy. The rate of application of the prestress load is important, but is typically only informed by experience and the 'observational method', whereby the extension of the fabric is observed during installation with tensioning applied as and when required. The time required for installation will vary substantially depending on environmental factors such as the temperature and wind loading during installation, the type of material, the shape of the structure and the method of installation. For example, PTFE-glass fibre fabric becomes very stiff at temperatures below 5°C, and can fail during installation unless the load is applied very slowly, over a period of weeks rather than days.

Figure 1-8. Installation of canopy, four linked conics (Dalton Park, County Durham, UK; images – Arup)

1.1.4 Architectural fabric material properties

Coated woven fabrics are used for roofs and canopies as they are lightweight (0.7-1.4kg/m^2), translucent (typically 10-20% light transmission), cheaper than glass and impervious to water. The low weight of the material means lightweight supporting steelwork and the possibility of retrofitting fabric roofs to buildings which could not support the additional load from, for example, a glass roof.

There are two principal types of architectural fabric: glass fibre fabric with a PolyTetraFluoroEthylene (PTFE) coating and polyester fabric with a PolyVinylChloride (PVC) coating. PVC-polyester benefits

from low cost and good flexibility – reducing the risk of damage during fabrication and installation. Low shear stiffness enables surfaces with high levels of double curvature to be achieved without wrinkling or buckling of the fabric surface. Disadvantages of PVC/polyester, compared to PTFE-glass, include relatively high levels of creep which can necessitate re-tensioning, lower resistance to dirt build-up and a shorter lifespan (12-15 years). PTFE coated glass-fibre is a much stiffer material, which reduces the overall deflections of the membrane under load, but conversely means that it is more susceptible to folding damage, which can occur when the brittle glass fibre yarns break. Higher shear stiffness prevents the material being used for forms with high levels of double-curvature. PTFE-glass has a lifespan in excess of 30 years, does not suffer UV degradation and is self-cleaning. It is however around five times more expensive than PVC-polyester.

The coating processes used for applying the PVC and PTFE coatings are different and significantly affect the final material properties. The PTFE coating is sprayed on to the base cloth in multiple applications until the required thickness is achieved. Between each application the fabric passes through heaters which sinter the coating onto the base cloth at 350 to 380°C (Mollaert & Forster, 2004). This is necessary to adhere the PTFE to the glass fibre yarns. The PVC adheres more easily to the base cloth. Excess coating is poured onto the fabric which is then scraped to the correct thickness before being gently heated to set the coating.

Recent research and developments in architectural fabric materials try to combine the flexibility of PVC-polyester with the long life-span and self cleaning properties of PTFE-glass. The aim of fabric development is to make a fabric which is:

- Strong,
- Durable - in particular resistant to UV degradation,
- Weldable,
- Self-cleaning,
- Not damaged by folding,
- Not prohibitively expensive and,
- Provides high levels of light transmission.

Recent fabric developments meet many of these aims, but not all. Woven PTFE yarns with a PTFE coating provide an extremely flexible fabric with 40% light transmission. Research is ongoing into coating polyester fabric with silicon to achieve similar properties.

All of these fabrics are composed of an open weave mesh of orthogonal yarns with a coating that encloses the mesh on both sides (Figure 1-9). The characteristics of the two main types of fabric are different, but the underlying deformation mechanisms are very similar. Under biaxial tensile loading the behaviour of

coated woven fabrics is highly non-linear and anisotropic (Skelton, 1980a; Tan & Barnes, 1980). Material non-linearity is evident in the load extension characteristics of both the yarn fibres and the coating. Geometric non-linearity occurs in the yarns (due to the complex twisted fibre structure) and in the finished fabric due to *crimp interchange*. Crimp interchange is the balancing of out-of-plane forces due to interaction between orthogonal warp and fill yarns, which leads to fundamentally non-linear stress-strain behaviour.

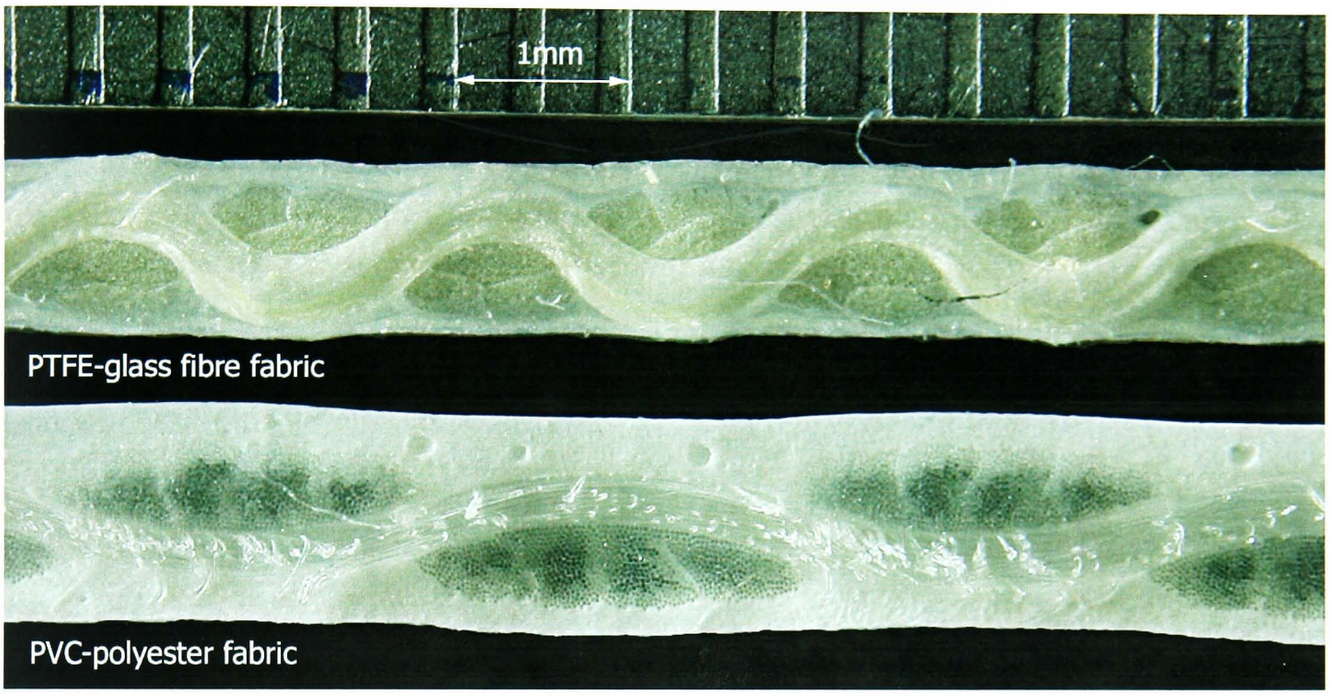

Figure 1-9. Fabric cross sections

The material response is hysteretic due to the coating and fibre properties and due to frictional effects (inter-fibre and inter-yarn friction). Long-term creep is also significant. Fabric response varies between batches of fabric and even across the width of a single roll. The weave pattern is changed by variation in the fabric tension during weaving and coating. Gripping of the edge of the fabric to move it through the loom can result in bowing of the fill yarns. The exact temperature used to sinter PTFE coating on to glass fibre fabric affects the shape of the yarns and the level of bond between them at intersections.

1.1.5 Fabric testing

Uniaxial tensile strip tests are routinely carried out by fabric manufacturers to determine the tensile strength of the fabric, and are clearly defined by standards (BS EN ISO 1421:1998). Uniaxial testing can be carried out with standard tensile test machines, the only modification being specialist jaws to grip the fabric without damaging it.

Biaxial fabric testing is much more specialist with no European standards, limited published guidance and few suitable test rigs. Contractors commonly carry out biaxial testing at low load to determine compensation values, but test rigs capable of testing to design loads for architectural fabrics are rare. Prior

to this work, one of the only such test rigs in Europe was at Laboratorium Blum (www) in Stuttgart. The biaxial test rig needs to accommodate large strains (20 to 25%) in two orthogonal directions, without excessive restraint from the clamps. Measurement of fabric strain in the area of interest is difficult without affecting the stress field in the fabric. There is no standard test procedure for determining the biaxial properties of architectural fabrics. Fabric stress-strain behaviour is inelastic, non-linear, time dependent (both short and long term) and temperature dependent. This means that the test procedure must be appropriate for the intended use of the test results.

1.2 AIMS & OBJECTIVES

The aim of this research is to increase understanding of the biaxial behaviour of coated woven fabrics used in tensile structures. There are two distinct parts to the work. Firstly, the development of a method for accurately representing non-linear biaxial fabric stress-strain behaviour for use in structural analysis. Secondly, formulation of a fabric model *in silico* to predict the biaxial stress-strain response of architectural fabrics without the need for biaxial testing. Fundamental to both parts of the project is the experimental determination of the biaxial stress-strain characteristics of architectural fabrics.

The implementation of this research aims to provide improved representations of the fabric behaviour which can feasibly be included in structural analysis. This will increase the accuracy of the design process, and should result in reduced factors of safety, fewer incidences of membrane failure and greater confidence to explore new fabric forms.

Specific objectives are to:

- Carry out an extensive literature review to establish the current state-of-art in all topics relating to this work,
- Design and fabricate a biaxial test rig,
- Develop a test protocol which rigorously investigates the response of architectural fabrics to biaxial in-plane loading,
- Carry out biaxial fabric testing to investigate and characterise the stress-strain behaviour of coated woven fabrics at design loads for a range of commonly used architectural fabrics (to include both PVC coated polyester and PTFE coated glass fibre),
- Develop an outline of how the biaxial test data can be implemented in structural analysis software,
- Develop a predictive model to determine the biaxial stress-strain behaviour of architectural fabrics when biaxial test data is not available. All model parameters should be determined from

standard tests without the need for specialist equipment, to ensure that the model can realistically be used by the design engineer (for detailed aims see §5.2).

- Perform suitable tests to inform the predictive model parameters (e.g. uniaxial strip tests, fabric imaging).
- Demonstrate the capability of the predictive model through comparison with biaxial test data for a range of fabrics.

1.3 SCOPE

The first part of this research is principally experimentally based. The biaxial test protocol will be developed iteratively through a series of fabric tests. Data for a range of fabrics will be acquired through biaxial testing. Finite element analysis using commercial software will be used to inform the design of the test rig.

An outline method of using the biaxial test data in finite element analysis of membrane structures will be developed. However, implementation in analysis software and finite element development are not within the scope of this work.

The second part of the research will involve developing a predictive model *in silico* to predict the response of coated woven fabric to biaxial loads. Modelling of inelastic behaviour, long term creep, shear and failure are not within the scope of this work. Whilst the model is theoretical, all necessary parameters will be determined experimentally, and detailed comparison will be carried out with biaxial test data.

The following aspects of fabric behaviour are not within the scope of this work: shear, long term creep, failure, strength, tearing and fatigue. However, the effect of these factors on the design of the biaxial test rig and test protocol is to be determined as appropriate. The effect of temperature on biaxial fabric behaviour will not be investigated.

1.4 THESIS STRUCTURE

Chapter 2 – Literature Review. Establishes previous work and the current state-of-the-art in all areas pertinent to the research: fibre, yarn, coating and fabric properties, fabric test methods, representation of biaxial test data, use of test data in membrane structural analysis, predictive models for fabric behaviour.

Chapter 3 – Fabric testing. Details of the design and fabrication of a biaxial test rig, with analysis of the specimen form and dimensions. Development of a new biaxial test protocol to provide full characterisation of the fabric behaviour suitable for structural design.

Chapter 4 – Biaxial test results and implementation. Presentation and discussion of biaxial test results. Review and assessment of methods used for the representation of non-linear biaxial stress-strain data. Proposed method for the use of test data from this work in structural analysis, and a novel method of quantifying fabric behaviour in terms of feasible strain states.

Chapter 5 – Predictive fabric model. Formulation of fabric unit cell models for both sawtooth and sinusoidal yarn waveforms. Implementation of constant yarn area and consistent geometry constraints. Comparison of model output with biaxial response surfaces for a range of fabrics.

Chapter 6 – Conclusions & recommendations for future work. Conclusions are presented at the end of each Chapter, with an overview of the key points in Chapter 6.

References. The Harvard system has been used, with references listed alphabetically by first author. Internet references are listed separately, alphabetically by title, and are denoted 'www' in the text.

1.5 PUBLICATIONS

B.N.Bridgens, P.D.Gosling (2005) *A predictive fabric model for membrane structure design*, Textile Composites and Inflatable Structures II, Stuttgart, Ed. E.Oñate & B.Kröplin, pp.287-296

B.N.Bridgens, P.D.Gosling (2004) *A new biaxial test protocol for architectural fabrics*, Journal of the International Association for Shell and Spatial Structures, 45, 3 (December) 175-181

B.N.Bridgens, P.D.Gosling & M.J.S.Birchall (2004) *Tensile fabric structures: concepts, practice & developments*, The Structural Engineer, 82, 14 (22 July), 21-27

B.N.Bridgens, P.D.Gosling & M.J.S.Birchall (2004) *Membrane material behaviour: concepts, practice & developments*, The Structural Engineer, 82, 14 (22 July), 28-33

B.N.Bridgens, P.D.Gosling (2004), *A new biaxial test protocol for architectural fabrics*, IASS 2004 Montpellier: Shell and spacial structures from models to realisation, Ed. R. Motro, 246-247

B.N.Bridgens & P.D.Gosling (2004), *Direct stress-strain representation for coated woven fabrics*, Computers and Structures, 82, 1913-1927

B.N.Bridgens & P.D.Gosling (2003) *Biaxial fabric testing to determine in-situ material properties*, Textile Composites and Inflatable Structures, Barcelona, Ed. E.Oñate & B.Kröplin, pp136-141.

B.N.Bridgens & P.D.Gosling (2002) *NURBS Representation of Coated Woven Fabric Behaviour*, Computational Structures Technology 2002, Prague, pp 219-220

1.6 AWARDS

Institution of Structural Engineers *Guthrie Brown Award* for *Tensile fabric structures: concepts, practice & developments* and *Membrane material behaviour: concepts, practice & developments*, awarded for the best paper published in the Structural Engineer by an author or authors under the age of forty,

2nd Hangai Prize awarded for the paper presented at IASS 2004, *A new biaxial test protocol for architectural fabrics*, for a young researcher showing innovative ideas related to the field of shell and spatial structures,

'ArtNomade 03:04' international architectural student design competition to design a demountable space for modern performance art, organised by the Languedoc Roussillon School of Architecture and the Grands Ateliers de l'Isle d'Abeau: joint second (Figure 1-6b, p.6),

Young Researchers' Conference 2003, Institution of Structural Engineers: first prize for best presentation,

Newcastle University Faculty Seminar, Civil Engineering: best poster 2002.

Chapter 2

Literature review

Contents

Figures

Tables

2.1 CHARACTERISTICS OF COATED WOVEN FABRICS

2.1.1 Fibre & yarn properties

How do the material properties of the yarns and their constituent fibres contribute to the behaviour of coated woven fabrics?

Bundles of fibres are twisted to form yarns, which are woven and then coated to form a stable, weatherproof fabric. The fibres are a fundamental component of the fabric, and their mechanical properties play an important role in fabric behaviour. Many types of fibre exhibit non-linear tensile behaviour, large strains and inelasticity (Buckley, 1980); *"It is clear that most common fibres extend in a non-linear fashion"* (Morris, Merkin & Rennell, 1999). Inter-fibre friction between parallel yarns is important in determining the properties of a twisted fibre bundle, or yarn. The frictional properties of fibres on the outside of the yarn enable woven fabrics to maintain their weave pattern and structure. This is known as the *dimensional stability* of the fabric.

The most common fibres used for architectural fabrics are polyester and glass. Other materials include Cotton, Polyamide 6.6 (Nylon), Aramid and extruded PTFE. Cotton is an organic fibre which was used by Frei Otto in his early garden show structures. Being organic, cotton is prone to damage from moisture and fungal attack, giving a maximum lifespan of around four years. Nylon is popular in the sailing industry for its high strength to weight ratio, but its poor resistance to ultraviolet light and water ingress mean that it is of little use for longer term architectural applications. Aramid fibres (e.g. Kevlar) have high tensile strength and chemical resistance but provide low levels of elastic strain and poor resistance to UV (Houtman & Orpana, 2000). Extruded PTFE fibres have good chemical and UV resistance and are not damaged by repeated bending and folding, making the material ideal for mountable/demountable structures (Figure 2-1). However, PTFE fibres have lower tensile strength than polyester or glass, and the low surface friction and chemical reactivity make coating application difficult. Recently a PTFE coated PTFE fabric has been developed (tradename *Tenara*, manufactured by Gore (Kelmartin, 2003; www: Gore)). This combines the benefits of PTFE fibres and PTFE coating, but is difficult to weld and is more expensive than other architectural fabrics.

Figure 2-1. Inner courtyard of the Prophet's Holy Mosque, Medina, Saudi Arabia

(reproduced from www: lega-musulmana)

Glass fibres and polyester fibres are fundamentally different in terms of micro-structure and hence stress-strain response (Figure 2-2). Glass fibres have an essentially linear stress-strain response, whereas polyester fibre response is complex and non-linear. This complexity is demonstrated by the inconsistency of the two polyester curves in Figure 2-2. The typical polyester stress-strain curve has three distinct parts (Figure 2-2b).

Polyester fibres have a high tensile strength and high elongation before yield, enabling adjustments to be made to a fabric canopy during installation. However, they do degrade significantly in sunlight and due to repeated stressing, and are prone to high levels of creep. The most common polyester used as a fibre is PET - *poly(ethylene terephthalate)* (Figure 2-3). This is a commonly available mass-produced fibre used, for example, in soft drink bottles.

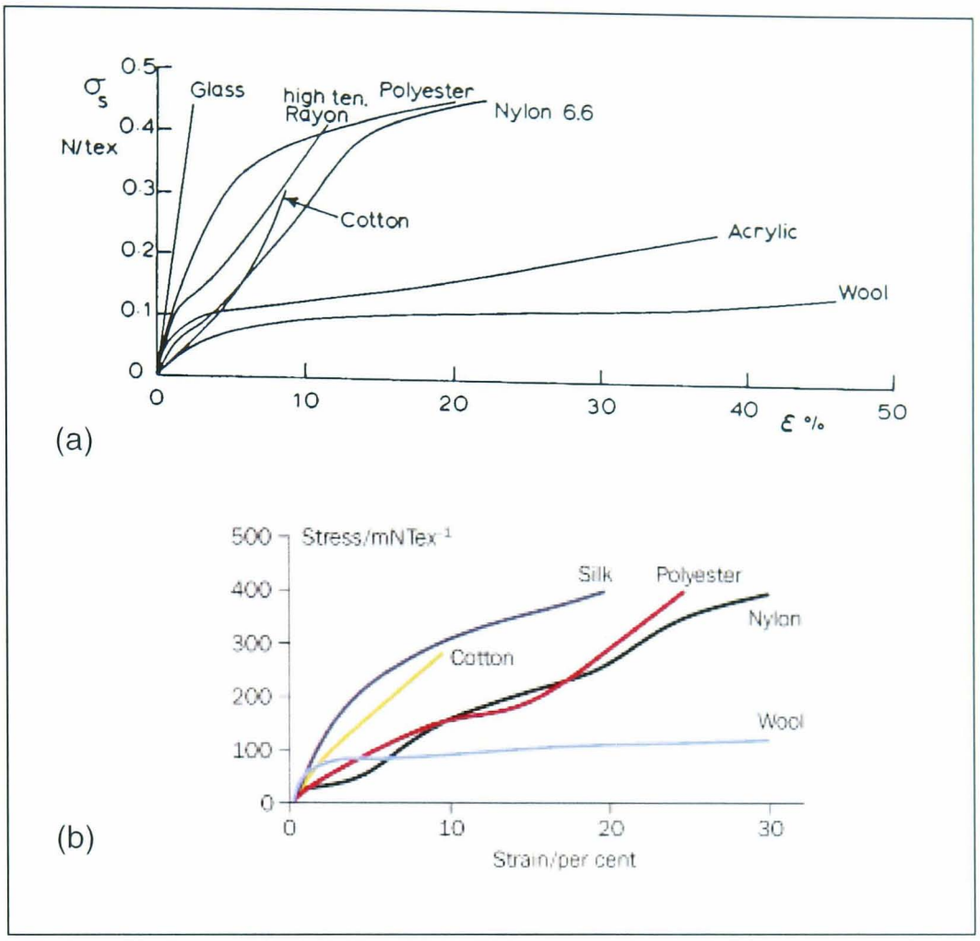

Figure 2-2. Stress-strain curves for various fibres[‡], reproduced from (a) Buckley, 1980, (b) Birkett, 2002.

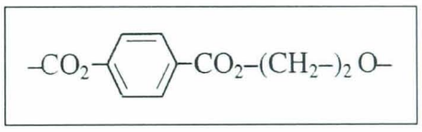

Figure 2-3. Polyester molecule, reproduced from Osswald & Menges, 1996, p. 41

Polyester fibres are composed of long-chain molecules, arranged approximately parallel and held together by lateral forces (Figure 2-4). It is this structure that gives fibres their distinctive

---

[‡] In most engineering applications stress is defined as load divided by cross-sectional area. However, the cross sectional area of a fibre is not necessarily well defined or constant. Variations are due to a non-constant yarn shape and changes in this shape under loading. It is therefore common to define the *specific stress* based on the mass of the fibre:

$$\textit{Specific stress} = \textit{load} / (\textit{mass} / \textit{unit length}) \quad \textit{Units: N/Tex}$$

The *Tex* is a measure of mass per unit length used for fibres, and is the weight in grams of a 1000m length of fibre.

tensile properties. Polymeric fibres are viscoelastic and "*at larger strains (typically beyond 0.001 to 0.01) the viscoelastic behaviour become measurably non-linear*" (Buckley, 1980).

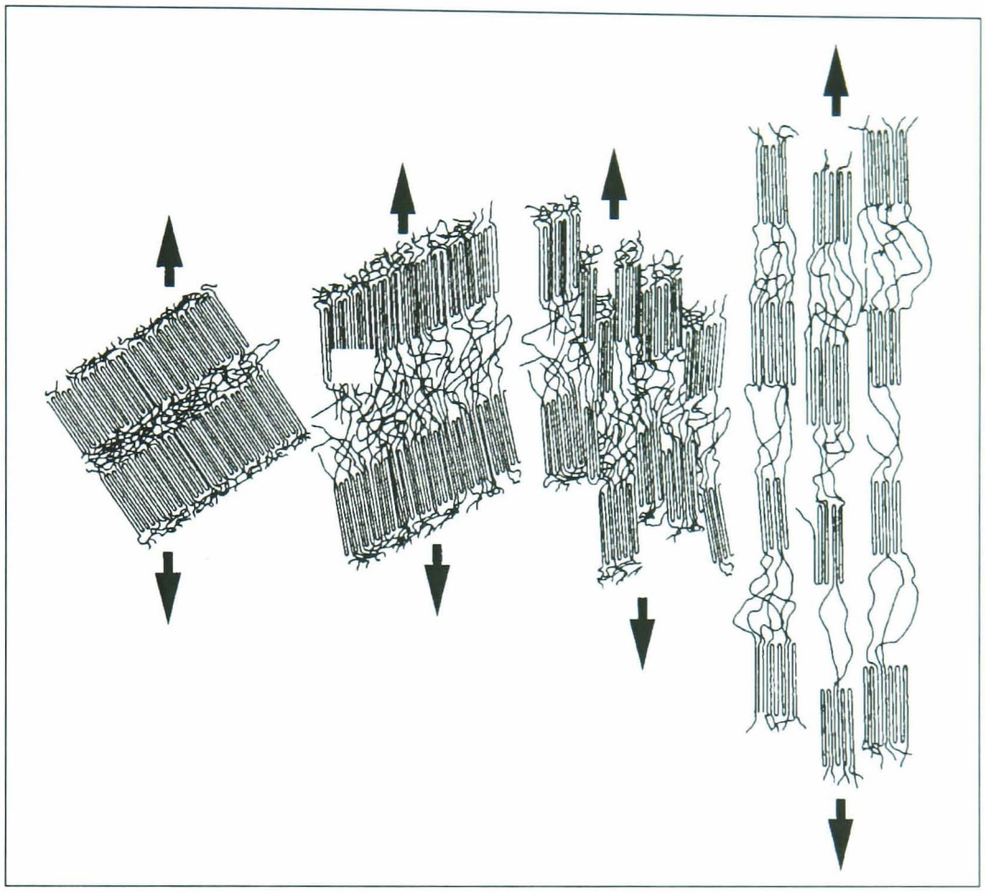

Figure 2-4. Molecular model of polymer tensile extension, reproduced from Osswald & Menges, 1996 (p.333)

Non-linear behaviour can be due to inelastic and/or time-dependent behaviour. Fibres under cyclic tensile loading take several cycles to become *mechanically conditioned* before following a hysteretic load-recovery pattern (Figure 2-5). The hysteretic behaviour is caused by energy loss due to internal friction.

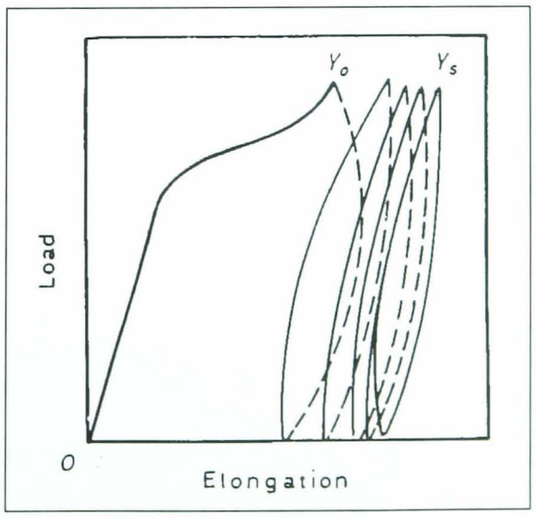

Figure 2-5. Cyclic loading of acetate to 90% of failure load, reproduced from Morton & Hearle, 1975.

The tensile response of fibres is dependant not only on their load history, but also the rate of loading. When a stress is applied there is an initial 'instant' deformation, followed by further deformation over time. *"On the application of a load to a fibre, it will, after an instantaneous extension, continue to extend as time goes on; and, on removal of the load, the recovery will not be limited to the instantaneous recovery, but will continue to take place"*, Morton & Hearle, 1975. The total extension can be subdivided into three parts; immediate elastic deformation (virtually instantaneous and recoverable), primary creep (recoverable in time), secondary creep (non-recoverable). Another time effect is the relaxation of stress under constant loading: *"When a fibre is held stretched, the stress in the fibre gradually decays. It may drop to a limiting value or it may disappear completely"*, Morton & Hearle, 1975.

Polymeric fibres exhibit significant levels of creep under sustained loading (Figure 2-6). If the creep data is plotted on a log-log graph *"in the majority of cases, the creep curves reduce to straight lines as shown for polypropylene"* (Figure 2-6b), (Osswald & Menges, 1996, p 27). It follows that polymer creep behaviour can be represented by a power law:

$$\epsilon(t) = M(\sigma, T)t^n, \qquad \text{Equation 2-1}$$

where M and n are parameters used to define the material.

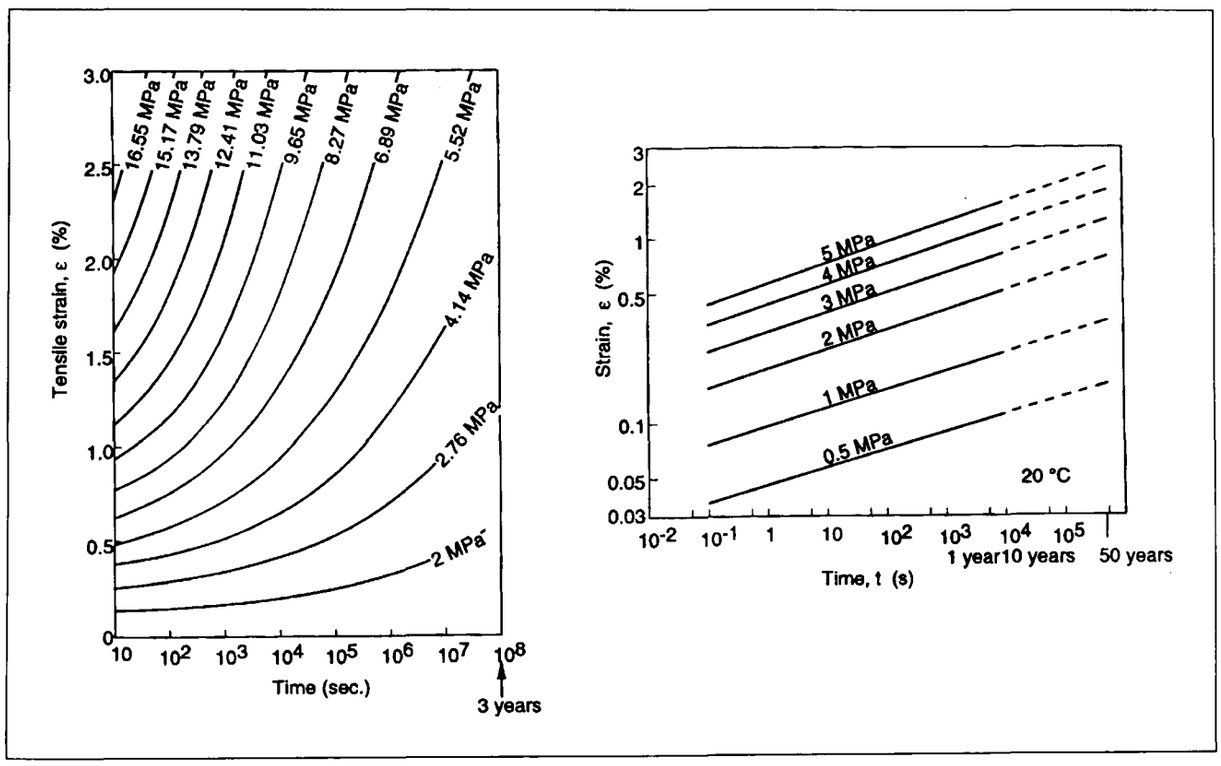

Figure 2-6. Polymer creep response, reproduced from Osswald & Menges, 1996 (p. 272)

In contrast to polyester fibres, glass fibres have higher tensile strength and are less susceptible to ageing, with sunlight having little effect on the material. *"According to experimental data, the high strength of glass fibres in comparison with massive glass is determined by the more isotropic structure of the high-temperature glass melt from which the fibres are produced and*

by their high rate of cooling, which prevents the formation of microdefects and microcracks on the surfaces of the fibres during their formation", Kostikov, 1995, pp 117-118. Compared to polyester, glass fibres have low elastic strain making accurate determination of compensation values and cutting patterns critical for successful installation. Glass fibres are brittle in bending and require careful handling during fabrication, transportation and erection (Ansell, Hill & Allgood, 1983). They are weakened if water penetrates the fabric: *"It is known that the strength of glass filaments is reduced in wet air and in water, irrespective of their chemical composition"*, (Kostikov, 1995, p 107).

Glass fibres are drawn from a glass melt; the physical and chemical properties of the melt, and rate of solidification, dramatically affect the final fibre properties. There are two generic types of fibre: continuous and staple (Kostikov, 1995, pp 24-25). Continuous fibres are long (tens to hundreds of kilometres) and are often arranged in parallel in the yarn. Staple fibres are shorter (several millimetres to two metres) and must be twisted in the yarn to achieve tensile strength through inter-yarn friction. Architectural fabrics typically use three to five micron diameter continuous fibres which are spun to form the yarn.

The tensile stress-strain behaviour of glass fibres is essentially linear (Figure 2-2a), hence use of a single value of Young's modulus to describe the fibre extension is appropriate. Glass fibres exhibit a low level of hysteresis; loading and unloading behaviour are similar with low residual strain.

Typical material properties for fibres used in architectural fabrics are summarised in Table 2-1.

	Polyester fibre[1]	Glass fibre[1]	Aramid fibre[2]	PTFE fibre[2]
Tensile strength (N/mm^2)	400-800	3400-3700	up to 2700	160-380
Elongation at break (%)	25-50	3.3-4.8	2-4	13-32
Elastic modulus (N/mm^2)	3500-15000	72000-77000	130000-150000	700-4000
[1] Osswald & Menges (1996), [2] Houtman & Orpana (2000)				

Table 2-1. Architectural fabric fibre material properties

Inconsistencies in the behaviour of fibres of the same type are important in defining their properties. As properties are not consistent between fibres of the same type then the best that can be achieved is a statistical distribution to represent the probable fibre properties. This adds a further non-linear aspect to fibre behaviour. Buckley (1980) discusses the variations in fibre behaviour, not just between different types of fibre but between individual fibres of the same

type. He states that the *"degree of molecular orientation... and the effect of any subsequent thermomechanical treatment"* affect the stress-strain curves. For example, it is not only the environmental conditions (temperature and relative humidity) at the time of the test that affect the behaviour of the fibre, but the conditions to which it has been previously exposed. Any quantification of fibre behaviour is very complex, and must account for test conditions and previous history – both in terms of loading and environment.

How does the yarn structure contribute to the non-linear behaviour of the fabric?

Several hundred fibres are assembled together (often twisted) to form a yarn. As with any engineering material, yarn behaviour can be characterised in terms of response to various forms of loading: tensile, bending, shear and torsion. The *"mechanical behaviour of a yarn depends on the properties of the fibres of which it is composed, and their arrangement"*, (Hearle, 1958). The movement of the fibres within the yarn must be considered – in bending the fibres slide relative to one another, hence bending is resisted by inter-fibre friction. Because of variations in the constituent fibres and yarn structure it is apposite to describe yarn properties using a statistical distribution of probable values.

Fabric structures resist load by deformation in the plane of the fabric, resulting in tension and shear in the fabric. The primary load condition of the yarns is therefore tensile. When a tensile load is applied to a typical engineering material the resultant stress is equal to the applied force divided by the cross-sectional area. Subjecting a yarn to a tensile load gives both elongation of the constituent fibres and a change in the angle between the fibres and the yarn, i.e. part of the tensile force results in untwisting of the yarn. Yarn extension is *"characterised by a progressive stiffness at low loads, which is due to the initial stretch of the yarn until the fibres are in contact with each other"* Dimitrov & Schock (1986). An identical mechanism in cords (i.e. several yarns twisted together) is described by Zimliki, Kennedy et al (2000a): *"...the act of straining a cord structure produces both elongation of the filaments and straightening of the angle that the ply makes with the cord axis"*. Furthermore *"there is also energy dissipated by interfilament slippage"*. Conversely, Thwaites (1980) states that inter-fibre movement does not result in a significant loss of energy: *"The ratio of energy lost per cycle to maximum energy stored for the yarn is very little different from that for the fibre material itself (in tension). This shows that there is little or no frictional energy loss due to relative motion between filaments"*.

The simplest type of yarn is composed of parallel, untwisted fibres but is prone to severe deformation and damage, but *"...to overcome fibre slippage, and to form fibres into a functional yarn, strands are usually given some amount of twist"* (Naik & Madhavan, 2000). Untwisted yarns have the advantage that they *"permit a relative sliding of the fibres in case of yarn curvature and the stress state in the yarn remains in form"* (Boisse, Gasser & Hivet,

2001). If all fibres were identical (to each other, and along their lengths) then little would be gained in terms of tensile strength by twisting yarns together. However all fibres have a varying cross-section and consequently have weak points. Twisting bundles of fibres together introduces radial forces which increase inter-fibre friction and so enable more effective load sharing to prevent weak fibres breaking. Twisting also increases yarn surface friction (improving handling and the *dimensional stability* of the finished fabric), reduces fibre slippage and "*tends to make the yarns more monolithic*" (Naik & Madhavan, 2000). It is for these reasons that yarns used for architectural fabrics are typically of a twisted construction.

The idealised structure of a continuous twisted yarn is often represented as being composed of uniform helices varying from a straight fibre at the centre of the yarn with helix angle increasing with increasing radius. This would suggest that the yarn properties are geometrically linear, the resistance to extension being similar to that of a spring It has been noted however (Morris, Merkin & Rennell, 1999) that the actual structure of yarns has a 'random' element due to the interaction of the fibres. "*The highly idealized form of structure... would not only be useless if it existed; it could not even be made...*" (Morton, 1956, p.325). "*...effects such as micro-buckling and migration have been observed. Because of these effects, the perfect helix assumption is not valid*" (Naik & Madhavan, 2000).

Migration is the "*entanglement of the fibres within the yarn*" (Morris, Merkin & Rennell, 1999). The central fibre is straight and the outer fibres have significant helical curvature, but all of the fibres are initially the same length. Hence the outer fibres are highly stressed, and they will move towards the centre of the yarn. "*Those* [fibres] *momentarily forming the surface layers will therefore tend to move in toward the core position, displacing the less highly tensioned fibres already there, and in due course are themselves displaced when their tension has fallen*" (Morton, 1956, p.325). Hence the path a given fibre takes will vary along the yarn, traversing through the cylindrical zones of the structure. Migration can be quantified by considering the ratio between the length of the outermost filament after migration, and the length of the outermost filament assuming a perfect helix. A 'migration zone' can then be determined, and the effect of migration is to make the path lengths in this zone equal, i.e. the twist for all filaments in the zone is equal (Figure 2-7).

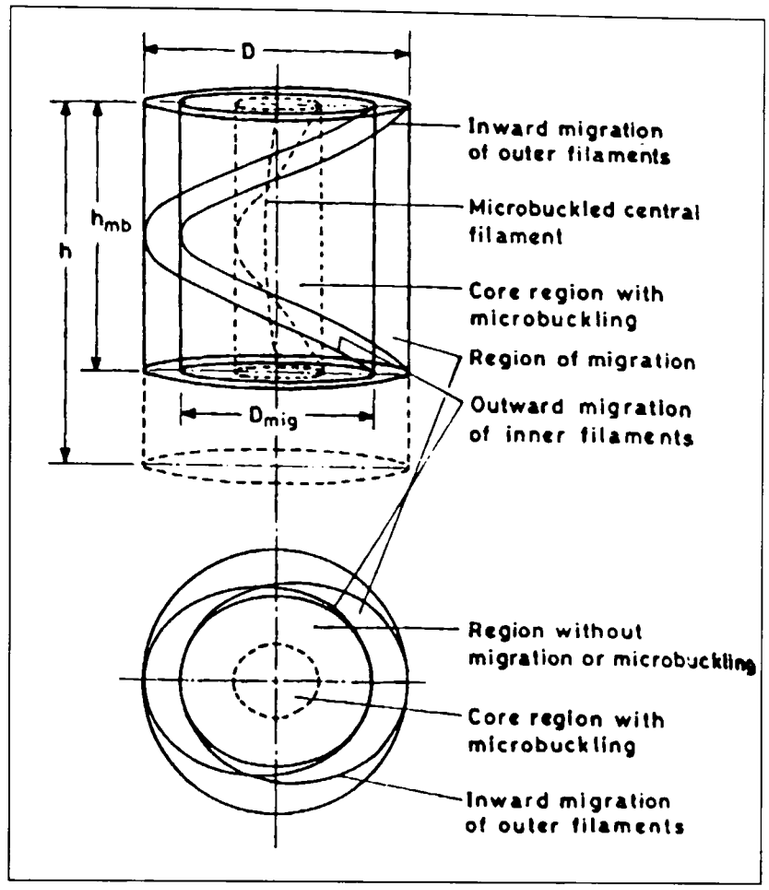

Figure 2-7. Migration and microbuckling, reproduced from Naik & Madhavan (2000)

The central filaments of a yarn undergo microbuckling - *"The effect of microbuckling is to reduce the pitch length of the yarn"*, (Naik & Madhavan, 2000) (Figure 2-7). Without microbuckling the central filament would be straight. However, the central filament does have some twist, and there is *"a zone where all filaments have the same length as they had prior to twisting"* (Naik & Madhavan, 2000). Microbuckling is quantified in a similar way as migration, by comparing the ideal pitch length to a reduced value for the microbuckled yarn.

Changes in yarn diameter are important in determining the exact geometry of the fabric, and hence its behaviour (§2.4.2 and Chapter 5). Pierce (1937) described the distortion of yarns at crossover points as *"much too great in most fabrics to ignore"*. There are three mechanisms which may result in a change in yarn radius:

- Initial bedding down (inelastic),
- Yarn crushing due to contact with orthogonal yarn (elastic or partially inelastic),
- Reduction in yarn radius due to tensile extension, i.e. Poisson's effect (elastic or partially elastic).

Both tensile stresses and transverse loads result in changes to the cross-sectional area of the yarn, *"...the reduction in yarn radii is caused by the coupled effect of the crushing force that is present at crossover points and the axial force in the yarn"* (Pargana, Lloyd Smith & Izzuddin,

2000). Hearle & Sakai (1978) use a "*diameter shrinkage function*" to model the change in yarn diameter, which is based on a constant Poisson's ratio. Morris, Merkin & Rennell (1999) use a function of fibre packing density and fibre Poisson's ratio to determine the overall Poisson's ratio of the yarn at any given location. This function, combined with a randomised fabric structure, gives a varying value of Poisson's ratio along the yarn. Under constant tensile load the yarn diameter varies along the length of the yarn.

The yarn diameter changes due to "*bedding-down of one yarn into the opposite one. This effect is due to the initial slack between the individual fibres... It may be assumed that the bedding down is irreversible*" (Dimitrov & Schock, 1986). This initial *bedding down* of the yarn (i.e. reduction in yarn radius when the fabric is first loaded) is influenced by:

- initial slack between fibres in the yarn,
- coating penetration into the yarn between the fibres,
- bending stiffness of fibres,
- lateral compressibility of fibres,
- spinning characteristics of the yarn.

The difficulty is that there is "*a most apparent lack of data on any of these factors*", (Dimitrov & Schock, 1986). Yarn crushing tests show an increase in tensile stiffness as the yarn is crushed, and some hysteresis during recovery when the load is removed (Figure 2-8b) (Kawabata, Niwa & Matsudaira, 1985; Sasai & Kawabata, 1985). However, the results are not conclusive, with the authors stating that "*the experiments must be measured more precisely*" (Sasai & Kawabata, 1985).

The bending resistance (or flexural rigidity) of yarns is very low compared to their resistance to tensile load along their length. Thus in the interest of simplicity the flexural rigidity is often ignored in fabric analysis. Boisse et al (1997) dismiss not only the bending stiffness of fibres, but also of the yarn and fabric: "*Yarns consist of very small section fibrins whose bending stiffness is negligible, therefore these of yarns and fabric are negligible too.*"

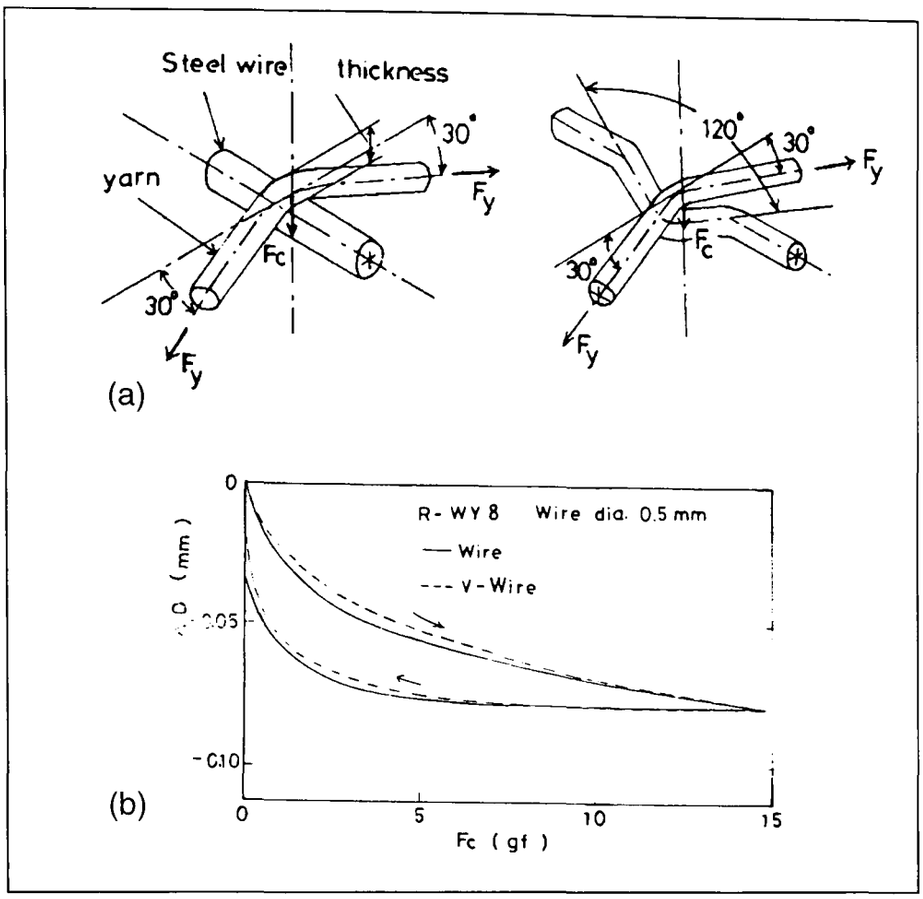

Figure 2-8. (a) Methods for testing crushing of yarns, (b) change in diameter with load; reproduced from Kawabata, Niwa & Matsudaira (1985)

Cooper (1960) compares the flexural stiffness of three types of yarn structure; independent filaments, adhering filaments and twisted yarns. Twisted yarns allow little inter-fibre movement, and so might be considered to behave similarly to a yarn model with 'adhering filaments'. On the contrary, Cooper suggests that "*twisted yarns are often found to have bending lengths close to those expected for free fibre movement*". This observation led to investigation of the relationship of twist to bending length for continuous filament viscous rayon. He found that values were close to those expected for independent filaments, but "*slightly increased stiffness was sometimes found with the yarns of higher twist*". This increase in yarn stiffness due to the twisted yarn structure is dependent on the level of inter-yarn friction, and so will be greater for high friction polyester fibres than for lower friction glass fibres. However, the conclusion of Cooper's work is that the bending stiffness of all yarns is very low, usually little higher than the sum of the fibre bending stiffnesses.

Yarn bending stiffness is generally regarded as negligible for the typical small changes in curvature which occur in membrane structures (§2.1.4.4). However, the yarn bending stiffness may be significant on the scale of individual yarn crossovers in the fabric. Crimp interchange results in large changes in curvature at small radii compared to the yarn diameter. A limiting bending condition can be reached when the cross-sectional shape of one yarn prevents further bending of the orthogonal yarn (Peirce, 1937).

2.1.2 Woven fabric

Yarns are woven on looms to form a fabric. Many weave patterns are possible (e.g. twill and panama, Figure 2-9) but architectural fabrics are typically plain woven. This is the simplest weave pattern in which alternate yarns pass under and over one another (Figure 2-9a).

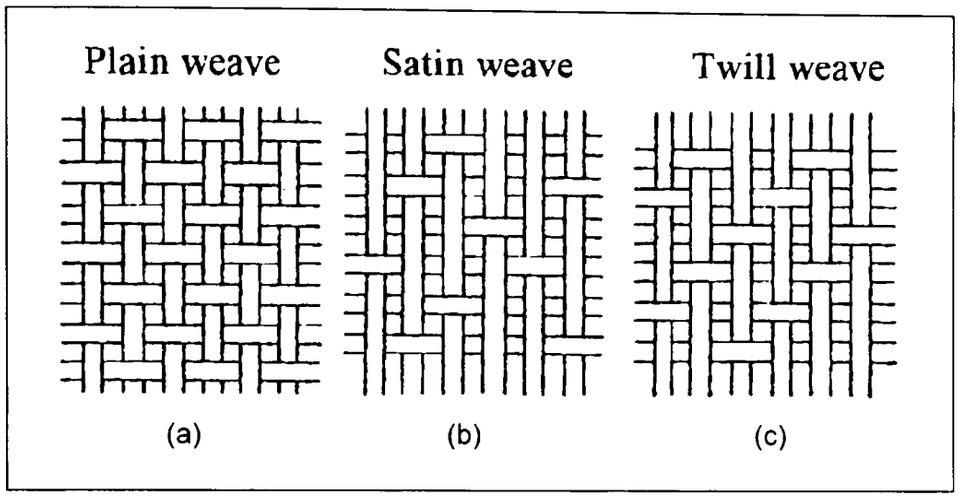

Figure 2-9. Common weave patterns, reproduced from MSAJ/M-02-1995

The similar weave pattern of most architectural fabrics means that the same principles govern their mechanical behaviour. However, the actual fabric behaviour varies widely between fabrics and the dominant effect governing the fabric behaviour is not necessarily the same for all fabrics. This is due to significant differences in fibre, yarn and coating properties.

The weaving process strongly influences the behaviour of the finished fabric. During manufacture, when the fabric is being transferred from roll to roll, a skew or bowing can be introduced to the weave pattern (Skelton and Freeston, 1971; Reumann, R.-D., 2000). This non-orthogonality can compromise the *dimensional stability* of the fabric. The resultant inconsistency in material properties across the width of the roll should be considered when cutting test samples. The weaving process involves bending the yarns, especially the fill yarn, as the warp and fill are interwoven. This can result in damage of the yarn fibres, particularly for a glass fibre fabric. The level of strength reduction varies with the material, weaving process (hydraulic, pneumatic or shuttle) and yarn direction (warp or fill) but is broadly in the region of ten percent (Kostikov, 1995, pp.107-108).

2.1.3 Coating

Coating is applied to open weave architectural fabrics to make them watertight. The coating also stabilises the fabric weave pattern and protects the yarns from damage. Any bowing of the fill yarns during weaving will be fixed in place by the coating: *"The act of coating sets fabric in its bowed or skewed configuration"* (Skelton and Freeston, 1971). The addition of the coating

further complicates the mechanical properties of a woven fabric. The coating will restrain the yarn movements and interactions, and adds a visco-elastic effect to any deformation mechanism (Testa, Stubbs & Spillers, 1978). Depending on the coating material, the mechanical behaviour of the coating can be "*highly non-linear and time dependent*" (Schock, 1991). Creep of the coating causes fabric strain to slowly increase, tending toward that of uncoated fabric.

The coating can impregnate the yarns during the coating process, changing their mechanical properties: "*The bedding down will usually be restrained by the coating material which will have penetrated the yarns to some degree*", (Dimitrov & Schock, 1986). However, the extent of this impregnation is variable and difficult to determine. In uncoated yarns it is frequently assumed that yarn crushing due to gaps between fibres is irreversible. If these gaps contain coating then the level of yarn crushing would be reduced, and may exhibit some elasticity. Coating of yarns increases their strength by bonding the fibres together and thereby localising the effect of broken fibres: "*In an unimpregnated yarn consisting of fibres only, the deformability of the fabric is provided through yarn sliding... However, in an impregnated yarn the deformability of the fabric is greatly reduced*", Naik and Madhavan (2000).

The tear resistance of the fabric is actually reduced by the coating because the yarns cannot move as easily to resist tearing forces (www: Architectural fabrics, 2004). The lateral contraction of the coating under tensile load could affect the fabric behaviour; "*As the Poisson's ratio of PTFE is rather high it is worth considering*" (Dimitrov & Schock, 1986). The bending stiffness of the coating is usually deemed to be negligible for structural applications (Testa, Stubbs & Spiller, 1978).

The two most commonly used coating materials are polytetrafluoroethylene (PTFE) on glass fibre fabric and polyvinyl chloride (PVC) on polyester fabric (Table 2-2). PTFE has recently been applied to PTFE-fibre fabric. This presents manufacturing problems in trying to adhere the coating to the base fabric when both have low surface friction and are chemically unreactive. The benefit is an extremely flexible, durable fabric with high (around 40%) light transmission (Kelmartin, 2003).

	Polytetrafluoroethylene	Polyvinyl Chloride
Tensile strength (N/mm^2)	25-36	10-25
Elongation at break (%)	350-550	170-400
Tensile modulus of elasticity (N/mm^2)	410	1000-3500

Table 2-2. PVC and PTFE material properties, reproduced from Osswald & Menges (1996)

Polytetrafluoroethylene (PTFE) is formed by the addition polymerization of tetrafluoroethylene (Figure 2-10). It is distinguished by its complete resistance to attack by virtually all chemicals and by its low surface friction. It maintains its physical properties over a large temperature range (-270° to 385°C) (www: Polymers, 2004).

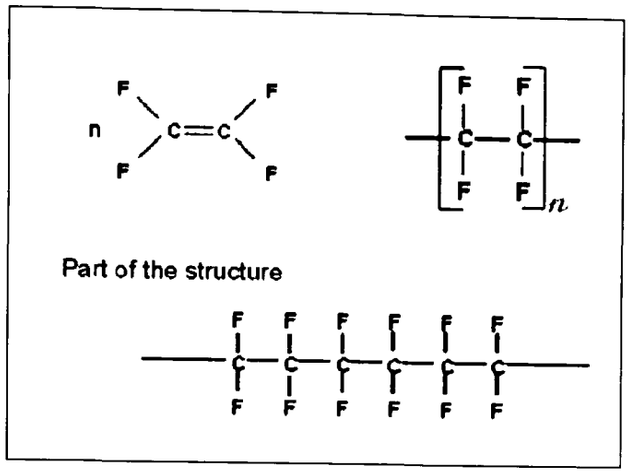

Figure 2-10. PTFE structure, reproduced from www: Addition polymers, 2004

The coating comprises three main layers (www: Taconic, 2004):

- Base coat: ensures adhesion of subsequent layers to the glass fibre fabric,
- PTFE and filler: this main layer is built up from repeated applications of PTFE dispersion, with the fabric being heated between applications to sinter the PTFE onto the base fabric. The 'filler' usually consists of glass beads,
- Top coat: an FEP (Fluorinated Ethylene Polymer) layer which increases impermeability, fungal resistance and weldability.

PTFE coating, combined with the long lifespan of glass fibres, results in a fabric with a service life in excess of thirty years (Houtman & Orpana, 2000). Silicone coating is also used on glass fibre fabric, providing high levels of light transmission (up to 25%) compared with 8-13% for PTFE or PVC coatings. The silicone rubber protects the brittle glass fibre yarns, reducing the tight radii which damage the fabric when it is creased or folded (Houtman & Orpana, 2000). Research is ongoing into coating polyester fabric with silicon to provide a highly translucent flexible fabric.

Polyvinyl chloride (PVC) is commonly used to coat polyester fabric, and also woven aramid. Polymerization of vinyl chloride produces a polymer similar to polyethylene, but having chlorine atoms at alternate carbon atoms on the chain (Figure 2-11). In this form PVC is rigid and somewhat brittle. When blended with a plasticizer such as phthalate ester it becomes pliable and is used for flexible articles such as raincoats and shower curtains. It is this plasticized PVC that is used to coat architectural fabrics. Over time the plasticizer migrates to the surface and breakdowns due to UV exposure. This results in dirt retention and weakening of

the coating (www: Architectural fabrics, 2004); consequently various top-coats are applied to modify the surface properties (Houtman, 2003). When choosing the top coat a compromise must be made between resistance to soiling and weldability. The PVC coating is applied as a liquid which is scraped off to the correct thickness and then gently heated to dry the fabric.

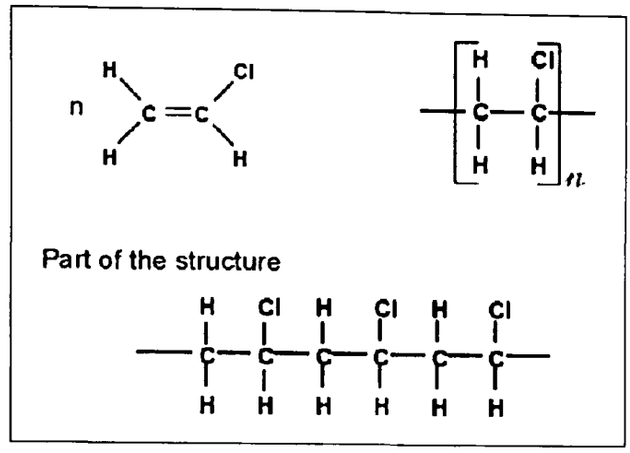

Figure 2-11. Polyvinyl Chloride structure, reproduced from www: Addition polymers, 2004

2.1.4 Mechanical behaviour of architectural fabrics

2.1.4.1 Material types and properties

The most commonly used architectural fabrics are PVC coated polyester (Figure 2-12) and PTFE coated glass fibre (Figure 2-13). They have distinct characteristics, often making the choice of material obvious for a given application. PVC-polyester is quite flexible, reducing the risk of damage during fabrication and installation. It does suffer UV degradation and dirt build up, resulting in a life expectancy of 12-15 years. PVC-polyester is produced in a range of weights, the heaviest fabrics being extremely strong (tensile strength up to 200kN/m). The flexibility of the fabric results in low resistance to shear; enabling highly double-curved shapes to be developed without wrinkling.

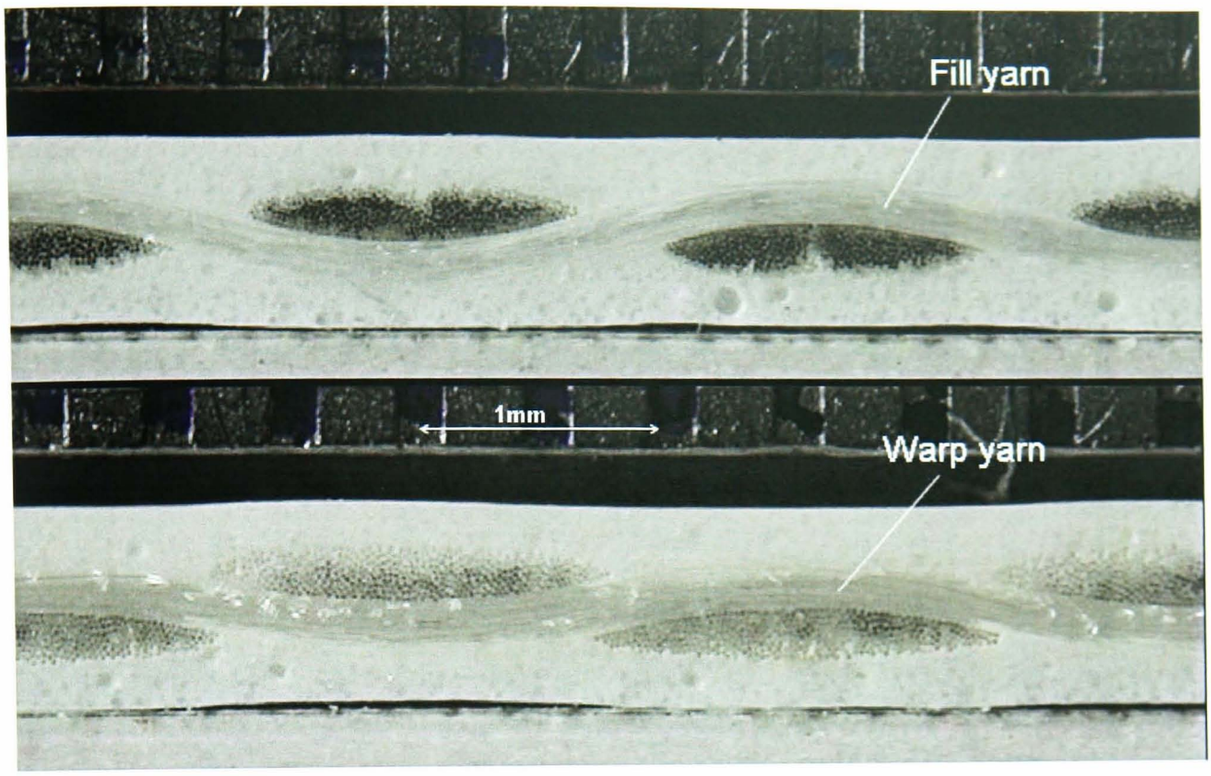

Figure 2-12. PVC-polyester fabric cross-section

PTFE-glass has a life expectancy greater than 30 years, but does cost around five times as much as PVC-polyester. PTFE-glass is easily damaged by folding or creasing, and so requires great care in handling and erection. The fabric is self cleaning and highly fire retardant. An uncoated glass fibre fabric has very low shear resistance due to the low level of friction between the yarns at crossovers. The PTFE increases the shear resistance substantially, giving a fabric which is less conformable and more likely to wrinkle than PVC-polyester (§2.1.4.3). PVC-polyester and PTFE-glass provide similar levels of light transmission (8-13%). Other types of fabric include silicone coated fabrics and PTFE yarns with a PTFE coating (§2.1.3).

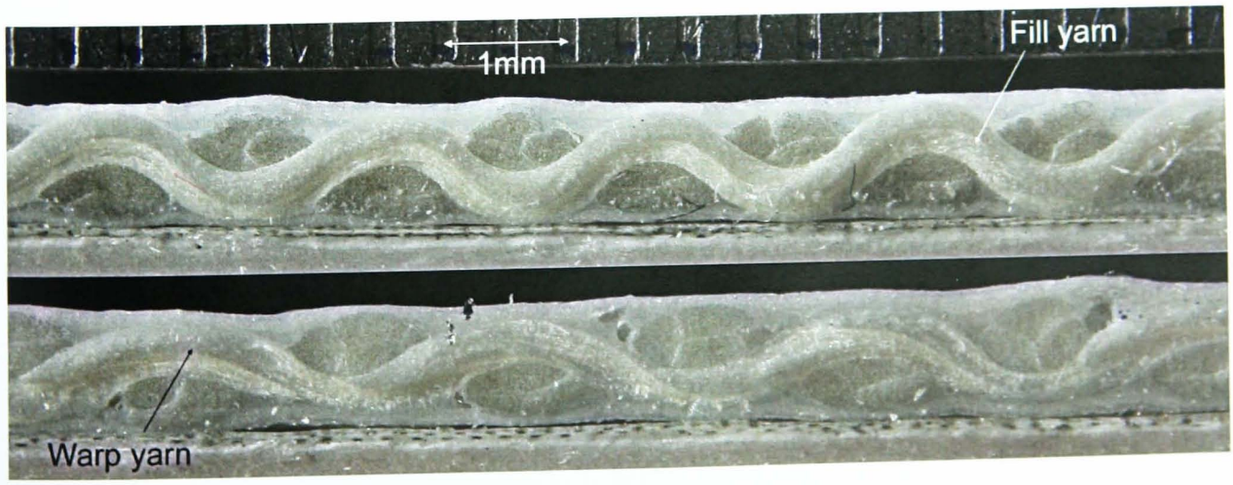

Figure 2-13. PTFE-glass fabric cross-section

It is clear from the fabric cross sections (Figure 2-12 & Figure 2-13) that the weave geometry of PVC-polyester and PTFE-glass fabrics are different; the PTFE-glass fabric has a notably higher level of crimp than the PVC-polyester. It is a combination of the weave geometry with the yarn and coating properties that determine the mechanical properties of the fabric (Figure 2-14 and Figure 2-15).

Fabric/ Coating	Weight g/m2 Din 55352	Fire retardant DIN 4102	Tensile strength Warp/weft N/50mm DIN 53354	Tensile strain Warp/weft % DIN 53354	Tear strength N DIN 53363	Bending capacity	Seam strength N/50mm
Cotton-Polyester/-	350	B2	1700/1000	35/18	60	Very good	
	520	B2	2500/2000	38/20	80		
Polyester/PVC							
Type 1	750	B1	3000/2800	15/20	300/280	Very good	2400 (30mm, 700c)
Type 2	1050		4200/4000	15/20	550/500		2850 (60mm, 700c)
Type 3	1050		5600/5600	15/25	800/650		3350 (60mm, 700c)
Type 4	1350		8000/7000	15/30	1200/1100		4600 (60mm, 700c)
Type 5	1500		10000/8000	20/30	1600/1400		4600 (60mm, 700c)
Fiberglas/PTFE	800	A2	3500/3000	7/10	300	sufficient	6000 (60mm, 700c)
	1270	A2	6600/6000	7/10	570		
Fiberglas/Si	350	B1	2000/2000			Good	4800 (30mm, 700c)
	1156	A2	5000/5000				
Aramid/PVC	750	B1	7500/7500	5/6	500/500	Good	
	1050		8000/6500	5/6	600/600		
	2020		24500/24500	5/6	4450		
PTFE/-	300	A2	2390/2210	11/10	500	Very good	
PTFE/PVDF	630	B1	3000/2900	11/10	818/854		
PTFE/PVDF	830		4200/4000	18/9	925/925		
PVDF/PVDF	200	B1	1400/1300	34/25			
	260		1600/1500	39/30			
ETFE foil thickness			N/mm2 (DIN 53455)				
50 m	87.5		64 / 56	450 / 500	450 / 450	sufficient	
80 m	140		58 / 54	500 / 600	450 / 450		
100 m	175		58 / 57	550 / 600	430 / 440		
150 m	262.5		58 / 57	600 / 650	450 / 430		
200 m	350		52 / 52	600 / 600	430 / 430		
250 m	437.5		>40 / >40	>300/ >300	>300 / >300		

Figure 2-14. Typical mechanical properties of architectural fabrics (1), reproduced from Houtman (2003)

(a)

Type	1	2	3	4	5
Surface weight (g/m²)					
French design guide	720	1 000	1 200	1 400	2 000
WG Messe Frankfurt	800	900	1 050	1 300	1 450
Yarn linear density (dtex)					
French design guide					
WG Messe Frankfurt	1 100	1 100	1 670	1 670	2 200
Tensile strength warp/weft (kN/m)					
French design guide	60/60	84/80	110/104	120/130	160/170
WG Messe Frankfurt	60/60	88/79	115/102	149/128	196/166
Trapezoïdal test warp/weft (N)					
French design guide					
WG Messe Frankfurt	310/350	520/580	800/950	1 100/1 400	1 600/1 800
Yarn number per cm warp/weft					
French design guide					
WG Messe Frankfurt	9/9	12/12	10.5/10.5	14/14	14/14

(b)

Type	G1	G2	G3	G4	G5	G6	G7
Tensile strenght warp/weft (kN/m)	26/22	43/28	70/70	90/72	124/100	140/120	170/158
Filament diameter (micrometer)	9	6	3	6	3	3 or 6	3
Surface weight (g/m²)	500	420	800	1 000	1 200	1 500	1 600
Trapezoïdal tear warp/weft (N)			300/300	300/300	400/400	500/500	450/450

Figure 2-15. Mechanical properties of architectural fabrics (2): (a) PVC-polyester, (b) PTFE-glass fibre, reproduced from the Tensinet Design Guide (Mollaert & Forster, 2004)

2.1.4.2 In-plane tensile behaviour

The tensile behaviour of architectural fabrics is highly non-linear due to both material properties and geometric non-linearities. Uniaxial fabric strip tests give a non-linear stress-strain curve (Figure 2-16) which can be intuitively explained. Initial large strain at low load is principally due decrimping, particularly for a sample loaded in the fill direction. Some tensile stiffness is provided by the coating. Slack between yarn fibres, and between yarns at crossovers, can further decrease the fabric tensile stiffness when initially loaded. Once crimp interchange is complete, the fabric response is dominated by the yarn behaviour: a non-linear three part response for polyester (Figure 2-16) and a steep linear response for glass fibre (§2.1.1).

The response to biaxial loading is more complicated as geometric non-linearities are introduced. Fundamental to the behaviour of woven fabrics is the interaction of warp and fill yarns, known as *crimp interchange*. Testa, Stubbs and Spillers (1978) identified two stages in fabric deformation: initial crimp interchange followed by yarn extension at higher stresses. It is

crimp interchange that prevents the biaxial response being inferred directly from uniaxial test data, and hence necessitates biaxial testing.

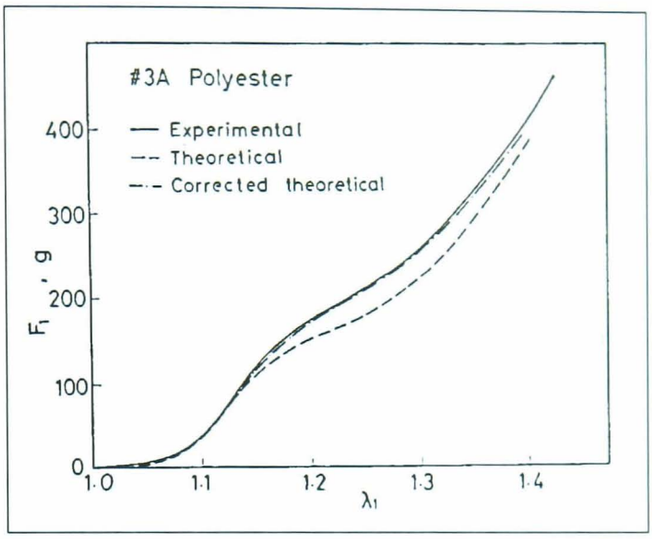

Figure 2-16. Polyester fabric under uniaxial extension, reproduced from Kawabata, Niwa & Kawai (1973b)

Pierce (1937) identified the fundamental deformation mechanisms that characterise the behaviour of woven fabrics under biaxial load, in particular *crimp interchange*. *Loom-state* (i.e. as produced) fabric has a high level of crimp in the fill direction (across the loom) and a low level of crimp in the warp direction (along the length of the roll of fabric) (Figure 2-17a).

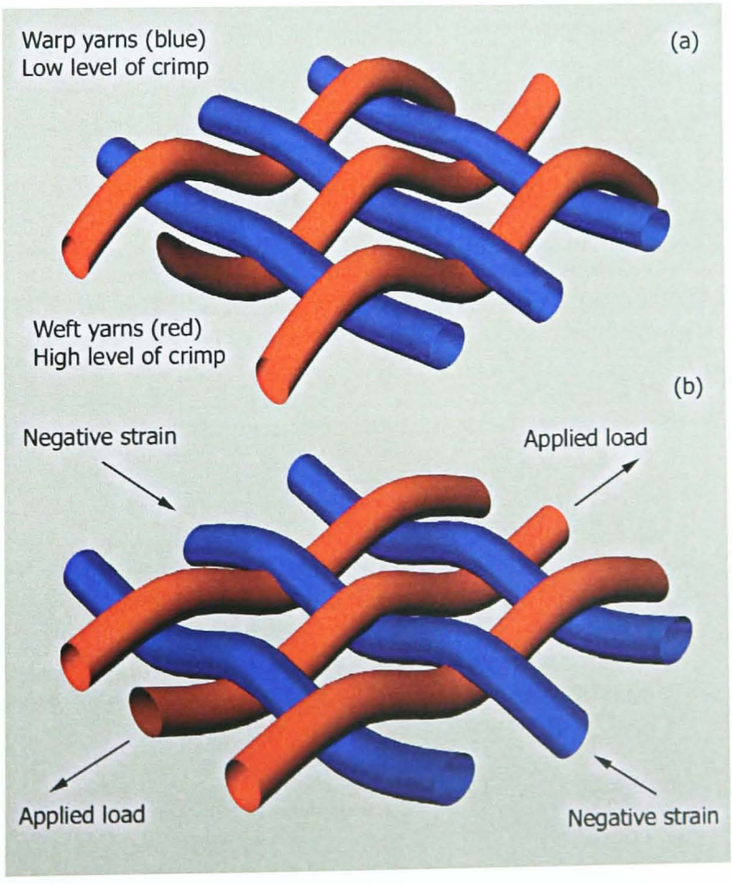

Figure 2-17. Crimp interchange mechanism.

An applied load in the fill direction straightens the fill yarns and increases the crimp in the warp – resulting in a negative strain in the warp direction (Figure 2-17b). Under biaxial load the ratio of the applied loads will determine the equilibrium configuration of the crimp, (Schock, 1991). This balancing of the crimp results in a highly variable level of strain in the orthogonal direction, which is normally related by Poisson's ratio for homogeneous materials (§4.2.1). Typical stress-strain curves for the *initial* behaviour of a PTFE-glass fibre fabric tested at warp to fill stress ratios of 5:1, 1:1 and 1:5 are reproduced from the work of Day (1986), Figure 2-18. The key features of the fabric response are:

1. Sudden changes in gradient (Figure 2-18a,b),
2. Gradient reversal (i.e. multiple values of stress for a given strain) (Figure 2-18a),
3. Negative strain (Figure 2-18b,c).

Initial large strains at low stresses (Figure 2-18a,c) are due to crimp interchange and slack in and between the yarns. The subsequent increase in tensile stiffness occurs when crimp interchange is complete and yarn stretching becomes the dominant deformation mechanism.

The response of coated woven fabrics to biaxial loads is even more complex than is shown by Day's results, which only give the response to initial loading. The material response is hysteretic due to the coating and yarn-fibre material properties and due to frictional effects (inter-fibre and inter-yarn friction). Long-term creep is also significant. Fabric response varies between batches of fabric and even across the width of a single roll. The weave pattern is changed by variation in the fabric tension during weaving and coating. Bowing of the fill yarns is caused by the way the fabric edges are gripped as it moves through the loom. The exact temperature used to sinter PTFE coating on to glass fibre fabric affects the shape of the yarns and the level of bond between them at intersections.

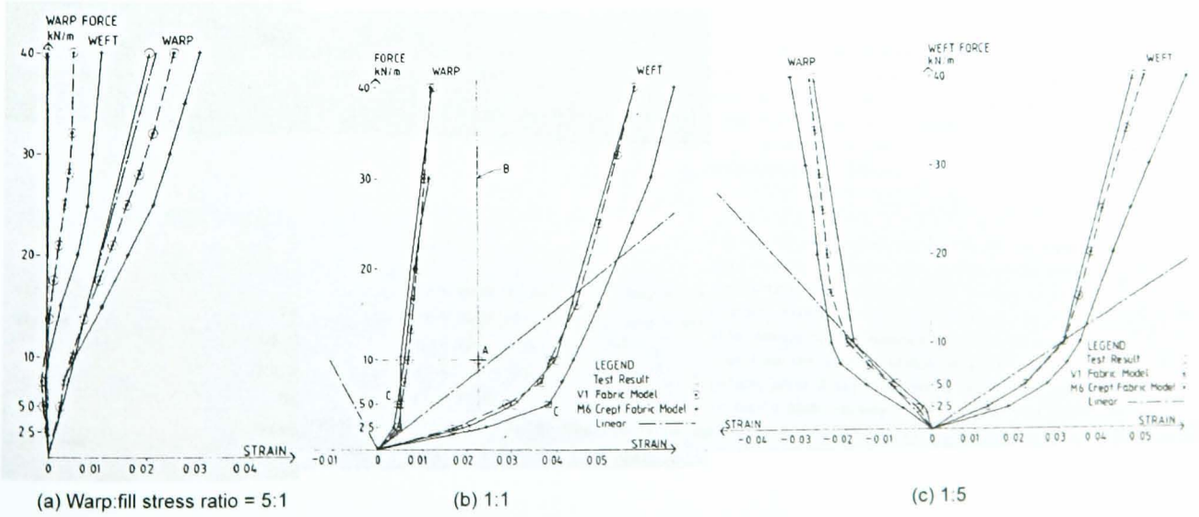

(a) Warp:fill stress ratio = 5:1 (b) 1:1 (c) 1:5

Figure 2-18. Stress-strain graphs for varying stress ratios, reproduced from Day (1986)

The addition of coating further complicates the crimp interchange mechanism. The coating restrains the movement of the yarns such that a greater force is required for complete crimp interchange to occur (Schock, 1991). Schock suggests that large initial fabric stiffnesses are "*possibly due to partial separation of coating*" from the yarns. This is contrary to usual observation of initial low tensile stiffness which increases when crimp interchange is complete (Testa, Stubbs & Spillers, 1978; Day, 1986). The addition of coating increases the non-linearity of fabric behaviour. The increase in stress required for full development of crimp interchange means that a greater part of the stress-strain curve is highly non-linear. The coating also adds a time-dependent, hysteretic element to the crimp interchange mechanism. Testa and Yu (1989) show through a series of tests that the load history of the fabric has a significant influence on its response to applied load. This is confirmed by Freeston, Platt and Schoppee (1967) who consider the effects of loading sequence and loading rate on the stress-strain characteristics of the fabric.

2.1.4.3 Shear

"A woven fabric may be bent into single curvature without any shear deformation; but if a fabric is bent into double curvature... then shearing must occur. In most fabrics, this shearing is likely to be largely explained by a change of angle between intersecting threads, but may also be a result of bending and twisting of the yarns between the intersections."

Cusick (1961)

Shear of fabrics is fundamental to the development of surfaces with double curvature from flat panels of fabric. "*The very low resistance to shear deformation compared with tensile deformation makes it easier for the cloth to cover a curved surface without buckling*", Kawabata, Niwa & Kawai (1973c, p.62). The level of shear deformation that can be mobilised will determine the curvature that can be achieved, and will affect the number of flat panels that are required. The majority of work on fabric shear behaviour has been carried out on non-coated fabrics, usually for modelling drape and conformability for the clothing industry (Amirbayat & Hearle, 1989; Chen, Hu & Teng, 2001; Postle & Norton, 1991; Collier et al, 1991) and more recently in simulating the placement of woven glass base cloth in the manufacture of composites (Tan, Tong & Steven, 1997; Buet-Gautier & Boisse, 2001). For this type of application the shear response under biaxial load is not required, but for fabric structures direct and shear stresses will always be coexistent (§6.2.5).

"*The problem is complicated by the fact that the usual 'shear' test on a woven fabric does not correspond exactly to simple shear*", (Spivak & Treloar, 1968, p.964). Simple shear in engineering terms is a constant area deformation; fabric shear (Figure 2-19) is not. Simple shear

requires the material to extend on the diagonals of the parallelogram (Figure 2-20a). For a given shear force the tensile extension of the yarns will be negligible compared to the large shear deformation (commonly 5 to 15° at working loads). Hence shear deformation leads to a reduction in area (Figure 2-20b).

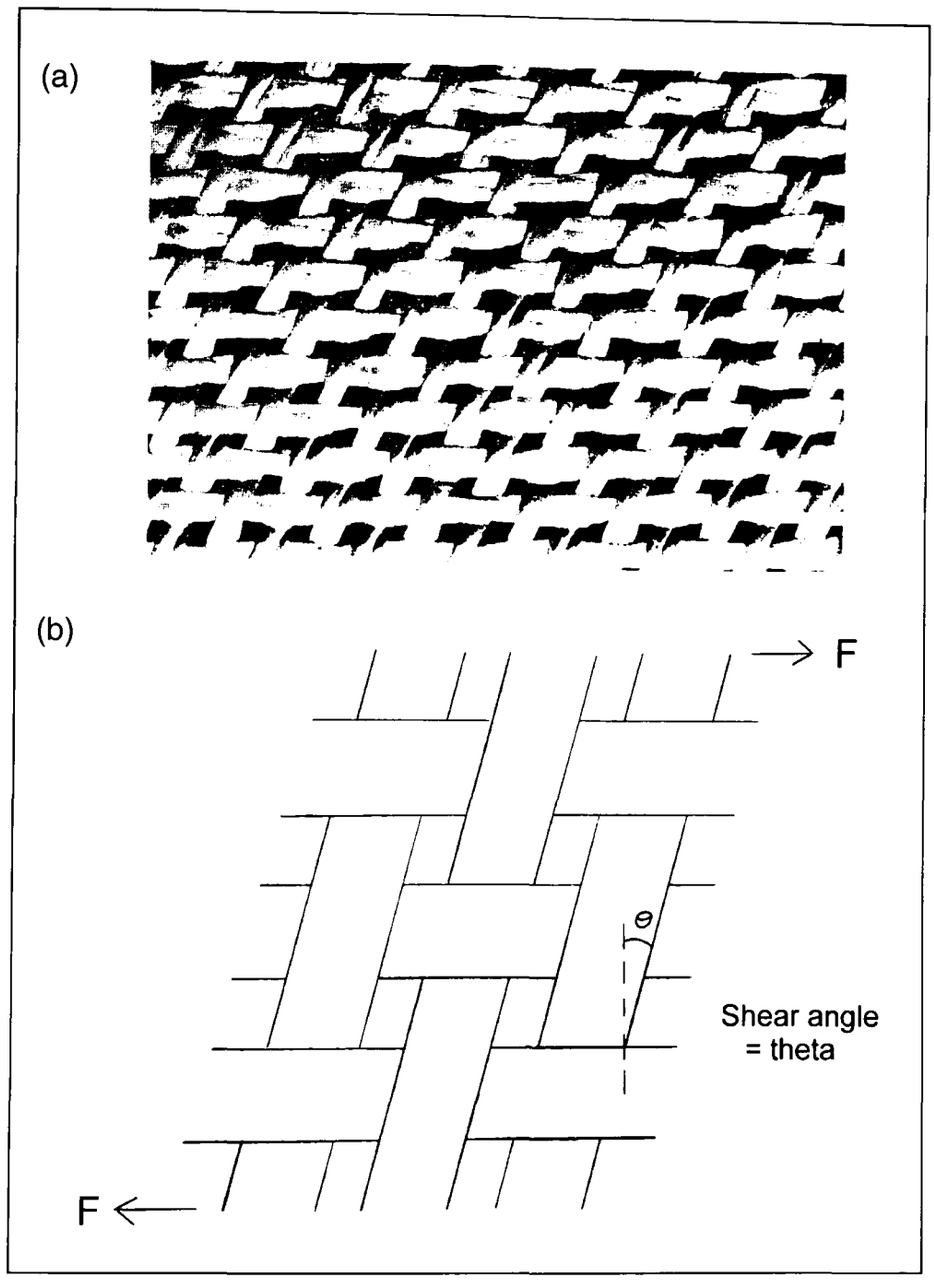

Figure 2-19. Shear in plain weave fabric; (a) reproduced from Leaf & Sheta, 1984

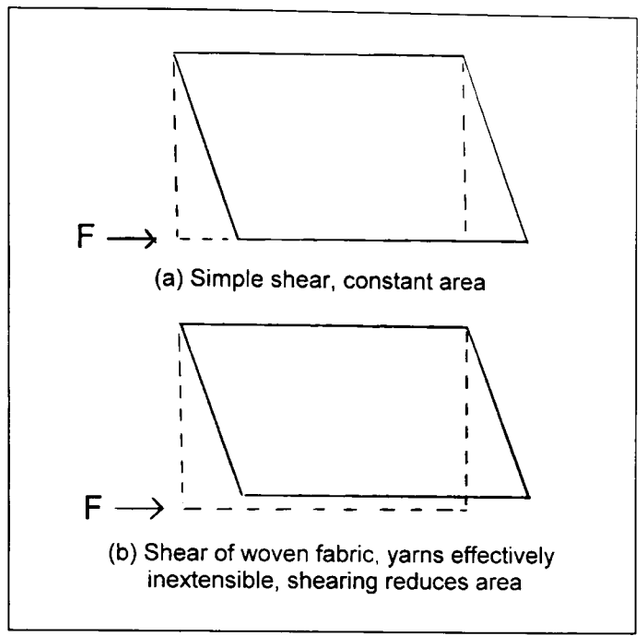

Figure 2-20. Comparison of shear mechanisms

"The shear stiffness of a fabric is fundamentally different from the shear modulus of a lamina as considered in normal engineering practice" (Skelton, 1976, p.862). Shear area is defined in terms of the area *"perpendicular to the plane of the lamina"*, but in a woven fabric the shear resistance is provided by inter-yarn friction and *"there is no relevant out of plane dimension"* [p.862-3]. Any attempt to use the fabric thickness is misleading. *"The resistance to deformation can be expected to be proportional to the number of yarn crossovers per-unit-area of the fabric"* [Skelton (1976), p.863]. A thick fabric will have greater yarn spacing and so lower shear resistance than a thin fabric. This is the antithesis of continuous sheet materials (e.g. steel) where an increase in thickness leads to an increase in shear resistance. Skelton proposes a definition of fabric shear stiffness (Figure 2-21).

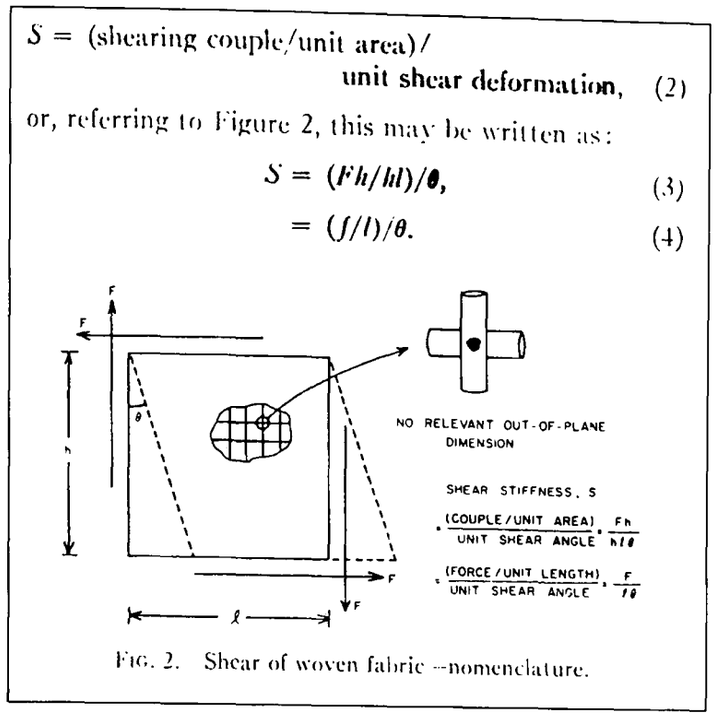

Figure 2-21. Shear of woven fabric, reproduced from Skelton (1976)

The hysteretic shear response of fabrics under repeated loading can be represented using envelopes of stress-strain curves (Figure 2-22).

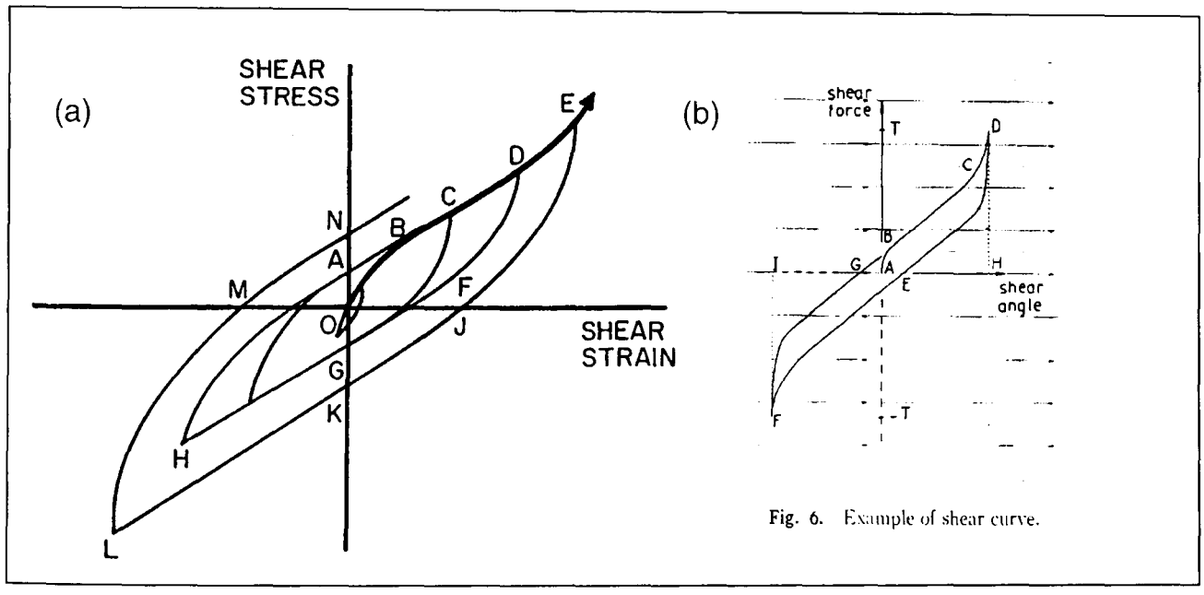

Figure 2-22. Typical stress-strain curves for shear deformation, reproduced from (a) Skelton, 1980b; (b) Behre, 1961

During the initial decreasing stiffness region (Figure 2-22b, AB) the shear stress is initially too low to mobilise rotation of the yarn intersections, and they act as if rigidly fixed. Deformation is by bending of the yarns between the intersections (Figure 2-23). This is linear elastic as it depends purely on yarn bending properties (Grosberg & Park, 1966). Skelton (1980b) describes the decreasing stiffness (Figure 2-22a, OB) as being due to gradual rotational mobilisation of yarn crossovers. For architectural fabrics the coating shear stiffness will dominate the shear response at low loads, as the yarn bending stiffness is low.

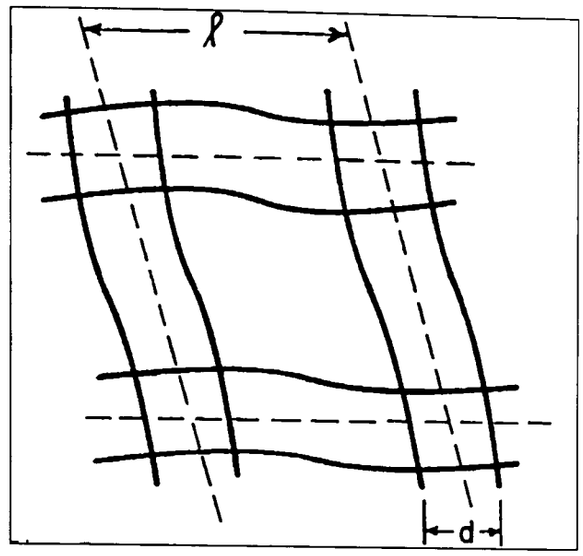

Figure 2-23. Fabric shear deformation at low shear stress, reproduced from Skelton (1980b)

After the initial deformation, fabric shear is essentially bilinear (Figure 2-22b; BC, CD). Once the yarn intersections are mobilised *"shearing hysteresis is produced as a result of yarn slippage at the intersections of the yarn in the fabric"*, Grosberg & Park (1966, p.420). This rotational 'slippage' involves friction and hence energy is lost. This essentially linear response (Figure 2-22a, BCD) is due to continued rotation with all joints mobilised (Skelton, 1980b).

"*Further increase in the shear force results in a non-linear region which is most probably a result of the jamming of the structure*", Grosberg & Park (1966, p.421). A sharp increase in shear stiffness occurs when *shear lock-up* occurs (Figure 2-22b, CD). The shear resistance of an uncoated woven fabric is commonly considered to be negligible until this *locking limit* is reached (Boisse, Gasser & Hivet, 2001). The locking limit, also referred to as *shear jamming* or *shear lock-up*, is a fundamental omission in many papers on woven fabric shear. "*A limiting condition... can occur when adjacent elements of a structure come into side-by-side contact*" (Skelton, 1980b, p.215). Shear lock-up is a geometric phenomenon; if the shear deformation of a specimen is increased to a certain angle the adjacent yarns in a given direction will come into side-by-side contact (Figure 2-24). It is often stated that, for uncoated fabrics, shear lock-up will not occur at angles relevant to fabric usage, "*the applicability of this idealization increases with the ratio of yarn spacing to diameter and, for relatively large ratios, the phenomenon of fibre jamming is unlikely*" (Testa, Stubbs & Spillers, 1978).

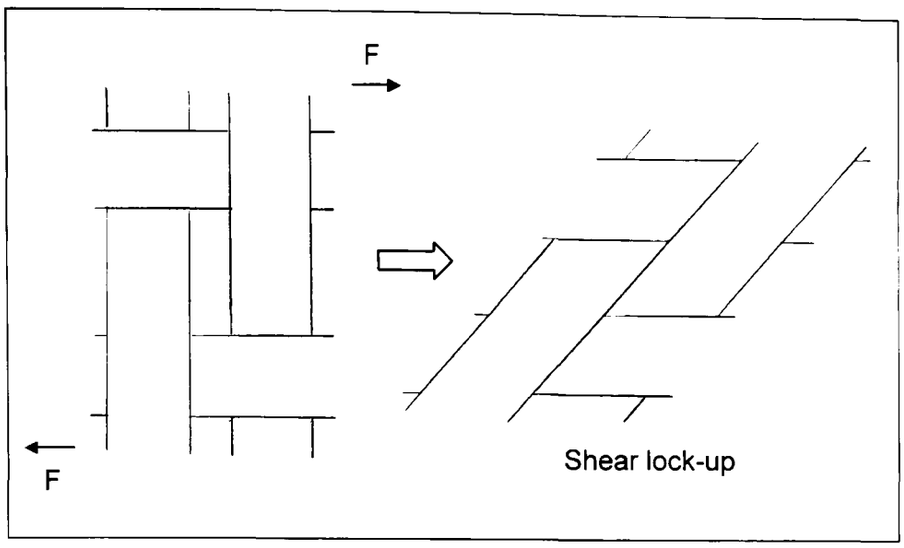

Figure 2-24. Geometric shear lock-up

Side-by-side yarn contact leads to a very large increase in shear resistance. It is important to note that shear lock-up is not as straightforward as it appears to be in Figure 2-24, which only shows the fabric structure on plan. In a woven fabric, the three dimensional weave geometry will cause orthogonal yarns to come into contact at lower angles than are required for side-by-side contact. Skelton (1976, 1980b) considers the 'shear limit' of interwoven circular cylinders (Figure 2-25).

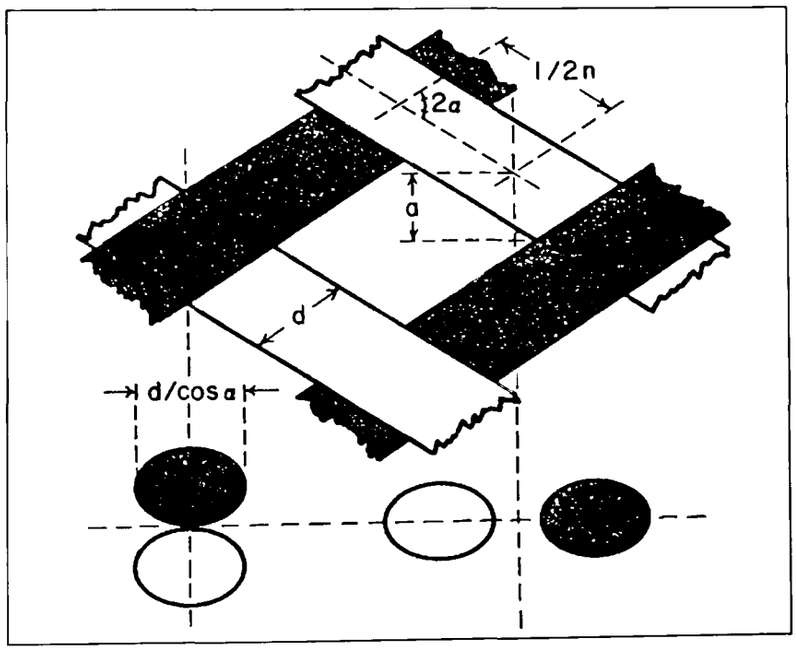

Figure 2-25. Shear lock-up of three-dimensional fabric structure, reproduced from Skelton (1980b)[§]

[§] In Figure 2-25 dimension 'd' is drawn incorrectly. It is the yarn diameter and so should be shown perpendicular to the longitudinal axis of the yarn.

Skelton's criterion for the shear limit is that parallel yarns come into contact midway between intersections. This is an oversimplification: non-circular yarns and yarn crimp mean that other parts of the parallel yarns may come into contact at lower shear angles. The exact shape of the yarn crimp will be crucial in determining the limiting shear. In a tightly woven fabric it easy to see that any shear deformation will cause yarns to come into contact, and yarn crushing will need to occur to enable shear deformation. Detailed analysis of three dimensional yarn shape, followed by modelling of shear deformation and comparison with experimental results is required to enable calculation of the lock-up angle (§6.2.5). Finite element models of woven fabric deformation are particularly well suited to this analysis (§2.4.2.1).

A comparison of the shear properties of an uncoated and coated fabric (Figure 2-26) shows the increase in shear stiffness due to the coating. Whilst the shear response of the uncoated fabric is approximately linear, the addition of coating results in a non-linear response. *"The reduction in slope of the curve for the coated fabric at deformations of 2-3° "* is attributed to *"the onset of buckling in the fabric and subsequent fall in effective shear modulus"* (Skelton & Freeston, 1971, p.878). Skelton and Freeston (1971) conclude that *"the shear stiffness of the coated fabric is determined principally by the shear stiffness of the coating material... and the direct contribution of the fabric is relatively insignificant"* [p.879]. However, this is only true if shear lock-up does not occur. For a coated fabric full shear lock-up with side-by-side contact of parallel yarns is unlikely as the coating will maintain yarn separation. However, the coating between the yarns will jam and increase the shear stiffness. This in turn will result in wrinkling or buckling of the fabric, and so may appear to be a reduction in shear stiffness. At what stage buckling occurs depends on the direct stresses in the fabric. The greater the direct biaxial stresses the greater the shear angle will be before buckling occurs. Little work has been carried out on combined biaxial tensile and shear testing, which is required to fully quantify the fabric behaviour (§6.2.5).

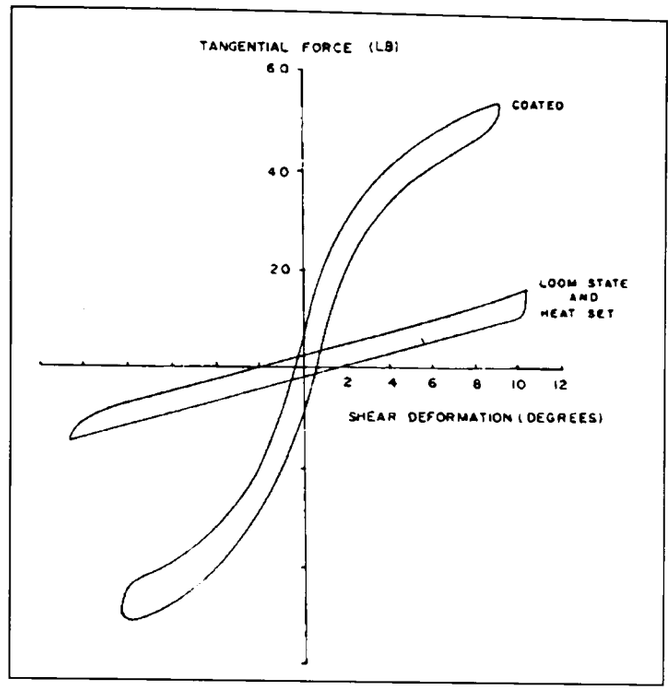

Figure 2-26. Comparison of shear behaviour of uncoated and coated fabric, reproduced from Skelton & Freeston (1971)

Accurate assessment of the fabric shear stiffness is vital for determining the level of double curvature that can be achieved in a fabric structure, and there are frequently problems with fabric wrinkling, for example at the top of a conic. Despite this *"it appears to be common practice to neglect the influence of shear when modelling fabric structures"* (Schock, 1991, p.286). Frequently shear is considered, but it is usually assumed to be linear elastic (Day, 1986; Chen, Lloyd & Harlock, 1995). *"Resistance to shear deformations arises almost entirely from the coating"* and so is *"essentially elastic"* (Testa & Yu, 1989, p.1636, referring to Teflon coated fibre-glass). A qualitative assessment of the fabric shear stiffness is commonly carried out to decide which type of fabric to use on a given project, i.e. for high curvature use PVC-polyester. However, detailed knowledge of the shear response would enable an assessment of whether a given form could be achieved using a given fabric without wrinkling.

2.1.4.4 Bending

"As to bending stiffness, it is not easy to measure because it is so weak that the woven reinforcements under consideration do not support their own weight"

(Boisse, Gasser & Hivet, 2001)

The bending stiffness of architectural fabrics is often neglected as it is very low compared to its tensile stiffness (Boisse et al, 1997). *"The mechanical behaviour of dry* [uncoated] *fabrics is very specific. Bending, shear and compression stiffnesses are near zero"*, (Gasser, Boisse & Hanklar, 2000). Shear stiffness is increased by coating and lock-up: should bending stiffness be considered negligible for a coated woven fabric?

"For a simple body the flexural rigidity is directly related to the tensile modulus by a geometrical factor, this is not so for a fabric" (Cooper, 1960). He recommends defining fabric flexural rigidity *"only in terms of the couples resisting bending, and symbols such as (EI), implying a direct relationship with tensile properties, should be avoided"*. The treatment of bending in typical engineering plates and shells does not apply to fabrics; *"... in textile materials the structure is not homogeneous; bending cannot usually be treated as a response of a series of layers through the fabric"*, (Shanahan et al, 1978). *"Textile fabrics... do not deform as a series of parallel layers... Thus a textile fabric must be treated either microscopically as a structure or macroscopically as a sheet material characterized by independent membrane and bending properties"* (Amirbayat & Hearle, 1989) (Figure 2-27).

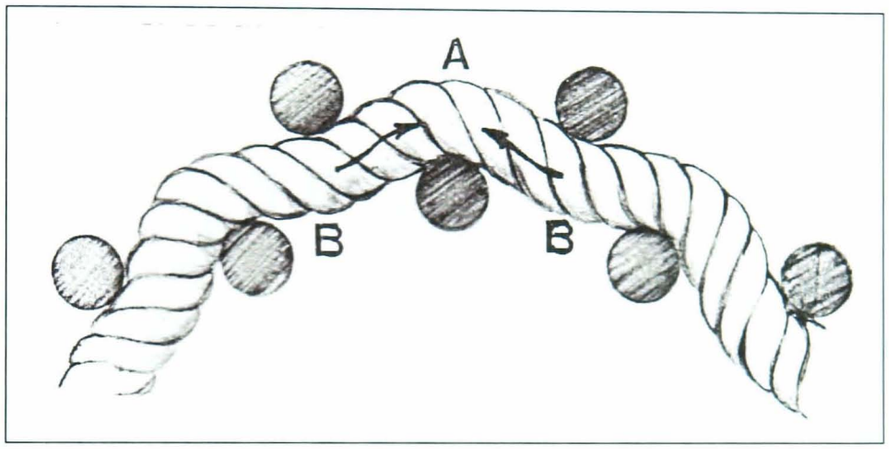

Figure 2-27. Bending of woven fabric, reproduced from Amirbayat & Hearle, 1989

Figure 2-27 shows how the yarns parallel to the bending axis provide virtually no increase in bending stiffness *in a loosely woven fabric*. The flexural rigidity of fabrics depend on the weave spacing - categorised as 'very open' or 'very tight' (Cooper, 1960). For a 'very open' weave the crimp is ignored and the fabric is assumed to be made up of straight, parallel yarns. With a 'very tight' weave *"the relative movement of fibres within yarns and yarns within the fabric structure may be inhibited. The stiffness would then increase towards that of a solid sheet of material"* (Cooper, 1960). The weave pattern of architectural fabrics varies depending on the weight, material and manufacturer. PVC-polyester tends to have a more open weave with less crimp (Figure 2-12 & Figure 2-13) and could be classified as 'very open'. PTFE-glass tends towards the description of 'very tight' with closer yarn spacing and high levels of crimp.

The form of fabric structures is typically defined by large spans and hence large radius curvature. Under load the fabric undergoes large in-plane strains (up to around 10%) and large out-of-plane displacements (of the order of metres, rather millimetres for a steel structure), but the change in curvature is small. The low bending stiffness of architectural fabrics combined with the small changes in curvature ensure that bending is not significant for the large scale analysis of fabric structures. However, the bending stiffness is significant for predicting when

wrinkling will occur and the form it will take, particularly for fabrics with low in-plane stresses (Amirbayat & Hearle, 1989; Rossi et al, 2003).

2.1.4.5 Fabric classification

Fabric strength and failure is not within the scope of this research, but an appreciation of these factors is required to determine appropriate test loads and ensure safety during testing. PVC-polyester fabrics are commonly described by their strength class (type 1 to 5), Figure 2-14 (p.38). PTFE-glass has a similar system with strength classes G1 to G7, Figure 2-15. The permissible stress used in the analysis of a fabric structure is limited by the stress at which a tear in the fabric will propagate (Happold et al, 1987). This ensures that minor damage does not lead to catastrophic collapse under design loads (§1.1.2). The material factor of safety applied to the fabric ultimate tensile strength (UTS, §2.2.1) is typically four, consequently 25% UTS is used as a maximum test load for this research.

2.1.5 Conclusions

The mechanical behaviour of coated woven fabrics is highly non-linear due to the properties of the constituent materials (fibres and coating) and geometric effects:

1. Crimp interchange,
2. Limiting configurations in shear and bending,
3. Deformation of the helical yarn structure.

These effects are all significant in architectural fabrics. High levels of crimp, especially in PTFE-glass fibre fabrics, result in negative strain and highly variable values of Poisson's ratio under biaxial load. The level of shear achievable before 'lock-up' occurs determines the level of double-curvature achievable with a given fabric. Bending stiffness is negligible on the scale of a fabric structure, but limiting bending configurations may be significant on the level of individual woven yarns.

Coated woven fabrics exhibit a hysteretic stress-strain response with residual strain after unloading. Long term creep is also significant. This inelastic behaviour is largely due to the polymeric properties of PVC, PTFE and polyester. The properties of these polymers vary with temperature, and glass-fibre yarns become increasingly brittle at low temperatures.

This research focuses on the two mostly commonly used architectural fabrics: PVC coated polyester and PTFE coated glass-fibre. An awareness of other architectural fabrics, which may move into prominence in the future, has enabled the test rig and protocol (Chapter 3) to be

designed to be flexible enough to accommodate other materials. Similarly, the predictive model formulation has been kept suitably general to be applicable to any plain woven fabric with little modification (Chapter 5).

Knowledge of fabric properties has informed the design of the biaxial test rig and test protocol (Chapter 3). For example, bowing of the weft yarns across the width of the roll led to the adoption of the 'floating' test rig to accommodate non-orthogonal test pieces. Mechanical conditioning has been used to provide medium to long term fabric properties, which are different to the initial response of the fabric. Whilst measurement of the shear response is clearly important, it is beyond the scope of this research.

An understanding of fabric properties is vital for the formulation of predictive models (Chapter 5), in particular for indentifying which deformation mechanisms and material properties are most significant, which enables a simple but accurate model to be formulated.

2.2 TEST METHODOLOGIES

2.2.1 Uniaxial fabric strip testing

Uniaxial strip tests are used to determine the ultimate tensile strength (UTS) of fabrics in both warp and fill directions. They also provide an indication of the stress-strain response of the fabric. Uniaxial strip tests for coated woven fabrics are defined by BS EN ISO 1421:1998 "Rubber- or plastics-coated fabrics - Determination of tensile strength and elongation at break".

2.2.2 Yarn crushing stiffness

Yarn crushing stiffness (i.e. radial compressive stiffness) is an important parameter in many models used to predict fabric biaxial behaviour (Chapter 5). There is no standard method for testing yarn crushing stiffness. Tests used include parallel plate, channel and wire methods (Figure 2-8 and Figure 2-28). The plate and channel methods measure the crushing stiffness independently of tensile load, but the wire method better represents the crushing forces acting at a yarn crossover in a woven fabric.

The results of crushing tests on as-produced yarns may not be representative of the yarn in a coated woven fabric for several reasons:

- The weaving process bends the yarns resulting in damaged fibres and reduced yarn strength (§2.1.1),
- The coating may penetrate into the yarn between the fibres (§2.1.1),
- For PTFE coated fabrics, the coating process involves sintering the coating onto the base cloth, which may affect the mechanical properties of the yarn,
- The crushing resistance of an ex-situ yarn with no tensile load is very low as it is solely the twisted yarn structure that prevents rearrangement of the fibres into the crushed configuration (an untwisted yarn would have negligible crushing stiffness using the parallel plate method). A yarn in a coated woven fabric is restrained by the coating, which may greatly increase the crushing stiffness.

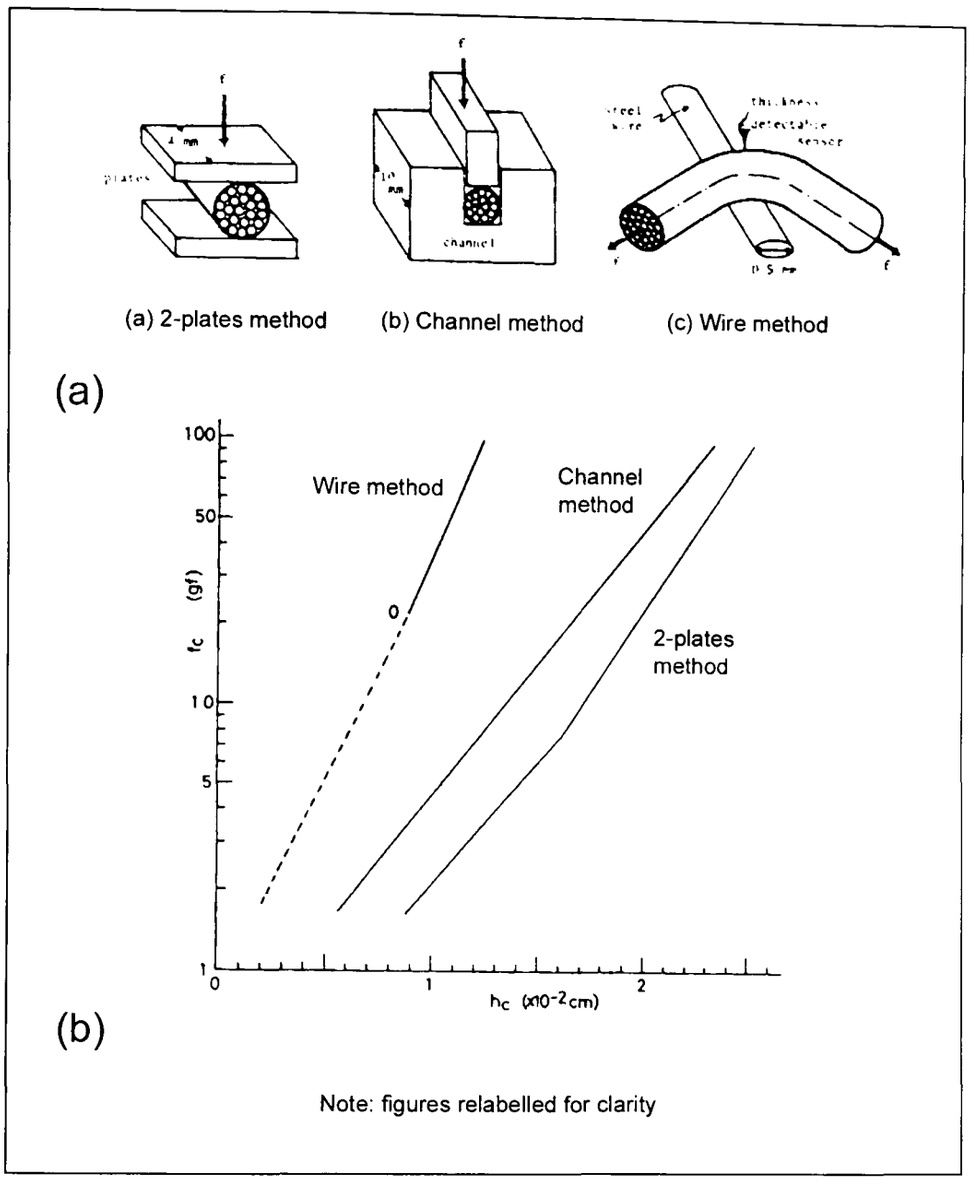

Figure 2-28. Yarn compression: (a) test methods, (b) results, reproduced from Sasai & Kawabata, 1985

The first three points could be addressed by removing yarns from a coated fabric and then testing them. This removal process presents difficulties (§3.1.2). The fourth point can only be addressed by testing the crushing stiffness of the in-situ yarn, i.e. the crushing resistance of the fabric. It then becomes difficult to distinguish between the effect of the yarn and the coating.

2.2.3 Biaxial fabric tensile testing

Crimp interchange, the interaction of warp and fill yarns, makes a major contribution to the stress-strain response of woven fabrics (§2.1.4.2). Hence the response of architectural fabrics to biaxial loads cannot be directly inferred from uniaxial strip tests (Reichardt, Woo & Montgomery, 1953). Without the use of predictive models (Chapter 5) biaxial testing is essential to quantify the fabric response.

2.2.3.1 Test equipment

There are three main types of biaxial test (Bassett, Postle & Pan, 1999a): the bursting test, the cylinder test (Mott, Huber & Leewood, 1985) and the plane biaxial test (Ansell, Barnes & Williams, 1984). The bursting test comprises a flat circle of fabric which is clamped at the edges and is then inflated. The inflation pressure can be used to calculate the load on the fabric. The major drawback with this test is that the ratio of warp stress to fill stress cannot easily be varied, and for structural applications fabrics must be tested at several stress ratios appropriate to the expected loading. The cylinder test uses inflation pressure to load the fabric along one axis, and applied displacement of the cylinder ends to load the fabric in the orthogonal direction (Figure 2-29). Results from the cylinder test are affected by the seam unless specially woven samples are used. This is impractical for architectural fabrics, especially as the coating process could not be replicated on a cylindrical sample. The bursting and cylinder tests have therefore not been used for this research. The plane biaxial test consists of a flat fabric specimen clamped on four edges, to which load is applied. This test best represents the loading of a fabric structure and is commonly used in industry (Ansell, Barnes & Williams, 1984; Architen-Landrell (www); Laboratorium Blum (www); Ferrari (www)).

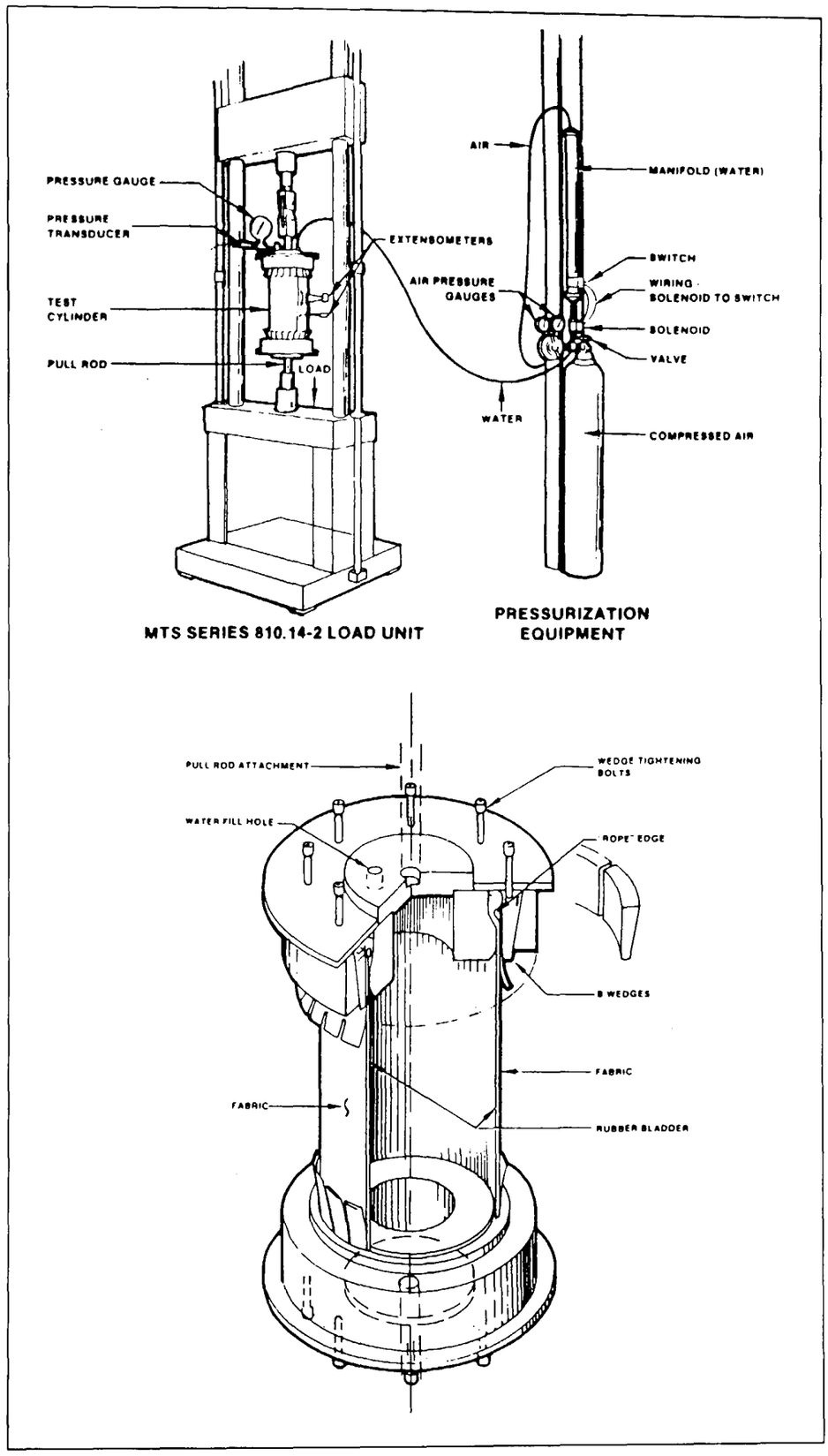

Figure 2-29. Cylindrical fabric test, reproduced from Mott, Huber & Leewood, 1985

Early work on biaxial fabric testing involved gripping the sides of a square of fabric (Reichardt, Woo & Montgomery, 1953). However, a key consideration is the application of uniform warp and fill stresses with large strains (10-15%) without disruption from the clamps. This led to the use of a cruciform test piece (Klein, 1959; Clulow & Taylor, 1963). The arms of the cruciform allow strain to occur orthogonal to the load applied by that arm, reducing the restraint imposed

by the clamp plate. Further developments included adding slits to the cruciform arms and loading the resultant strips independently (Reinhardt, 1976). The only international standard to give detailed guidance on biaxial fabric testing specifies a *"slitted cross-shaped specimen"* (MSAJ/M-02-1995). The same result can be achieved with a square test piece with many point loads along each edge – with the load application points free to move as the fabric strains in both directions (MacRory & McNamara, 1977). Bassett, Postle & Pan (1999b) studied in detail the effect of loading a square specimen with 'pin grips' (Figure 2-30). However, their treatment does not consider issues of damage caused to the fabric by the pin grips at high loads. The advantage of the cruciform is that rigid clamps which are well removed from the area of interest can apply high loads to the specimen.

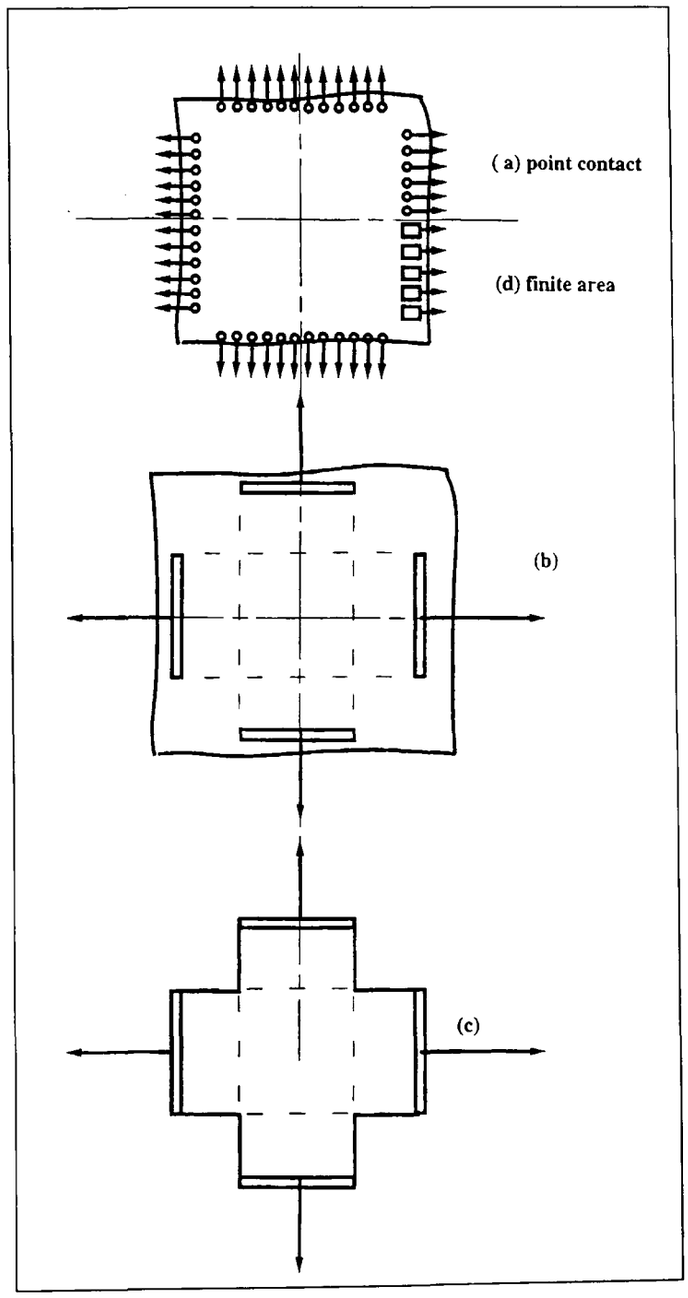

Figure 2-30. Cruciform options, reproduced from Bassett, Postle & Pan, 1999b

2.2.3.2 Test method

Fabric tests frequently only measure initial stress-strain behaviour with no repeated stressing (Clulow & Taylor, 1963; Day, 1986). However, changes occur in the fabric such that the initial behaviour is significantly different to the behaviour after repeated stressing: *"...internal changes in the cloth, in the density and degree of flattening of the yarns, may occur with repeated stressing"*, (Clulow & Taylor, 1963, p.T324). Clulow and Taylor addressed this problem by applying a constant load in one direction whilst cycling the load in the orthogonal direction: *"complete super-position of consecutive hysteresis cycles occurs after about the 8th cycle"* (p.T329). These tests were not carried out on architectural fabrics, but the principles behind the material behaviour are very similar.

"...It is necessary during biaxial tests to simulate the behaviour in the building structure, in other words under real conditions. Real loads are snow and wind." (Blum, 2002; p.12). It is not sufficient to apply these test loads to the virgin fabric because when load is removed the strain does not return to zero, Blum & Bidmon (1987). This hysteresis reduces as more load cycles are applied; when the hysteresis is negligible (i.e. the fabric behaviour is consistent for repeated load cycles) the fabric is said to be mechanically conditioned (Figure 2-31).

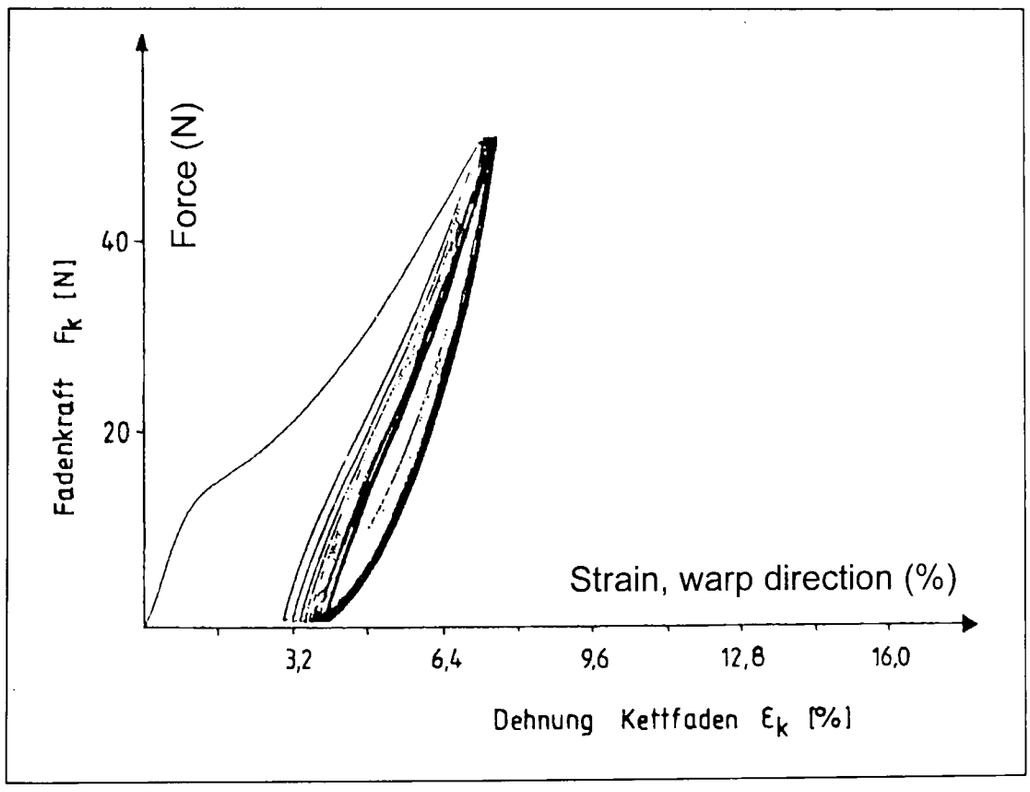

Figure 2-31. Stress-strain response under biaxial load cycling, reproduced from Blum & Bidmon, 1987

Standards specifying biaxial test methods are very limited. British Standards for fabric testing only provide guidance for uniaxial testing (BS EN ISO 1421:1998). The British Standard for *"Design, construction and maintenance of single-skin air supported structures"* (BS 6661:

1986) states that *"information on the biaxial stress-strain properties of coated fabrics is necessary for a more accurate prediction of the magnitude of stresses"*. Research papers are referenced but *"further research work is necessary if the results of the work on biaxial stress-strain behaviour are to be fully utilized in the design"* (BS 6661: 1986, p.12). Similarly the American Society of Civil Engineers standard for air-supported structures (ASCE 17-96) requires that *"all analysis and design shall give appropriate attention to behaviour due to the effects of large deflection nonlinearities and nonlinear material properties"* (p.6). Situations in which non-linear relationships for load-deformation behaviour must be used are listed, but there is no guidance on how these material properties should be determined. American Standards relating to fabric test methods only provide details of uniaxial tests (ASTM D 4851-97). The only standard which explicitly defines a biaxial test procedure is published by the Membrane Structures Association of Japan (MSAJ/M-02-1995), in which a series of load ratios is defined (Table 2-3).

Direction	Ratio of applied loads				
Warp	1	2	1	1	0
Fill	1	1	2	0	1

Table 2-3. Load ratios for biaxial test, MSAJ/M-02-1995

The cruciform is loaded at a rate of between 2 and 4 mm per minute up to 25% of its tensile strength and then unloaded at the same rate. This is repeated three times, and then the specified load ratio from Table 2-3 is applied. This sequence is repeated for each load ratio. The results are used to determine elastic constants to define the fabric behaviour (§2.3.3).

The lack of a clearly defined and justified standard biaxial test procedure for coated woven fabrics necessitates consideration of current practice (in both academic research and industry) and preliminary testing to determine an appropriate test regime for this research (Chapter 3). To determine fabric stress-strain properties Blum (2002) applies cyclic loading in one direction (either warp or fill) with constant low load in the other, and then changes over. The upper stress level is then increased and the cycle is repeated (Figure 2-32). As is often the case, there is no published justification for this test procedure. In a similar manner to the Japanese standard, the results are used to determine elastic constants in an attempt to define the fabric behaviour (§2.3.3).

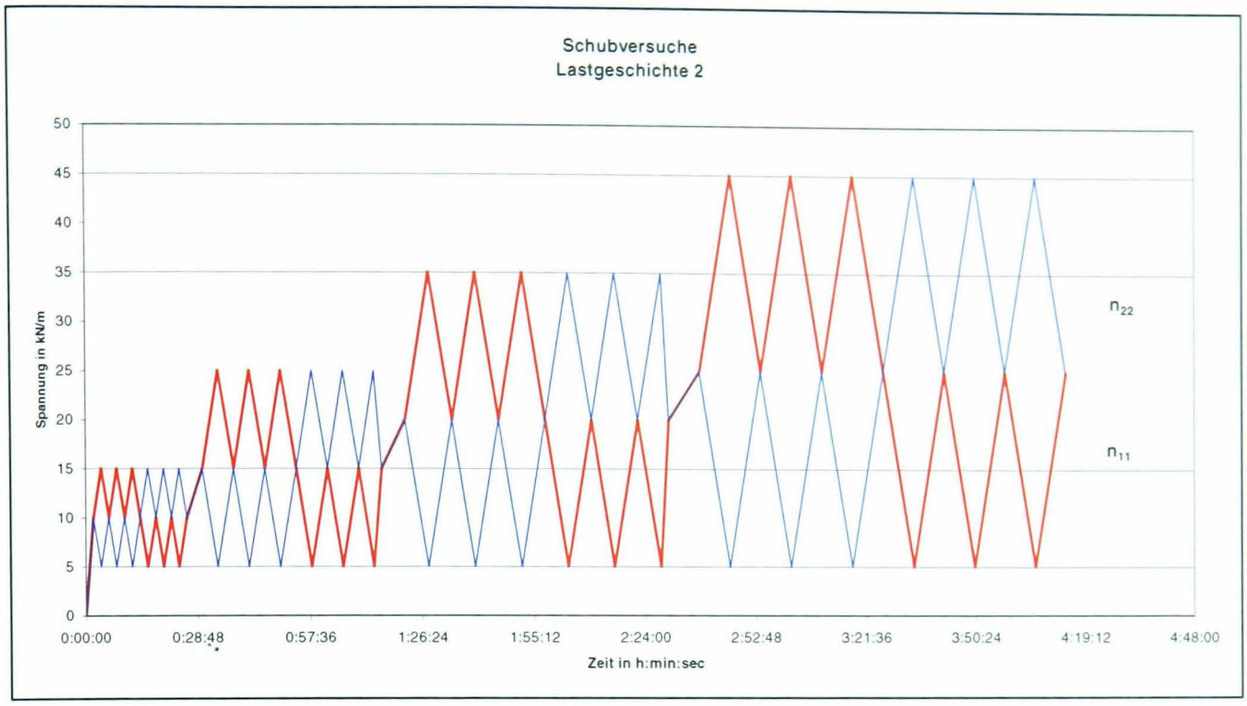

Figure 2-32. Stress history for the determination of the elastic moduli, reproduced from Blum (2002).

Test regimes used in industry (e.g. Laboratorium Blum, Stuttgart (www; Blum & Bidmon, 1987; Blum & Bögner, 2002) and national standards (MSAJ/M-02-1995) are typically developed to provide suitable data to inform a plane stress model rather than fully explore the response of the fabric (Chapter 3).

Mott, Huber & Leewood (1985) determine fabric elastic constants using cyclic biaxial testing of a pressurised fabric cylinder. *"The cylinder is cycled five times from prestress to prestress + 17.5 N/mm and returned to the original prestress load. The cyclic loading removes the majority of initial visco-elastic strain that is characteristic of TFE coated fabrics"* (p.14). Doering (1993) carried out a thorough investigation of the biaxial stress-strain behaviour of Type II, III and IV PVC-polyester fabrics (defined in Figure 2-14). Three stress levels were defined:

- Initial or base load – a small load to tension the fabric on the rig, approximately 1% of maximum stress, 0.4 to 0.6 kN/m,
- Lower stress level similar to prestress - Doering suggests that prestress is between 3 and 7 kN/m, and adopts 20% of the upper stress level,
- Upper stress level – upper working stress level, 25% of manufacturer specified failure load. Hence the applied stresses lie in the region of normal design loads with a factor of safety of four (Figure 2-33).

The stressing procedure involves cycles between the base load and lower stress level, followed by cycles between lower and upper stresses, separated by three 20 minute pauses (Figure 2-34). The resultant stress-strain response clearly shows the difference between initial behaviour and the mechanically conditioned response (Figure 2-35).

		Type 11	Type 111	Type IV
Baseload W=F (10% of the lower stress level)	kN/m	0.4	0.5	0.6
Lower stress level W=F (20% of the upper stress level)	kN/m	4.0	5.0	6.0
Upper stress level W=F (Approx. 25% of the breakload)	kN/m	20.0	25.0	30.0
Breakload W/F (According to manufacturer)	kN/m	88.0/ 79.0	115.0/ 102.0	149.0/ 128.0

Figure 2-33. "Stress levels of the various fabric types", reproduced from Doering (1993).

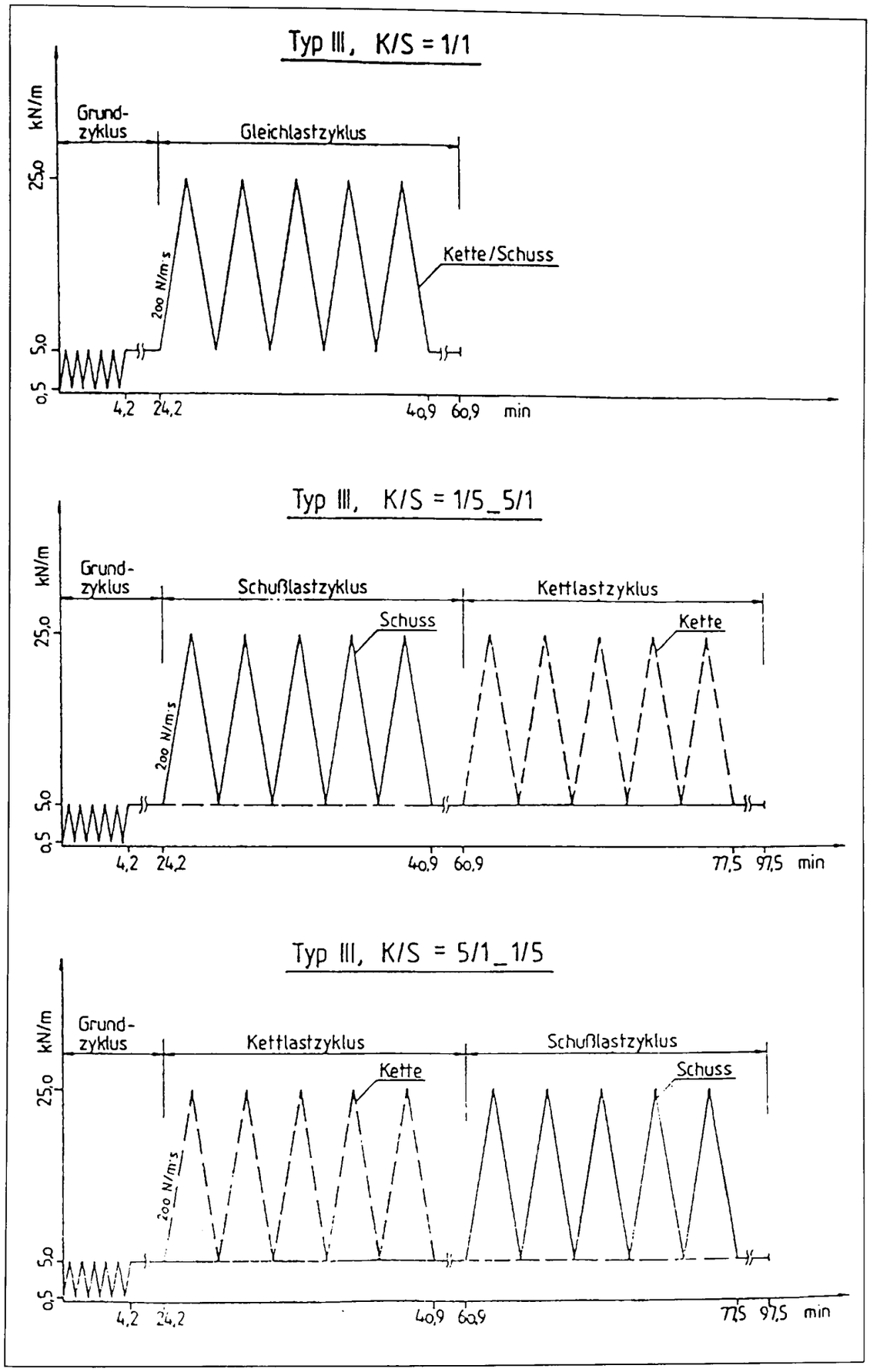

Figure 2-34. Stressing programme, reproduced from Doering (1993)**.

** Translation of German: *Schuss* = fill, *Kette* = warp

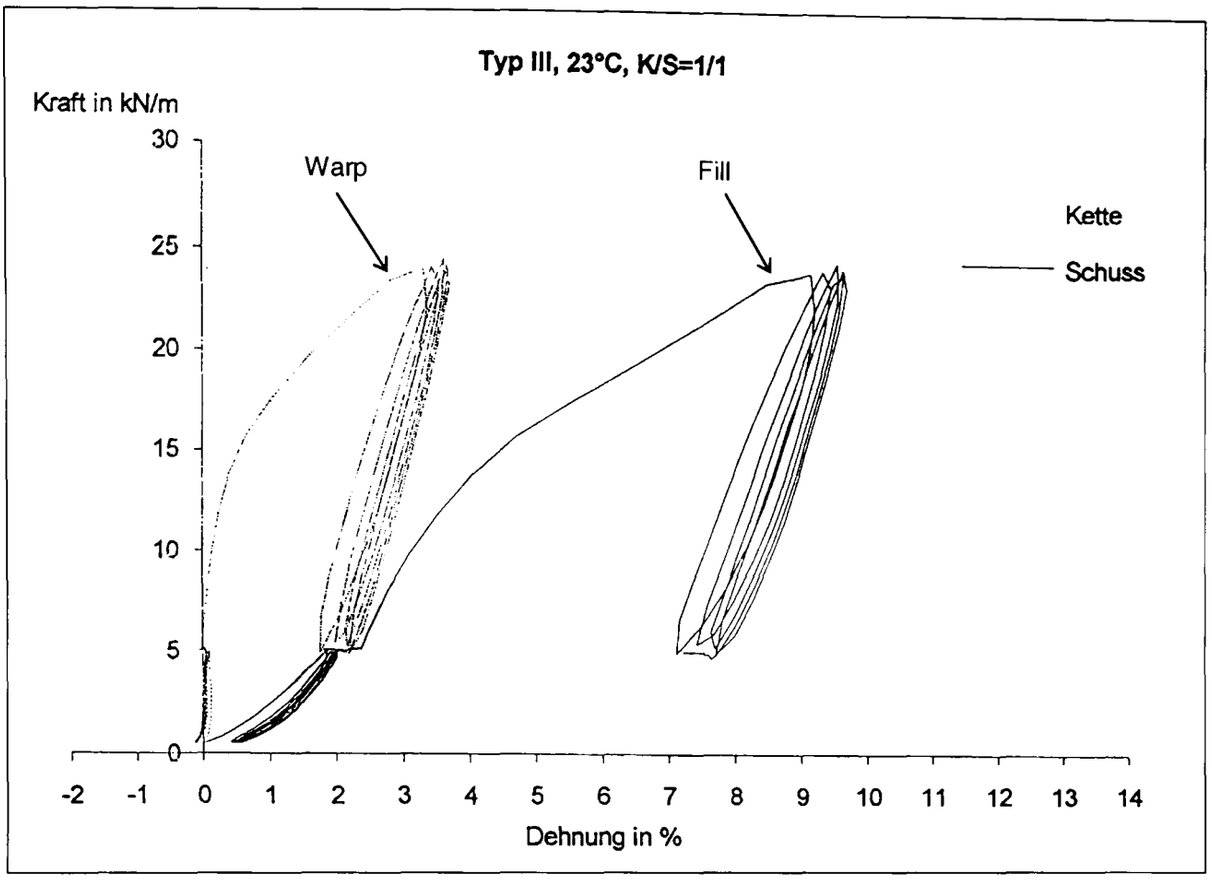

Figure 2-35. Stress-strain response under cyclic load, reproduced from Doering (1993)

Contractors who specialise in fabric structure erection usually have their own procedure for determining compensation values. Whilst not trying to determine long-term stress-strain properties, they condition the fabric to give the expected level of strain after a given period (some weeks or months) in-situ. Architen-Landrell (www) use variable load and temperature cycles to simulate long term installation loads. Birdair (www) employ a more rapid protocol using cyclic loading applied alternatively in warp and fill directions, details of which are confidential.

These compensation test procedures may provide a starting point for developing a mechanical conditioning regime. Ansell, Barnes & Williams (1984) suggest that compensation values should be *"recorded as long term values after fairly random stress cycling of the biaxial sample to simulate service conditions"* (p.35). Compensation values need to be appropriate for the period of installation and expected loads during this time (both installation loads and environmental loads). Long term values should inform the design of re-tensioning capabilities, and be used for long term structural analysis.

2.2.4 Conclusions

A uniaxial test method is defined by British Standards and is commonly used in industry to determine fabric tensile strength. This provides a reliable basis for defining test loads (Chapter 3). With the addition of strain measurement the standard uniaxial test provides easily attainable stress-strain data, from which material properties can be inferred for use in predictive models (Chapter 5).

Yarn testing involves removing the yarns from the coated fabric, which is difficult to achieve without damaging the yarns. Determination of the yarn crushing stiffness is potentially useful for predictive modeling. However, there is no standard test and trying to simulate the correct form of crushing is problematic. Yarn testing has therefore not been used in this research, instead all material properties have been inferred from standard uniaxial tests.

Biaxial testing is fundamental to this research for determining the response of architectural fabrics to applied loads, which are resisted as stresses in the plane of fabric. The plane cruciform test has been identified as being the most appropriate for membrane structures and as being the industry standard (Laboratorium Blum, Architen-Landrell; www). There are several variations on this type of test, with little published analysis or guidance as to their benefits or limitations. Analysis is therefore required to determine the optimum cruciform configuration (§3.3.1).

There is also little published guidance on biaxial test methods. Many have been developed in industry and are not publicly available. Frequently testing is carried out at low load for compensation, not to provide values for analysis. Those tests that do provide data for structural analysis typically aim to inform a plane stress model (i.e. to provide Young's moduli and Poisson's ratio(s)), rather than to fully quantify the non-linear fabric behaviour. Published work on fabric testing points to two key concepts:

1. Mechanical conditioning (i.e. load cycling) to enable typical medium to long term properties to be measured, as opposed to the initial behaviour,
2. Application of varying warp to fill load ratios (e.g. 1:5, 1:2, 1:1, 2:1, 5:1) to explore the fabric response.

These concepts will be used as a departure point for developing a new test protocol to fully determine the fabric response as design loads. With limited published work, the test protocol which will be used for this research will be based on extensive fabric testing.

2.3 REPRESENTATION OF BIAXIAL TEST DATA

2.3.1 Data fitting

The non-linear characteristics of fabric stress-strain behaviour make it difficult to establish a single function which fully represents the fabric response. A bi-linear representation may be appropriate for the two stage deformation mechanism of woven fabrics (§2.1.4.2). This method gives some limited degree of fit to the test data, but the 'change point' must to be modified for each stress ratio (Testa, Stubbs & Spillers, 1978; Kageyama, Kawabata & Niwa, 1988). Testa & Yu (1989) modelled non-linear biaxial fabric response using strain energy functions:

$$\varepsilon_{ef} = p_1 A_1 \sigma_f^{p_1 - 1} + A_3 \sigma_w p^3 + p_4 A_4 \sigma_f^{p_4 - 1} \sigma_w + A_5 \sigma_w,$$

Equation 2-2

with a similar expression for ε_{ew}, where σ = stress, ε = strain, and subscripts are defined as follows: e = elastic part of response, w = warp direction, f = fill direction. Nine parameters ($A_1 \ldots A_5$ and $p_1 \ldots p_4$) were used to fit this polynomial, but the resultant function did not adequately represent the test data. Chen, Lloyd and Harlock (1995) used a simpler second order polynomial, enabling the tensile modulus at a given stress level to be derived easily by differentiation. However, the second order polynomial fit failed to follow discontinuities in the test data.

Polynomial representations of fabric tensile stress-strain curves may not sufficiently match the fabric response. In particular they tend to smooth rapid changes in gradient. Conversion of the stress-strain curve into a modulus-strain curve exaggerates non-linearities, giving distinct peaks rather than subtle changes in gradient. This technique has been used to fit the non-linear stress-strain curves of polymeric yarns (Lucas, 1983; Zimliki et al, 2000b). The derivation of the modulus-strain curve involved calculation of the gradient of the stress-strain curve by fitting polynomials to a small moving window of data.

Neural networks, genetic algorithms and genetic programming are techniques for optimising a system using biologically analogous processes (Koza, 1992; Masters, 1995; Eiben & Schoenauer, 2002; Sette & Boullart, 2001; Brunetti, 2000). In this case the 'system' is a functional representation of the fabric test data. Neural networks take their structure and language from the human brain and learn relationships between data. Genetic algorithms are based on the processes of evolution, Darwinian selection and reproduction. Strings of parameter values are assessed for *fitness* (suitability to the problem) and the best are copied, split and recombined. Genetic programming has the same basis in evolution but is a more powerful tool

as functions are combined rather than parameter values. Virtually no prior knowledge of the form of the function is required. These powerful tools are gaining popularity for data fitting and problem solving in a wide range of fields (Nastran & Balic, 2002; Grosman & Lewin, 2002; Soh & Yang, 2000; Nikitas & Papageorgiou, 2001; Kim & Cho, 2000; Yang et al, 2002; Javadi et al, 1999). Genetic programming is clearly an appropriate technique for fitting a response surface to a highly non-linear scattered data set. However, there are problems with this type of functional representation:

(i) A function which passes through every data point may not provide sensible interpolation between the points (§4.2.3),

(ii) The function may also be very sensitive beyond the data set and provide poor extrapolation (§4.2.3),

(iii) Proprietry software incorporating these biologically analogous tools is currently very expensive. The aim of this research is to provide methods for using the test data which do not require specialist techniques and so can easily be adopted by the design engineer (§1.2).

2.3.2 Mechanical fabric model

To ensure good interpolation between data points, and realistic extrapolation beyond the data set, a representation of the test data with some physical relevance to the fabric response can be used. The non-linear fabric response to in-plane loads can be modelled using a set of equations based on force equilibrium in the fabric unit cell (for details of model formulation see §2.4.2) The unit cell is the smallest repeated unit in the fabric (Figure 2-36); for a plain woven fabric the unit cell is simply two crossed yarns, with the model including one half wavelength of each yarn (Peirce, 1937).

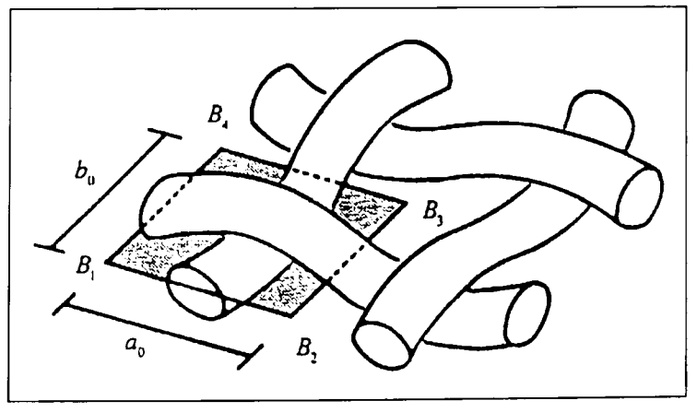

Figure 2-36. Fabric unit cell, reproduced from Kato, Yoshino & Minami (1999)

Model parameters include yarn and coating tensile moduli, yarn crushing modulus and initial fabric crimp geometry. Values are determined by a combination of physical testing and calibration against biaxial test data. If all parameters are determined independently from the biaxial test data then the model can be used as a predictive tool (§2.4.2). Frequently parameters are determined through comparison with biaxial test data, and the model is used as the basis for a set of equations which represent the fabric behaviour (Kato, Yoshino & Minami, 1999; Pargana, Lloyd-Smith & Izzuddin, 2000; Tan & Barnes, 1984; Uetani, Fujiwara and Ohsaki, 2002). Parameters in these equations are varied for a given set of data until the model reproduces the test data with an acceptable degree of accuracy.

Frequently researchers provide little evidence of the quality of the model, either providing no comparison with test data (Menges & Meffert, 1976) or only comparison with other models (e.g. Tan & Barnes, 1984). Authors commonly conclude their papers with unjustified statements that 'the correlation with test data is good'. Statistical assessments of the quality of the model, including comparisons with multiple sets of test data, are rarely found in the literature reviewed. For example, Pargana, Lloyd Smith & Izzuddin (2000) provide no comparison of theoretical and experimental results, only a comparison of theory with and without the yarn crushing mechanism. "*Although the model has not been calibrated against experimental test results, it offers the promise of high levels of accuracy and confidence*" (Pargana, Lloyd Smith & Izzuddin, 2000, p.13). However, the results shown (Figure 2-37) are very different to previous work. In particular there is no evidence of the negative strain which is typical of woven fabrics under biaxial load, clearly shown in the experimental results of Day (1986); Figure 2-18.

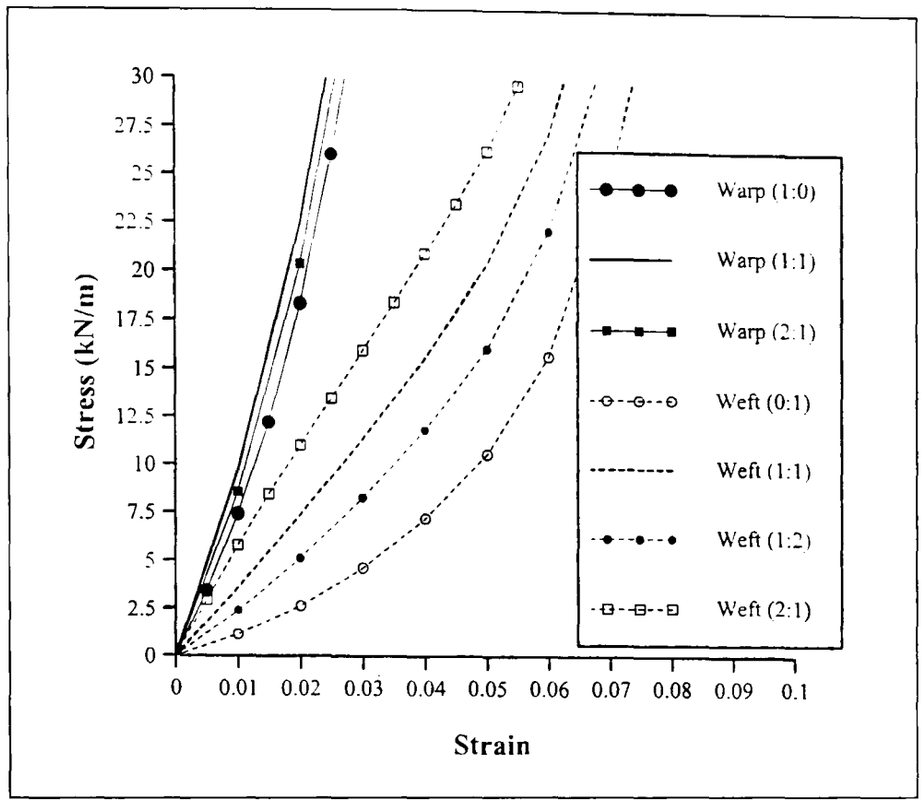

Figure 2-37. Material model output, reproduced from Pargana, Lloyd Smith & Izzuddin (2000)

Stubbs and Fluss (1980) compare experimental results from biaxial tests on Teflon coated glass-fibre fabric with their unit cell model output: "*For all three load ratios [1:2, 1:1, 2:1] there is satisfactory agreement between the theoretical and experimental results*" [Stubbs & Fluss (1980), p.57]. Typically this statement is not backed up by, for example, a percentage deviation for the whole data set. The results for stress ratios of 2:1 and 1:2 show significant differences between the theoretical and experimental curves (Figure 2-38).

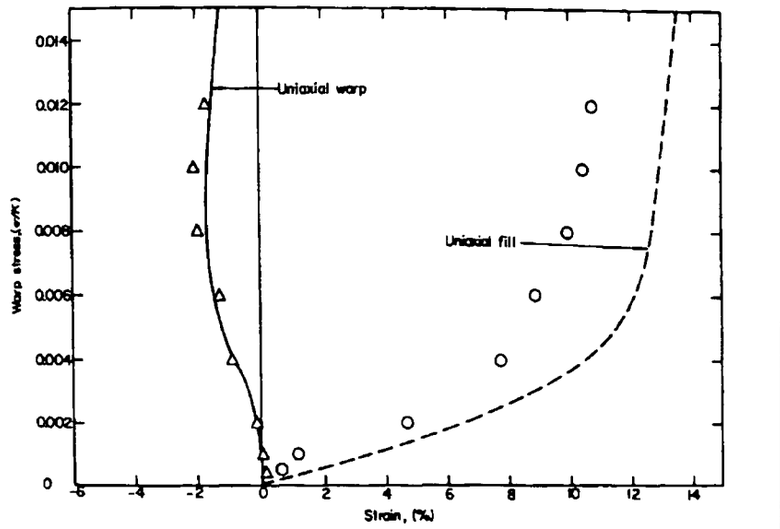

Figure 13 Theoretical and experimental comparisons. Warp: (—), theoretical; (△), experimental; Fill: (— — —), theoretical; (o), experimental. Fill load/warp load = 2

Space-truss model for fabrics: N. Stubbs and H. Fluss

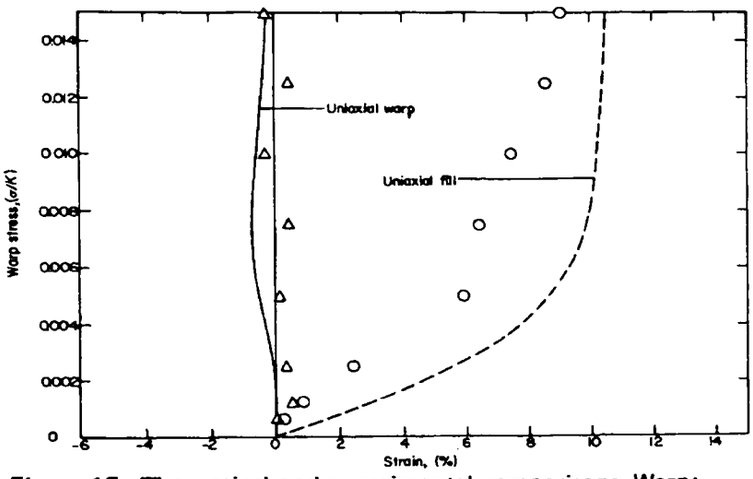

Figure 15 Theoretical and experimental comparisons. Warp: (—), theoretical; (△), experimental. Fill: (— — —), theoretical; (o), experimental. Fill load/warp load = 0.5

Figure 2-38. Theoretical and experimental comparison, Stubbs & Fluss (1980)

The output from Wang's (2002) sinusoidal unit cell model seems to provide a reasonable correlation with test data (e.g. Figure 2-39). Wang does provide percentage differences between calculated and measured strains, which vary from 0 to around 50% of the measured value.

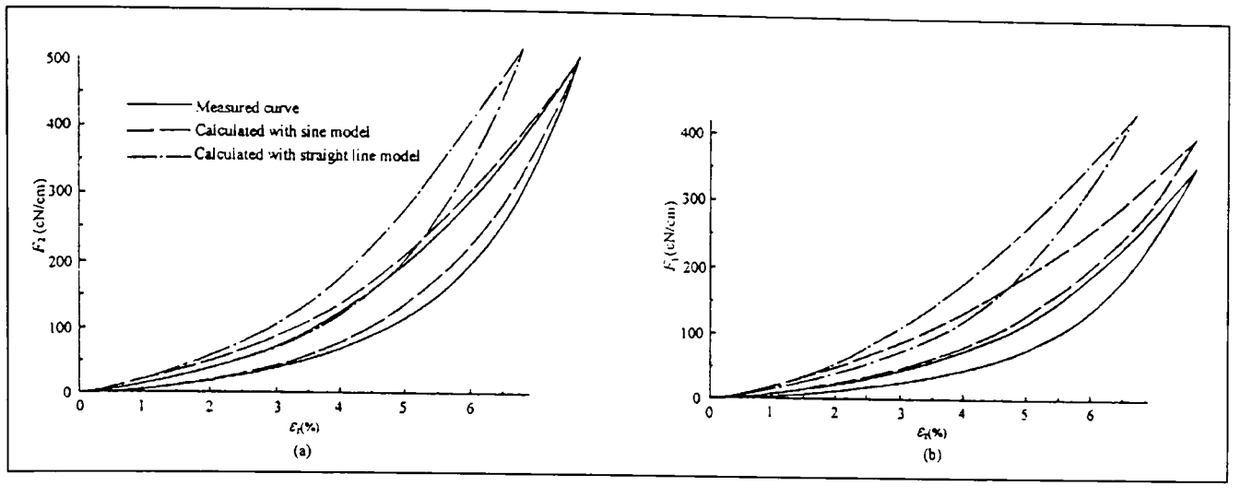

Figure 2-39. Theoretical and experimental comparison, Wang (2002)

The correlation between the unit cell models and test data is often surprisingly poor in view of the fact that the model parameters are informed by the test data, and the set of equations is based on the fabric deformation mechanism. With little more development the unit cell model can be used to predict the fabric response from measured parameters (§2.4.2). This is the approach used in this research, with simpler numerical methods used to represent the fabric response (§4.2.3)

The simultaneous equations which describe these models can be used in finite element analysis. Until recently simplified models were used to ensure rapid convergence of the non-linear equations describing the fabric unit cell. The equations derived by Freeston, Platt & Schoppee (1967) were difficult to solve without a good initial guess, and hence were better for fabric design than structural analysis. Tan & Barnes (1980) developed a simple model suitable for structural analysis, commenting that a solution involving simultaneous non-linear equations with many unknowns for each element in the structure can be prohibitively slow. With increases in computing power and '*robust solution procedures*' (Pargana, Lloyd Smith & Izzuddin, 2000) more comprehensive models can be included. However, until the models are shown to match the fabric response sufficiently accurately their utility for structural design is limited.

2.3.3 Current practice: plane stress representation

Accurate test data is commonly used for installation, but broad assumptions and simplifications are commonly made when it is applied to structural analysis. Even in specialist membrane analysis software (with membrane finite elements and form finding and prestress capabilities, e.g. *Oasys Software's GSA*, www: Oasys) the material behaviour is defined using plane-stress material properties (two Young's moduli and Poisson's ratios). Because of this, fabric test data is commonly manipulated to fit within a plane stress framework:

1. Two Youngs's moduli and one Poisson's ratio are determined from the secant moduli of warp and fill stress-strain curves at a stress ratio and magnitude deemed typical for the structure. These values remain constant throughout the structural analysis. Frequently this approach is further simplified. No testing is carried out and instead assumed values are used that are deemed typical for a given type of fabric. Values used by Arup (www), based on extensive experience, are:

	Warp modulus (kN/m)	Fill modulus (kN/m)	Poisson's ratio
PVC-polyester fabric	600	600	0.3 – 0.84
PTFE-glass fibre fabric	1200	1200	0.3 – 0.84

Table 2-4. Typical fabric material properties

According to plane stress theory Poisson's ratio cannot exceed 0.5. However, a value of 0.84 is used to model the large negative strains which occur in woven fabrics under biaxial load.

2. Use of elastic and interaction moduli (Blum & Bidmon, 1987; Blum & Bögner, 2002),

$$\begin{bmatrix} \sigma_{11} \\ \sigma_{22} \end{bmatrix} = \begin{bmatrix} E_{1111} & E_{1122} \\ E_{1122} & E_{2222} \end{bmatrix} \begin{bmatrix} \varepsilon_{11} \\ \varepsilon_{22} \end{bmatrix} \qquad \text{Equation 2-3}$$

where σ = stress, ε = strain, E = elastic modulus and subscripts *11* and *22* denote warp and fill directions respectively. Two Poisson's ratios (υ) are defined,

$$\upsilon_{12} = \frac{E_{1122}}{E_{1111}},$$

$$\upsilon_{21} = \frac{E_{1122}}{E_{2222}}. \qquad \text{Equation 2-4}$$

for warp-fill and fill-warp interaction respectively. Stresses and strains are replaced by small increments $\Delta\sigma$ and $\Delta\varepsilon$ to linearise an interval of the non-linear stress-strain curve. For example, the three moduli (E_{1111}, E_{1122} and E_{2222}) can be determined between an assumed prestress and an upper value. Incremental loading (both positive and negative) is used to simulate different environmental loads (e.g. wind and snow) and elastic moduli are assessed at different stages of the load history. However, in undertaking tests in two orthogonal directions two values of E_{1122} are obtained. Typically these are averaged and reported as a single value.

3. Determination of elastic constants using response surfaces, (Minami et al, 1997). Response surfaces provide a useful visualisation of the fabric stress-strain response (Figure 2-40). Orthogonal stresses (σ_w, σ_f) and strains (ε_w, ε_f) (subscript w denotes warp direction, f denotes fill) from biaxial tests form surfaces in the σ_w, σ_f, ε_w and σ_w, σ_f, ε_f coordinate systems. Five stress ratios are considered, and elastic constants are established using a multi-step linear approximation. The surface is divided into quadrilaterals and for each quadrilateral the elastic constants are determined. The size of the quadrilaterals is critical in ensuring discontinuities in the fabric behaviour are accurately captured.

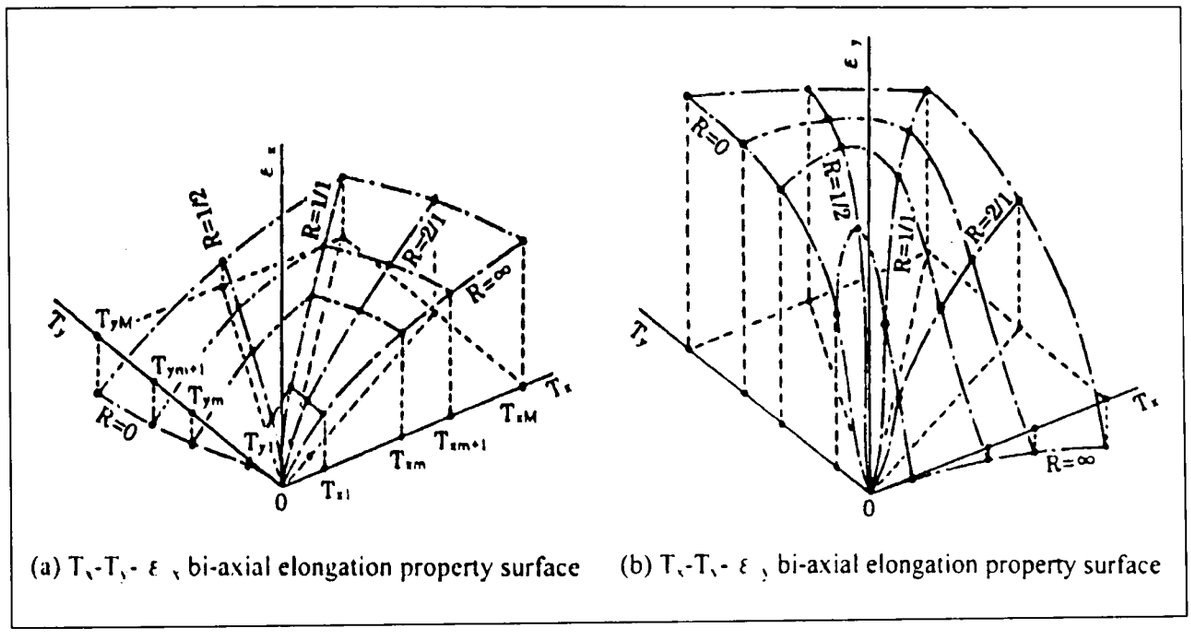

(a) T_x-T_y- ε_x bi-axial elongation property surface (b) T_x-T_y- ε_y bi-axial elongation property surface

Figure 2-40. Stress-stress-strain response surface, reproduced from Minami et al, 1997

4. Use of elastic constants for each stress ratio (MSAJ/M-02-1995), *"From the load-strain curves obtained for each load ratio in the warp and weft directions by the biaxial tensile tests, tensile stiffness and Poisson's ratio of warp and weft directions are calculated"* (MSAJ/M-02-1995, p.2). However, this will give multiple values to be used in the analysis, *"If we set a membrane material constant corresponding to each case, a large number of material constants will need to be used. Although this may actually be necessary, it is not realistic"* (MSAJ/M-02-1995, p.6). Hence equations are given to calculate two Young's moduli and two Poisson's ratios.

These four methods are very similar – they all involve linearisation of the fabric response which enables values of Young's modulus and Poisson's ratio to be determined. How well these elastic constants represent the fabric response is rarely evaluated.

2.3.4 Stress and strain mean and difference functions

Day (1986) provides a completely different approach based on the representation of non-linear stress-strain behaviour in soil mechanics [Day (1972)] in which the mean and difference of the principal strains are related. Principal stresses lie in warp and fill directions and the shear stresses are dealt with independently, such that,

$$\sigma_a = \frac{(\sigma_x + \sigma_y)}{2}, \qquad \text{Equation 2-5}$$

$$\varepsilon_a = \frac{(\varepsilon_x + \varepsilon_y)}{2}, \qquad \text{Equation 2-6}$$

$$T = \frac{(\sigma_y - \sigma_x)}{2}, \qquad \text{Equation 2-7}$$

$$g = \frac{(\varepsilon_x - \varepsilon_y)}{2}, \qquad \text{Equation 2-8}$$

$$\sigma_a = f^1(\varepsilon_a) + f^2(g), \qquad \text{Equation 2-9}$$

$$T = f^3(\varepsilon_a) + f^4(g), \qquad \text{Equation 2-10}$$

where σ_x = warp stress, σ_y = fill stress, σ_{xy} = shear stress, ε_x = warp strain, ε_y = fill strain and f^1 to f^4 are functions that are to be determined using test data. Shear stress and strain are related by an independent linear function f^5 (Day, 1986). Discontinuities in the test results make reproduction of the test curves impossible using algebraic functions (e.g. polynomials) for f^1 to f^4. Therefore Day used arbitrary functions defined by a set of points, requiring linear interpolation between them. Test data and predictions show good correlation using the mean and difference functions (Figure 2-18).

This work represents a major shift in conceptualising fabric behaviour for structural analysis: it attempts to encapsulate the data for three different stress ratios in two simultaneous equations, and it is contrary to the universally adopted plane stress approach. Day's work is discussed in more detail in Chapter 4 (§4.2.2).

2.3.5 Conclusions

Plane stress representations (i.e. two Young's moduli and Poisson's ratios) are almost universally used to represent the biaxial behaviour of architectural fabrics (Laboratorium Blum, Arup (Oasys' GSA), Tensys, MSAJ/M-02-1995). The elastic constants are, at best, based on secant moduli from biaxial stress-strain curves, but frequently use typical values for all fabrics.

"Membrane materials have strong material non-linearity. Although linearization in membrane materials poses a problem, in the present structural analysis of membranes, material linearity is assumed within a certain stress range in many cases."

"If we set a membrane material constant corresponding to each case [stress ratio], a large number of material constants will need to be used. Although this may actually be necessary, it is not realistic."

MSAJ/M-02-1995

The method used by the Laboratorium Blum results in two values of Poisson's ratio, which are then averaged to provide a single value which can easily be used in analysis software. The aim of this research is to fully quantify the fabric response, with no constraining assumptions of plane stress which may not be appropriate for coated woven fabric behaviour (Chapter 4).

The non-linear characteristics of fabric stress-strain behaviour make it difficult to establish a single function which fully represents the fabric response. Biologically analogous methods (e.g. genetic programming) could be used to determine a suitable function to represent the test data, but interpolation and extrapolation would be unreliable without extensive checks on the form of the function. To ensure good interpolation between data points, and realistic extrapolation beyond the data set, a representation of the test data with some physical relevance to the fabric response can be used. Day (1986) provides a different approach based on the representation of non-linear stress-strain behaviour in soil mechanics in which the mean and difference of the principal strains are related. This approach is analysed in more detail in Chapter 4. A set of equations based on force equilibrium in the fabric unit cell can be used to model the test data. This is an effective method of data fitting, but in this research the unit cell model has been utilised as a predictive tool (Chapter 5) with a simpler approach sought for representing the test data (Chapter 4).

2.4 PREDICTIVE MODELLING

2.4.1 Yarn models

Considerable research has been carried out in this area (Morris, Merkin & Rennell, 1999; Hearle & Sakai, 1978; Hearle, 1969; Naik & Madhavan, 2000; Zimliki et al, 2000a, b; Thwaites, 1980), the aim being to predict yarn properties from knowledge of the fibre properties and spinning process (§2.1.1).

It is difficult to accurately predict the behaviour of a yarn in a coated woven fabric because the yarn undergoes changes during the coating and weaving processes (§2.1.2 & 2.1.3). For this research the yarn has been taken as the fundamental unit of the fabric (§5.2.1). Incorporation of a yarn model (e.g. Moghe, 1980) would be useful for reverse engineering of the yarns, to determine the effect on fabric behaviour of changes to the yarn structure (§5.6). Yarn modelling has recently been incorporated successfully in finite element fabric models (Durville, 2003; §2.4.2.1).

2.4.2 Predictive fabric models

"*Fibres, yarns and fabrics are not regular structures capable of description in mathematical form, even to the degree of approximation attainable by the simplest physical measurements. To reduce observations on actual specimens to quantitative relations of any general validity, statistical methods are necessary, with all their reservations of error, variation and uncertainty.*"

Peirce (1937), p. T45

Fabric models models are typically developed for one of two purposes:

1. As the basis for a set of equations which represent fabric biaxial test data (Kato, Yoshino & Minami, 1999; Pargana, Lloyd-Smith & Izzuddin, 2000; Tan & Barnes, 1984; Uetani, Fujiwara and Ohsaki, 2002). Parameters in the equations are varied for a given set of data until the model reproduces the test data with an acceptable degree of accuracy (§2.3.2). The model is only predictive in that it provides stress-strain data in the intervals between the experimental data points.
2. To predict the fabric biaxial stress-strain behaviour without the need for biaxial testing, using measurements of weave geometry and yarn and coating properties as input data.

Fabric models are typically formulated to describe the behaviour of the fabric *unit cell*, which is the smallest repeated unit in the fabric. In a plain woven fabric the unit cell is simply two crossed yarns, with the model including one half wavelength of each yarn (Figure 2-36).

Fabric shear strain is frequently assumed to be uncoupled with direct strains (Pargana, Lloyd Smith & Izzuddin, 2000; Day, 1986) and hence rarely forms an integral part of the biaxially loaded unit cell model.

Realistic modelling of weave geometry, and how it changes under applied load, is the key to developing an accurate fabric model. In 1937 Peirce wrote his seminal work "*The Geometry of Cloth Structure*". This describes the fundamentals of fabric geometry and Peirce's formulations have been utilised in virtually all fabric models to the present. Peirce identified the measurements required to define the weave structure, assuming infinitely flexible, cylindrical yarns (Figure 2-41).

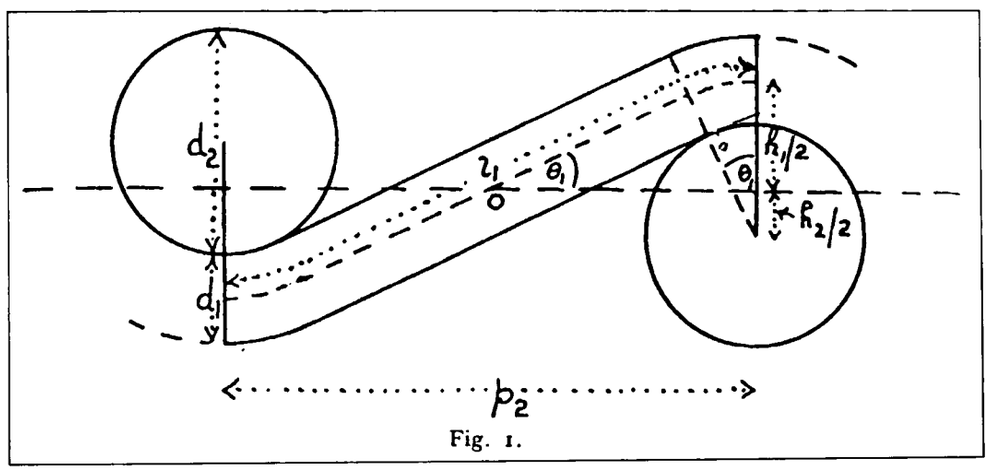

Figure 2-41. Notation for geometry of plain weave fabric, Peirce (1937)

Crimp (c) is defined as "*the percentage excess of length of the yarn axis over the cloth length*" (p.T50). The level of crimp is fundamental for determining the lateral contraction of the fabric which results from *crimp interchange*. Peirce describes a limiting condition called '*crimp jamming*': assuming a circular yarn cross-section, a maximum level of crimp is reached once the thread is in a semi-circular configuration. Architectural fabrics tend to have an open weave and non-circular (flattened, elliptical) yarns so this should not affect their behaviour. Using the notation in Figure 2-41 geometric relationships are derived to describe the fabric structure:

$$c_1 = \left(\frac{l_1}{p_2}\right) - 1$$

Equation 2-11[††]

$$p_2 = (l_1 - D\theta_1)\sin\theta_1 + D(\cos\theta_1)$$

Equation 2-12

$$h_1 = (l_1 - D\theta_1)\sin\theta_1 + D(1 - \cos\theta_1)$$

Equation 2-13

$$h_1 + h_2 = d_1 + d_2$$

Equation 2-14

Peirce (1937) considered ways in which a real fabric differs from his idealised structure:

- The neglect of yarn rigidity cannot always be justified,
- Shear forces, bending moments and lateral pressures have a considerable influence on the balance of crimp,
- Compression of the threads (yarns) at crossovers will result in an elliptical yarn cross-section, and a resultant change in the level of crimp. Peirce identified that determining the contact length or area between the yarns is critical for modelling the crushing behaviour.
- Peirce accepted that threads do not behave in an elastic manner, but decides to carry out the analysis as if they were elastic, "*modified by such estimation of the effect of deviations as is possible*" (Peirce, 1937, p.T73).

Two key aspects of the model formulation are the shape of the yarn cross-section and the shape of the yarn wave-form. For models with a point contact between yarns at crossovers these are independent. For a geometrically consistent model with a finite contact length they are fundamentally linked.

Peirce (1937) realised that under load an ellipse would better represent the yarn cross-section than a circle. This was modelled by substituting the circular radius with the minor axis of the ellipse. However the effect of an elliptical thread was not rigorously considered. Peirce's use of circular cross-section yarns with flattening corrections led to fundamental errors in the geometrical relationships (Olofsson, 1964; 1966). An alternative is the 'racetrack' section, consisting of a rectangle with semi-circular ends, Kemp (1958), Figure 2-42.

[††] Equation 2-11 to Equation 2-14 are reproduced from Peirce, 1937

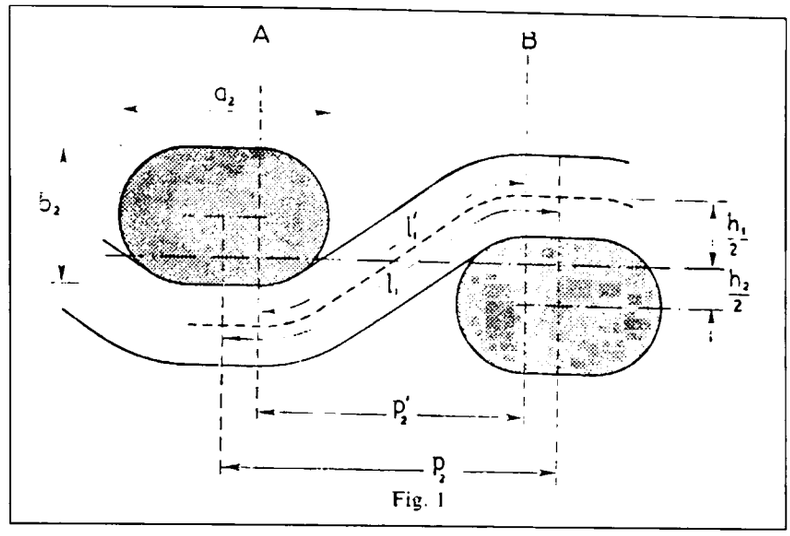

Figure 2-42. 'Racetrack' yarn cross section, reproduced from Kemp (1958)

The racetrack yarn shape provides more realistic fabric geometry, is better for determining limiting conditions due to crimp jamming and provides an intermediate step to the more general analysis of non-circular yarns (Kemp, 1958). For the flat yarns used in architectural fabrics (Figure 2-12 & Figure 2-13, p.37) the rhombus provides a more accurate representation of the yarn cross-section (Pargana, Lloyd Smith & Izzuddin (2000)). Finite element models impose fewer limitations on the form of the yarn cross-section which can be modelled (§2.4.2.1).

Yarn crushing, i.e. changes in the yarn out-of-plane thickness (or 'radius'), result in significant variation in the level of crimp in the unit cell and hence influence the warp and fill strains (Kawabata, Niwa & Kawai, 1973a; Pargana, Lloyd Smith & Izzuddin, 2000), Figure 2-43. The main simplification in Peirce's (1937) model of the fabric unit cell is that the crushing of yarns (due to contact with other yarns and tensile extension) is not considered, Menges & Meffert (1976). Changes in yarn radius are caused by out-of-plane crushing forces at crossovers and contraction under tensile extension (i.e. yarn Poisson's effect).

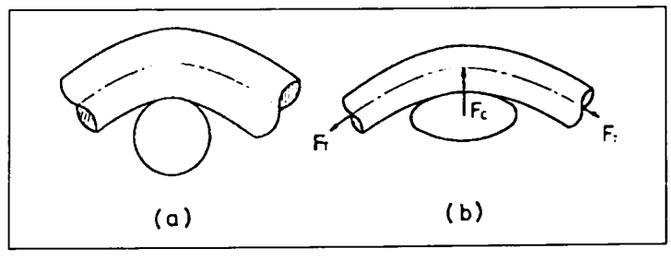

Figure 2-43. (a) Incompressible yarn, (b) compressible yarn; reproduced from Kawabata, Niwa & Kawai (1973a)

A simple crushing spring between orthogonal yarns at cross-overs can be used to model crushing due to out-of-plane contact forces (Menges & Meffert, 1976). Determination of the spring constant for this element is problematic (§2.2.2); Dimitrov and Schock (1986) suggested that the determination of this value would be pure guesswork, and so the resulting curve would be "*mere cosmetic*" [p.861]. Dimitrov and Schock (1986) developed Menges & Meffert's

(1976) model of PTFE-coated glass fibre, extending it to include "*bedding down of yarns*" (the take-up of any initial gap between the yarns) which is assumed to be irreversible. An initial gap between yarns is assumed, expressed as a fraction of weave length in terms of a "*dimensionless bedding factor*". Results are only given for a stress ratio of 1:1. A discontinuity in the stress-strain response is introduced by the yarns coming into contact once 'bedding down' has taken place. This discontinuity is more severe than that which occurs in reality; it is suggested that the initial gap between yarns could be changed to a progressive spring element to dampen the effect of bedding down. This would be particularly relevant for coated fabrics in which the coating would dampen any yarn movement.

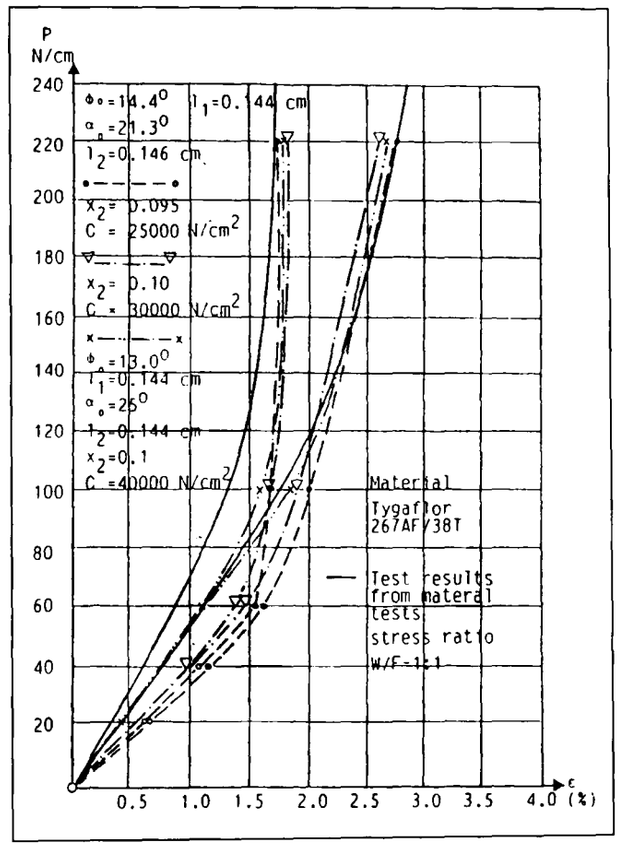

Figure 2-44. Comparison of model and test data, reproduced from Dimitrov & Schock, 1986

Dimitrov and Schock (1986) state that the fit of their model to the test data is not good for stress ratios other than the fabric's *natural* stress ratio. This is the ratio of applied loads which does not result in any crimp interchange, equal to 1:1 for a balanced fabric. This implies that the model formulation does not provide a good representation of the crimp interchange mechanism.

The coupling of yarn extension and crushing force at crossovers to give the total change in yarn out-of-plane thickness has a "*profound impact on the overall response of fabrics*", Pargana, Lloyd Smith and Izzuddin, 2000, p.2. The rhomboid yarn is modelled as a mechanism of elastic elements and rigid links, and yarn crushing causes the lateral and axial stiffness of the yarns to change (Figure 2-45).

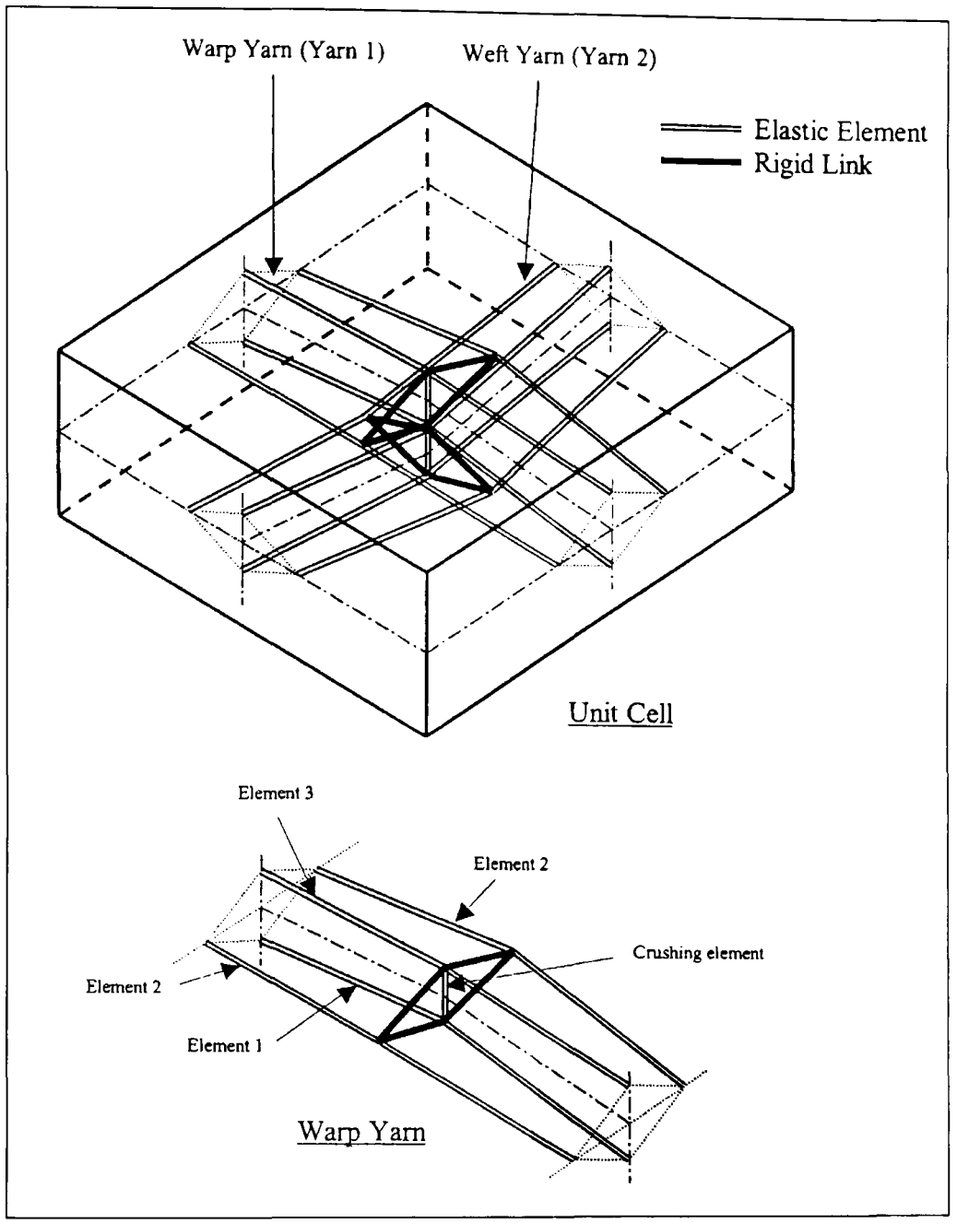

Figure 2-45. Fabric unit cell and modelling of yarn, reproduced from Pargana, Lloyd Smith & Izzuddin (2000)

The unit cell can be modelled with a point contact between yarns (Figure 2-46a) or a finite contact length (Figure 2-46b), (Peirce, 1937).

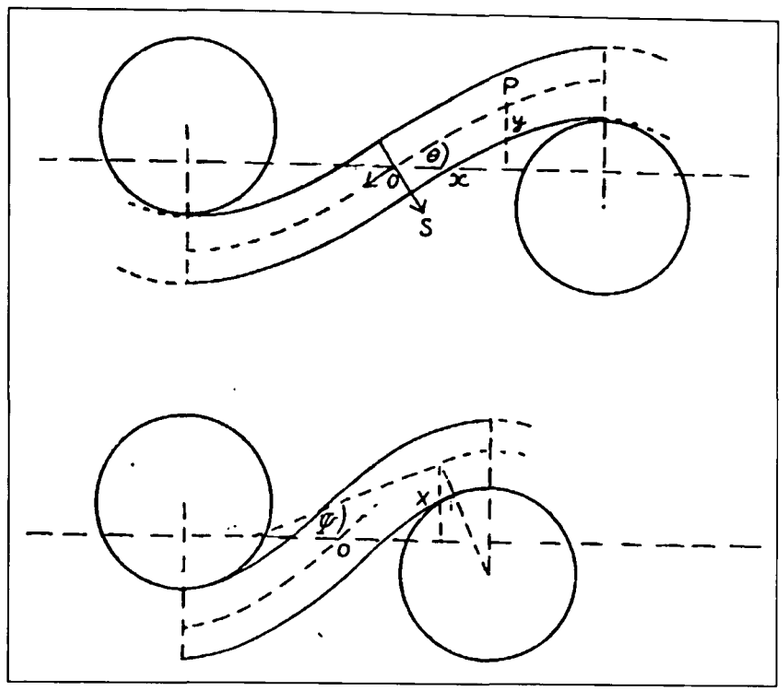

Figure 2-46. Two options for yarn contact (Peirce, 1937)

A point contact combined with negligible bending stiffness provides the familiar *sawtooth* model (Tan & Barnes, 1980; Menges & Meffert, 1976; Dimitrov and Schock, 1986; Pargana et al, 2000). The sawtooth model enables crimp interchange to be modelled using force equilibrium (Menges & Meffert, 1976; Figure 2-52) or minimisation of strain energy in the unit cell (De Jong & Postle, 1978). Use of a point contact results in a lack of geometric consistency between the warp and fill yarns. Paragana et al (2000) represent the yarn cross-section as a rhombus, but a point contact is used and hence the yarn cross-section is not consistent with the crimp shape of the orthogonal yarn (Figure 2-47). The result is a gap between the yarns. This gap may occur in uncoated fabrics with a high yarn bending stiffness, but would be unlikely in coated architectural fabrics.

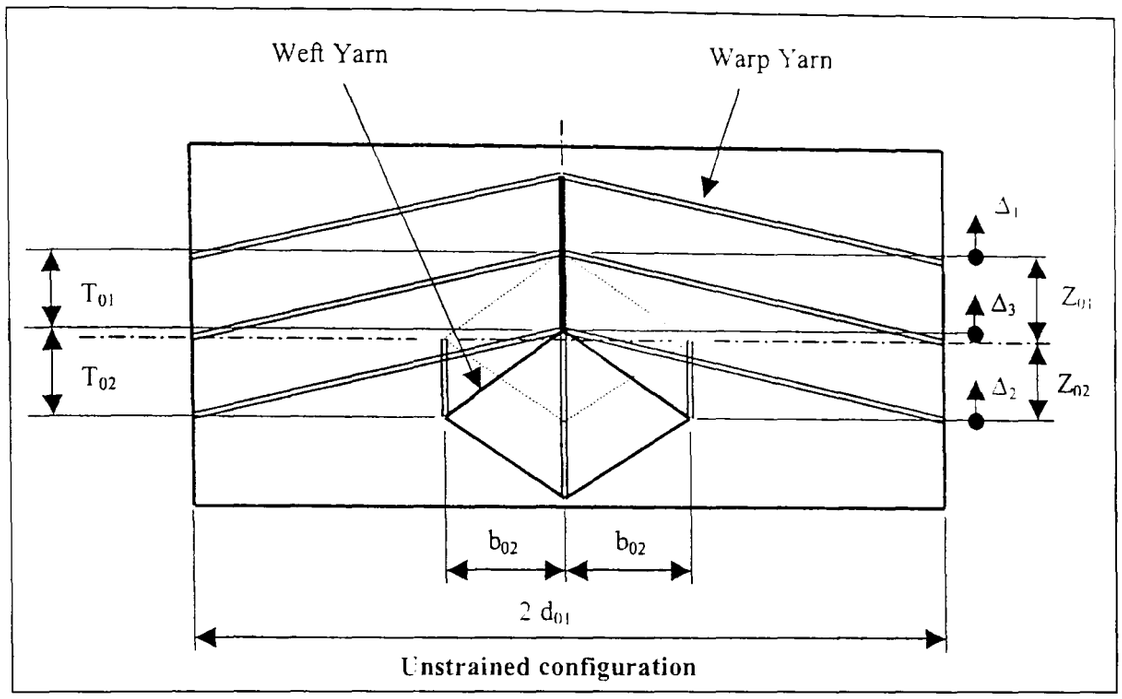

Figure 2-47. Unit cell configuration, reproduced from Pargana et al (2000)

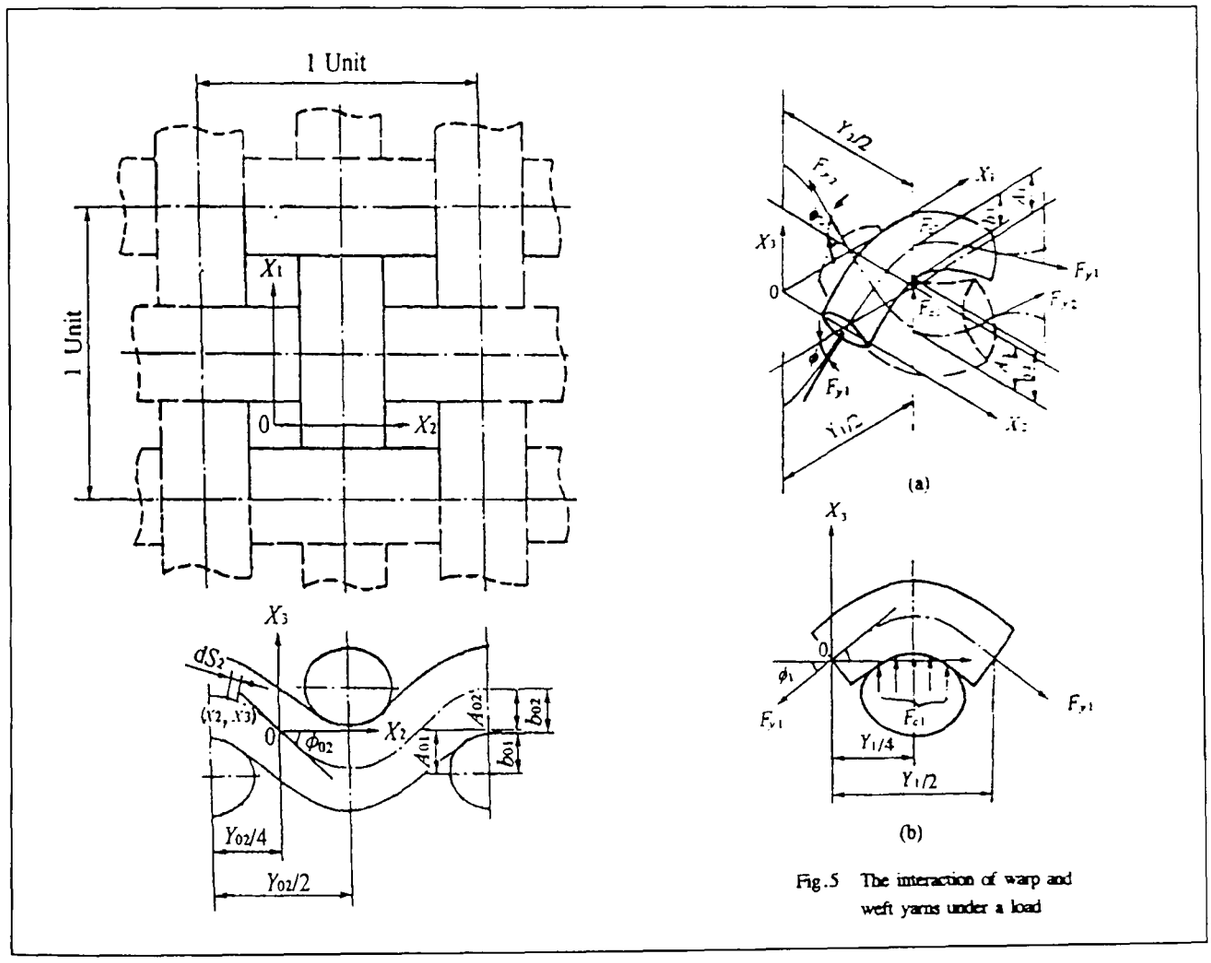

Figure 2-48. Sinusoidal yarn configuration, reproduced from Wang (2002)

Wang (2002) uses a similar formulation to the sawtooth model but instead of a triangular sawtooth a sinusoidal yarn shape is adopted. This provides a more realistic representation of the yarn waveform, and should give a more accurate measure of *decrimping strain* (i.e. the difference in length between a crimped yarn in the as-woven fabric and a straightened yarn).

The sinusoidal model is not fully utilised; the vertical force developed by the yarns (F_c in Figure 2-48) is calculated simply as the vertical component of the force in the yarn when the yarn is at its steepest gradient. This gives an out-of-plane force similar to that provided by the sawtooth model, and does not account for the variation in out-of-plane force along the yarn. A full analysis of the vertical forces generated by the curved yarn provides scope for further development. To determine these out-of-plane forces the contact area between the warp and fill yarns must be considered.

For architectural fabrics orthogonal warp and fill yarns are in contact with each other for almost their entire length (Figure 2-12 & Figure 2-13, p.37). Hence consideration of a finite contact length with out-of-plane contact forces occurring along this length is appropriate. Olofsson (1964; 1966) developed a model with no a *priori* assumptions about the yarn wave form: the yarn weave geometry is a function of the forces applied to the yarn, the *initial set* (i.e. the residual yarn crimp when it has been removed from the fabric) and the yarn bending stiffness (Figure 2-49). This provides a fabric model which more closely resembles the fabric as seen under the microscope than the sawtooth model.

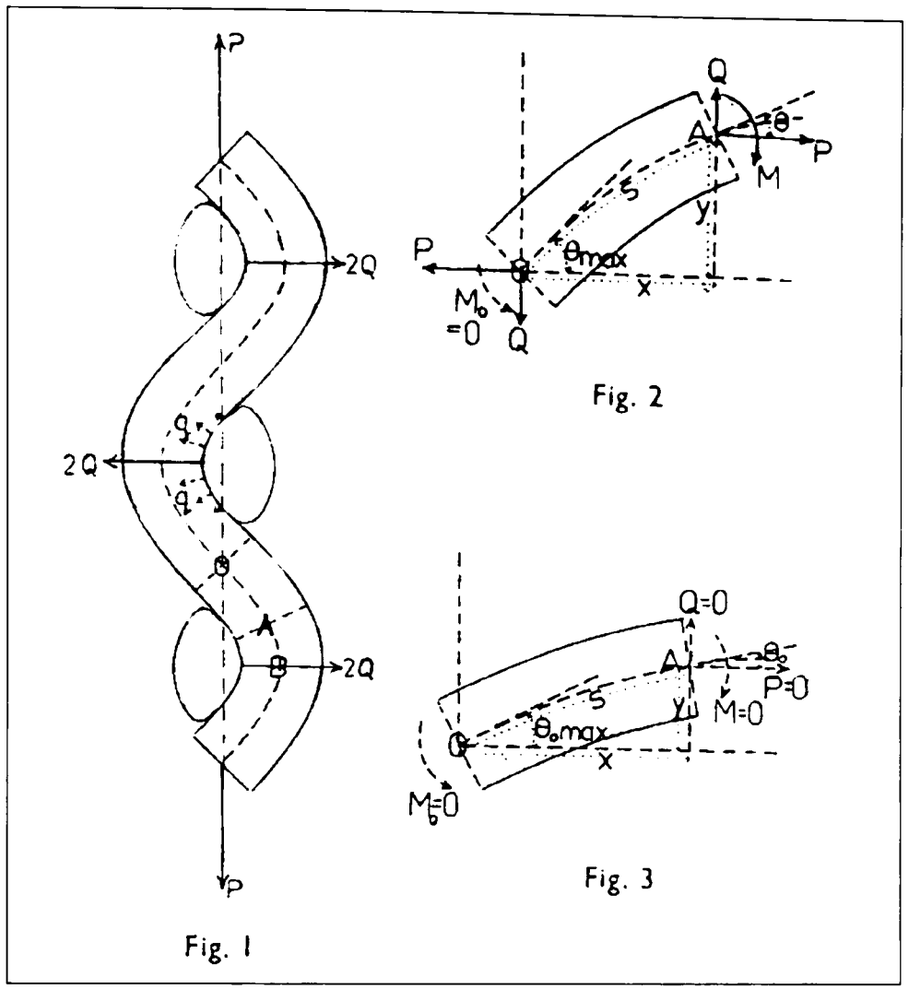

Figure 2-49. Elastic thread model, reproduced from Olofsson (1964)

"*If we consider the geometric-mechanical interdependence as fundamental, it* [Peirce's (1937) model] *is quite inadequate*" [Olofsson (1964), p.T542]. A finite contact length at yarn crossovers results in a model with geometric consistency between the warp and fill yarns, rather than the yarn section just being defined by its 'radius'. The yarn waveform fits the orthogonal yarn cross-section throughout the contact length, Figure 2-50. This enables the yarn volume to be taken into account (Freeston, Platt & Schoppee, 1967; Boisse, Gasser & Hivet, 2001) and gives an inherent interaction between changes in yarn cross sectional area (due to both tensile extension and inter-yarn forces), out-of-plane thickness and weave shape. The assumption of a constant yarn cross-sectional area and consistent yarn geometry negates the need to define the yarn crushing stiffness: "*Ideally the yarn can also vary its cross-sectional shape (although not area)...*" [Glaessgen et al (1996), p. 44]. Finite element unit cell models are well suited to modelling consistent yarn geometry (§2.4.2.1).

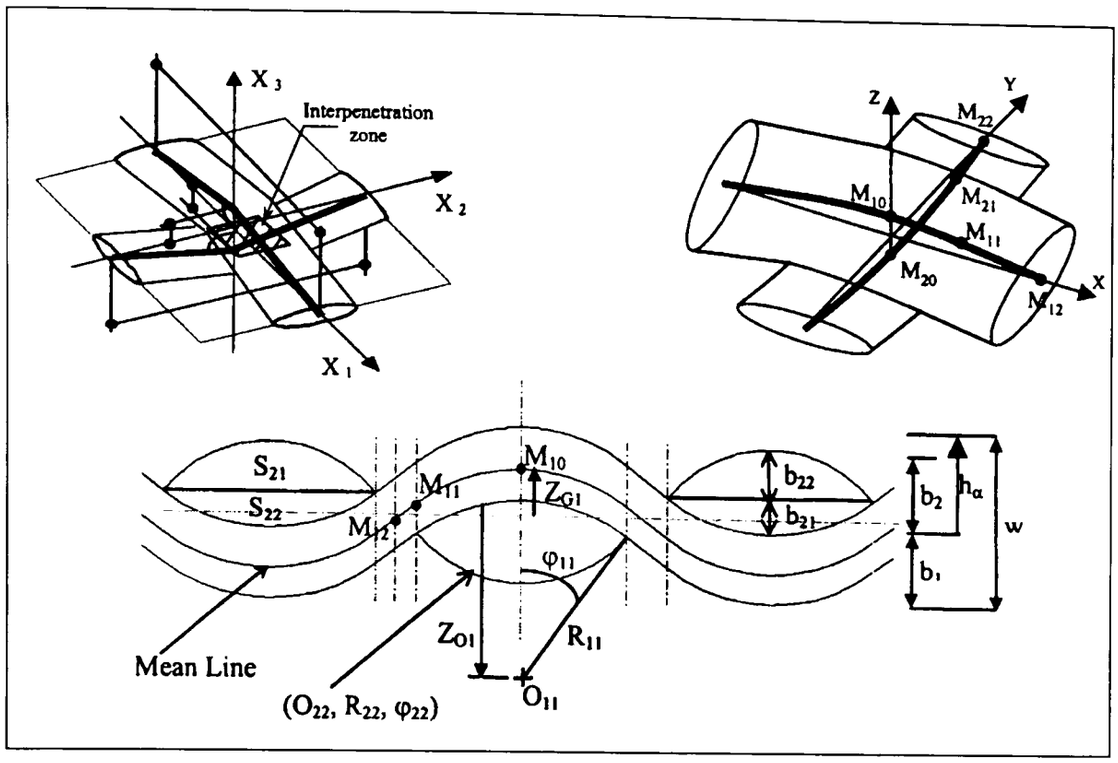

Figure 2-50. Geometrically consistent model, reproduced from Boisse, Gasser & Hivet (2001)

Menges & Meffert (1976) carried out the first significant work on *coated* woven fabrics; analysing a model of PVC-coated polyester fabric including the effect of the coating. This was the first fabric model directly applicable to architectural fabrics. The model uses a typical sawtooth formulation; the fabric is "*considered to be a load-bearing structure consisting of deformable bars that lie in the direction of the warp and woof* [fill] *axes. These bars are connected together by flexible joints located at the crossovers of the fibres in the fabric*", Menges and Meffert (1976), p.12, Figure 2-51 & Figure 2-52.

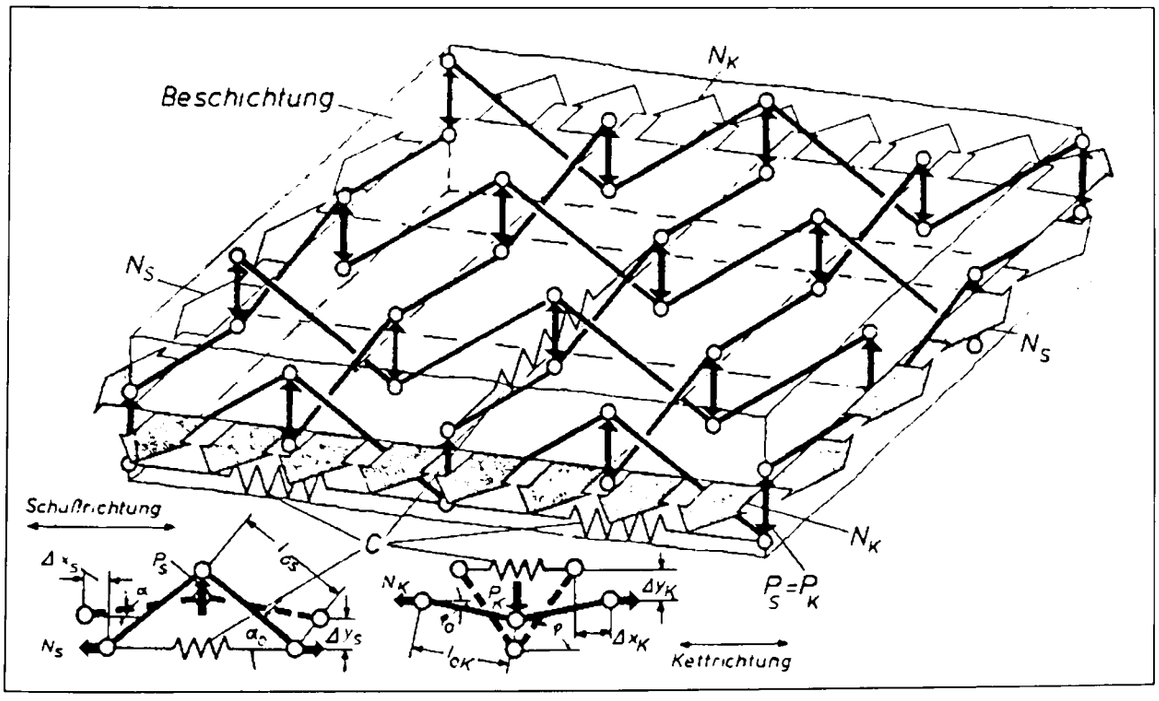

Figure 2-51. "Model for calculating the biaxial stress-strain characteristic", reproduced from Menges & Meffert (1976)

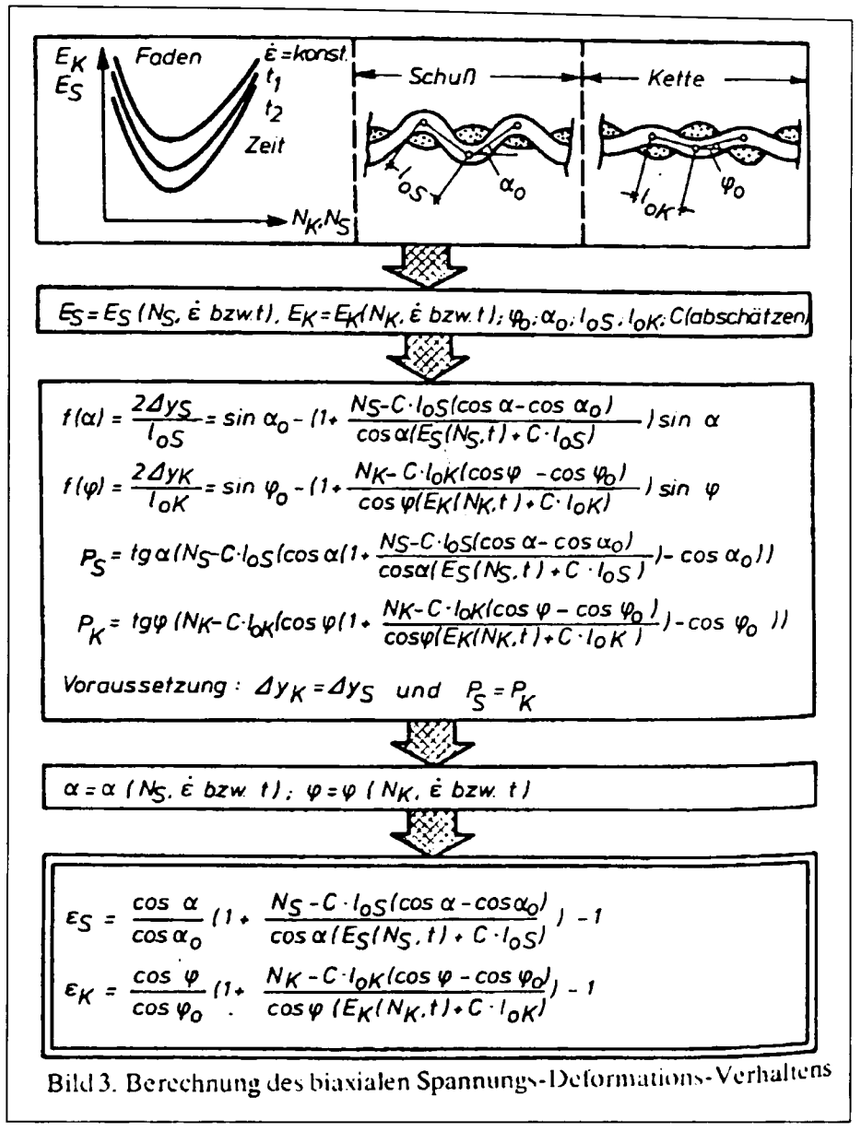

Bild 3. Berechnung des biaxialen Spannungs-Deformations-Verhaltens

Figure 2-52. Calculating the biaxial stress-deformation characteristic, reproduced from Menges & Meffert (1976)

The coating simply consists of spring elements joining the yarn crossovers, arranged in parallel with the warp and fill directions. The shear resistance of an uncoated plain woven fabric is commonly assumed to be negligible (§2.1.4.3), hence fabric shear resistance is attributed to the coating. This can be modelled by introducing coating springs diagonally between crossovers (Figure 2-51), or by modelling the coating as an isotropic linear elastic panel (Tan and Barnes, 1980).

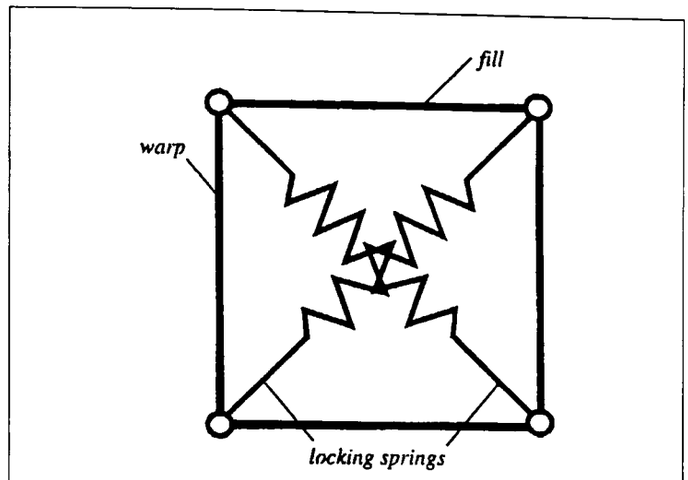

Fig. 4. The model of the RC.

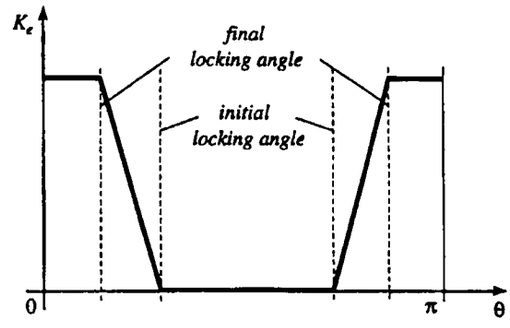

Fig. 5. Locking springs stiffness, K_c, versus angle between fibers, θ.

Figure 2-53. Inclusion of shear in fabric model, reproduced from Tanov & Brueggert (2003)

PTFE coating has a high Poisson's ratio and can contribute to lateral fabric contraction under load (Dimitrov and Schock, 1986). Both PVC and PTFE coatings exhibit significant creep under sustained load. As a result, time-stress curves are required for accurate modelling of the coating response (Dimitrov and Schock, 1986). The effect of the coating stiffness on the fabric biaxial response is shown in Figure 2-54.

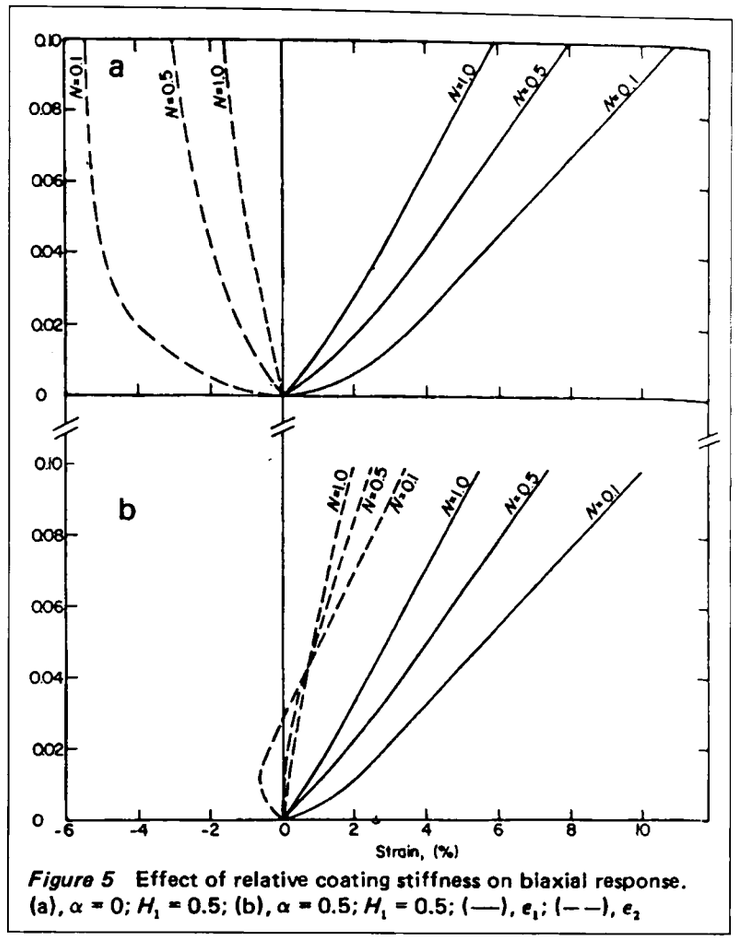

Figure 5 Effect of relative coating stiffness on biaxial response. (a), $\alpha = 0$; $H_1 = 0.5$; (b), $\alpha = 0.5$; $H_1 = 0.5$; (—), e_1; (– –), e_2

Figure 2-54. Effect of coating stiffness on biaxial behaviour, reproduced from Stubbs & Fluss (1980)

The sawtooth model consists of straight yarns with infinitely flexible joints, with yarn bending stiffness assumed to be negligible (Testa, Stubbs & Spillers, 1978; Menges & Meffert, 1976; Kawabata, Niwa & Kawai, 1973a). Whether yarn bending stiffness should be included in the unit cell model is a moot point. The bending stiffness of the fabric as a whole is commonly assumed to negligible for tensioned structural applications (§2.1.4.4). However, the yarn bending stiffness may be significant on the scale of the unit cell model. In his 1937 treatise, Peirce stated that the neglect of yarn rigidity cannot always be justified. Stubbs & Fluss (1980) suggest that the lack of agreement of their model with test results at low load is due to yarn bending stiffness (and 'other effects') being ignored. Similarly, Olofsson (1964; 1966) stated that Peirce's work was flawed because yarn bending and yarn torsional resistance are neglected. Skelton (1980a) developed a unit cell model based entirely on the bending of circular arcs (Figure 2-55).

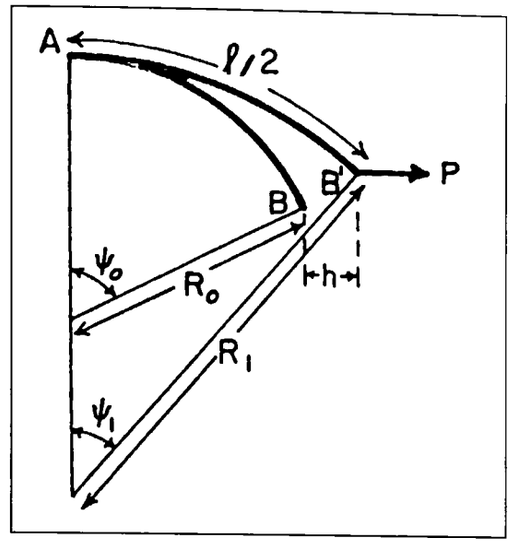

Figure 2-55. Circular arc geometry, reproduced from Skelton (1980a)

Clearly the determination of the yarn flexural rigidity, G, is fundamental to the accuracy of this model. Yarn bending can be modelled with varying degrees of association between the constituent fibres, and the model of yarn bending in which there is no movement between fibres is adopted. Skelton considered the fibres as being arranged in a rectangular array, with the bending stiffness calculated as for a beam. Many papers on yarn modelling since 1980 show this approach to be over simplistic for yarns in non-coated fabrics (§2.1.1). However, in coated fabrics the coating impregnates the yarn reducing the interfibre movement. The model output "*appears to be adequate for the determination of trends, but it is not good enough for detailed predictive purposes*" [Skelton (1980a), p.467]. Any limitations in the model are blamed on uncertainty in determination of the yarn flexural rigidity and inter-yarn forces. For example, a finite contact length would give different yarn bending moments compared to the typical point contact. For architectural fabrics composed of flat yarns (Figure 2-12 & Figure 2-13, p.37) the changes in curvature of the yarns will be small during crimp interchange, making significant bending effects less likely.

Fabric models are commonly formulated with the assumption of *elastic behaviour* for both the yarns and coating (Menges & Meffert, 1976; Stubbs & Fluss, 1980; Pargana et al, 2000). Peirce notes that yarns behave in an inelastic manner, but adopts an elastic analysis, "*modified by such estimation of the effect of deviations* [from elasticity] *as is possible*" (Peirce, 1937, p.T73). Non-linear yarn behaviour can be included using a multi-linear or polynomial representation of the yarn stress-strain curve (assuming yarn test data is available and representative of the in-situ yarn; §3.1.2). Yarn stiffness for glass fibres can be "*described analytically by a parabola fitting. For the nether* [lower] *regions the load extension behaviour can be approximated by a second order polynomial*" (Dimitrov & Schock, 1986), p.862).

Yarn and coating properties are *time dependent* with significant hysteresis and creep (§2.1.1 & 2.1.3). The end use of the model can preclude the inclusion of time-dependent effects.

Typically fabric models are developed to represent the fabric response for use in structural analysis (§2.3.2), with no scope in the analysis for inclusion of time dependent effects (§6.2.4). Uetani, Fujiwara and Ohsaki (2002) formulated a simple model for visco-elastic fabric behaviour. The aim was to model fabric response for approximately one week after construction for cutting pattern calculation (§1.1.3). Each yarn was represented by three parameters (Figure 2-56). The viscoelastic property was modelled by the Voigt element consisting of a spring and dashpot connected in parallel. If the rate of loading or unloading is large the dashpot is effectively fixed, giving elastic behaviour determined by spring 'E'. If the rate of loading is small the dashpot can be ignored and the elastic behaviour is determined by the two springs in series. The parallel part is called the 'viscoelastic part'; the remaining spring is called the 'elastic part'.

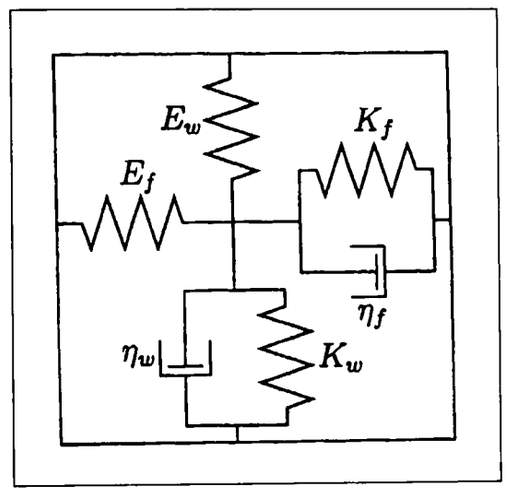

Figure 2-56. Orthogonal three-parameter model, reproduced from Uetani, Fujiwara and Ohsaki (2002)

The results provided by Wang's (2002) model clearly show hysteretic loading and unloading curves, but with no residual strain (Figure 2-39). This is achieved by using yarn stress-strain curves directly in the model to relate yarn tensile stresses and strains. In this way most models which use a value of Young's modulus to describe the elastic yarn behaviour can readily be modified to model viscoelastic behaviour. However, determination of the visco-elastic yarn (and coating) response is not straightforward.

Models which aim to represent a given set of test data (§2.3.2) are calibrated against that data to determine various parameters. These parameters may represent physical quantities (e.g. crimp amplitude or yarn crushing stiffness) but still be determined by trial and error to give the best fit to the data set (Kato, Yoshino & Minami, 1999).

For a truly predictive model the input parameters must be independent of the biaxial test data. The aim of the model developed in this research is to determine the biaxial response of the fabric without biaxial testing (§5.2). Fabric weave geometry and yarn shape can be determined by measuring fabric cross-section images, but specific details relating to how the measurements

are taken are rarely mentioned in research papers. The key material properties required for most unit cell models are the yarn and coating tensile stiffnesses. To avoid the difficulties associated with removing yarns from the fabric and testing them, another approach is to infer yarn and coating properties from standard uniaxial strip tests (Menges & Meffert, 1976; Dimitrov & Schock, 1986). The initial part of the uniaxial stress-strain curve, before the initial crimp in the yarns has been straightened, can be attributed to the coating stiffness. This is best seen in the fill direction. Once the yarns have been straightened the uniaxial strip test will closely resemble the yarn tensile response (Testa, Stubbs & Spillers, 1978). The coating stiffness should be deducted from this uniaxial strip stiffness to give the yarn stiffness. Stubbs and Fluss (1980) developed a model with parameters based on two uniaxial tests. Model parameters are varied until the theoretical uniaxial stress-strain curves are mapped onto the experimental curves. In this way other inaccuracies or simplifying assumptions in the model are corrected, at least for the uniaxial parts of the model response. This does not compromise the predictive nature of the model, as no biaxial test data is required for the calibration.

2.4.2.1 Finite element fabric models

"*...a new approach based on the combination of geometric and mechanical models*"

Tarfaoui & Akesbi, 2001, from Abstract

Finite element (FE) modelling of the fabric unit cell is a recent development from the mechanical models described above (§2.4.2). The earliest paper cited here was published in 1996 (Glaessgen et al, 1996), and the majority of the work has been carried out in the last couple of years. Whilst FE modelling has been deemed unsuitable for use in this research (Chapter 5) there is much to be learnt from FE unit cell models, in particular about the realistic modelling of yarn waveforms and interyarn contact.

The majority of research on FE unit cell models is applied to woven composites; typically untwisted glass fibre yarns set in a resin matrix (Glaessgen et al, 1996; Gasser, Boisse & Hankler, 2000; Boisse, Gasser & Hivet, 2001). Because the yarn is untwisted the fibres can slide relative to one another, resulting in negligible bending stiffness. During composite forming the matrix is liquid and does not impede yarn movements, thus effectively requiring an analysis of an uncoated fabric.

FE models of woven fabrics are similar to mechanical unit cell models in their approach: modelling the geometric and material non-linearities of the fabric by consideration of the fabric unit cell. The unit cell analysis provides an understanding of fabric behaviour which can then be applied to the whole continuum. The principal advantage of FE models is the reduction in the number of simplifications required to generate a viable model, in particular less

simplification of the yarn geometry is necessary. Boisse, Gasser & Hivet (2001) present a model "*consistent with the geometry of the plain weave woven mesh*" [p.1395], (Figure 2-57). Yarn undulation and interyarn contact can be modelled, allowing the unit cell to be modelled "*without any restriction and any simplifying assumption*" (Tarfaoui & Akesbi, 2001).

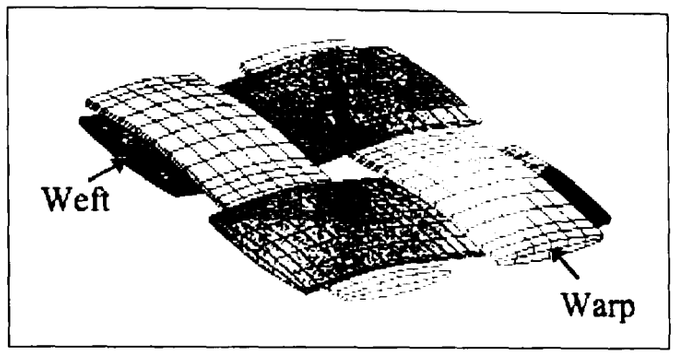

Figure 2-57. Finite element unit cell model, reproduced from Gasser, Boisse & Hankler, 2000

Tarfaoui & Akesbi (2001) considered using Peirce's flexible yarn model (i.e. the basic sawtooth), Peirce's elliptical model and Kemp's racetrack model (Figure 2-58). However, all three of these yarn structures were abandoned in favour of a sinusoidal yarn structure.

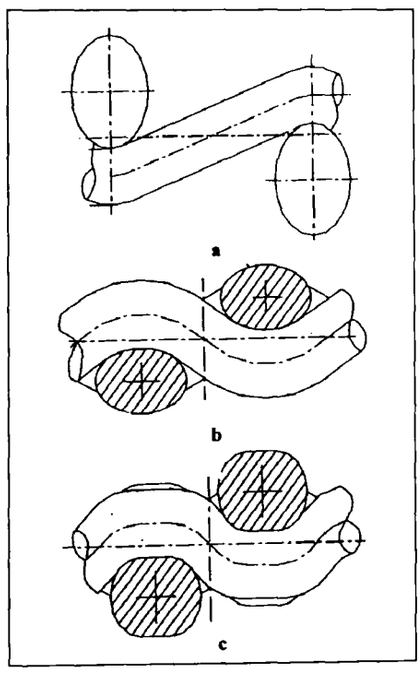

Figure 2-58. Yarn configuration in three fabric models, reproduced from Tarfaoui & Akesbi, 2001

Better utilising the flexibility of the FE model, Glaessgen et al (1996) defined the centreline of each yarn with a Bézier curve which interpolates a set of support points. Ellipses located at intervals along the Bézier curves are used to generate the yarn surface.

Durville (2003) made no initial assumption about the yarn waveform. An arbitrary starting configuration was used (Figure 2-61a) and, with a simple definition of the weave pattern, contact detection ensures a realistic yarn configuration. Different parameters gave different

weave patterns with no change to the model formulation (Figure 2-61b, c). Traditional mechanical models are well suited to plain weave fabric, but the model formulation requires substantial modification for twill or other weave patterns (Tarfoui & Drean, 2001). This method works well for uncoated fabrics with minimal *crimp set*. To apply this approach to architectural fabrics the model would need to include a target level of crimp in each direction, to account for the crimp set that is introduced during weaving and particularly coating.

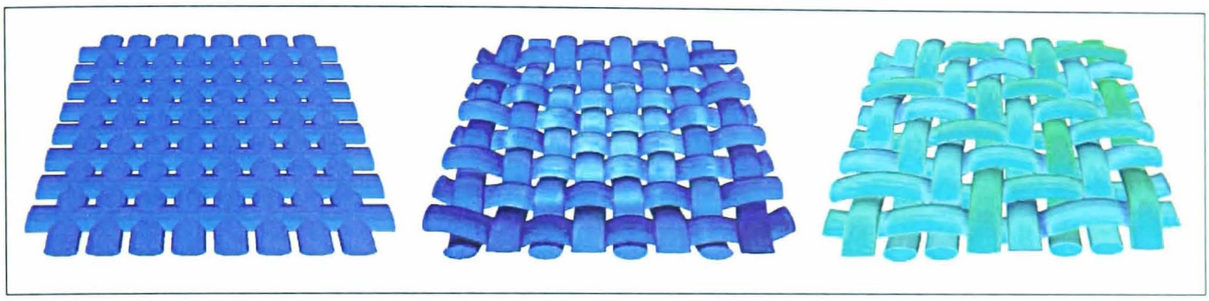

Figure 2-59. Weave patterns, reproduced from Durville, 2003

Full account can be taken of the contact area between yarns and the variation in contact forces across this area. With the correct formulation the model can account for yarn interaction (and consequent yarn crushing) and effects on behaviour due to changing yarn geometry. Whilst coating is absent from the models reviewed, the coating could be modelled as a geometrically consistent entity, not approximated by spring elements between crossovers. FE models are potentially extremely useful for modelling shear behaviour as no additional modelling or formulation is required, just a change in the applied loading (Durville, 2003; Figure 2-60).

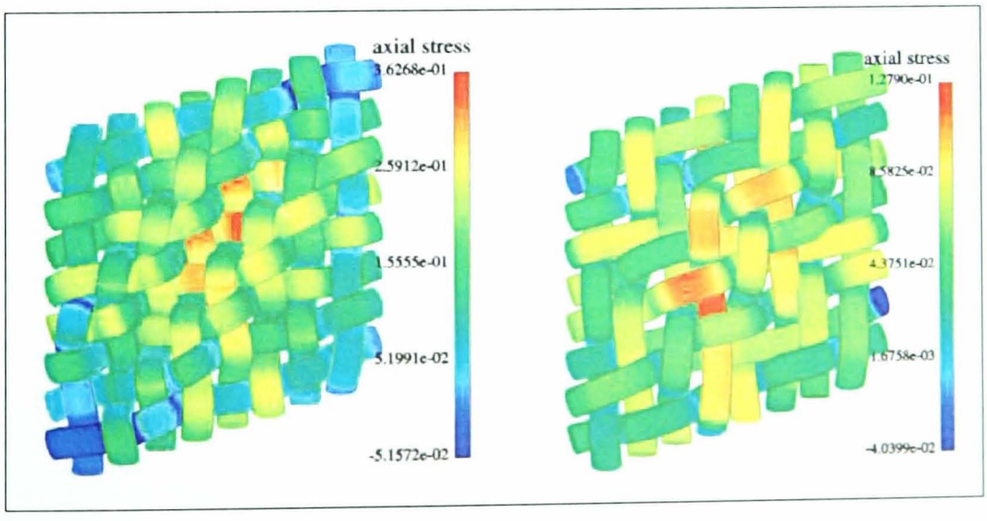

Figure 2-60. Model of shear deformation, reproduced from Durville, 2003

Determination of appropriate non-linear, viscoelastic yarn and coating properties is crucial for FE fabric models. As for mechanical models (§2.4.2) establishing the level of yarn crushing, due to both transverse compression, longitudinal tension and the interaction between them, is critical (Boisse, Gasser & Hivet, 2001).

To accurately determine crushing parameters requires either:

- Yarn testing involving removal of the yarns from the fabric and dedicated test equipment (Figure 2-8 & Figure 2-28),
- Test data from as-produced yarns, ideally modified to account for the effect of the weaving and coating process on the yarn properties,
- Calibration of the model against uniaxial or biaxial test data,
- Predictive yarn models based on fibre properties.

Gasser, Boisse & Hankler (2000) determined yarn crushing stiffness empirically, but commented that it would be beneficial to determine the crushing behaviour from yarn structure. The yarn crushing modulus is increased as transverse and/or longitudinal strains increase. Use of yarn models is more popular in FE models than mechanical models. FE analysis is better suited to modelling the fibre interactions (including migration and microbuckling, §2.1.1, Figure 2-7), whereas formulating equations to describe these mechanisms would be cumbersome. Durville (2003) modelled the unit cell with the yarn fibre as the fundamental unit: *"The unknown initial configuration is obtained as a first result of the simulation by tightening a starting arbitrary assembly of fibres"* (Figure 2-61).

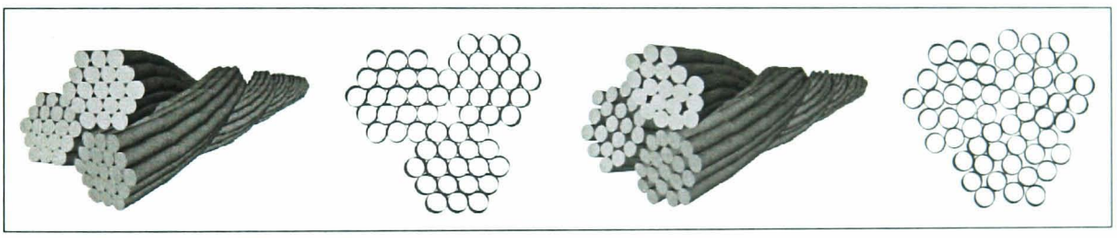

Figure 2-61. Yarn model, reproduced from Durville, 2003

Bigaud & Hamelin (1997) conducted their analysis at three levels, with the first 'miscroscopic' level being used to predict the behaviour of the yarn.

- Microscopic: determine the material properties based on constituents (fibre + matrix)
- Mesoscopic: define properties of meso-element (8 micro-elements)
- Macroscopic: mechanical properties of unit cell (aggregate of meso-elements)

Typically an energy minimisation approach is applied, with energy penalties for overlapping yarns used to ensure a feasible configuration (Bigaud & Hamelin, 1997; Glaessgen et al, 1996). Glaessgen et al (1996) used Lagrange's principle of minimum work is used to determine the initial fabric geometry:

$$L = \sum_{i=i}^{n} (W_t^i + W_b^i + W_\theta^i) + W_p - A_e, \qquad \text{Equation 2-15}$$

$$W_t^i = \frac{1}{2} \int C_t^i \varepsilon_i^2 \, dl_i, \qquad \text{Equation 2-16}$$

$$W_b^i = \frac{1}{2} \int C_b^i \kappa_i^2 \, dl_i, \qquad \text{Equation 2-17}$$

$$W_\theta^i = \frac{1}{2} \int C_\theta^i \theta_i^2 \, dl_i, \qquad \text{Equation 2-18}$$

where L is the total energy in the system, C_t^i, C_b^i and C_θ^i correspond to tension, bending and twist coefficients of the ith yarn, ε_i is the longitudinal strain, κ_i is the local curvature, and θ_i is the linear twist of the ith yarn. N is the number of yarns forming the unit cell, l_i is the arc length along the centreline of the ith yarn, W_p is the penalty for yarn intersection and A_e is the work done by applied external loads. If two yarns overlap the energy penalty prevents that structure being accepted. A high penalty is used for rigid yarns, and a carefully chosen penalty is used to represent yarn deformation.

Similar to the mechanical unit cell models (§2.4.2), published papers rarely provide detailed comparison of the model output with biaxial test data. Glaessgen et al's (1996) model exhibits a typical stress-strain response for a woven fabric; at low strain the response is non-linear due to crimp interchange, at higher strains linear yarn extension is dominant. Comparison of the model output with experimental results shows that the model fails to predict important parts of the response (Figure 2-62).

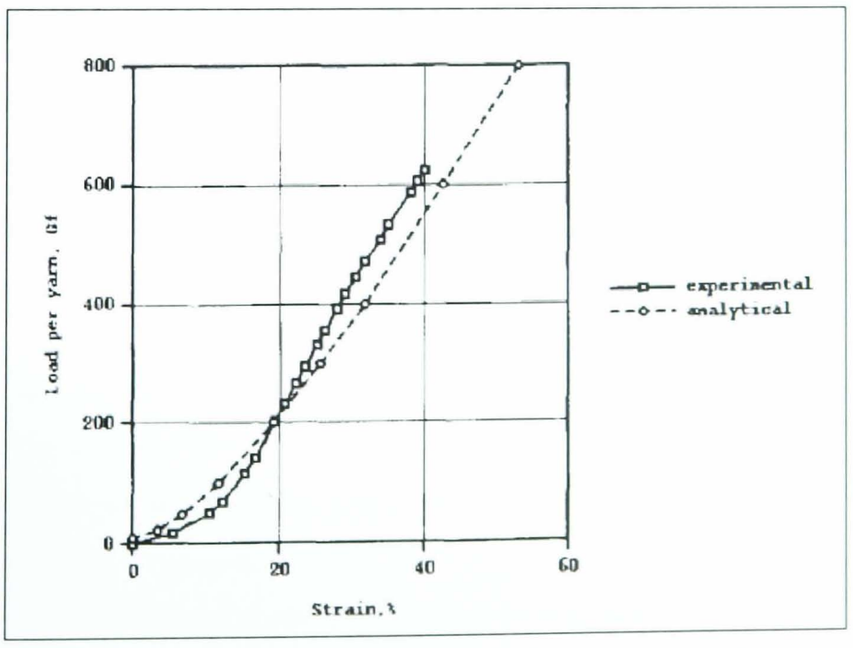

Figure 2-62. Comparison of experimental and predicted axial stress-strain response of plain weave fabric, reproduced from Glaessgen et al, 1996

Gasser, Boisse & Hankler's (2000) model shows reasonable agreement between the experimental results and model prediction (Figure 2-63). However, the behaviour of the uncoated, glass-fibre yarns used in composite forming is much simpler than the behaviour of architectural fabrics. For example, the results show no negative strain due high levels of crimp interchange.

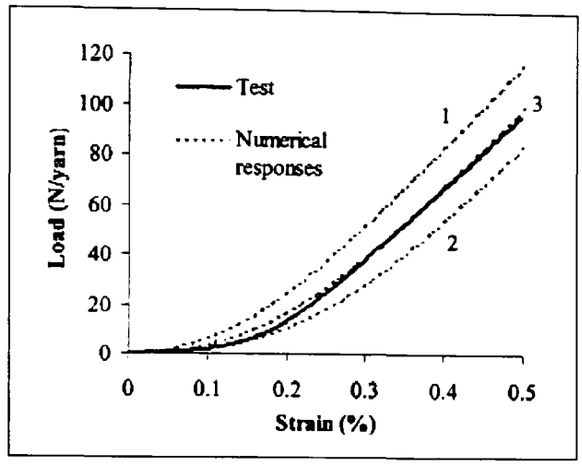

Figure 2-63. Comparison of model and test data, reproduced from Gasser, Boisse & Hankler, 2000

2.4.3 Conclusions

A mechanical model of the unit cell, the smallest repeated unit in the fabric, can be used to predict the fabric response to in-plane loads. The key deformation mechanism, crimp interchange, is easily modelled using a simple sawtooth representation of the weave shape. Many models described in published papers seek to represent the test data rather than predict the fabric response without biaxial testing. These models, with parameters calibrated against test data, often poorly match the fabric stress-strain curves. These comparisons are typically carried out at a limited number of stress ratios and for only a single type of fabric. In this research the model will be kept as general as possible (i.e. appropriate for PTFE-glass fibre and PVC-polyester fabrics in range of weights), using comparison with comprehensive test data to assess the model validity.

The fundamentals of the sawtooth model are well established (Peirce, 1937; Menges & Meffert, 1976) and will be used as a basis for this research. In recent papers on fabric models a good correlation between model and test data still has not been achieved, but several useful possibilities for further development are identified which will be pursued in this research. These include use of a sinusoidal yarn waveform, use of a constant yarn cross-sectional area and maintaining consistent geometry between the yarn waveform and the cross-section of the orthogonal yarn (Chapter 5).

Finite element models of the unit cell present fewer constraints than the mechanical models discussed above. However, they are difficult to modify for different fabrics, and accurate assessment of the constituent material properties (in particular yarn crushing stiffness) is vital. Key aims of the unit cell model developed in this research are ease of use, general applicability and accessibility to the design engineer. Because of this the simple mechanical unit cell model has been used.

Chapter 3

Fabric testing

Contents

Figures

Tables

3.1 UNIAXIAL TESTING

3.1.1 Fabric strip testing

Uniaxial strip tests for coated woven fabrics are defined by BS EN ISO 1421:1998 "Rubber- or plastics-coated fabrics - Determination of tensile strength and elongation at break". This test is commonly used in industry to determine fabric ultimate tensile strength. The British Standard specifies that 50mm wide strips are used, with a gauge length of 100mm and the jaws of the tensile tester at least 200mm apart.

The choice of strip width is a compromise. As strip width is increased, lateral contraction (due to crimp interchange, and possibly Poisson's effect in the coating) increases. The distance between clamps must be increased to prevent lateral restraint from the clamps causing a significant biaxial state of stress in the strip. If the strip is too narrow, accurate measurement of the strip width becomes critical. This is problematic when fabrics can only effectively be cut to the nearest thread, which may be around 1mm for a heavy PVC fabric (e.g. Ferrari 1502). For a strip width of 50mm, whether the cut is made on one side of a thread or the other results in a 2% variation in width. Strips are cut from the roll of fabric in warp and fill directions (Figure 3-1). Ideally warp strips are cut from the centre of the roll to avoid shear effects in the strip due to bowed fill yarns. This is not always possible as the strips may need to be arranged around the cutting of biaxial test specimens (§3.3) if the available fabric for testing is limited. This was the case during the initial stages of this research. Strips used in this research were cut no closer than 20mm from the edge of the roll; the edge fabric may not be typical due to inconsistencies in the coating or the effects of edge grips used during the manufacturing process.

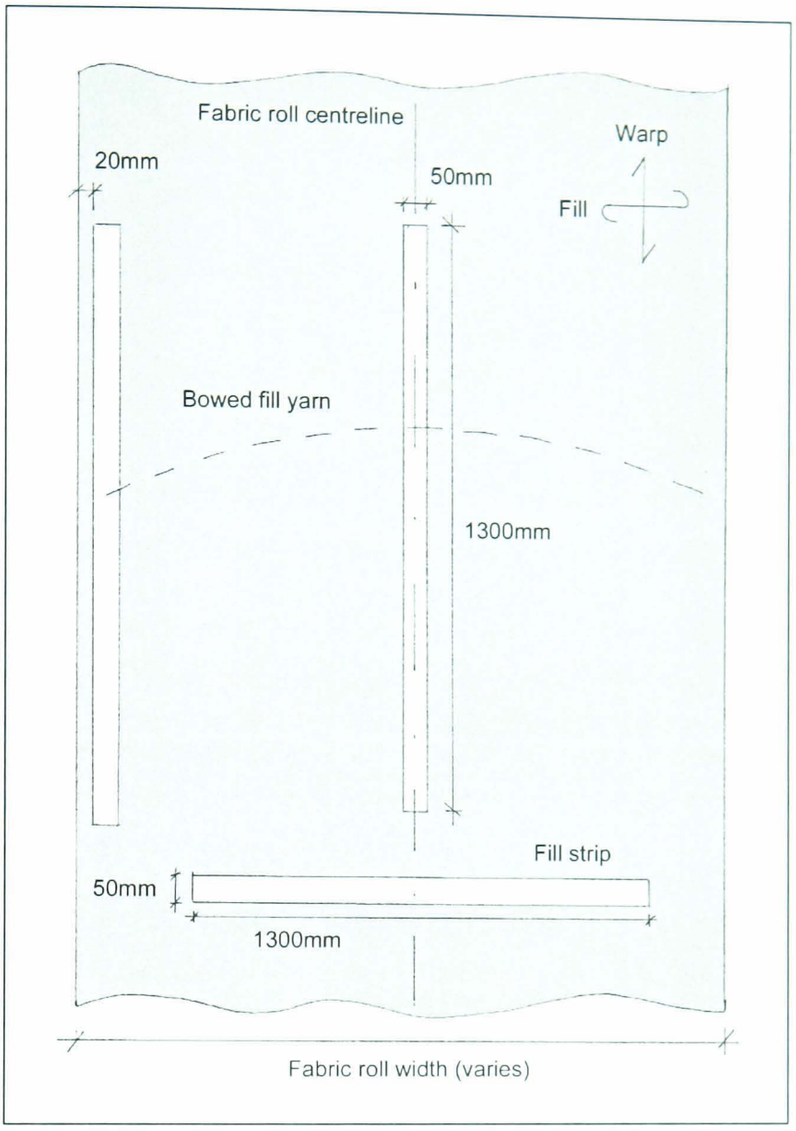

Figure 3-1. Cutting uniaxial strips

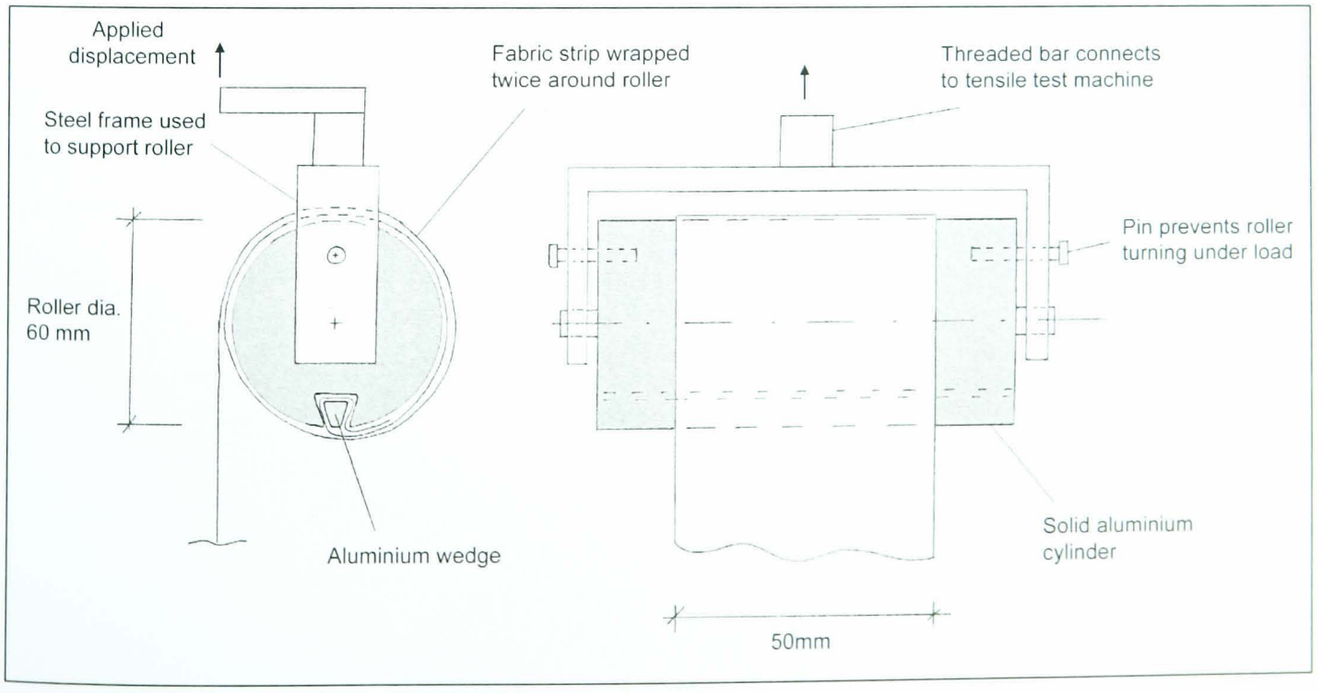

Figure 3-2. Jaws for fabric strip testing.

Clamping of woven fabrics without weakening the fabric at the jaw or allowing the fabric to slip is problematic and requires careful clamp design. The roller jaw with triangular inset (Figure 3-2) was developed for testing geotextiles and provides a good starting point. The two main types of architectural fabric present different clamping problems:

1. PTFE coated glass-fibre has a low coefficient of friction and is easily damaged if folded or loaded over an edge. The roller system does not provide enough friction: load is transferred back to where the fabric is wrapped round the triangular insert, and fails prematurely because the fabric is loaded over an edge. If the PTFE-glass fibre fabric is wrapped around the roller with a piece of PVC-polyester fabric the level of friction is increased and failure is remote from the rollers.
2. PVC-polyester fabric has a higher coefficient of friction, hence the load tends to be held by friction and is not evenly distributed around the roller. This can lead to instantaneous slippage which liberates slack fabric from further round the roller, resulting in a sudden drop in load. The solution is similar to before; by wrapping the PVC-polyester with a strip of PTFE-glass fibre the level of friction is decreased and a smooth loading curve is achieved. Again failure is remote from the rollers.

Strain was measured over a 100mm gauge length using a laser extensometer which scans between two reflective strips adhered to the fabric surface (Figure 3-3). Recording the cross-head displacement would not be sufficiently accurate as slippage at the clamps would be recorded as fabric strain. Using the laser extensometer, clamp slippage gives no reduction in strain measurement accuracy. Because the test is displacement controlled (see below), slippage at the clamp does give a drop in load and should be minimised.

The test is carried out at a constant rate of strain, i.e. constant cross-head speed. For the rate of strain of the fabric strip to be the same the initial distance between the clamps must be the same for each test. This is because it is the rate strain per unit length which is important. The test standard specifies a strain rate of 100mm/min. The fabric is tested to failure (Figure 3-4 & Figure 3-5).

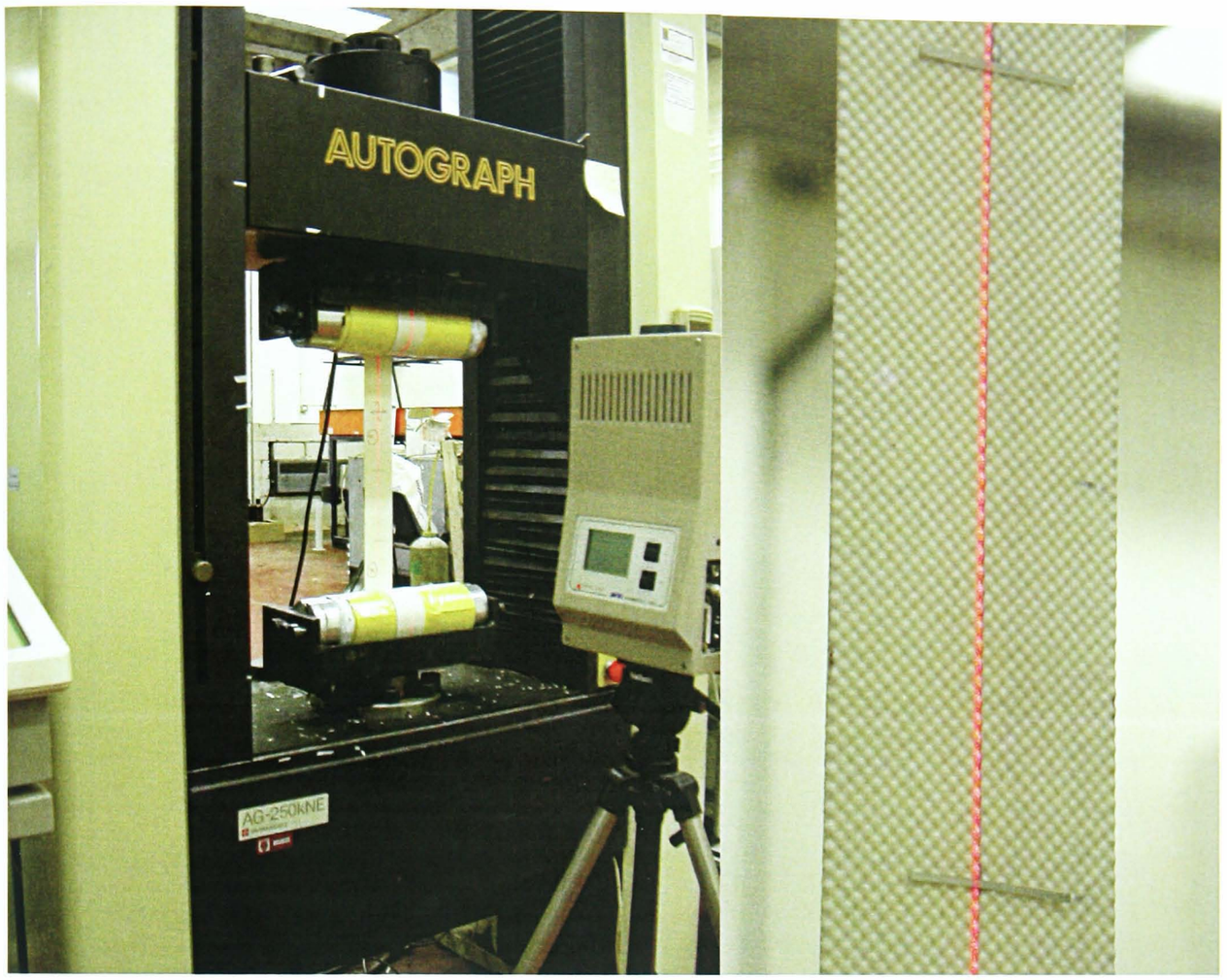

Figure 3-3. Uniaxial fabric testing

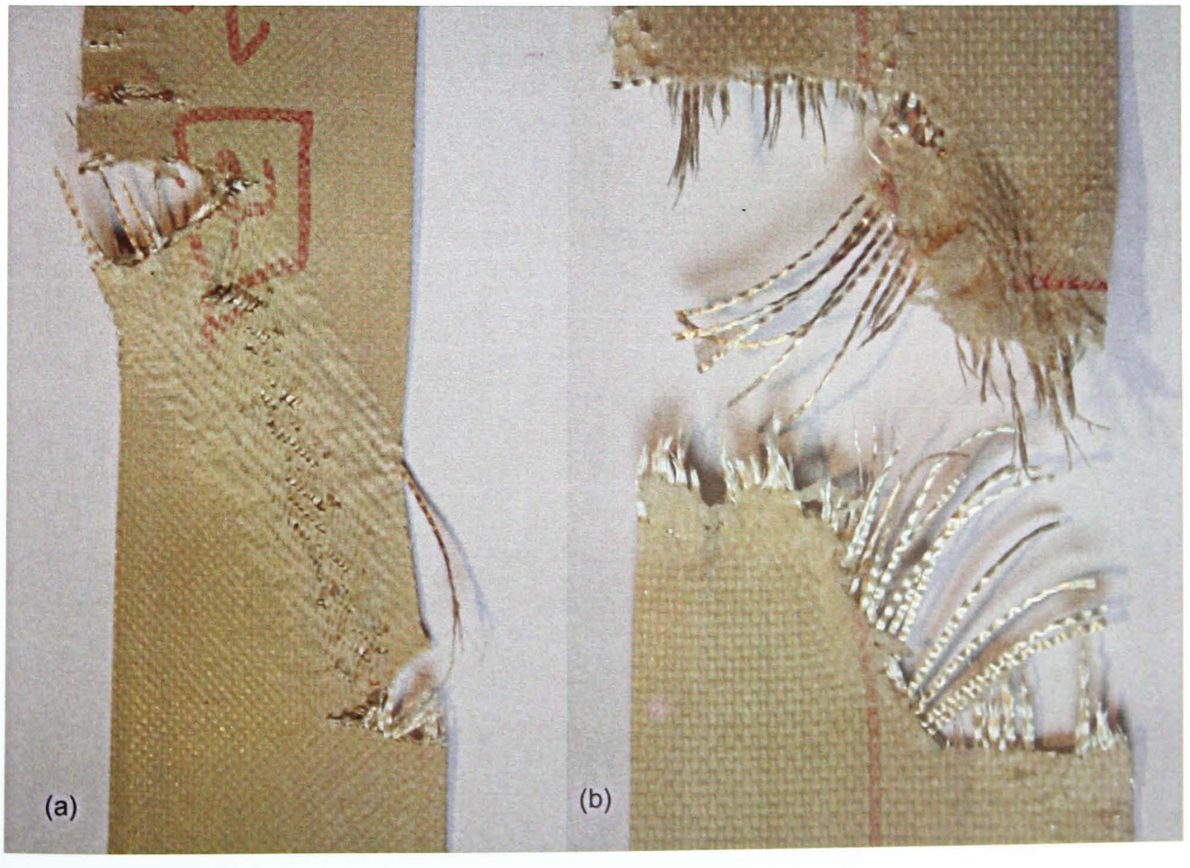

Figure 3-4. Failure of PTFE / glass-fibre strip

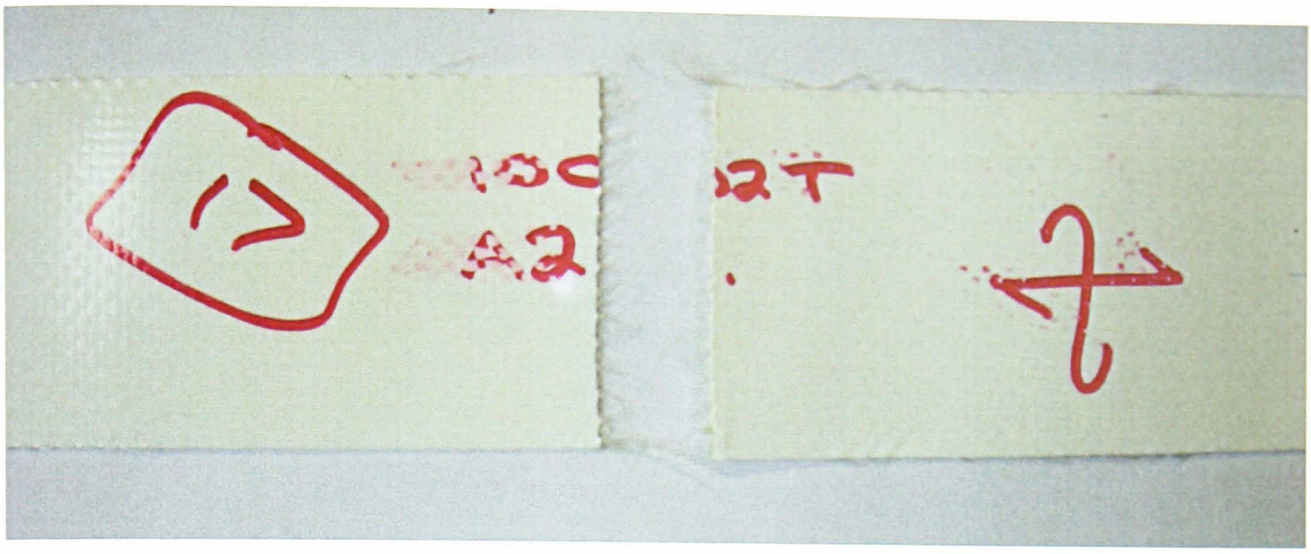

Figure 3-5. Failure of PVC / polyester strip

The uniaxial test procedure adopted for this research was initially based on BS 3424-21: 1993 "Testing coated fabrics – Part 21: Method 24. Method for determination of elongation and tension set". The test piece dimensions are the same as BS EN ISO 1421:1998, the difference being that the rate of straining specified in BS 3424-21: 1993 is 5mm/min. The aim of this testing is to determine the stress-strain response of the fabric; this is not the specific purpose of either standard, and hence neither has more validity than the other. Tests were carried out at a range of loading rates (e.g. 100, 50, 20, 10, 5 & 2mm/min) to determine the effect of rate of loading on the stress-strain response of both PTFE-glass fibre fabric and PVC-polyester fabric (Figure 3-6 & Figure 3-7).

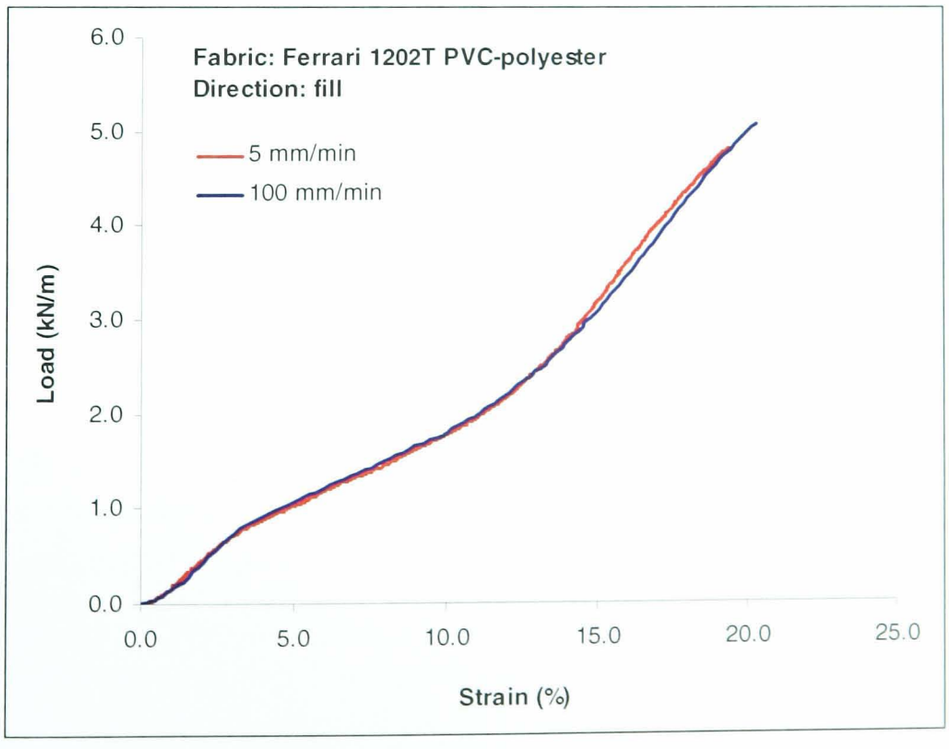

Figure 3-6. Rate of loading, PVC-polyester

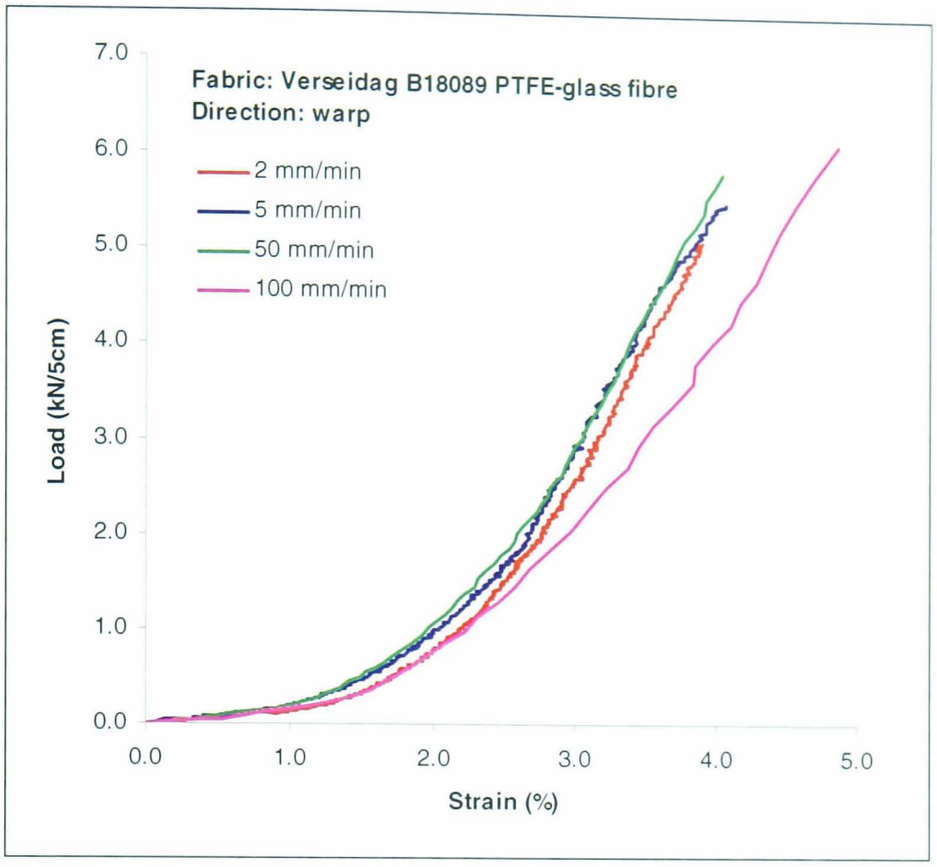

Figure 3-7. Rate of loading, PTFE-glass fibre

The tests show that for PVC-polyester fabric the rate of straining (within the range tested) has virtually no effect on the stress-strain response, or on the failure stress. For PTFE-glass fibre fabric strain rates up to 50mm/min give similar results. However, for a strain rate of 100mm/min the results are significantly different (but still very similar for loads up to typical design stress of 25% UTS). At 100mm/min the PTFE-glass fabric exhibits increased levels of strain at higher loads compared to lower rates of loading. This part of the fabric response is dominated by yarn tensile extension, and the increased strain may be due to brittle failure of glass fibres. Because of this tests on PTFE-glass fibre have been limited to 50mm/min, whereas tests on PVC-polyester have been carried out at a range of strain rates up to 100mm/min (Figure 3-6 & Figure 3-7).

Cyclic load tests were carried out on a limited number of fabrics to investigate hysteresis effects (Figure 3-8). The aim was to determine how the initial behaviour of the strip (measured by a single load application to failure, described above) compares with the behaviour after cyclic loading, so called 'mechanically conditioned' behaviour (§3.3.3.3). Six load cycles were applied between a low 'prestress' load (approximately 0.1 kN/m) and 25% UTS. A further six cycles were applied between 0.1 kN/m and 50% UTS. The control system on the tensile test machine failed to enable exact upper and lower loads to be used. However, the resulting cyclic loading is sufficient to show trends in the fabric behaviour. The loading and unloading curves are distinct, but after each hysteretic load the cycle the residual fabric strain is small. After six load cycles the subsequent stress-strain curve is almost identical to the results without load cycling. This low level of residual strain may be due to the high rate of load application

(100mm/min). This is appropriate for wind loading of fabric structures which occurs rapidly, but less appropriate for longer term snow loading which is more likely to lead to high levels of residual strain.

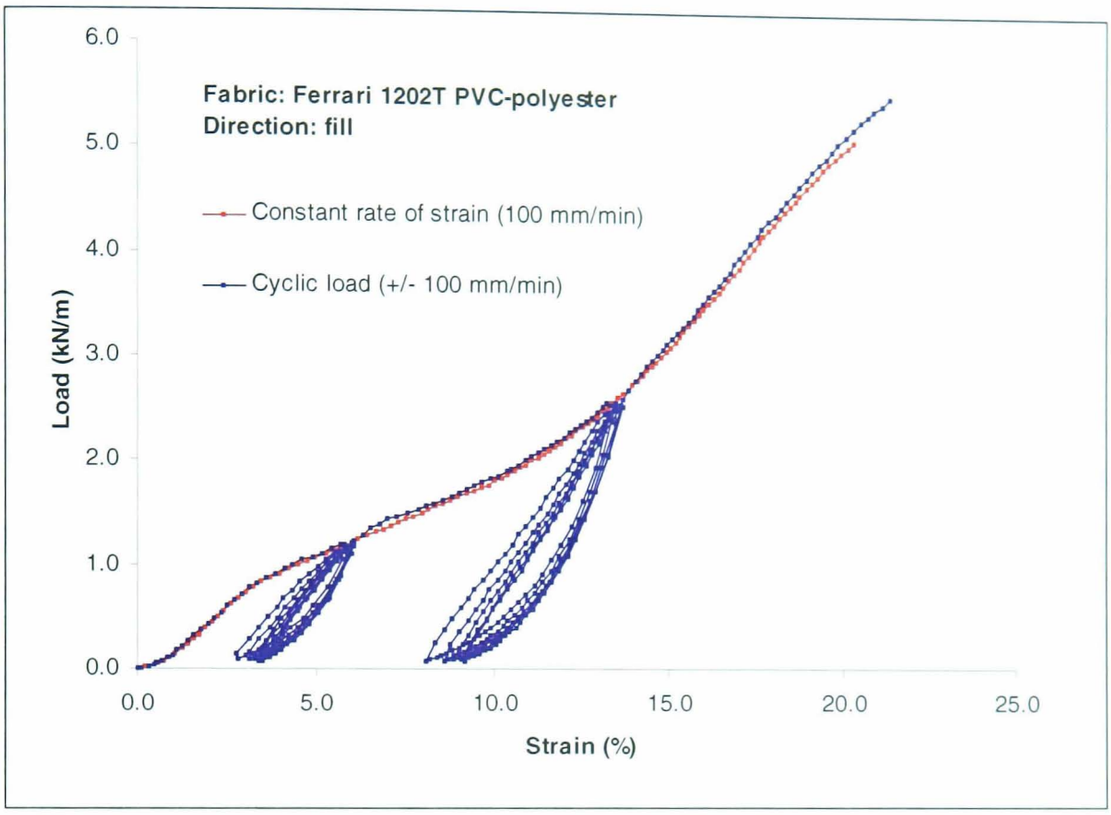

Figure 3-8. Cyclic uniaxial strip test

3.1.2 Yarn testing

Yarns can be removed from both PTFE-glass fibre and PVC-polyester fabrics by pulling the yarn from the edge of the fabric. First the fabric is cut in line with the yarn direction, and then a small cut is made behind the first yarn from the edge. The resulting 'tab' is gripped with pliers and the yarn is pulled from the edge of the fabric. This is achieved much more easily for heavier fabrics in which the stronger yarns are less likely to break during extraction. This is particularly true of PTFE-glass fibre fabrics; yarns can be easily removed from Taconic Solus 1410, but tend to break during removal for lighter fabrics. The extracted yarns can be used to determine tensile and transverse crushing properties (§2.2.2). The level of residual crimp in the yarn (or *crimp set*) can be determined by comparing the length of the removed yarn with zero axial load and with a small axial load (sufficient to straighten the yarn but not stretch it).

As the yarns frequently break during extraction, it is clear that the load necessary to pull the yarn from the fabric is very close to its failure load. It is inevitable that some of the removed yarns will have been damaged, and this will alter subsequent test results. Measurement of crimp set may not be a true reflection of the level of crimp in the fabric, as the yarn will have been straightened and/or inelasticity strained during extraction.

Alternative methods for removing the yarn from a coated fabric include burning the PTFE coating from a glass-fibre fabric or dissolving the PVC coating from a polyester fabric using a suitable solvent. These techniques have not been tried for this project, the concern being that the base fabric would be altered during the stripping process. When two pieces of fabric are welded together and then peeled apart the weak point is often the bond of the coating to the base cloth, and so the coating is peeled away (Figure 3-9). However, the yarns are still held in place by the coating on the other side, and extraction frequently causes the yarns to fail.

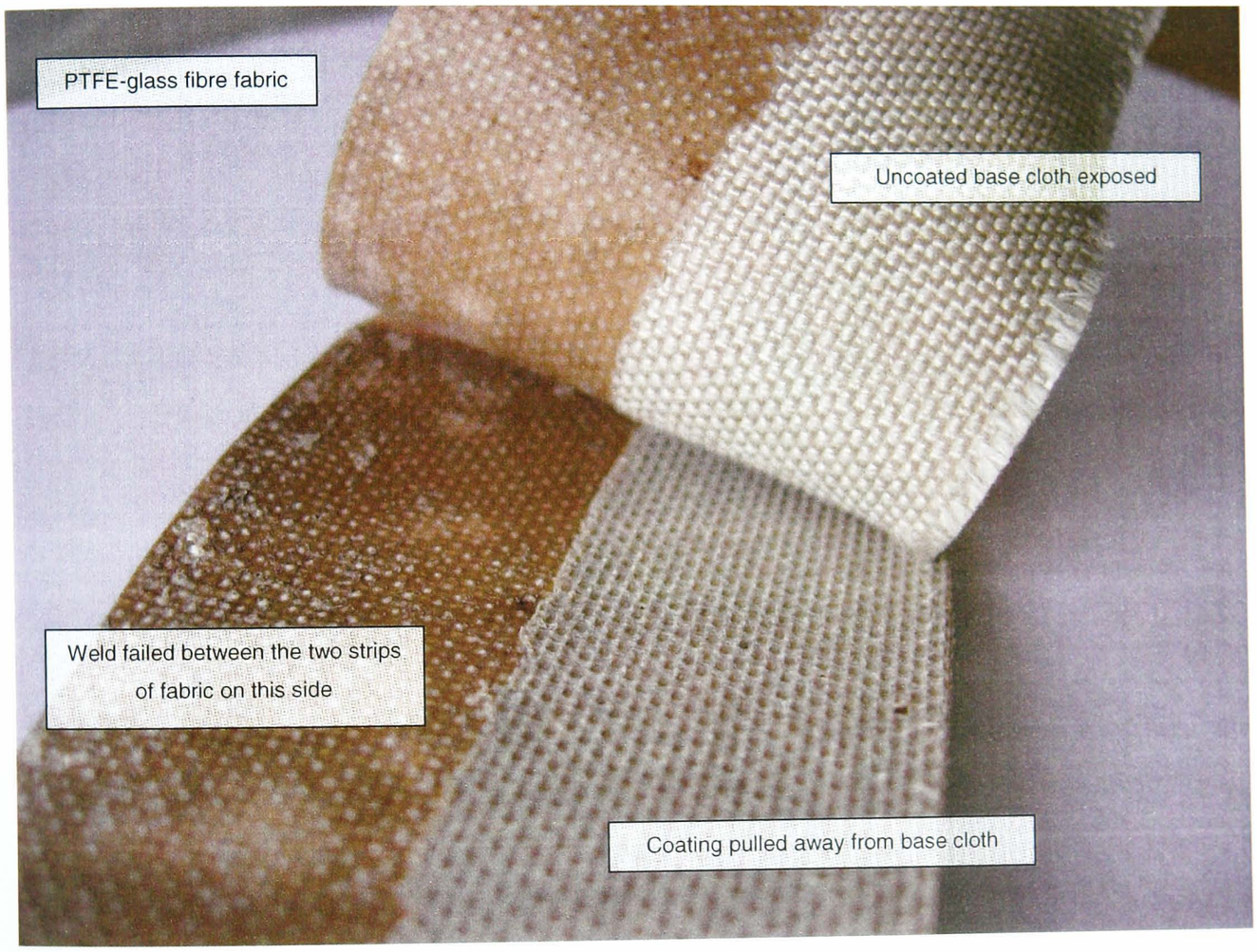

Figure 3-9. Peeling weld to remove coating

These difficulties are avoided if the yarns are removed from the uncoated base fabric. Non-coated polyester and glass-fibre fabrics have little dimensional stability and yarns can easily be slid out of the fabric. If the fabric testing is project specific, non-coated samples may be difficult to obtain. As material properties may vary between rolls or batches, a sample would need to be cut from a particular roll before coating. Samples of the finished fabric are easily acquired as they are always available for compensation testing. The coating process may change the yarn properties; sintering of PTFE onto glass fibre fabric and coating penetration between yarn fibres in a polyester fabric (§1.1.4). For this research, the yarn properties are needed to inform a predictive model which aims to not require specialist testing (§5.2). Testing a single yarn requires specialist jaws, and strain measurement presents difficulties.

Determination of the visco-elastic yarn and coating properties would be beneficial to enable a viscoelastic fabric model to be developed. Thorough investigation of the time dependent response of the yarn, including the effect of loading rate from wind gust to long term prestress would require extensive testing. The effect of ambient temperature is also significant. The coating has a significant effect on the visco-elastic behaviour of coated woven fabrics (§2.1), hence it may be more useful to carry out this type of test on the finished fabric rather than individual yarns.

Yarn properties are required for use in the predictive fabric model (§5.4.2), but a key aim of the model development is that all input parameters can be measured from standard tests that do not require overly specialist equipment. Hence yarn testing was deemed to be unsuitable, and yarn properties were inferred from uniaxial strip tests (§3.1.1). No yarn tests were carried out for this project.

3.2 FABRIC IMAGING

The predictive fabric model developed in Chapter 5 requires measurements of the fabric cross-section geometry (crimp amplitude and wavelength, yarn cross-section dimensions), without the use of specialist equipment. This is to ensure that the model can be used widely in industry without prohibitively expensive investment in equipment.

Scanning electron microscopes [Ansell, Hill & Allgood (1983), Happold et al (1987)] or specialist C.C.D. (Charged Cathode Device) digital imaging equipment [Blum & Bidmon (1987)] have been used historically to obtain images of the fabric cross-section. Both techniques provide high quality images suitable for fabric geometry measurement. In particular the scanning electron microscope provides extremely detailed images which are useful for studying the yarn structure, coating composition and fabric damage. Fortunately, recent advances in digital camera technology mean that high quality, low cost C.C.D. imaging is now available, with sufficient resolution to be used for measurement of the fabric geometry.

In this research a *Nikon Coolpix 4500* digital camera was used, with an additional macro lens (cost in 2002: camera £400, macro lens £50). Over the next few years it is expected that these costs will drop and image quality will increase. The key features of the camera are:

- 4.0 effective megapixel C.C.D. with a true (non-interpolated) image resolution of 2,272 x 1,704 pixels,
- Macro mode enabling images to be taken of objects 20mm from the lens, reduced to 10mm with the addition of a 1.5x macro lens.

Subject lighting is always difficult for macro photography; the camera lens is so close to the subject that it tends to block incident light and cast a shadow. For this research diffuse natural light was used, but a

macro lighting unit is available consisting of a ring of light emitting diodes mounted around the lens to evenly illuminate the subject. Use of the 4x optical zoom also enabled the camera to be further from the subject than would otherwise have been possible. Use of digital zoom is not recommended as it results in a reduction in image quality.

The fabric is held between two supports. The upper support has a steel rule with 0.5mm graduations mounted flush with the edge of the fabric. The lower support is recessed so that it is out of focus and does not distract from the subject of the image (Figure 3-10). The fabric is lit using natural light. Typical images of PVC-polyester and PTFE-glass fibre fabric are shown in Figure 3-11 and Figure 3-12.

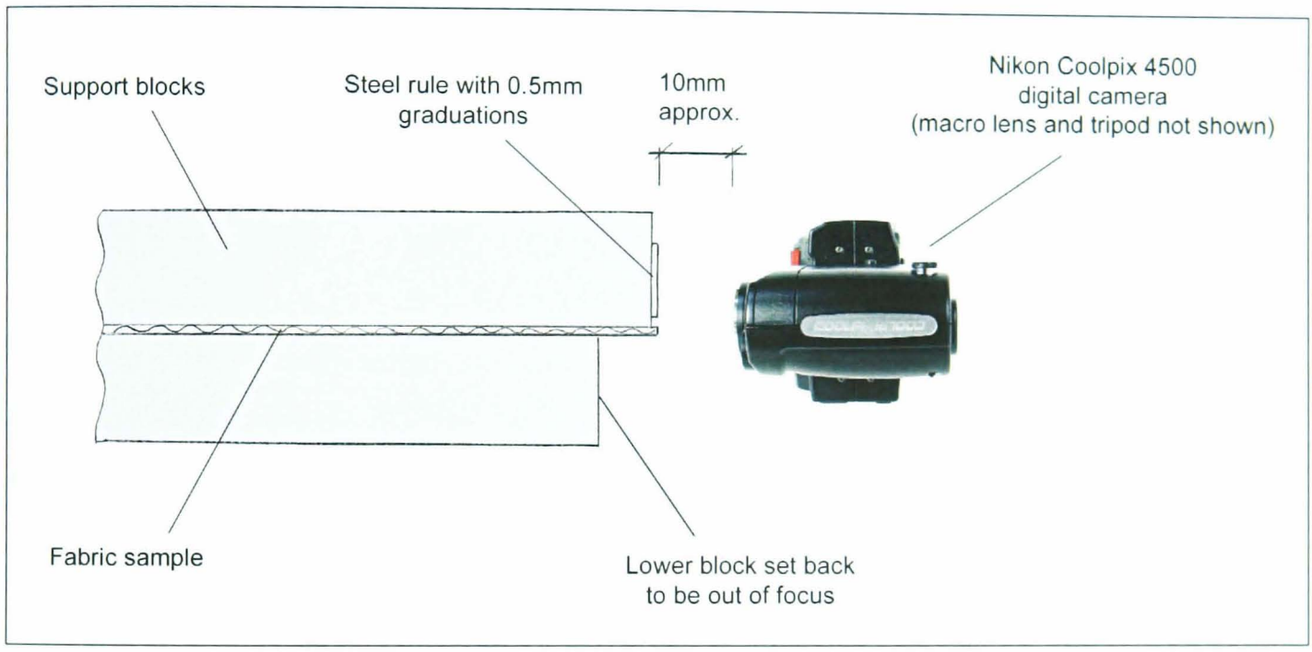

Figure 3-10. Fabric imaging set-up

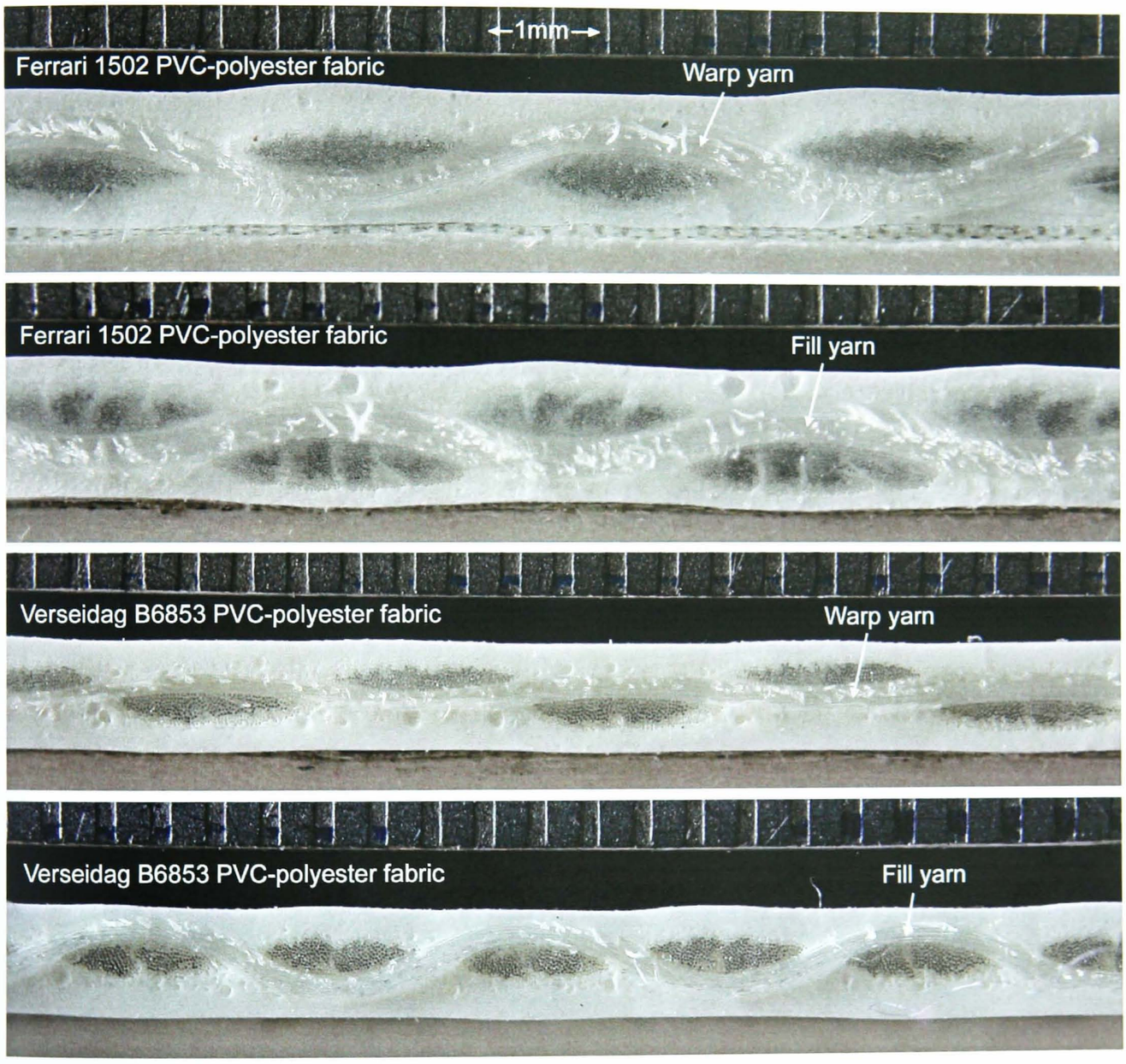

Figure 3-11. PVC-polyester fabric cross sections

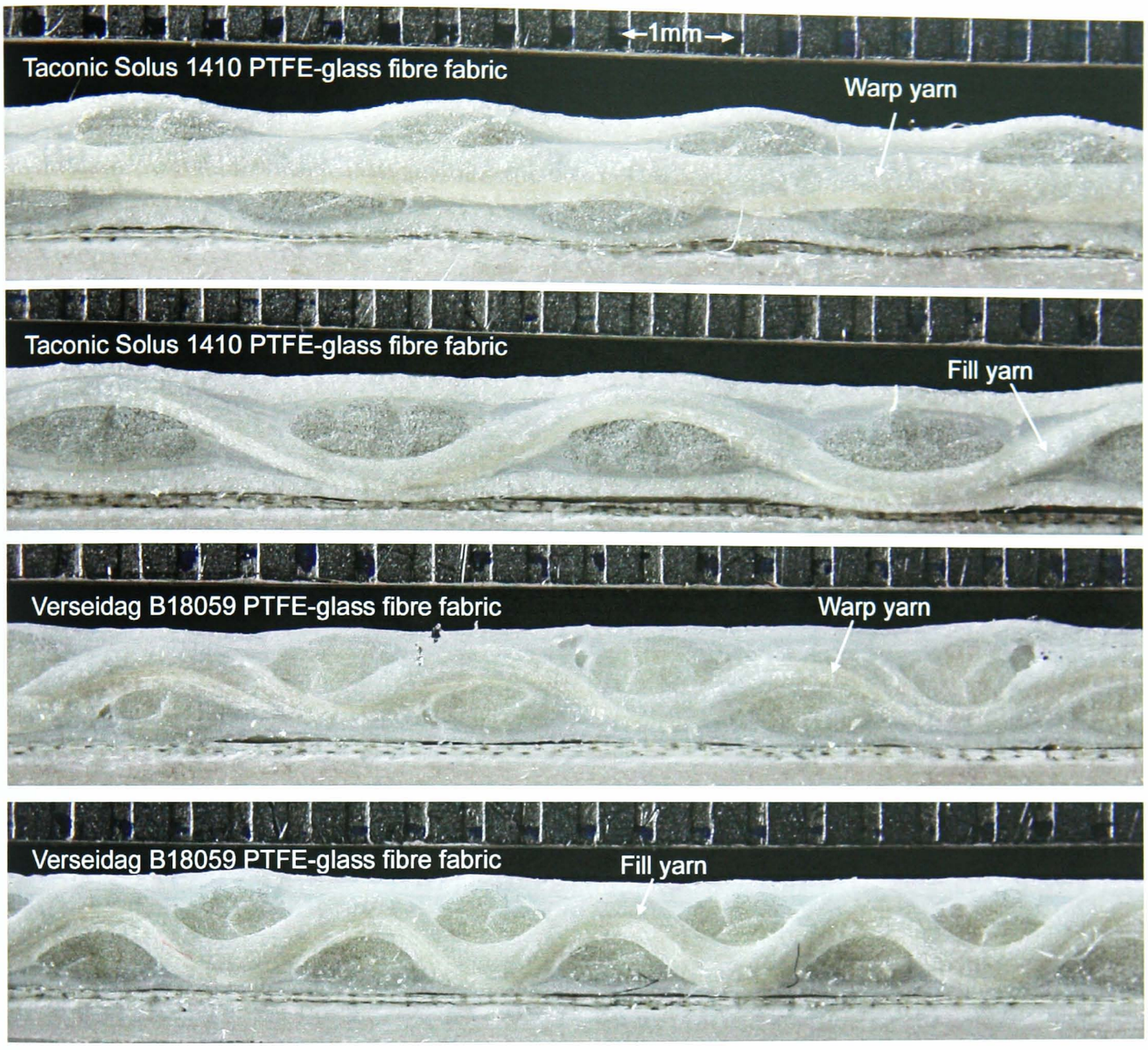

Figure 3-12. PTFE-glass fibre fabric cross sections

Camera settings used are as follows:

- Image quality: Maximum. High quality non-compressed image (TIFF format), approximately 10MB per image,
- Lens Converter set to 'Wide', appropriate for Macro Lens add-on,
- Exposure mode: Aperture Priority. Aperture set as small as possible – i.e. f9.8 or f10.7, giving long exposure (not a problem as tripod mounted) and maximum depth of field. This is important as close-up photography can result in a very small depth of field (e.g. 1mm); maximizing the depth of field is vital to ensure all of the fabric cross section is in focus.
- White balance: Auto, appropriate for natural lighting,
- Zoom: optical zoom slightly less than maximum (maximum optical zoom interferes with macro focusing),

- Spot metering: the camera focuses on a single user-selected point i.e. on the fabric at the centre of the frame,
- No flash,
- Macro mode,
- Timed shutter release used to avoid camera shake.

3.3 BIAXIAL TESTING

There are currently no British or European standards for biaxial fabric testing; however the European collaborative group *TensiNet* (www) has recently published a design guide which collates current good practice and recommendations on all aspects of fabric structure design (Mollaert & Forster, 2004). Development of the biaxial test protocol presented in this thesis (§3.3.3) is based on this guide, previous published work, numerical modeling, methods used in industry and the few available relevant international standards.

The plane biaxial test best represents the loading of a fabric structure and is commonly used in industry [Ansell, Barnes & Williams (1984); used by Architen-Landrell (www), Laboratorium Blum (www) & Ferrari (www)], and hence has been adopted for this research (§2.2.3).

It is vital to distinguish between the initial behaviour (appropriate for compensation values and installation planning) and the medium to long-term behaviour of an in-situ fabric which has been subjected to repeated loading. It is this in-situ behaviour which should be used for structural design, and which this research aims to quantify.

3.3.1 Analysis of cruciform test piece

The aim of a biaxial test is to develop an area of fabric with a known, uniform stress field over which the strain can be measured. The shape of the fabric sample, method of load application and location in which the strain is measured are all critical in achieving this. Geometrically non-linear finite element models have been used to investigate the stress field in a cruciform test piece under biaxial loading. The effect of slits in the cruciform arms and variations in load ratio and material properties have been considered. The aim of the numerical analysis is to determine:

1. The effect of slit configurations and clamp types to inform the design of cruciform test piece,
2. A suitable gauge length for measuring fabric extension,
3. How the stress level within this gauge length relates to the applied load.

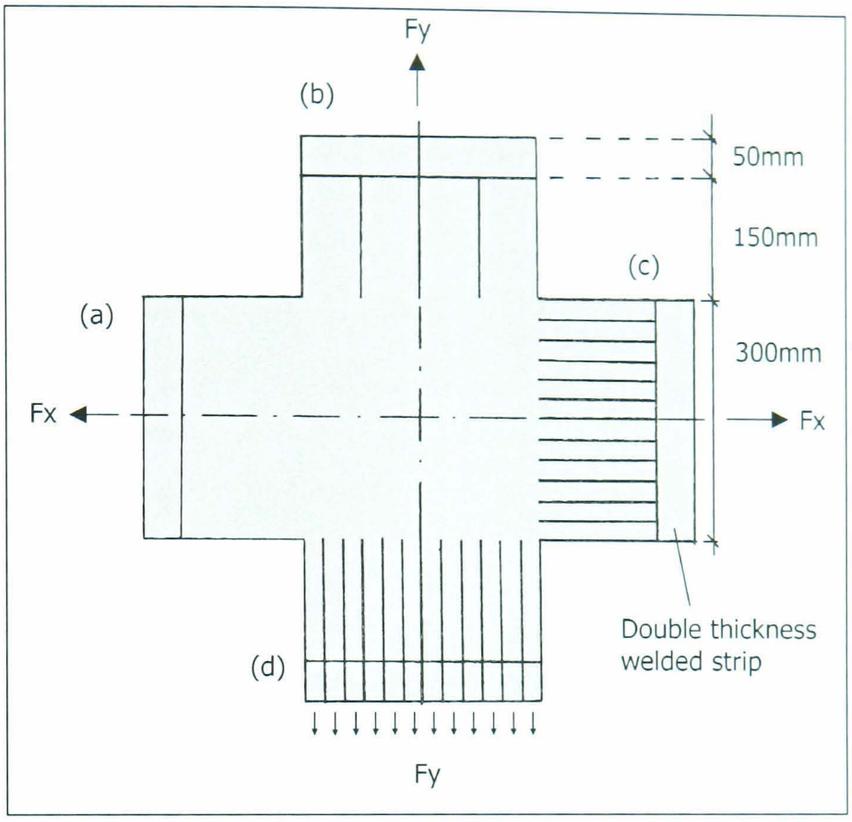

Figure 3-13. Cruciform options.

Four cruciform configurations have been analysed (Figure 3-13):

(a) No slits in the cruciform arms,

(b) Three 150mm long slits,

(c) Eleven 150mm long slits,

(d) Eleven full length slits with each strip loaded independently and free to move transverse to the direction of the applied load.

Cruciform dimensions are those used by Architen-Landrell (Chepstow, UK, www). The central square of the cruciform is 300mm on each side. Cruciforms used in industry vary from around 100mm (Ferrari, www) to 1000mm (Laboratorium Blum, www). The 300mm central square is large enough to ensure that a sufficient number of yarns have been included to avoid significant inaccuracies due to a single broken yarn or inconsistencies in the number of yarns included in the area of interest. Even for the heaviest fabrics tested (e.g. Taconic Solus 1410 or Ferrari Fluotop 1502) a 300mm square will contain approximately 400 yarns – sufficient to give a good distribution of yarn properties and ensure any single yarn is negligible. A larger cruciform would lead to practical problems with the increased test rig dimensions and high loads required, particularly as the rig is expected to be used in future for biaxial failure testing.

To model the fabric cruciform typical material properties for a balanced weave Type III PVC-polyester fabric have been used: $E_{warp} = E_{fill} = 600kN/m$, $G = 30kN/m$ and $\nu = 0.3$; where E = Young's modulus, G

= shear modulus and ν = Poisson's ratio. This fabric model is crude: coated woven fabrics have highly variable material properties depending on the applied stresses. To make the analysis widely applicable the sensitivity of the model to changes in material properties has been investigated. The double thickness welded strips (used to form a loop for clamping) have been modeled with values of elastic and shear moduli doubled. Direct stresses have been recorded along the centre-lines of the 300mm central square of the cruciform.

Initial results from the cruciform model using a membrane finite element formulation in *Oasys'* (www) *GSA* software produced unexpected asymmetric results (Figure 3-14).

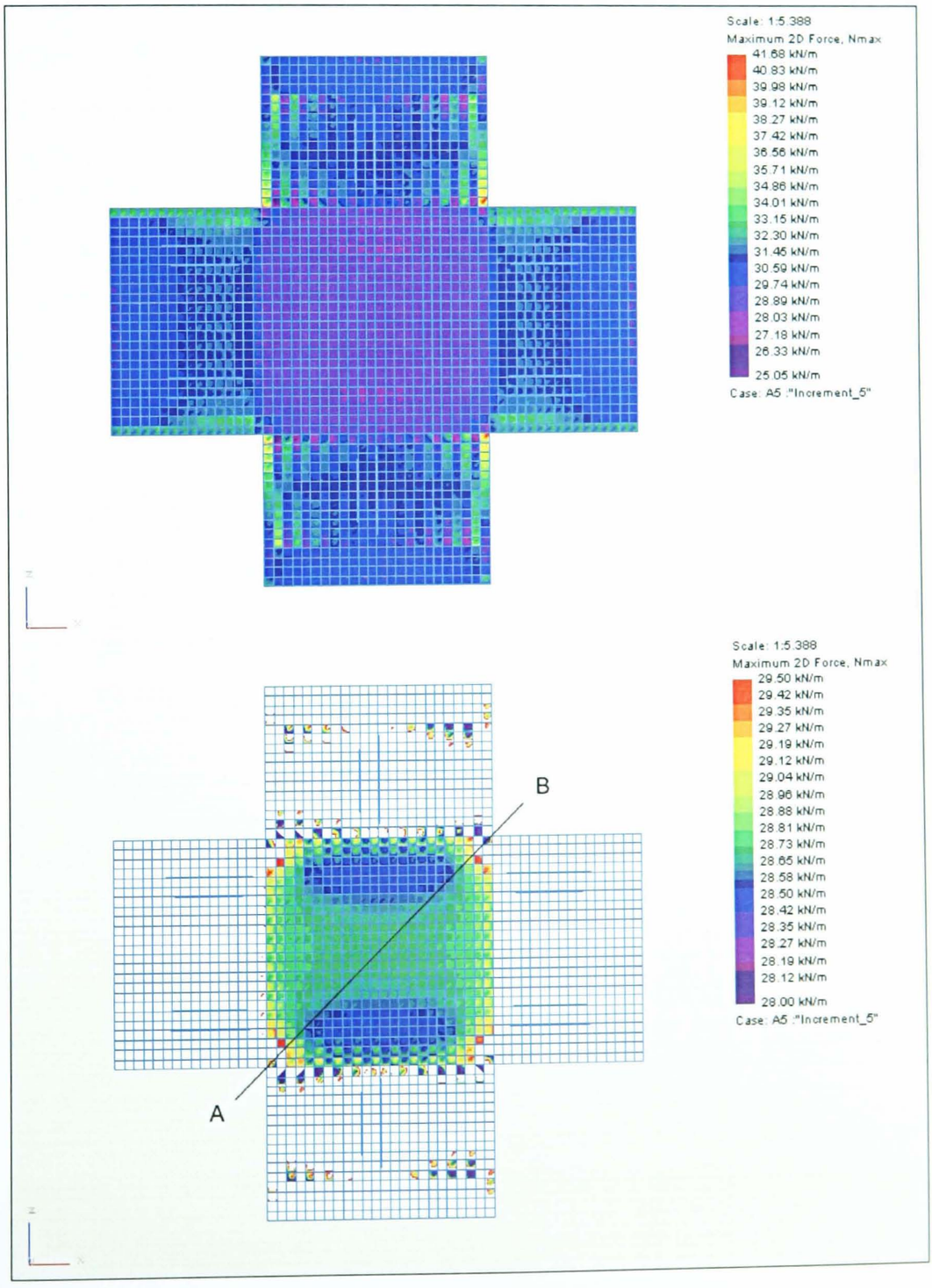

Figure 3-14. Asymmetric results of cruciform model

For example, the stress distribution is non-symmetric about the line A-B, despite a symmetrical stress state being applied to a perfectly symmetrical model. The cause of this asymmetry has been identified as the inability of the finite element formulation to accurately model the effect of combined large direct and shear strains. The resolution of this problem is outside the scope of the research presented in this thesis. This finite element formulation is not unique to *Oasys' GSA*, but is widely used throughout the industry. A new membrane element formulation without this limitation is being developed as part of a PhD research project at the University of Newcastle (2003-2006). The importance of this research is highlighted by the fact that the research is being funded by a consortium of interested companies (Architen-Landrell, Arup, Tensys and Ferrari).

As an alternative, the cruciform model has been analysed using *LUSAS* (www). An orthotropic plane-stress model has been used with eight-noded quadrilateral thin-shell finite elements. This is not subject to the small strain assumptions referred to above. Unlike a membrane element, the thin-shell element does not have zero bending stiffness. However, in this analysis the bending stiffness is irrelevant as the cruciform is flat and is fully restrained in the out-of-plane (z) direction to avoid instability at unsupported fabric edges. All four cruciform types give a uniform stress distribution in the middle of the central square, with edge effects becoming significant around 50mm from the edge (Figure 3-15, Figure 3-16 & Figure 3-17).

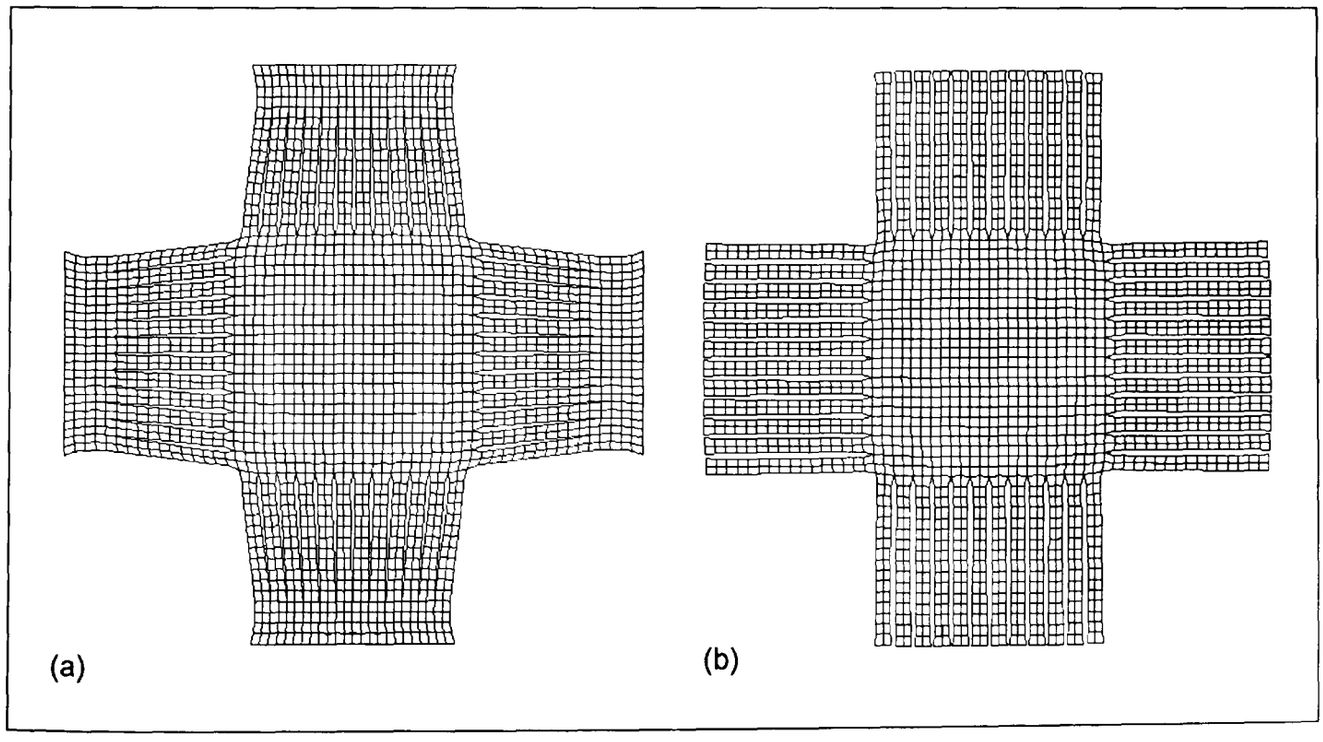

Figure 3-15. Two clamping methods, (a) single clamp & slits; (b) individual clamps

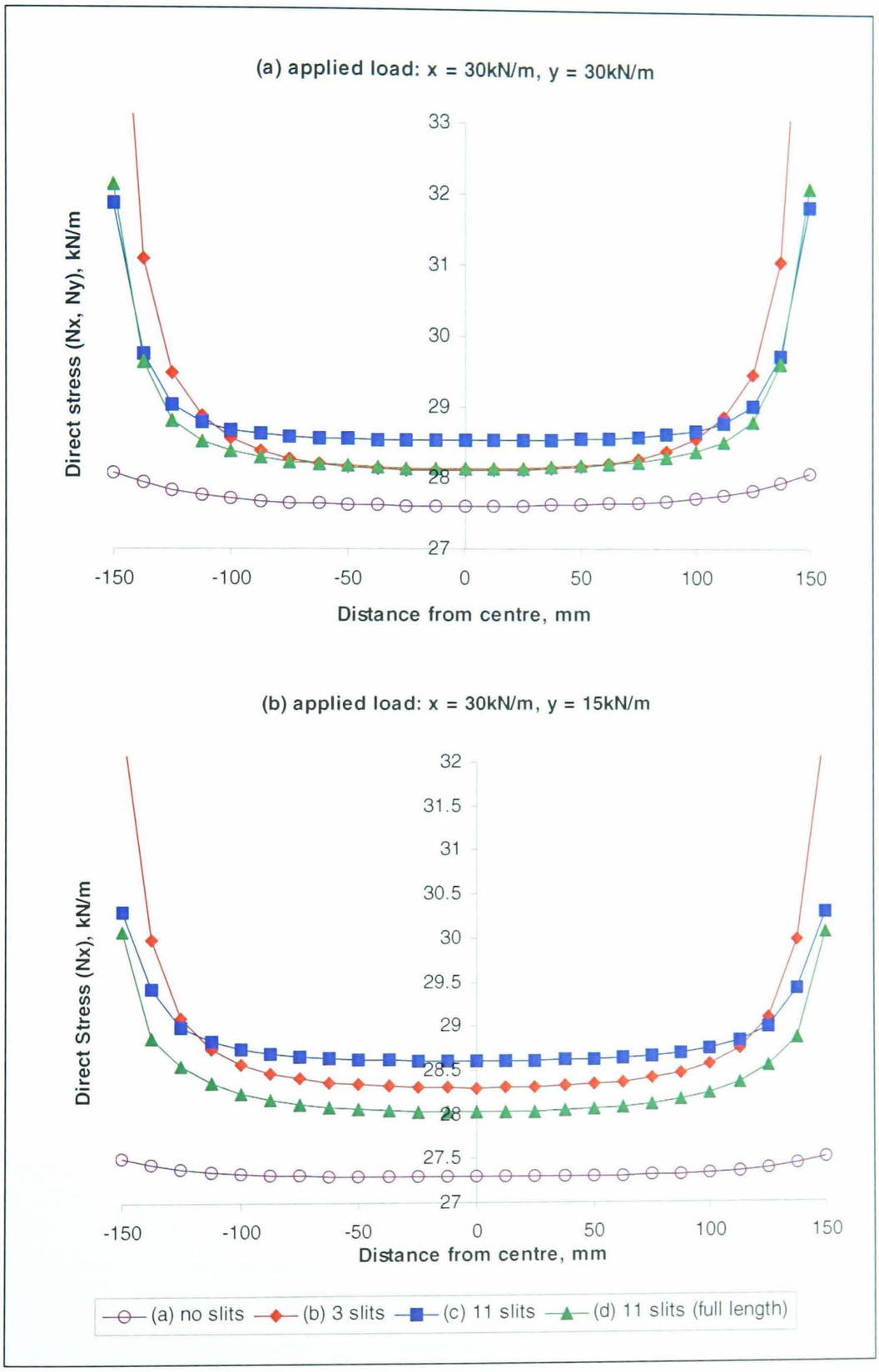

Figure 3-16. Stress variation along cruciform centreline.

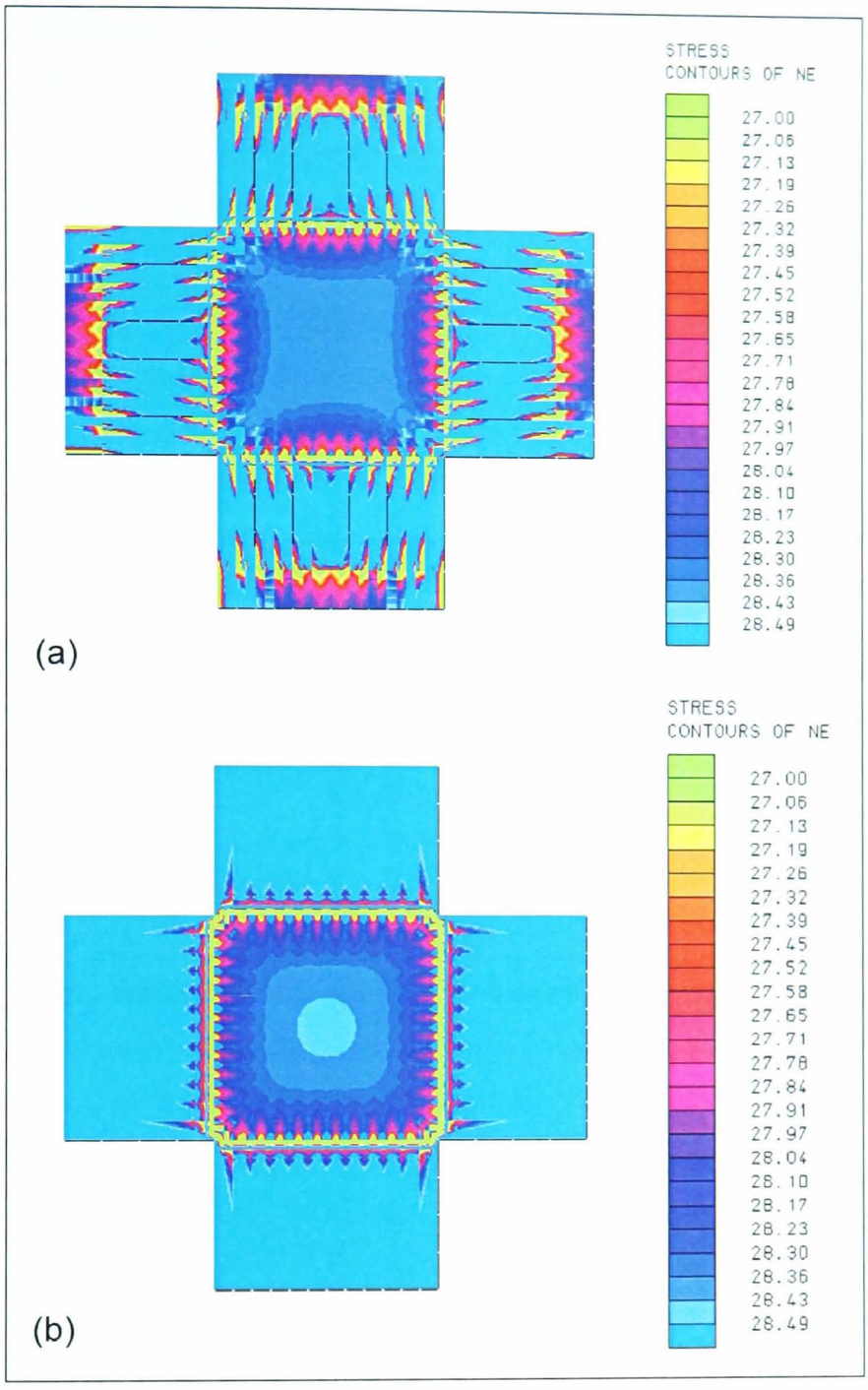

Figure 3-17. Stress distribution in cruciform.

The cruciform with no slits (Figure 3-13a & Figure 3-16) gives the least variation across the 300mm central square. The increased stress between 100mm and 150mm in the other three specimens is largely due to stress concentrations at the ends of the slits. However, the cruciform with no slits gives the lowest level of stress in the central square. With a ratio of applied loads of 2:1 (Figure 3-16b) the direct stress (N_x) at the centre of cruciform (a) is 27.1kN/m, only 90.3% of the applied load. With 11 slits (type c) the stress is 28.6kN/m, 95.3% of the applied load. The slits in the cruciform arms allow the arms to spread providing less transverse restraint to the transfer of load to the central square. Similar results are discussed in the commentary to MSAJ/M-02-1995 (p.10); without slits the analysis gives a stress at the centre of the specimen of 72.1% of the applied load. This is a much greater reduction than the 90.3% reported above.

This may be due to differences in cruciform dimensions or the type of material being tested. With slits the stress at the centre of the cruciform is 92.1% of the applied (MSAJ/M-02-1995, p.10).

The slits may be more important than is suggested by these analyses. During a real test a combination of decrimping and creep can give strains in the fill direction in the order of 25%. A large shear deformation of the cruciform arms would be required and shear lock-up could occur; restraint from the cruciform arms with no slits could be very significant. Because of this it is advantageous to use as many slits as is practicable. Use of independent clamps (Figure 3-13, type d; Figure 3-17b) solves the problem of shear in the cruciform arms, but results in a slightly higher variation in stress across the central square of the cruciform than the 11-slit, single clamp option. Independent clamps are much more difficult to realise than a single clamp plate; the individual clamp units need to be mounted on a track with bearings to allow them to move perpendicular to the direction of load, even when under high levels of load. The 11-slit, single clamp configuration (Figure 3-13, type c) provides the best combination of load transfer and even stress distribution, combined with simplicity of manufacture and operation.

For all of the cruciform models the stress level in the central square is significantly less than the applied stress. Part of the applied load goes into spreading the transverse cruciform arms: in the central portion of the specimen the load is acting on a width greater than the 300mm to which it was applied. It is common to report biaxial stress-strain data as applied load (per unit length) against measured displacement. These results show that a stress reduction factor should be used to reduce the applied load per unit length to the stress level in the central square predicted by the model. This reduction factor could alternatively be seen as an *effective width* over which the load is acting.

The sensitivity of the analysis to variations in material properties has been investigated. Modification of the elastic moduli (between 600kN/m and 1200 kN/m) resulted in changes in the stress level in the cruciform for the same applied load (Figure 3-18a). The difference between the highest and lowest values in Figure 3-18a is 0.73kN/m or 2.4% of the applied load. This suggests that for fabrics with large variations between warp and weft properties further investigation of the stress field in the sample may be justified. For example, during initial fabric loading the weft modulus can be negative (due to crimp interchange) – this could lead to a very different stress state to that implied by the applied load.

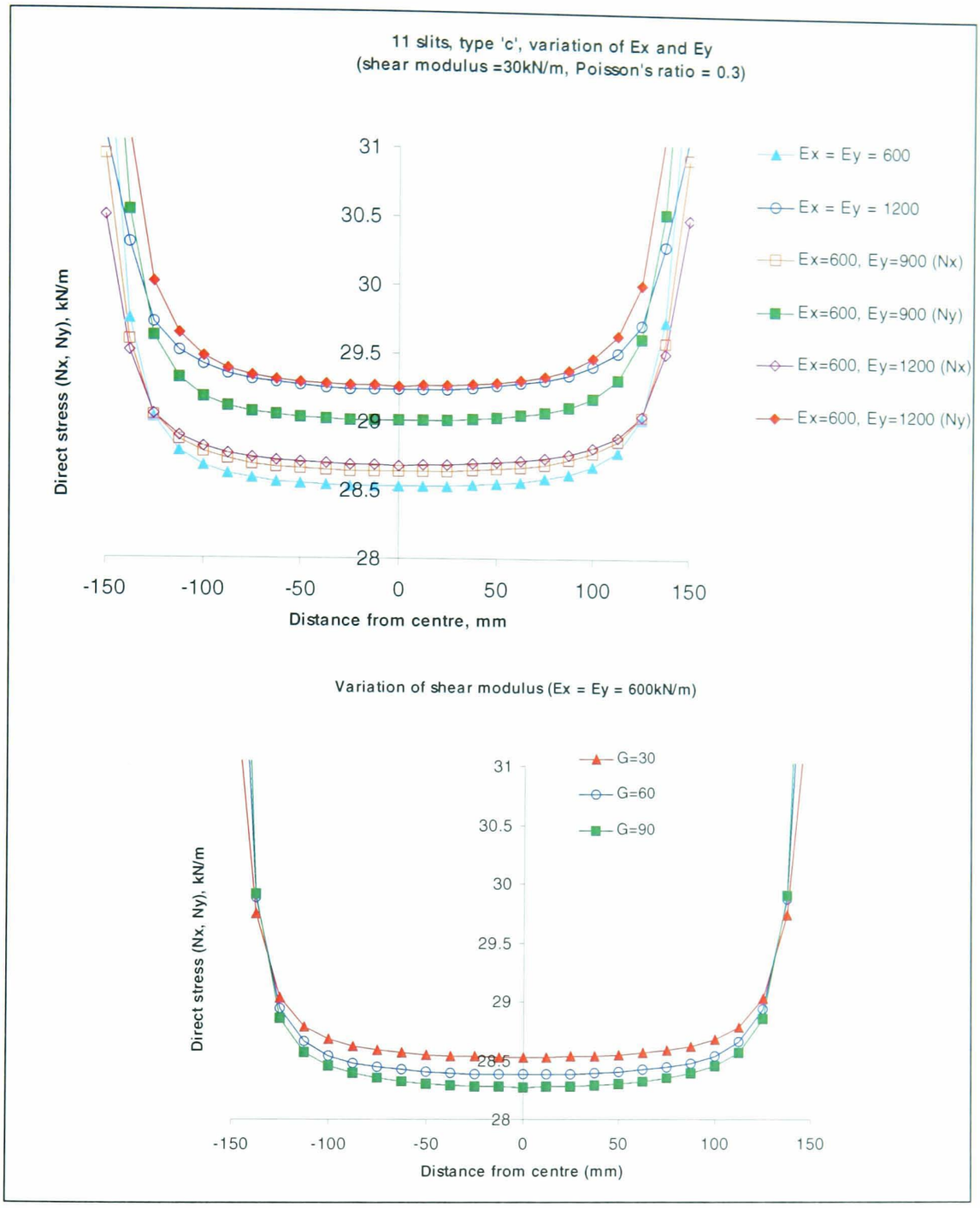

Figure 3-18. Effect of material properties on cruciform stress distribution.

Anisotropic material properties give asymmetric stress fields; for E_x = 600kN/m and E_y = 1200kN/m the difference between N_x and N_y is 0.58kN/m, giving a stress ratio of 0.98:1. This difference is small and is expected to be neglible compared to fabric variability and experimental error (§2.2).

An increase in shear modulus led to a small reduction in the stress level in the area of interest (Figure 3-18b). Fabric shear response is known to be non-linear and prone to 'lock-up' when adjacent yarns come into side-by-side contact [Skelton, 1976] – leading to a sudden increase in shear stiffness. This would reduce the ability of the cruciform to transfer load to the central square.

The ratio of the applied loads has little effect on the stress level. Changing from 1:1 (F_x = F_y = 30kN/m) to 5:1 (F_x = 30kN/m, F_y = 6kN/m) increased the direct stress (N_x) at the centre of the specimen by 0.12kN/m or 0.4% (Figure 3-19). This suggests that any results determined at one particular stress ratio should be widely applicable to any combination of loads. As discussed previously, the effect of shear lock-up or highly non-linear fabric behaviour may change these results, which should only be seen as an indication of the cruciform response.

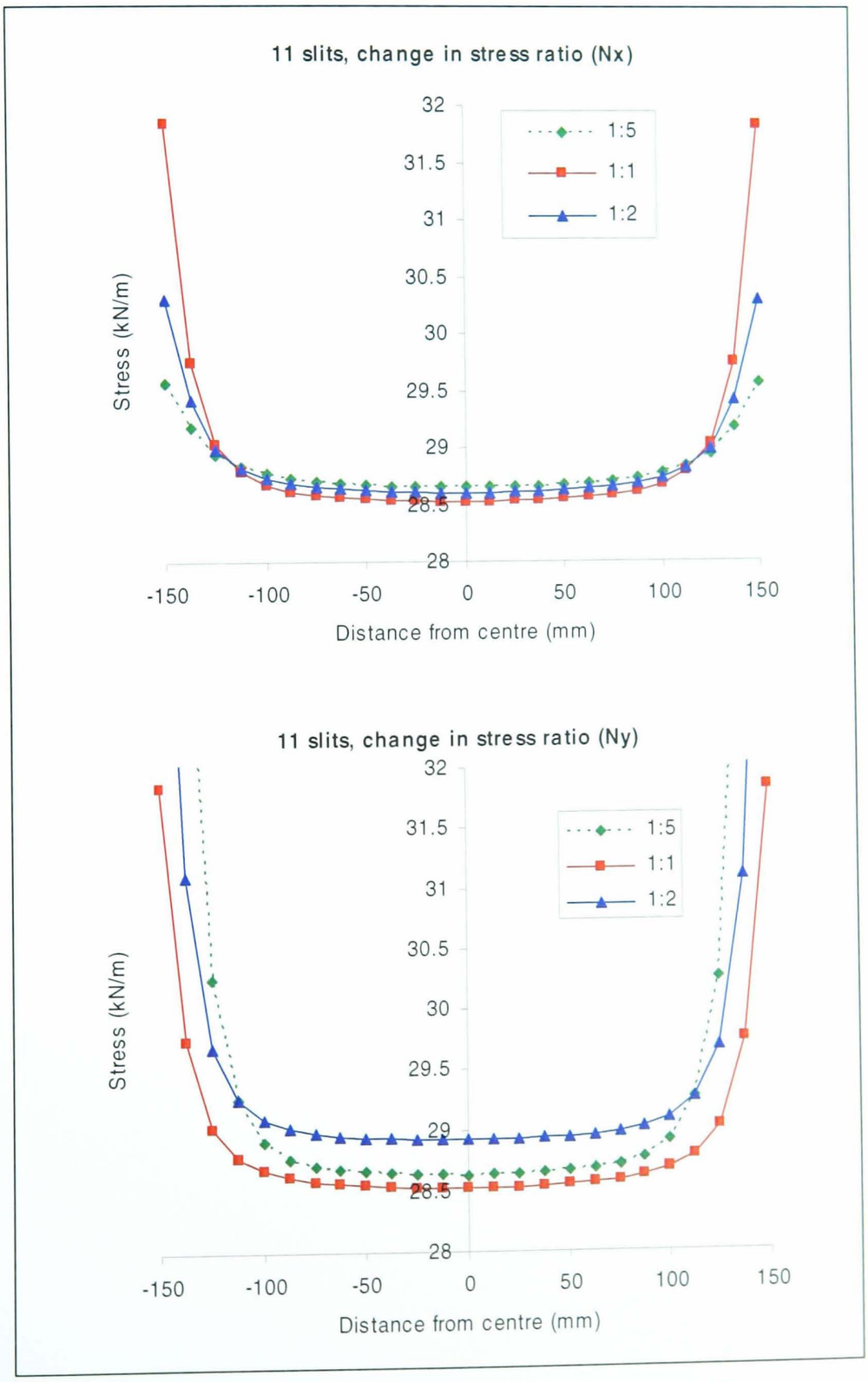

Figure 3-19. Effect of stress ratio on cruciform stress distribution.

A load reduction factor should be used to modify the applied load to the expected stress level in the area of interest. The load ratio has little effect on the resultant stress level. For the balanced PVC-polyester material properties the mean direct stress (N_x) over the 200mm gauge length varies with load ratio as follows: 1:1 → 28.57kN/m, 2:1 → 28.60kN/m, 5:1 → 28.69kN/m. This gives a reduction factor of around 0.95, or an effective width of 315mm.

3.3.2 Test rig design

The test rig built for this research is based on the 'floating' design innovated by Architen-Landrell (Chepstow, UK). Loads are applied in warp and weft directions by two reaction frames (Figure 3-21, Figure 3-22 and Figure 3-20). The upper frame is mounted on four spherical bearings and is free to move in the plane of the fabric.

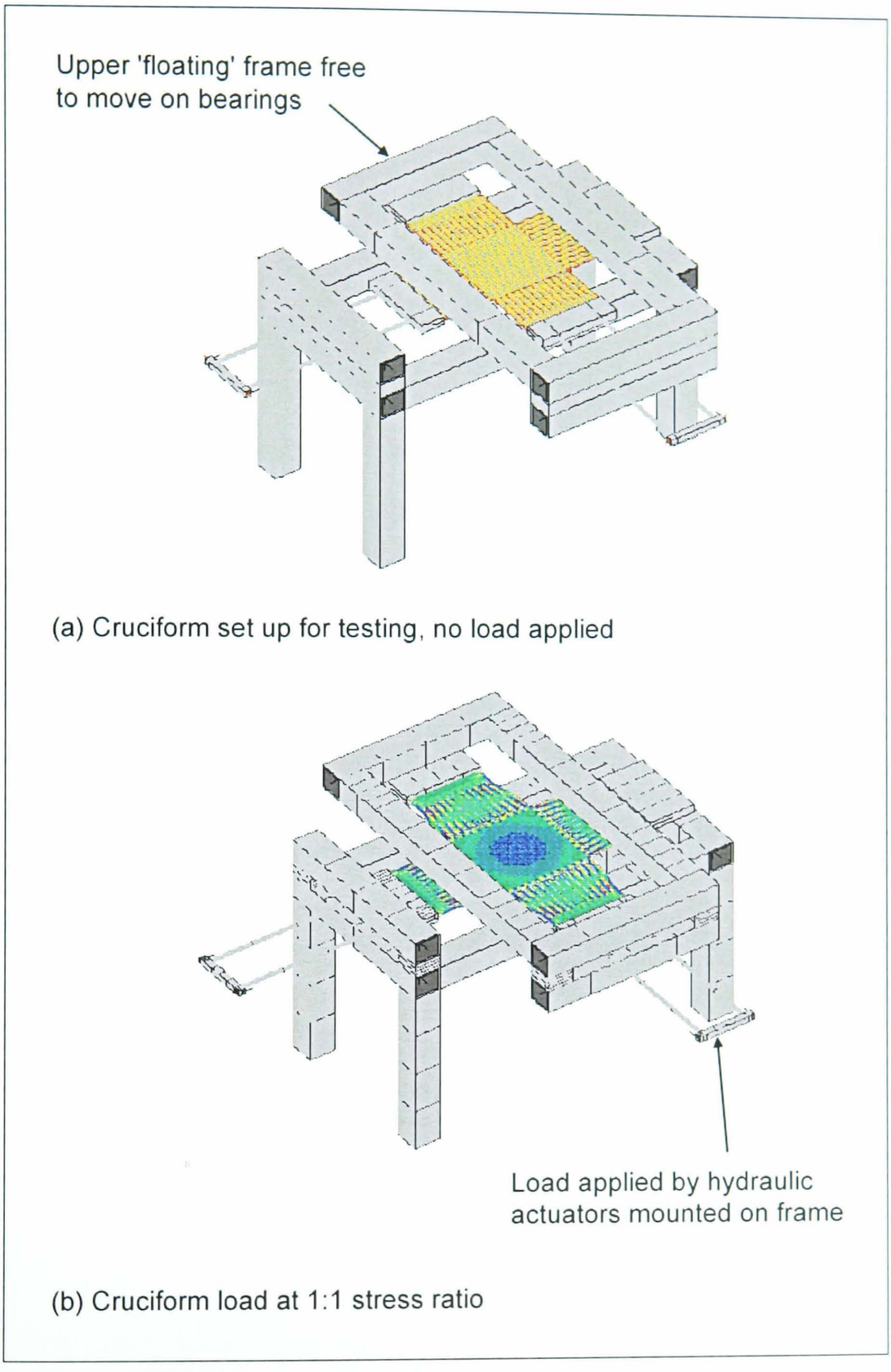

Figure 3-20. GSA model of test rig and fabric cruciform

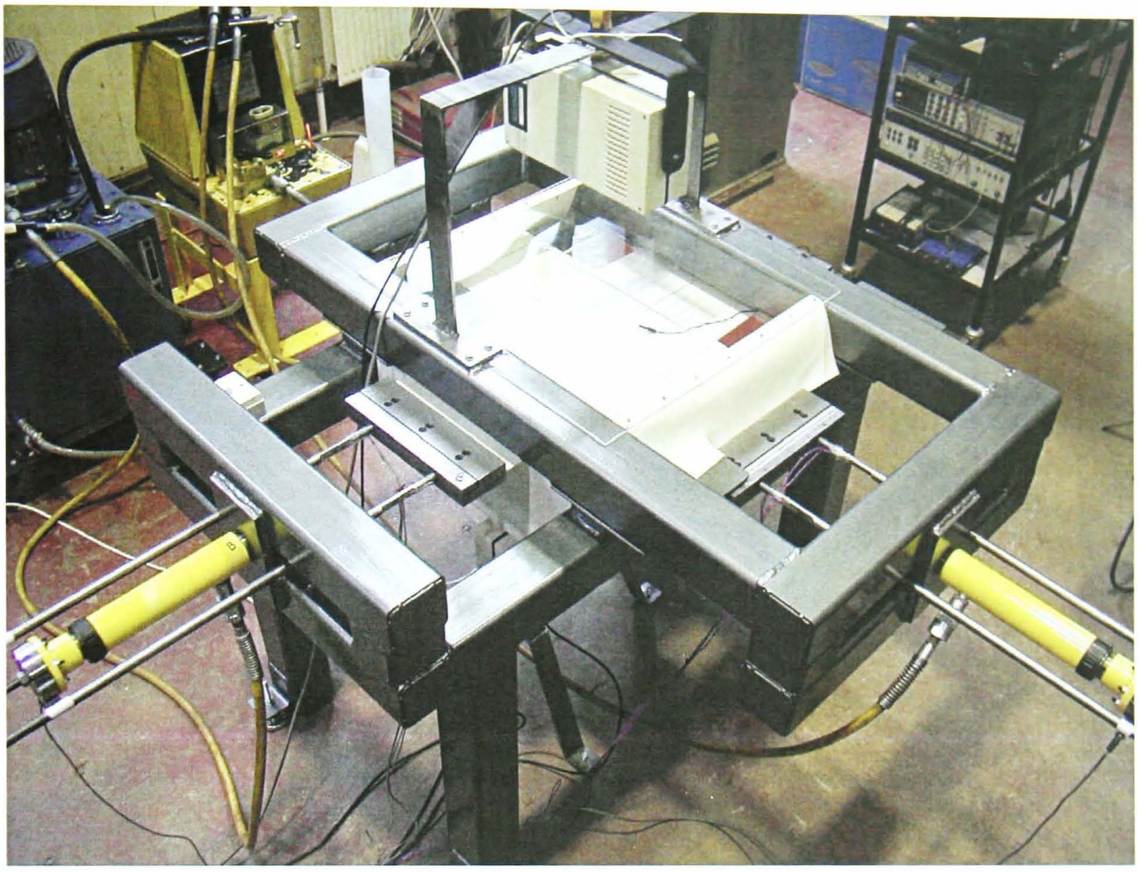

Figure 3-21. Biaxial test rig (1)

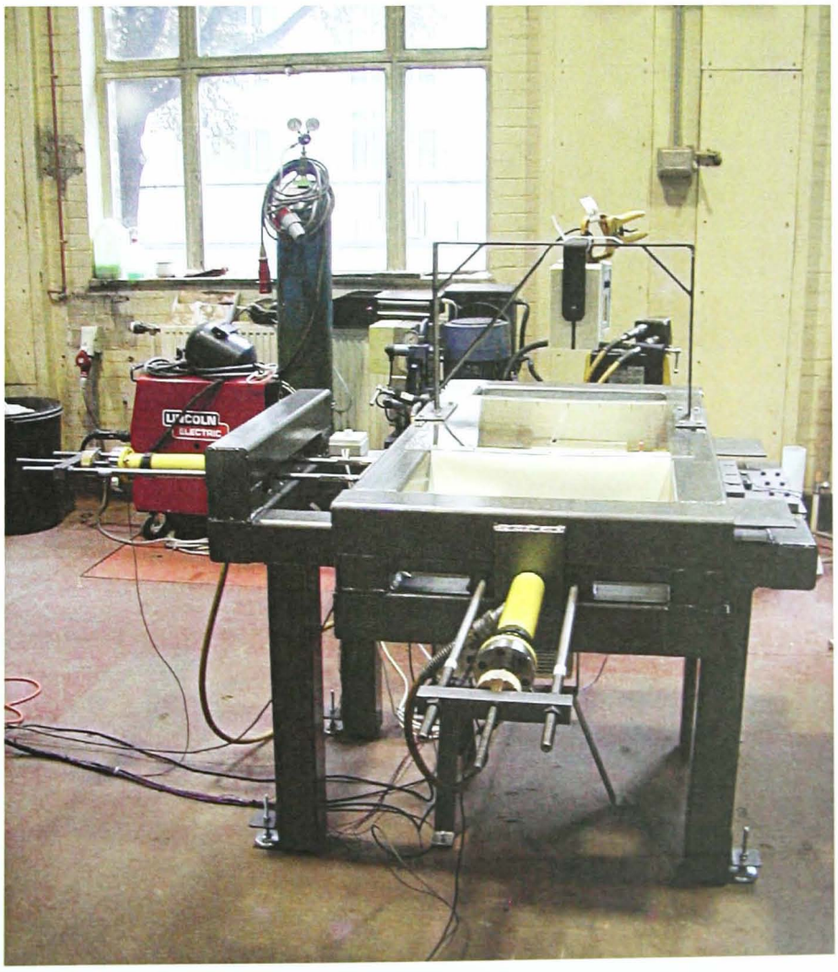

Figure 3-22. Biaxial test rig (2)

The fabric manufacturing process results in bowing of the weft yarns and hence the warp and weft yarns are not necessarily orthogonal: for the fabrics tested the angle between warp and fill varied between 89.4° to 85.6°. Angles were measured at the centre of each cruciform before testing. For PVC-polyester fabrics the angle varied from 89.4° to 88.3° with a mean value of 89.1°. The bowing is often more severe in PTFE-glass fibre fabrics, with measured values of 89.3° to 85.6° (mean value of 88.1°). Because of this, the cruciform samples have been cut in line with the warp and weft yarns, not necessarily orthogonally. This is appropriate as fabrics will always resist loads along the line of the yarns because the yarns are stiffer than the coating, and the fabric shear stiffness is relatively low (until lock-up occurs, §2.1.4.3).

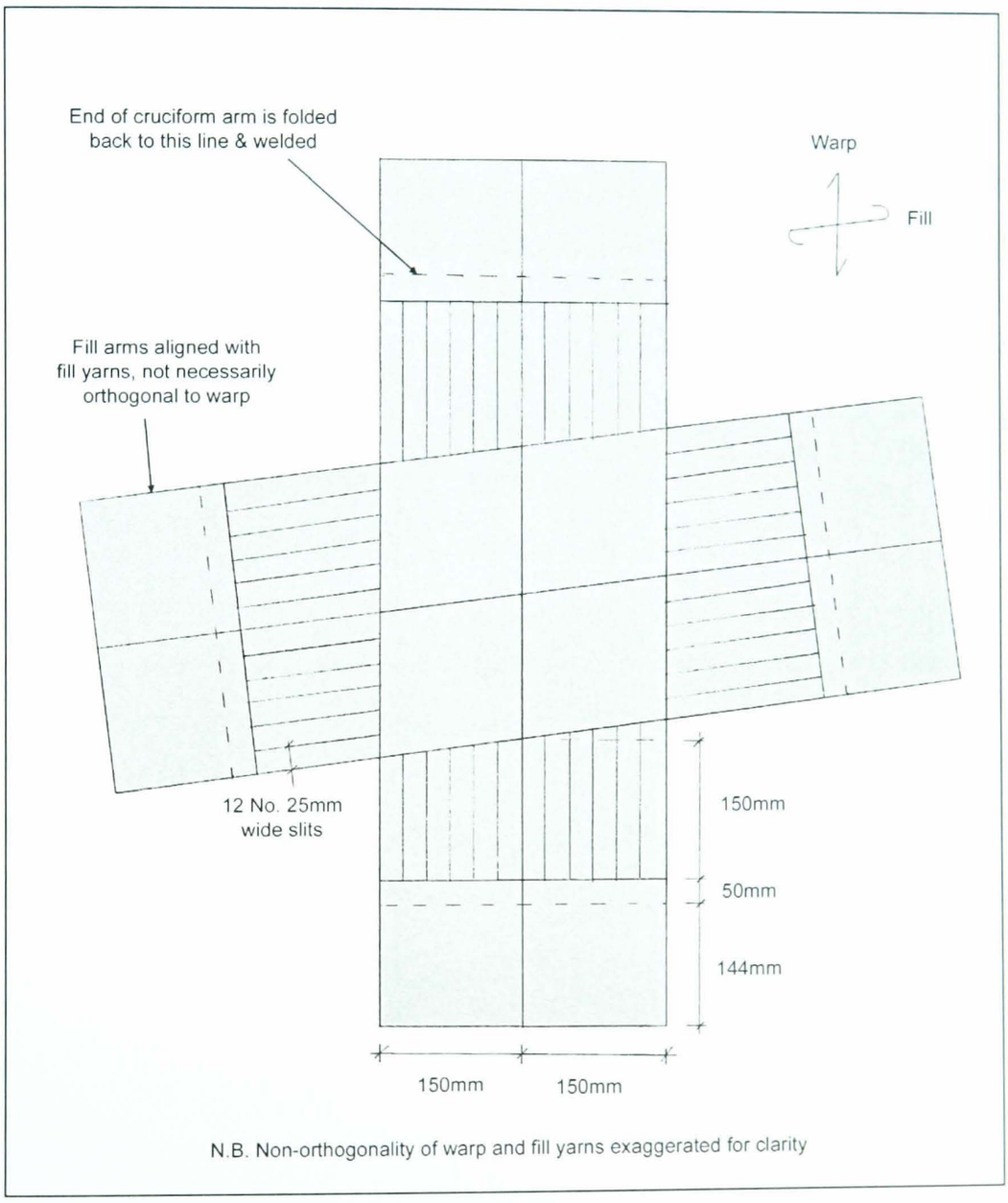

Figure 3-23. Cruciform cut in line with yarn directions

When load is applied to the cruciform the 'floating' upper frame becomes aligned with the cruciform / fabric axes. This allows more accurate measurement of fabric biaxial behaviour without introducing unwanted shear effects. Warp and weft strains have been measured using two laser extensometers, one

positioned above the cruciform and the other below. The top laser extensometer has been mounted on the frame such that it follows the fabric centre-line position and orientation (Figure 3-24 & Figure 3-27).

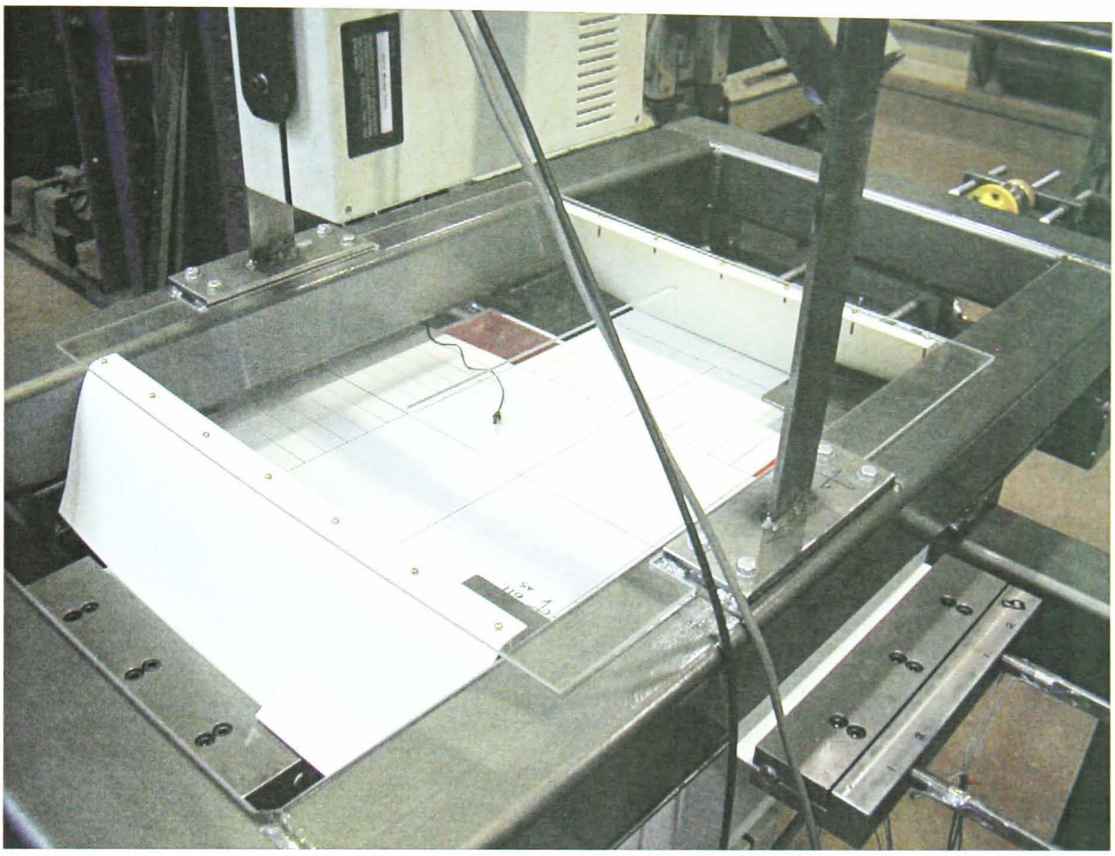

Figure 3-24. Biaxial test rig, cruciform during test

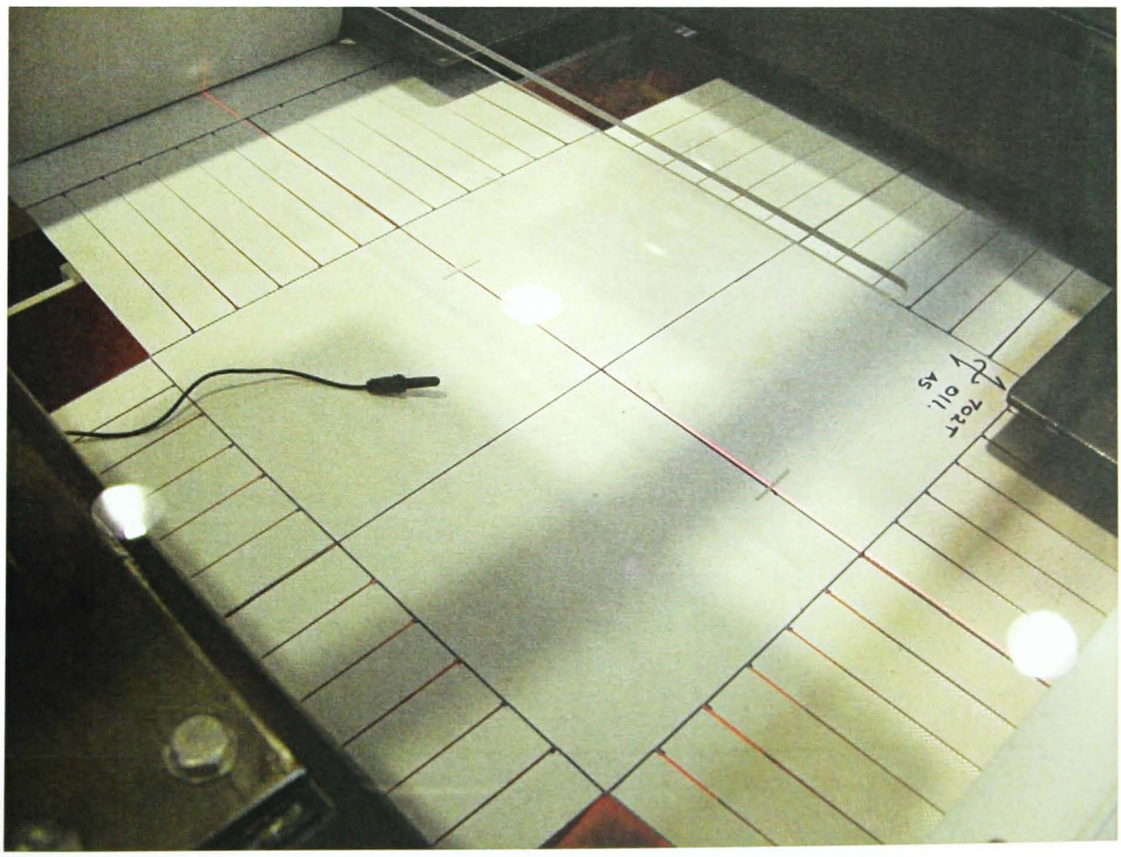

Figure 3-25. Biaxial test rig, close-up of cruciform during test

Load is applied using hydraulic actuators and is measured with load cells mounted on the actuator ends. The reaction frame allows equal and opposite loads to be applied to the specimen in a given direction whilst only having to control one hydraulic cylinder per axis.

3.3.2.1 Design details

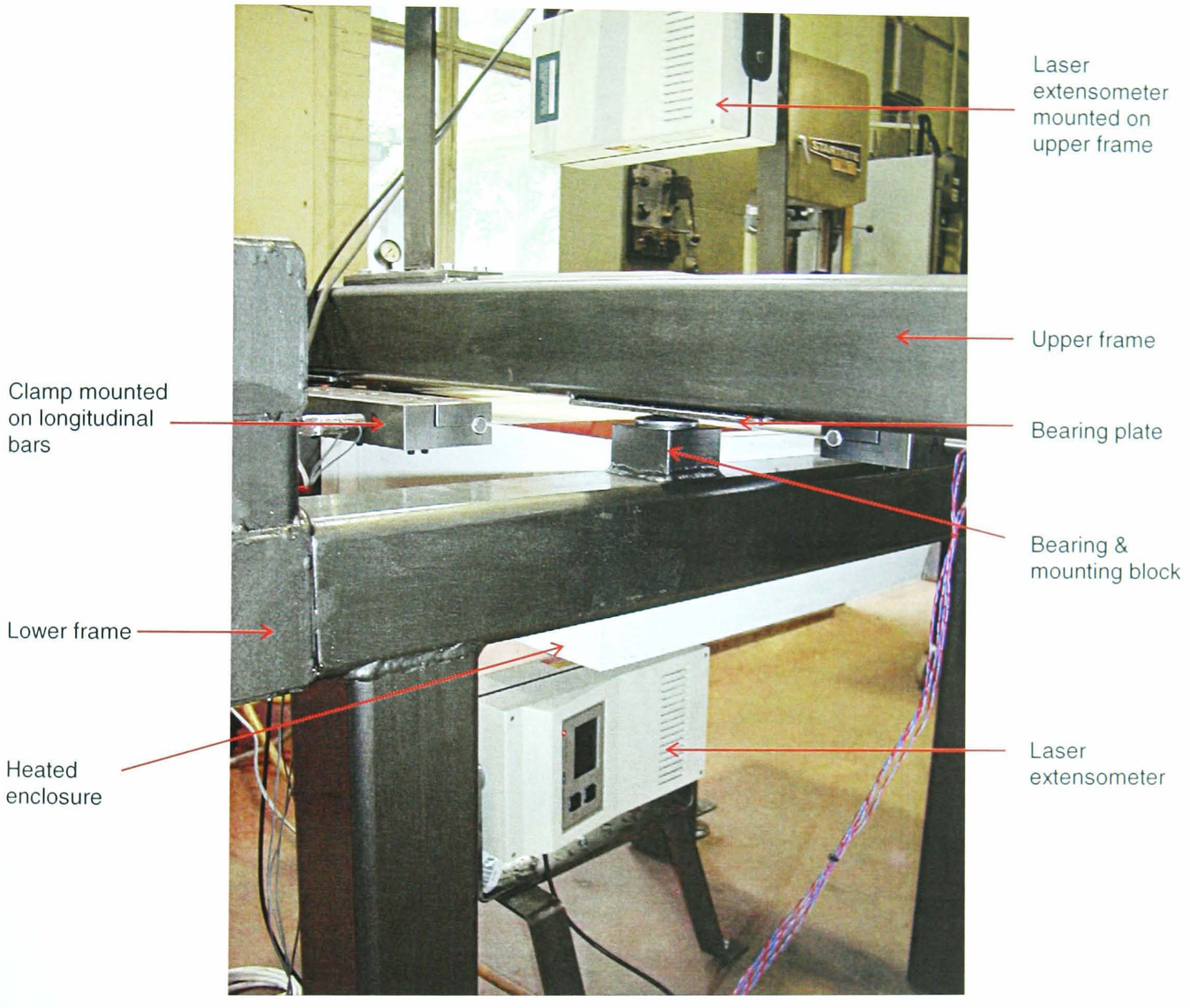

Figure 3-26. Biaxial test rig, side view showing clamp and bearings

Bearing plates have been sized to allow for combined translation (25% strain in fill direction of 700mm sample = 175mm displacement) and rotation (up to 10°).

Adjustable feet have been attached to the four legs to enable the frame to be levelled. This is vital to ensure that there is no load on the fabric due to gravity acting on the considerable weight (approximately 145kg) of the floating upper frame. For example, if the frame was 1° off level then the horizontal force acting on the fabric would be, ignoring friction, equal to: sin 1° x 145kg x 9.81 ms^{-2} = 24.8 N = 0.084 kN/m width. With the lower frame level and the upper frame seated on bearings there is negligible restraint to the movement of the upper frame.

Clamp plates have been designed to hold the fabric up to failure load, whilst minimising damage to prevent premature failure at the clamp. A circular steel bar (10.0mm or 12.5mm diameter depending on fabric thickness) is held within a circular enclosure formed between two steel plates which are bolted together (Figure 3-27). For the biaxial tests carried out for this research the ends of the cruciform arms were bent over and welded and the steel bar was inserted in the resulting sleeve (Figure 3-28a). This method of clamping is extremely robust, but does require specialist welding equipment (cruciforms were welded by Architen-Landrell). However, the same clamp arrangement will satisfactorily hold non-welded samples (Figure 3-28b). The fabric is wrapped around the bar with an additional piece of PVC-polyester fabric on each side. The internal piece increases friction between the fabric and the bar, the outer piece protects the cruciform arm from damage where it is loaded against the clamp. This method has been shown to give no slippage up to failure, and failure occurs away from the clamp plate.

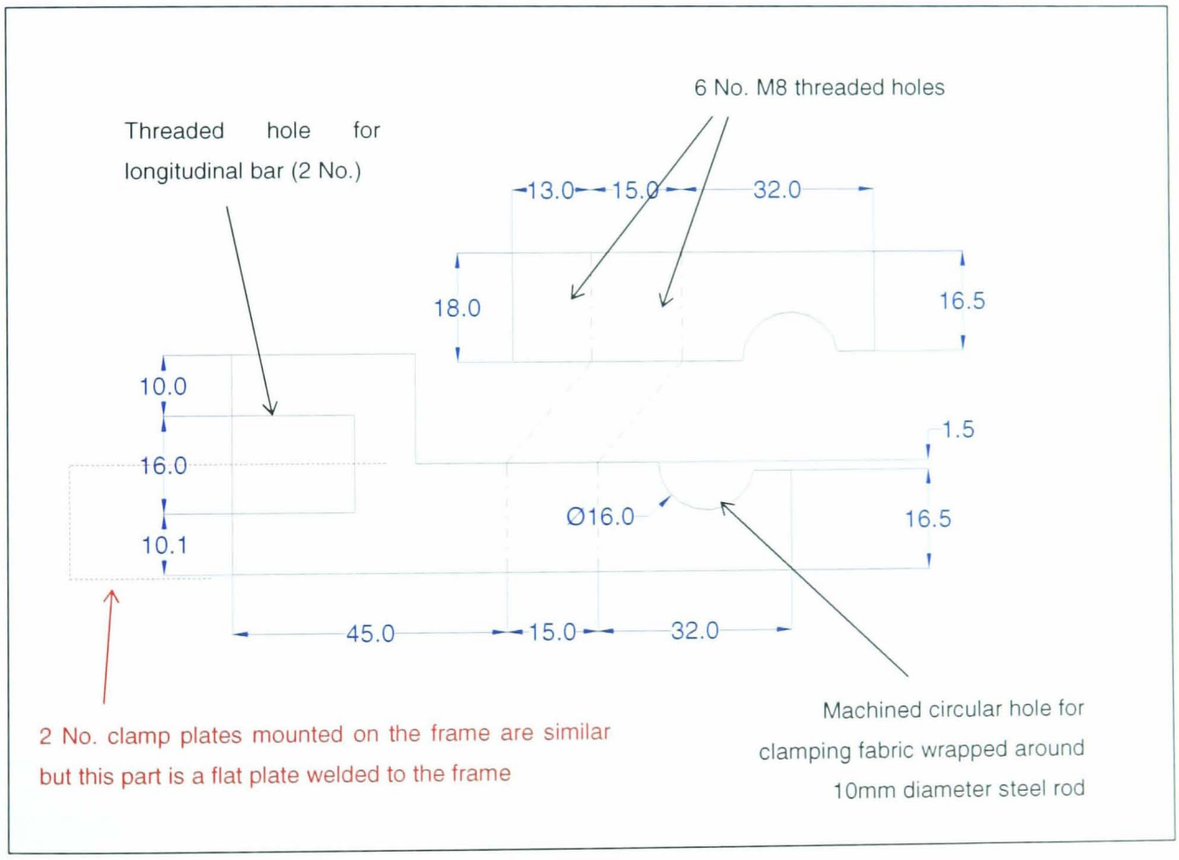

Figure 3-27. Section through clamp plate mounted on longitudinal bars

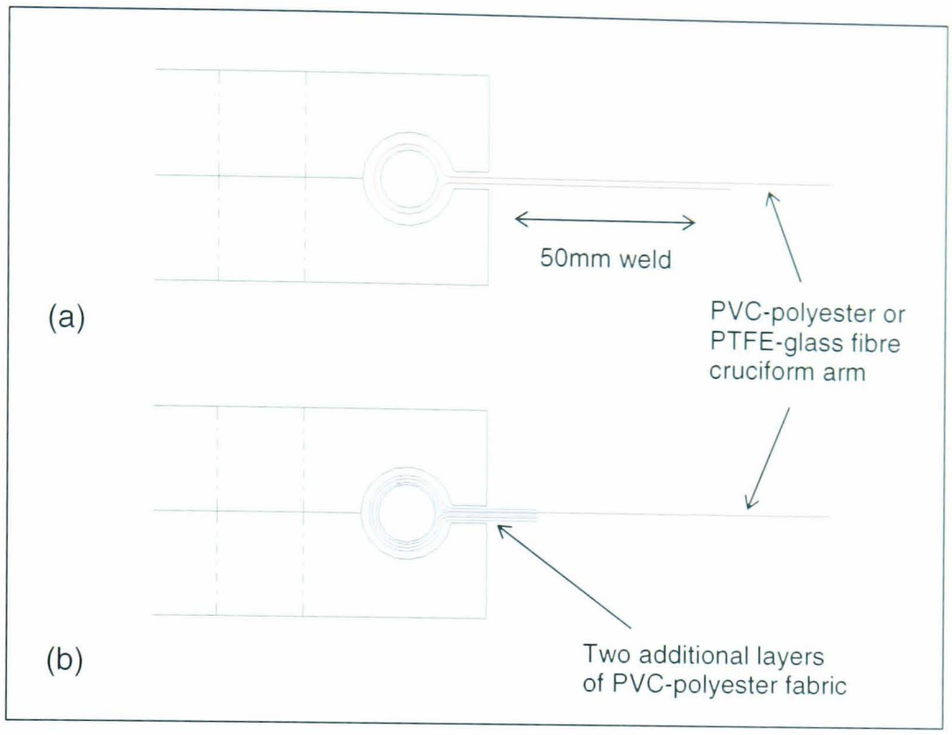

Figure 3-28. Two clamping methods

Use of a scanning **laser extensometer** (Hounsfield 500L, www) enables accurate, automated, non-contact strain measurement between two reflective strips adhered to the fabric surface. The extensometer can be set to measure either tensile or compressive strain, giving an output of zero to one volt which represents zero to 100% strain. Strains ranging from around -10 to +25% need to be measured based on the assumed upper stress level of 25% UTS (§3.3.3.2). A method has been developed to enable the extensometer to be used to measure both positive and negative strain.

The laser is normally calibrated by zeroing the readout whilst it is reading the distance between the reflective strips on the unstrained sample. All subsequent strain readings are relative to this initial gauge length. To enable positive and negative strains to be measured a smaller initial calibration length (L_0, Figure 3-29) is used, so that the strain reading on the unstrained sample is, say, 15% (ε_{init}). By subtracting this 15% from all subsequent readings the laser can measure from -15 to +85% strain (ε_r). However, these strains are a proportion of the initial calibration length, not the gauge length. This means that the recorded strain values (ε_r) need to be modified to give the percentage strain of the gauge length.

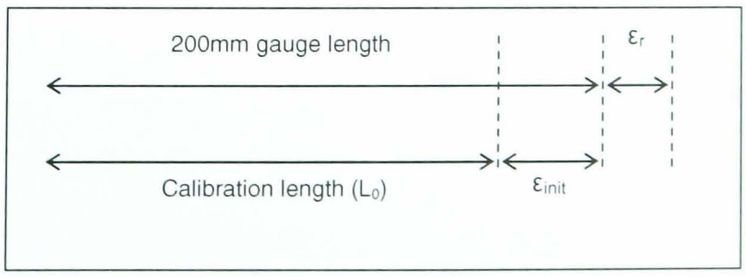

Figure 3-29. Laser calibration nomenclature

$$L_0 = \frac{200}{1 + \varepsilon_{init}}$$ Equation 3-1

$$\varepsilon_{R'} = \frac{\varepsilon_R L_0}{200}$$ Equation 3-2

where ε_r' is the recorded strain (ε_r) expressed as a percentage of the gauge length. Combining Equation 3-1 and Equation 3-2 gives:

$$\varepsilon'_R = \frac{\varepsilon_R}{1 + \varepsilon_{init}}$$ Equation 3-3

For each test the initial strains (ε_{init} in warp and fill directions) were noted, and strain readings were adjusted as per Equation 3-3.

A **heated enclosure** is used to maintain the cruciform at a constant temperature. A wooden box mounted under the cruciform holds two adjustable strip lights which provide a variable level of heating. A sheet of Perspex above the cruciform with PVC-polyester flaps at the sides reduces heat loss. Slits in the Perspex and wood allow the laser extensometer to operate. A digital thermometer is used with a remote probe placed on the fabric surface to monitor the temperature. The level of heating is controlled manually. There is no provision for cooling, but the ambient temperature did not exceed the target temperature at any time. A temperature of 23 ± 2°C is maintained.

The **hydraulic cylinders are controlled manually** using two pressure relief valves. The hydraulic cylinders are powered by two independent constant pressure pumps. This means that the cylinders will deliver a constant load even if high levels of strain occur in the test piece and hence in the cylinder. In practice the applied load can vary for a given position of the pressure relief valve, and frequent adjustments can be required to maintain a given pair of loads.

Knurled brass wheels on threaded bars mounted on the end of the hydraulic actuators have been used to apply low loads, up to around 1 kN, or 3.3 kN/m. It is difficult to control the hydraulic actuators at low load with sufficient accuracy, and so knurled brass wheels have been used to enable manual application of low loads. This method works well and enables low levels of load (e.g. prestress) to be applied very accurately. However, any creep strain in the fabric leads to a rapid drop in load and so frequent adjustment is required to maintain a constant load.

Strain gauges on the bars just behind the clamp plates ensure that the load measured by the load cell at the end of hydraulic cylinder has been successfully transferred to the clamp plate, and hence to the fabric.

3.3.2.2 Safety

The key safety concern for the biaxial test rig is ensuring that the floating upper frame, weighing in excess of 145kg, does not fall off the bearings. When a cruciform is clamped in place it holds the upper frame in position. However, if the sample were to fail or when the sample is removed the upper frame is free to move and could easily slide off the bearings. Several approaches have been adopted to ensure the safe operation of the test rig:

- Loops of rope have been tied around upper and lower frames at each of the four corners. They are slack enough to ensure that they do not interfere with the test. The frame might leave the bearings, but the ropes would come tight and prevent it falling off the lower frame.
- When the cruciform is being removed and replaced the upper and lower frames are clamped together at one corner using a piece of steel angle and two G-clamps.
- If the test rig is used for biaxial failure testing it is recommended that the upper frame is supported from above (e.g. by overhead crane in a heavy engineering workshop) to prevent damage to the bearings and bearing plates due to sudden movement when the cruciform fails.

There is also scope for the upper frame to pivot on the bearings and fall. Calculations were carried out to check that the upper frame was stable in all feasible positions. Other safety considerations when using the test rig are:

- Wearing safety boots at all times,
- Not reaching between the upper and lower frames in case fabric failure results in sudden movement of the upper frame,
- Not standing by the ends of the hydraulic cylinders, again in case fabric failure results in sudden movements,
- Checking the hydraulic connections are secure and in good condition,
- Avoiding skin contact with hydraulic fluid,
- Avoid looking directly into the laser beam emitted by the laser extensometers.

3.3.2.3 Test rig specification

- Extremely stiff steel frame ensures negligible frame deflection at working loads,
- Level frame ensures no unwanted load effects from floating upper reaction frame,
- Maximum strain 25%,
- Maximum rotation of fabric warp and fill axes from orthogonal: ±10°,

- Applied load, limited to 20kN (= 66.7kN/m width) by operating range of loadcell. Hydraulic cylinders will apply 100kN (333.3kN/m width). Load cell measurement accurate to ±0.05kN.
- Strain measurement. Laser extensometer accurate to 1 part in 50 000; gauge length = 200mm giving accuracy of ±0.004mm, i.e. accuracy will not be compromised by extensometer but by other factors, for example distortion of the analogue signal from the laser extensometer to the data logger,
- Data logging: synchronised readings have been logged at a specified frequency of up to one per second. Data recorded are two applied loads, two strains and output from eight strain gauges.
- Temperature control is manual hence accuracy depends on the operator; ±2°C can be achieved easily, usually ±1°C. Maximum and minimum temperatures have been recorded for each test.

3.3.3 Test protocol development

3.3.3.1 Overview

Cyclic loading is required to provide data on fabric service behaviour rather than initial behaviour. The cyclic load pattern aims to simulate loading on a fabric structure: prestress plus wind and snow loads. Test protocols used in industry and previous research (Doering, 1993) provide a starting point for development of a biaxial test protocol. However, with little published work in this area and little justification or explanation available for existing procedures, the protocol proposed in this research has primarily been developed through extensive testing.

Test regimes used in industry e.g. Laboratorium Blum, Stuttgart (Blum, 1980; Blum & Bidmon, 1987; Blum & Bögner, 2002) and national standards [MSAJ/M-02-1995] have typically been developed to provide suitable data to inform a plane stress model rather than fully explore the response of the fabric. This test protocol has been developed with no preconceptions about how the test data will be used; the aim is to explore the fabric behaviour as thoroughly as possible.

Current test methods require a new sample to be used for each biaxial stress ratio. However, a general mechanical conditioning regime has been developed which enables a series of biaxial tests to be carried out quickly and efficiently on the same sample. This enables the stress-strain response of the fabric to be explored thoroughly, not just tested at a limited number of stress ratios. The validity of this method has been checked by re-applying stress states at different stages of the test and comparing the resultant strains. These repeat readings show whether the test regime affects the subsequent behaviour of the sample.

The principal limitation of the biaxial test rig, as currently functioning, is that the rate of loading cannot be controlled accurately. Proposed modifications to the test rig include using servo-controlled valves to automate testing and improve load accuracy (§6.2.2). The biaxial test rig is designed to maintain constant

loads, hence cyclic load regimes must be based around maintained constant loads (square wave) rather than constantly changing loads at a given rate (sawtooth). Uniaxial tests have been carried out to determine the sensitivity of the fabric response to the rate of loading (§3.1.1, Figure 3-6 & Figure 3-7).

The test protocol was initially developed from tests on PVC-polyester fabrics (a range of weights and thicknesses manufactured by Ferrari and Verseidag), with subsequent testing of PTFE-glass fibre fabric (manufactured by Taconic and Verseidag). The framework for the test protocol is three stages: prestress, mechanical conditioning and testing. Factors that have been investigated in developing the protocol are:

- Load levels (§3.3.3.2),
- Mechanical conditioning (§3.3.3.3),
- Residual strain (§3.3.3.4),
- Load history (§3.3.3.5).

3.3.3.2 Load levels

The test regime is stress controlled, which is appropriate as the range of expected stresses is known and the strains are required.

The cruciform is held at prestress prior to testing to prevent initial high levels of creep from interfering with test results, and to simulate the normal load condition of an in-situ fabric. The prestress level is based on typical levels used in structural design, and is defined as a percentage of the strip ultimate tensile strength (UTS): 1.3% UTS for PVC/polyester fabric and 2.5% UTS for PTFE/glass fibre fabric. The strip UTS provides a useful basis for defining test loads as it is usually provided by manufacturers and is defined by BS EN ISO 1421:1998. These percentages are typical of values used in industry. However, values vary widely depending on factors such as geometry and expected load patterns. The values given here simply provide a standard base load level for testing. If the test was being carried out for a particular project, the prestress levels could be modified to ensure the test data was as accurate as possible for that application. It is important to note that the aim of the initial application of prestress is **not** to determine compensation values (§1.1.3). Compensation values are particular to each project and depend on exact prestress levels in warp and fill directions, and are routinely determined by specialist contractors such as Architen-Landrell (www).

The maximum design / test load is based on tear propagation, which occurs at approximately 25% UTS (Happold et al, 1987). The conditioning load (§3.3.3.3) is 10% higher than the design / test load, the aim being to subject the fabric to loads slightly beyond the extremes which will be experienced during the test.

3.3.3.3 Mechanical conditioning

The fabric must be mechanically conditioned such that the behaviour measured is *not* the initial behaviour but the typical behaviour of an in-situ fabric. The aim is that a conditioned fabric will exhibit the same strains for a given state of stress for repeated applications of this stress state. For materials which exhibit significant levels of creep, the effect of creep must be removed before this comparison can be made (§3.3.3.4). This will give consistent results throughout a test, and enable repeat readings to be taken using a single sample. The results should represent the behaviour of an in-situ fabric that has been exposed to environmental loads (e.g. wind and snow) better than a test on a virgin fabric. The purpose of the cyclic conditioning can easily be seen from the behaviour of a uniaxial strip test under cyclic load (Figure 3-30).

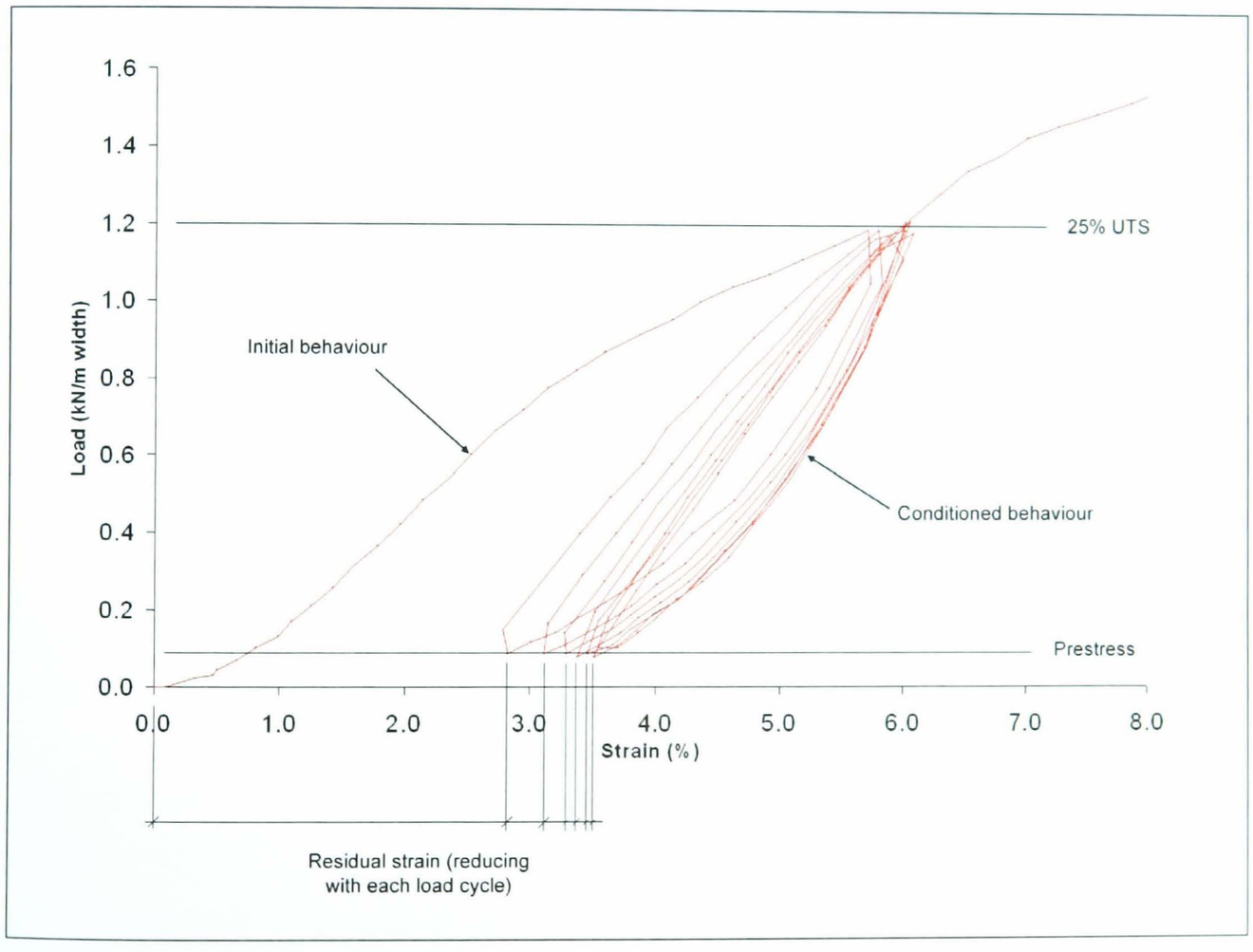

Figure 3-30. Cyclic uniaxial strip test

A cyclic load pattern is applied (Table 3-1 & Figure 3-31); the three load states aim to subject the fabric to all feasible extremes of loading.

Time (minutes)	Warp load	Fill load
0 - 5	Prestress	Prestress
5 – 10	Conditioning load	Conditioning load
10 – 15	Prestress	Prestress
15 – 20	Conditioning load	Prestress
20 – 25	Prestress	Prestress
25 - 30	Prestress	Conditioning load

Table 3-1. Single conditioning cycle

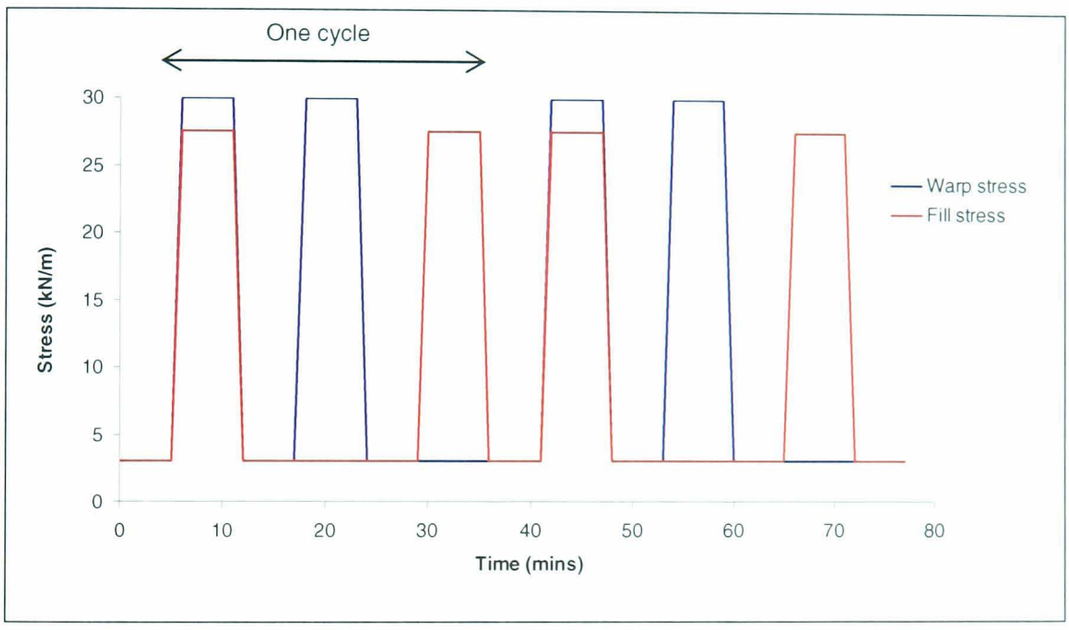

Figure 3-31. Typical conditioning cycle

The mechanical conditioning cycle is applied repeatedly until the warp and fill strains are similar for repeated applications of a given stress state. However, after loading, coated woven fabrics exhibit high levels of residual strain due to creep and hysteresis of the yarns and coating, and internal frictional effects. To determine whether a fabric is conditioned the strains during each cycle have been compared *after residual strain has been subtracted* from the readings (§3.3.3.4).

A variation in strain between cycles of less than 5% of the actual strain is deemed to be acceptable. Testing on various PVC/polyester fabrics has shown that typically three, and occasionally four, cycles are sufficient. If the actual value of strain is small then the 5% criterion may be too onerous, in which case a variation of no more than 0.1% strain has been deemed to be acceptable.

3.3.3.4 *Residual strain*

Preliminary biaxial tests have been carried out which involved applying various combinations of loads up to the design load for around three hours. The test was repeated at twenty-four hour intervals, with the applied load being approximately maintained at prestress between tests. After four tests there was a gap of seventy-two hours and then one final test (Figure 3-32). After each test the fill strain has increased significantly. The creep at prestress is negligible over the period of time required for testing, it is the residual strain in the fabric after a test at high loads which is significant. Similarly, during a cyclic uniaxial test the strain at prestress steadily increases (Figure 3-30).

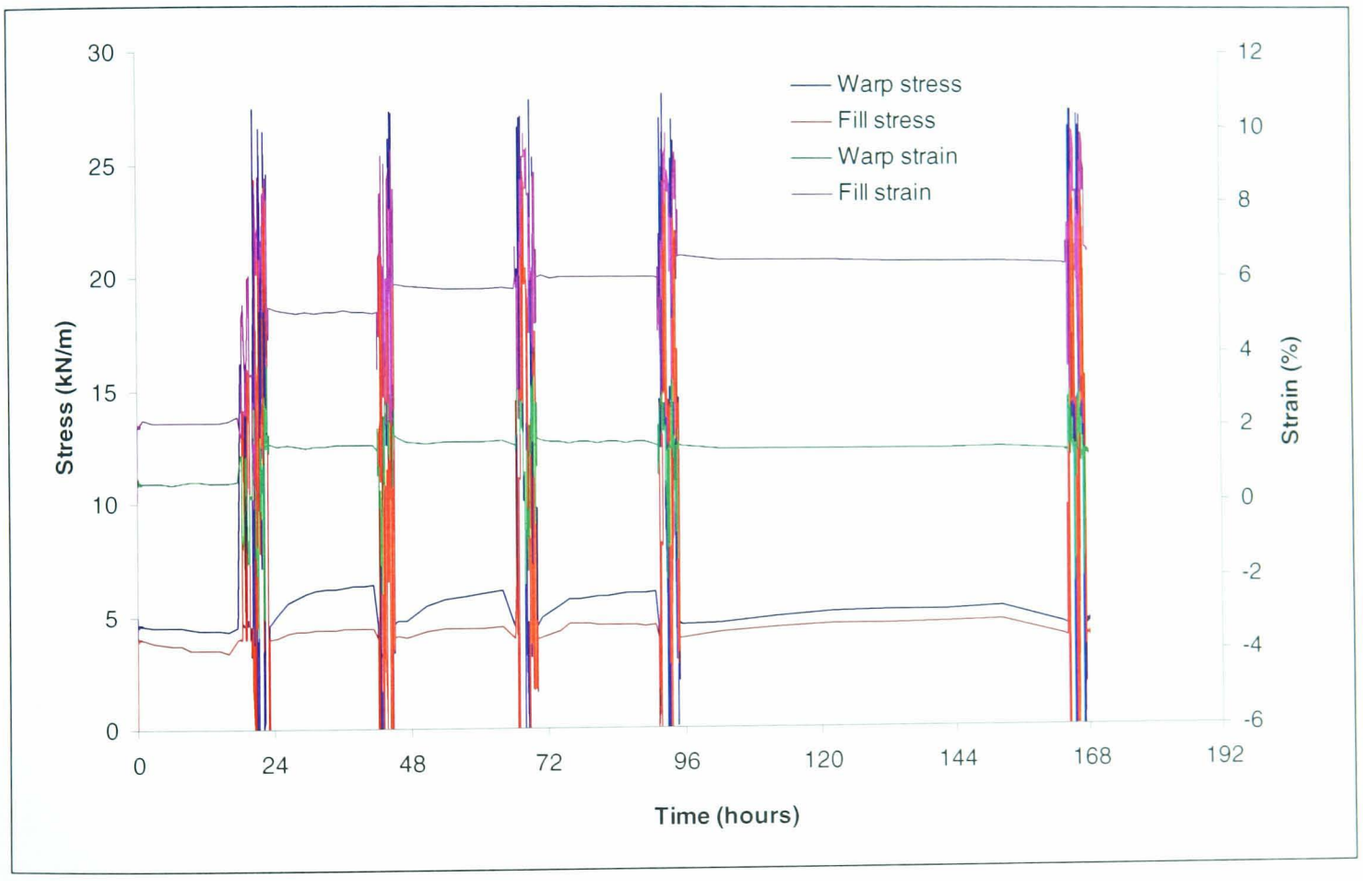

Figure 3-32. Residual strain in test on PVC-polyester fabric.

For results from repeat tests (and within a single test) to be compared meaningfully it is necessary to subtract the residual strains from the results. In fact, it is useful to remove the effect of residual strain from the results for several reasons:

- Strains from conditioning cycles can be compared directly with one another to establish when the fabric is sufficiently conditioned,
- The stress-strain response can be compared for repeat readings on the same sample, and for different samples which may have been loaded at different levels or for different times and hence have different levels of residual strain (Figure 3-33 & Figure 3-34),
- Skewing of the results due to increased levels of residual strain at high loads is avoided.

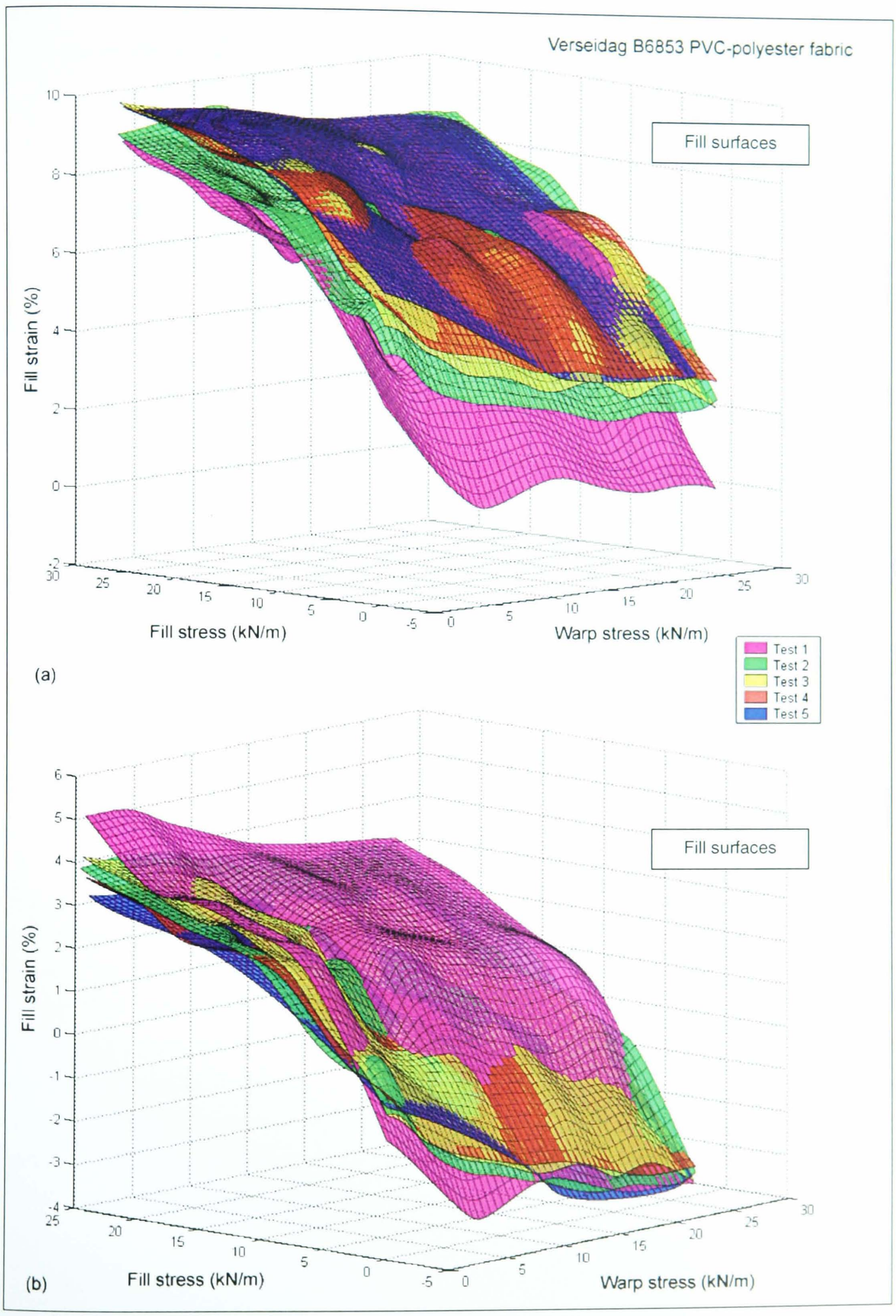

Figure 3-33. Five tests on PVC-polyester fabric, (a) with creep and (b) with creep removed

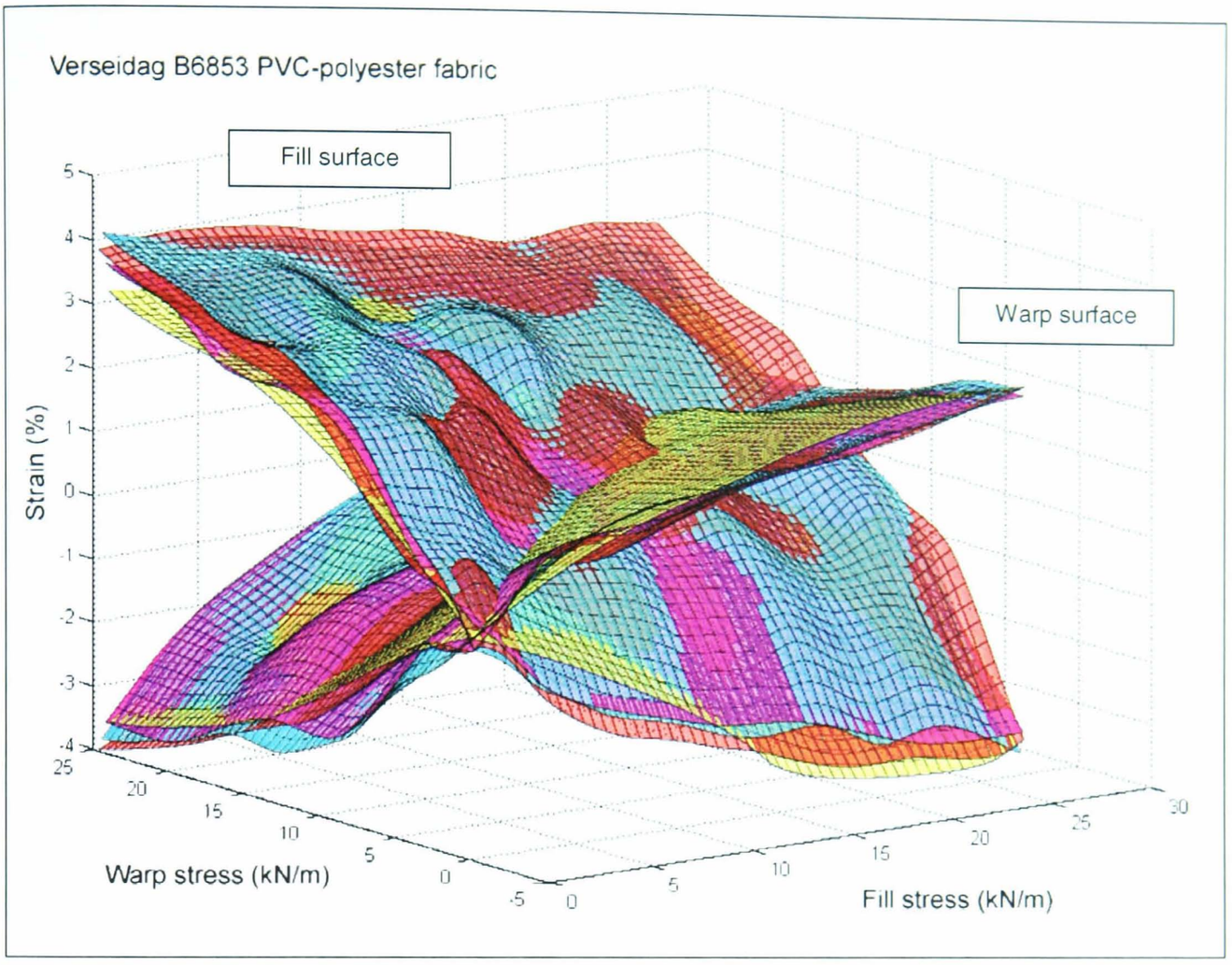

Figure 3-34. Warp and fill surfaces with creep removed

The Japanese standard on membrane material testing (MSAJ/M-02-1995) is the only reference where a similar process of removing residual strain has been found: *"if we assume a low level of pretension, it may sometimes be necessary to set the stress under this condition as the starting point"*, *"the initial point of the curve in the tensile test is set individually for each stress ratio"* (p.6). **Prestress has been chosen as a reference state; the modified warp and fill strains have been deemed to be zero under prestress.** This is an arbitrary choice – any stress state could have been chosen for zero strain. The reference stress state must be applied regularly during the test to enable residual strains to be subtracted accurately. Hence prestress is a natural choice as it will be applied at the start and end of the test and between each part of any load regime. Strains have been compared each time prestress is applied (in both warp and fill directions simultaneously) and the residual strain is deducted from the strain readings in that interval. The reduction in strain is proportional to the applied load and the time for which it has been applied; based on the assumption that the greater the applied load the greater the rate of creep (Figure 3-35).

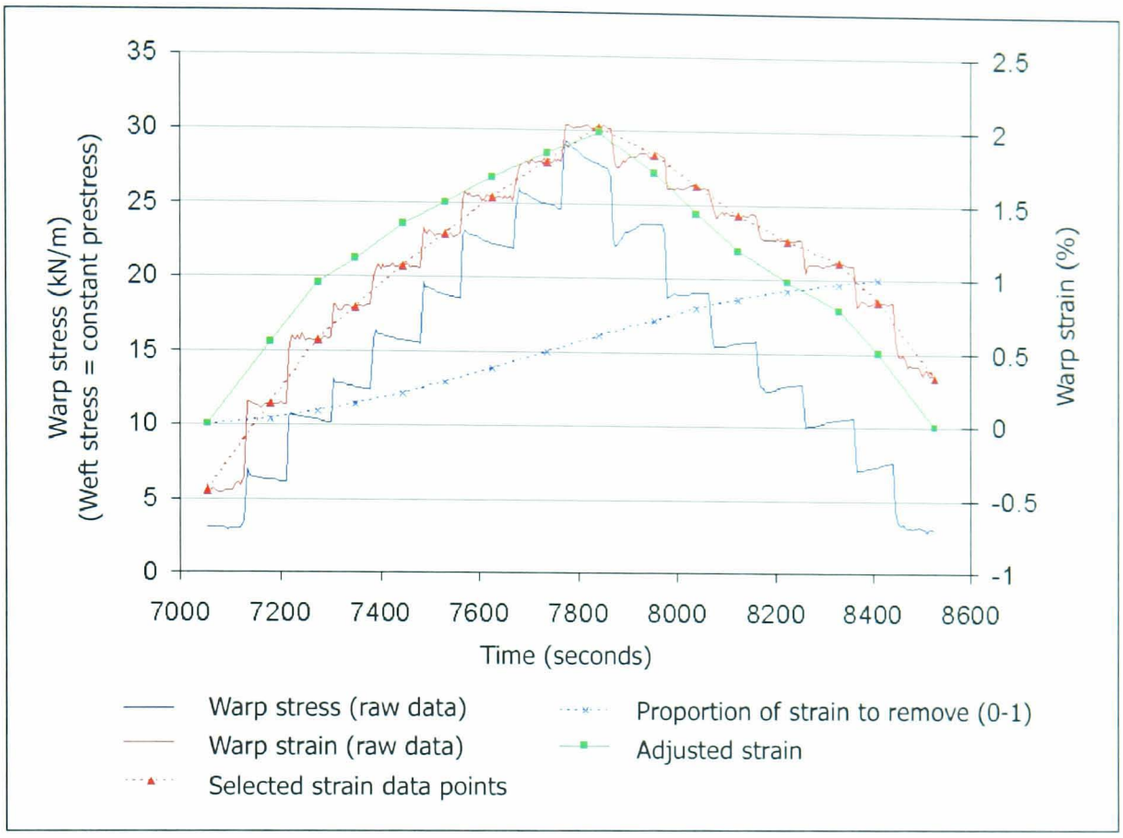

Figure 3-35. Removal of residual strain

Results with residual strain removed are appropriate for elastic structural analysis. Residual strains must be included in the analysis, however, for calculation of long term stress states and re-tensioning requirements.

3.3.3.5 Load history

A fundamental question is: "Does the maximum load which has been applied to a fabric recently (or ever) affect the subsequent response of the fabric?" The concern is that once a fabric has been subjected to the maximum design load (e.g. 25% UTS), the test results may not be valid for medium term behaviour (e.g. 2 year expected loading) where the maximum load may never exceed, say, 10% UTS. Tests have been carried out with two different maximum load levels with the aim of determining whether separate tests are required for different load levels. The fabric was mechanically conditioned to a load 10% higher than the maximum load for each test (§3.3.3.3).

The results (Figure 3-36) show the response to medium term loads (purple & yellow) and long term loads (blue and red) for a PVC-polyester fabric. Residual strain has been removed from all results following the convention that strain at prestress is deemed to be zero (§3.3.3.4). The similarity of these surfaces indicates that the maximum load applied to the sample during the test does not significantly affect the subsequent behaviour. A single test has therefore been adopted for all load levels.

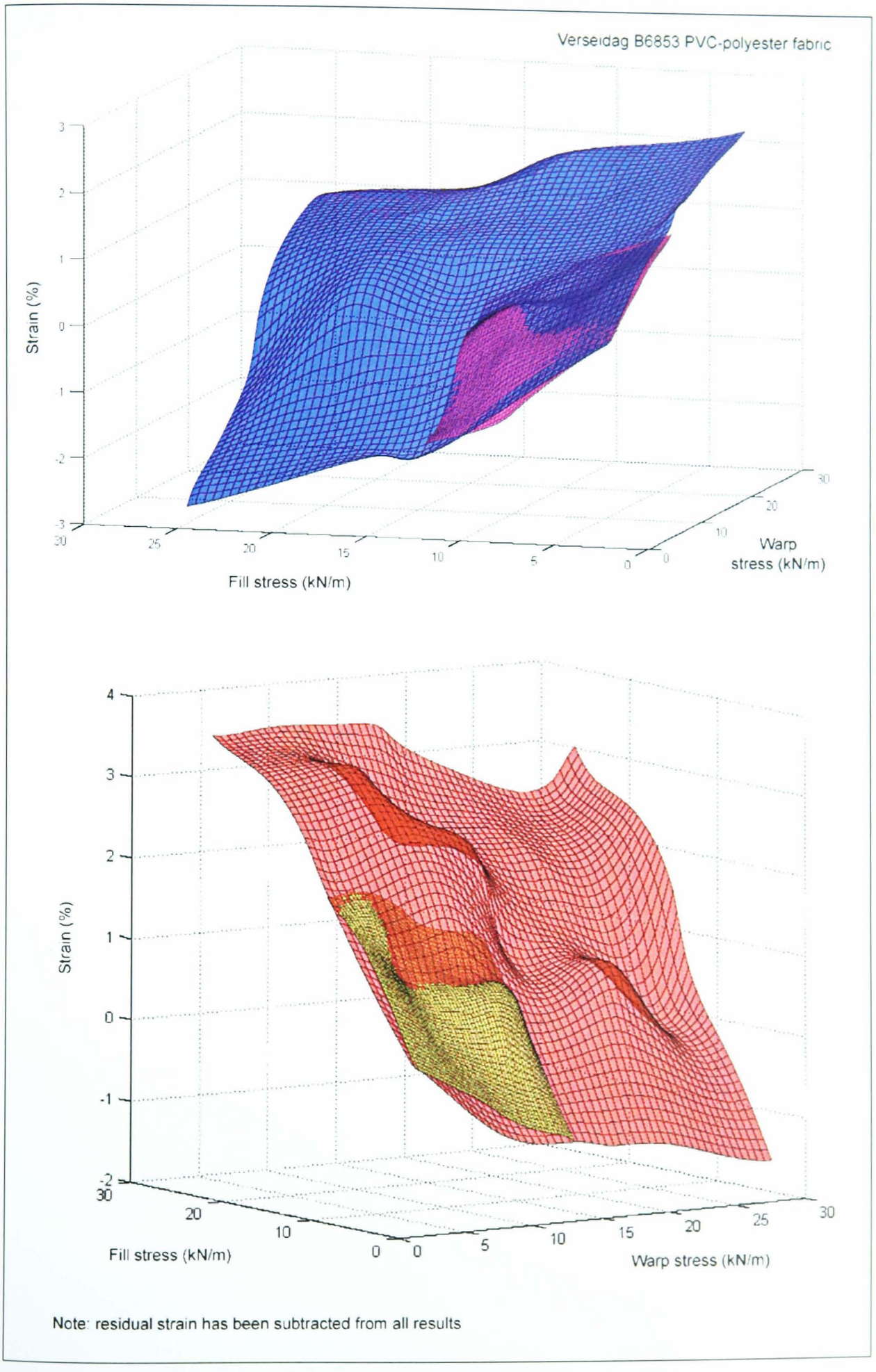

Figure 3-36. Stress-strain response for medium and high loads

Once the fabric is conditioned it is important to ensure that the sequence of test loads do not affect the subsequent response of the fabric. The effect of recent load history on the biaxial response of the fabric has been investigated. A reference stress state was chosen, which was then approached from eight different previous stress states (Figure 3-37).

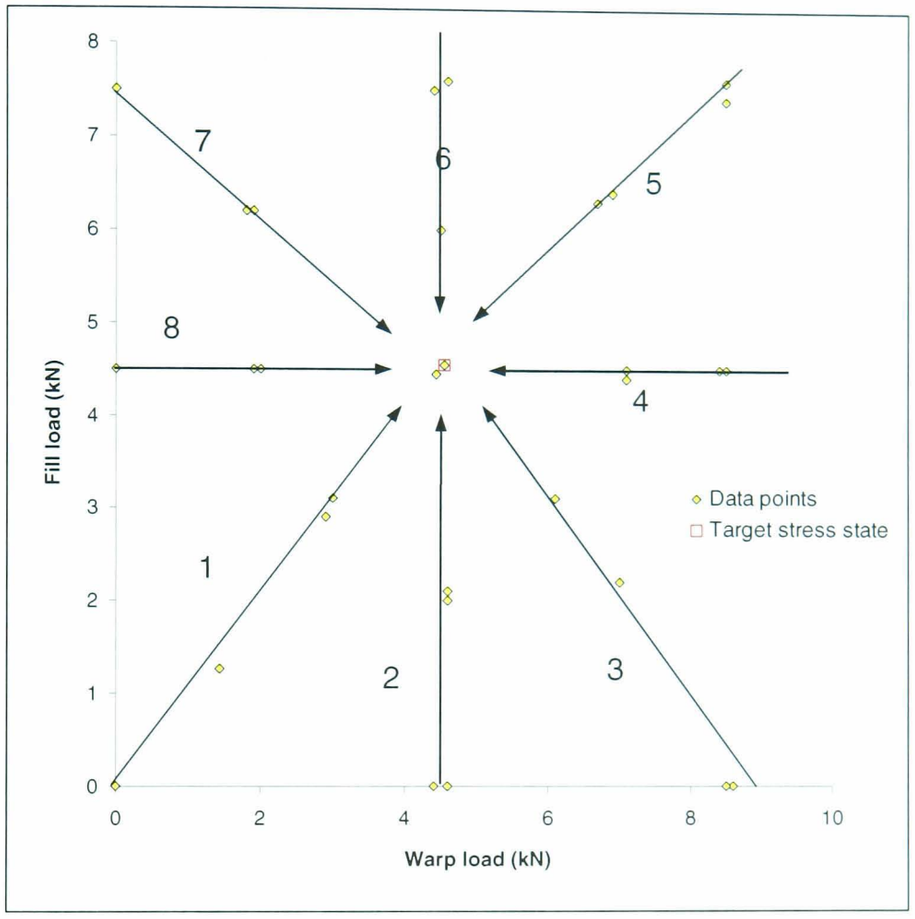

Figure 3-37. Load paths to investigate recent load history

The level of strain variation due to recent load history is significant; 0.62% in the warp direction and 0.76% in the fill direction, compared with mean strain values of 0.16% and 1.33% respectively (Figure 3-38). A high stress in warp or fill direction results in a high strain in that direction (Figure 3-38, load paths 4 and 6 respectively).

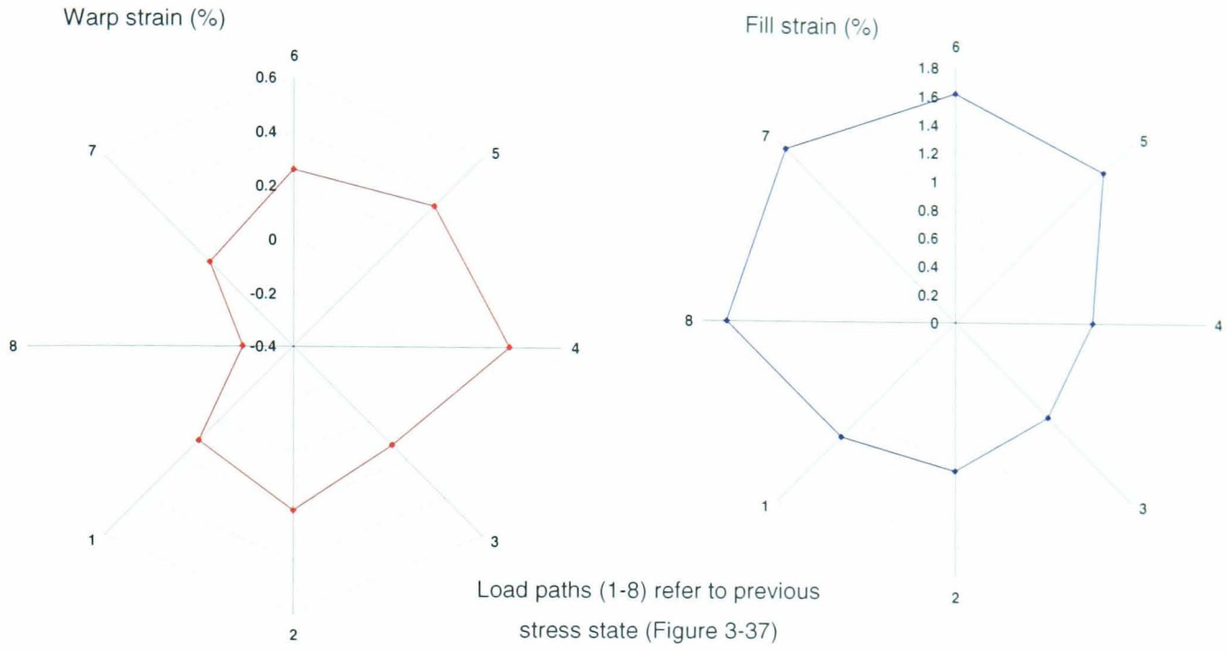

Note: 1. Values are averages for five tests on Verseidag B6853 PVC-polyester fabric,

2. Residual strain has been removed from all strain values.

Figure 3-38. Spider diagrams of effect of recent load history

Further investigation was carried out using four different reference states of stress, and approaching each from various prior load states (Figure 3-39).

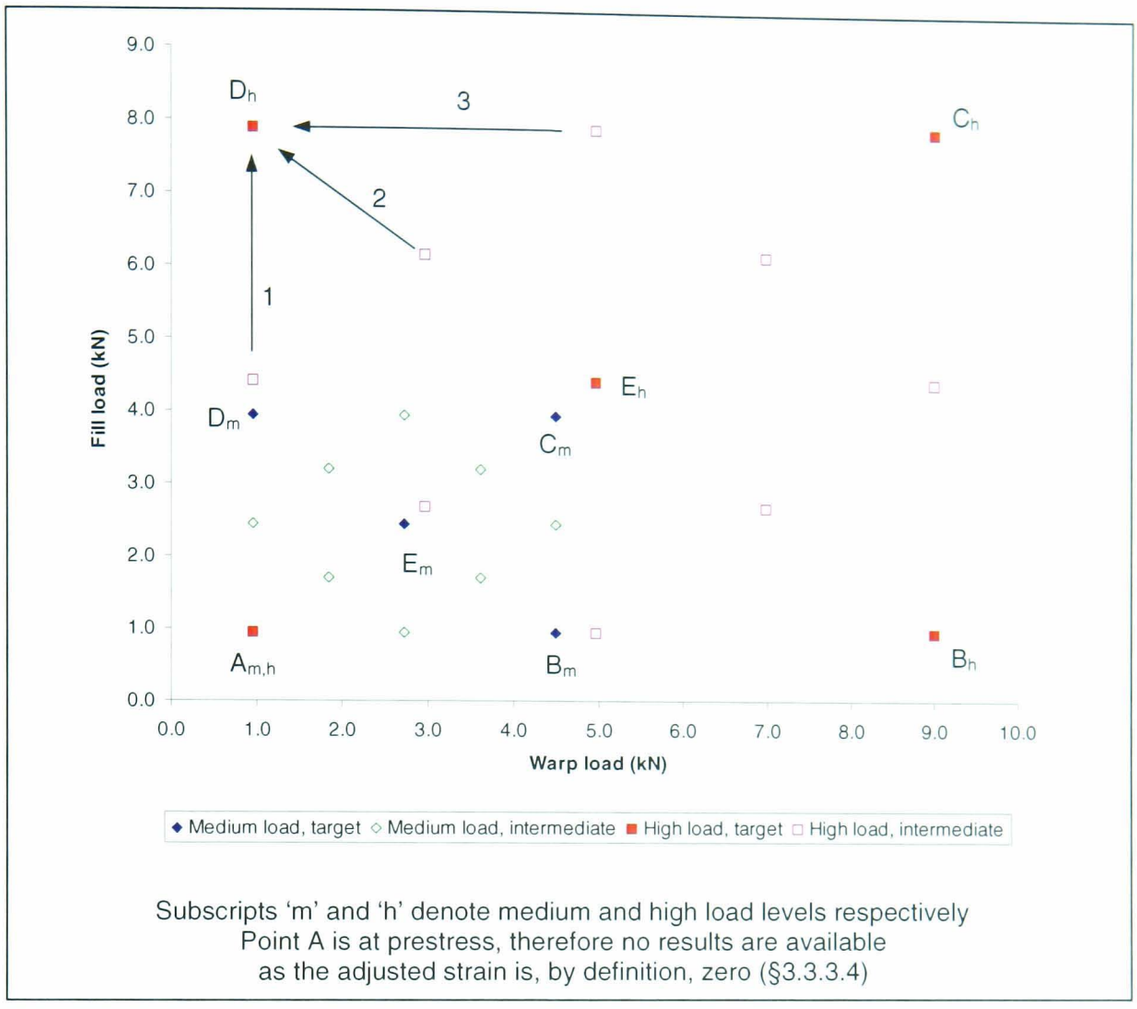

Figure 3-39. Load paths to investigate recent load history, multiple reference states

Two different maximum load levels were used, described as medium and high. For each load level four different target stress states were used. Stress states B, C and D were approached using three different load paths, state E was approached using four different load paths. The aim of the tests was to assess the level of strain variation due to recent load history for a wide range of stress ratios and magnitudes.

Results are the average of two separate tests on Verseidag B6853 PVC-polyester fabric. All results have had residual strains removed. There is good agreement between repeat readings (mean difference between the two tests: warp, 0.13% strain, fill 0.10% strain; maximum difference between repeat tests: warp 0.38% strain, fill 0.21% strain), and a fairly good correlation between medium and high levels of applied load. The strain variations due to different previous stress states are very significant (Table 3-2).

Stress state (Figure 3-39)	Stress level	Strain variation (percentage strain)		Strain variation (percentage of mean strain)	
		Warp	Fill	Warp	Fill
B	Medium	0.21	0.25	-2.31	2.52
B	High	0.35	0.10	-2.44	0.54
C	Medium	0.35	0.42	3.50	13.86
C	High	0.54	0.54	2.17	6.64
D	Medium	0.23	0.22	1.42	-1.48
D	High	0.53	1.02	1.68	-4.22
E	Medium	0.48	0.36	10.72	-50.00†
E	High	1.19	0.73	9.97	14.66

All values are for adjusted test data, i.e. with residual strain removed

Values are means of two tests on Verseidag B6853 PVC-polyester fabric

† If the mean strain is small, the 'percentage of mean strain' becomes prone to large variations

Table 3-2. Effect of recent load history

Thorough testing of all 'approach directions' (i.e. previous stress states) for all stress states is clearly too time consuming. Hence it is proposed that radial load paths (from prestress) are used to give loading and unloading behaviour (Figure 3-40). This is appropriate because:

1. It is the type of load path the structure will typically experience for a single load event (a gust of wind, snow load), i.e. from prestress to a loaded condition and back to prestress,
2. The loading and unloading behaviour will give a good indication of the variability due to recent load history,
3. It gives frequent applications of prestress to enable accurate residual strain removal for determining the underlying elastic characteristics of the fabric.

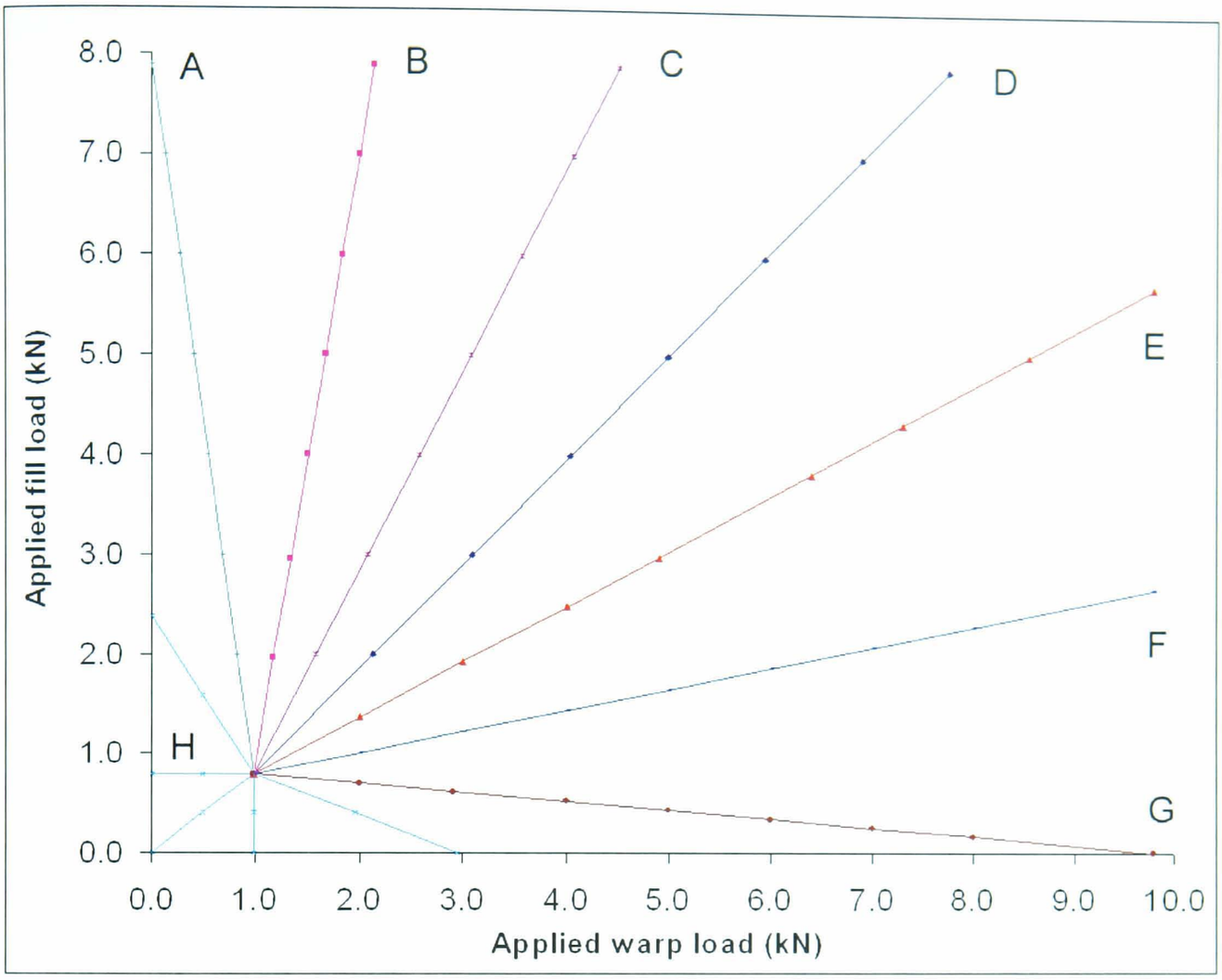

Figure 3-40. Radial load regime

3.3.4 Biaxial test protocol

The test is carried out at 23 ± 2°C. The protocol consists of three parts: prestressing, conditioning and testing.

Prestress of 1.3% UTS (strip ultimate tensile strength, BS EN ISO 1421:1998) for PVC/polyester fabric and 2.5% UTS for PTFE/glass fibre fabric is applied for approximately 17 hours.

Conditioning cycles (Figure 3-31) are applied until the strain difference between repeated stress states is less than 5% of total strain. Strains are compared with residual strain removed. A concession in this criterion is required for very low strains where 5% may not be achievable.

A **test protocol** consisting of radial load paths extending from prestress to 25% UTS is proposed (Figure 3-40). 25% UTS is the maximum design load based on a factor of safety of four to prevent tear propagation. The cruciform is subjected to evenly spaced radial load paths (Figure 3-40, A-G), applied in the order D, B, E, H, C, G, A, F to distribute high warp and fill loads throughout the test (Figure 3-41). Load path H determines the fabric response at loads below prestress. Strains are recorded for both the loading and unloading parts of each radial arm, each stress state is held for at least one minute to allow

initial rapid creep to subside. Warp and fill loads and strains are logged every five seconds throughout the test. The average of at least five consecutive readings is taken to define a data point.

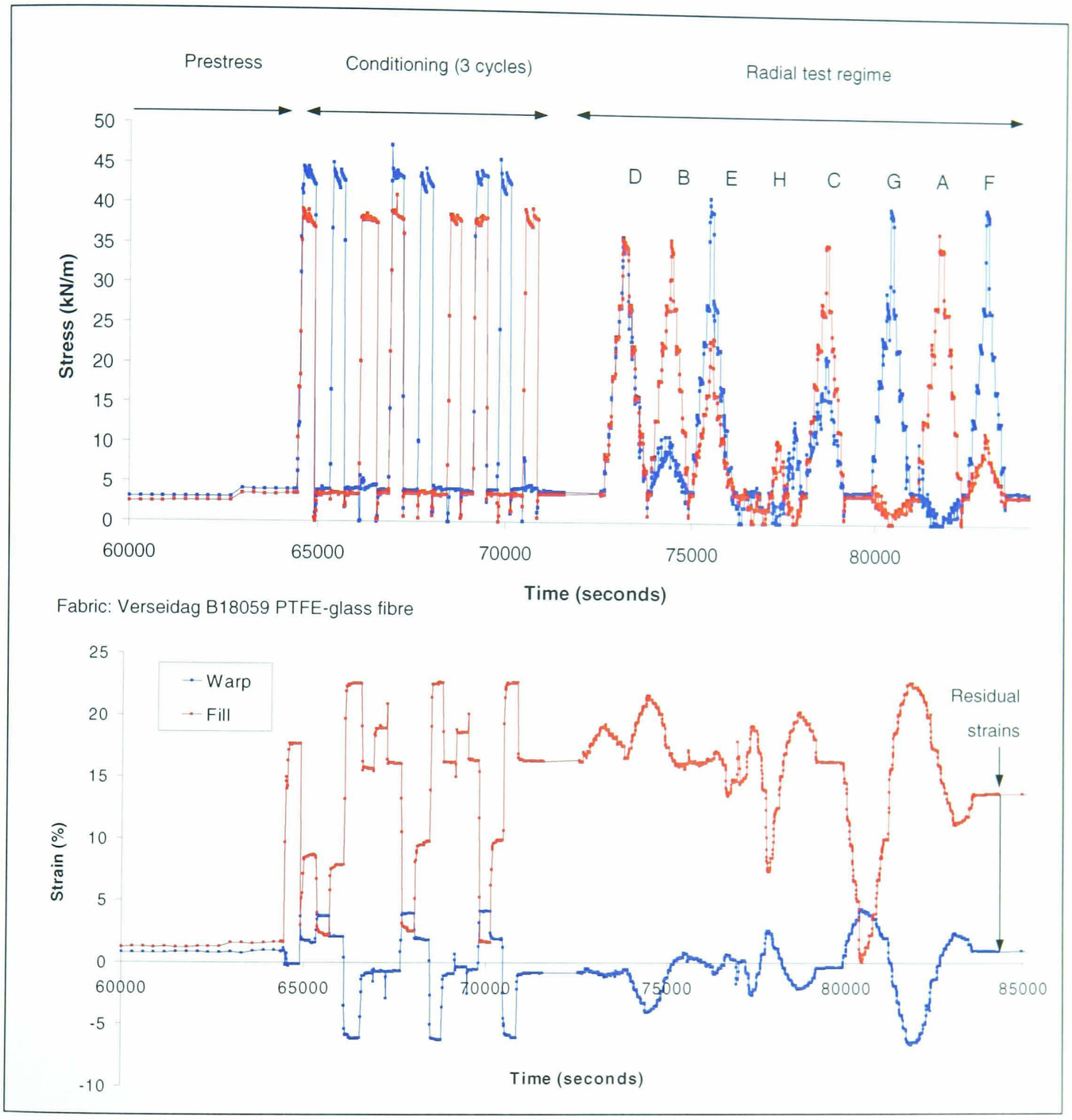

Figure 3-41. Typical load and strain histories

This protocol efficiently populates the stress space with strain data and frequently returns to prestress to enable accurate removal of residual strains. Thorough testing of the effect of load history on each stress state is infeasible; the loading and unloading results give a good indication of the level of variability. Each radial arm of the load regime is typical of the load paths the structure will experience in a single load event (a gust of wind or snow load), i.e. from prestress to a loaded condition and back to prestress. The high residual strains at the end of a typical test (warp strain = 0.9% , fill strain = 13.8% in Figure

3-41) show the importance of removing residual strain from the test results to prevent distortion of the response surface.

The test protocol demonstrates a principle for biaxial testing. The details are not fixed; for example, the number of radial arms and data points will vary depending on practical considerations, time constraints and the level of detail required. Further testing can be carried out for stress states that are important to a particular design.

3.4 TEST PROGRAM

Fabric	Material (Type†)	Strip tensile strength (kN/m)		Prestress (kN/m)		Design / test load (kN/m)		Conditioning load (kN/m)	
		Warp	Fill	Warp	Fill	Warp	Fill	Warp	Fill
Taconic Solus 1120	PTFE-glass (G5)	124	100	3.10	2.50	31.0	25.0	34.1	27.5
Taconic Solus 1300	PTFE-glass (G6)	150	116	3.75	2.90	37.5	29.0	41.3	31.9
Taconic Solus 1410	PTFE-glass (G7)	160	160	4.00	4.00	40.0	40.0	44.0	44.0
Verseidag B18059	PTFE-glass (G6)	140	120	3.50	3.00	35.0	30.0	38.5	33.0
Verseidag B18089	PTFE-glass (G6/G7)	160	140	4.00	3.50	40.0	35.0	44.0	38.5
Ferrari 702T	PVC-polyester (I)	56	56	0.73	0.73	14.0	14.0	15.4	15.4
Ferrari 1002T	PVC-polyester (II)	84	80	1.09	1.04	21.0	20.0	23.1	22.0
Ferrari 1202T	PVC-polyester (III)	112	112	1.46	1.46	28.0	28.0	30.8	30.8
Ferrari 1502T	PVC-polyester (IV/V)	200	160	2.60	2.08	50.0	40.0	55.0	44.0
Verseidag B6853	PVC-polyester (III)	114	100	1.48	1.30	28.5	25.0	31.4	27.5

† For definition of fabric types see Chapter 2, §2.1.4.1, Figure 2-15

Table 3-3. Fabrics tested & stress levels for testing

The loads to apply to the fabric were calculated from the values in Table 3-3. The stress levels were multiplied by 0.3 to give the load to be applied to the 300mm wide cruciform, and then divided by 0.95 to account for the reduction in stress in the centre of the cruciform (§3.3.1). Two samples of each fabric were tested, both taken from the same roll.

3.5 SUMMARY & CONCLUSIONS

There are no British or European standards on biaxial fabric testing, and little published justification of test regimes used in industry. Test regimes are typically developed to inform a plane stress model rather than fully explore the fabric response.

A biaxial test rig has been built based on the 'floating' concept innovated by Architen-Landrell, which applies load to a cruciform test piece in the direction of the warp and fill yarns (not necessarily orthogonally). The cruciform with slit arms has been adopted, and the stress state within the cruciform has been analysed using finite element models. This enabled the appropriate gauge length to be determined. The cruciform analysis indicated that a load reduction factor (equal to 0.95) is required to convert the applied load to the expected stress in the area of interest.

A new biaxial test protocol for architectural fabrics has been developed based on extensive testing of architectural fabrics. Application of prestress followed by mechanical conditioning provides repeatable stress-strain data suitable for medium to long term structural design. The test protocol efficiently populates the space of feasible stress states; it is not restricted to a limited number of stress ratios. A method of removing residual strain from the test data has been developed to prevent skewing of the response surface due to creep during the test. Removal of residual strain also enables accurate comparison between repeat tests and with predictive models. Test results with residual strain removed are appropriate for the elastic analysis currently used for membrane structure design.

PVC coated polyester and PTFE coated glass-fibre are by far the most commonly used architectural fabrics. Tests have been carried out on both types of fabric in a range of weights from several manufacturers (PVC/polyester, types I-IV/V; PTFE-glass types G5-G7). Two tests have been carried out on each fabric.

Chapter 4

Biaxial test results and implementation

Contents

Figures

Tables

4.1 RESULTS & DISCUSSION

The biaxial test regime developed in this research (§3.3.4) provides a more thorough population of the stress-strain data space than previous work in the field (§2.2.3.2). Testing has been carried out on a range of PVC-polyester and PTFE-glass fibre fabrics at stresses from zero to 25% of their ultimate tensile strength. The data can be represented as a series of conventional two dimensional stress-strain plots (§4.1.1) or, to comprehensively visualise the fabric response, as a pair of three dimensional response surfaces (§4.1.2).

4.1.1 Classical stress-strain plots

This familiar form is useful for identifying characteristics of the fabric response and comparing fabric behaviour with other materials. It enables comparison with previous fabric test data, which typically consists of stress-strain data for a small number of warp to fill stress ratios, e.g. 2:1, 1:1, 1:2. (§2.2.3.2). Stress-strain plots can be produced using results from the new test protocol by plotting the stress-strain results along each arm of the radial load regime (§3.3.4). Strain measurements have been recorded for both increasing and decreasing load; the hysteretic behaviour of coated woven fabrics results in distinct loading and unloading curves. In previous work the warp and fill strains are typically plotted against the warp stress, the corresponding fill stress being defined by the stress ratio. Because the radial load paths start at prestress (rather than zero load) the stress ratio along a radial arm is not constant. Specifying one stress level (e.g. warp) on the graph would not fully describe the stress state in the sample. Instead the root-mean-square of the warp and fill stresses have been used to give an indication of the stress magnitude. Reference to the radial load arm diagram is required to determine the applied loads for a given data point. This shows the limitations of trying to plot a relationship between four variables on a two-dimensional graph, and led to the use of response surfaces (§4.1.2).

The stress-strain plots are useful for examining the fabric behaviour in detail: non-linear response characteristics (e.g. sudden changes in gradient and gradient reversal), hysteretic response envelopes and comparison between repeat tests and between different fabrics are all easily examined using stress-strain plots. The high levels of residual strain in the fill direction (Figure 4-1 & Figure 4-2) are caused by the initial crimp in the fill yarns straightening during the conditioning cycles and during the test. This straightening of the fill induces additional crimp in the warp, giving some negative residual strain in the PTFE-glass fabric (Figure 4-1). The same mechanism occurs in the PVC-polyester, but the creep of the yarn fibres ensures that strains in both warp and fill are positive (Figure 4-2).

To minimise skewing of the test results a method has been developed to remove residual strain from the test data (§3.3.3.4). To assess the difference between repeat tests it is beneficial to use these adjusted results. Raw test data for two tests each on Taconic Solus 1300 PTFE-glass (Figure 4-1) and Ferrari

1202T PVC-polyester (Figure 4-2) show poor correlation between the repeat tests. The Solus 1300 results show a strain difference of approximately 2% in the fill direction, the 1202T results differ by 0.5% in the warp direction. The adjusted results for the same tests (Figure 4-3 & Figure 4-4) show extremely good correlation: the strain differences between the original sets of data are largely due to differing levels of residual strain. This variation in residual strain levels may be caused by a different number of conditioning cycles being required, or the samples having been held at prestress for different lengths of time prior to testing. The adjusted data facilitates comparison of differences in the stress-strain response between the two tests, between different stress ratios and between different fabrics. A more rigorous assessment of the difference between repeat tests has been carried out by subtracting stress-stress-strain response surfaces fitted to the test data (§4.1.2, Table 4-2).

Notes on Figure 4-1 to Figure 4-12:

1. 'Warp 1' and 'Warp 2' denote strains measured in the warp direction for tests 1 and 2 on different fabric samples,
2. Results are not given for load path H (both stresses below prestress) as the limited number of data points at each stress ratio are not appropriate for plotting stress-strain curves. Load path H results are included in the response surface plots (Figure 4-13 to Figure 4-24),
3. The root-mean-square (RMS) stress is used to represent the magnitude of the applied stresses, but it is important to realise that at high stress ratios the applied load in one direction will be considerably lower than that shown on the axis. This difficulty in representing biaxial stress-strain behaviour on two axes led to the use of stress-stress-strain response surfaces (§4.1.2),
4. Red circles ○ have been used to identify outlying data points which do not appear to fit with the trend of the test data. Due to the limited number of tests (two per fabric type) these potentially erroneous points have been identified using subjective judgement, not statistical analysis.

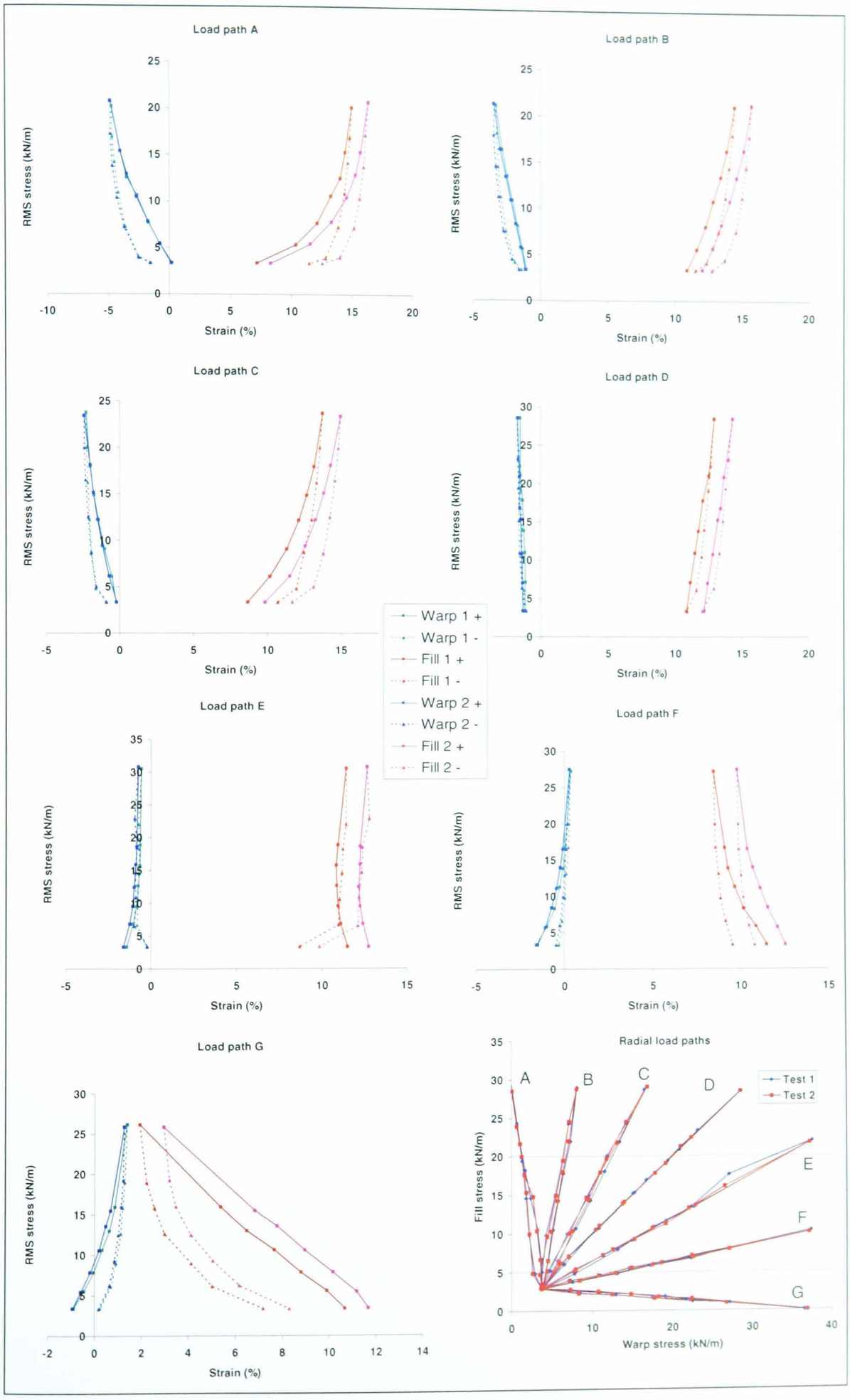

Figure 4-1. Non-adjusted stress-strain curves, Taconic Solus 1300, PTFE/glass

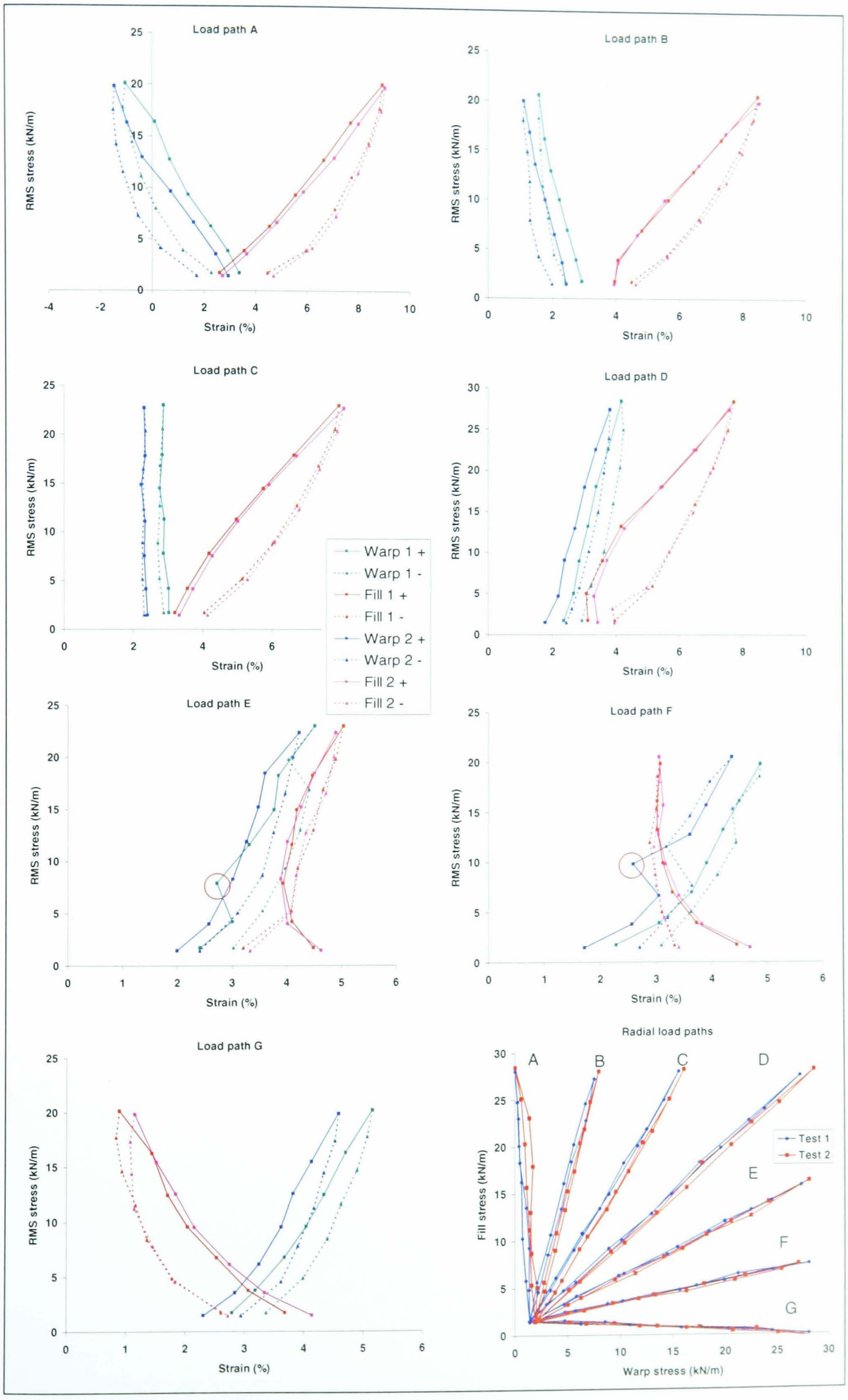

Figure 4-2. Non-adjusted stress-strain curves, Ferrari 1202T, PVC/polyester

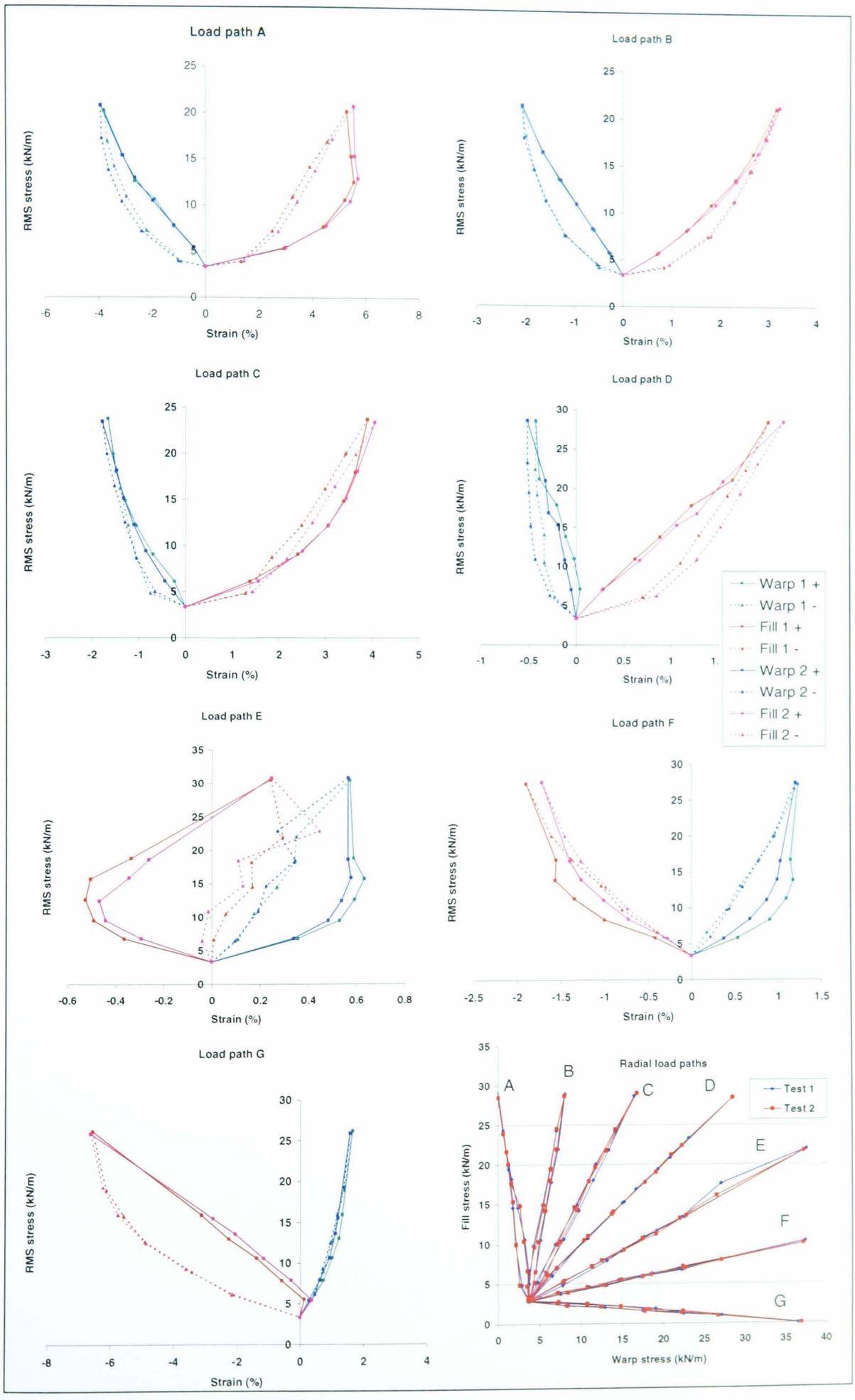

Figure 4-3. Stress-strain curves, Taconic Solus 1300, PTFE/glass

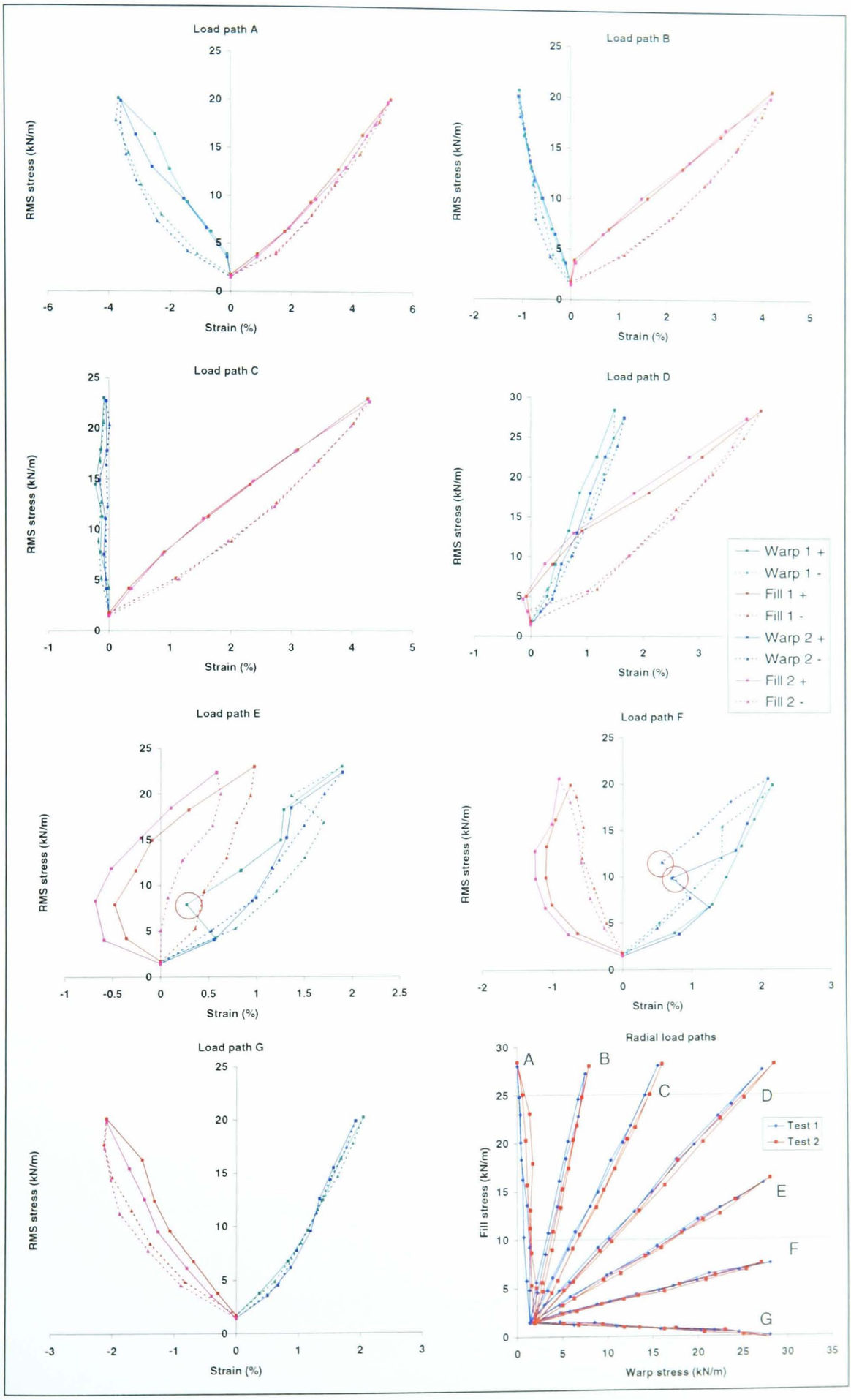

Figure 4-4. Stress-strain curves, Ferrari 1202T, PVC/polyester

The non-linear characteristics of coated woven fabric behaviour are clear from the test results for all fabrics. There are numerous examples of gradient reversal (e.g. Figure 4-3 and Figure 4-4: load path E, fill) and sudden changes in gradient (e.g. Figure 4-3: load path A, fill; load path E, warp). Negative strain is common in the warp direction. There are three types of negative strain: negative values of strain (Figure 4-1, load paths A-F, warp), negative stress-strain gradient (Figure 4-3, load paths A – D (warp), load paths E – G (fill); Figure 4-4, load paths A & B (warp), load path E - G (fill)) and negative residual strain (Figure 4-1, load paths A-F, warp).

Tests were carried out on a wide range of fabrics (§3.4) and the test results for all of the samples show distinct similarities (Figure 4-3 to Figure 4-12). The structure of all of the fabrics is fundamentally the same, and these common stress-strain properties can be explained in terms of the balance of crimp in the fabric:

Load paths A to D. High fill loads result in large strains in the fill direction. Straightening of the fill yarns introduces crimp into the warp, giving negative stress-strain gradients. As the warp load increases through load paths B, C and D the negative warp stress-strain gradient decreases, becoming positive by load path D for the PVC-polyester fabrics (Figure 4-4 & Figure 4-9 to Figure 4-12). The balance of crimp gradually shifts as the stress ratio changes.

Load path E. A transition point is reached when the level of crimp is more or less balanced and hence the warp and fill strains are both low.

It may be expected that this would occur around load path D, for which the warp to fill stress ratio is approximately 1:1. In fact, the crimp transition zone can be seen in the load path E results for all fabrics tested, with a warp:fill stress ratio that varies between 1.5:1 at low load to 1.7:1 at maximum load. This transition point, where for a given stress ratio no crimp interchange occurs, is called the *natural stress ratio*. When biaxial load is applied to a fabric *"there exists a load ratio at which no crimp interchange is generated"* (MSAJ/M-02-1995). The natural stress ratio is not necessarily constant for a given fabric as it may vary with stress magnitude. During a test it is difficult to ascertain whether strain is occurring due to crimp interchange or yarn tensile extension. A more workable definition of the natural stress ratio is the *stress ratio which results in minimum strain in both warp and fill directions*. Minimum strain refers to minimum absolute values of strain, with negative and positive strain being kept to a minimum. Because crimp interchange results in large strains at low load, minimising fabric strain should minimise crimp interchange.

The fabric response at stress ratios close to the natural ratio is highly non-linear. Small changes in load ratio result in a change in the crimp configuration that gives large variations in strain levels and stress-strain gradient (Figure 4-3 to Figure 4-12, compare load paths D and F). The fabric is considerably stiffer in this crimp transition zone than for other stress ratios. Particularly for PTFE-glass fabrics, the yarn tensile extension is low at test loads, and the majority of fabric strain is the result of crimp interchange. In

the crimp transition zone the level of crimp interchange is minimal and the strain levels are low. For example, the adjusted results for Taconic Solus 1120 PTFE-glass (Figure 4-5) give maximum strains in warp and fill directions of around 0.7% for load path E, with strains at maximum load (25% UTS) of only 0.1%. This suggests that the stress ratio at high load (1.7:1) is very close to the conditioned natural stress ratio for the fabric. These strains are extremely low given the strain ranges of -7% to 6% (fill, load path G and A respectively) and -5% to 2% (warp, load path A and G). For typical biaxial tests carried out at a limited number of stress ratios (e.g. 5:1, 2:1, 1:1, 1:2 and 1:5) this behaviour at 1.5 to 1.7:1 might not be apparent.

Load paths F – G. Beyond the crimp transition zone the warp stress dominates the fabric response. Straightening of the warp yarns gives a positive warp stress-strain gradient, and a negative fill gradient due to crimp interchange.

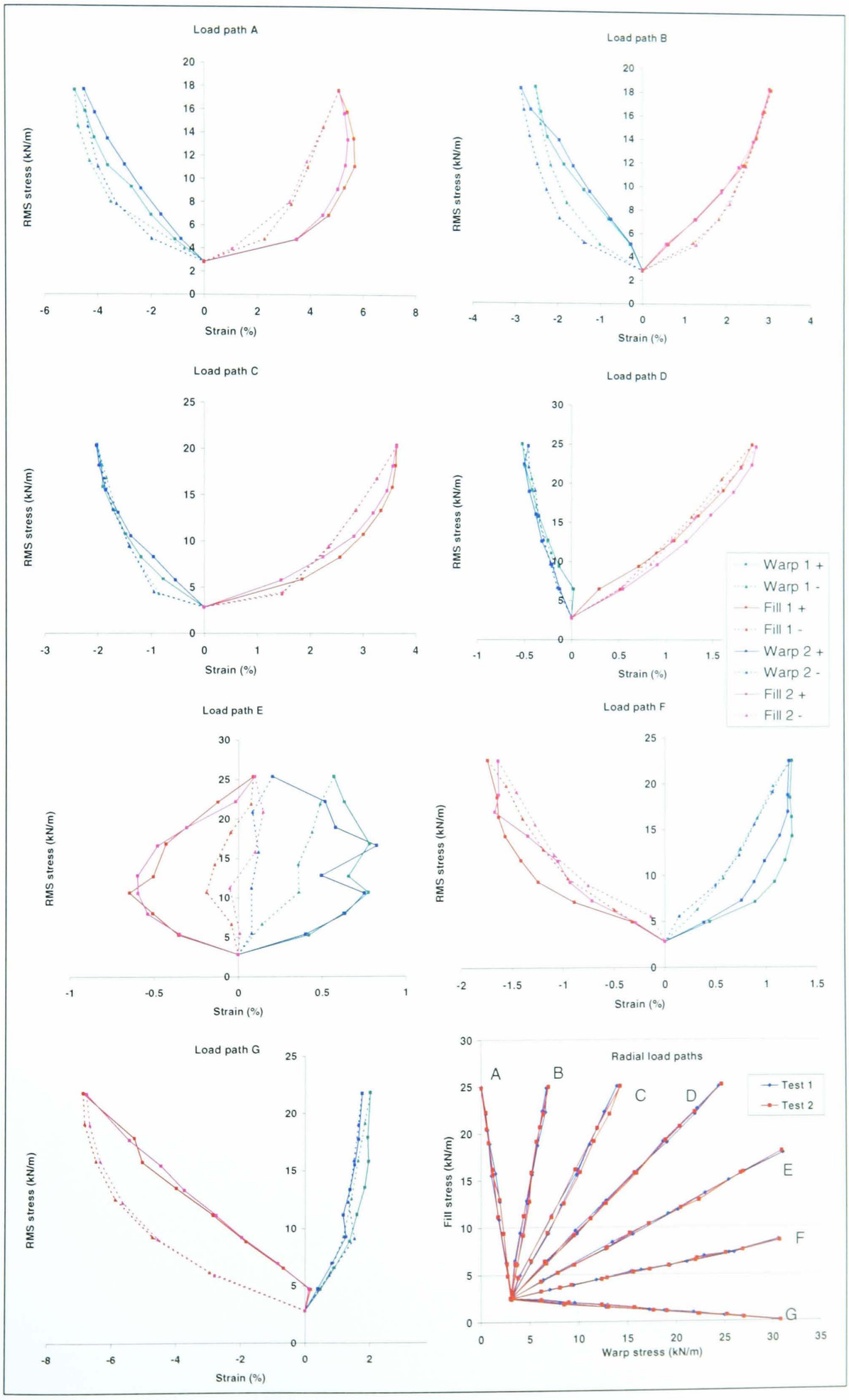

Figure 4-5. Stress-strain curves, Taconic Solus 1120, PTFE/glass

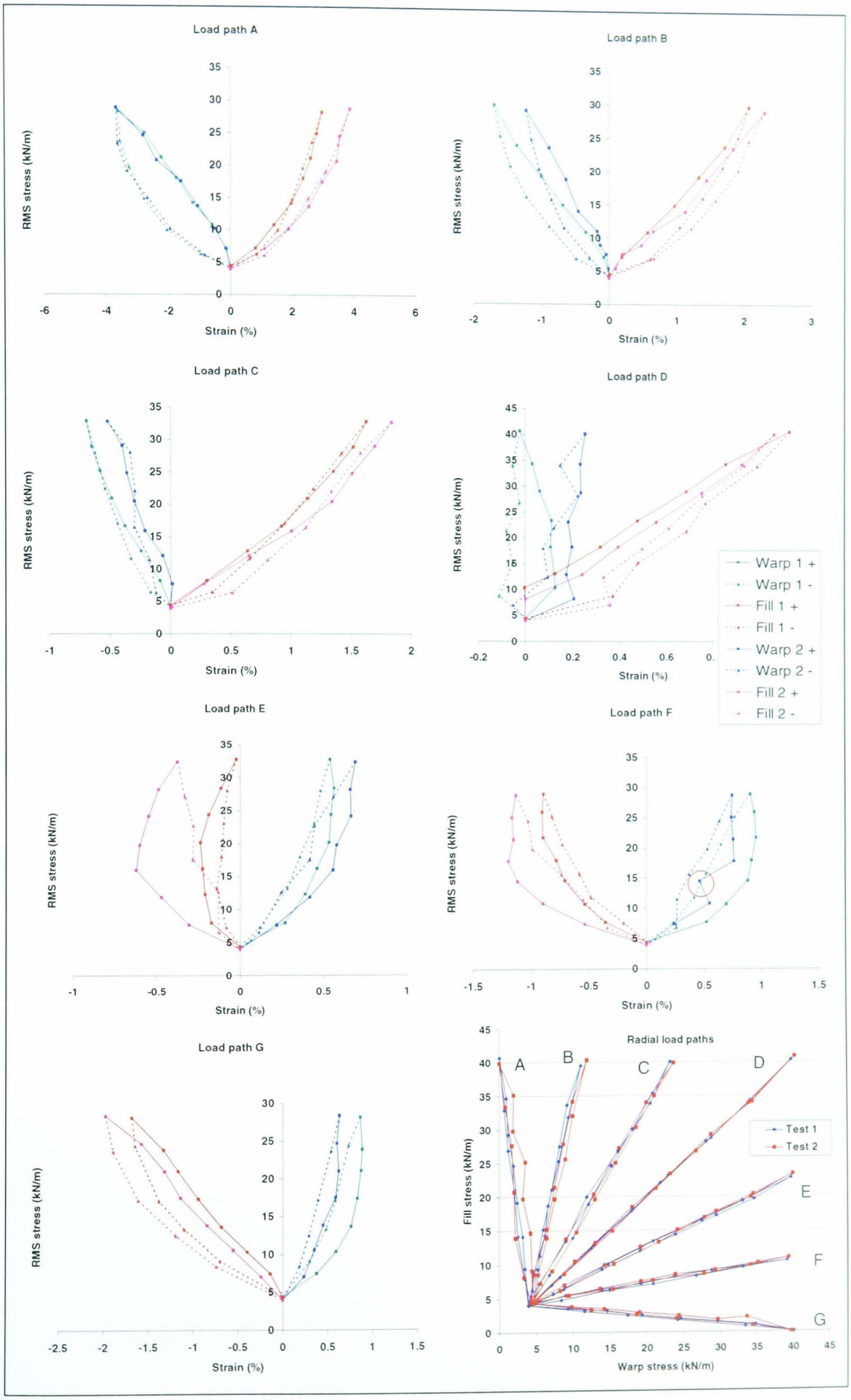

Figure 4-6. Stress-strain curves, Taconic Solus 1410, PTFE/glass

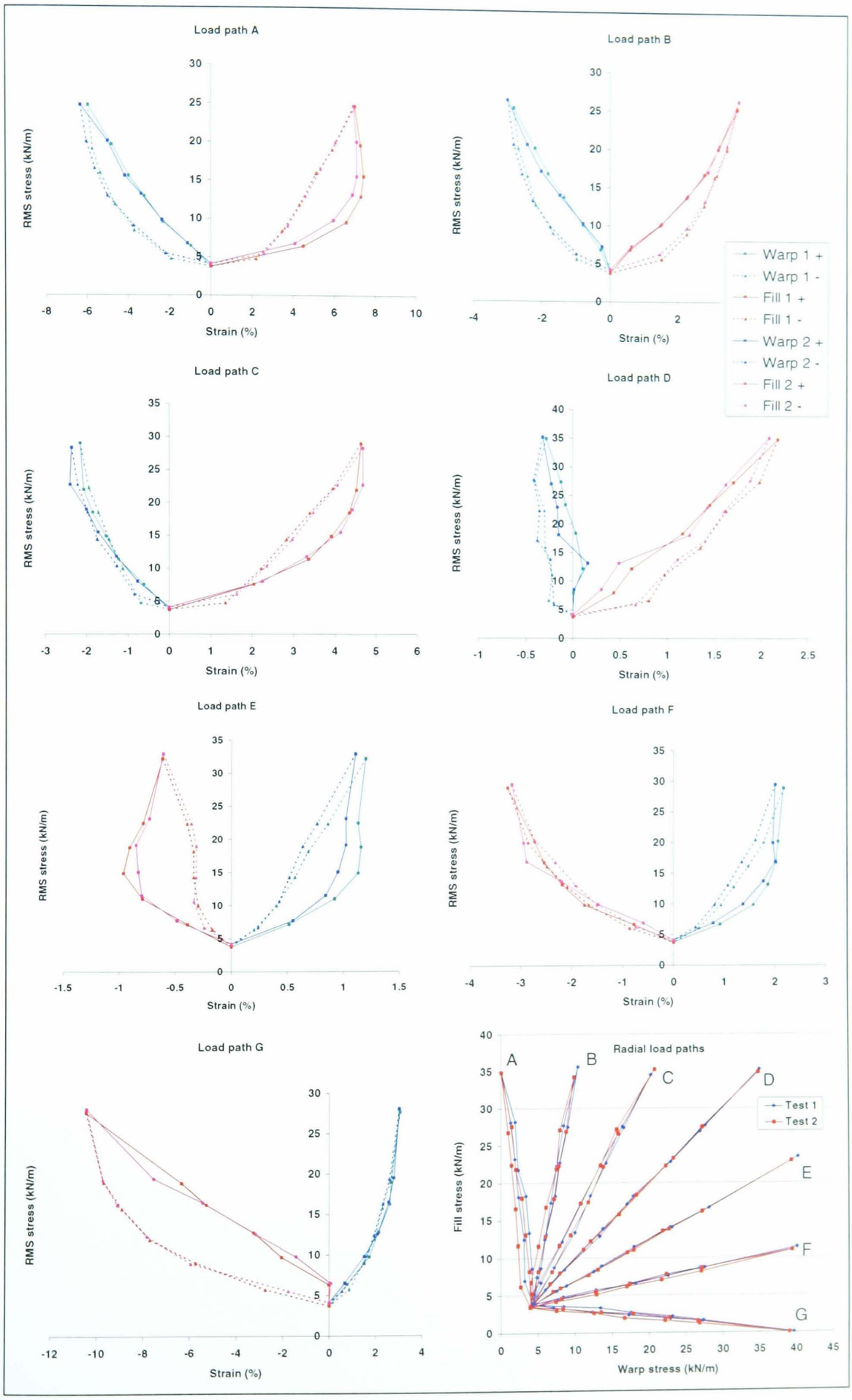

Figure 4-7. Stress-strain curves, Verseidag B18059, PTFE/glass

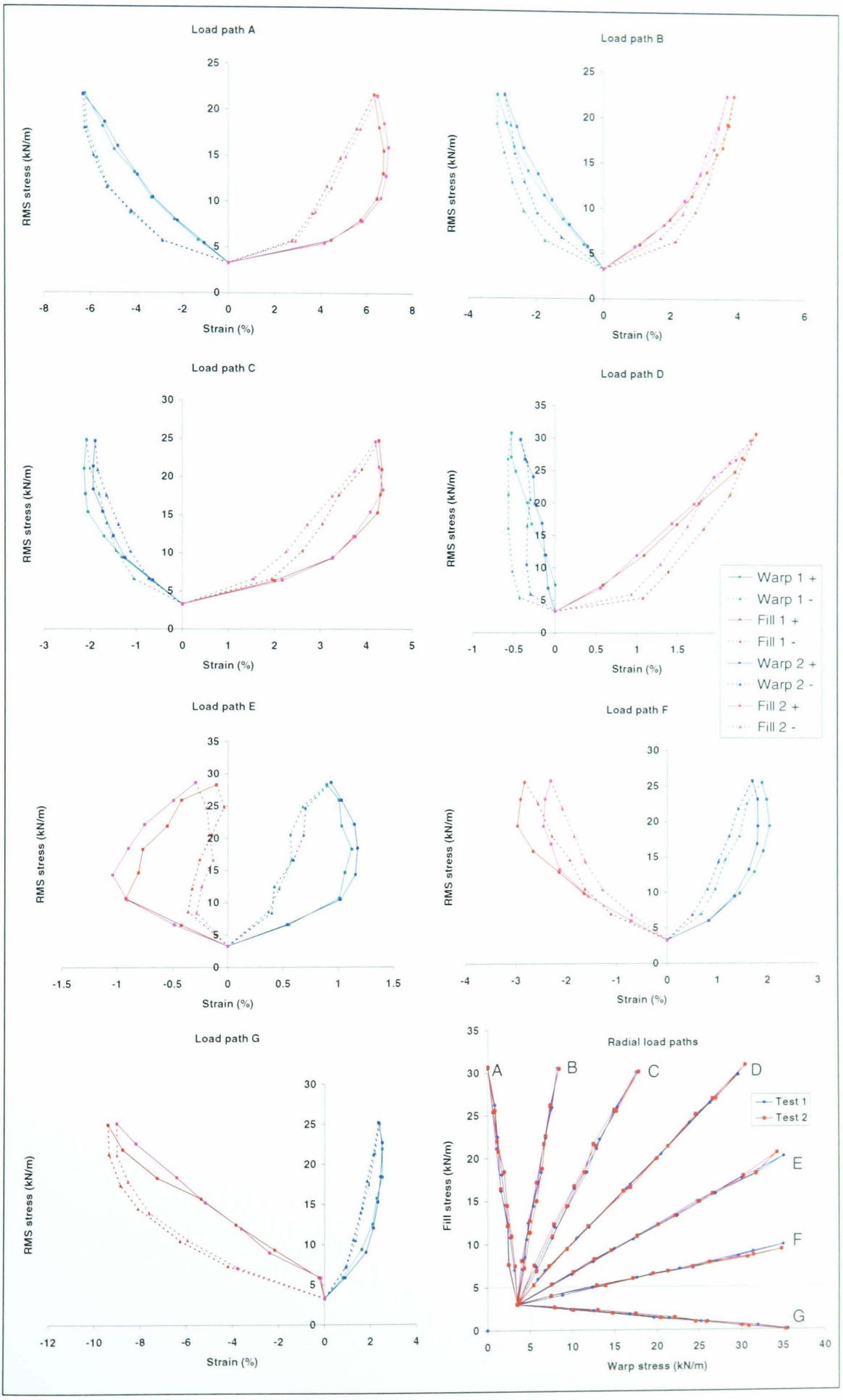

Figure 4-8. Stress-strain curves, Verseidag B18089, PTFE/glass

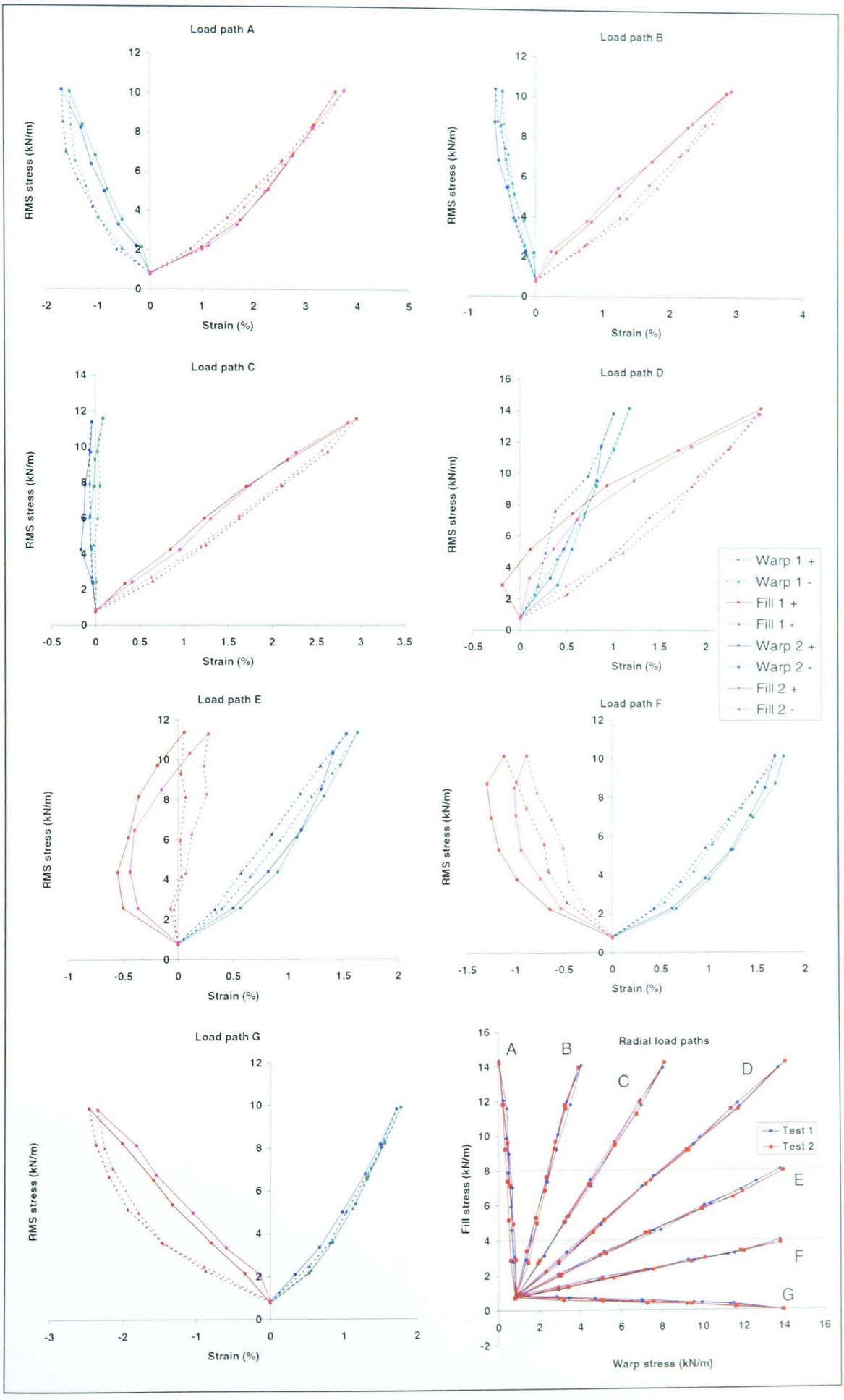

Figure 4-9. Stress-strain curves, Ferrari 702T, PVC/polyester

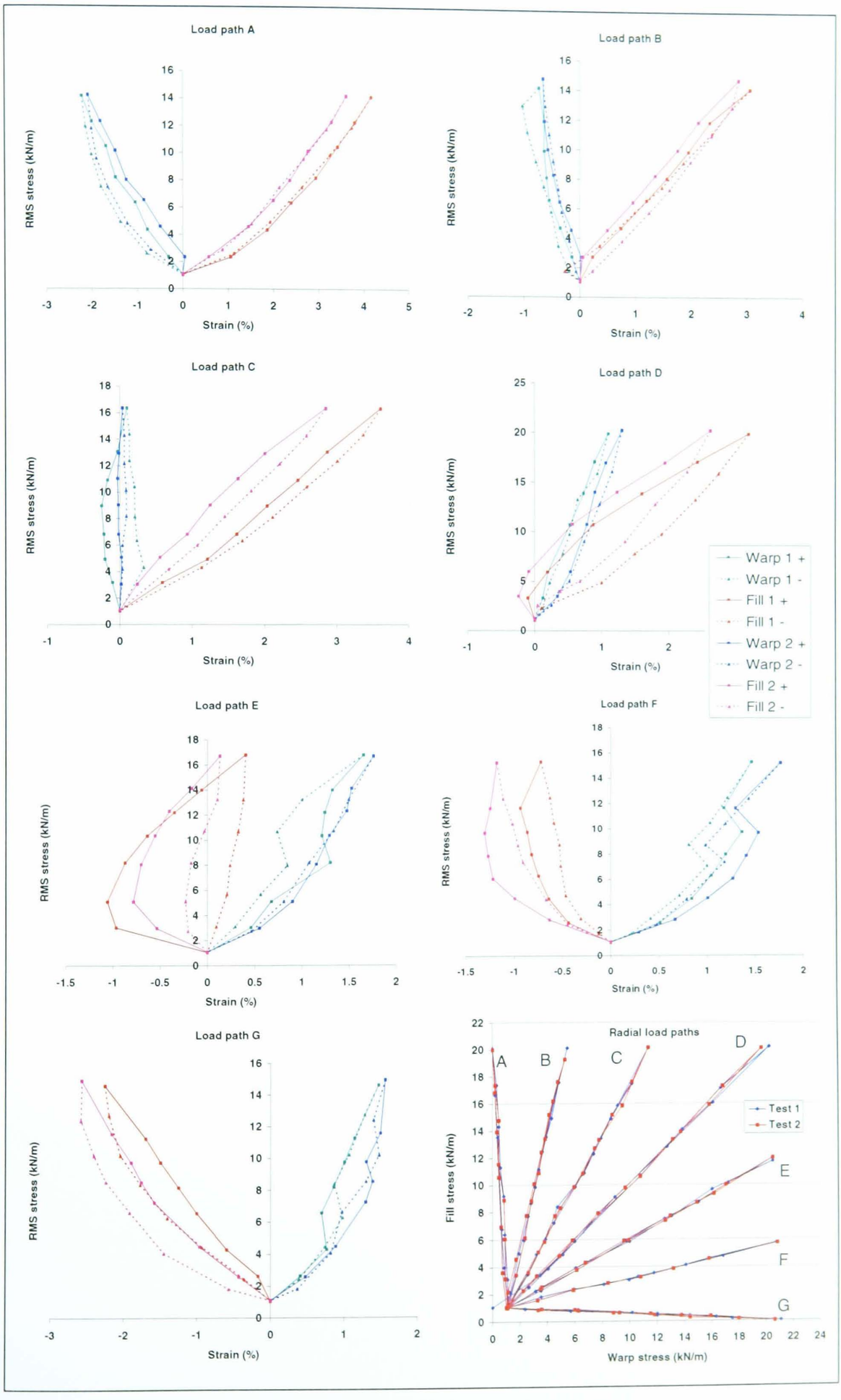

Figure 4-10. Stress-strain curves, Ferrari 1002T, PVC/polyester

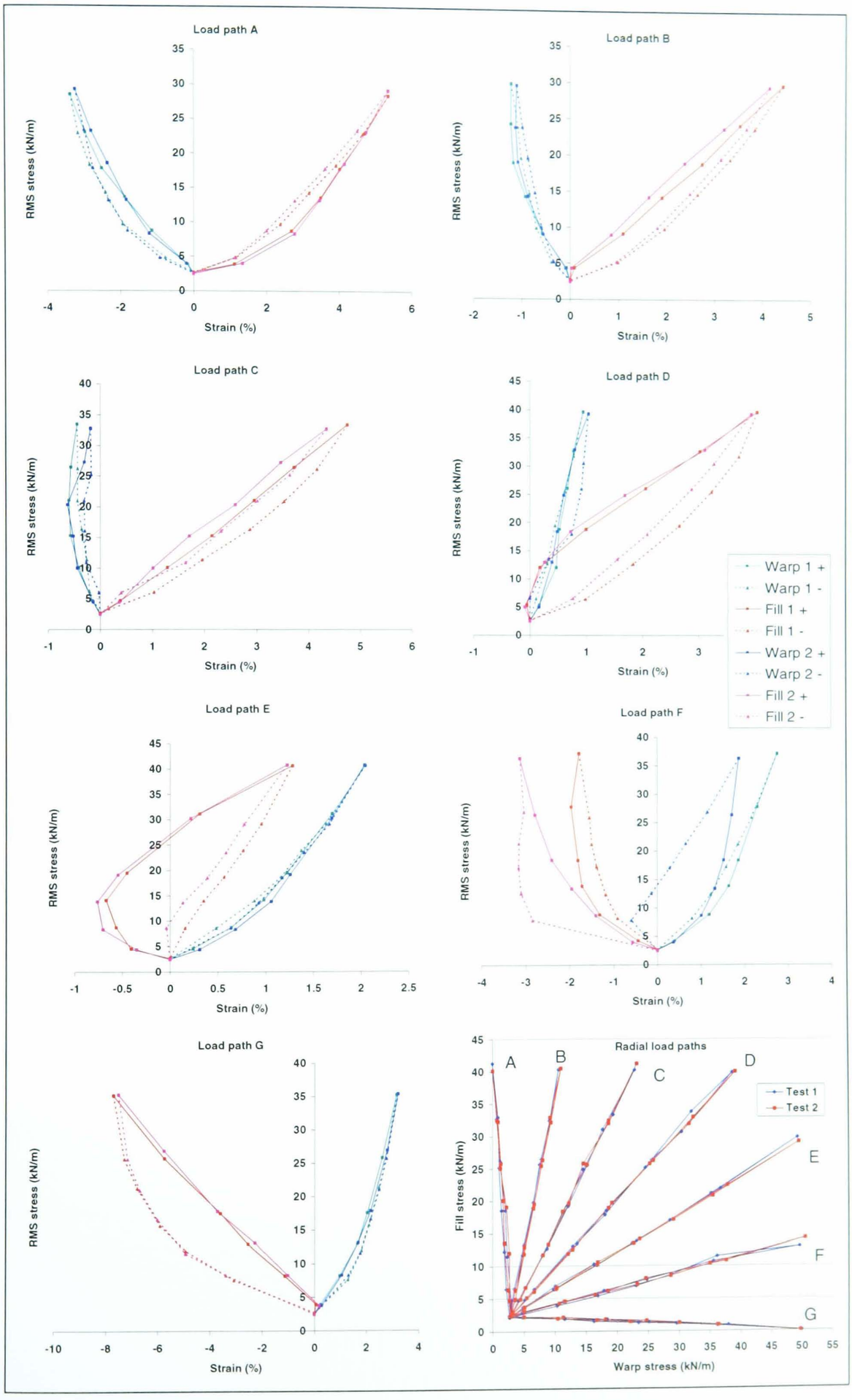

Figure 4-11. Stress-strain curves, Ferrari 1502T, PVC/polyester

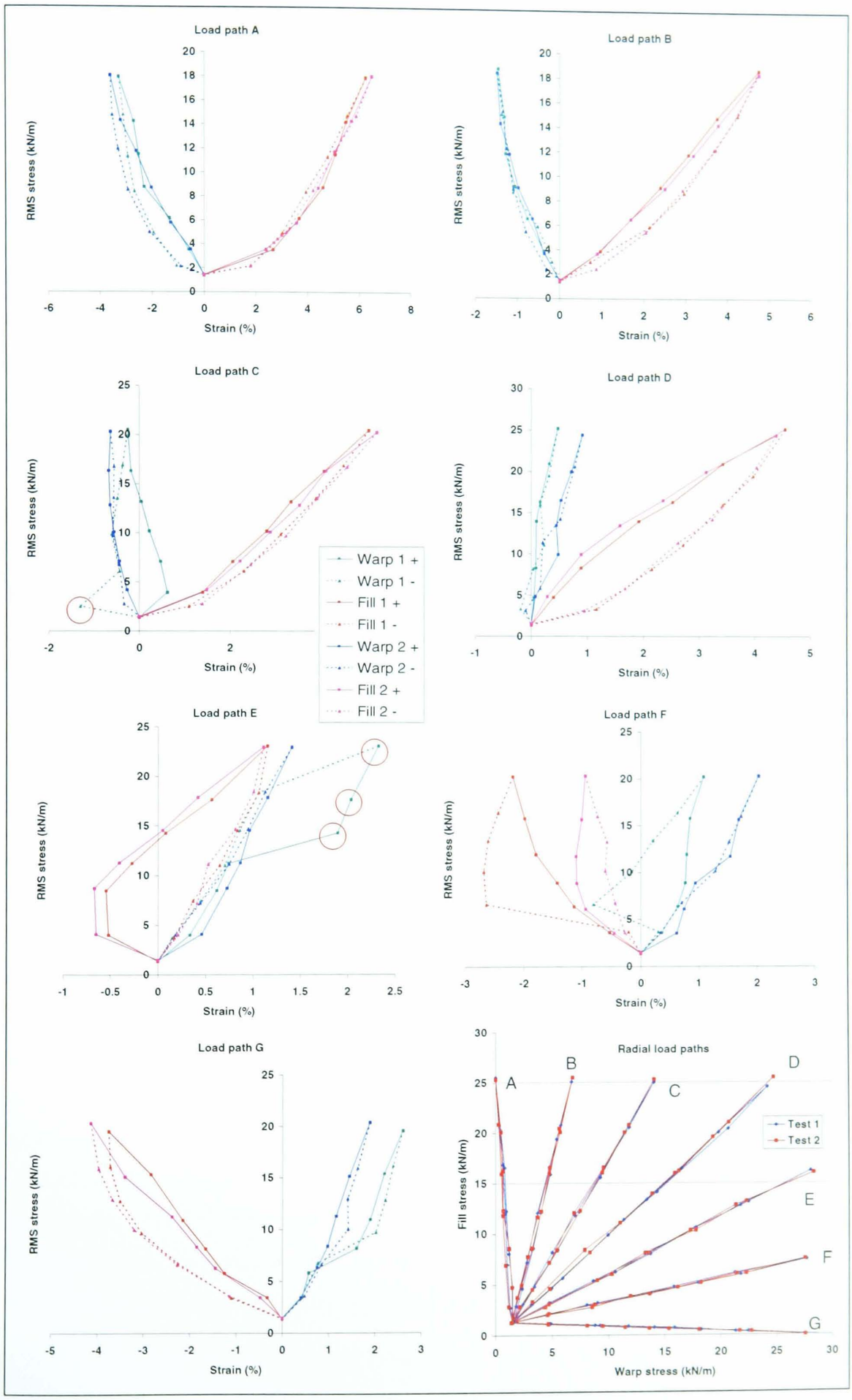

Figure 4-12. Stress-strain curves, Verseidag B6853, PVC/polyester

When seen in isolation, stress-strain plots for some load paths suggest that the fabric response is essentially linear (e.g. Figure 4-5, load path D; Figure 4-9 load paths B, C and G). This highlights the risk of testing at a limited number of stress ratios, which may suggest that the fabric response can be approximated with a linear or bi-linear function. This may be true for each individual stress ratio, but the fabric behaviour at the transition between these stress ratios will not be captured. The complete stress-stress-strain response can be better understood using a response surface representation (§4.1.2).

The loading and unloading curves demonstrate the complex hysteretic behaviour of the fabric. When trying to understand the hysteretic response it is necessary to look at the adjusted results (e.g. Figure 4-3 & Figure 4-4) in conjunction with the actual strain values (Figure 4-1 & Figure 4-2). The hysteresis curves are quite straightforward to explain for the original strain values; the unloading strain lags behind the loading strain for a given applied load. If the strain increases with increasing load, then the unloading strain is greater than the loading strain (e.g. Figure 4-1, load path A, fill). Conversely, when the strain decreases on loading, the unloading strain is less than the loading strain (e.g. Figure 4-1, load path A, warp). The level of hysteresis is small for PTFE-glass fabrics compared to the large strain variations for PVC-polyester. This is easily understood by considering the material properties: glass fibres are essentially linear elastic with minimal hysteresis, polyester fibres are highly hysteretic with large differences between loading and unloading response (§2.1.1).

The loading and unloading behaviour appears to be more complex once the residual strain has been removed (e.g. Figure 4-3 & Figure 4-4). The unloading curve can be to the left or right of the loading curve, and for some stress ratios the loading and unloading curves are virtually coincident. This is simply a question of what proportion of the fabric strain is elastic for each load path. With little residual strain (e.g. Figure 4-1, load path B and D, fill) the adjusted values are very similar to the raw data. With higher levels of residual strain (e.g. Figure 4-2, load path A and C, fill) the hysteresis loop is reversed. The exact shape of the hysteresis loop is not as important as the level of hysteresis. For some load paths the difference between loading and unloading strain is high: for example up to 3.5% with a strain range of 7% (Figure 4-3, load path G, fill) or up to 3% with a strain range of 8% (Figure 4-11, load path G, fill). The variation between loading and unloading strains varies from zero to 50% of the strain range. This is very significant for the characterisation of the fabric and for understanding the variability of the fabric response (§6.2.6 & 6.2.8). Because the fabric is conditioned these variations in loading and unloading response are not due to initial effects such as the 'bedding down' of yarns and local de-lamination of the coating. The variations are medium to long term properties of the fabric response, caused by the constituent material properties and possibly by gradual recovery of the coiled yarn structure (§2.1).

There are several anomalous points on the test data graphs. Because the correlation between the two tests on each fabric is typically very good, it is often clear when a particular data point is erroneous. The potentially outlying points have been identified by inspection as insufficient data (two sets for each fabric) was available to statistically check for outliers. Data points which are deemed to be erroneous are

circled in red on the graphs (e.g. Figure 4-12, load path C, warp). Because of the subjective nature of the selection of the erroneous points they have not been removed from the test data for the purposes of comparison (e.g. between loading and unloading behaviour, and between repeat tests). The comparisons given are for all data points, and so represent the worst case. Occasional strain measurement errors may have occurred due to the laser beam being reflected back to the extensometer from the fabric surface. This was particularly problematic for PTFE-glass fibre fabrics, and led to a non-reflective surface (a piece of paper) being placed on the cruciform between the reflective strips to reduce reflections from the fabric. The manual hydraulic control system used for this research was very sensitive and care was required to avoid suddenly increasing the load on the fabric. Rapid loading would give a different stress-strain response to the gradual load increments specified by the test protocol (§6.2.1).

4.1.2 Response surface representation

The test protocol proposed in this research (§3.3.4) effectively quantifies the biaxial stress-strain behaviour of coated woven fabrics for all feasible stress states up to the maximum design stress. More accurately this should be described as the *stress-stress-strain-strain* behaviour. Each data point consists of four values: warp stress, fill stress, warp strain, fill strain. Ideally a representation in four dimensional space (perhaps using a hypercube as the basis for the axes?) would fully encapsulate the test data. Given the limitation of two-dimensional media, two three-dimensional surfaces have been used, enabling all of the data for each test to be plotted on one graph (Figure 4-13).

Response surfaces allow test data for *all feasible stress-states* to be represented on one graph. The lower bounds of the surface (x and y axes) are absolute as the compression stiffness of architectural fabrics is negligible, hence significant compressive stresses do not occur. The upper limits of the surface are bounded by the maximum design load, assumed to be 25% UTS (§3.3.3.2). This is sufficient for all stress states that will be encountered using current design principles.

The stress-stress-strain surface representation enables visualisation of the complete data set and hence provides a better understanding of the fabric behaviour. The stress-strain graphs (Figure 4-3 to Figure 4-12) show that initial high levels of strain at low load give way to stiffer fabric behaviour when crimp interchange is complete. However, response surfaces are required to see how the response changes as the load changes from, for example, high warp/low fill to low warp/high fill. Surface representations also provide the means to comprehensively assess the validity of predictive models (Chapter 5).

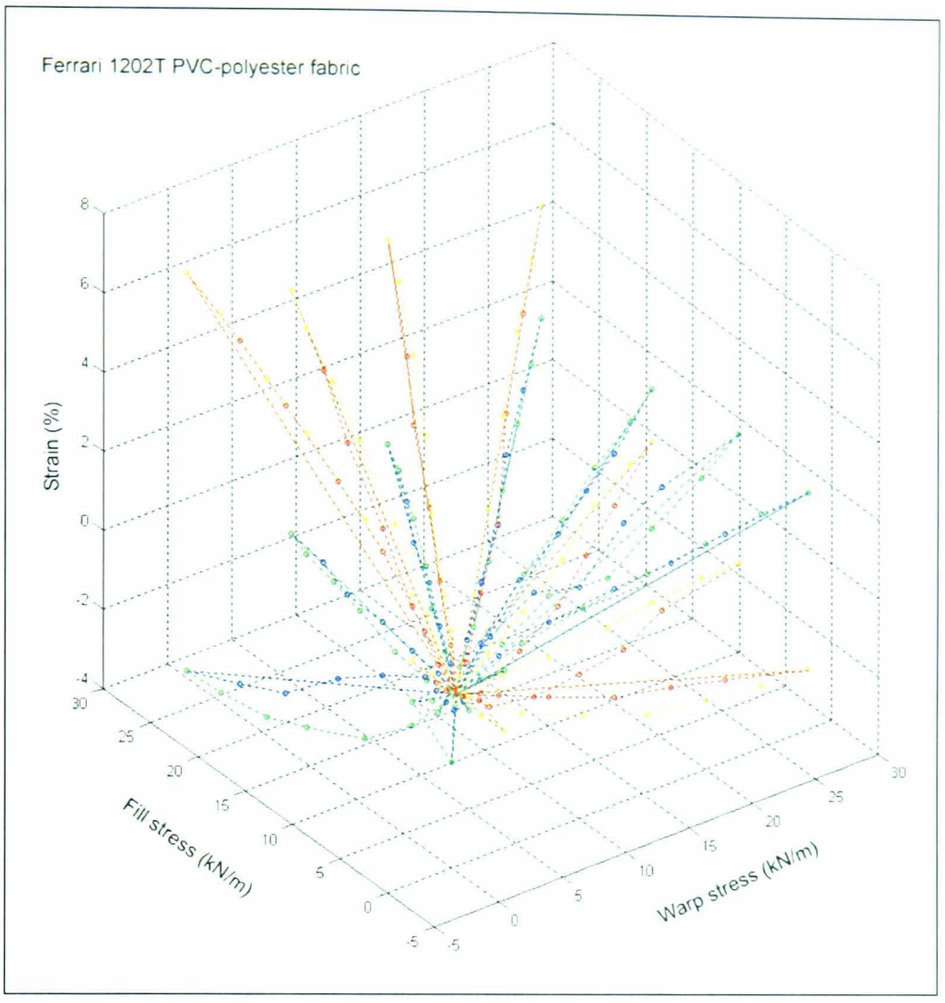

Figure 4-13. Test data plotted on stress-stress-strain axes, Ferrari 1202T PVC-polyester

Minami et al (1997) joined biaxial test curves at several stress ratios to form response surfaces in the stress-stress-strain space (§2.3.3). This concept has been applied to the test data: a facetted surface has been generated in *Matlab* passing through all of the test points (Figure 4-14 & Figure 4-15). The test protocol provides loading and unloading data, hence two surfaces are plotted for each fabric axis (warp and fill). The surface should pass through all data points, but there are data points around the edge which are not interpolated by the surface. This is due to difficulties in defining the limits of the surface. The surface has straight sides (aligned with the axes) in the x-y plane; if all of the scattered data points were included in the surface then some extrapolation would be necessary. To avoid this the *Matlab* function which defines the surface misses some points at the extremes of the data set. However, the surface is sufficient for visualising the test data. For implementation in structural analysis use of all data points is required (§4.2.3).

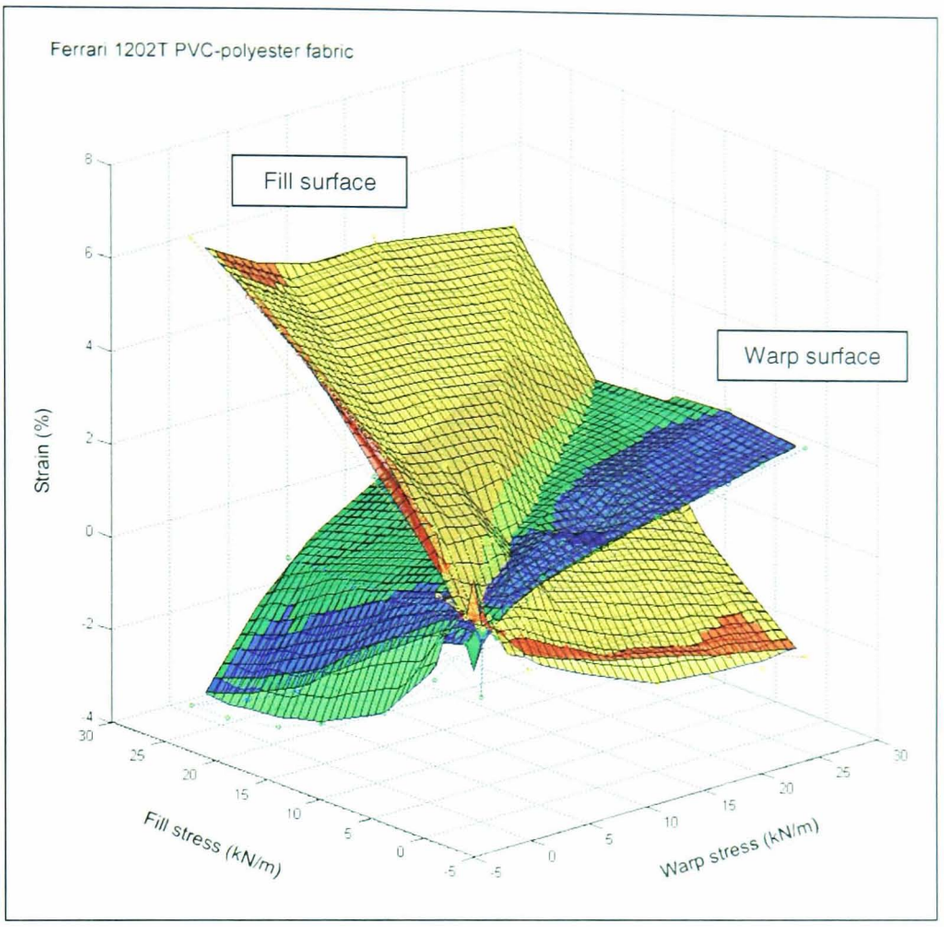

Figure 4-14. Surface representation of loading and unloading data, Ferrari 1202T PVC-polyester

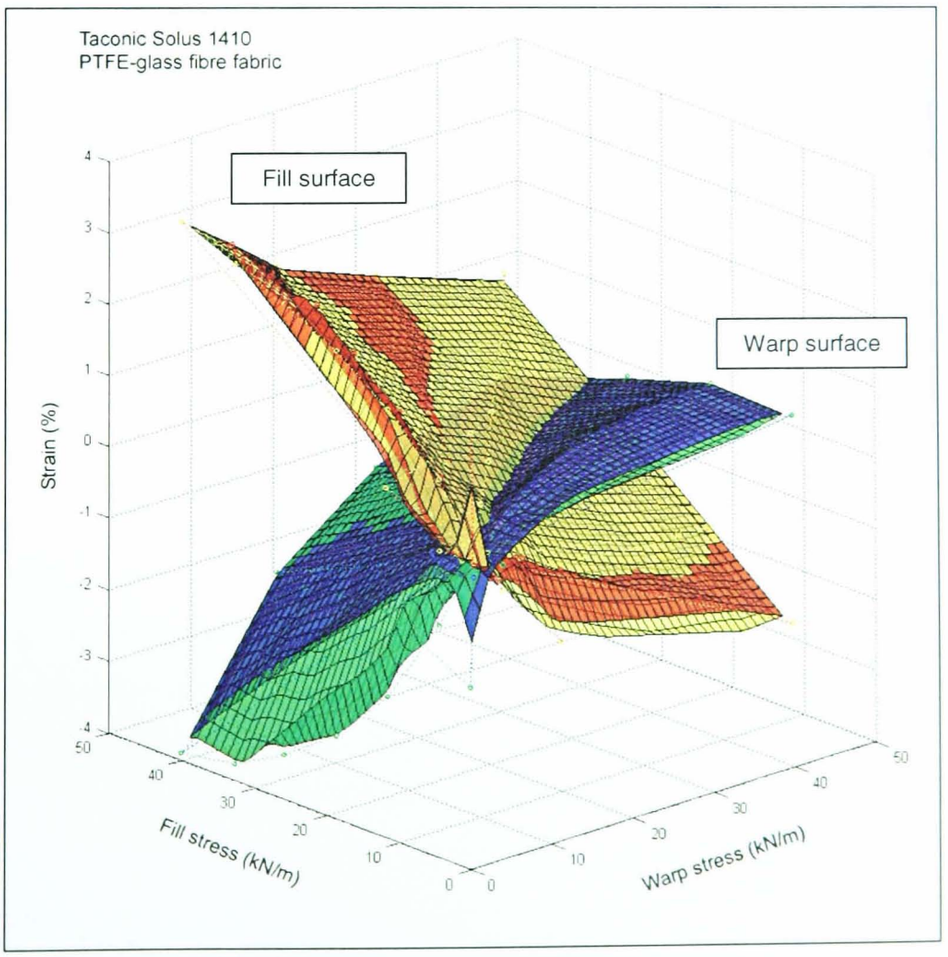

Figure 4-15. Surface representation of loading and unloading data, Taconic Solus 1410 PTFE-glass

Loading and unloading surfaces could be used as the upper and lower bounds of the fabric response, but neither consistently provides higher or lower values for a given stress state. It would be better to 'drop' upper and lower bounding surfaces onto the whole data set. Multiple sets of test data could be combined to define these upper and lower bounds. Alternatively, and more readily applicable to structural analysis, a mean surface can be used (Figure 4-16 & Figure 4-17) with the deviation of the loading and unloading data points from the mean providing a measure of confidence in the results (Table 4-1). This is appropriate as the measurement of loading and unloading data points has been included in the test protocol to give an indication of the variability due to recent load history (§3.3.3). Any real load event (e.g. a gust of wind) will give a complex load history dependent on wind direction, duration, canopy shape, etc. The loading and unloading results should be seen as the expected variability during any analysis. The difference of the two curves from their mean is given as the standard deviation of the data-set, which is the root-mean-square deviation of the data points from their mean. The level of deviation of the data points from the mean surface is fairly consistent for all fabrics, but the values are different for PVC-polyester and PTFE-glass and in warp and fill directions (Table 4-1). Calculating the deviation as a percentage of the strain range gives a better idea of the significance of the variation. The mean deviations in warp and fill directions are 2.2 and 2.8% of the strain range, giving a range of values of around 5% of the strain range. This suggests that the overall effect of recent load history is quite small, and that it may be reasonable to use the mean response surface in analysis.

This appears to be in stark contrast to the large differences (up to 100% of the measured strain) between loading and unloading curves discussed in section 4.1.1. Reasons for this apparent discrepancy are as follows:

1. The values given above are deviations from the mean surface, whereas in section 4.1.1 the differences quoted are between the loading and unloading curves.
2. The differences discussed in section 4.1.1 are maximums; those given in Table 4-1 are mean values for all stress states tested. The difference between the loading and unloading curves is always zero at the two extremes of the curve. At maximum load the curves meet at a single data point, at minimum load (i.e. prestress) the curves intersect because the strain at prestress is zero by definition for the adjusted data.
3. In section 4.1.1 the strain difference is compared to the strain values at a single point and it is seen that the difference is up to 100% of the measured strain. For example, if the loading and unloading strains are 1% and 2%, the difference is 1% which is 100% of the loading strain and 50% of the unloading strain). In Table 4-1 the strain differences are compared with the total strain range for the test, which results in the difference being expressed as a smaller proportion.

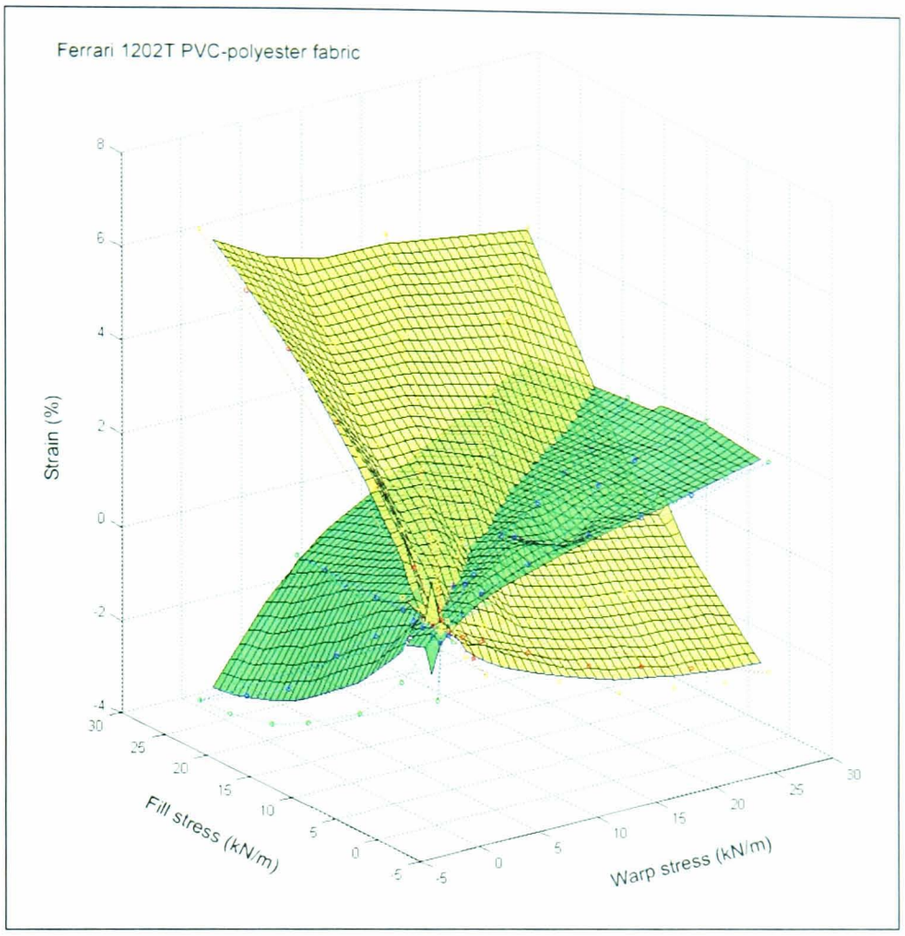

Figure 4-16. Mean surface, Ferrari 1202T PVC-polyester

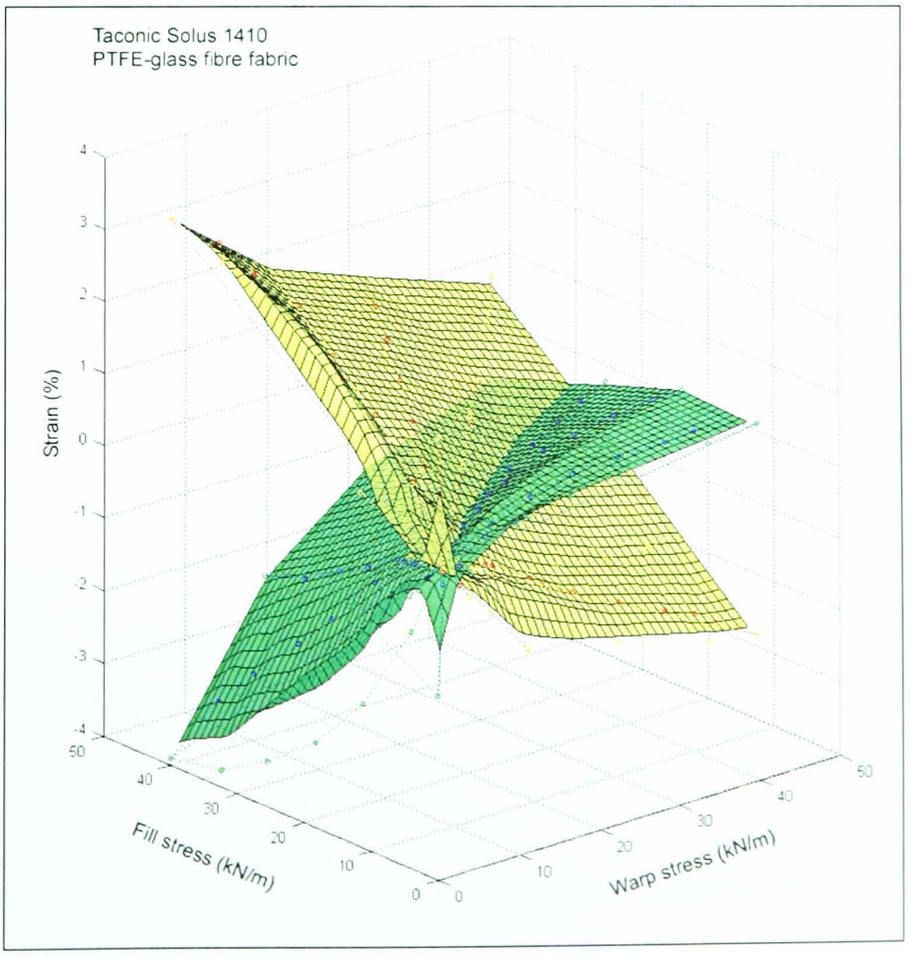

Figure 4-17. Mean surface, Taconic Solus 1410 PTFE-glass

Fabric	Material (Type†)	Combined standard deviation of loading & unloading surfaces from their mean (percentage strain)		Combined standard deviation of loading and unloading surfaces from their mean (percentage of the strain range)	
		Warp	Fill	Warp	Fill
Taconic Solus 1120	PTFE-glass (G5)	0.15	0.29	2.37	2.46
Taconic Solus 1300	PTFE-glass (G6)	0.13	0.31	2.40	2.67
Taconic Solus 1410	PTFE-glass (G7)	0.15	0.08	3.31	1.46
Verseidag B18059	PTFE-glass (G6)	0.19	0.43	2.11	2.51
Verseidag B18089	PTFE-glass (G6/G7)	0.21	0.38	2.53	2.43
Mean values for PTFE-glass		0.17	0.29	2.54	2.31
Ferrari 702T	PVC-polyester (I)	0.06	0.18	1.71	3.23
Ferrari 1002T	PVC-polyester (II)	0.07	0.22	1.98	3.63
Ferrari 1202T	PVC-polyester (III)	0.12	0.30	2.10	4.31
Ferrari 1502T	PVC-polyester (IV/V)	0.09	0.35	1.54	2.90
Verseidag B6853	PVC-polyester (III)	0.11	0.28	2.11	2.80
Mean values for PVC-polyester		0.09	0.27	1.89	3.37
Overall mean values		0.13	0.29	2.22	2.84

All values are for adjusted test data, i.e. with residual strain removed.

† For definition of fabric types see Chapter 2, §2.1.4.1, Figure 2-15

Table 4-1. Deviation of loading and unloading surfaces from their mean

The results of two tests on the same type of fabric can be compared by overlaying the mean response surfaces (Figure 4-18 & Figure 4-19) and subtracting one from the other (Figure 4-20 & Figure 4-21). The root-mean-square value of the difference between the surfaces gives an indication of the variability between tests (Figure 4-2).

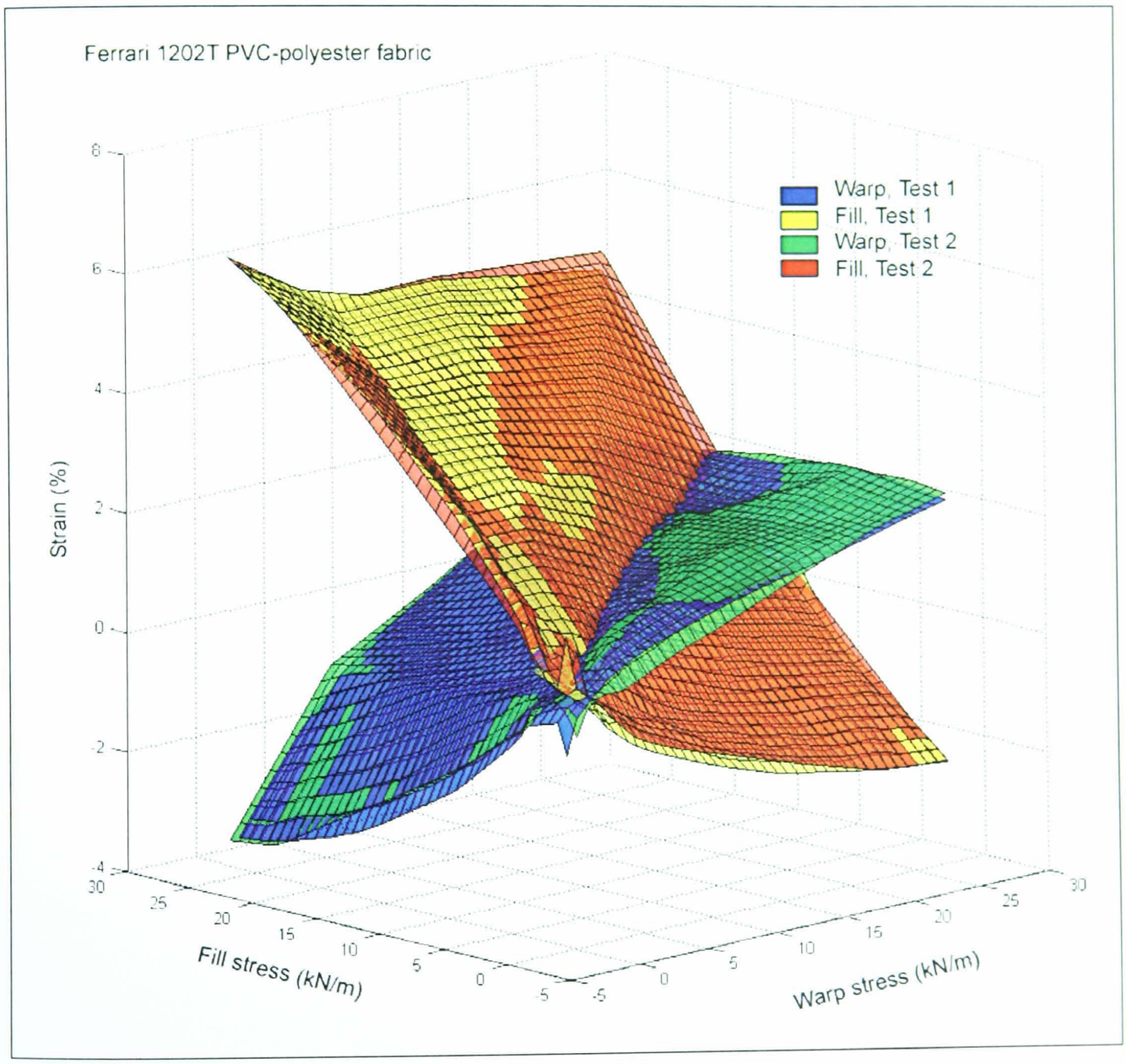

Figure 4-18. Comparison of repeat tests, Ferrari 1202T PVC-polyester

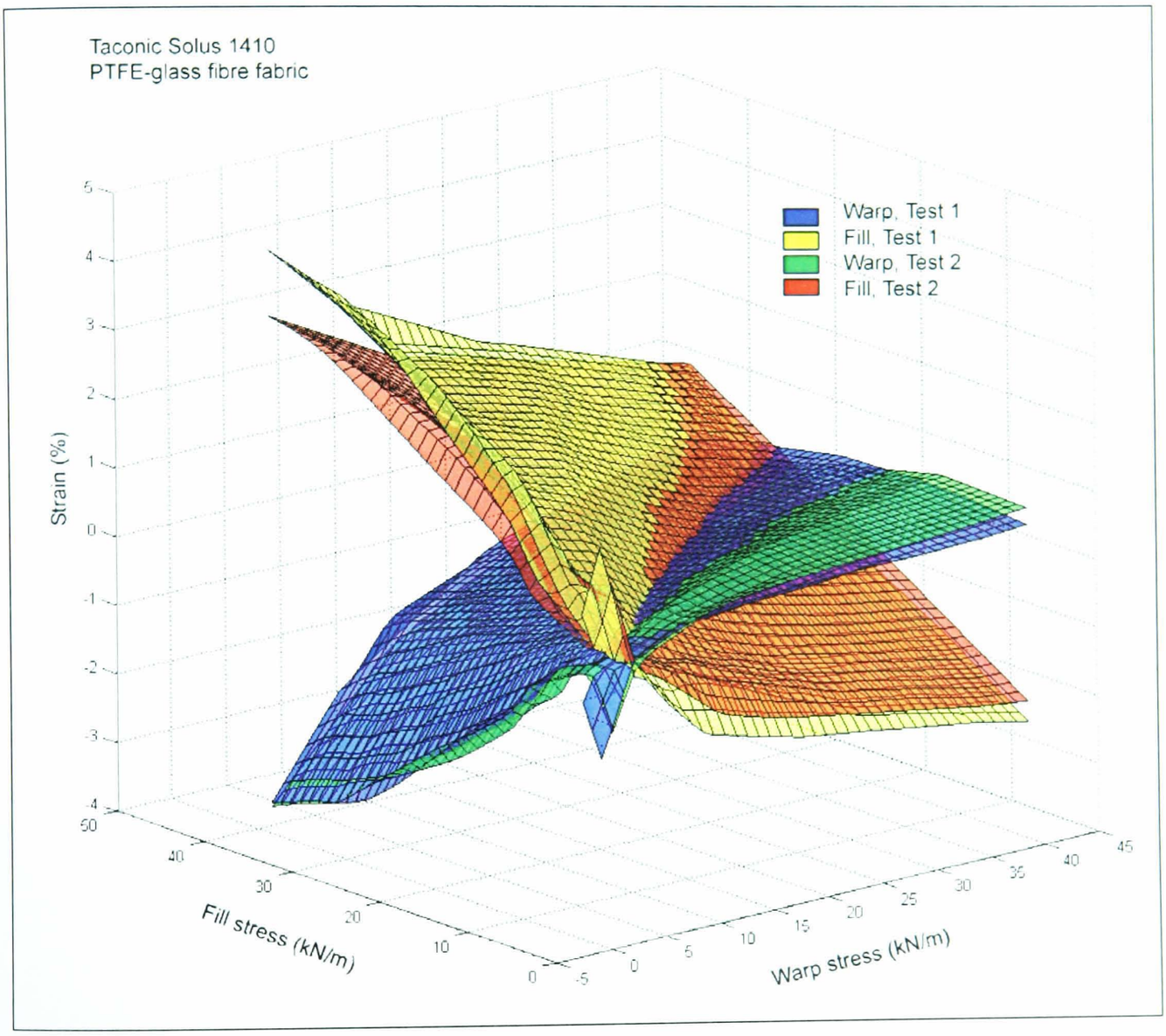

Figure 4-19. Comparison of repeat tests, Taconic Solus 1410 PTFE-glass

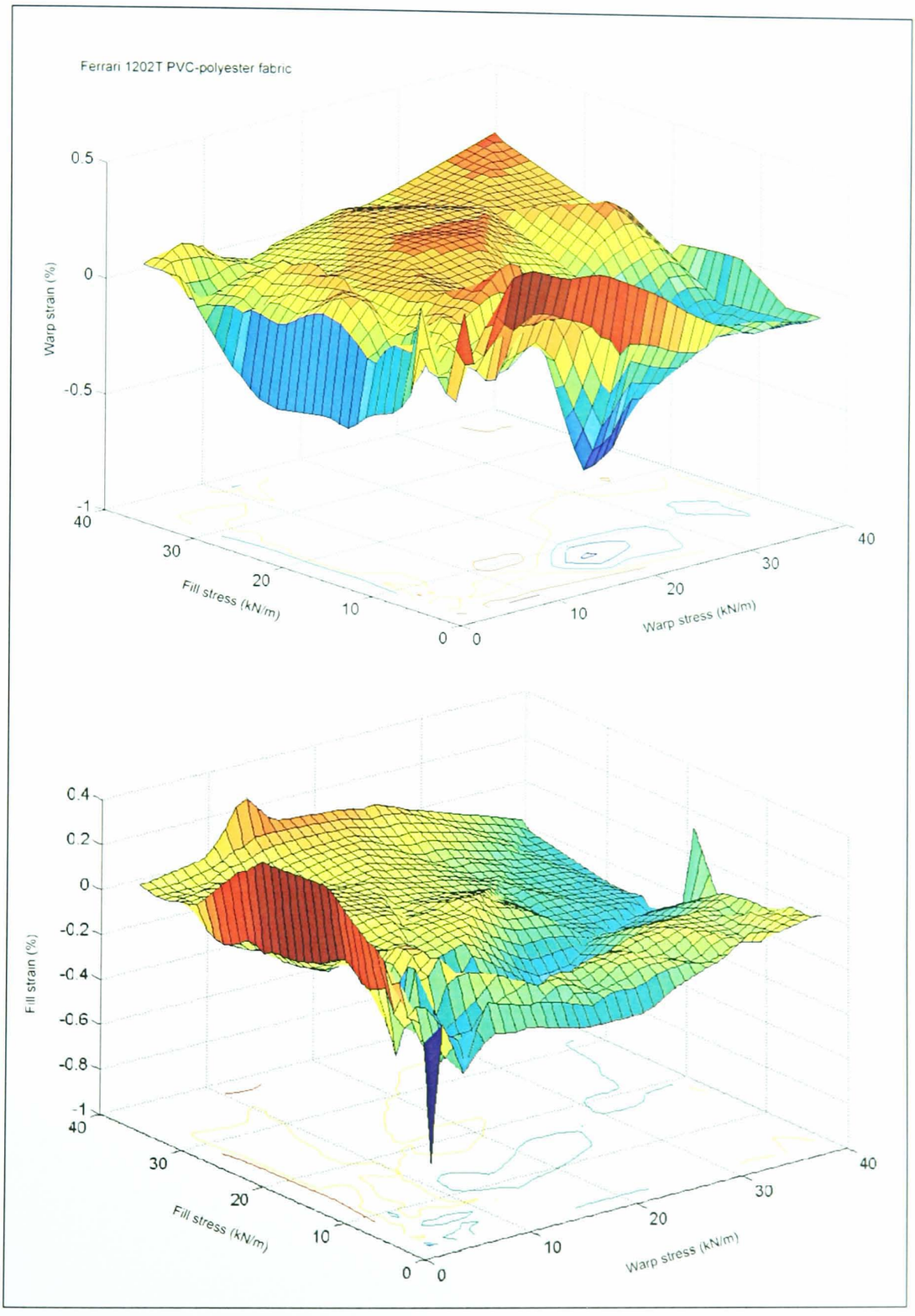

Figure 4-20. Repeat test difference surfaces, Ferrari 1202T PVC-polyester

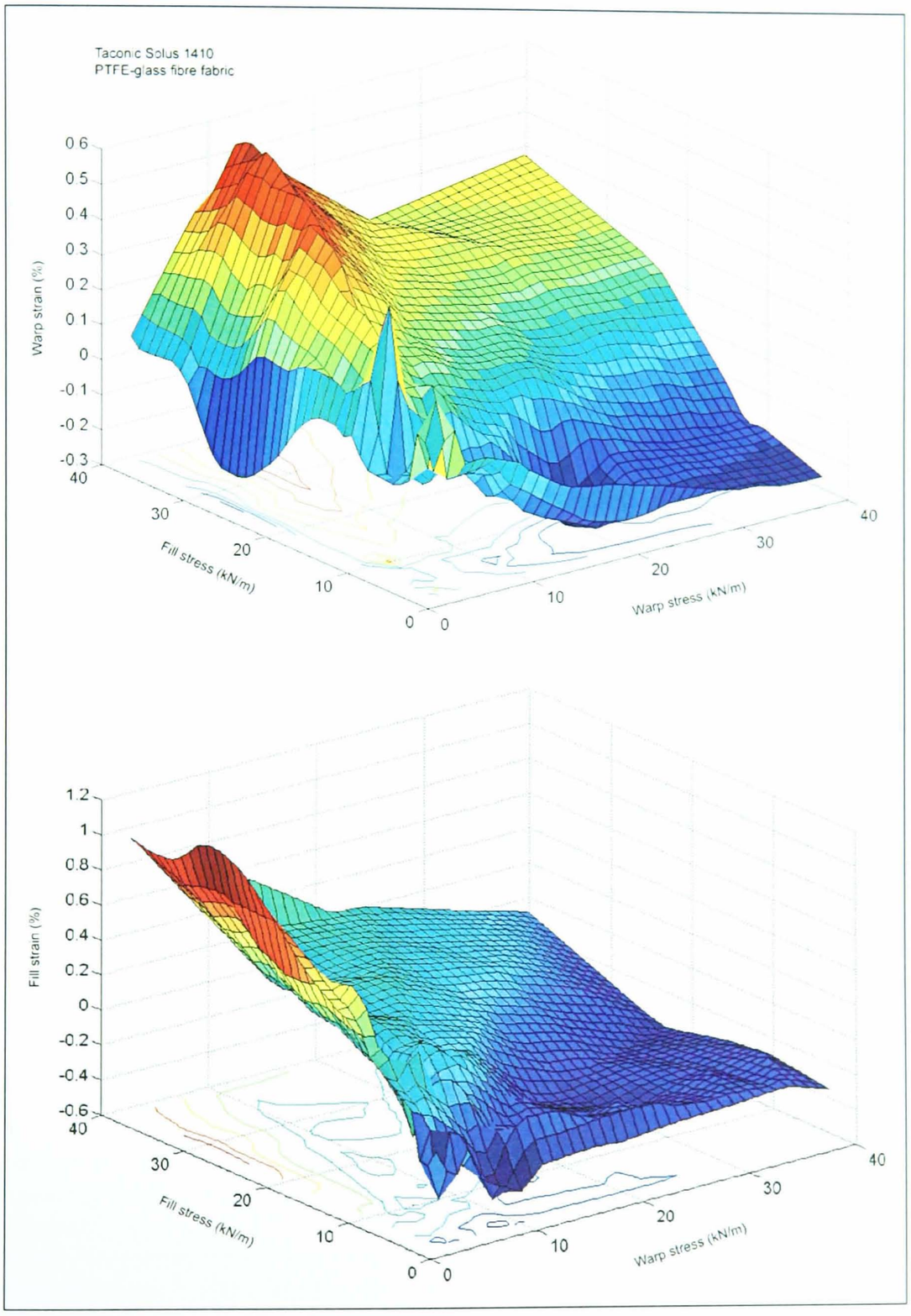

Figure 4-21. Repeat test difference surfaces, Taconic Solus 1410 PTFE-glass

Fabric	Material (Type†)	RMS difference between repeat tests (percentage strain)		RMS difference between repeat tests (percentage of the strain range)		Standard deviation of RMS difference between repeat tests (percentage of the strain range)	
		Warp	Fill	Warp	Fill	Warp	Fill
Taconic Solus 1120	PTFE-glass (G5)	0.13	0.09	2.11	0.79	1.92	0.70
Taconic Solus 1300	PTFE-glass (G6)	0.06	0.11	1.1	0.96	0.67	0.69
Taconic Solus 1410	PTFE-glass (G7)	0.21	0.24	4.79	4.82	4.12	4.81
Verseidag B18059	PTFE-glass (G6)	0.16	0.17	1.83	0.98	1.18	0.98
Verseidag B18089	PTFE-glass (G6/G7)	0.15	0.20	1.70	1.27	1.50	1.26
Mean values for PTFE-glass		0.14	0.16	2.31	1.76	1.88	1.69
Ferrari 702T	PVC-polyester (I)	0.10	0.11	3.07	1.94	1.11	1.23
Ferrari 1002T	PVC-polyester (II)	0.19	0.44	5.25	7.19	2.45	2.93
Ferrari 1202T	PVC-polyester (III)	0.14	0.11	2.52	1.48	2.48	1.27
Ferrari 1502T	PVC-polyester (IV/V)	0.29	0.45	4.75	3.67	4.62	2.26
Verseidag B6853	PVC-polyester (III)	0.34	0.39	6.37	3.92	6.37	3.50
Mean values for PVC-polyester		0.21	0.30	4.39	3.64	3.41	2.24
Overall mean values		0.18	0.24	3.35	2.70	2.64	1.96

All values are for adjusted test data, i.e. with residual strain removed.

† For definition of fabric types see Chapter 2, §2.1.4.1, Figure 2-15

Table 4-2. Difference between repeat tests

With only two tests carried out on each fabric, the results in Table 4-2 cannot be taken as a conclusive measure of fabric variability. However, the values do provide a general idea of the level of variability and show some broad trends. Overall, PTFE-glass fibre fabrics give slightly more consistent results than PVC-polyester; explained by the almost linear elastic tensile properties of glass fibres, coupled with the high tensile modulus which results in a large proportion of the fabric strain being due to crimp interchange – a predictable, repeatable mechanism. The mean level of variability between tests for all fabrics is small: the difference between repeat tests being similar to the difference between loading and unloading results. Any further deductions would be speculative: extensive testing is required to establish the statistical distribution of fabric properties for a particular fabric type, batch or roll (§6.2.8).

4.1.3 Creep & recovery

Most of the results discussed above (§4.1.1 & §4.1.2) have been presented with residual strain removed, such that the strain at prestress is deemed to be zero throughout the test. This is valid for calculating the load-extension behaviour of the fabric. However, for patterning, installation and design of provision for re-tensioning, the actual levels of strain are required. Analysis of the levels of residual strain during the course of a test gives an indication of the expected in-service fabric strains.

The biaxial test protocol provides frequent measures of the strain at prestress; Table 4-3 provides values at three stages of the test. Prestress values used in these tests (§3.3.3.2) are,

PVC-polyester: 0.13 x strip ultimate tensile strength (**BS EN ISO 1421:1998**),

PTFE-glass: 0.25 x strip ultimate tensile strength (**BS EN ISO 1421:1998**),

with fabric strengths from manufacturers' data sheets.

Fabric	Material (Type†)	Sample number	Approximately 17 hours at prestress		After three conditioning cycles		After test (after 5 minutes at prestress)	
			Warp strain (%)	Fill strain (%)	Warp strain (%)	Fill strain (%)	Warp strain (%)	Fill strain (%)
Taconic Solus 1120	PTFE-glass (G5)	023	1.44	-0.29	-0.33	6.39	0.57	5.41
		024	1.04	-0.15	-0.93	6.19	0.27	5.47
Taconic Solus 1300	PTFE-glass (G6)	042	0.07	2.04	-1.49	12.20	-0.45	10.87
		043‡	-	-	-1.18	10.87	-0.33	9.50
Taconic Solus 1410	PTFE-glass (G7)	013	0.57	1.74	-0.20	6.93	0.40	1.78
		014	0.96	0.84	0.14	4.79	0.70	4.22
Verseidag B18059	PTFE-glass (G6)	018	0.60	2.31	-1.26	13.88	0.45	11.61
		021	0.88	1.33	-0.81	13.66	0.87	11.59
Verseidag B18089	PTFE-glass (G6/7)	028	1.02	1.94	-1.19	13.69	-0.06	12.27
		029	1.15	2.85	-0.87	13.85	0.25	12.61
Ferrari 702T	PVC-polyester (I)	040	1.17	-0.76	1.12	1.79	1.88	1.14
		041	0.19	-1.85	0.22	0.50	0.94	-0.03
Ferrari 1002T	PVC-polyester (II)	002	1.31	-2.00	1.73	1.10	2.00	1.55
		004	0.44	-0.26	0.64	2.93	1.10	2.73
Ferrari 1202T	PVC-polyester (III)	037	1.41	-1.86	1.75	3.52	2.51	3.38
		038	1.48	-1.54	2.03	3.72	2.92	3.16
Ferrari 1502T	PVC-polyester (IV/V)	036	0.53	-4.15	1.10	0.55	2.10	-0.02
		037	1.41	-1.85	1.78	3.53	2.54	3.38
Verseidag B6853	PVC-polyester (III)	032	0.65	0.16	-0.71	5.97	-0.16	5.76
		034	0.54	0.03	0.12	7.42	2.10	9.82

All values are for non-adjusted test data, i.e. including residual strain.

‡ Data for initial stages of test lost due to a data-logging error.

† For definition of fabric types see Chapter 2, §2.1.4.1, Figure 2-15

Table 4-3. Residual strain levels at prestress

The Verseidag PTFE-glass fabrics give consistent values of residual strain, and the results can be explained in terms of fabric deformation mechanisms. After seventeen hours at prestress the initially highly crimped fill yarn has straightened to give a positive strain, while the less crimped warp yarn has straightened slightly to give a small strain (§3.2, Figures 3-11 & 3-12). These values are similar to those that would be used for compensation. After three conditioning cycles the fill strain has increased substantially to around 13%. This is higher than the 11.1% and 10.5% theoretical decrimping strains calculated from fabric cross-section images for the two fabrics (§5.4.1, Table 5-6). The additional strain may be due to inelastic strain of the yarn. Whilst glass fibre tensile behaviour is essentially linear elastic, changes to the twisted yarn structure may result in inelastic strain (§2.1.1). The total decrimping of the fill yarns caused by the conditioning results in an increase in warp crimp and corresponding negative warp strain. After testing at a wide range of load levels and ratios the balance of crimp has been partially restored, giving a decrease in fill strain and an increase in warp strain.

The results for some fabrics are inconsistent and difficult to explain. After seventeen hours at prestress the PVC-polyester fabrics and the Taconic Solus 1120 PTFE-glass exhibited higher levels of strain in the warp direction than the fill. All of these fabrics, except Verseidag B6853, gave negative fill strains. This is contrary to the explanation given above for the Verseidag PTFE-glass fabric behaviour. One reason for the increased warp strains is that for some fabrics the prestress level used for this test protocol is higher in the warp than the fill. This is because the fabrics are stronger in the warp direction than the fill, and the prestress level is based on the strip ultimate tensile strength (§3.4). This may explain the high warp strain for the Taconic Solus 1120, Ferrari 1002T and Ferrari 1502T. However, Taconic Solus 1300 and the Verseidag PTFE-glass fabrics also have high warp prestress levels but behave as expected with high fill strain and low warp strain.

All of the Ferrari fabrics consistently give low warp strains (zero to -4%) and positive fill strains. These fabrics are manufactured using the *Précontraint* system which tensions the fill yarns during coating to give more balanced crimp in warp and fill directions in the finished fabric. This reduces the level of decrimping available in the fill direction, and provides more balanced fabric behaviour. However, with the exception of 1502T, the results show that these fabrics do have a greater level of crimp in the fill than the warp.

The exact way in which prestress is applied may affect the resultant levels of warp and fill strain. Due to difficulties in manually controlling the hydraulic actuators on the biaxial test rig at low loads, prestress has been applied manually by using a wheel on a threaded bar (§3.3.2.1). This enables very accurate control at low loads, with no risk of an accidental sudden increase in load. Load application using this method is displacement controlled. This means that as load is applied in one direction the load in the other direction changes due to crimp interchange. An iterative series of adjustments is required to achieve the desired prestress in both directions. The order in which the warp and fill loads are applied to the cruciform may affect the strain levels. Prestress has, principally, been applied in two or three increments.

with warp and fill directions being increased alternately. An automated control system is being installed (§6.2.2) which will enable loads to be applied simultaneously at constant rates. However, for this research there was no set system for which direction the load was applied in first. The two resultant loading scenarios are:

- Load applied in fill direction first. Crimp interchange results in loading of warp direction, so virtually all load application is made by extension in the fill direction.
- Load applied in warp direction first. Extension of warp yarns only results in minimal crimp interchange, hence extension in fill direction is also required. Only a small extension in the fill is required to reach prestress as less crimp interchange occurs with the already tensioned warp yarns.

If crimp interchange was a linear elastic mechanism then the order in which the displacements/loads were applied would be immaterial. However, the effect of friction (inter-yarn and yarn-coating), inelastic coating extension and creep all result in inelastic behaviour; hence the order of load application may result in significant changes in strain level. These effects are particularly significant at low loads. Load cycling between zero (or a minimal holding load) and prestress (Doering, 1993) may negate these effects and prevent the initial load sequence affecting the prestress strains.

This effect may be significant for compensation testing which requires accurate determination of strains at prestress. This also highlights the importance of the installation sequence: the order in which, for example, edge cables are tensioned and masts are jacked up may give different levels of warp and fill prestress for given applied displacements (§6.2.7). For the research presented in this thesis any discrepancies resulting from the initial application of prestress should not significantly affect the test results after mechanical conditioning. This can be seen in the strains at prestress after conditioning and testing (Table 4-3), which are more consistent than those before conditioning.

After conditioning and testing, the PTFE-glass fabrics all give high fill strains (between 4.2 and 12.6%) with fairly consistent results for repeat tests (Table 4-3). For three fabrics (Taconic Solus 1120 and both Verseidag fabrics) the mean difference between repeat tests after conditioning is less than 0.6% strain. However, for the Taconic Solus 1300 and 1410 the differences are 1.33% and 2.14% respectively. Similarly, after testing the Taconic Solus 1120 and both Verseidag fabrics gave very consistent results (mean difference of 0.14%), whereas for Taconic Solus 1300 and 1410 the differences were 1.38% and 2.44%. The differences are very similar after conditioning and after testing, suggesting that they are a feature of the fabric samples. Whilst this suggests that the heavier Taconic fabrics may have less consistent material properties, further testing would be required to make any conclusive statements.

Warp strains after conditioning and after testing range from 0.14% and -1.49%. Decrimping of the highly crimped fill yarns at high fill stresses is inelastic, leading to high levels of fill strain when the fabric is returned to prestress. The *Précontraint* Ferrari fabrics give much lower fill strains due to the more

balanced initial crimp configuration. The Ferrari results contrast with the Verseidag B6853 PVC-polyester which has high fill and low warp strains similar to the PTFE-glass fabrics. While not providing an exact prediction of the fill strains, the theoretical decrimping strains calculated from fabric geometry measurements do fit the trends described above (§5.4.1, Table 5-6).

Strains of around 14% suggest that scope for significant re-tensioning may be required in some structures to prevent loss of prestress and subsequent excessive movement of the fabric. It is important to assess how these strain values relate to a real structure. The test protocol applies stresses up to a design load of 25% UTS. An in-situ fabric will infrequently be exposed to these stress levels, and they will tend to occur in localised areas (e.g. the top of conics and clamped corners). The structure will be exposed to loading between prestress and design load throughout its design life, not just for the five hours which it takes to complete a test. Long term strains (i.e. maximum expected in the design life of the structure) may be even higher than those in Table 4-3, due to a combination of extreme load events and long term creep. A stress-area assessment of the structure, combined with expected load levels and durations, would be required to give some idea of an expected overall level of residual strain (§6.2.8). Care must be taken with re-tensioning: after long term creep materials may have a failure strain independent of their failure load. With excessive re-tensioning this failure strain could be reached, leading to failure at low loads (§6.2.4).

The recovery of the fabric after an extreme load event is important. If the high residual strains are temporary they may not contribute to long term strain. They would still be significant for ponding: if snow load results in excessive deflections, melt-water will accumulate, potentially leading to fabric failure (§1.1.2). Following one biaxial test the stress in the fabric was maintained at prestress for nearly four days to monitor recovery (Table 4-4). This data was not recorded for any other fabrics.

	Approx. 17 hours at prestress	Immediately after test	47 hours after test	90 hours after test
Warp strain (%)	0.71	0.86	0.80	0.76
Fill strain (%)	1.07	11.63	11.70	11.68

Table 4-4. Recovery of Verseidag B18059 PTFE-glass

Recovery of the fabric is negligible: the strain in the fill direction is largely due to inelastic decrimping. The fill strain can only be reduced by high loads in the warp direction re-introducing the crimp.

4.2 REPRESENTATION & IMPLEMENTATION OF TEST RESULTS

4.2.1 Comparison of test data with plane stress model

Use of biaxial fabric test data in structural analysis is typically set within a plane stress framework using elastic moduli and interaction terms (§2.3.3). The suitably of this approach for representing non-linear fabric behaviour has been assessed by comparing test data from this research with the 'best fit' plane stress model. Residual strain has been removed from the test results and the mean value of the loading and unloading curves has been calculated (Figure 4-22). This simplification approximates the inelastic hysteretic fabric behaviour with an elastic response. This simplification is necessary before trying to represent the fabric behaviour with a plane stress model.

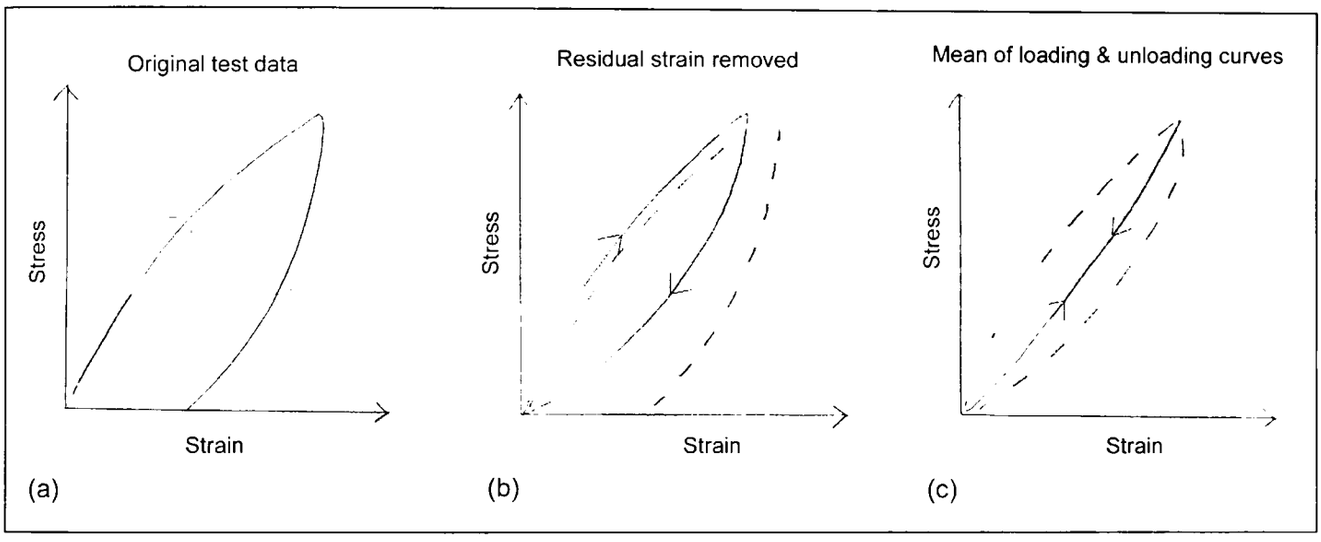

Figure 4-22. Simplification of test data

Plane stress theory defines strains in terms of stresses, Young's moduli and Poisson's ratios. Applying plane stress theory to the principal warp and fill fabric axes gives:

$$\varepsilon_w = \frac{\sigma_w}{E_w} - \frac{\sigma_f \nu_{fw}}{E_f}, \qquad \text{Equation 4-1}$$

$$\varepsilon_f = \frac{\sigma_f}{E_f} - \frac{\sigma_w \nu_{wf}}{E_w}, \qquad \text{Equation 4-2}$$

where ε = strain, σ = stress, E = Young's modulus, subscripts w and f denote warp and fill directions respectively, and ν = Poisson's ratio, defined as:

ν_{wf} = fill direction strain caused by unit strain in the warp direction,

ν_{fw} = warp direction strain caused by unit strain in the fill direction.

The results for each pair of tests on one type of fabric have been combined into one data-set, and values of Young's modulus and Poisson's ratio have been determined to minimise the root-mean-square deviation of the plane stress values from the test results (Table 4-5). This has been carried out using *Microsoft Excel 2003* and the standard *Solver* add-in. No constraints were imposed on the values of Young's modulus and Poisson's ratio. For each stress state tested the strains predicted by Equation 4-1 and Equation 4-2 have been compared with the test results (Table 4-5). The plane stress equations define planes in the stress-stress-strain space which can be used to visualise the representation of the test data (Figure 4-23 & Figure 4-24).

Fabric	Material (Type†)	Young's modulus (kN/m width)		Poisson's ratio‡		RMS strain difference for all test data points (percentage strain, sd = standard deviation)		RMS strain difference (percentage of test strain range)	
		Warp	Fill	ν_{fw}	ν_{wf}	Warp	Fill	Warp	Fill
Taconic Solus 1120	PTFE-glass (G5)	960.7	371.7	1.87	0.57	0.53, sd = 0.50	0.96, sd = 0.91	7.21	6.41
Taconic Solus 1300	PTFE-glass (G6)	1229.3	416.7	2.02	0.50	0.41, sd = 0.37	0.88, sd = 0.81	6.82	5.99
Taconic Solus 1410	PTFE-glass (G7)	2246.9	1161.7	1.36	0.60	0.49, sd = 0.45	0.34, sd = 0.33	9.72	4.93
Verseidag B18059	PTFE-glass (G6)	755.5	356.2	1.78	0.58	0.64, sd = 0.58	1.38, sd = 1.27	6.29	6.49
Verseidag B18089	PTFE-glass (G6/G7)	852.2	341.5	1.91	0.54	0.75, sd = 0.7	1.29, sd = 1.23	7.93	6.61
Mean values for PTFE-glass		1208.9	529.6	1.79	0.56	0.56, sd = 0.52	0.97, sd = 0.91	7.59	6.09
Ferrari 702T	PVC-polyester (I)	592.0	342.9	1.01	0.35	0.20, sd = 0.18	0.33, sd = 0.30	5.35	4.47
Ferrari 1002T	PVC-polyester (II)	772.8	463.0	0.98	0.37	0.34, sd = 0.32	0.46, sd = 0.45	7.95	5.71
Ferrari 1202T	PVC-polyester (III)	877.9	506.0	0.79	0.42	0.51, sd = 0.47	0.46, sd = 0.42	8.08	5.23
Ferrari 1502T	PVC-polyester (IV/V)	1192.2	536.1	1.59	0.37	0.45, sd = 0.41	1.02, sd = 0.94	6.33	6.58
Verseidag B6853	PVC-polyester (III)	825.7	341.6	1.20	0.38	0.5, sd = 0.45	0.66, sd = 0.60	7.54	5.18
Mean values for PVC-polyester		852.1	437.9	1.11	0.38	0.4, sd = 0.37	0.59, sd = 0.54	7.05	5.43

All values are determined from adjusted test data, i.e. with residual strain removed.

‡ According to plane stress theory Poisson's ratio cannot exceed 0.5. However, higher values are required to model the high level of warp-fill interaction and large negative strains which occur in woven fabrics under biaxial load,

ν_{wf} = fill direction strain caused by unit strain in the warp direction,

ν_{fw} = warp direction strain caused by unit strain in the fill direction.

† For definition of fabric types see Chapter 2, §2.1.4.1, Figure 2-15

Table 4-5. Plane stress representation of fabric test data

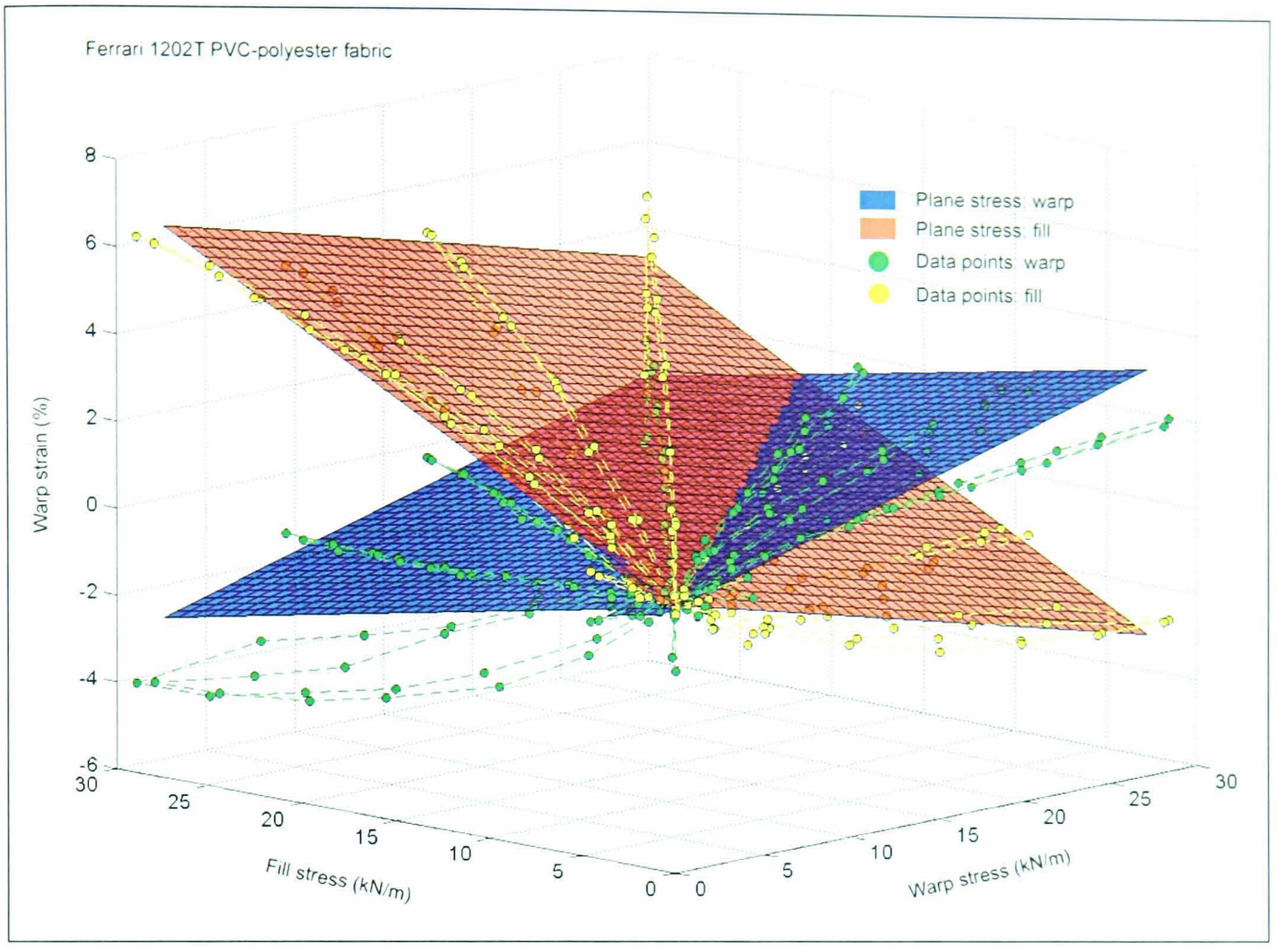

Figure 4-23. Test data for two test and best fit plane, Ferrari 1202T PVC-polyester

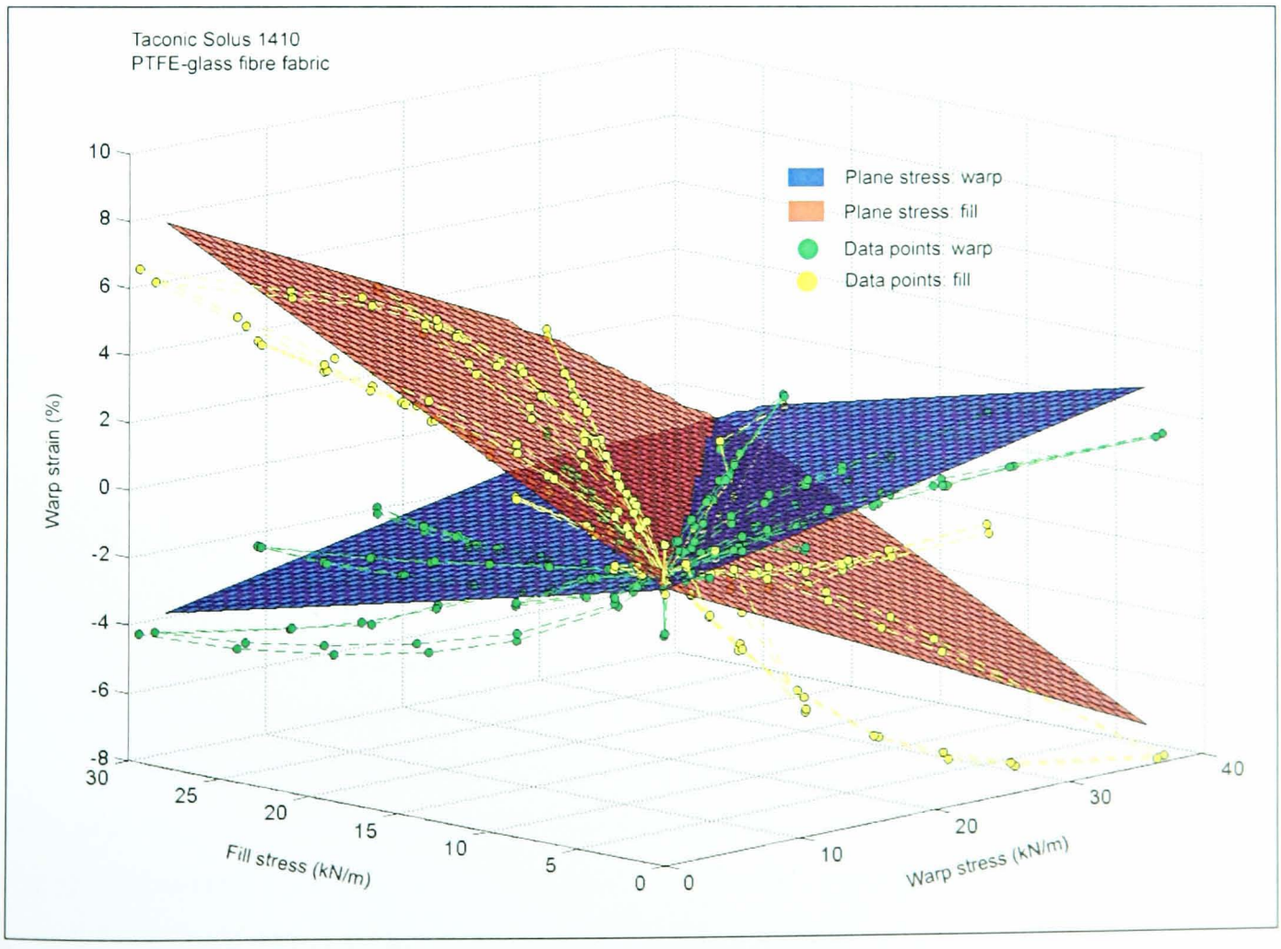

Figure 4-24. Test data for two test and best fit plane, Taconic Solus 1410 PTFE-glass

The overall correlation between the test data and plane stress representation is good. For PVC-polyester fabrics the variation between the test data and plane stress model is only twice as much as the variation between the two repeat tests (Table 4-6). The plane stress representation is only slightly less accurate for the PTFE-glass fabrics, but the fabric response is more consistent between tests making the mean 6 to 7.5% discrepancy between the test data and plane stress model more significant. The good fit of the plane stress model to the PVC-polyester test data can be attributed to the low level of crimp in the fabric, and the low tensile modulus of the polyester yarns. The low level of crimp (compared to PTFE-glass fabrics) results in less marked non-linearity. The low tensile modulus reduces the effect of the transition between crimp interchange at low load and yarn extension at higher loads. Whilst the mean deviation of the plane stress representation from the test data is good, the standard deviation is large (similar to the difference, Table 4-5). For some stress ratios and load levels the correlation is not so good, as can be seen in Figure 4-23 & Figure 4-24.

Even when mechanically conditioned, the response of PTFE-glass fabrics is highly non-linear due to significant crimp interchange at low load and tensile extension of the stiff glass yarns at high loads. The repeat tests on PTFE-glass give much closer results than for PVC-polyester because the tensile properties of glass fibres are essentially linear elastic, unlike the non-linear, time dependent polyester yarn behaviour (§2.1.1). For the PTFE-glass fabrics, in the fill direction the RMS difference between the plane stress model and test data is 3.5 times greater than the difference between repeat tests.

Material	RMS difference between two tests as a percentage of the strain range, from Table 4-2.		RMS difference between best plane stress representation and test data, as a percentage of strain range, from Table 4-5.	
	Warp	Fill	Warp	Fill
PTFE-glass	2.31	1.76	7.59	6.09
PVC-polyester	4.39	3.64	7.05	5.43

Table 4-6. Comparison of plane stress model with difference between repeat tests

The relatively close correlation between the plane stress model and test data seems to be in stark contrast with previous work on the non-linear nature of coated woven fabrics (§2.1.4). One reason for this is that some previous research used stress-strain data for initial fabric behaviour (Clulow & Taylor, 1963; Day, 1986), which exhibits greater non-linearities than the mechanically conditioned response measured in this research. However, it is the conditioned behaviour which is appropriate for structural analysis, for which medium to long term material properties are required. Another reason for the apparent discrepancy is the way in which the results are visualised. Conventional stress-strain plots at a single warp to fill stress ratio may show significant non-linearities which are unsuitable for linear representation. Comprehensive data giving an overview of the fabric behaviour for all stress states may show that these non-linearities are not

as significant. However, the plane stress representation does involve considerable approximation; a method which fully utilises the test data without simplification would enable more accurate structural modelling and give higher levels of confidence in the design process.

For a linear elastic orthotropic material subjected to biaxial stress, the Young's moduli and Poisson's ratio are related by Equation 4-3:

$$\frac{\nu_{wf}}{E_w} = \frac{\nu_{fw}}{E_f} \qquad \text{Equation 4-3}$$

where: $\mathbf{E_w}$ is the warp direction Young's modulus,

$\mathbf{E_f}$ is the fill direction Young's modulus,

$\boldsymbol{\nu_{wf}}$ is the fill direction strain caused by unit strain in the warp direction and

$\boldsymbol{\nu_{fw}}$ is the warp direction strain caused by unit strain in the fill direction.

The values of Young's modulus and Poisson's ratio determined above (Table 4-5) do not fit this relationship. Consider the mean values for each fabric material from Table 4-5:

PTFE-glass fibre: $E_w / \boldsymbol{\nu_{wf}} = 1209 / 0.56 = 2157$,

$E_f / \boldsymbol{\nu_{fw}} = 530 / 1.79 = 296$,

$\rightarrow E_w / \boldsymbol{\nu_{wf}} \neq E_f / \boldsymbol{\nu_{fw}}$

PVC-polyester: $E_w / \boldsymbol{\nu_{wf}} = 852 / 0.38 = 2242$,

$E_f / \boldsymbol{\nu_{fw}} = 438 / 1.11 = 395$,

$\rightarrow E_w / \boldsymbol{\nu_{wf}} \neq E_f / \boldsymbol{\nu_{fw}}$

It is proposed here from inspection of the values of Young's modulus and Poisson's ratio in Table 4-5 shows that these values adhere more closely to an inverse of the plane stress relationship for an orthotropic material. However, a constant (C) also needs to be introduced for the relationship to hold:

$$\frac{\nu_{wf}}{E_f} = C\left(\frac{\nu_{fw}}{E_w}\right) \qquad \text{Equation 4-4}$$

Values of C are reasonably consistent for each fabric material:

PTFE-glass fibre: Mean value of C = 1.40 (standard deviation = 0.11),

PVC-polyester: Mean value of C = 1.51 (standard deviation = 0.33).

For comparison, if a similar constant is introduced in Equation 4-3 the values are much more variable:

PTFE-glass fibre: Mean value of C = 7.32 (standard deviation = 2.82).

PVC-polyester: Mean value of C = 5.70 (standard deviation = 2.54).

The inverse relationship introduced in Equation 4-4 is more apposite for coated woven fabrics than the plane stress relationship (Equation 4-3). Whilst having little association with plane stress theory, Equation 4-4 provides a simple relationship between the Young's modulus and Poisson's ratios which best represent the biaxial response of architectural fabrics.

Informal peer review of this research questioned the validity of the values in Table 4-5 and the relationship defined by Equation 4-4:

> "This material would violate the reciprocal theorem and the conservation of energy.
>
> Consider a unit square of material. I will use s for stress and e for strain. If we consider two load conditions
>
> 1. s_a and s_b in the x and y directions respectively
> 2. s_c and s_d in the x and y directions respectively
>
> If we apply 1 followed by 2 the strain energy is
>
> $$W = \tfrac{1}{2} (s_a.e_a + s_b.e_b) + \tfrac{1}{2} (s_c.e_c + s_d.e_d) + (s_a.e_c + s_b.e_d)$$
>
> If we apply 2 followed by 1 the strain energy is
>
> $$W = \tfrac{1}{2} (s_a.e_a + s_b.e_b) + \tfrac{1}{2} (s_c.e_c + s_d.e_d) + (s_c.e_a + s_d.e_b)$$
>
> Now the strain energy should be independent of how we get there for conservation of energy so that implies that
>
> $$\tfrac{1}{2} (s_a.e_a + s_b.e_b) + \tfrac{1}{2} (s_c.e_c + s_d.e_d) + (s_a.e_c + s_b.e_d) =$$
>
> $$\tfrac{1}{2} (s_a.e_a + s_b.e_b) + \tfrac{1}{2} (s_c.e_c + s_d.e_d) + (s_c.e_a + s_d.e_b)$$
>
> or
>
> $$(s_a.e_c + s_b.e_d) = (s_c.e_a + s_d.e_b)$$
>
> Using a strain-stress relationship
>
> $$e_x = A.s_x + B.s_y$$
>
> $$e_y = C.s_x + D.s_y$$
>
> we get that
>
> $$(s_a.s_c.A + s_a.s_d.B + s_b.s_c.C + s_b.s_d.D) = (s_a.s_c.A + s_b.s_c.B + s_a.s_d.C + s_b.s_d.D)$$
>
> or
>
> $$(s_a.s_d.B + s_b.s_c.C) = (s_b.s_c.B + s_a.s_d.C)$$

> Which is only satisfied if B = C. Or the standard relationship between E and nu for an orthotropic material; i.e. the nu values are not independent."
>
> Hendry, 2005

This query is correct in the context of a homogeneous material. Fundamental to this research is the fact coated woven fabrics are not homogeneous materials: the interaction of warp and fill yarns and the behaviour of the twisted yarn structure mean that they are better described as a *mechanism*. It is this mechanical interaction, analysed in detail in Chapter 5, which causes the elastic moduli and Poisson's ratios to not fit the relationship for a homogeneous material (Equation 4-3). This effect is augmented by the fact that the fabric is composed of two different materials. The mechanical properties of the fibres and the coating dominate the fabric response at different load levels (essentially coating at low load load, fibre/yarn at high load). The lack of conservation of energy is due to frictional effects at crossovers, inelastic yarn crushing and inelastic coating extension.

The values of elastic modulus and Poisson's ratio provide a useful tool for approximating the non-linear fabric response surface with a best fit plane. It may be more appropriate to refer to these as arbitrary parameters which define a best fit plane, as opposed to than mechanical parameters or elastic constants.

These values enable the test data to be used in analysis software with little or no modification (§4.2.3). The values provide convenient notation to define the extension and lateral contraction of the fabric for a given load state. Definition of elastic moduli and Poisson's ratios is not meant to suggest that the fabric behaves as a typical homogeneous material. It has already been established that fabric shear and bending do not correspond to the conventional definitions used for engineering materials. For example, simple shear is defined as a constant area deformation, whereas shear of woven fabrics results in a reduction in area (§2.1.4.3). It is proposed here that the biaxial tensile behaviour is also fundamentally different to other materials. Whilst Young's moduli and Poisson's ratios can be used to approximate this behaviour, it is clear that plane stress theory is inappropriate for accurately describing the non-linear biaxial behaviour of architectural fabrics.

4.2.2 Stress-strain mean and difference functions

Day (1986) proposed a novel method of representing biaxial fabric behaviour, without the constraining assumptions of plane-stress. Day carried out this research for Arup's design of the roof of the Schlumberger Research Centre (Cambridge, UK; Figure 4-25).

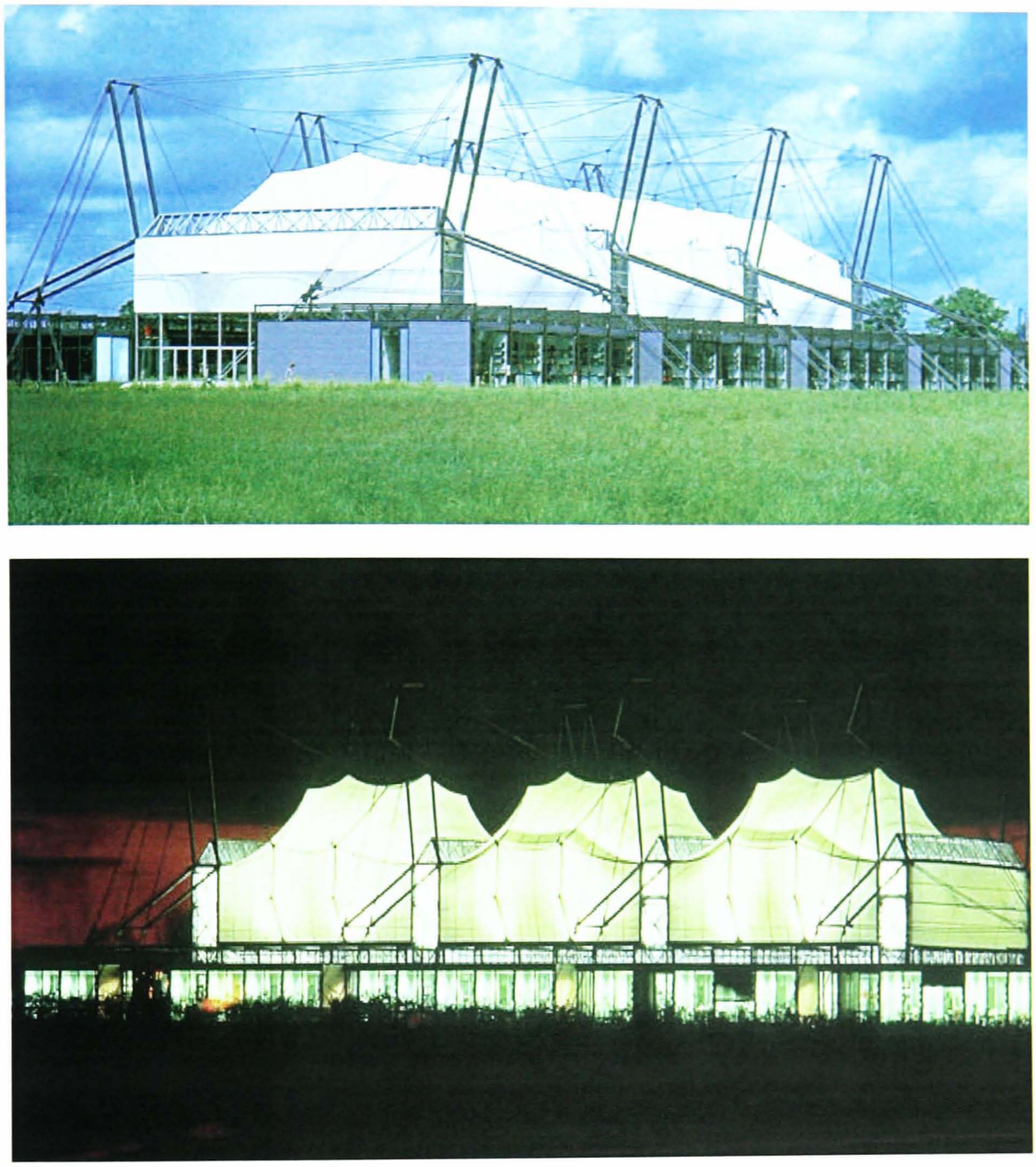

Figure 4-25. Schlumberger Research Centre (photographs: Arup)

The original fabric test data has been retrieved from archives (Table 4-7 and Figure 4-26) so that Day's work can be reproduced, and its utility as a departure point for this research can be assessed.

Warp:fill stress ratio = 1:1						
Warp stress (kN/m)		0	2.5	5	10	40
Strain (%)	Warp	0	0.53	0.52	0.5	1.26
	Fill	0	1.93	3.06	3.99	5.74
Warp:fill stress ratio = 5:1						
Warp stress (kN/m)		0	2.5	5	10	40
Strain (%)	Warp	0	0.11	0.27	0.53	2.01
	Fill	0	-0.05	-0.08	-0.04	-0.01
Warp:fill stress ratio = 1:5						
Warp stress (kN/m)		0	2.5	5	10	40
Strain (%)	Warp	0	-0.17	-0.78	-1.8	-2.67
	Fill	0	1.27	2.17	3.17	4.77

Table 4-7. Original test data from Schlumberger archive

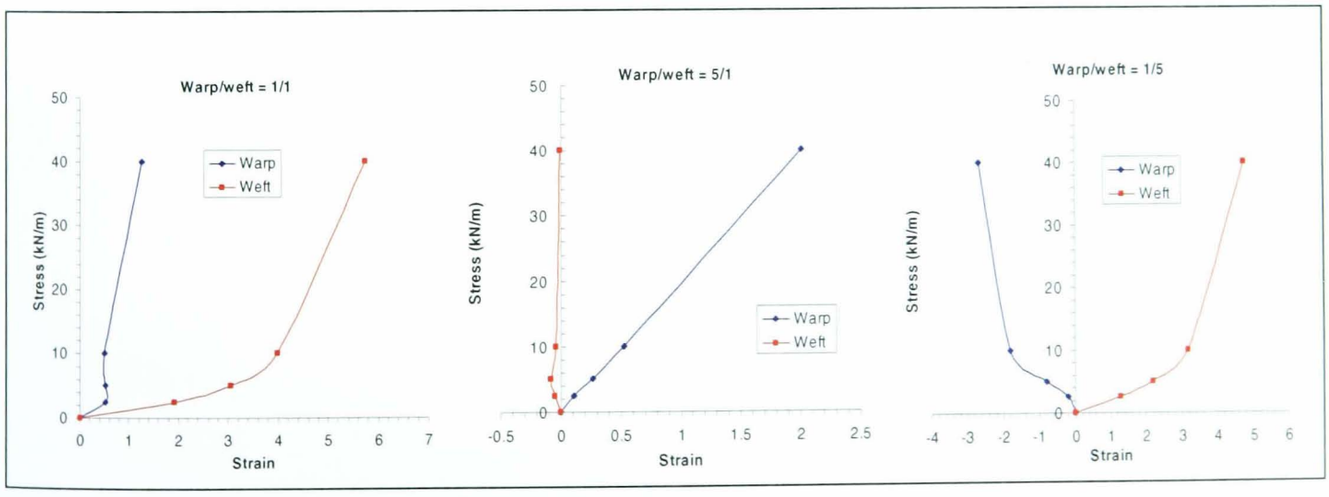

Figure 4-26. Stress-strain curves for Day's (1986) results.

Day used stress and strain mean and difference functions to represent biaxial test data for three stress ratios:

$$\sigma_a = \frac{(\sigma_x + \sigma_y)}{2}, \qquad \text{Equation 4-5}$$

$$\varepsilon_a = \frac{(\varepsilon_x + \varepsilon_y)}{2}, \qquad \text{Equation 4-6}$$

$$T = \frac{(\sigma_y - \sigma_x)}{2}, \qquad \text{Equation 4-7}$$

$$g = \frac{(\varepsilon_x - \varepsilon_y)}{2}, \qquad \text{Equation 4-8}$$

$$\sigma_a = f^1(\varepsilon_a) + f^2(g), \qquad \text{Equation 4-9}$$

$$T = f^3(\varepsilon_a) + f^4(g), \qquad \text{Equation 4-10}$$

where σ_x = warp stress, σ_y = fill stress, σ_a = mean stress, ε_x = warp strain, ε_y = fill strain, ε_a = mean strain, T = stress difference, g = strain difference and f^1 to f^4 are functions that are to be determined using test data. This work has been repeated to assess how well these functions model the complete fabric response, i.e. at stress ratios other than those tested. Day used 'arbitrary curves' for the mean and difference functions; this has been interpreted to mean multi-linear functions used to join the data points. Polynomials have also been used for this research (Figure 4-27), to assess whether Day's method enables simple functions to be used to model fabric behaviour.

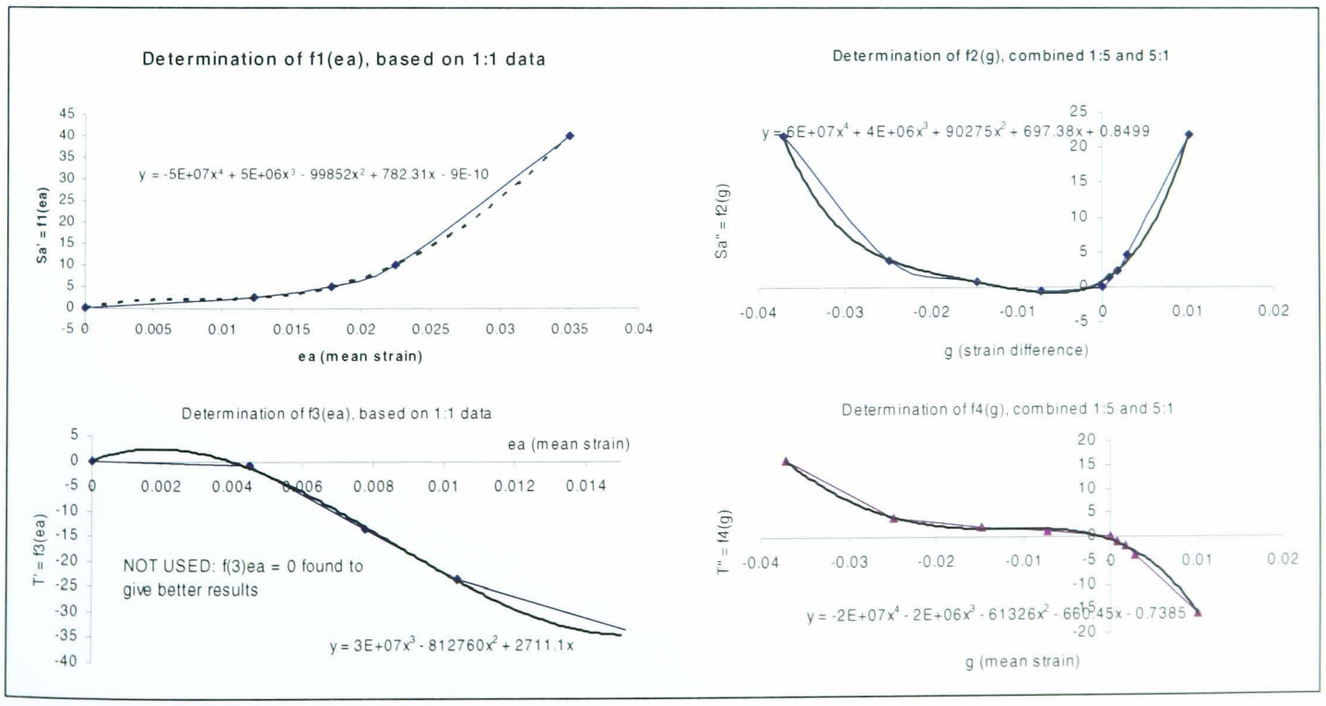

Figure 4-27. Representation of stress-strain mean-difference equations using fourth order polynomials.

Both multi-linear and polynomial functions initially gave poor correlations when used to calculate stresses from known strains. However, with $f_3(ea)$ set to zero (i.e. $T = f_4(g)$) a reasonable correlation is seen between predicted values and test data (Figure 4-28). The correlation is good considering that polynomial functions were used and that iterative improvement (optimisation) of the functions has not yet been carried out. An even better correlation is achieved using multi-linear functions, again with $f_3(ea)$ equal to zero (Figure 4-28).

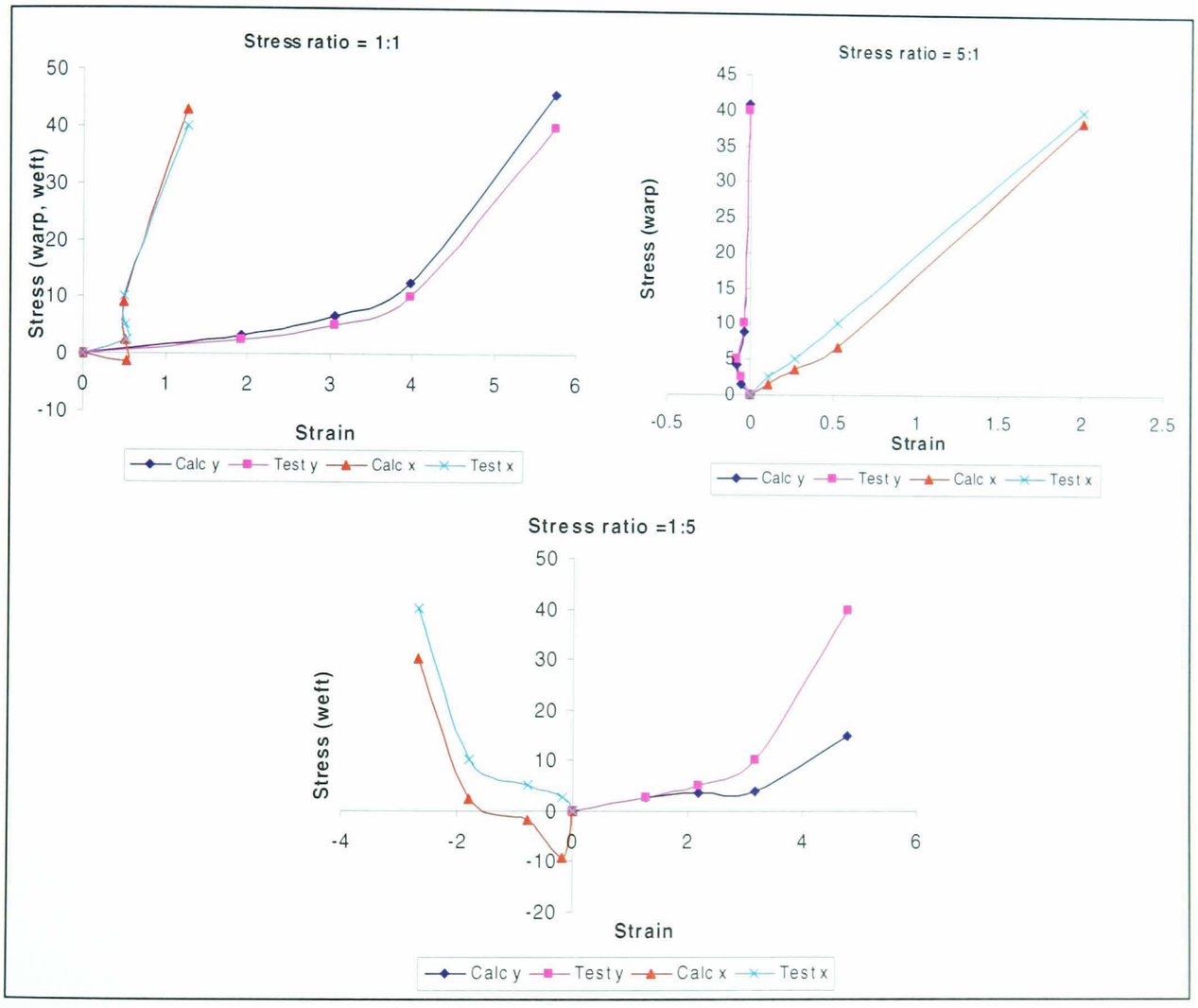

Figure 4-28. Curve fitting using polynomial functions to model stress-strain mean-difference relationships.

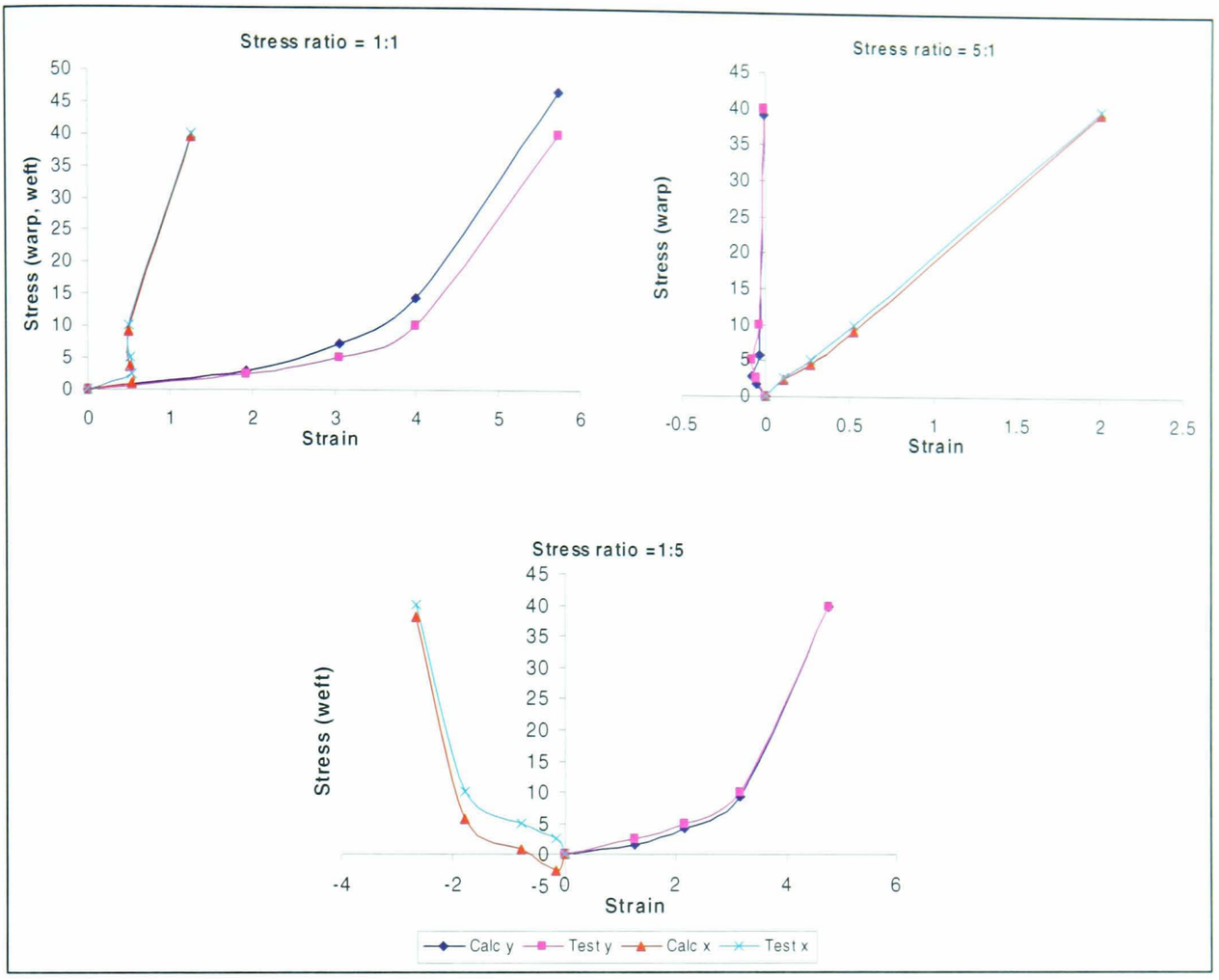

Figure 4-29. Curve fitting using linear interpolation to model stress-strain mean-difference relationships.

Consider the calculation of the function for mean stress, **Sa**, equal to $\mathbf{f_1(ea) + f_2(g)}$. For a stress ratio of 1:1, $f_1(ea)$ is large compared to $f_2(g)$ and so $f_1(ea)$ dominates the response. This gives a good correlation between test data and function output as $f_1(ea)$ is determined from 1:1 test data. For stress ratios of 1:5 and 5:1, $f_1(ea)$ is small compared to $f_2(g)$ hence the response is dominated by $f_2(g)$. Again good correlation is achieved as $f_2(g)$ is determined from the 1:5 and 5:1 test data.

A similar argument applies to the stress difference function, **T**, equal to $\mathbf{f_3(ea) + f_4(g)}$. For this example, $f_3(ea) = 0$ seems to provide a good correlation between the predicted response and test data. For a stress ratio of 1:1, $f_4(g)$ is small compared to Sa, hence a value of $f_4(g) = 0$ would give an exact fit to the 1:1 curve. Non-zero values of $f_4(g)$ give some deviation from the test data. For stress ratios of 1:5 and 5:1, $f_4(g)$ is determined by the relevant test data and so produces a good fit to the test curves.

Whilst providing a good correlation with the test data upon which they are based, an important question arises regarding their general applicability: do these functions provide reasonable values for other stress states? Thus far the equations have essentially been used to curve fit the test data, with no evidence that the mean and difference functions are suited to representing the overall fabric response. Can these functions be further informed, and encapsulate information from, other stress ratios? Data for warp to fill stress ratios of 2:5 and 5:2 have been derived by linear interpolation between the 1:5, 1:1 and 5:1 test

data. These values for stress ratios of 2:5 and 5:2 are not expected to accurately represent the material behaviour, but they do represent a feasible response with which to test the utility of Day's method. For Day's method to be applicable to multiple stress ratios, the additional data points provided by mean and difference functions for 2:5 and 5:2 ratios must further inform the $f_2(g)$ and $f_4(g)$ functions. This is not the case. The strain difference, g, for the hypothetical 5:2 data bears no relation to the other curves (Figure 4-30). To achieve a good fit to test data for other stress ratios $f_2(g)$ and $f_4(g)$ would need to be represented by a different polynomial for each stress ratio. This reduces the process to a curve fitting exercise.

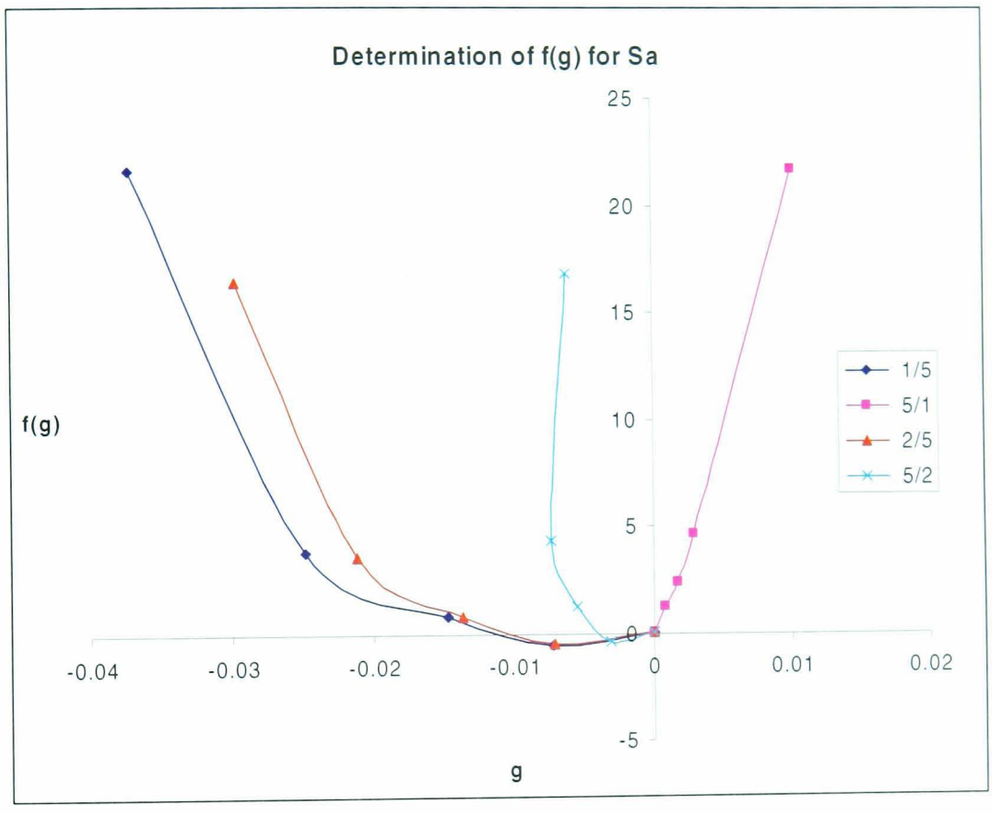

Figure 4-30. Possible definitions of $f_2(g)$ for four stress ratios.

Do the existing functions (based on the 1:5, 1:1 and 5:1 test data) give a reasonable (i.e. feasible) prediction of the fabric response at other stress ratios? The correlation between the interpolated test results and the calculated values is limited for the 5:2 and 2:5 ratios, in particular for the warp (x) direction (Figure 4-31). The general form of the response is predicted, but the magnitude of the stresses varies considerably. There are two possible explanations for this poor correlation:

1. The stress-strain mean-difference functions are providing a better informed representation of the fabric behaviour, and hence do not match the crude linear interpolation between stress ratios used as the 'test' values in these graphs.

2. The validity of the stress-strain mean-difference functions does not hold for stress ratios other than those tested.

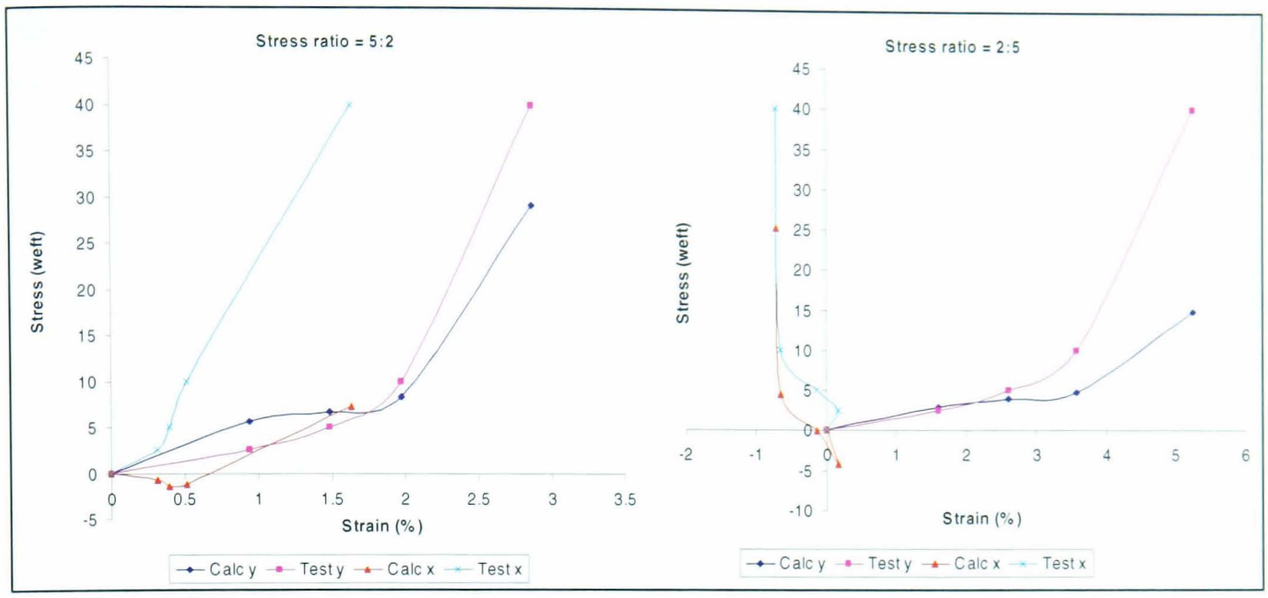

Figure 4-31. Comparison of linearly interpolated test results and prediction using polynomial representation of stress-strain mean-difference functions.

To gain a better understanding of the stress-strain mean-difference functions, and how they will behave at intermediate stress ratios, response surfaces can be plotted to represent the functions. Day's method is devised to enable the stresses to be determined for a given known state of biaxial strain. It is therefore logical to consider strain-strain-stress surfaces, as shown in Figure 4-32.

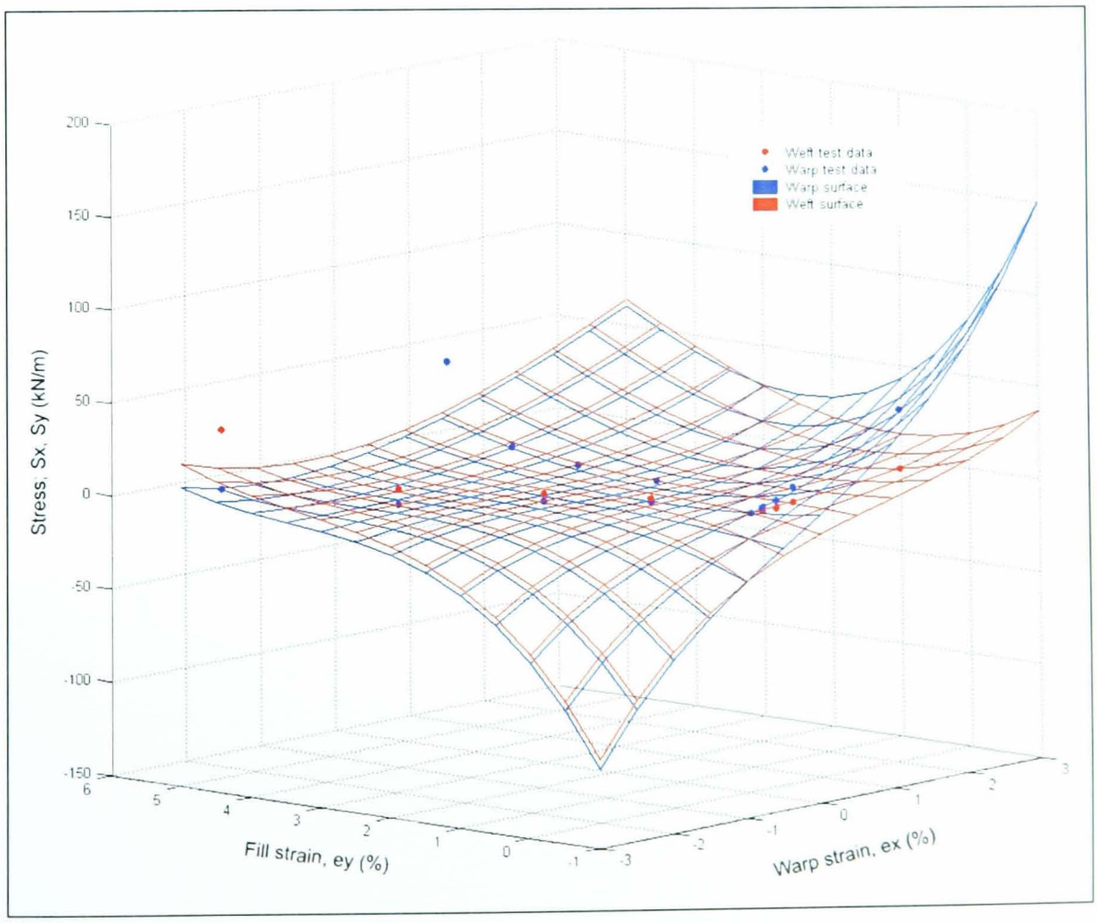

Figure 4-32. Response surface derived using stress-strain mean-difference functions.

The response surface is largely flat providing stable interpolation between the data points, however two data points (at high fill strain) clearly do not lie on the surface. The response functions can also be represented as stress-stress-strain surfaces for comparison with other surface fitting techniques (Figure 4-33 & Figure 4-34; scattered points represent the surface). The results are similar for the polynomial functions (not shown). The surfaces generated using Day's method have very steep gradients, i.e. a small change in stress leads to a large change in strain. These areas of instability occur at design stresses and could lead to great uncertainty in the accuracy of the analysis. The surfaces tend towards very high strain values at stress levels which may be required for structural design. The shape of an interpolating surface fit (Figure 4-35) is totally different: the spline surface is flatter giving a more controlled response, and a more intuitive interpolation between the data points.

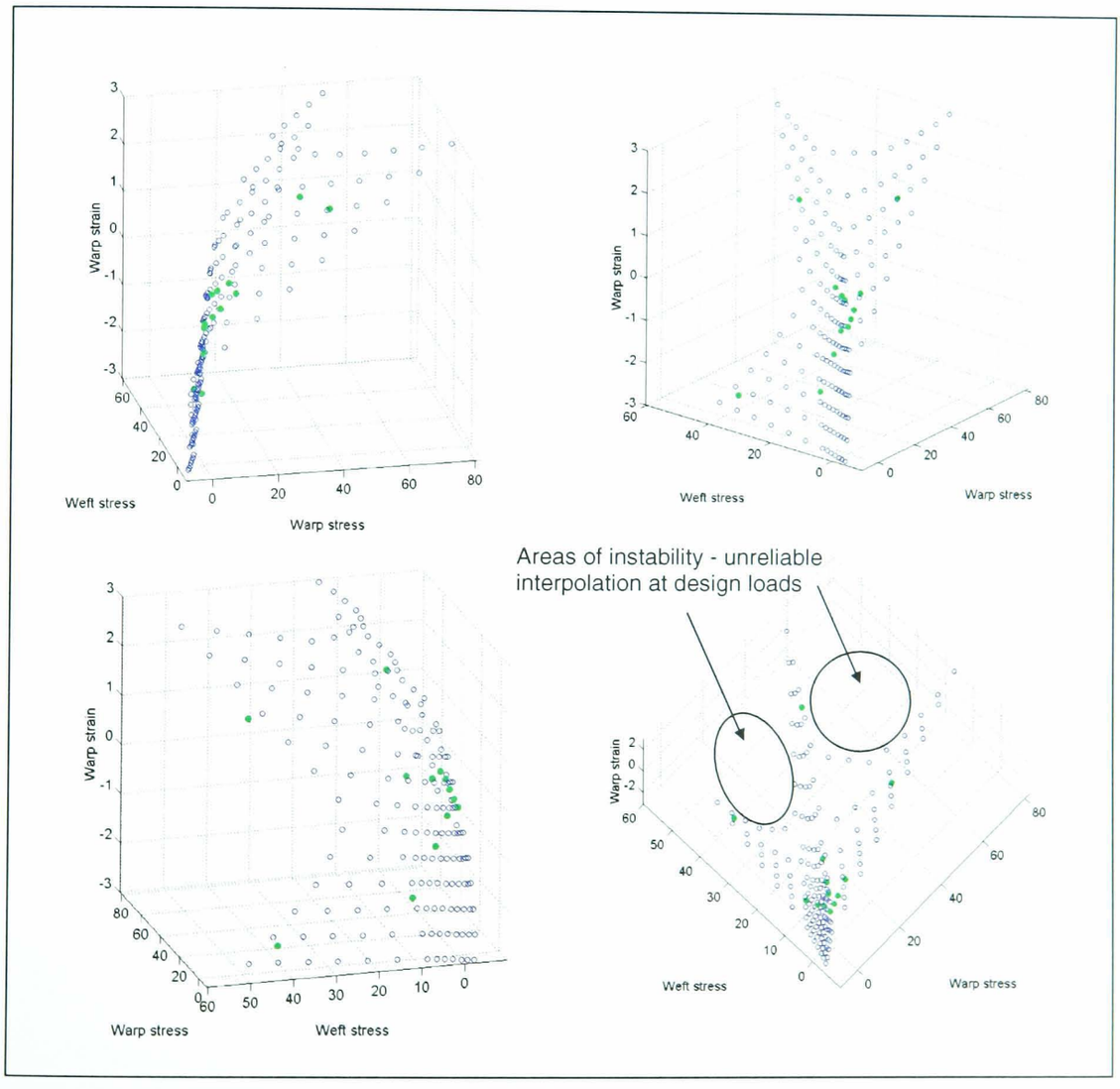

Figure 4-33. Biaxial stress-strain response surface for warp strain generated from linear representation of Day's stress-strain mean and difference equations.

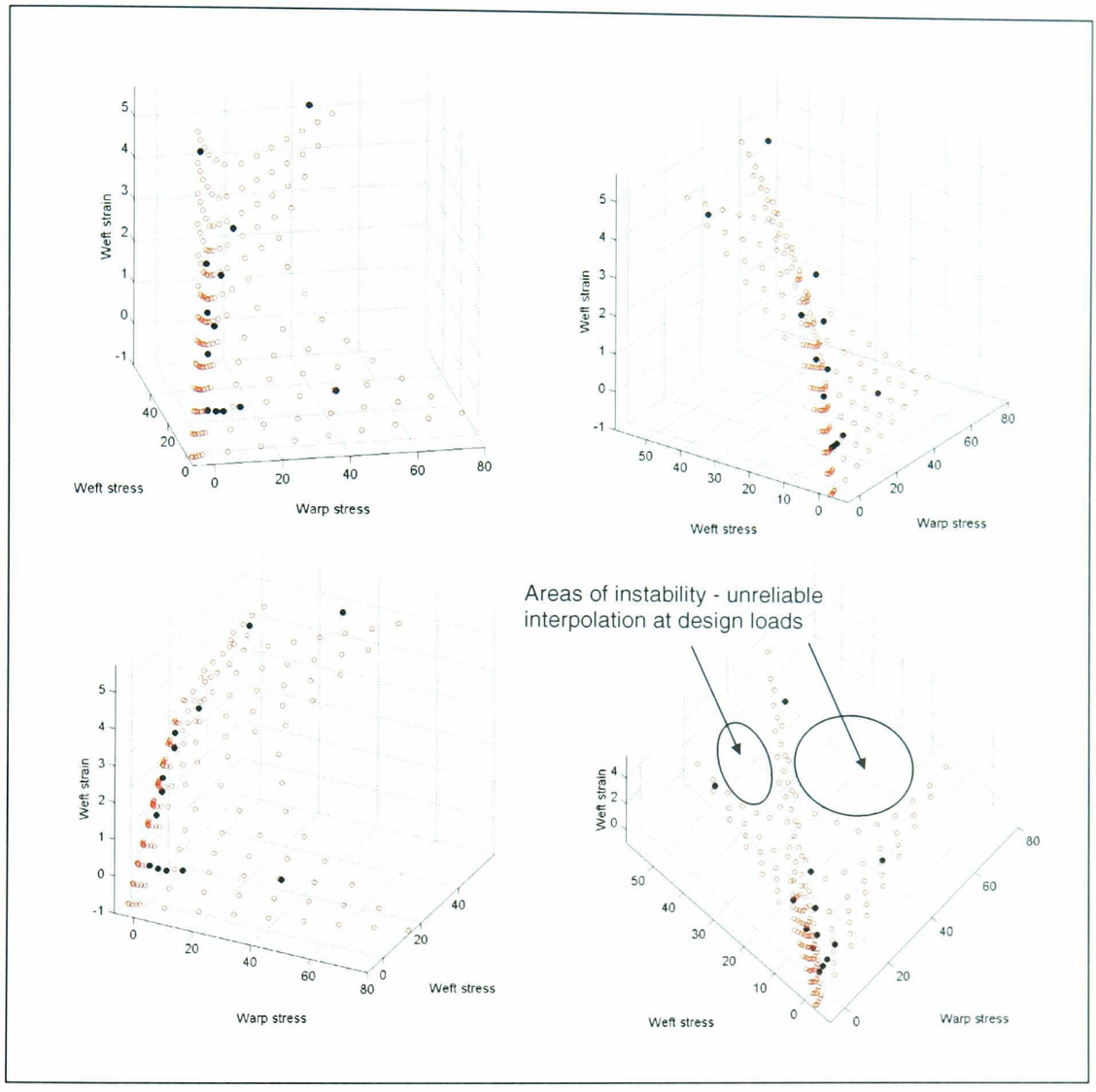

Figure 4-34. Biaxial stress-strain response surface for fill strain generated from linear representation of Day's stress-strain mean and difference equations.

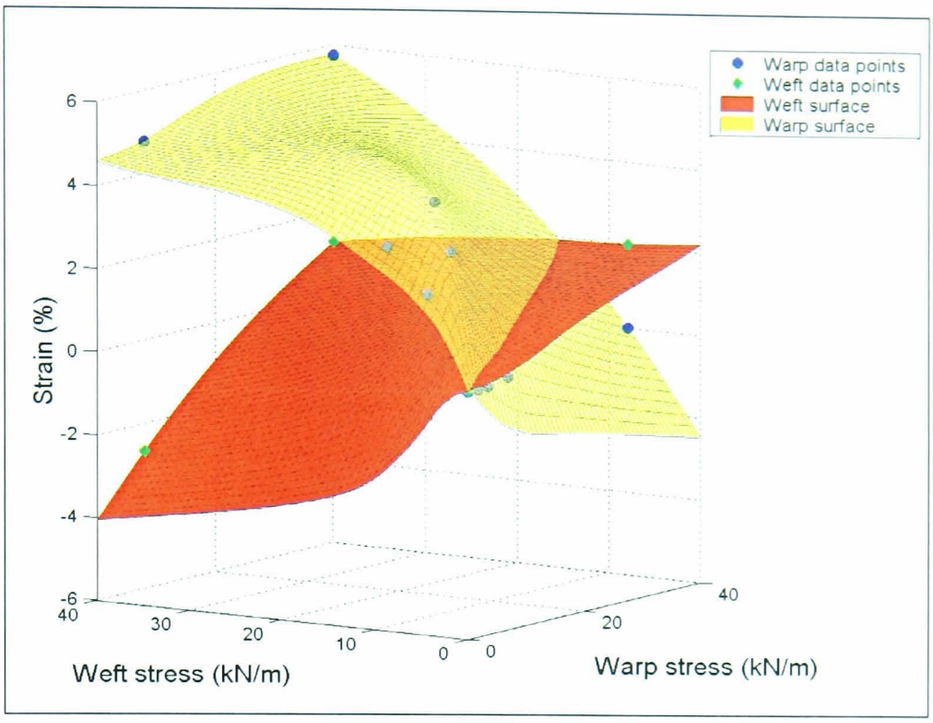

Figure 4-35. Biaxial stress-strain response surface for warp and fill strain generated using an interpolating spline in Matlab.

Day's 'stress-strain mean-difference' functions provide a method of fitting non-linear fabric stress-strain curves using polynomials or multi-linear functions. Data for warp and fill behaviour for three stress ratios is modelled with little function interaction. Surface plots of the functions show that they do not provide stable interpolation between the tested stress states (Figure 4-33 & Figure 4-34). Whilst calculation at a wide range of stress ratios and magnitudes will always be required in structural analysis, there is no evidence to suggest that these functions will successfully model fabric behaviour at stress ratios other than those tested.

4.2.3 A new approach

To successfully represent complex non-linear fabric test data for a wide range of fabrics (including as yet untested fabrics) requires a method with no *a priori* assumptions about the form of the response, the level of warp-fill interaction or the distribution of the data points. Development of the planar response surface given by plane-stress theory (§4.2.1) leads to surface fitting methods such as bi-linear or polynomial representations (§2.3.1). Any such method will result in some simplification of the original data, and may need to be modified for different types of fabric. For example, Testa, Stubbs and Spillers' bi-linear representation of fabric stress-strain behaviour requires the 'change point' to be modified for each test. It has already been established that fabric shear and bending do not correspond to the conventional definitions used for engineering materials (§2.1.4.3 & 2.1.4.4). It is proposed that response surfaces are used, but without the constraining assumptions of plane-stress which are not appropriate for describing architectural fabric behaviour (§4.2.1).

Previous researchers have used fabric tests carried out at a limited number of stress ratios (Day, 1986; MSAJ/M-02-1995; Minami et al, 1997; Blum, 2002). Using the new test protocol (§3.3.4), numerous stress states have been explored giving a much wider population of the data space. The test regime is stress controlled, which is appropriate as the range of expected stresses is known and the strains are required. However, during finite-element structural analysis, displacements are calculated from which warp and fill strains are determined and the corresponding stresses are required. Hence strain-strain-stress response surfaces are required to visualise the material response as it will be used in finite element analysis (Figure 4-36 & Figure 4-37). It is proposed that direct correlation between pairs of strains and corresponding pairs of stresses can be used for structural analysis. This avoids the inherent approximations and inaccuracy incurred when non-linear fabric behaviour is represented using a plane stress model (§4.2.1).

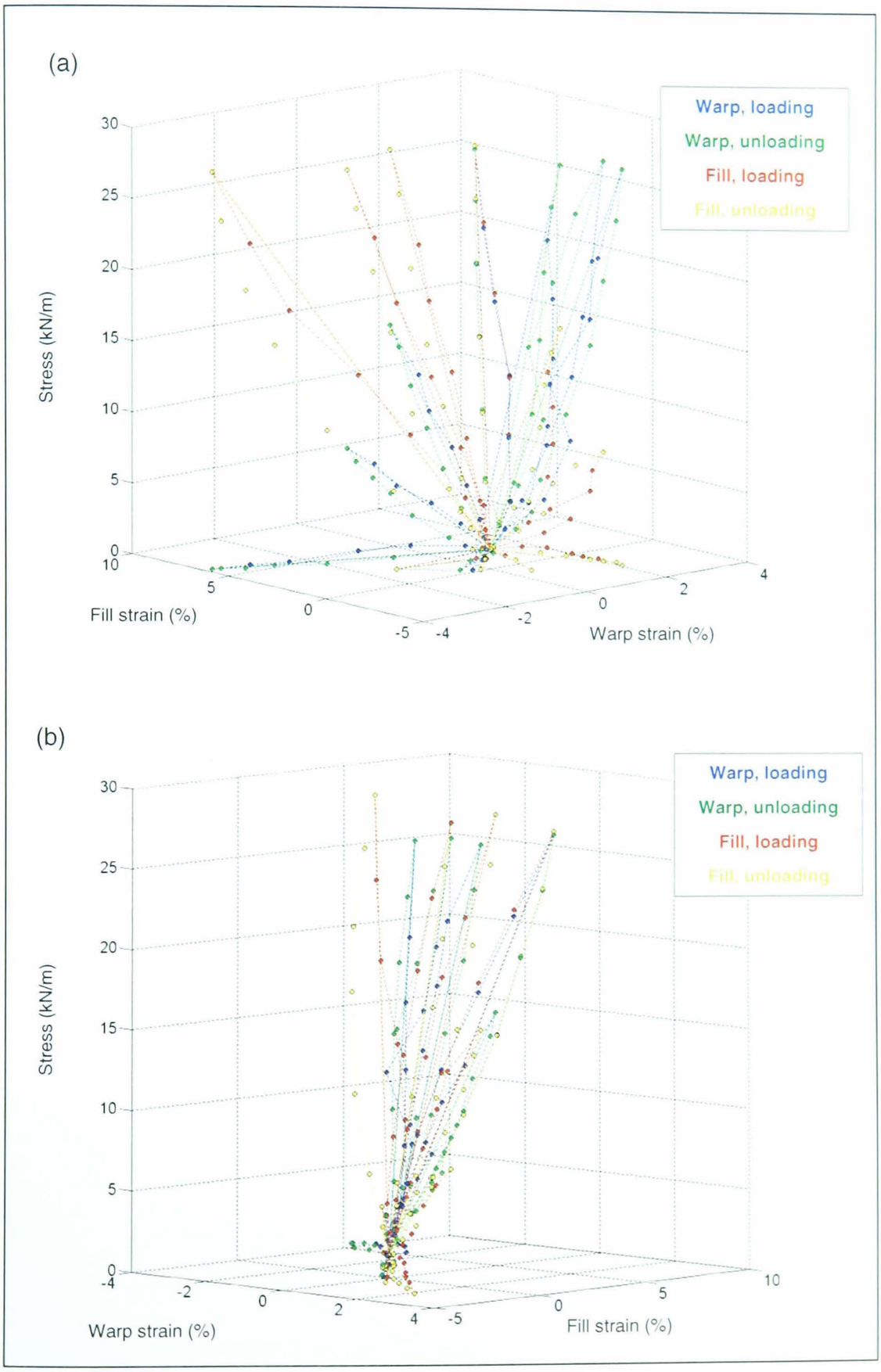

Figure 4-36. Strain-strain-stress representation of test data, Ferrari 1202T PVC-polyester, two views

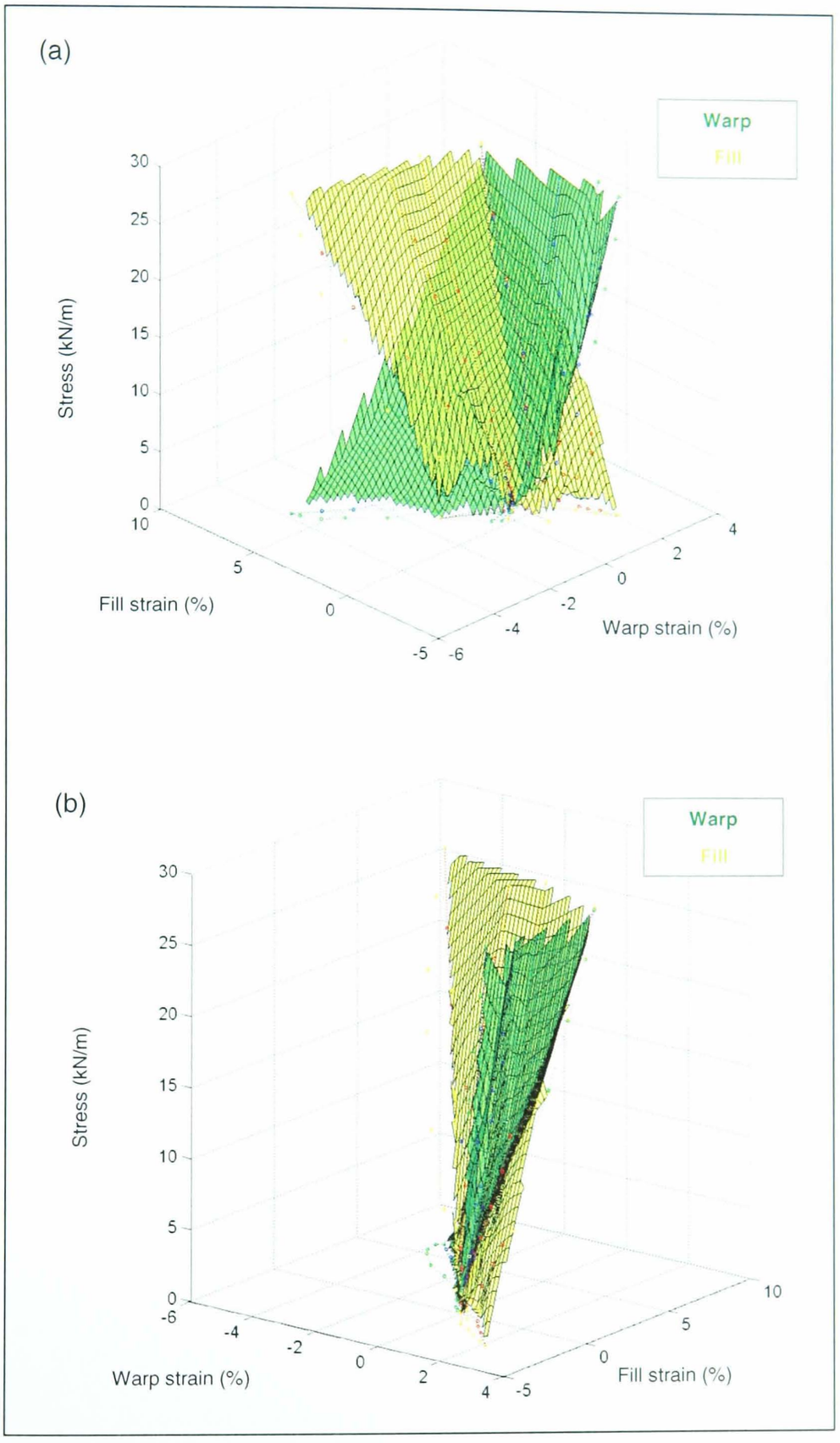

Figure 4-37. Strain-strain-stress mean surfaces, Ferrari 1202T PVC-polyester, two views

The strain-strain-stress surfaces are very steep compared with the corresponding stress-stress-strain surface. Small changes in displacement (strain) give large changes in stress. This will potentially make analysis using this data unstable. However, this is not a problem caused by this method; it is an inherent characteristic of the fabric response. For accurate representation of fabric behaviour this highly sensitive response must be included in the analysis. Numerical stabilisation techniques such as arc length control found in elasto-plastic analysis may need to be employed. The steep gradient of the strain-strain-stress surfaces increases the importance of including the variability of the test results (§6.2.6).

When direct correlation between strains and stresses is used in a finite element anlysis, surface gradients are not required. Consequently, a differentiable surface function does not need to be defined. A 'look-up' table of warp and fill strains and stresses may be used to replace elastic constants in the analysis. This avoids the need to linearise the test data using elastic constants (§4.2.1); the test data is included in the analysis with little modification, and no prior assumption about the form of the response. However, for an elastic analysis residual strain will need to be removed (Figure 4-22b, p.188).

Various interpolation schemes exist to fit local surface patches on to a specified number of 'nearest neighbours' to the point of interest (Chivate & Jablokow, 1995; Jüttler & Felis, 2002; Weiss et al, 2002). For simplicity, use of a triangular interpolation scheme is proposed to provide reliable, linear interpolation. Three pairs of strains (data points) are chosen which form a triangle enclosing the pair of strains for which stresses are required (Figure 4-38). The position of the strain data point within the triangle is used to interpolate between the three pairs of stresses at the corners of the triangle.

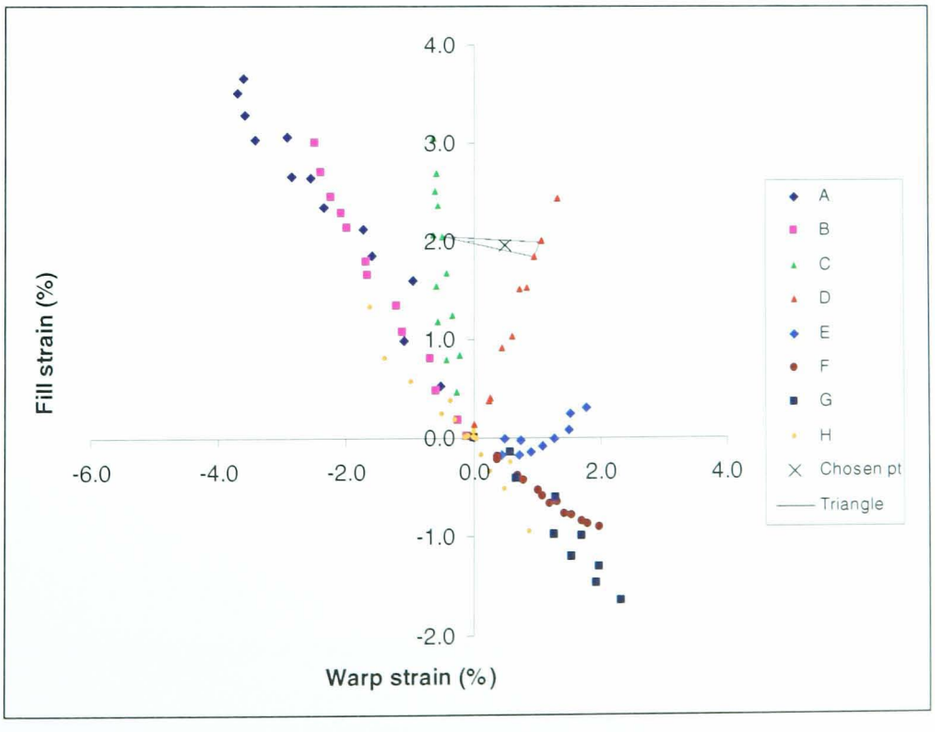

Figure 4-38. Interpolation between pairs of strains

Interpolation within the triangle can be carried using *natural* or *area coordinates* which are defined as ratios of areas (Figure 4-39, Equation 4-11; Cook et al, 1989).

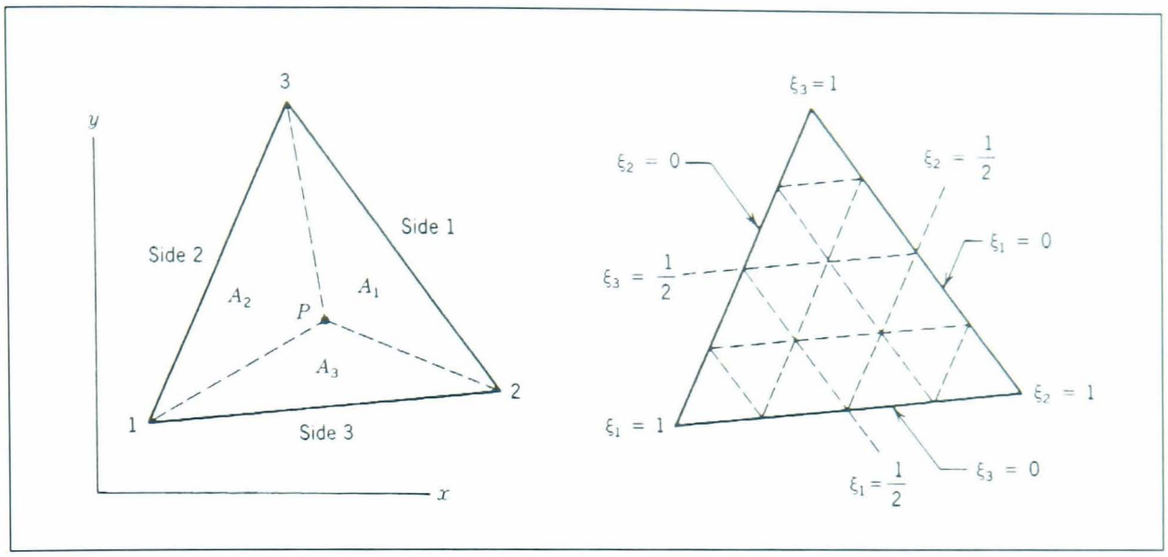

Figure 4-39. Natural (area) coordinates for a triangle, reproduced from Cook et al (1989)

$$\xi_1 = \frac{A_1}{A} \qquad \xi_2 = \frac{A_2}{A} \qquad \xi_3 = \frac{A_3}{A}$$

Equation 4-11

The x and y coordinates of point P are known, these are the warp and fill strains for which the stresses are required. Points 1, 2 and 3 are the nearest three data points which form a triangle around the point of interest. The areas A_1, A_2 and A_3 can be calculated by considering the projection of the four points (P, 1, 2 & 3) onto the x, y plane. Hence ξ_1, ξ_2 and ξ_3 can be calculated using Equation 4-12 (Cook et al, 1989),

$$\begin{pmatrix} \xi_1 \\ \xi_2 \\ \xi_3 \end{pmatrix} = [A]^{-1} \begin{bmatrix} 1 \\ x \\ y \end{bmatrix}$$

Equation 4-12

where, with $x_{ij} = x_i - x_j$ and $y_{ij} = y_i - y_j$,

$$[A]^{-1} = \frac{1}{2A} \begin{bmatrix} x_2y_3 - x_3y_2 & y_{23} & x_{32} \\ x_3y_1 - x_1y_3 & y_{31} & x_{13} \\ x_1y_2 - x_2y_1 & y_{12} & x_{21} \end{bmatrix}$$

Equation 4-13

The stress at point P is determined by multiplying the stress value of each data point by its area coordinate and summing, that is:

$$\begin{pmatrix} \sigma_w \\ \sigma_f \end{pmatrix} = \sum_{i=1}^{3} \left[\xi_i \begin{pmatrix} \sigma_{wi} \\ \sigma_{fi} \end{pmatrix} \right]$$

Equation 4-14

where i refers to the three data points and subscripts w and f denote warp and fill directions.

This interpolation scheme provides a simple, workable solution. Another method would be to fit a polynomial 'patch' surface to a given number of neighbouring points and use this to determine the stresses at the point of interest. A different approach would be to use genetic algorithms or genetic programming (§2.3.1) to generate two functions for the warp and fill strain-strain-stress response

surfaces. This would avoid the need for a database of test values and interpolation during the analysis. However, a function which correlates perfectly with the test data (i.e. passes through all data points) may not provide sensible results between data points (similar to the poor interpolation provided by mean and difference functions, §4.2.2, Figure 4-33 & Figure 4-34). The deviation of the function from a faceted multi-linear surface would need to be checked (and minimised) to avoid fluctuating functions which could give spurious results between data points. This is demonstrated in Figure 4-40 for a curve fit to 2D data points; this is analogous to a surface fit to 3D data points but clearer. Linear interpolation also keeps the computation time to a minimum. This is important for geometrically non-linear finite element structural analysis which requires an iterative solution and a potentially large number of elements.

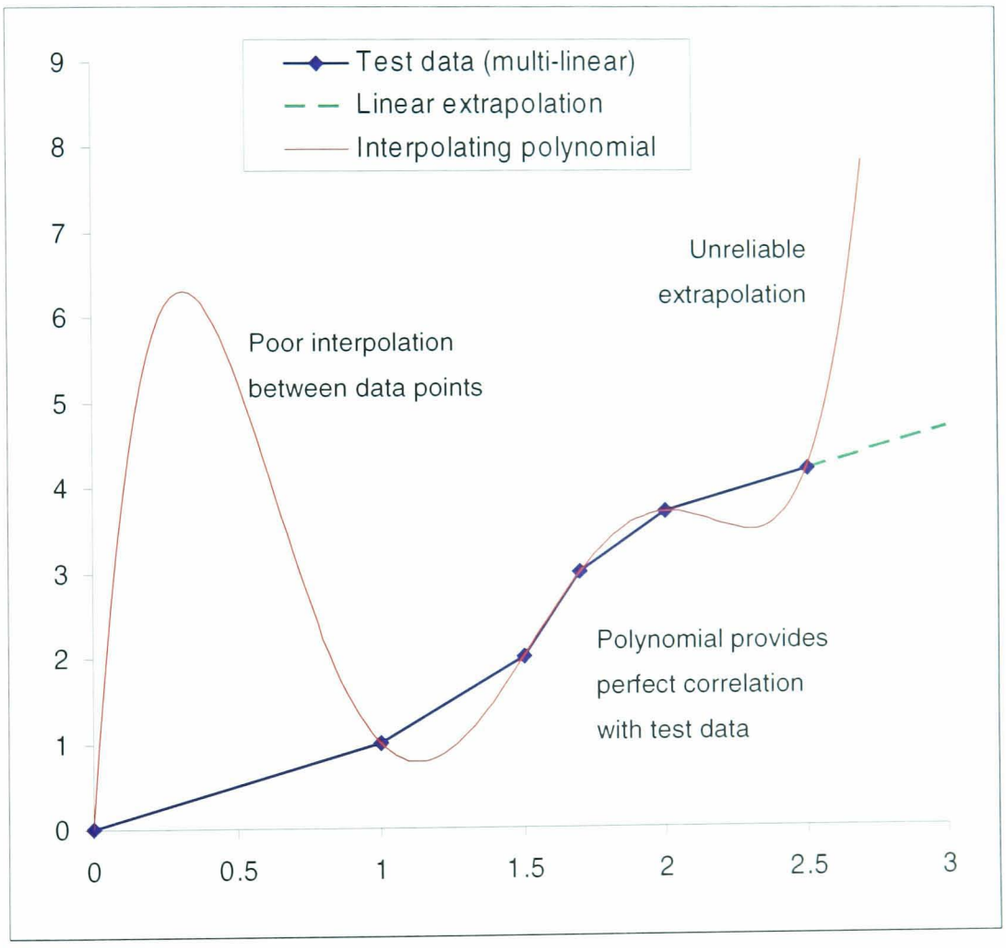

Figure 4-40. Interpolating polynomial fit to test data

Unless testing is carried out to failure, extrapolation beyond the tested stress states will be required. For this research stress states from zero to 25% of the ultimate tensile strength of the fabric have been tested. This provides data for all expected design stresses. However, several scenarios will require data for higher stresses in the analysis:

1. A structure with higher stresses which will need some modifications to reduce the fabric stress. Whilst the accuracy of the predicted stresses is not critical because the structure will not be built in this form, an indication of the stress distribution would aid the design process,

2. Small areas of high stress are common, for example at the top of conics and around clamp plates. These increased stresses may be allowable in areas of double-thickness reinforcement. Alternatively, some stress concentrations may be deemed to be due to limitations of the FE model (for example, due to an overly course mesh or unrealistically rigid edge constraints) and so may be ignored,
3. Higher stresses may occur during the geometrically non-linear iterative analysis before the model converges on the final solution.

In each of these situations it is important that the analysis is able to continue for stress states beyond the extremes of the data set and return feasible values. Extrapolation beyond the data set is therefore required. For the triangular interpolation method, the three points nearest the stress-state of interest will define a plane (in the strain-strain-stress space) which gives the level of strain at the point of interest. The two-dimensional analogue of this is linear extrapolation from the last segment of a multi-linear fit (Figure 4-40). This provides a robust solution which will give reasonable values. Alternatively, nominal values can be used beyond the edges of the data set (for both high and negative stresses) to maintain numerical stability. Use of a functional representation (e.g. polynomial patch or surface function determined using genetic algorithms or genetic programming) would make extrapolation straightforward but unreliable. Steep gradients can result in very high or low results with even a small extrapolation beyond the limit of the test data (Figure 4-40). This is difficult to mitigate as there are, by definition, no test data to provide a linear surface to check the function against.

4.2.4 Feasible fabric strain states

The population of the strain-strain space can be examined by plotting the data points on the strain-strain axes (Figure 4-41); effectively looking down the z-axis on the graphs in Figure 4-36 and Figure 4-36. The strain-strain space is unevenly populated; particularly for PTFE-glass there is a concentration of data points around the origin. With the highly sensitive strain-stress response it may be beneficial to use knowledge of the fabric response to modify the test protocol to further populate the sparse areas in Figure 4-41b. However, a strain controlled system is not recommended: it would be easy to specify strains which require stresses beyond the design stress, potentially resulting in fabric failure. The data points in Figure 4-41 are from multiple tests on a range of fabrics at stresses from zero through prestress to 25% UTS. Hence the population of the strain space indicates the bounds of the feasible fabric response for that material type.

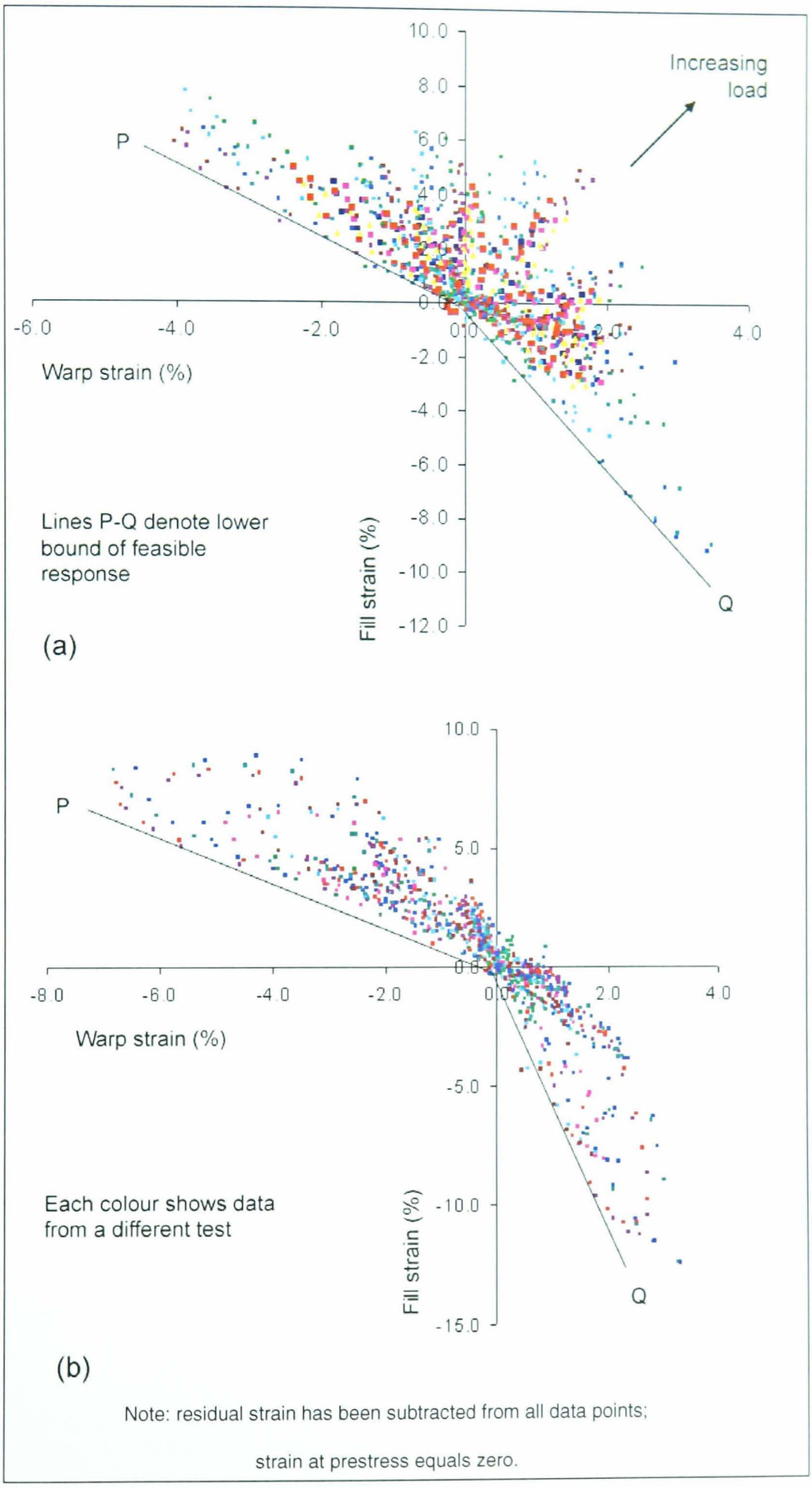

Figure 4-41. Population of strain space; multiple tests on (a) PVC-polyester, (b) PTFE-glass fibre

The PTFE-glass fabric has a very discrete response envelope; the behaviour is dominated by crimp interchange with little extension of the stiff glass fibre yarns. In contrast the polyester yarns are more easily extensible giving a greater range of possible strain states. This type of diagram provides a new tool for quantifying and understanding the biaxial behaviour of different fabric types. Test data for individual fabrics can be plotted in the same way to characterise the feasible fabric strains. This could be used as a tool for choosing fabrics depending on the required strain behaviour. For example, a barrel vault roof may be installed by tensioning in the fill direction to induce prestress in the warp by crimp interchange. These strain-strain plots show what level of negative strain is available in each fabric. A similar plot on three axes showing feasible warp, fill and shear strains would be extremely useful (§6.2.5).

In Figure 4-41 the test data has been adjusted to remove residual strain during the test, which is necessary to avoid skewing of the data. However, for consideration of feasible strain states for use in design it is necessary to include residual strains (Figure 4-42). In this plot the residual strains are those determined during biaxial testing (Table 4-3). In this example strain levels after 17 hours at prestress have been taken as 'installation' values, i.e. expected post-installation or compensation strain levels (§1.1.3). 'Medium term' refers to fabric strains after the test, which may approximate strain levels after several extreme load events, perhaps after two to five years in service. With further compensation and medium to long term strain testing it would be possible to include the likely level of variation in the creep strains, to give larger zones of feasible stress for medium and long term design cases (§6.2.4).

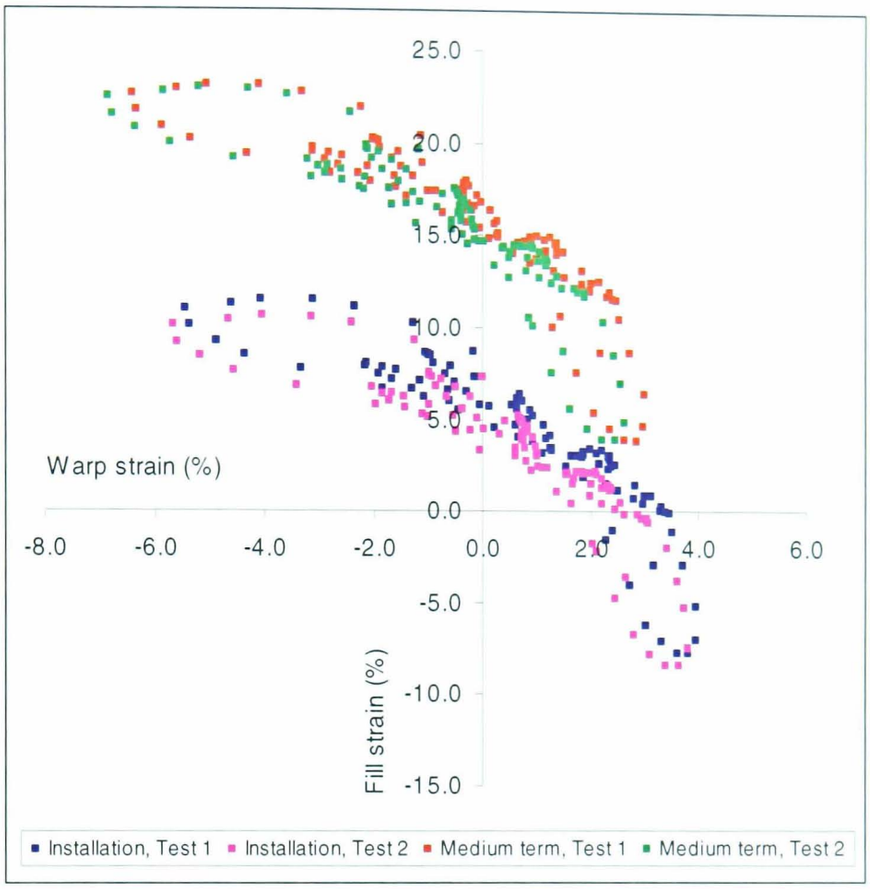

Figure 4-42. Strain-strain plots with residual strain

4.3 SUMMARY & CONCLUSIONS

A new biaxial test regime has been proposed and implemented that fully explores the design stress states of a fabric. Fabric samples have been mechanically conditioned to provide data relevant to medium to long term fabric behaviour, suitable for use in structural design. Biaxial test results for a range of PVC-polyester and PTFE-glass fibre fabrics have been presented.

Stress-strain plots for each radial arm of the test protocol show the variation in response at varying load ratios, including negative strain, gradient reversal and sudden changes in gradient. Loading and unloading curves give an indication of the potential variation in strain for a given stress state due to recent load history. Values vary considerably depending on fabric type and stress ratio, but are commonly 1 to 2% strain which can be up to 100% of the total strain (e.g. Figure 4-4, load path D, fill at 5kN/m).

To better understand the fabric response, and to enable comprehensive comparison between repeat tests, response surfaces in the stress-stress-strain space have been used. When the overall fabric response is considered the loading/unloading variation and non-linearities are less significant than for individual load paths. The mean deviation between loading and unloading surfaces for all fabrics tested is 2.2% (warp) and 2.8% (fill) of the strain range. All fabrics exhibited high residual strains in the fill direction after testing, in particular PTFE-glass fibre fabrics with fill strains of around 13%. One long term recovery test was carried out which indicated that this is non-recoverable; however, thorough creep and recovery testing is beyond scope of this research. Further work on creep and recovery would be useful to aid design of re-tensioning details and ensure that prestress is maintained for the design life of a structure (§6.2.4).

Current representations of fabric stress-strain behaviour are based on plane-stress assumptions, and tend to simplify the available data (e.g. use of secant elastic moduli). Young's moduli and Poisson's ratios were determined for each test so as to provide the best fit plane to the scattered data points. These planar representations provided a surprisingly good correlation with test data. The elastic constants do not comply with plane stress theory: this is reasonable because coated woven fabrics are not homogeneous materials: they are composites with the interaction of orthogonal yarns making them act as a constrained mechanism.

It is therefore appropriate to move away from plane stress theory and develop a new method for representing architectural fabric behaviour. Day's (1986) work on stress and strain mean and difference functions has been reproduced to see if this provides a useful basis for defining fabric behaviour. However, the utility of his method seems to be limited to curve fitting data at a limited number of stress ratios, with poor interpolation between these stress ratios. Day's method employs a limited number of equations and is not suited to representing test data from a wide range of stress states, such as that from the test protocol developed in this research.

A new approach to incorporating fabric test data in structural analysis is proposed here: use of direct correlation between pairs of stresses and strains. This avoids the inherent approximation in defining elastic constants or other parameters to quantify the fabric behaviour. A simple triangular interpolation scheme has been proposed which is robust and avoids the risk of unreliable interpolation and extrapolation when using a functional representation of the data.

The proposed method for using the test data in structural analysis is as follows. Prestress is applied to the model to determine the fabric geometry (*form finding*). This provides a reference geometry which is deemed to be 'zero strain'; and hence is compatible with the adjusted test data for which stresses are equal to prestress and strains are equal zero. The finite element analysis is then carried out using the test data with residual strain removed. The test data is incorporated directly in the analysis as a look-up table of values. Applied loads (e.g. wind and snow) cause displacements, which are resolved into warp and fill strains. Interpolation between data points determines the warp and fill stresses appropriate to the strain state. An iterative process gives consistent strains and stresses. Finally the membrane stresses can be checked against allowable stresses or incorporated in a reliability based analysis. This analysis procedure does not include residual strain or shear, both of which must be incorporated and are discussed in Chapter 6.

Strain-strain-stress surfaces show that the fabric is very sensitive to changes in strain: small changes in strain result in large changes in stress. This makes inclusion of strain variability due to load history and fabric variability vital. Because the test protocol provides results for all feasible stress states (from zero to 25% ultimate tensile strength), plotting the test data on strain-strain axes demonstrates the range of feasible strain states which a given fabric can attain. The differing characteristics of PTFE-glass fibre fabric and PVC-polyester fabric are clear from the form of the strain response envelope. This type of diagram provides a new tool for quantifying and understanding the biaxial behaviour of different fabric types, and can easily be extended to include shear and creep behaviour.

Chapter 5

Predictive fabric models

Contents

Figures

Tables

5.1 INTRODUCTION

Architectural fabrics have different mechanical properties due to variations in material properties and weave geometry (yarn diameter, weave pattern and coating thickness). Variability in the manufacturing process leads to inconsistency in properties between fabric batches, and even across the width of a single roll. Biaxial testing is frequently carried out at prestress to determine compensation values, but rarely at working loads to determine fabric stress-strain behaviour for structural design. There are few biaxial test rigs with sufficient load capacity for this type of testing. Prior to the development of a test rig at the University of Newcastle for this work, one of the only suitable test rigs in Europe was at the Laboratorium Blum, Stuttgart (www). The specialist nature of fabric biaxial testing makes accurate determination of material properties prohibitively expensive, especially for small structures.

Uniaxial strip tests are routinely carried out by manufacturers to determine the ultimate tensile strength of a fabric in warp and fill directions. However, measurements of load and extension from these tests give limited information about the biaxial stress-strain behaviour of the fabric. The interaction of warp and fill yarns (*crimp interchange*) results in complex, non-linear biaxial behaviour that cannot directly be inferred from uniaxial results alone. Despite considerable work in the field, predictive models based on constituent material properties and fabric geometry have so far failed to determine fabric response sufficiently accurately for use in structural design (§2.4). Previous work has typically focused on either PTFE-glass or PVC-polyester fabric. It would be useful to develop a model applicable to both types of fabric. Whilst the material properties are different for the two types of fabric, the fundamental deformation mechanisms are the same for both. A model which is sufficiently general for both PTFE-glass and PVC-polyester has scope for more general application: for other architectural fabrics (e.g. silicon coated glass and Tenara, manufactured by Gore, www) and fabrics used in other fields (e.g. medical textiles; Gupta, 1998).

A model which predicts the biaxial behaviour of coated woven fabrics up to design working loads with no specialist testing or software would be of benefit for:

- Determination of material properties for fabric structure design,
- Rapid comparison of different types and weights of fabric,
- Assessment of the impact on a structure of using several different fabrics,
- Reverse engineering of fabric, i.e. understanding how fabric parameters (e.g. weave spacing, initial crimp balance) can be varied to give the required fabric properties. This iterative process could be automated; the user would input the desired material properties and the necessary fabric parameters would be determined. This could be used to select the best fabric for a project from those available, or for a large project it would enable the designer to specify the fabric parameters. For example, Ferrari (www) can control the relative levels of warp and fill crimp using their *précontraint* system. Initially the system was developed to provide balanced fabrics

with equal warp and fill crimp. For some structures this actually makes installation more difficult, specifically when fill prestress is introduced by tensioning the fabric in the warp direction with the fabric restrained in the fill direction. Crimp interchange results in negative fill strain, and hence an increase in fill stress. This is particularly useful for installing barrel vault canopies. A predictive fabric model combined with the Ferrari *précontraint* system would enable designers to specify the required levels of crimp to give the correct fill prestress for a given structure.

Predictive fabric models typically consider the fabric 'unit cell', the smallest repeated unit in the fabric. For a plain weave fabric this is simply half a wavelength of two orthogonal yarns intersecting on plan (Figure 5-1).

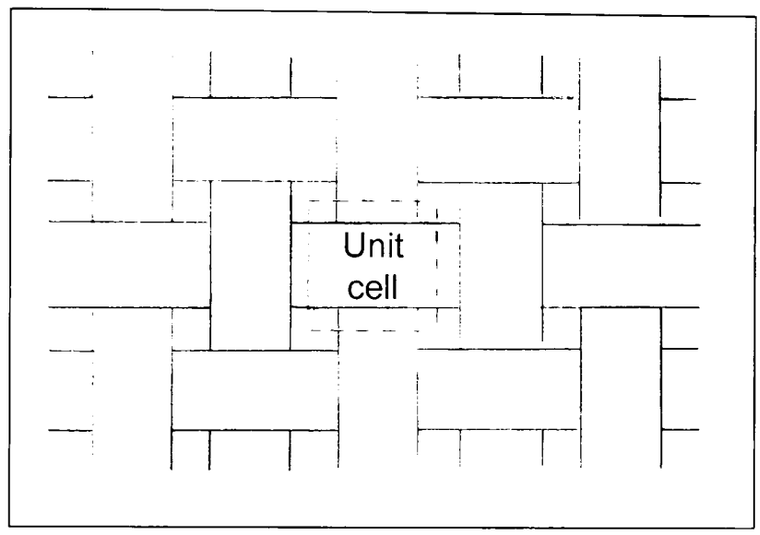

Figure 5-1. Plain weave unit cell

Fabric properties which are typically incorporated in the model include the initial fabric geometry and the yarn/fibre and coating mechanical properties. For this work the yarn and coating have been taken as the fundamental fabric units. Predictive models have been developed to determine the yarn tensile behaviour from knowledge of the fibre properties and spinning process (§2.4.1). This extra level of analysis would not benefit this work because:

1. Determining yarn properties directly is experimentally easier than testing individual fibres,
2. Predicting the yarn properties would add another level of complexity to the model which might reduce its accuracy,
3. The weaving and coating processes significantly affect the yarn properties: at best the yarn model would predict the properties of an as-spun yarn rather than an in-situ yarn in the coated fabric.

One benefit of including a yarn model is that the reverse engineering discussed above could be taken a step further, enabling the effect on the fabric properties of changes to the fibre type and spinning parameters to be determined.

5.2 AIMS

To develop a predictive model that is:

1. Capable of determining the in-plane stress-strain characteristics of coated woven fabrics under biaxial load, suitable for use in structural design,
2. Truly predictive and that requires no adjustment of parameters to fit a given data set,
3. Applicable to a wide range of fabric materials, types and weights,
4. Easily accessible to the design engineer; with input parameters which can be measured using standard tests and/or commonly available equipment,
5. Simple to set-up for different fabrics and does not require overly specialist software or computer hardware,
6. Proven to work through numerical comparison with a range of fabric test data.

5.3 MODEL FORMULATION

5.3.1 Nomenclature

Subscripts $_1$ and $_2$ denote warp and fill directions respectively,

' modified value under load, e.g. A = initial amplitude (unstrained), A' = modified amplitude with applied load,

'' value after two load increments,

r yarn radius; for non-circular yarns r is half the yarn thickness in the out-of-plane (z) direction (mm),

$\mathbf{r}_{area1,2}$ value of r required to give a constant yarn cross-sectional area (mm),

w half the yarn width, equal to r for a circular yarn (mm),

x warp direction,

y fill direction,

z out-of-plane direction, orthogonal to x and y,

A crimp amplitude (mm),

Area yarn cross-sectional area (mm^2),

B segment of yarn cross-section used in sinusoidal model (Figure 5-13), B + D = cross-sectional area,

C yarn crushing stiffness (kN/mm per yarn intersection, i.e. the spring constant for each yarn = C/2),

D segment of yarn cross-section used in sinusoidal model (Figure 5-13), B + D = cross-sectional area,

E yarn tensile modulus (kN/mm per yarn),

$\mathbf{E_j}$ coating compressive stiffness (kN/mm per yarn),

$\mathbf{E_k}$ coating tensile modulus (kN/mm per half unit cell width, L),

F applied load per unit cell, equal to the load per yarn for a plain weave fabric (kN),

$\mathbf{F_c}$ crushing force (out-of-plane (z) force developed by yarn) per crossover (kN),

$\mathbf{F_k}$ force acting on coating (kN) per unit cell width ($F_{k1,2}$ acts over a width $L_{2,1}$),

$\mathbf{F_y}$ tension force in yarn (kN),

L half the length of unit cell (L = yarn wavelength/4) (mm),

P applied load per metre width of fabric (kN/m width),

Q curve bounding sinusoidal yarn cross-section (Figure 5-13),

T fabric thickness (mm),

$\mathbf{T_n}$ yarn tension between nodes n and n-1 (sinusoid formulation, Figure 5-10),

Y yarn length, half the length of yarn in a unit cell (mm), equal to one quarter of the yarn wavelength,

ε strain (%),

θ angle between yarn and fabric plane (°),

5.3.2 Sawtooth model

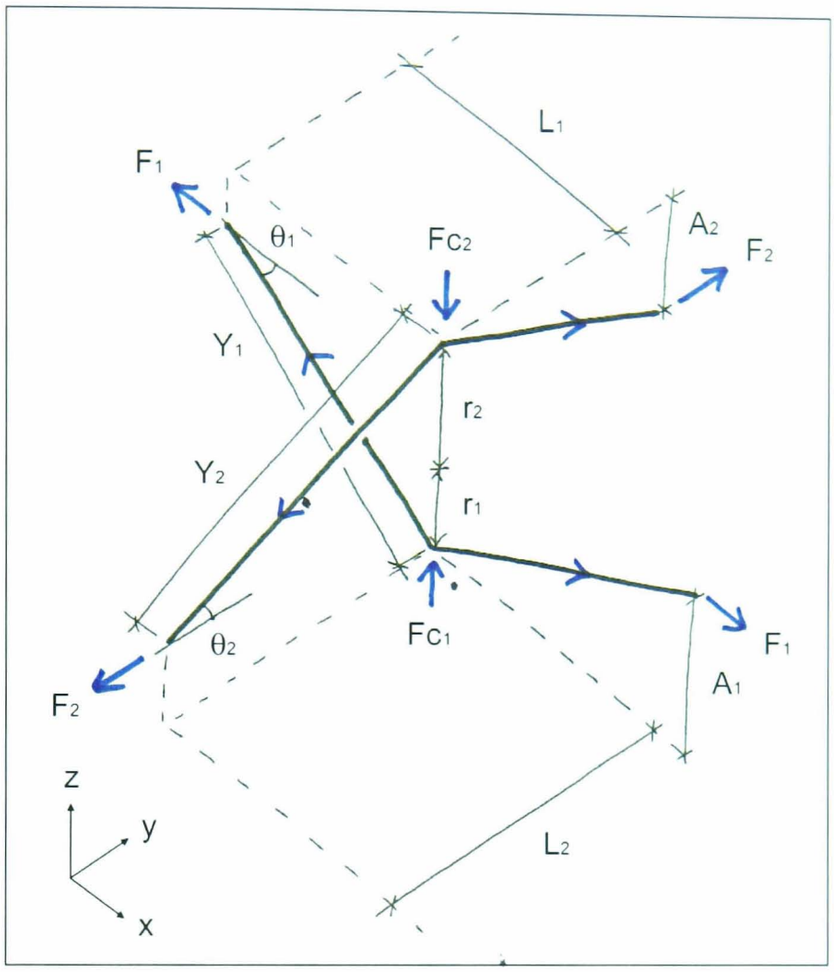

Figure 5-2. Fundamentals of the sawtooth unit cell model

Initially a simple sawtooth model (Peirce, 1937; Menges & Meffert, 1976; §2.4.2) was developed with inextensible yarns, no yarn crushing and no coating (Figure 5-2). These elements were then added to the model sequentially. The model behaviour is elastic – there is no consideration of energy loss and viscoelastic effects. Three equations are used to define crimp interchange equilibrium (terms are defined in §5.3.1):

$$r_1 + r_2 = A_1 + A_2$$ Equation 5-1 (Peirce, 1937)

$$Fc_{1,2} = Fy_{1,2} \sin \theta_{1,2}$$ Equation 5-2

$$Fc_1 + Fc_2 = 0$$ Equation 5-3

Equation 1 is a simple geometric relationship that is evident from Figure 5-2. The sum of vertical forces in the unit cell must be zero as (assuming negligible bending stiffness) the fabric provides no restraint to out-of-plane forces (Equation 2). The force in the yarn is a component of the applied force (Figure 5-5, Equation 5-4).

$$Fy_{1,2} = \frac{F_{1,2}}{\cos \theta_{1,2}}$$ Equation 5-4

This is true if the orthogonal yarns do not slide over one another; i.e. inter-yarn friction is modelled as being infinite. As inter-yarn friction tends to zero, $Fy_{1,2}$ tends to $F_{1,2}$. Any slippage at crossovers would be seen during testing, a proportion of the strain would occur at the edge of the fabric sample (Figure 5-3). As the coating restrains the yarn movements and prevents slippage, the high friction (no slip) model has been adopted. As some slippage may occur, the two types of model may bound the actual fabric response, and ideally partial slippage may be required.

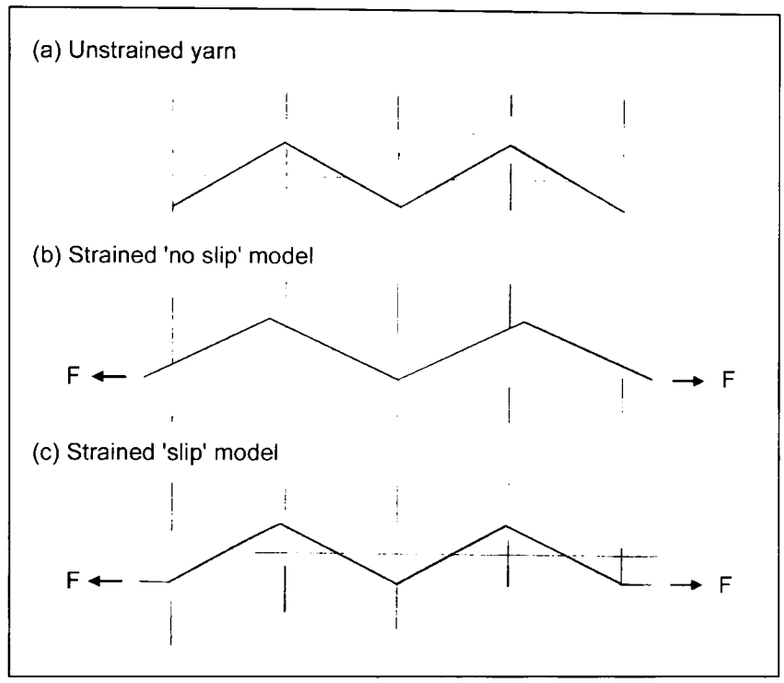

Figure 5-3. 'Slip' and 'no-slip' models

To determine the yarn tension ($Fy_{1,2}$) the applied load per metre width must be scaled down to the load per unit cell; for a plain weave fabric this is the load per yarn (Equation 5-5).

$$F_{1,2} = \frac{P_{1,2}}{2L_{2,1}}$$

Equation 5-5

Equations 5-1 to 5-5 provide the fundamental model of crimp interchange based on force equilibrium in the fabric. **Yarn extension** has been incorporated into the model with the yarn assumed to be linear elastic (Equation 5-6). However, the elastic modulus can be varied (with stress or strain) using a multi-linear representation to model non-linear tensile extension.

$$Y'_{1,2} = Y_{1,2}\left[1 + \left(\frac{Fy'_{1,1}}{E_{1,2}}\right)\right]$$

Equation 5-6

During model development a **yarn crushing** mechanism has been included, initially using a crushing modulus ($C_{1,2}$) to determine the reduced yarn radius (Equation 5-7). The yarn crushing modulus is defined per yarn.

$$r'_{1,2} = r_{1,2}\left[1 - \frac{Fc_{1,2}}{C_{1,2}}\right]$$

Equation 5-7

Poisson's effects of a yarn are more significant than for a single fibre. The tightening of the twisted fibre bundle under load results in a reduction in cross-sectional area (§2.1.1 & 2.4.2). Yarn extension should be coupled to yarn crushing (Pargana et al, 2000): in this model the crushing force is a function of the yarn force (Equation 5-2), which in turn is dependent on the applied load. Hence yarn extension and crushing are implicitly linked.

Determination of yarn crushing stiffness from tests is problematic:

1. Testing of virgin yarns may not be representative of the yarn properties after weaving and coating,
2. Removal of yarns from a coated fabric is difficult without damaging the yarn,
3. Testing of yarns removed from the coated fabric does not account for the effect of the coating around the in-situ yarn on it's crushing behaviour,
4. Yarn crushing tests are not standard practice or easy to carry out, and so do not comply with the objectives of this model (§3.1.2).

Because of these difficulties, the yarn crushing stiffness ($\mathbf{C}_{1,2}$) has been used as a parameter for calibrating the model against test data. The aim is to determine a crushing stiffness value that does not need to be modified for each fabric, as this would compromise the predictive nature of the mode. Acceptable options are:

1. A single value which is constant for all fabrics,
2. A value for each fabric type (e.g. PTFE/glass, PVC/polyester),
3. A value which is a function of measured fabric attributes, C = f (fabric weight, fabric thickness, yarn wave form, yarn cross-section shape, yarn and coating tensile properties).

If a different value of $\mathbf{C}_{1,2}$ is required for each fabric the model becomes useless as a predictive tool. Yarn crushing in the model has been limited such that $\mathbf{r}_i'$ is always greater than half the original yarn radius. This is an arbitrary constraint and is open to modification based on comparison with test results. Alternatively a progressively stiffening spring can be used (Dimitrov & Schock, 1986). Problems with the determination of the yarn crushing modulus (§3.1.2) prompted a search for an alternative method for calculating the change in yarn radius under load. One alternative is to maintain a constant yarn cross sectional area (Freeston, Platt & Schoppee, 1967; Glaessgen et al, 1996). As well as obviating the need to define the yarn crushing stiffness, this enables the yarn cross-section to be modelled such that it is consistent with the wave-form of the orthogonal yarn. This is preferable to the yarn cross-section being defined only by a radius, with the implicit assumption that the yarn is circular, or an undefined ellipse.

The transverse compressive forces vary with the sine of the angle of yarn. The angle between the sawtooth yarn and the horizontal varies between zero and approximately 45° depending on the fabric type

and stress ratio. The yarn crushing force varies from close to zero to around 70% of the applied load. However, it has been assumed that the compressive deformation of the yarn fibres is negligible. This is reasonable for glass fibres, but for polyester fibres crushing may be significant. Determination of the fibre crushing stiffness, and what level of fibre deformation would occur in preference to rearrangement, would make the model overly complicated (§6.2.9). Hence it has been assumed that yarn crushing is dominated by the rearrangement of the yarn fibres, which will occur with constant yarn cross sectional area. Initial 'bedding down' of the yarn fibres may cause a reduction in yarn cross-sectional area when the fabric is first loaded, but this has been assumed to be negligible in this work. This initial affect is more important for calculation of compensation values and residual strain than predicting the medium to long term elastic stress-strain behaviour.

A yarn cross-section consistent with the sawtooth unit cell geometry can be defined by four straight lines. From the elliptical initial yarn geometry it is appropriate to model the cross section using an equilateral parallelogram, or rhombus (Figure 5-4). As load is applied to yarn 1 (Figure 5-5b) the width of yarn 2 must increase to maintain a constant yarn area. This may be reasonable initially, but as θ_1 tends to zero (Figure 5-5c) the width of yarn 2 will tend to infinity and the area to zero.

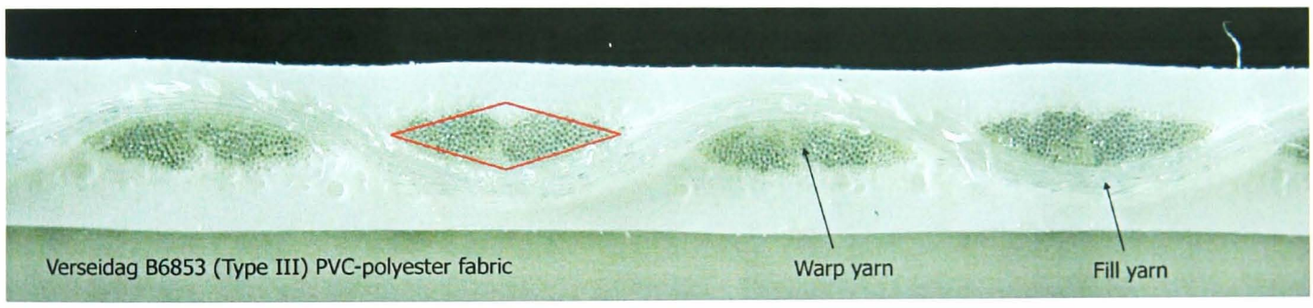

Figure 5-4. Rhombus yarn cross section

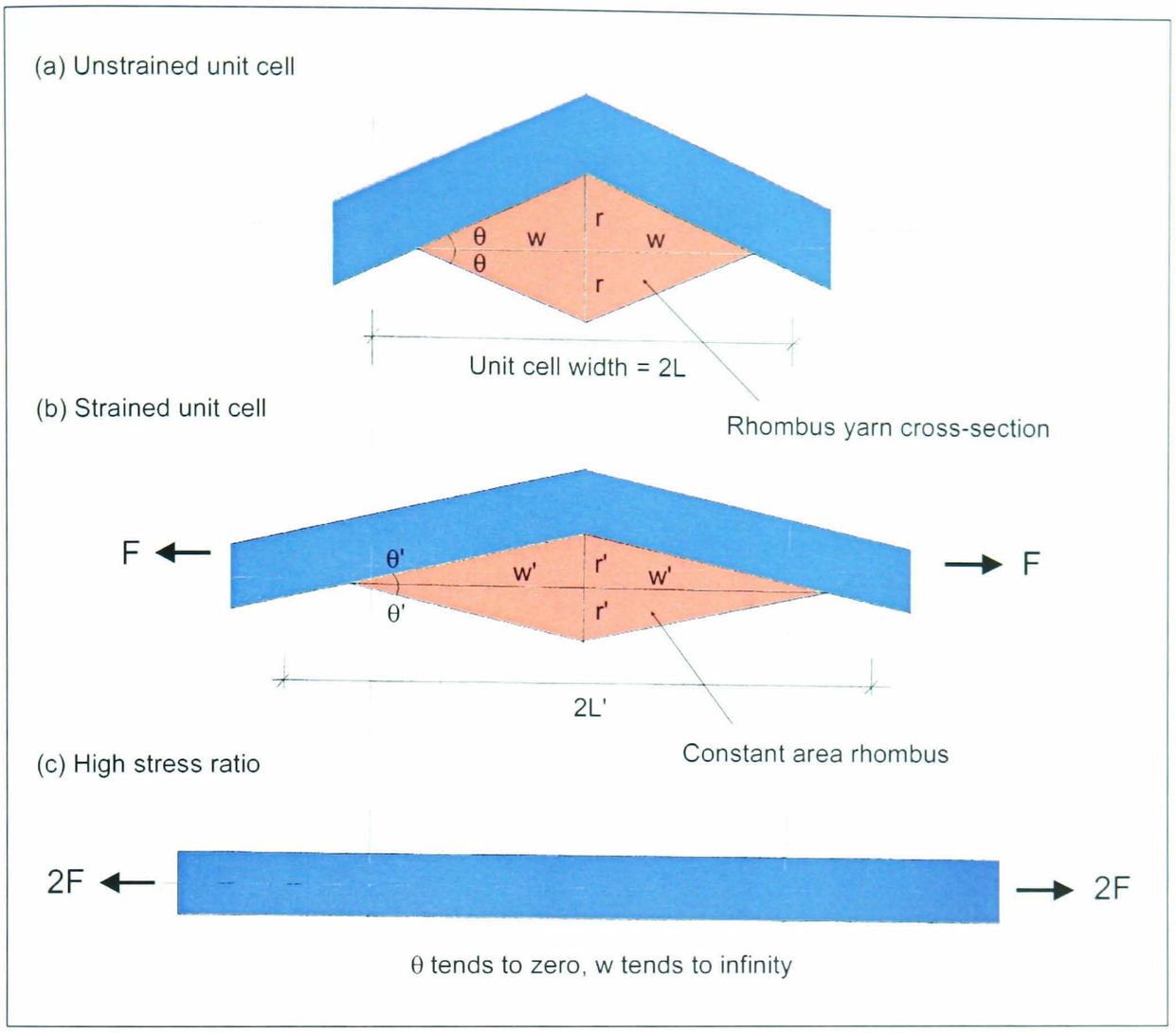

Figure 5-5. Rhombus yarn cross section deformation

The rhombus is clearly inappropriate for modelling the deformed yarn cross section. An alternative is to use a quadrilateral with one line of symmetry, or *kite shape* (Figure 5-6). The initial geometry is modelled with a rhombus, which is used to calculate the yarn area from measurements of width and thickness. When the unit cell deforms the yarn cross section changes from rhombus to a kite shape (Figure 5-6b). In the limiting case of yarn 1 being straight, the cross section of yarn 2 will be an isosceles triangle with height 2r' and width 2w' (Figure 5-6c).

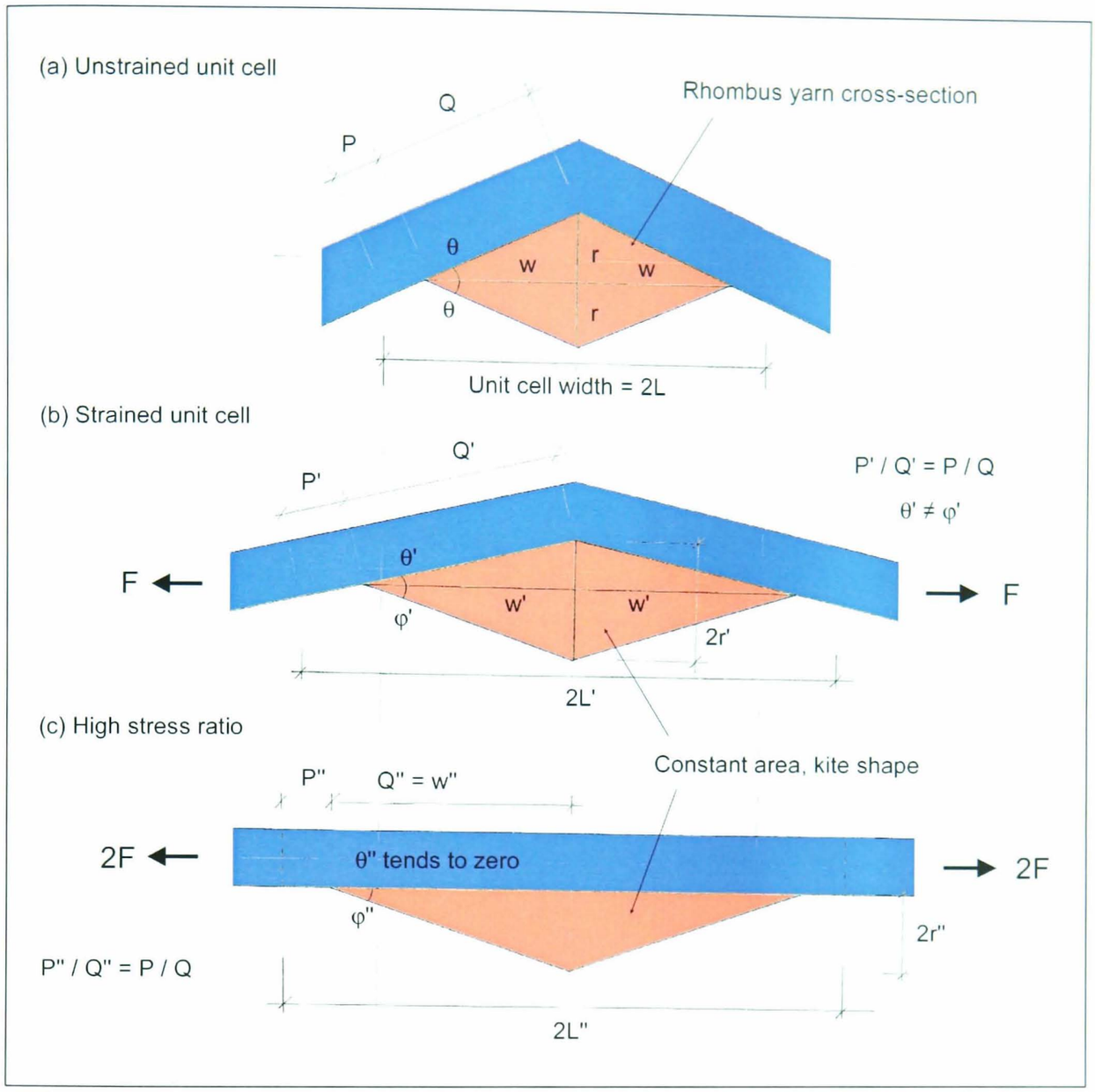

Figure 5-6. Kite shape yarn cross-section

The relative position of point A is maintained as yarn 1 moves; i.e. as yarn 1 extends the ratio P:Q is kept constant, the width of yarn 2 increases as yarn 1 extends. The movement of point A to maintain a constant ratio P:Q is not intended to model inter-yarn friction which will be small, particularly for glass-fibre yarns. It is proposed that it is the extension of the coating (which corresponds to the extension of the yarn) which determines the dimensions of the yarn cross section. It is difficult to measure the exact geometry of the fabric as it deforms. To observe the fabric geometry under load would mean cutting the sample, which would profoundly affect the state of stress and balance of forces in the fabric. Some researchers have attempted to accurately measure the fabric thickness during biaxial loading and make inferences about the fabric deformation from these measurements (Fontaine, Durand & Freyburger, 2002). This type of measurement requires specialist equipment and is not within the scope of this project. Even with these thickness measurements it is difficult to determine how the yarns and coating are contributing to the fabric thickness, although this can be helped by measuring the maximum and minimum fabric thicknesses, i.e. at the peaks and troughs of the yarn waveform.

The quadrilateral representation of the yarn cross-section provides a feasible, approximate model of the yarn which enables the yarn thickness in the out-of-plane direction ($r_{1,2}$) to be determined such that the yarn cross-sectional area is constant and the yarn shape is consistent with the orthogonal yarn. A constant yarn *volume* has also been modelled, such that tensile extension of the yarn leads to a decrease in yarn cross-sectional area (in effect a yarn Poisson's effect). Difficulty in determining a value for the yarn Poisson's ratio led to a constant *area* model being adopted for simplicity. Use of a constant area or volume constraint removes the need to define the yarn crushing stiffness, the yarn thickness being determined geometrically.

The final step in building up the sawtooth model was to add the **coating** (Figure 5-7). This is modelled as a spring between the peaks of the sawtooth wave-form (Menges & Meffert, 1976). For simplicity, lateral contraction of the coating under tensile load (i.e. Poisson's effect) has not been included (§6.2.9). The coating is largely responsible for the time dependent aspects of fabric behaviour. In this model the fabric behaviour is assumed to be elastic; viscoelasticity could be introduced by modelling the coating as a spring and damper (Uetani, Fujiwara & Ohsaki, 2002).

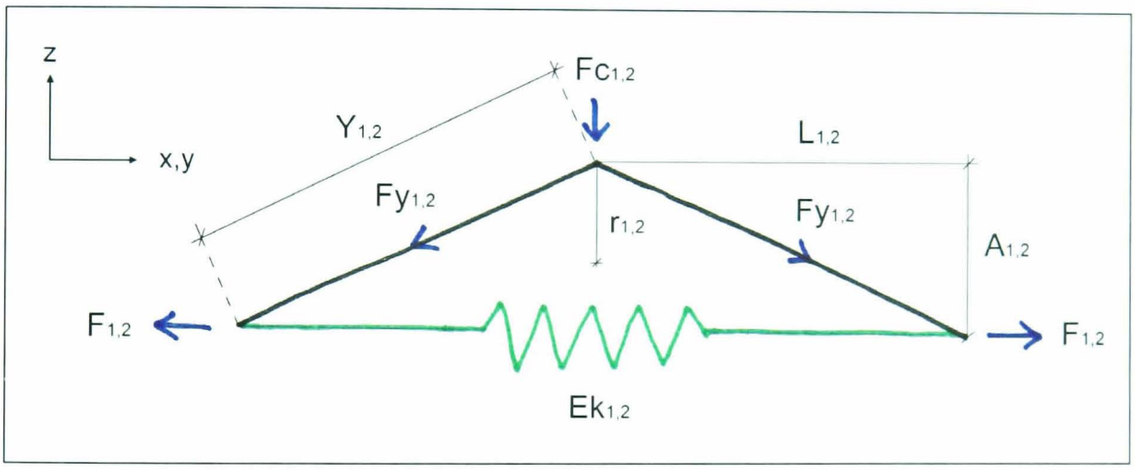

Figure 5-7. Inclusion of coating in unit cell model.

Calculation of the effect of the coating is not as straightforward as calculation of the yarn extension or change in yarn radius. An iterative process has been used to determine how much force should be applied to the coating (i.e. using direct substitution). The equilibrium configuration of the unit cell is calculated without the coating, and the resultant change in unit cell length provides a first approximation to the coating strain. The force required to give this level of strain in the coating is calculated from the coating stiffness, and subtracted from the applied load acting on the yarn. The equilibrium configuration of the unit cell is then recalculated using the modified yarn force; hence the coating strain is modified and so on until a consistent set of forces and strains is achieved. This iterative process is necessary as the force cannot be distributed to the yarn and coating in proportion to their relative stiffness because the yarn stiffness is dependent on a combination of yarn modulus (constant) and crimp interchange (stiffness varies with yarn angle, which varies with yarn force).

Whether the coating should act in tension only or both tension and compression is debatable. The way in which the coating stiffness is determined from uniaxial tests only provides data on the tensile stiffness (§5.4.2). Measurement of the compressive resistance of the coating is problematic; any in-plane compressive load on the fabric on a large scale will simply result in bending. Out-of-plane compression of coating removed from the fabric would be valid if the material was isotropic, but the polymeric nature of both PVC and PTFE coatings result in anisotropic properties (§2.1.3). Removal of coating and small scale compressive testing are not standard techniques, and are therefore not suitable for this model. However, during crimp interchange negative strains do occur, and hence compressive forces are exerted on the coating. Compressive coating stiffness and its effect on the model output is discussed further in Section 5.5.2.

Three elements of the model require an iterative solution: yarn extension, determination of the yarn cross-section and coating extension. This would make the model cumbersome to include directly in a finite element analysis as it would add a further iterative step to the already time consuming non-linear large displacement analysis. However, the model does not need to be used directly in the analysis. For a given fabric a set of data points can be generated at a number of expected stress states, for example for warp and fill stresses from 0 to 25% UTS at 1kN intervals. Interpolation between this database of values could then be used in the analysis. Areas of the fabric response which are sensitive to small changes in stress or strain can be identified and additional data points calculated to reduce interpolation errors. This check could be carried out automatically; limits could be set for the maximum allowable stress and/or strain difference between neighbouring points, and further data points would be calculated to achieve this. This method of implementation is very similar to that proposed for the biaxial test data generated by this research (§4.2.3).

Initially programming was carried out in *Matlab* (www: Matlab). However, it was found that the *Excel Solver* (a standard *Microsoft Excel* add-in) provides an effective tool for solving the model, and is universally available. For model development which requires many runs of the model, speed has been increased by installing the *Premium Solver Platform* (www: Solver), a third-party add-in to *Excel*. The standard *Excel Solver* is adequate once the model is finalised. The input to the *Excel Solver* is a list of variables, constraints and target values (Table 5-1). Multiple loadcases are analysed using a *Visual Basic* routine, and results are exported to *Matlab* (using the *Matlab 'Excel Link'* toolbox) for visualisation and comparison with test data.

Parameter	'Slip' model	'No slip' model
Initial values from fabric geometry	$L_{1,2}$, $r_{1,2}$, $A_{1,2}$, $w_{1,2}$	As slip model
Material properties from uniaxial tests	$E_{1,2}$, $E_{k1,2}$	As slip model
Initial values calculated from fabric geometry	$Area_{1,2} = 2\, r_{1,2}\, w_{1,2}$ $Y_{1,2} = \sqrt{(A_{1,2}^2 + L_{1,2}^2)}$	As slip model
Applied load	$F_{1,2}$	As slip model
New values for yarn geometry	$L'_{1,2} = \sqrt{(Y'^2_{1,2} - A'^2_{1,2})}$ $A'_{1,2} = Y'_{1,2} \sin \theta'_{1,2}$ $w'_{1,2} = (w_{1,2} / L_{2,1})\, L'_{2,1}$ $\varepsilon_{1,2} = (L_{1,2} - L'_{1,2}) / L_{1,2}$ $F_k'_{1,2} = E_{k1,2}\, L'_{2,1}\, \varepsilon_{1,2}$ $Fy'_{1,2} = (F_{1,2} - F_k'_{1,2})$ $Y'_{1,2} = Y_{1,2} [\, 1 + (Fy'_{1,2} / E_{1,2})]$ $r_{area}'_{1,2} = Area_{1,2} / (2w'_{1,2})$	As slip model except: $Fy'_{1,2} = (F_{1,2} - F_k'_{1,2}) / \cos \theta'_{1,2}$
Excel Solver parameters: variables modified by solver	$r'_{1,2}$, $Y'_{1,2}$, $\varphi'_{1,2}$	As slip model
Excel Solver parameters: constraints	$r'_{1,2} = r_{area}'_{1,2}$ $A'_1 + A'_2 = r'_1 + r'_2$ $Fy'_1 \sin \theta'_1 = Fy'_2 \sin \theta'_2$ $(A'_{1,2} / L'_{1,2}) - \tan \theta'_{1,2} = 0$	As slip model
Subscripts 1 and 2 denote warp and fill directions respectively, ' = modified value under load, e.g. A = initial amplitude (unstrained), A' = modified amplitude with applied load.		

Table 5-1. Sawtooth model summary.

5.3.3 Sinusoid model

It is clear from images of the fabric cross-section that the sawtooth arrangement does not provide the best possible representation of the yarn wave-form (Figure 5-8).

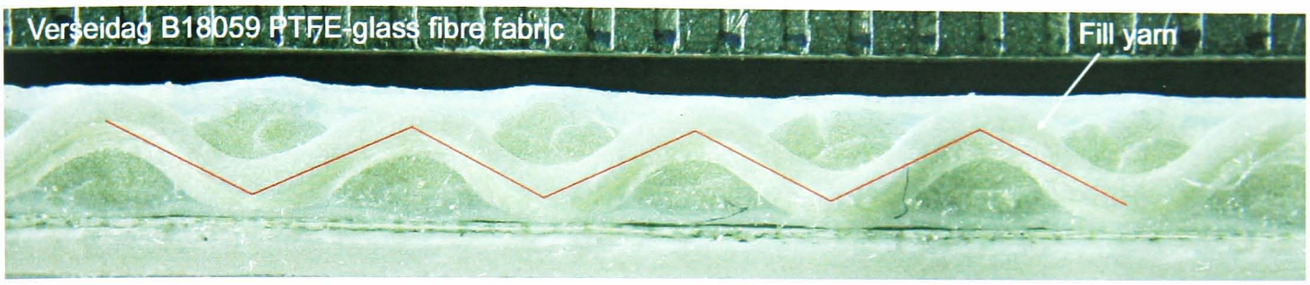

Figure 5-8. Sawtooth representation of yarn wave-form

Use of a more realistic representation than the ubiquitous sawtooth may benefit model accuracy (Olofsson, 1964 & 1966; Wang, 2002). Sinusoidal or other curved yarn representations are frequently used in finite element unit cell models, which impose fewer restraints on the geometry (§2.4.2.1). Methods used to model curved yarns include:

- A series of control points interpolated by a Bézier curve with ellipses defining the yarn cross section (Glaessgen et al, 1996),
- A sinusoidal waveform (Tarfaoui & Akesbi, 2001; Wang, 2002),
- A model with no *a priori* assumptions about the yarn wave form, the geometry of the yarn being a function of the applied loads and initial set (Olofsson, 1964 & 1966). The initial set is the residual shape of a yarn when it is removed from the fabric.

Fourier analysis (Stroud, 1996) has been carried out on points measured along in-situ yarns to determine the most appropriate function to represent the shape of the yarn. Twelve points were measured along one wavelength of the yarn and the difference between the first three harmonics and the measured points was calculated (Figure 5-9). With the addition of each harmonic the function, by definition, provides a better fit to the test data. However, the correlation of the simple sine curve (or fundamental, $a_0 + a_1 \sin x$) is extremely good (Table 5-2). The mean deviation from the measured points is only 2.5% of the amplitude for the Taconic Solus 1120 PTFE-glass fibre and 1.7% for the Verseidag B6853 PVC-polyester. To define a simple sine function only requires measurement of the yarn amplitude and wavelength (§5.4.1). If additional harmonics were used then further points would need to be measured on the yarn cross-section to determine the required constants (a_2, a_3 etc.) for each fabric. Additional harmonics would also increase the complexity of the calculations of yarn length and unit cell equilibrium. For this work the fundamental sine function has been used.

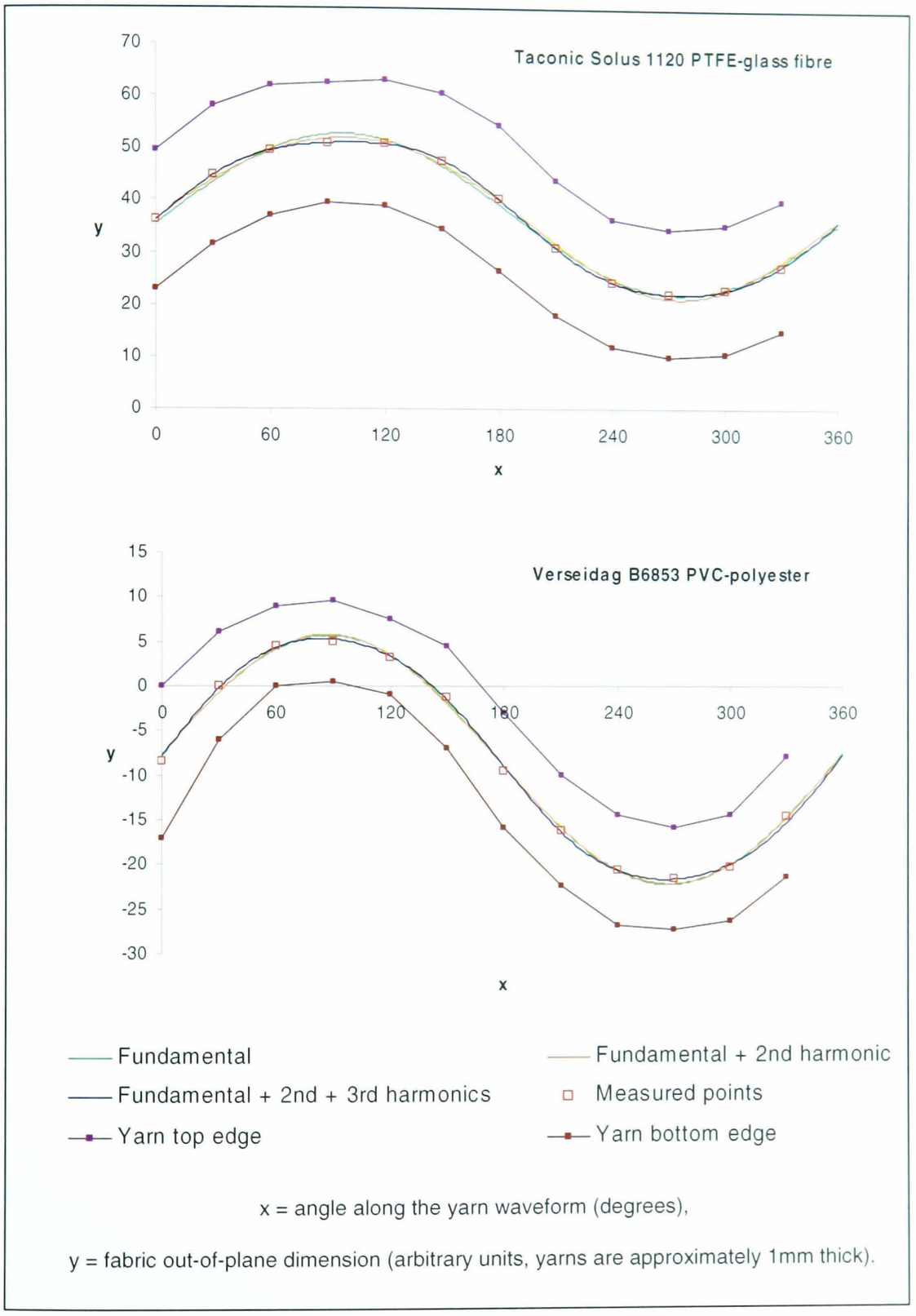

Figure 5-9. Fourier analysis of weave shape

Material	Fabric	All values expressed as a percentage of the measured yarn centreline amplitude (standard deviation)		
		1st harmonic $a_0 + a_1 \cos x$	1st + 2nd harmonics $a_0 + a_1 \cos x + a_2 \cos 2x$	1st + 2nd + 3rd harmonics $a_0 + a_1 \cos x + a_2 \cos 2x + a_3 \cos 3x$
PTFE/glass fibre	Taconic Solus 1120	2.54 (1.63)	1.88 (1.15)	0.43 (0.32)
PVC/polyester	Verseidag B6853	1.66 (0.90)	1.59 (0.92)	1.06 (0.72)

Table 5-2. Fourier analysis of weave shape

Use of a sine wave to represent the yarn provides a more accurate measure of yarn length for a given wavelength and amplitude, and hence may provide a more accurate determination of decrimping strain. It should also allow the out-of-plane 'crushing force' generated by the yarn to be calculated more accurately. Recent research using a sinusoidal yarn wave-form (Wang, 2002) involved simplification of the calculation of the out-of-plane contact forces between the two yarns. Wang used the vertical component of the force in the yarn at the steepest part of the sinusoid (§2.4.2). A synergy of Wang's sinusoidal waveform with Olofsson's (1964, 1966) concept of the applied loads determining the yarn wave form has been developed for this research. Contact forces at multiple points along the yarn are calculated which provide a sinusoidal yarn geometry with the correct yarn length. These forces are summed to give the out-of-plane forces which are necessary to determine crimp equilibrium.

Yarns have negligible bending stiffness (§2.1.1) and so it is only the applied load and contact forces which determine the yarn shape. Theoretically, in the area where the yarn is not in contact with an orthogonal yarn it should be straight (§2.4.2; Figure 2-41, Peirce, 1937). There are several reasons why a sinusoid (as opposed to sections of sinusoid joined by straight lines) is appropriate for modelling the yarn wave-form in architectural fabrics:

- Yarns are in almost constant contact with the orthogonal yarns, giving a short (or non-existent) length of 'free' yarn (Figure 5-8),
- Where the yarns are not in contact is at the start, mid-point and end of the sine curve (i.e. 0°, 180° and 360°); these are points of inflection with a low rate of change of curvature – the sine curve provides a good approximation to a straight line in these areas,
- The fourier analysis used to fit sine curves to the yarn images showed that a simple sine wave provides an extremely a good fit to the fabric geometry throughout its length.

The yarn has been modelled as being composed of many pinned bars with vertical forces (Fv_n) applied at each node and a horizontal force (F) applied at one end (Figure 5-10). The total length of the yarn in the unit cell is twice the sum of the yarn segments (ΣY_n) shown in Figure 5-10. For clarity the quarter wavelength shown has only been divided into four, in the model twenty-five subdivisions have been used to approximate the curve.

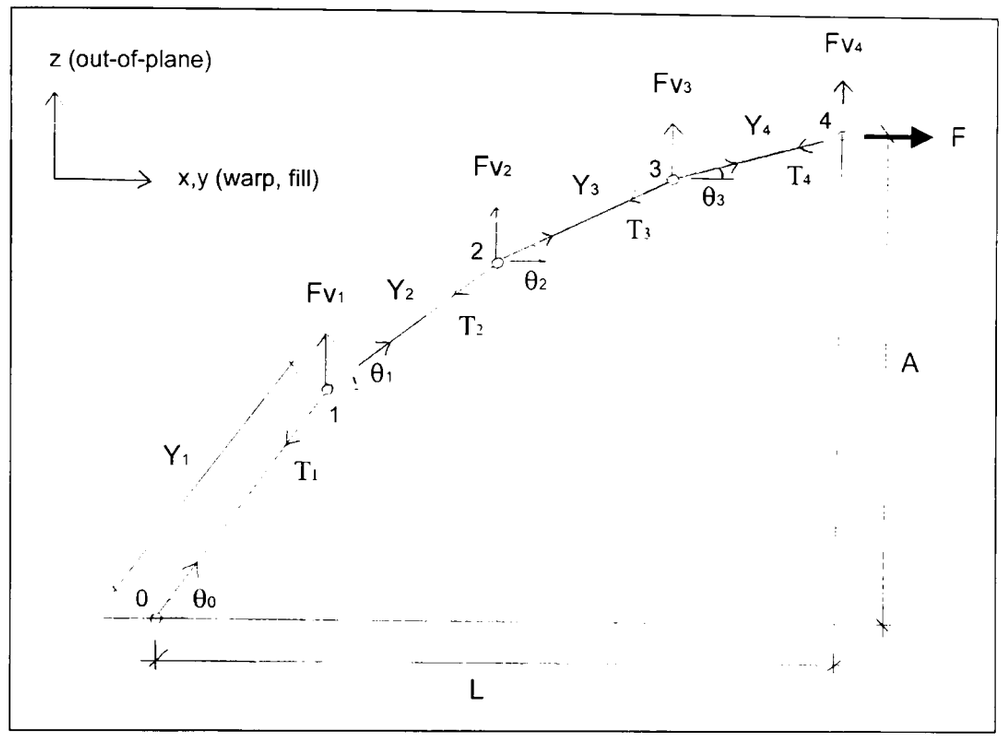

Figure 5-10. Sinusoidal yarn model

Measurements of fabric geometry provide the amplitude and wavelength, from which the initial shape of the sinusoidal yarn curve are known. Hence angles θ_1 and θ_2 are known at each node. As in the sawtooth model, there are two options for modelling inter-yarn friction:

1. 'Slip'- zero friction between yarns at crossovers. The yarn is modelled as if it passes over a series of rollers: the yarn tension, T, is equal to the applied load (minus any load taken by the coating) and so is constant. This is less realistic but simpler to model than,

2. 'No slip' – infinite friction, no inter-yarn movement at crossovers, yarn tension varies throughout its length due to contact forces with the orthogonal yarn.

The actual fabric behaviour may lie somewhere between these two extremes, but certainly closer to the 'no slip' model as evidenced by the lack of yarn pull-out at the edges of a test piece. The 'slip' version of the sinusoid model has initially been developed as it is considerably simpler with fewer iterative steps. The no-slip version has then been developed with varying tension along the yarn (§5.3.3.2).

5.3.3.1 Slip formulation

The sinusoid model has initially been formulated assuming constant tension along the yarn ($T_1 = T_2 = \ldots = T_n$). Hence the vertical forces ($F_{v1}, F_{v2}, \ldots, F_{vn}$) are the only unknowns (Figure 5-10). The horizontal reaction on the orthogonal yarn (necessary for force equilibrium with constant yarn tension) has been ignored. Resolving forces at each node provides a series of out-of-plane forces acting on the yarn.

$$T = F_H \qquad \text{Equation 5-8}$$

$$F_{vn} = T(sin\theta_2 - sin\theta_1) \qquad \text{Equation 5-9}$$

The distribution of forces varies dependent on the ratio of wavelength to amplitude (Figure 5-11). This method provides a series of contact forces ($F_{v1}, F_{v2}, \ldots, F_{vn}$) appropriate to the weave shape.

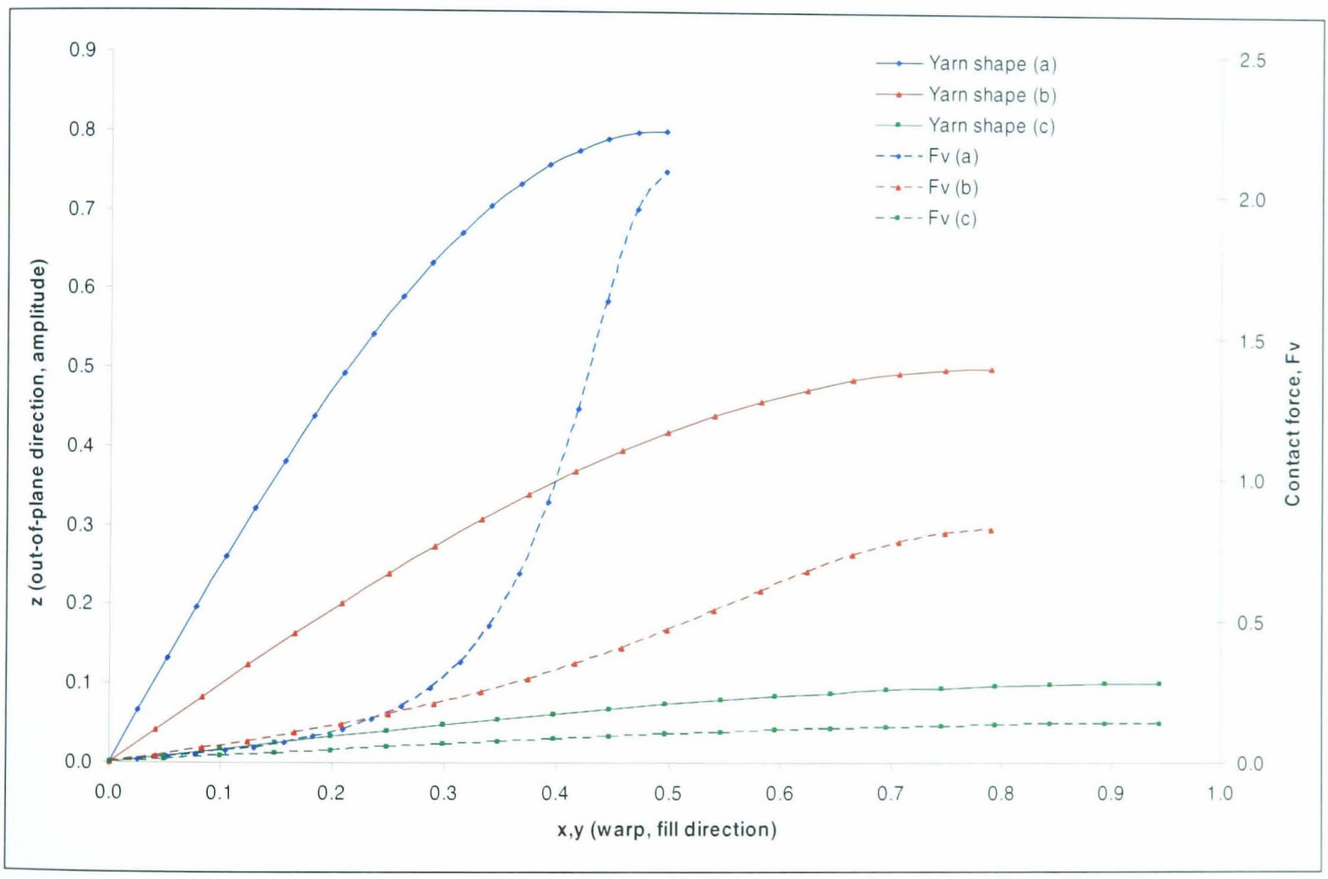

Figure 5-11. Variation of contact force distribution

The basic sinusoidal model formulation has been developed assuming a constant yarn radius and no coating. Yarn tensile extension is included in the simplest model as it is trivial to calculate; with constant yarn tension and no coating the yarn extension is constant for a given applied load. For equilibrium the sum of the out-of-plane forces must be zero, that is:

$$\sum F_{v1} = \sum F_{v2} \qquad \text{Equation 5-10}$$

For a given loading, the magnitude of the out-of-plane forces depends solely on the yarn wave form (i.e. amplitude and wavelength). The initial yarn length is calculated from the measured fabric geometry. The length of a since curve, s, is defined by an elliptic integral of the second kind (Stroud, 1996, p.155):

$$s = \int_0^L \sqrt{1 + \left(\frac{dz}{dx}\right)^2}\, dx$$

Equation 5-11

Let $z_{1,2}$ define the initial sinusoidal yarn geometry in terms of the measured crimp amplitude ($A_{1,2}$) and yarn wavelength ($L_{1,2}$ = wavelength / 4):

$$z_{1,2} = A_{1,2} sin\left(\frac{\pi x_{1,2}}{2L_{1,2}}\right)$$

Equation 5-12

It follows that:

$$\frac{dz}{dx} = \frac{\pi A_{1,2}}{2L_{1,2}} cos\left(\frac{\pi x_{1,2}}{2L_{1,2}}\right)$$

Equation 5-13

Hence:

$$s = \int_0^L \sqrt{1 + \left(\frac{\pi A_{1,2}}{2L_{1,2}}\right)^2 sin^2\left(\frac{\pi x_{1,2}}{2L_{1,2}}\right)}\, dx$$

Equation 5-14

The solution of this elliptic integral is not straightforward, but it can easily be evaluated numerically using Simpson's rule. The initial yarn length is calculated by dividing the unit cell (i.e. one quarter of the yarn wavelength) into a sufficiently large number of sections and applying Simpson's rule to sum the length of these straight lines (twenty-five segments were used for this work). With constant tension along the length of the yarn the strained yarn length for a given load is simply determined using the yarn elastic modulus (or moduli for a multi-linear representation of yarn behaviour) and remains constant for a given applied load.

With constant yarn radii, the only parameters that can be altered to balance the out-of-plane forces (Equation 5-10) are the unit cell lengths ($L_{1,2}$) and amplitudes ($A_{1,2}$). However, with a constant yarn length the unit cell length and amplitude are not independent but are related by Equation 5-14. In the model the yarn length (Y) is known, the amplitude (A) is a variable, and the corresponding unit cell length (L) is required. An iterative process is required to determine values of L for known values of Y and A. To avoid slowing the model down a database of values for L, Y and A has been used. Values of L have been calculated for all values of A from 0 to 1.5mm at 0.01mm increments, and values of Y from 0 to 2.2mm at 0.01mm increments. This range of values should be sufficient for all architectural fabrics for any reasonable applied loads. Clearly Y must be greater than A. For a given pair of values of Y and A

linear interpolation is carried out between four values in the look-up table to give a sufficiently accurate value of L (effectively rounding the values of Y and A to the nearest 0.005mm).

With constant yarn radii the values of A_1 and A_2 are not independent (Equation 5-1, p. 225). Hence, in the simple form of the sinusoid model the only variable is A_1, from which values of A_2, L_1, L_2, Fv_1 and Fv_2 can be calculated. To find the equilibrium configuration for a given pair of loads A_1 is varied by the *Excel Solver* until $Fv_1 = Fv_2$.

A **constant yarn cross-sectional area constraint** has also been included in the model. The approach is very similar to that used in the sawtooth model (§5.3.2), but with the yarn cross-section being bounded by two intersecting sinusoids as opposed to a rhombus (for the unstrained yarn) or kite shape (for the strained configuration). This provides a more realistic representation of the yarn cross-section, and a correspondingly more accurate calculation of the yarn cross-sectional area (Figure 5-12). As for the sawtooth model, the result is a geometrically consistent model of the orthogonal yarns that does not require definition of yarn crushing stiffness.

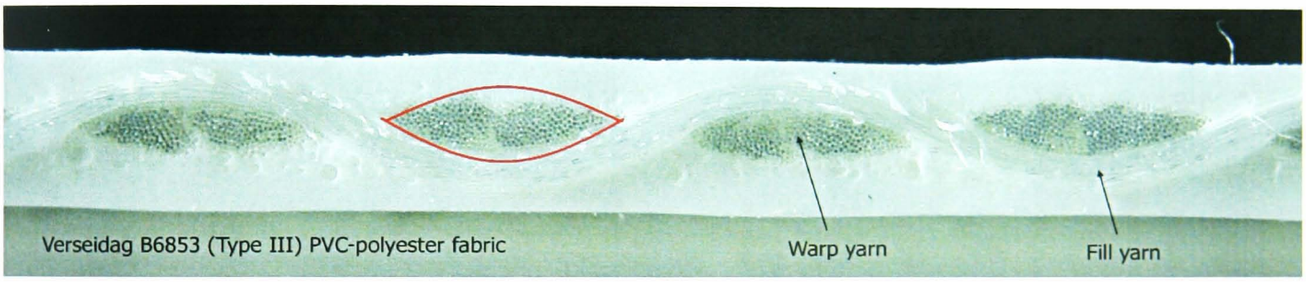

Figure 5-12. Sinusoidal representation of yarn cross-section

The initial cross-sectional area of the yarn (area B plus C in Figure 5-13) is calculated as follows:

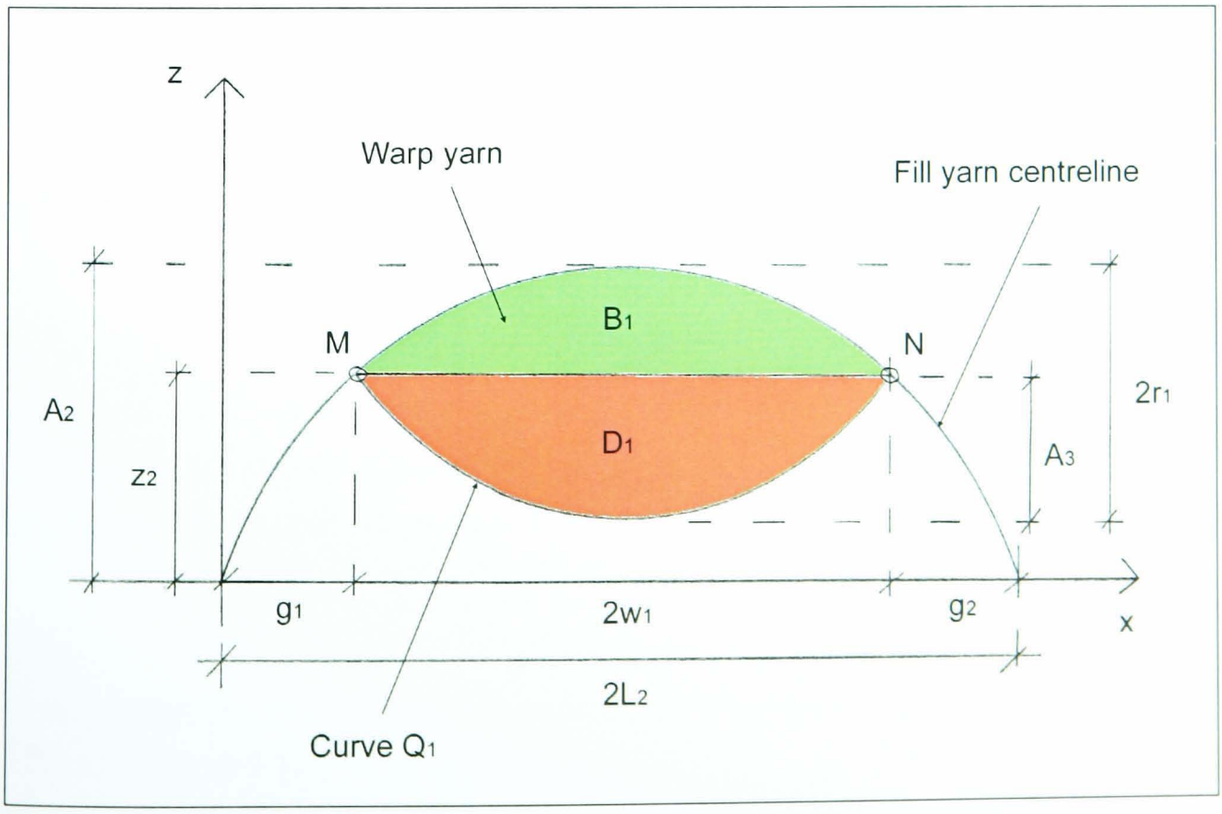

Figure 5-13. Calculation of sinusoidal yarn cross-section

$$B_{1,2} = \left[\int_{g1,2}^{g1,2+2w1,2} A_{2,1} sin\left(\frac{\pi x}{2L_{2,1}}\right) \right] - 2w_{1,2}z_{2,1} \qquad \text{Equation 5-15}$$

$$B_{1,2} = \left(\frac{2L_{2,1}A_{1,2}}{\pi} \left[-cos\left(\frac{\pi x}{2L_{2,1}}\right) \right]_{g1,2}^{g1,2+2w1,2} \right) - 2w_{1,2}z_{2,1} \qquad \text{Equation 5-16}$$

$$B_{1,2} = \left(\frac{2L_{2,1}A_{1,2}}{\pi} \left[-cos\left(\frac{\pi(g_{1,2}+2w_{1,2})}{2L_{2,1}}\right) + cos\left(\frac{\pi g_{1,2}}{2L_{2,1}}\right) \right] - 2w_{1,2}z_{2,1} \right) \qquad \text{Equation 5-17}$$

$$z_{Q1} = A_{3,1} \sin\left(\frac{\pi x}{2w_{1,2}}\right) \qquad \text{Equation 5-18}$$

$$A_{3,4} = 2r_{1,2} - A_{2,1} + z_{2,1} \qquad \text{Equation 5-19}$$

$$D_{1,2} = \int_0^{2w1,2} A_{3,4} \sin\left(\frac{\pi x}{2w_{1,2}}\right) = \frac{2w_{1,2}A_{3,1}}{\pi} \left[-cos\left(\frac{\pi x}{2w_{1,2}}\right) \right]_0^{2w1,2} \qquad \text{Equation 5-20}$$

$$D_{1,2} = \frac{4w_{1,2}A_{3,4}}{\pi} \qquad \text{Equation 5-21}$$

where A_3 and A_4 are the amplitudes of the curves Q_1 and Q_2 that bound the yarn cross-section. All terms are defined in §5.3.1. The wavelength of curve $Q_{1,2}$ is not equal to the yarn wavelength, it is equal to four times the yarn width (4w), Equation 5-20 & Equation 5-21. The intersection points of the two curves (M and N in Figure 5-13) lie at the end of half a wavelength of curve $Q_{1,2}$. Initially the model was set up with the wavelength of curve $Q_{1,2}$ equal to the yarn wavelength, but this made the calculation of $Q_{1,2}$ more involved because the appropriate amplitude and offset from the x-axis had to be determined to ensure that the two curves intersected at points M and N. With the wavelength of $Q_{1,2}$ equal to 4w, only the correct amplitude needs to be calculated (Equation 5-19) to ensure intersection at M and N. This avoids adding another iterative stage to the calculation. In this form the model has three principal constraints:

1. $r_1 + r_2 = A_1 + A_2$,
2. $F_{v1} = F_{v2}$,
3. $B'_{1,2} + D'_{1,2} = B_{1,2} + D_{1,2}$ i.e. the warp and fill yarn cross-sectional areas must remain constant.

Before the amplitude is modified (and the corresponding unit cell length is determined from the 'L,Y,A' look-up table) the out-of-plane forces ($Fv_{1,2}$) are equal. As the amplitude changes, the yarn radii are recalculated to ensure the cross-sectional areas remain constant. To ensure the first constraint is met, A_2 is calculated as the sum of the radii minus A_1. This enables the three constraints to be met as efficiently as possible.

Finally the **coating** has been added to the model using the same method developed for the sawtooth model (§5.3.2 & Figure 5-7).

5.3.3.2 *No slip formulation*

As discussed in the development of the sawtooth model (§5.3.2), the 'no slip' model may provide a better representation of fabric behaviour as inter-yarn friction and, more significantly, restraint by the coating prevents yarn slippage at crossovers. In the no-slip sinusoid the tension in the yarn will vary along the length of the yarn (T_1, T_2, T_3 and T_4 have different values, Figure 5-14).

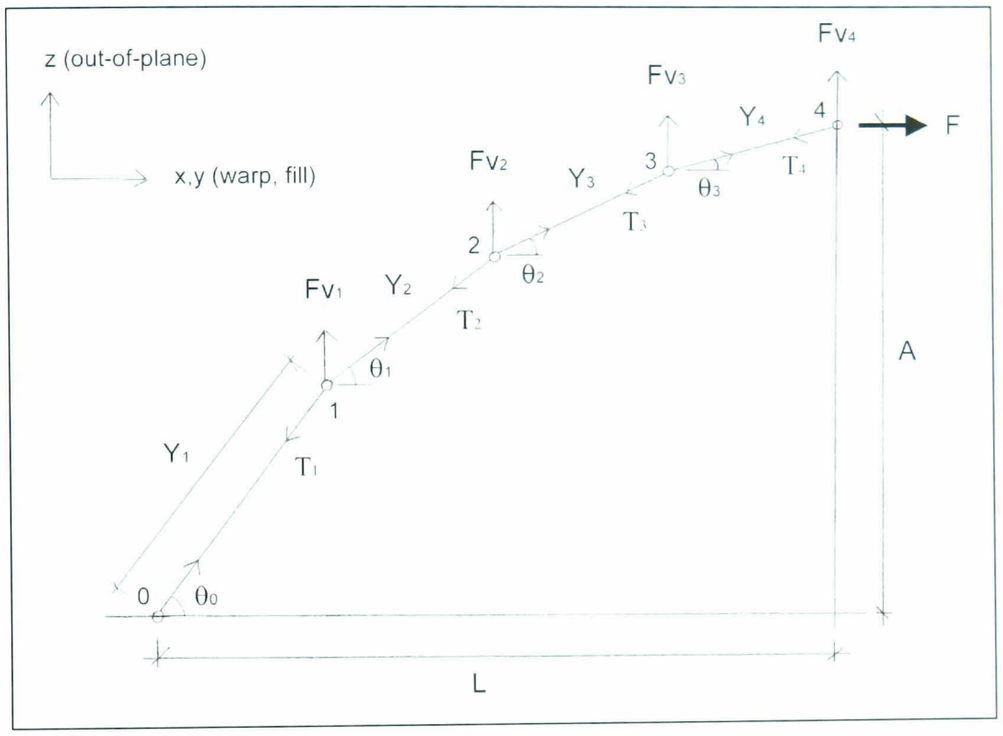

Figure 5-14. Sinusoid yarn model (*Figure 5-9 reproduced for ease of reference*)

Starting with the known applied load (F), forces can be resolved at node 4:

$$T_4 = \frac{F}{\cos\theta_3}$$ Equation 5-22

$$F_{v4} = \frac{T_4}{\sin\theta_3}$$ Equation 5-23

And then at subsequent nodes along the yarn:

$$T_3 = \frac{T_1 \cos\theta_3}{cos\theta_2}$$ Equation 5-24

$$F_{v3} = \frac{T_3}{sin\theta_2} - \frac{T_4}{sin\theta_3}$$ Equation 5-25

This calculation is carried out for the warp and fill yarns. As with the 'slip' model the amplitude is varied until the sum of the out-of-plane forces is zero (Equation 5-10). In the 'no-slip' model this results in a

change in yarn tension, hence a change in yarn tensile extension. This in turn changes the geometry of the unit cell, and hence the yarn tension. This adds another iterative element to the calculation of crimp equilibrium. All other aspects of the model, such as yarn cross-section calculation and coating stiffness, are identical to the slip model. All parameters for the slip and no-slip sinusoid models are given in Table 5-3.

Parameter	'Slip' model	'No slip' model
Initial values from fabric geometry	$L_{1,2}$, $r_{1,2}$, $A_{1,2}$, $w_{1,2}$	As slip model
Material properties from uniaxial tests	$E_{1,2}$, $E_{k1,2}$	As slip model
Applied load	$F_{1,2}$	As slip model
Initial values calculated from fabric geometry	$Area_{1,2}$ (see Equation 5-15 to Equation 5-20) $Y_{1,2}$ calculated using Simpson's rule	As slip model
New values for yarn geometry	$L'_{1,2}$ determined from look-up table which relates values of $Y'_{1,2}$ and $A'_{1,2}$ to $L'_{1,2}$ $A'_2 = r'_1 + r'_2 - A'_1$ $w'_{1,2} = w_{1,2}$ $\varepsilon_{1,2} = (L_{1,2} - L'_{1,2}) / L_{1,2}$ $F_k'_{1,2} = E_{k1,2} L'_{2,1} \varepsilon_{1,2}$ $Fy'_{1,2} = (F_{1,2} - F_k'_{1,2})$ $Y'_{1,2} = Y_{1,2} [1 + (Fy'_{1,2} / E_{1,2})]$ $r_{area}'_{1,2} = A_{3,4} + A_{2,1} - z'_1$,	As slip model except $F_{y1,2} = \Sigma T_{n1,2}$, $T_1 \neq T_2 \neq \ldots \neq T_n$ $Y'_{1,2} = \Sigma Y'_{n1,2}$
Excel Solver parameters: variables modified by solver	$r'_{1,2}$ A'_1 $A'_{3,4}$	As slip model
Excel Solver parameters: constraints	$r'_{1,2} = r_{area}'_{1,2}$ $A'_1 + A'_2 = r'_1 + r'_2$ (inherently true as A'_2 is calculated as $r'_1 + r'_2 - A'_1$) $Fv_1 = Fv_2$	As slip model
Subscripts 1 and 2 denote warp and fill directions respectively, ' = modified value under load, e.g. A = initial amplitude (unstrained), A' = modified amplitude with applied load.		

Table 5-3. Sinusoidal model summary.

5.4 MODEL INPUT DATA

5.4.1 Fabric geometry

Yarn dimensions and crimp characteristics have been determined using measurements of fabric cross-section images, Figure 5-15.

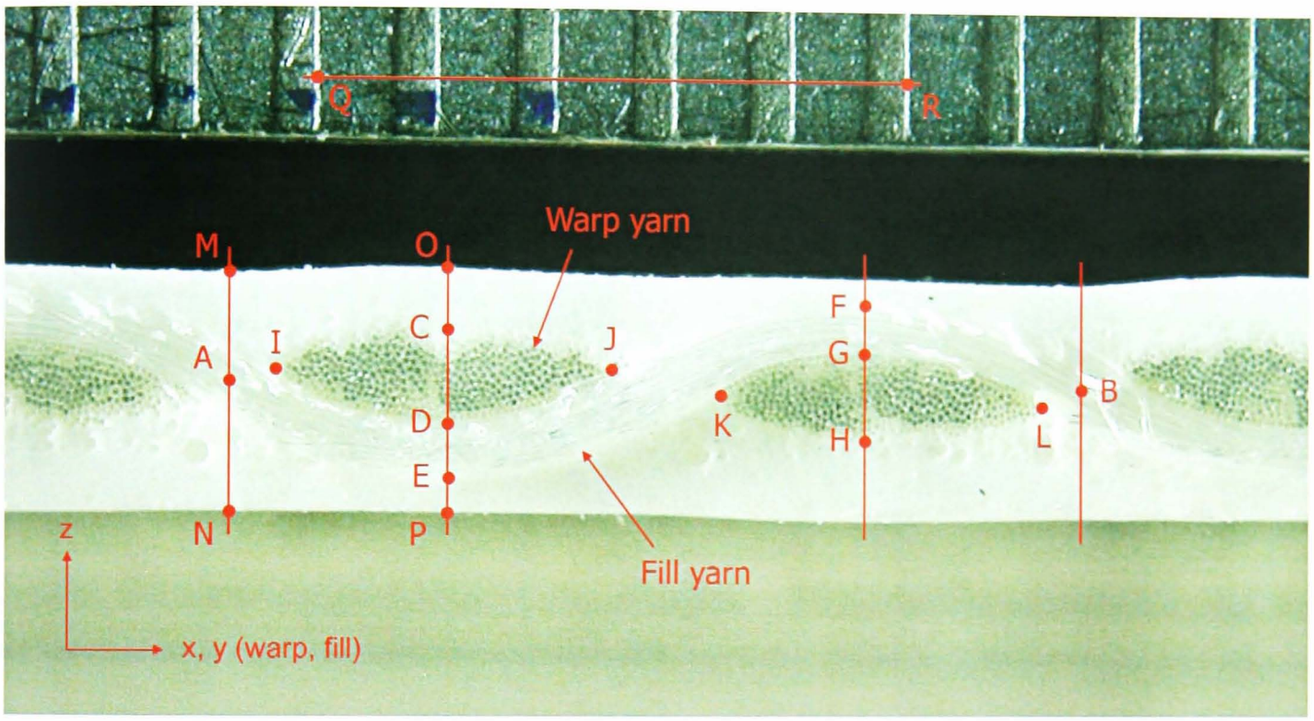

Figure 5-15. Measurements taken from fabric cross section

For each fabric ten images were taken, five in each direction, at different points along the sample (§3.2). The image in Figure 5-15 is described as a fill image as the fabric has been cut along a fill yarn. Of these ten images, the clearest three in each direction were measured and average values taken. For assessment of fabric variability many more measurements would be required (§6.2). For this work the aim is to assess the model against the test data from a particular fabric sample. It follows that using mean values of measurements from that fabric sample is appropriate.

Point (Figure 5-15)	Measurements required		Point (Figure 5-15)	Measurements required	
	x, y	z		x, y	z
A	✓		J	✓	
B	✓		K	✓	
C		✓	L	✓	
D		✓	M		✓
E		✓	N		✓
F		✓	O		✓
G		✓	P		✓
H		✓	Q	✓	
I	✓		R	✓	

Table 5-4. Fabric measurements

The measurements taken from the images are in arbitrary units dependent on the distance of the camera from the subject. The measurement of points Q and R on the steel ruler at the top of the each image enables the dimensions to be scaled. Q and R are separated by five half millimetre intervals (i.e. 2.5mm apart); subtracting Q from R and dividing by 2.5 gives a meaningful scale to the rest of the measurements.

The calculation of warp measurements are given, fill measurements are the same with subscripts reversed. Subscripts 1 and 2 are used to denote measurements taken on the warp and fill images respectively.

Warp yarn wavelength = $B_1 - A_1$

Warp yarn thickness = *maximum of* $(D_2 - C_2)$, $(H_2 - G_2)$, $(E_1 - D_1)$ *and* $(G_1 - F_1)$

Measurements taken on the fill image always provide the maximum (and most accurate) measurement of warp yarn thickness. On the warp image the warp yarn thickness will only be correct if the cut has passed exactly down the centreline of the yarn – which is very difficult to achieve. On the fill image (e.g. Figure 5-15) the warp yarns have been cut through in section and provide a reliable measurement of yarn thickness. This only provides measurements of yarn thickness at the crossover point – the yarn may have different dimensions between crossovers. This is appropriate for the model as the yarn thickness is modelled at the crossover.

Warp yarn crimp amplitude = *maximum of* $[(D_1 - F_1 + E_1 - G_1)/4]$ *and* $[(G_2 - C_2 + H_2 - D_2)/4]$

Warp yarn width = *mean of* $(J_2 - I_2)$ *and* $(L_2 - K_2)$

Fabric thickness (T) = mean of (N_1-M_1), (N_2-M_2), (O_1-P_1) and (O_2-P_2)

The sum '$A_1 + A_2 - r_1 - r_2$' (where A = crimp amplitude, r = yarn thickness and subscripts 1 and 2 denote warp and fill directions respectively) must equal zero for geometric consistency (Equation 5-1). This sum can be used as a measure of the quality and consistency of the fabric measurements (Table 5-5), and is best expressed as a percentage of the fabric thickness. Some variation from zero is expected because:

1. The geometry of several yarn sections has been averaged,
2. Some measurement inaccuracy is unavoidable,
3. The yarn geometry may be disturbed when the fabric is cut.

Fabric	Material (Type†)	Mean value of $A_1+A_2-r_1-r_2$ / T (%)
Taconic Solus 1120	PTFE-glass (G5)	2.00
Taconic Solus 1300	PTFE-glass (G6)	1.49
Taconic Solus 1410	PTFE-glass (G7)	0.49
Verseidag B18059	PTFE-glass (G6)	-2.23
Verseidag B18089	PTFE-glass (G6/G7)	1.70
Ferrari 702T	PVC-polyester (I)	-0.04
Ferrari 1002T	PVC-polyester (II)	3.15
Ferrari 1202T	PVC-polyester (III)	0.31
Ferrari 1502	PVC-polyester (IV/V)	5.42
Verseidag B6853	PVC-polyester (III)	2.12
† For definition of fabric types see Chapter 2, §2.1.4.1, Figure 2-15		

Table 5-5. Consistency of fabric measurements

For the fabric model consistent fabric geometry is required. Therefore the crimp amplitudes (A_1, A_2) and yarn thicknesses (r_1, r_2) must be adjusted. The adjustments have been made proportional to the magnitude of the value being adjusted to avoid, for example, a small warp crimp being modified out of all proportion to its value (Equation 5-26 & Equation 5-27),

$$A'_{1,2} = A_{1,2} + \left(\frac{A_{1,2}D}{S}\right)$$ Equation 5-26

$$r'_{1,2} = r_{1,2} + \left(\frac{r_{1,2}D}{S}\right)$$ Equation 5-27

where $S = A_1 + A_2 + r_1 + r_2$ and $D = A_1 + A_2 - r_1 - r_2$. This gives a consistent geometry which defines the initial state of the unit cell model, without excessive modification of any one value. These fabric measurements enable the theoretical maximum and minimum strains due to crimp interchange to be calculated (Table 5-6). These values provide some information about the fabric response, but other factors (e.g. restraint due to the coating and creep of the yarn and coating) may modify the actual maximum and minimum fabric strains. Decrimping strain is defined as the fabric extension from its unloaded state to a state where the yarns are straight, but no yarn tensile extension has yet occurred.

The differences between the values in Table 5-6 provide an insight into the difference in behaviour between the sawtooth and sinusoid models (Table 5-7). The sinusoidal representation always gives a greater yarn length than the sawtooth for a given yarn geometry, hence the decrimping strains are greater for the sinusoid model. The difference, between 17% and 20% of the mean value, is clearly significant to the model output.

Fabric	Material (Type†)	Sawtooth model				Sinusoid model			
		Positive decrimping strain (%)		Negative strain due to crimp interchange (%)		Positive decrimping strain (%)		Negative strain due to crimp interchange (%)	
		Warp	Fill	Warp	Fill	Warp	Fill	Warp	Fill
Taconic Solus 1120	PTFE-glass (G5)	1.75	7.12	-10.09	-13.63	2.14	8.55	-12.10	-15.79
Taconic Solus 1300	PTFE-glass (G6)	1.38	8.26	-10.34	-12.71	1.69	9.89	-12.41	-14.65
Taconic Solus 1410	PTFE-glass (G7)	0.55	4.31	-22.95	-1.90	0.68	5.23	-27.06	-2.28
Verseidag B18059	PTFE-glass (G6)	3.18	11.11	-18.91	-23.38	3.87	13.19	-22.13	-26.07
Verseidag B18089	PTFE-glass (G6/G7)	1.65	10.48	-18.70	-12.15	2.02	12.47	-22.08	-13.88
Ferrari 702T	PVC-polyester (I)	0.59	0.95	-2.68	-1.99	0.72	1.17	-3.28	-2.43
Ferrari 1002T	PVC-polyester (II)	0.43	1.27	-3.23	-1.72	0.53	1.55	-3.96	-2.10
Ferrari 1202T	PVC-polyester (III)	0.66	1.94	-9.48	-1.65	0.82	2.37	-11.45	-2.01
Ferrari 1502T	PVC-polyester (IV/V)	2.57	1.49	-4.50	-8.75	3.14	1.83	-5.43	-10.52
Verseidag B6853	PVC-polyester (III)	0.11	3.32	-4.85	-1.29	0.13	4.04	-5.93	-1.56

† For definition of fabric types see Chapter 2, §2.1.4.1, Figure 2-15

Table 5-6. Theoretical decrimping strains

Fabric	Material (Type†)	Difference, sinusoid minus sawtooth (% strain)				Difference, sinusoid minus sawtooth (% of mean value)			
		Decrimping strain (%)		Negative strain due to crimp interchange (%)		Decrimping strain (%)		Negative strain due to crimp interchange (%)	
		Warp	Fill	Warp	Fill	Warp	Fill	Warp	Fill
Taconic Solus 1120	PTFE-glass (G5)	0.39	1.43	-2.01	-2.15	20.2	18.3	18.1	14.6
Taconic Solus 1300	PTFE-glass (G6)	0.31	1.63	-2.07	-1.94	20.4	17.9	18.2	14.2
Taconic Solus 1410	PTFE-glass (G7)	0.13	0.92	-4.11	-0.38	20.7	19.3	16.4	18.2
Verseidag B18059	PTFE-glass (G6)	0.69	2.08	-3.21	-2.68	19.7	17.1	15.7	10.9
Verseidag B18089	PTFE-glass (G6/G7)	0.37	1.98	-3.38	-1.73	20.3	17.3	16.6	13.3
Ferrari 702T	PVC-polyester (I)	0.14	0.22	-0.60	-0.44	20.7	20.5	20.1	20.1
Ferrari 1002T	PVC-polyester (II)	0.10	0.29	-0.72	-0.38	20.7	20.4	20.1	19.9
Ferrari 1202T	PVC-polyester (III)	0.15	0.43	-1.97	-0.36	20.6	20.1	18.8	19.5
Ferrari 1502T	PVC-polyester (IV/V)	0.57	0.34	-0.92	-1.78	19.9	20.3	18.6	18.4
Verseidag B6853	PVC-polyester (III)	0.02	0.72	-1.08	-0.27	20.9	19.6	20.0	18.9

† For definition of fabric types see Chapter 2, §2.1.4.1, Figure 2-15

Table 5-7. Theoretical decrimping strain differences

Decrimping strains can be determined experimentally from uniaxial stress-strain data for PTFE-glass fibre fabrics in the fill direction (Figure 5-16). The high level of decrimping strain coupled with the high tensile modulus of the glass fibre yarns means that the decrimping part of the curve is distinct from the tensile extension. The tensile behaviour of PVC-polyester is more complex and the different parts of the curve cannot be attributed to a single deformation mechanism.

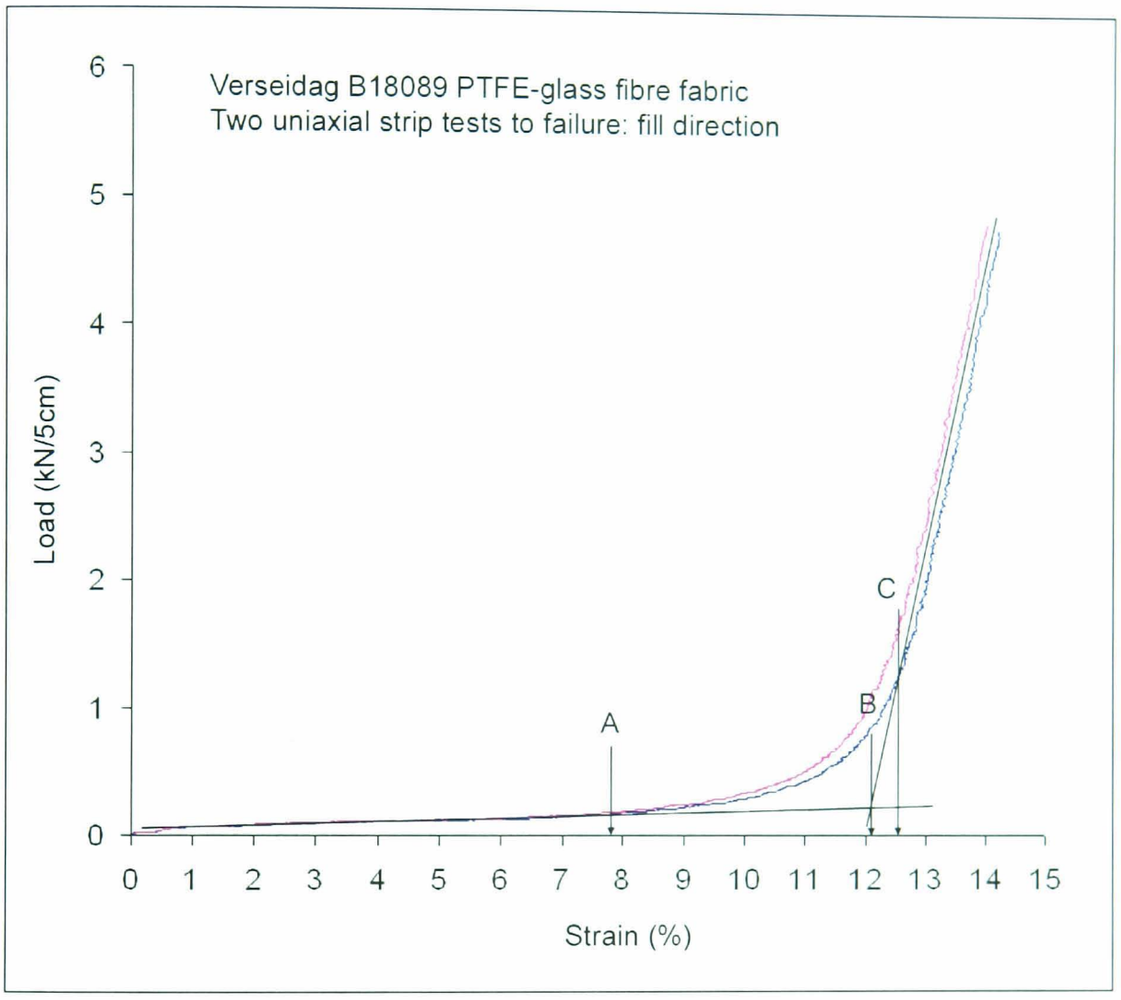

Figure 5-16. Determination of decrimping strain (experimental)

Comparison of the theoretical decrimping strains with values from test data may provide a starting point in determining which model, sawtooth or sinusoid, is more appropriate for modelling coated woven fabric behaviour (Table 5-8).

Fabric	Material (Type†)	Decrimping strain (% strain, FILL direction)				
		Experimental (see Figure 5-16)			Sawtooth model	Sinusoid model
		(A) Minimum	(B) Intersection	(C) Maximum		
Taconic Solus 1120	PTFE-glass (G5)	5.2	7.3	7.7	7.12	8.55
Taconic Solus 1300	PTFE-glass (G6)	6.8	10.0	10.5	8.26	9.89
Taconic Solus 1410	PTFE-glass (G7)	2.7	5.7	6.9	4.31	5.23
Verseidag B18059	PTFE-glass (G6)	6.8	11.9	12.4	11.11	13.19
Verseidag B18089	PTFE-glass (G6/G7)	7.9	12.1	12.5	10.48	12.47
† For definition of fabric types see Chapter 2, §2.1.4.1, Figure 2-15						

Table 5-8. Decrimping strains: theoretical and experimental

Even with the easily interpreted PTFE-glass uniaxial fill-direction curve, it is difficult to ascertain an exact value of decrimping strain. The initial shallow part of the curve corresponds to decrimping with the restraint to extension being provided by the coating. The minimum value for the decrimping strain is when the curve first deviates from this almost linear behaviour (Figure 5-16, point A). However, at point A decrimping is not complete, the yarn is not yet straight. The increase in stiffness from A to C is rapid but not instantaneous. As the fabric is loaded in the fill direction, the level of crimp increases in the orthogonal warp direction. This increase in crimp results in out-of-plane coating deformation. The increase in length of the coating over the highly crimped 'dimples' in the fabric surface will require additional load to be applied before crimp interchange is complete (Figure 5-17 & Figure 5-18).

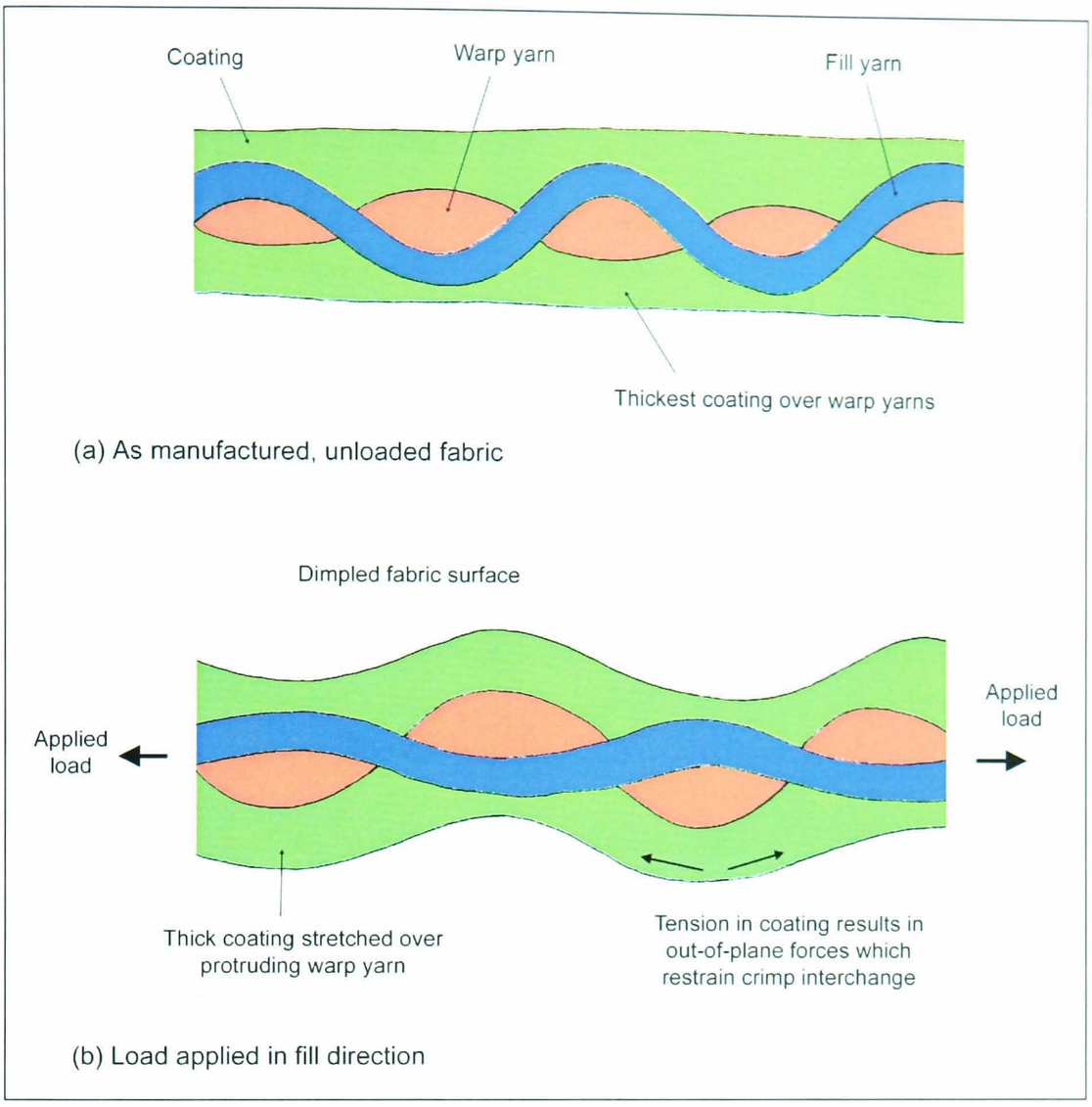

Figure 5-17. Coating strain over decrimping 'dimples'

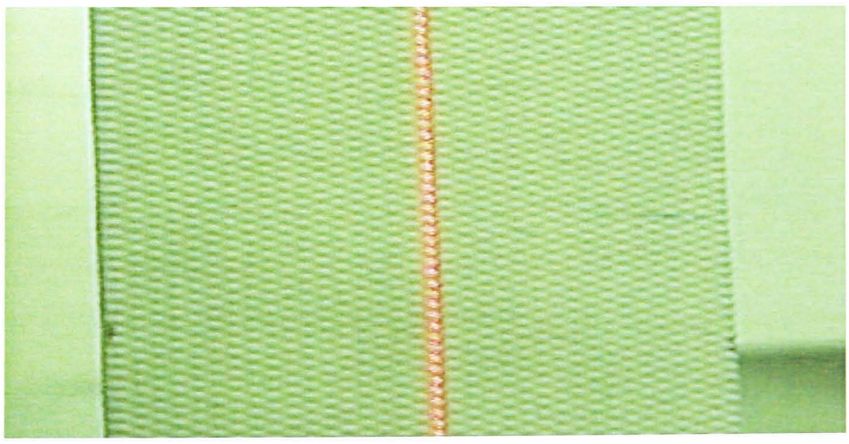

Figure 5-18. Dimpled fabric surface during uniaxial test

By point C (Figure 5-16) crimp interchange is clearly complete; the response is dominated by linear glass-fibre extension. This is the maximum value which could be attributed to decrimping. However, tensile extension of the yarn may have already started. The initial part of the yarn extension curve is shallower than the typical linear response due to slack in and between fibres in the twisted yarn structure. In fact, as the coating restrains crimp interchange, yarn tensile extension may start before the yarn is

completely straight. This means that the definition of decrimping strain given above (p.248) may not be appropriate for actual coated woven fabric deformation. It is more appropriate to calculate the decrimping strain from fabric cross-section measurements, with the sinusoid giving the most accurate measurement of yarn length (§5.3.3 & Figure 5-9).

Comparison of theoretical decrimping strains with points A, B and C is still useful for to assess how the sawtooth and sinusoid models relate to the fabric behaviour. As expected from the foregoing discussion, the sinusoid model decrimping strains compare well with the maximum experimental strains (C). The sawtooth model, giving lower strain due to the straight line approximation to the yarn curve, gives strains between A and B. This inaccuracy in the sawtooth model may actually make it more accurate as a predictive tool as it inadvertently counteracts some of the simplifications in the model. Explicitly, the out-of-plane restraint provided by the coating (Figure 5-17) is not included in the model, but this effect may be approximated by the shortened yarn length inherent in the sawtooth representation.

5.4.2 Material properties – elastic moduli

Determination of the tensile modulus of the yarns and coating is vital for the unit cell model. It is possible to remove yarns from the fabric and test them individually, but this is a specialist process that is not usually carried out and may damage the yarns (§3.1.2). Isolation of the coating for tensile testing is extremely difficult. Samples of PVC or PTFE, if available, would not necessarily yield the correct results. For example, the properties of the PTFE may be changed by sintering during the coating process. Even if the coating modulus was known, it is not straightforward to utilise in the model as the thickness of the coating is difficult to measure and varies considerably. Likewise samples of uncoated yarn may not be representative of the yarns in the coated fabric due to changes during the coating process and possible impregnation of the yarns by the coating (although in practice there is usually little impregnation).

Yarn and coating tensile properties have been evaluated using stress-strain data from standard uniaxial tests (§3.1.1). The principal is that the initial part of the stress-strain curve at low load corresponds to coating stiffness, with yarn tensile properties becoming dominant at high loads. This approach has been adopted by several previous researchers (e.g. Menges & Meffert, 1976; Testa, Stubbs & Spillers, 1978). This is appropriate for this work which aims to develop a predictive model which does not require specialist testing.

Uniaxial tests on PTFE-glass fabric give physically intuitive test results which are easy to interpret (Figure 5-19). In the warp direction the stress-strain curve rapidly becomes steep and near linear. With minimal crimp in the warp direction the response is dominated by the yarn and coating properties. In the fill direction there is an initial period with a large increase in strain at low load when the fill yarns are decrimping. Assuming negligible yarn bending stiffness (§2.1.4.4), the gradient of this part of the curve is equal to the coating stiffness. When decrimping is complete the yarns start to extend and the gradient

becomes similar to that in the warp direction. In Figure 5-19 the tensile modulus of the coating is gradient A, the warp and fill yarn moduli are 'C minus A' and 'B minus A' respectively.

The uniaxial test data shown in Figure 5-19 shows the fabric response to failure. For structural design stresses are limited to, at most, 25% of the ultimate tensile strength (line P, Figure 5-19). These extreme stress levels will occur rarely (for example during a 50-year wind) and only occur in certain areas of the structure (e.g. at the top of conics and in clamped corners), not throughout the canopy. Typical working loads may be between prestress and line Q. The uniaxial test data suggests that at this load level full decrimping in the fill direction may not occur. This explains why the residual strains of around 15% following the biaxial tests on PTFE-glass fibre fabrics may not occur for a real structure. The fabric is not fully decrimped during installation, or due to typical loads in, say, the first month or year before routine inspection and retensioning occurs. This may leave the structure prone to slackening following an extreme load event which would mobilise the 15% residual strain, but this would depend what area of the structure reaches stress levels near the design stress.

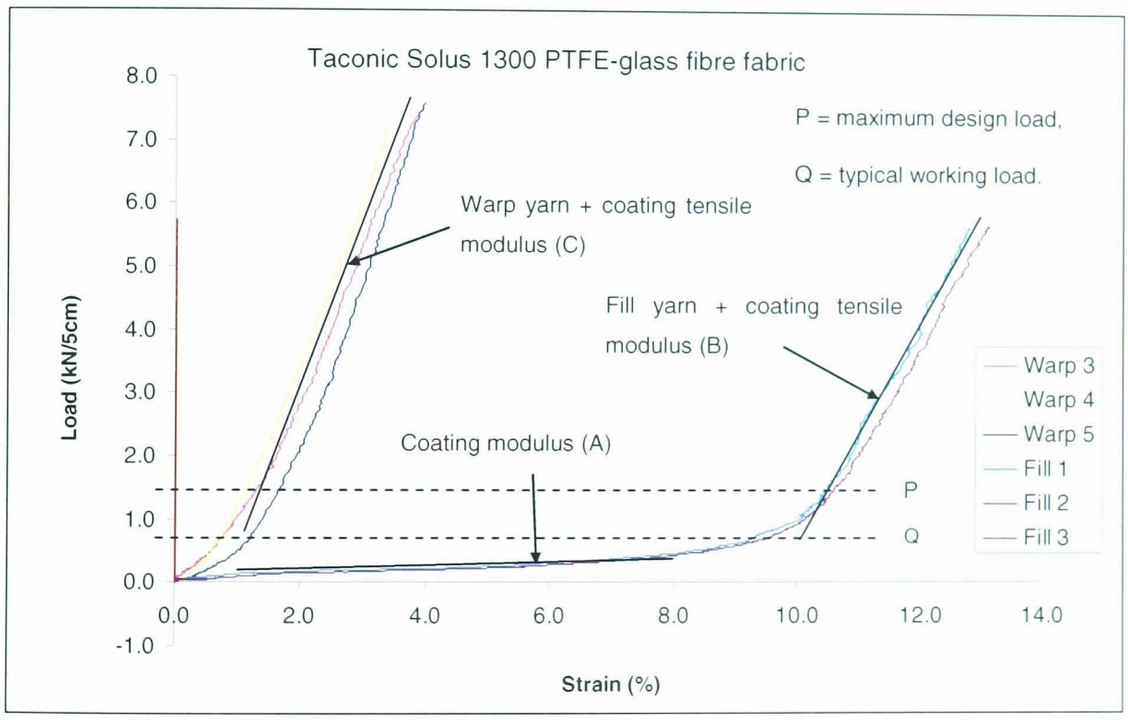

Figure 5-19. Uniaxial test data for PTFE-glass fabric

The interpretation of results for uniaxial tests on PVC-polyester is more difficult (Figure 5-20). As expected the fill strip gives large strains at low loads due to decrimping, hence gradient A_f can be used as a measure of coating stiffness. For the stress-strain response at higher loads it seems appropriate from the graph to use three values of elastic modulus to describe the yarn behaviour at different loads ($B_{w,f}$, $C_{w,f}$ and $D_{w,f}$). However, if the coating modulus (A_f) is subtracted from these gradients to give the yarn modulus (as used above for PTFE-glass) then gradient $C_{w,f}$ is reduced almost to zero. Consideration of typical polymer tensile properties (§2.1) suggests that the stiffness of the PVC coating may drop dramatically after a critical level of strain: the coating may not significantly affect the response in region

$C_{w,f}$. The gradients $B_{w,f}$, $C_{w,f}$ and $D_{w,f}$ were therefore used as the yarn stiffnesses with no modification. The uniaxial data shown in Figure 5-20 is for a test to failure, whereas for this work only the material properties up to the maximum working load (assumed to be 25% ultimate tensile strength) are relevant (Figure 5-21). Gradient $B_{w,f}$ dominates the yarn response at typical working loads, with gradient $C_{w,f}$ being significant for extreme load events. Comparison with test data during model development using a bilinear yarn stiffness (gradients $B_{w,f}$ and $C_{w,f}$) gave poor correlation at high loads. It was clear that use of single values of warp and fill yarn modulus equal to gradients B_w and B_f are appropriate.

Ferrari fabrics are made using the précontraint system which results in approximately equal crimp in warp and fill directions (known as a *balanced* fabric). This makes identification of the coating stiffness from uniaxial test data less obvious than for other PVC-polyester fabrics. For the fabrics tested for this work, the fill direction did have a slightly higher level of crimp than the warp, allowing the coating stiffness to be determined from the small initial part of the fill curve.

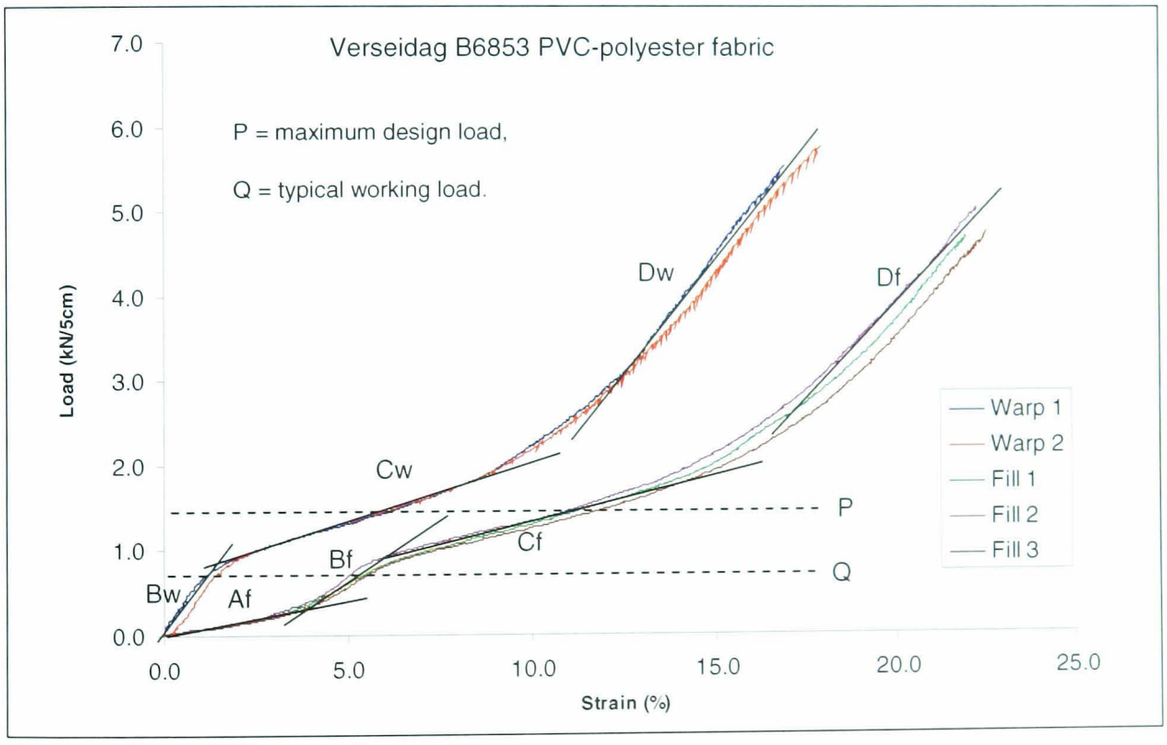

Figure 5-20. Uniaxial test data for Verseidag PVC-polyester fabric to failure

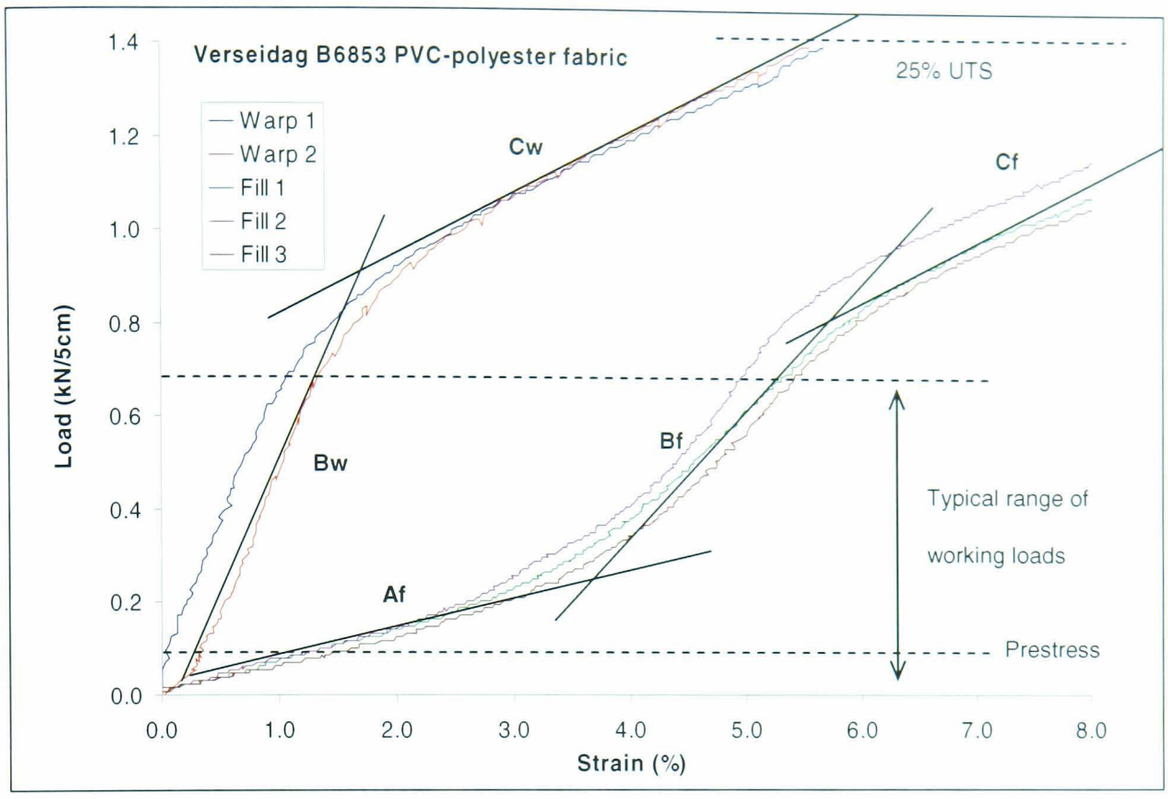

Figure 5-21. Uniaxial test data for Verseidag PVC-polyester fabric at working loads

Use of single values of Young's modulus (Table 5-9) based on the gradient of the initial part of the test curves has been found to give extremely good correlation with test data (§5.4.2).

The very high values of glass-fibre yarn stiffness (around 5000kN/m) confirm that virtually all extension of PTFE-glass fibre fabrics occurs due to crimp interchange. This concurs with the strain-strain plots in Chapter 4 (Figure 4-41) which show a discrete envelope of possible strain states for PTFE-glass fibre fabrics.

Fabric	Material (Type†)	Warp yarn elastic modulus (kN/m width)	Fill yarn elastic modulus (kN/m width)	Difference (as a percentage of warp modulus)
Taconic Solus 1120	PTFE-glass (G5)	5430	4320	20.4
Taconic Solus 1300	PTFE-glass (G6)	4910	3460	29.5
Taconic Solus 1410	PTFE-glass (G7)	8650	8650	0.0
Verseidag B18059	PTFE-glass (G6)	4440	4730	-6.4
Verseidag B18089	PTFE-glass (G6/G7)	5440	4600	15.4
Mean for PTFE-glass fabrics		5770	5150	11.8
Ferrari 702T	PVC-polyester (I)	450	340	24.9
Ferrari 1002T	PVC-polyester (II)	840	570	32.7
Ferrari 1202T	PVC-polyester (III)	850	560	34.0
Ferrari 1502T	PVC-polyester (IV/V)	1110	830	25.1
Verseidag B6853	PVC-polyester (III)	1260	480	62.0
Mean for PVC-polyester fabrics		900	550	35.8
† For definition of fabric types see Chapter 2, §2.1.4.1, Figure 2-15				

Table 5-9. Warp and fill yarn moduli (from uniaxial tests)

5.5 PREDICTIVE MODEL OUTPUT

5.5.1 Methods for representing model output and assessing model validity

Predictive models are typically used to generate stress-stress-strain response surfaces because computer analysis of the models lends itself to calculating strains for a wide range of stress states (Blum & Bidmon, 1987; Pargana, Lloyd Smith & Izzuddin, 2000). These response surfaces are rarely compared with comprehensive test data, making assessment of the validity of the models difficult. Clear comparison with appropriate test results is frequently absent (§2.4.2). The aim of this section is to assess the quality of the predictive unit cell model through comparison with test data from rigorous tests on a range of architectural fabrics (Chapter 4). Changes to model parameters to fit the model output to the test data are kept to a minimum. Any adjustments (such as variations in compressive coating stiffness) are carried out to optimise the model for a whole class of fabrics (e.g. all fabrics of a given material type) to ensure that the model is still valid as a predictive tool. The model input comprises measured values from cross-section images and uniaxial tests (§5.4), with no use of data from biaxial tests.

Both the sawtooth and sinusoid models provide the same output: for warp and fill loads the model predicts warp and fill strains. This is analogous to the load controlled biaxial test rig providing measured strains. A *Microsoft Visual Basic* routine running in *Microsoft Excel* increments the loads in the model by user selected increments from zero up to the maximum design load (for this work taken to be 25% of the ultimate tensile strength), until strains have been calculated for all load combinations. For each load-case the loads and resultant strains are exported to *Matlab* for visualisation.

The unit cell model developed here does not include visco-elastic effects or inelastic deformation. It is therefore appropriate to compare the model with test data which has had residual strain removed, such that the strain at prestress is deemed to be zero (§3.3.3.4). It is necessary to apply the same 'stress reduction' to the model output. The model is used to calculate the predicted warp and fill strains at prestress, and these values are subtracted from all subsequent calculated strain values. The response surfaces can then be compared (e.g. Figure 5-22).

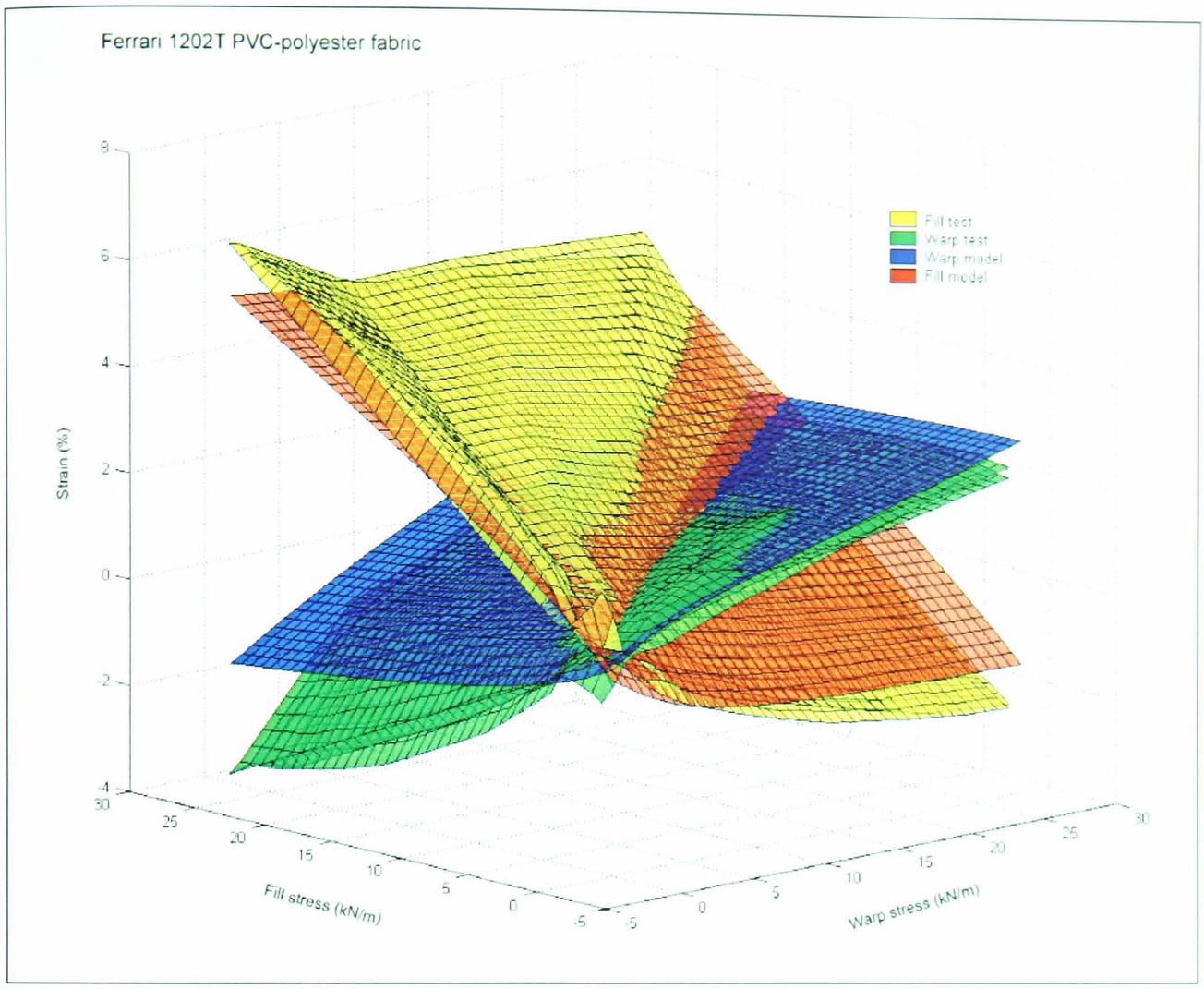

Figure 5-22. Typical response surface comparison

Subtracting the mean test surface (mean of loading and unloading data from two tests) from the predicted surface provides a 'difference surface'; an overall measure of model quality can be assessed by calculating the root-mean-square value of all the points on this 'difference surface'. However, this may not be best way to evaluate the quality of the model because:

1. The test protocol developed for this work provides loading and unloading data. For comparison of response surfaces the mean response is used. The model prediction may differ from this mean surface, but still lie within the loading-unloading envelope,
2. Whatever method of surface fitting is used (e.g. faceted surface between data points used in Figure 5-22) there will be some approximation in the interpolation between data points, which may not be representative of the fabric response.

The test protocol produces scattered data points that cover all feasible load states (i.e. zero to 25% UTS). Due to practical constraints and the radial nature of the test load paths (§3.3.4) the test data points do not lie on a regular grid. To enable a direct comparison of the model and test results, the model can be used to predict strains for the actual loads applied during a particular test. The applied loads for each test are input

into the model and the corresponding strains are calculated. For each set of test data the root-mean-square difference between the test and model strains can be determined to assess the quality of the model.

The test protocol measures fabric strains during increasing and decreasing load along each radial arm (§3.3.4). The model, however, is linear elastic, with time and load history effects being beyond the scope of this work. A perfect correlation with the test data is therefore impossible; the best that can be achieved is that the predicted stress-strain response lies between the loading and unloading curves. This means that consideration of the deviation of the model from a single data point can be misleading. The model must be assessed as to whether the predicted response lies within the envelope of loading and unloading behaviour. This is simple to assess visually for one 'arm' of the radial load regime; the predicted response should lie within the loading and unloading curves. It is more useful if the validity can be assessed mathematically for all data points. If the loading and unloading strain readings had been measured at exactly the same stress levels then this issue would be trivial; the predicted response could be compared with the mean test values. Limitations in the hydraulic control of the test rig means that the loading and unloading readings are not taken at identical stress values. The root-mean-square (RMS) deviation of the model output from the test data will never be zero: the best possible model will lie between the loading and unloading data points and hence deviate considerably from them. The difference between the predicted response and test data can be compared with the difference between the loading and unloading response to give a true measure of the model accuracy (§5.5.2, Table 5-11). The model output can be plotted on graphs of strain against RMS stress along each of the radial load paths, providing a good visual assessment of the quality of the model (Figure 5-23).

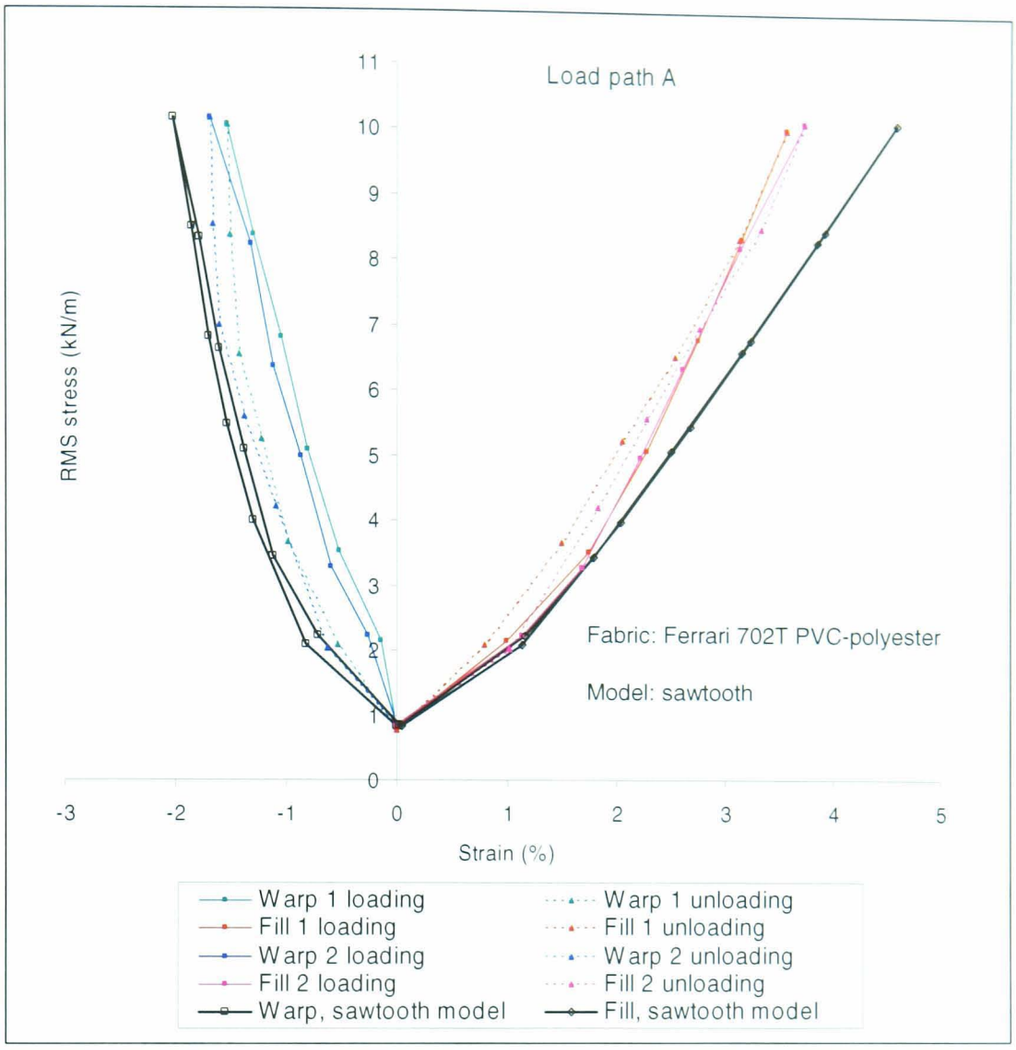

Figure 5-23. Comparison of predictive model and test data along a single radial load path

Standard stress-strain plots can also be drawn, which are useful for comparing the model with work by other researchers and previous test data which tend to be in this format. A *Visual Basic* routine enables the user select a constant stress ratio (Figure 5-24).

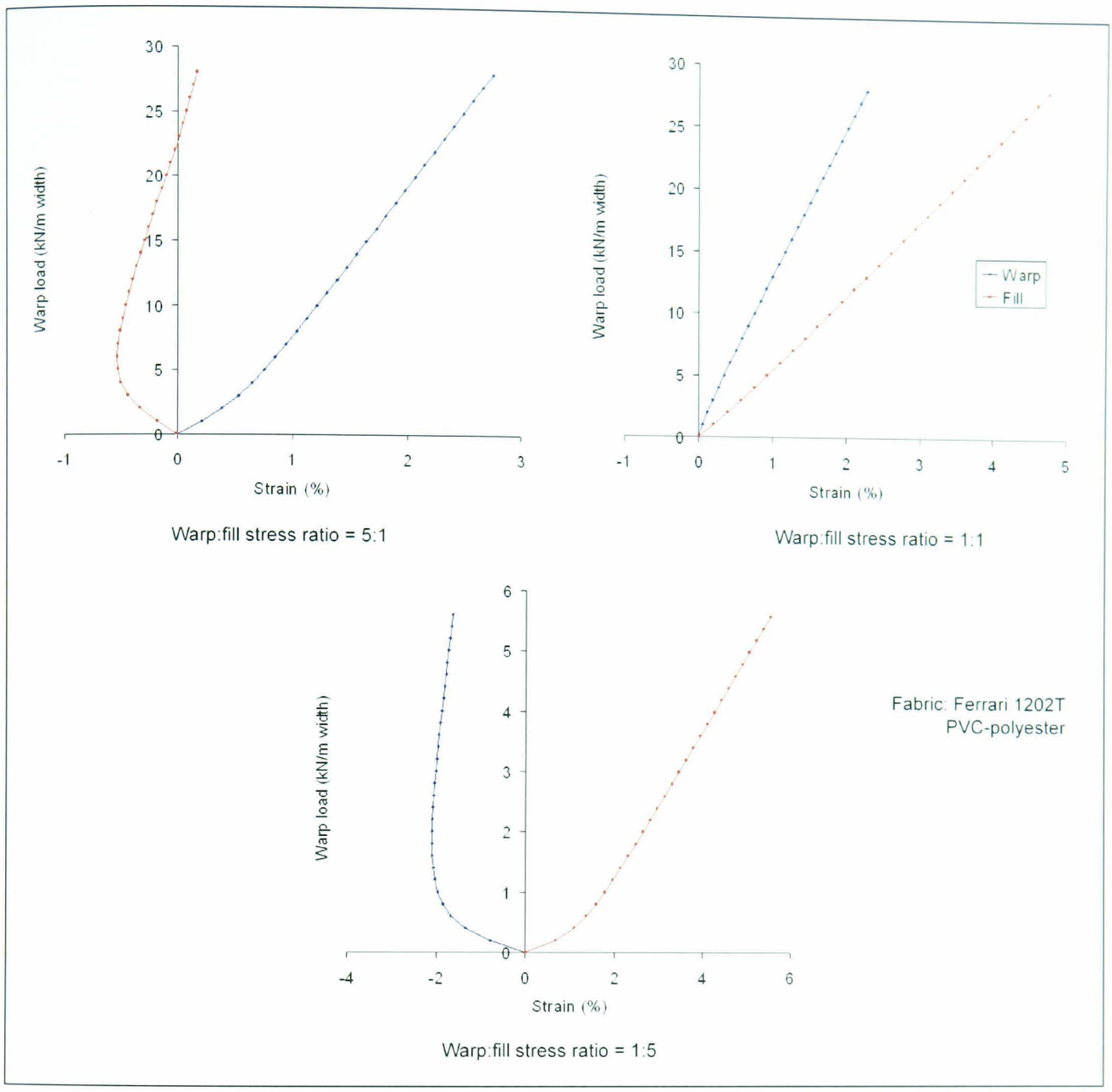

Figure 5-24. Stress-strain plots at constant stress ratio (sawtooth model)

Both the sawtooth and sinusoid models enable visualisation of the fabric cross section (Figure 5-25). This provides a useful check that the unit cell configuration is realistic, and provides a tool to assist in the understanding of the fabric response.

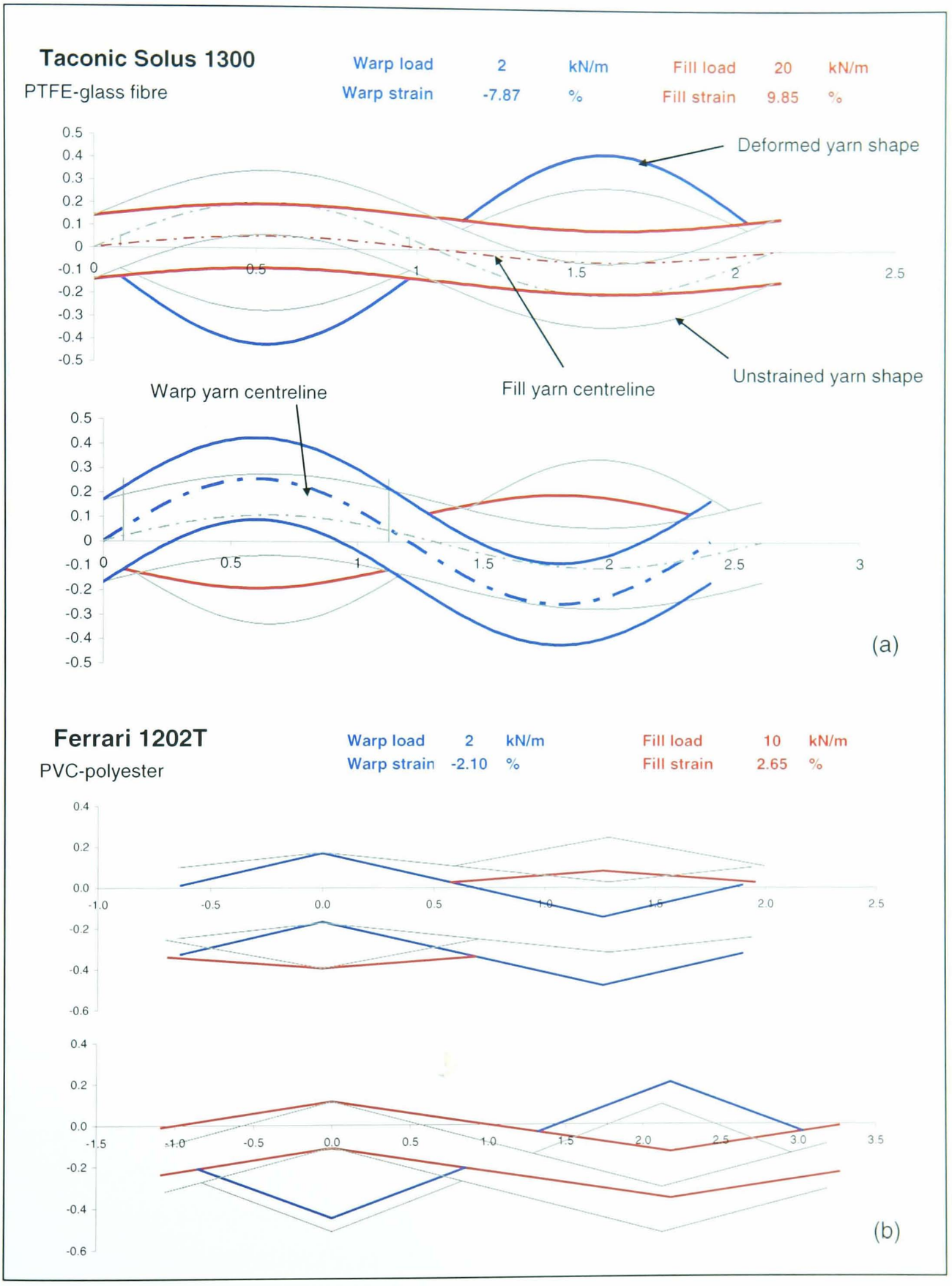

Figure 5-25. Yarn shapes (a) sinusoid, (b) sawtooth

5.5.2 Comparison with test data

With the inclusion of compressive coating stiffness, the sawtooth and sinusoid models both provide the correct form of stress-strain response curve, picking up the key non-linear characteristics of the material response (Figure 5-24). A sharp change in gradient is seen when crimp interchange is complete and yarn extension becomes the dominant deformation mechanism; gradient reversal and negative strain are also evident.

Initially both the sawtooth and sinusoid models predicted excessively large negative strains, particularly at high warp stress and low fill stress (Figure 5-26a, Figure 5-27a, Figure 5-28a & Figure 5-29a). It is clear from the values of 'maximum negative strain due to crimp interchange' (Table 5-6) that the model will tend to generate excessively large negative strains. There are several mechanisms that are not included in the model formulation which may prevent these negative strains occurring:

(i) Compressive resistance of the coating,

(ii) Coating between yarns restraining relative yarn movements,

(iii) Restraint due to out-of-plane coating deformation, resulting in local tension in the coating (Figure 5-17 & Figure 5-18),

(iv) Yarn bending stiffness and the possibility that a limiting bending configuration may be reached where further bending is prevented by the shape of the orthogonal yarn (§2.1.1).

The first three factors have been incorporated in the model by including a single value of compressive coating stiffness. Yarn bending stiffness has not been included in the model, but restraint due to the orthogonal yarn is modelled by the use of a constant yarn cross-sectional area and modelling of consistent orthogonal yarn shapes.

Because of difficulties in determining the coating compressive stiffness (§5.3.2), it has been used as a parameter for calibrating the model against the test data. To make the model generally applicable and ensure that it is truly predictive, the compressive coating stiffness function must be same for each type of fabric (i.e. for all PTFE-glass fibre fabrics and for all PVC-polyester fabrics) and preferably the same for both types of fabric. As a starting point the compressive coating stiffness was set to be equal to the tensile coating stiffness. The values of the compressive coating stiffness factor (a multiplier applied to the tensile coating stiffness) were then varied to give the best correlation with the test data (Figure 5-26, Figure 5-27, Figure 5-28, Figure 5-29 & Table 5-10). Better than a visual assessment, the root-mean-square (RMS) deviation of the predicted strains from the test strains can be calculated (Table 5-10). These values are expressed both as percentage strain and as a percentage of the strain range (i.e. for a given yarn direction, the maximum strain recorded during a test minus the minimum strain), in warp and fill directions. The

first row in Table 5-10 gives the difference for the basic models, as shown for the no-slip sawtooth in Figure 5-22. It is clear that different values are required for PVC-polyester and PTFE-glass, which is reasonable as the PVC and PTFE coatings have different material properties. The best fit has been achieved with a coating stiffness factor of 0.25 for PVC-polyester fabric and three for PTFE-glass fibre fabric. These values were determined by varying the coating stiffness factor and assessing the model output using the response surface plots and mean deviations.

Description	Direction	Compressive coating stiffness parameters		Mean deviation of predicted strain from test data (percentage of strain range, percentage strain)					
				Sawtooth, no-slip		Sawtooth, slip		Sinusoid, slip	
		PVC/ poly.	PTFE/ glass	PVC/ poly.	PTFE/ glass	PVC/ poly.	PTFE/ glass	PVC/ poly.	PTFE/ glass
(1) Zero compressive coating stiffness	Warp	0.0	0.0	15.6, 0.85	49.9, 3.46	15.7, 0.86	52.0, 3.61	23.2, 1.23	70.5, 5.30
	Fill	0.0	0.0	8.6, 0.84	20.5, 3.37	8.5, 0.83	21.8, 3.61	17.9, 1.85	31.9, 5.09
(2) Compressive coating stiffness = tensile coating stiffness	Warp	1.0	1.0	9.3, 0.50	11.6, 0.91	9.2, 0.50	12.7, 1.01	13.4, 0.68	23.7, 1.84
	Fill	1.0	1.0	9.2, 0.94	8.8, 1.37	9.1, 0.93	9.5, 1.50	17.2, 1.78	21.3, 3.25
(3) Parameters optimised for sawtooth models	Warp	0.25	3.0	7.8, 0.31	8.1, 0.40	7.8, 0.31	8.4, 0.43	-	-
	Fill	0.25	3.0	8.7, 0.53	7.6, 0.72	8.4, 0.50	7.6, 0.74	-	-
(4) Parameters optimised for sinusoid model	Warp	0.25	3.5	-	-	-	-	14.3, 0.73	14.3, 1.07
	Fill	0.25	3.5	-	-	-	-	17.5, 1.81	16.8, 2.5

Table 5-10. Sawtooth & sinusoid models, comparison with test data.

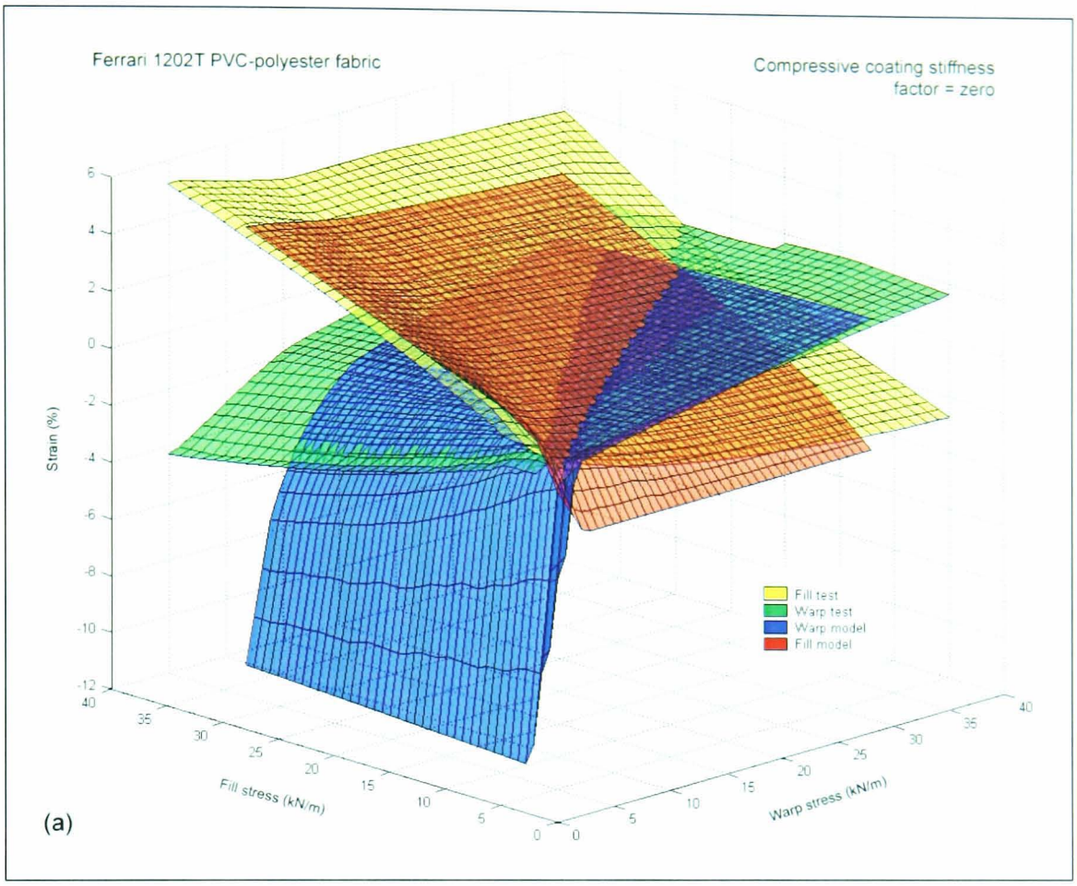
Ferrari 1202T PVC-polyester fabric
Compressive coating stiffness factor = zero
Strain (%)
Fill stress (kN/m)
Warp stress (kN/m)
Fill test
Warp test
Warp model
Fill model
(a)

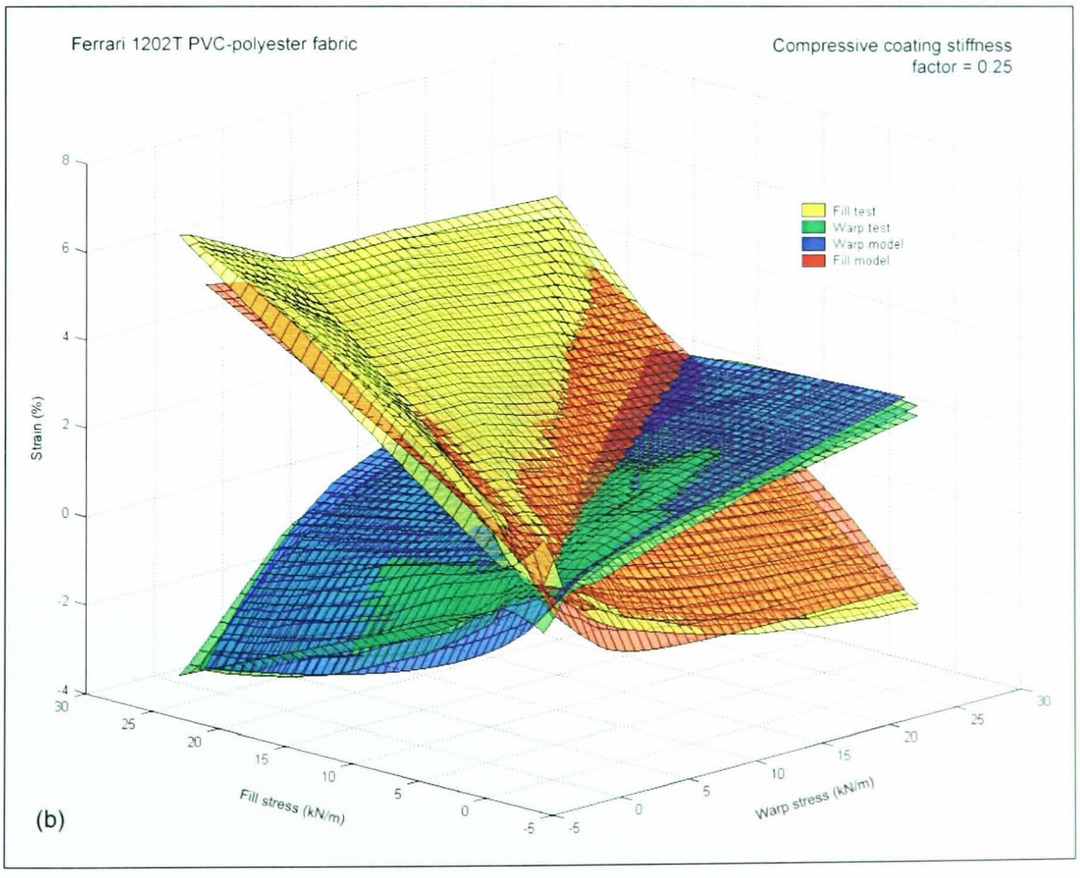
Ferrari 1202T PVC-polyester fabric
Compressive coating stiffness factor = 0.25
Strain (%)
Fill stress (kN/m)
Warp stress (kN/m)
Fill test
Warp test
Warp model
Fill model
(b)

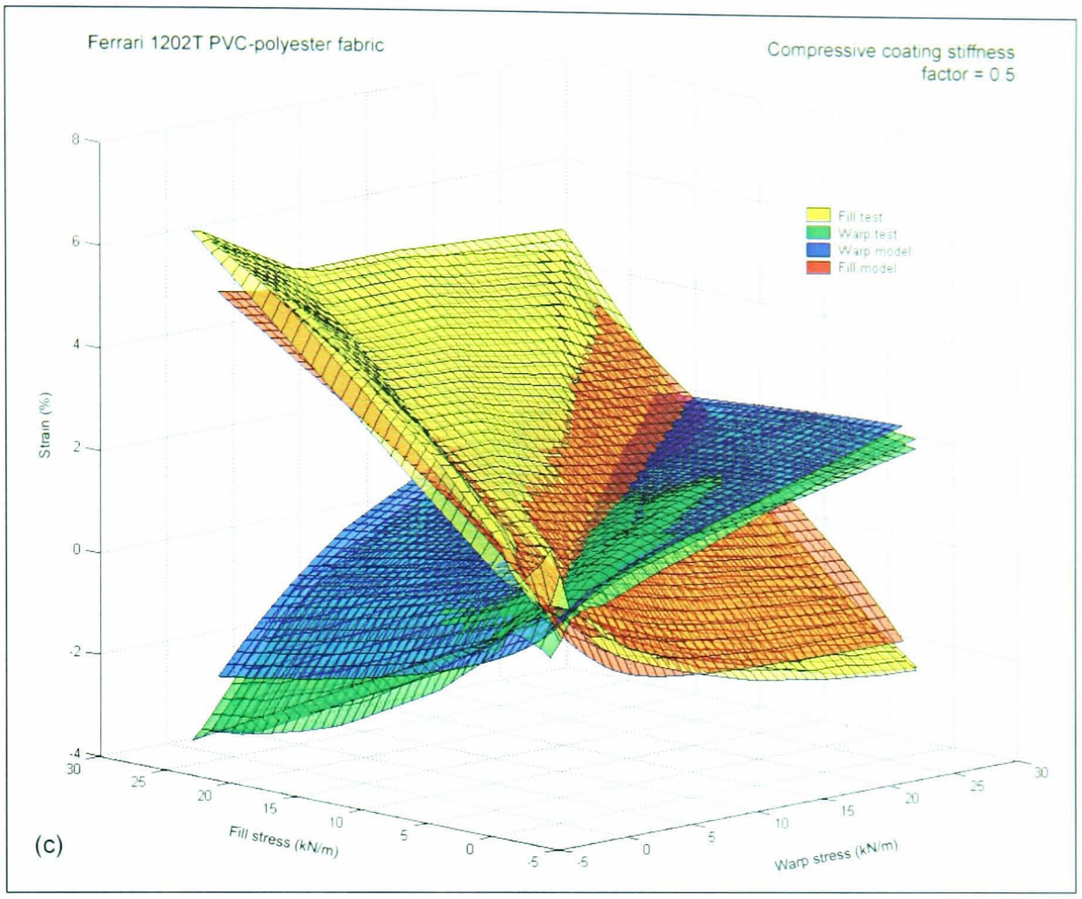

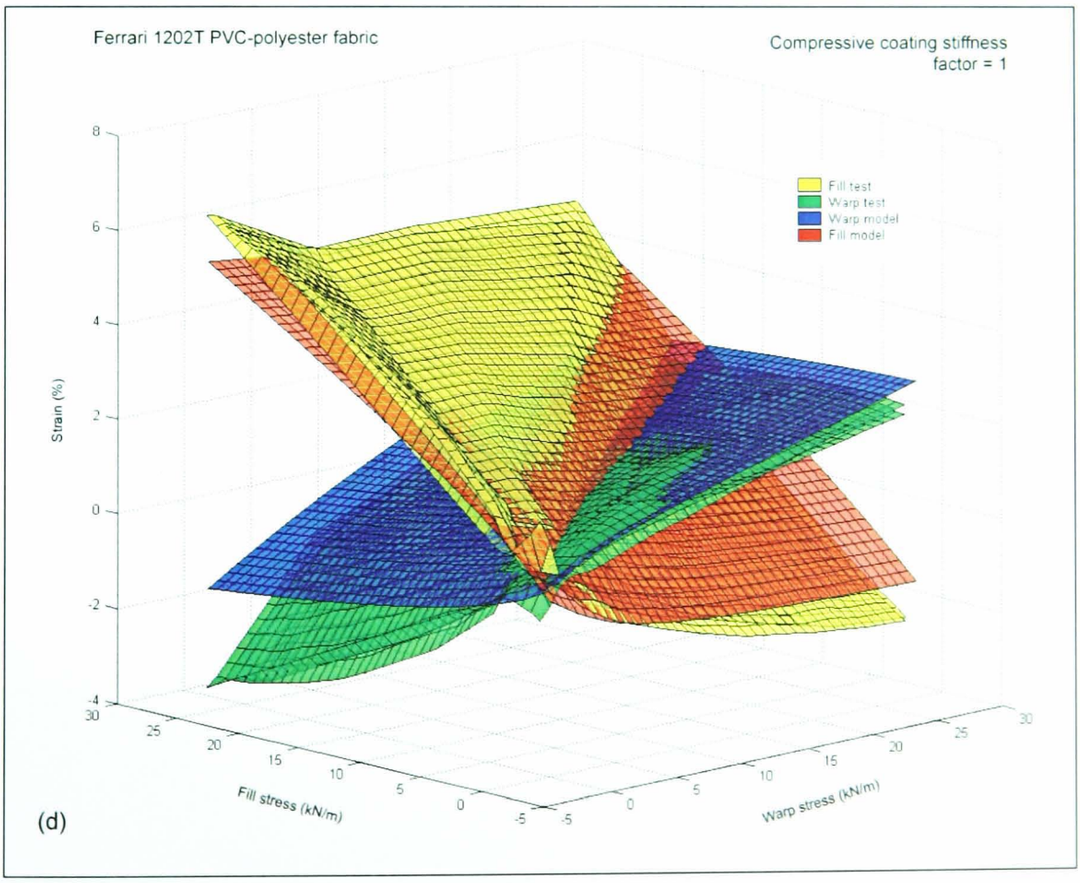

Figure 5-26. Variation in coating compressive stiffness: sawtooth, no-slip model, PVC-polyester

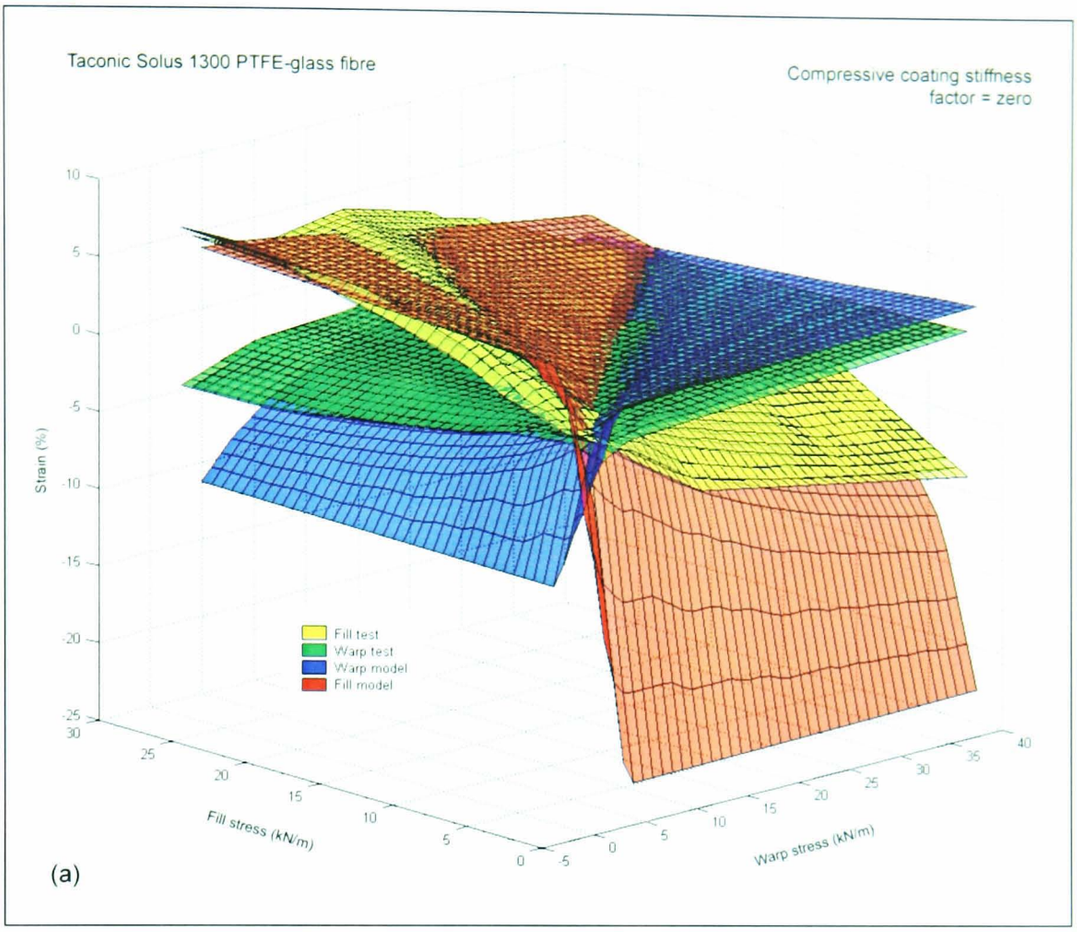
Taconic Solus 1300 PTFE-glass fibre
Compressive coating stiffness factor = zero
Strain (%)
Fill test
Warp test
Warp model
Fill model
Fill stress (kN/m)
Warp stress (kN/m)
(a)

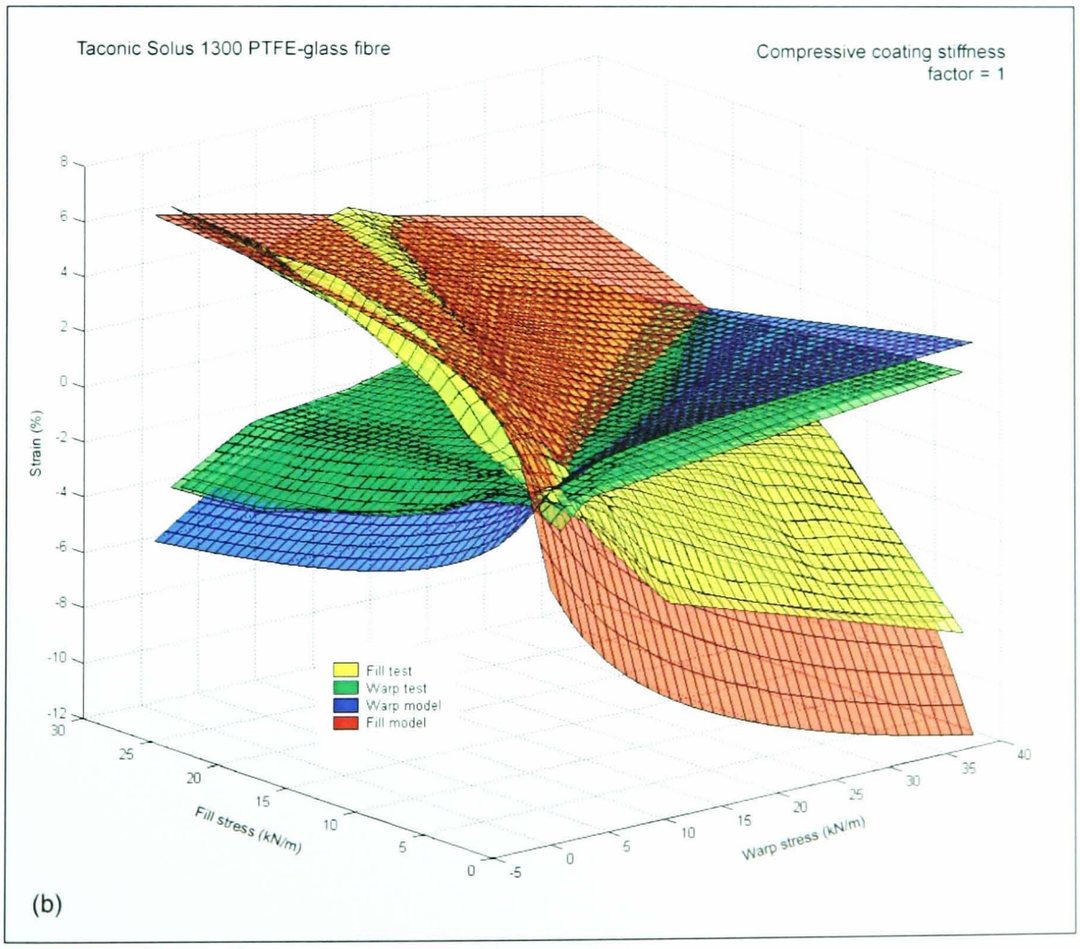
Taconic Solus 1300 PTFE-glass fibre
Compressive coating stiffness factor = 1
Strain (%)
Fill test
Warp test
Warp model
Fill model
Fill stress (kN/m)
Warp stress (kN/m)
(b)

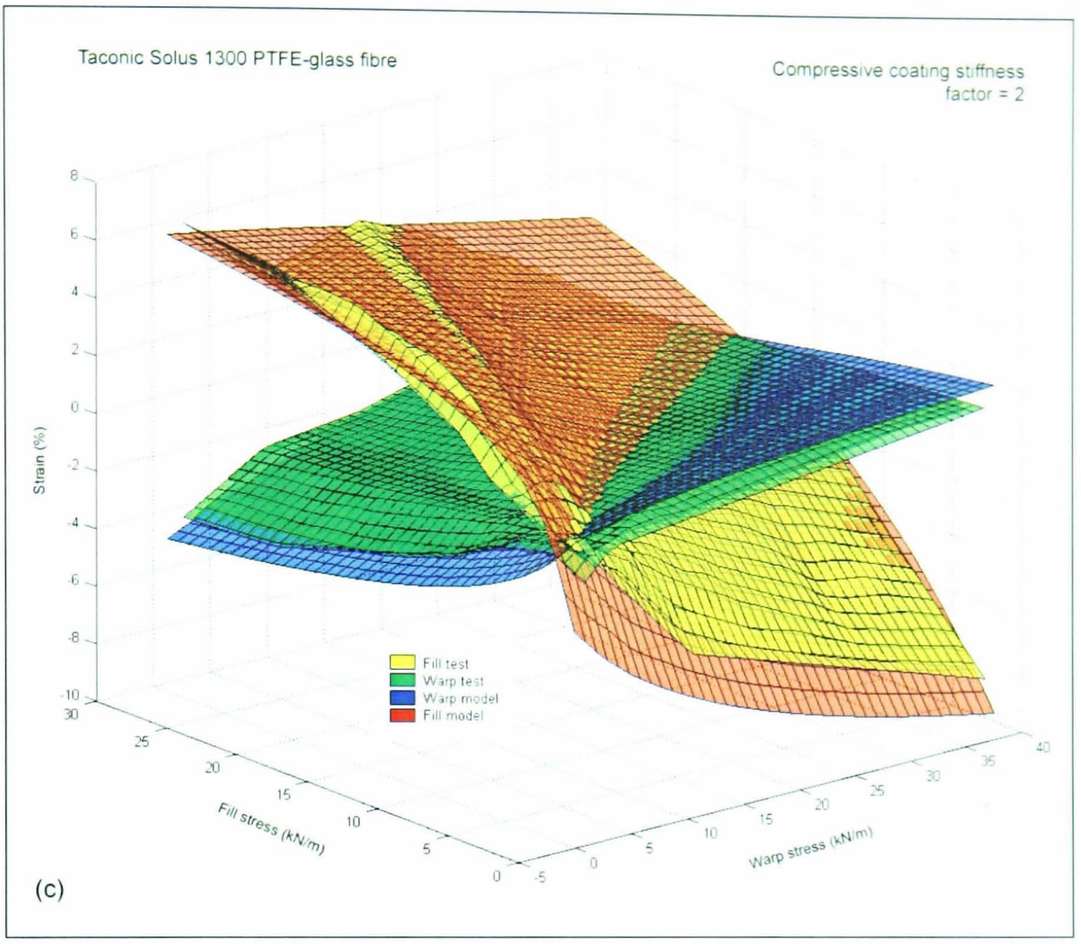
Taconic Solus 1300 PTFE-glass fibre
Compressive coating stiffness factor = 2
Strain (%)
Fill test
Warp test
Warp model
Fill model
Fill stress (kN/m)
Warp stress (kN/m)
(c)

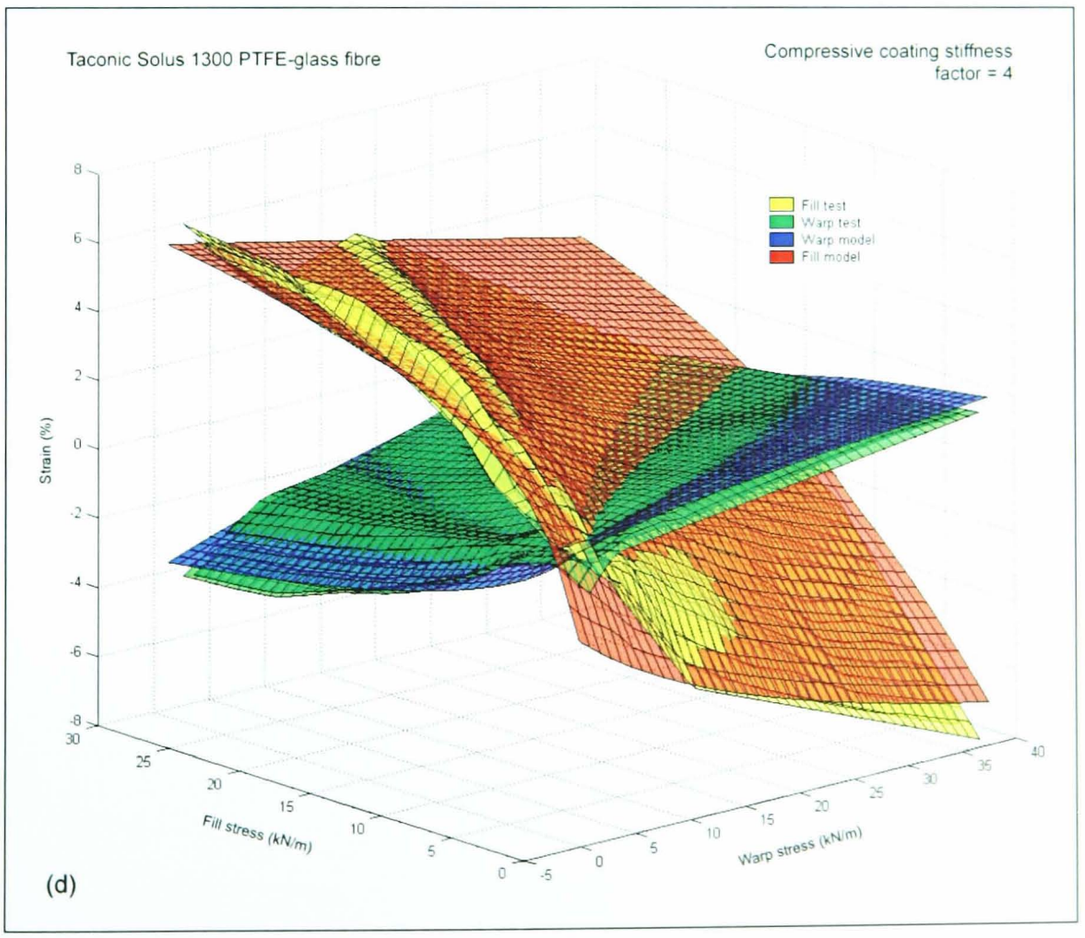
Taconic Solus 1300 PTFE-glass fibre
Compressive coating stiffness factor = 4
Strain (%)
Fill test
Warp test
Warp model
Fill model
Fill stress (kN/m)
Warp stress (kN/m)
(d)

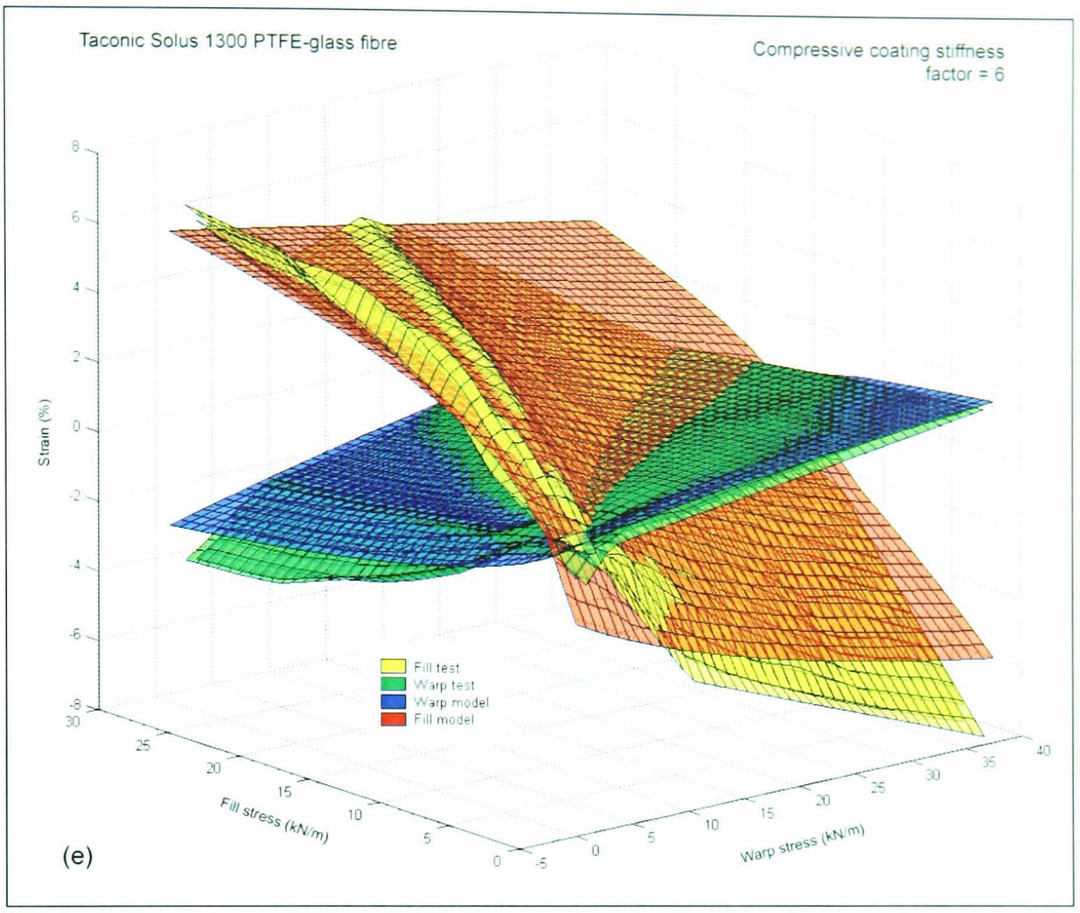

Figure 5-27. Variation in coating compressive stiffness: sawtooth, no-slip model, PTFE-glass fibre

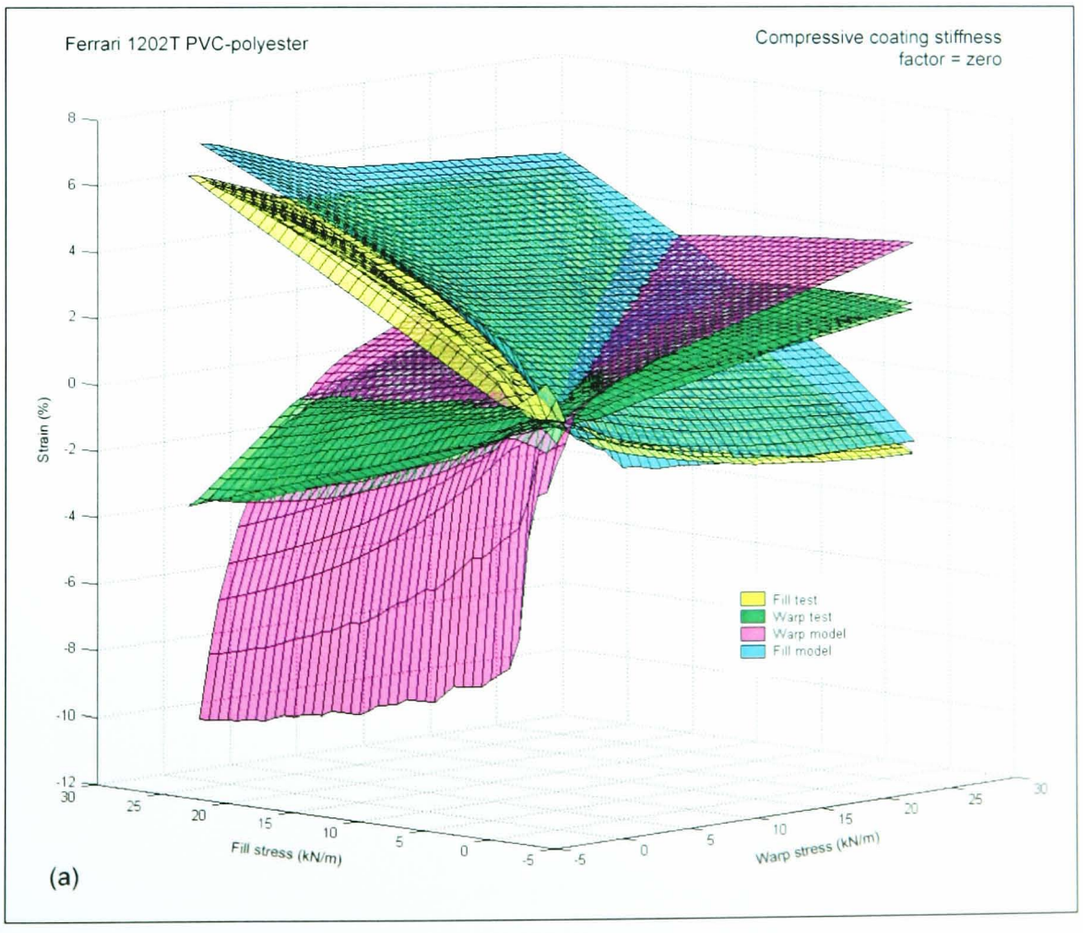

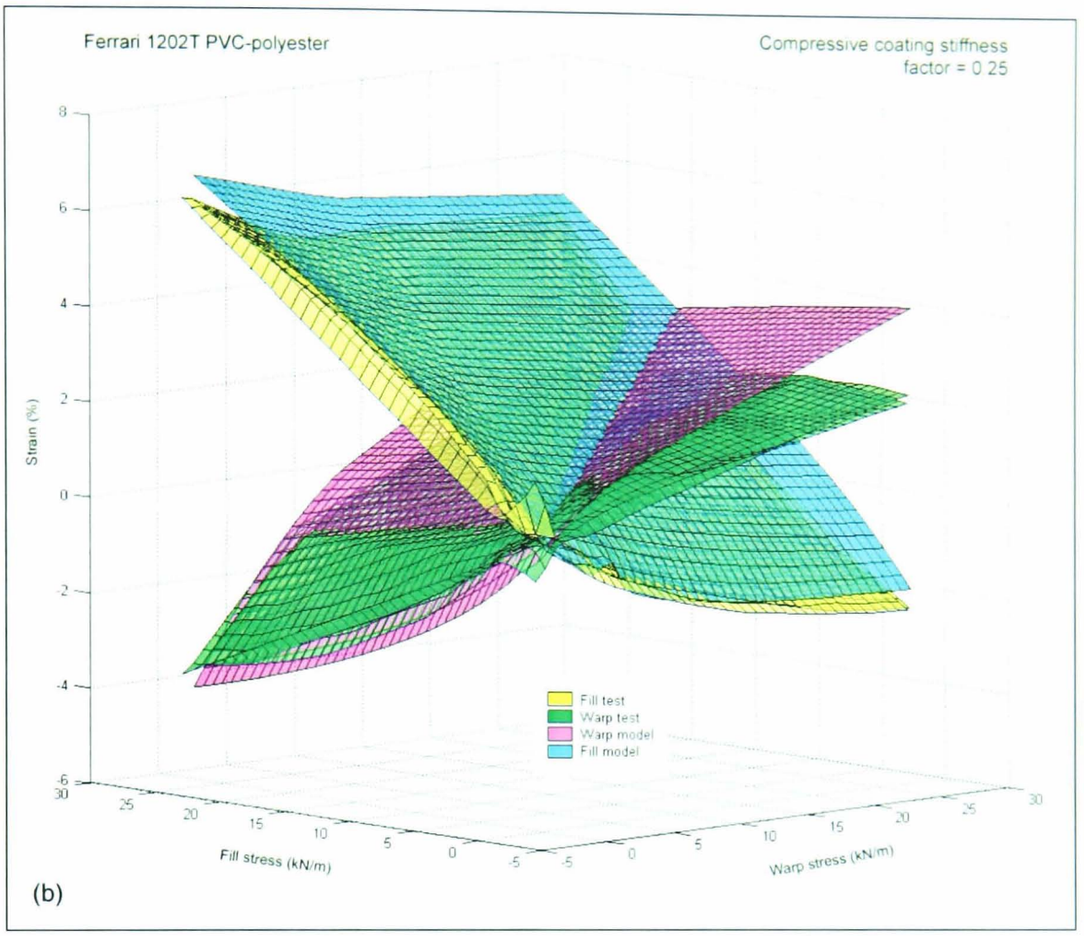

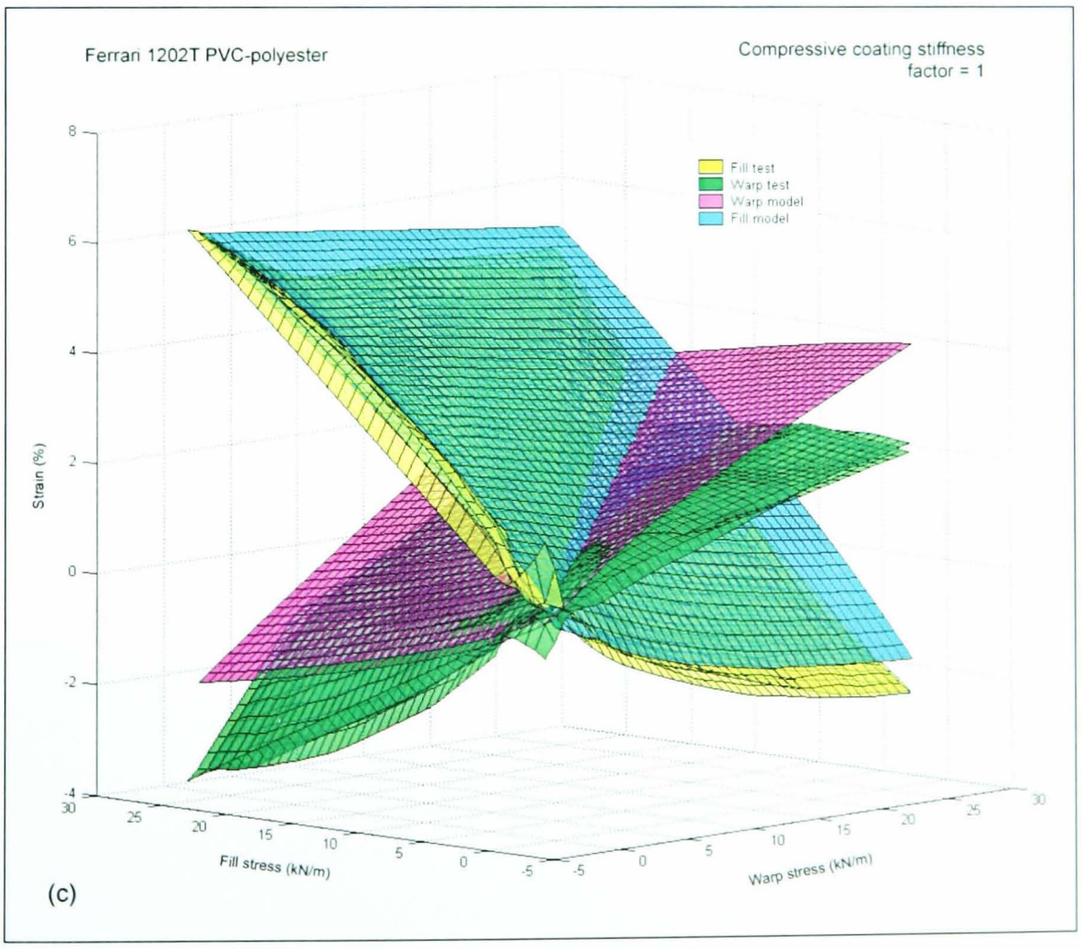

Figure 5-28. Variation in coating compressive stiffness: sinusoid model, slip model, PVC-polyester

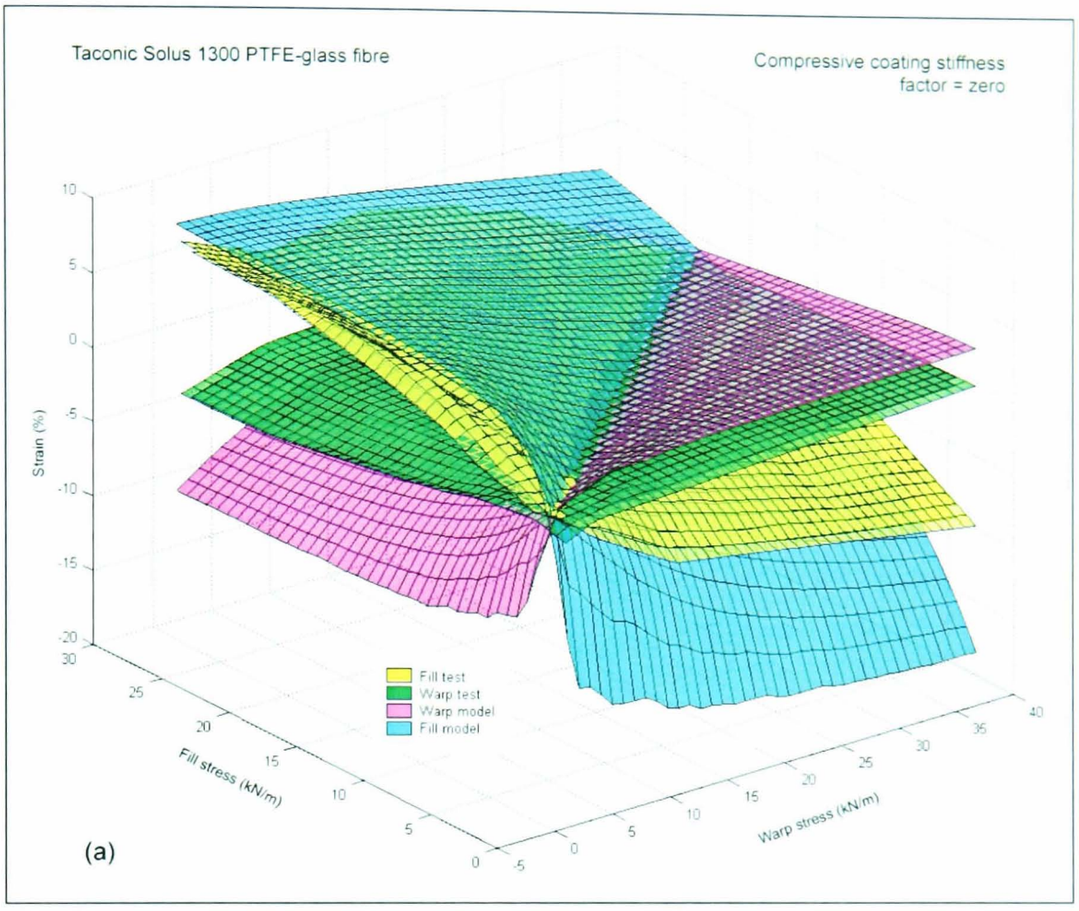
Taconic Solus 1300 PTFE-glass fibre
Compressive coating stiffness factor = zero
Strain (%)
10
5
0
-5
-10
-15
-20
Fill stress (kN/m)
30
25
20
15
10
5
0
Warp stress (kN/m)
-5
0
5
10
15
20
25
30
35
40
Fill test
Warp test
Warp model
Fill model
(a)

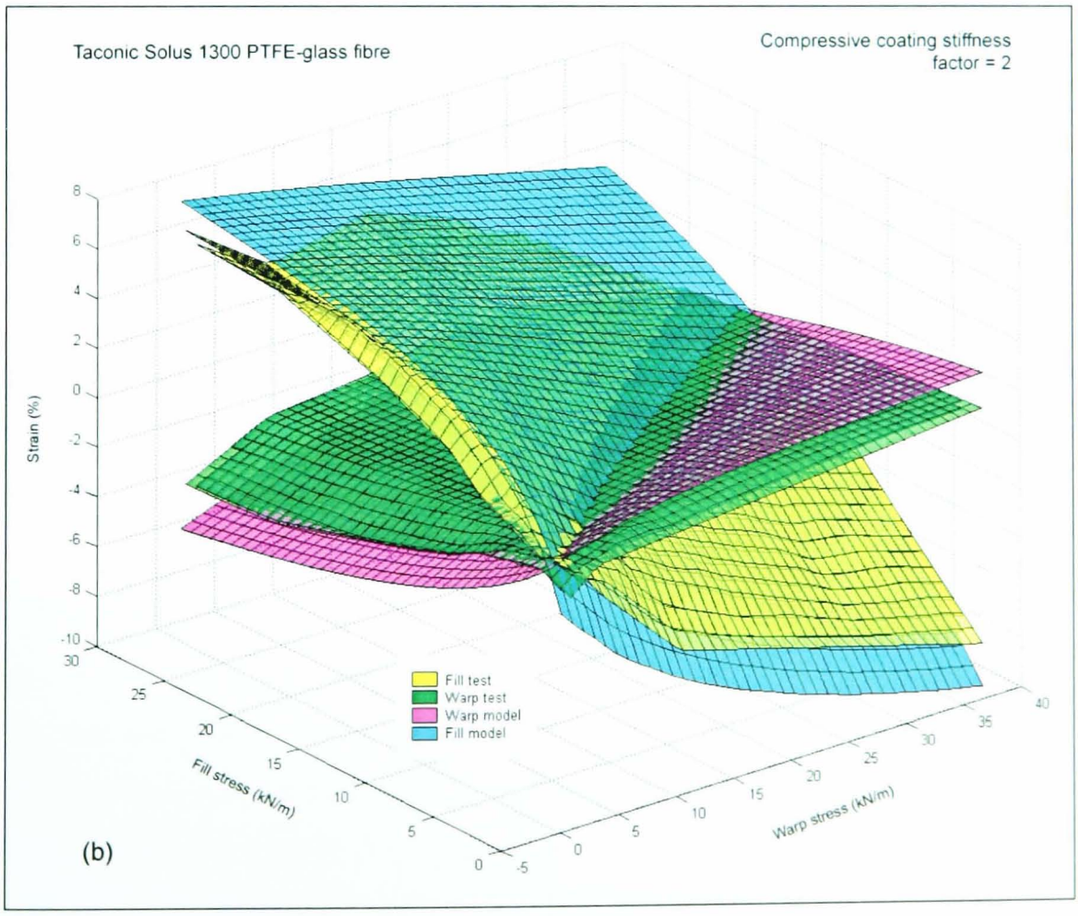
Taconic Solus 1300 PTFE-glass fibre
Compressive coating stiffness factor = 2
Strain (%)
8
6
4
2
0
-2
-4
-6
-8
-10
Fill stress (kN/m)
30
25
20
15
10
5
0
Warp stress (kN/m)
-5
0
5
10
15
20
25
30
35
40
Fill test
Warp test
Warp model
Fill model
(b)

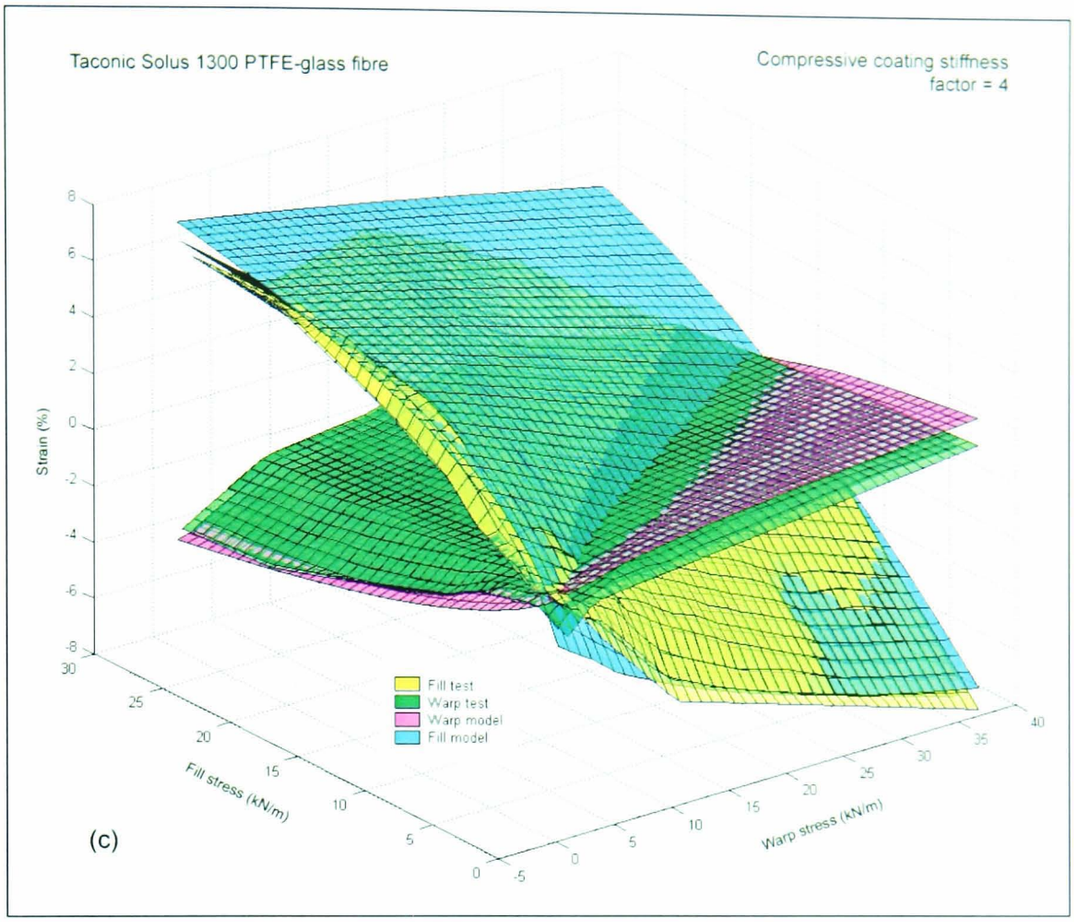

Figure 5-29. Variation in coating compressive stiffness: sinusoid model, slip model, PTFE-glass fibre

It is possible to have different compressive coating stiffness factors for warp and fill directions, but from the evidence in Figure 5-26, Figure 5-27, Figure 5-28 and Figure 5-29 there appears to be little benefit in having differing values. This fits with the compressive coating stiffness representing a physical property which would have a similar value in both warp and fill directions.

With the optimised values of coating compressive stiffness factor the correlation with test data is extremely good for PTFE-glass fibre fabrics (e.g. Verseidag B18089, Figure 5-31). The form of the response is modelled well for all load paths except G. This corresponds approximately to the *natural stress ratio* (§4.1.1, p.161), at which point the level of crimp is virtually balanced, the strains are very low, and the response is highly sensitive to small changes in stress ratio. Whilst the model output does not exactly match the test data for load path G, the model has predicted that the crimp is balanced at this stress ratio, and gives appropriately low levels of strain.

The correlation for PVC-polyester fabrics (e.g. Ferrari 702T, Figure 5-30) is good at high and low stress ratios, but the transition point described above is not as well predicted, with poor correlation for load path E. However, the overall correlation is good considering that no parameters have been varied for each particular fabric, ensuring the model is truly predictive. The correlations given in Table 5-10 (typically 7.5 to 8.5% of the strain range for the sawtooth model) are particularly good because the single model surface is being compared with loading and unloading test data, hence a deviation of zero could never be

achieved. The model deviation can be put in context by comparing the test data with a mean surface derived from the loading and unloading data (Table 5-11).

Direction	Deviation of loading and unloading test data from mean surface		Difference between no-slip sawtooth model and test data (Table 5-10, row 3)		Difference = model accuracy	
	Percentage of the strain range (percentage strain) 'sd' denotes standard deviation for two tests on each of the fabrics tested (Table 3-3)					
	PVC-polyester	PTFE-glass	PVC-polyester	PTFE-glass	PVC-polyester	PTFE-glass
Warp	1.9 (0.08)	2.5 (0.12)	7.8 (0.31, sd = 0.40)	8.1 (0.40, sd = 0.60)	**5.9 (0.23)**	**5.6 (0.28)**
Fill	3.4 (0.21)	2.3 (0.22)	8.7 (0.53, sd = 0.84)	7.6 (0.72, sd = 1.12)	**5.3 (0.32)**	**5.3 (0.50)**

Table 5-11. Model accuracy

More complex functions for the compressive coating stiffness factor may provide an even better correlation with the test data. For example, for PVC-polyester fabrics a function of the form:

$$E_{j1,2} = \left[a - \left(\frac{F_{2,1}}{F_{max2,1}}\right)\right] E_k$$

Equation 5-28

is proposed, where a and b are parameters to be determined and F_{max} is the maximum design load. The function has been derived by determining the coating stiffness factor which gives the best correlation at various load ratios, and then making a formula that provides the appropriate change in factor with stress ratio. However, this formula does not provide a significant improvement on the single value factor, and so the simpler approach has been adopted.

The sawtooth model predicts the stress-strain response of PVC/polyester and PTFE/glass fabrics from several manufacturers in a wide range of types (PVC/polyester, type I-IV/V, PTFE-glass type G5-G7), (Table 5-11). However, the model should be used with caution on other types of fabric (e.g. PTFE coated PTFE yarns, or *Tenara*) until further calibration of the coating compressive stiffness is carried out against test data.

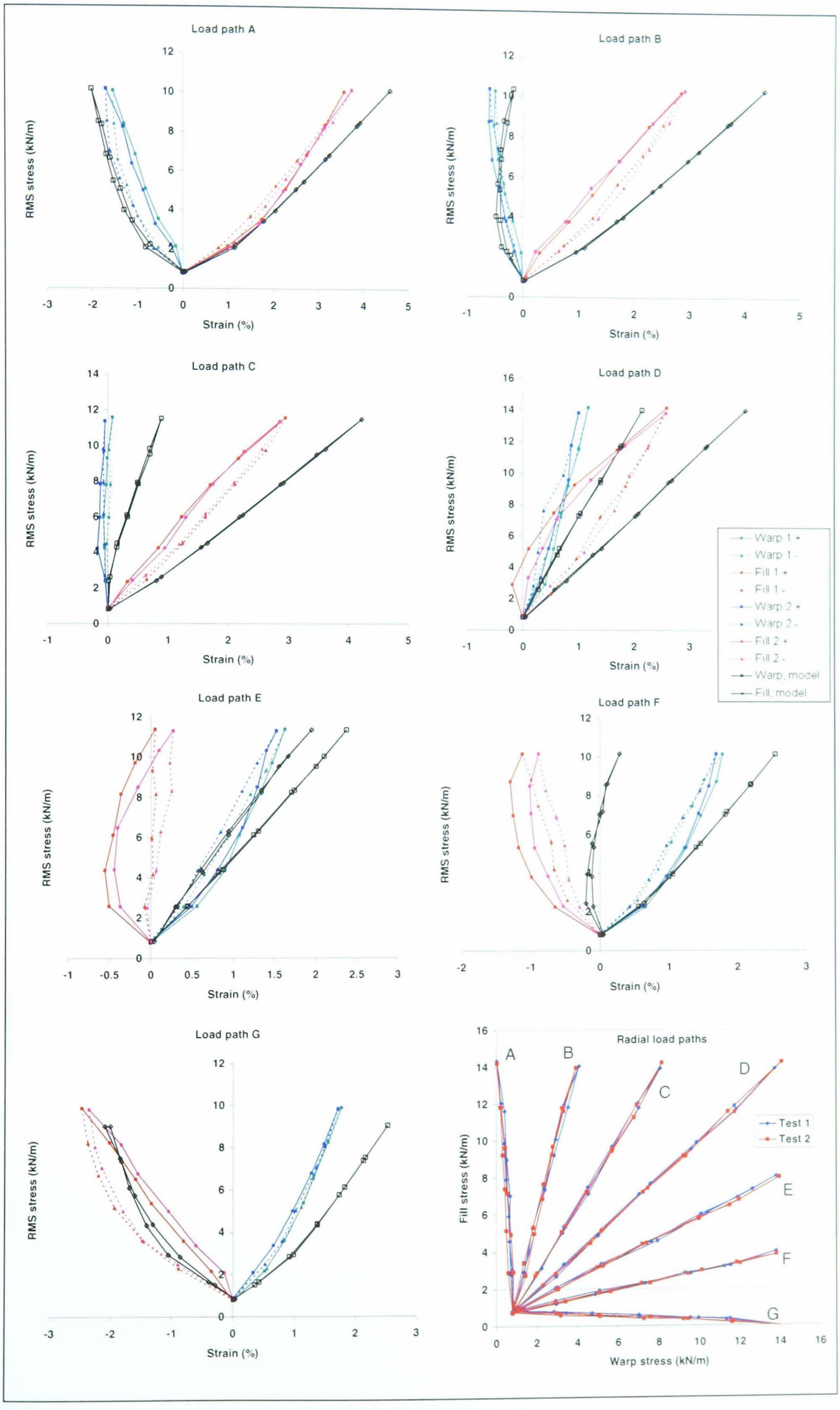

Figure 5-30. Comparison along radial load arms, sawtooth model, Ferrari 702T PVC-polyester

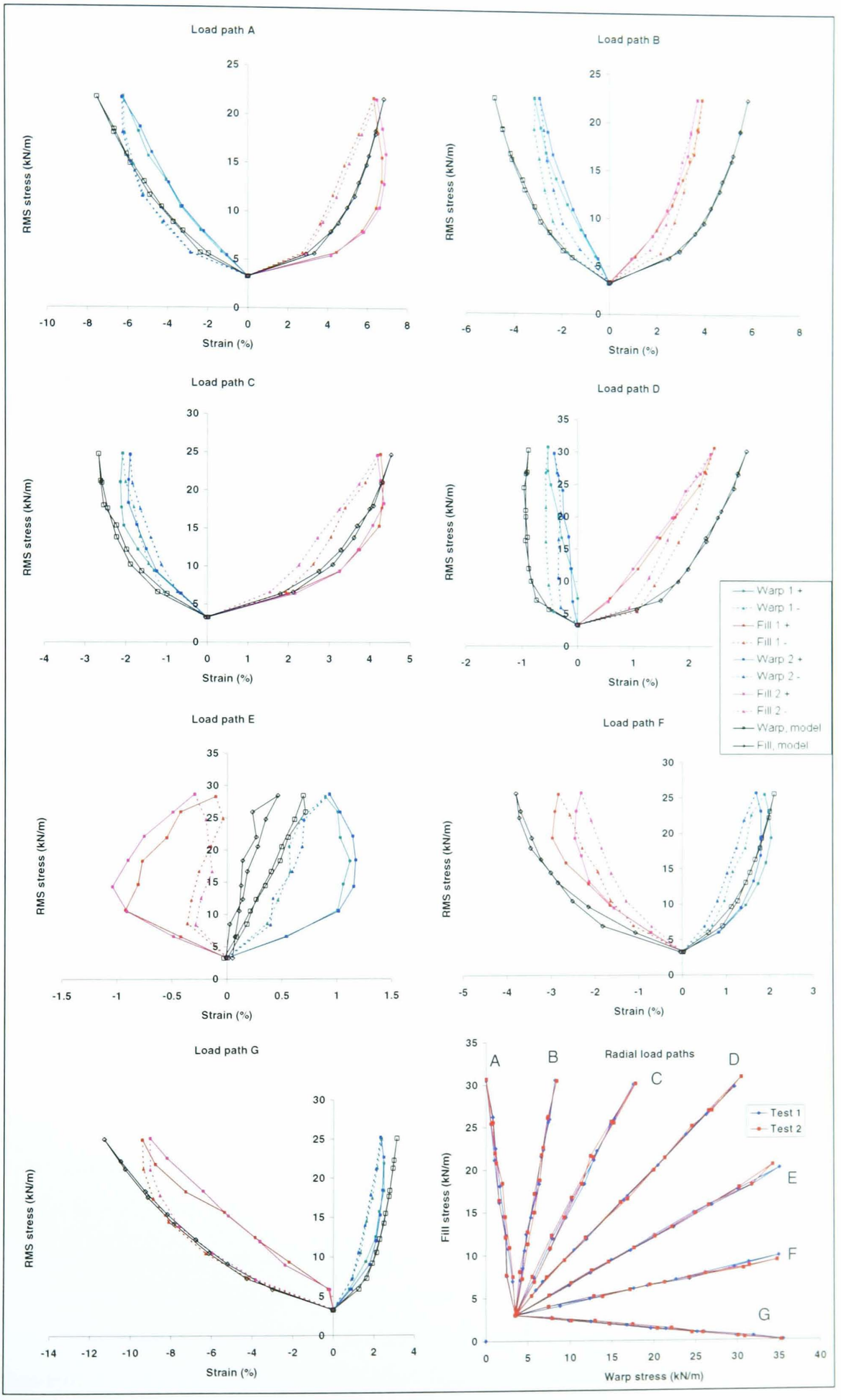

Figure 5-31. Comparison along radial load arms, sawtooth model, Verseidag B18089 PTFE-glass fibre

The hypothesis during the model formulation was that the slip and no-slip models would bound the fabric response, with the optimum model being somewhere between the two (Figure 5-32 & Figure 5-33). This does not appear to be the case, but the variation between the slip and no-slip models is typically small. For the Ferrari 702T PVC-polyester (Figure 5-32) the slip model matches the test data best in the fill direction, with little difference between the slip and no-slip models in the warp direction. For the Verseidag B18089 PTFE-glass (Figure 5-33) the two models are very similar, with the no-slip model providing a slightly better correlation with the test data in the fill direction. These observations concur with the numerical assessment in Table 5-10 which shows virtually no difference between the slip and no-slip models.

The sinusoid model output has only been provided for the slip model. The formulation of the no-slip model (§5.3.3.2) adds one more constraint to the already complex set of equations which must be satisfied to achieve equilibrium in the unit cell. The modification of the yarn tension, and hence yarn length due to the resultant change in tensile extension, presented difficulties in convergence for some loadcases using the *Excel Solver*. As a result, output is not available for the no-slip sinusoid model. However, for the sawtooth model the difference between the slip and no-slip versions is small (Table 5-10, Figure 5-32, Figure 5-33) and the no-slip sinusoid should therefore give a good indication of the model's capabilities.

A novel method has been proposed for determining crimp equilibrium for a sinusoidal yarn based on contact forces and geometric constraints, which provides a new approach to realistically modelling coated woven fabrics. Despite this, the sinusoid model as formulated here does not provide as good a correlation with the test data as the sawtooth model. The theoretical decrimping strains (Table 5-6) suggest that the sawtooth model gives a better prediction of decrimping strain than the sinusoid. This is fundamental for predicting woven fabric behaviour. Conversely, visual inspection of the fabric cross-section (Figure 5-9) clearly shows that the sinusoid model is a more appropriate model of the yarn geometry. Wang's (2002) model confirms this, with the sinusoid model providing a better fit to test data than a straight line (sawtooth) model (§2.4.2). However, Wang simplified the sinusoid model by calculating the out-of-plane force as the vertical component of the yarn tension at the point of inflection of the sine wave. This gives the model substantial similarity to the sawtooth model, the only difference being the calculation of yarn length. Wang's model has been developed for uncoated fabrics, and uses yarn crushing stiffness to calculate changes in yarn thickness. This means that direct comparison with the model developed here is difficult.

The sawtooth model, giving lower strains with its straight line approximation to the yarn waveform, may be more accurate as a predictive tool as it inadvertently counteracts some of the simplifications in the model. Explicitly, the out-of-plane restraint provided by the coating is not included in the model. At high stress ratios crimp interchange results in a 'dimpled' fabric surface with the coating being stretched over the yarns at crossovers (§5.4.1, Figure 5-17 & Figure 5-18). It is postulated here that this effect may be

approximated by the shortened yarn length inherent in the sawtooth representation. Further work modelling the tension in the coating over the crimp interchange 'dimples' may be beneficial (§6.2.9).

Yarn bending stiffness has also been neglected in the model. The large scale bending stiffness of architectural fabrics is generally regarded as negligible, but the yarn bending stiffness may be significant on the scale of the unit cell. Inclusion of these additional factors with the sinusoid formulation may provide an even more accurate model than the sawtooth model presented here.

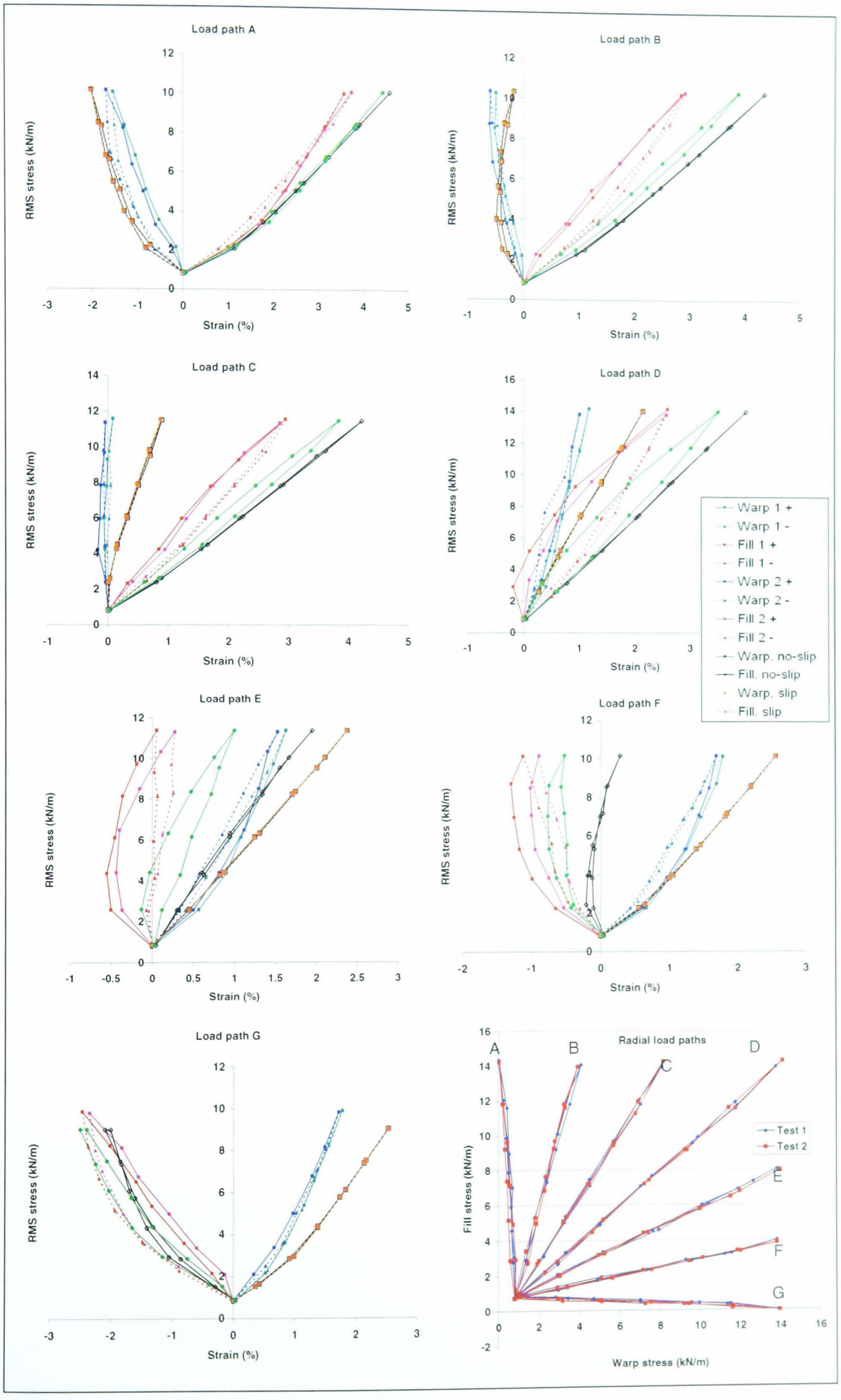

Figure 5-32. Slip and no-slip sawtooth; comparison with test data, Ferrari 702T PVC/polyester

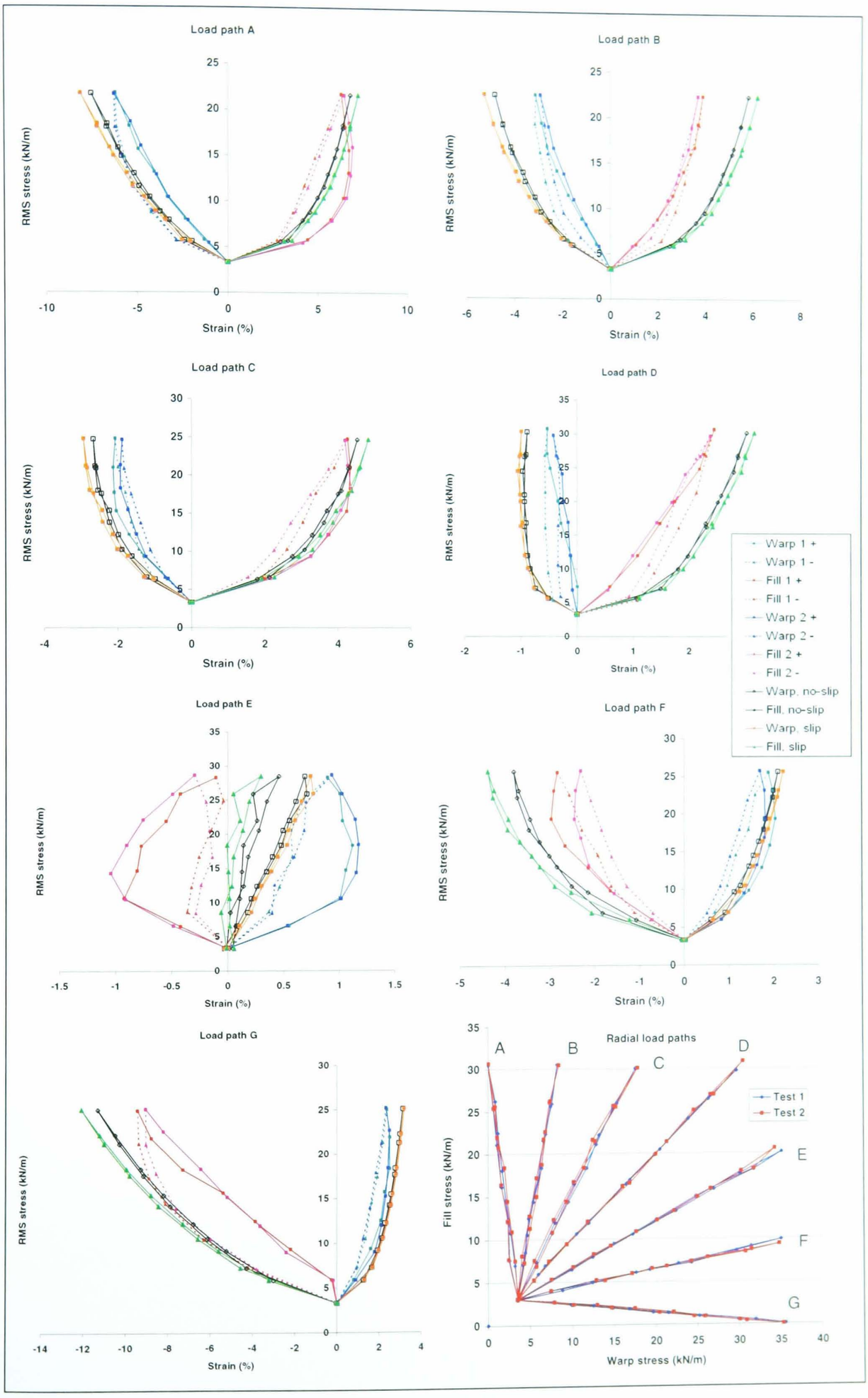

Figure 5-33. Slip and no-slip sawtooth; comparison with test data, Verseidag B18089 PTFE-glass fibre

5.5.3 Comparison with plane stress model

The model provides a more accurate representation of fabric behaviour than current industry best practice (i.e. elastic constants based on biaxial test data), but without specialist testing or equipment. The difference between the sawtooth model and the test data is similar to the difference between the test data and the plane stress representation discussed in Chapter 4 (Table 5-12). The fundamental difference is that the plane stress representation uses elastic moduli and Poisson's ratios which are evaluated using the test data, and are changed for each fabric. The sawtooth model provides a similar level of accuracy but with no biaxial testing and no modification for each fabric. The values of elastic moduli and Poisson's ratios used to give the values in Table 5-12 vary significantly between the fabrics, if a single value of each parameter was used for each fabric type (PVC-polyester and PTFE-glass) the correlation would be much worse than that provided by the sawtooth model.

Direction	RMS difference between plane stress representation and test data (percentage of strain range)		RMS difference between no-slip sawtooth model and test data (percentage of strain range)	
	PVC-polyester	PTFE-glass	PVC-polyester	PTFE-glass
Warp	7.6, sd = 7.0	**8.2, sd = 7.4**	**7.8, sd = 7.1**	8.1, sd = 7.4
Fill	6.5, sd = 6.15	**7.3, sd = 7.0**	**8.7, sd = 9.1**	7.6, sd = 7.3

Table 5-12. Comparison of unit cell model and plane stress representation.

In industry architectural fabric properties are typically modelled using two elastic moduli and Poisson's ratios. These will typically comply with plane stress theory (Equation 4-3), which has been shown in this work to be inappropriate for coated woven fabrics (§4.2.1). Frequently assumed values will be used with no reference to biaxial test data for a particular fabric (§2.3.3). Use of the sawtooth model would provide more accurate material properties.

5.6 SUMMARY & CONCLUSIONS

A predictive model has been developed to determine the biaxial stress-strain response of architectural fabrics, without the need for biaxial testing. The model provides a more accurate representation of fabric behaviour than current industry best practice (i.e. elastic constants based on biaxial test data), but without specialist testing or equipment.

Initially a sawtooth unit cell model was formulated, with spring elements between crossovers used to represent the coating. The sawtooth model formulation builds closely on previous work (§2.4.2). A sinusoidal crimp shape was then introduced to provide a more realistic representation of the unit cell geometry, and to enable more accurate calculation of decrimping strain. A significant development in both models is that a constant yarn cross-sectional has been maintained, resulting in a relationship between unit cell length and yarn thickness, eliminating the need to determine the yarn crushing stiffness. The constant yarn area constraint has been coupled with the requirement that consistent geometry is maintained for the orthogonal yarns (i.e. the shape of the yarn cross-section corresponds to the orthogonal yarn wave form throughout the contact length). Yarn crushing stiffness is difficult to measure and is commonly used as a parameter to calibrate models against specific sets of test data. Whilst providing a realistic model of the deformed fabric, the geometric constraints remove the need to determine yarn crushing stiffness. Compressive coating stiffness has been introduced to prevent excessive negative strain due to unrestrained crimp interchange.

All model parameters are determined from standard tests: yarn and coating tensile moduli are inferred from uniaxial strip tests, weave geometry is measured from digital photographs of the fabric cross-section. The model is truly predictive, requiring no calibration against test data for individual fabrics, and as such provides a significant benefit compared with previous work. The compressive coating stiffness factor has been chosen following comparison with the test data, but a single value has been used for each type of fabric (PVC-polyester and PTFE-glass fibre). The model has been compared with biaxial test data for both PTFE-glass and PVC-polyester fabrics from several manufacturers in a range of weights, and it provides a good correlation with all test data. The root-mean-square deviation of the model from the mean test data (i.e. mean of loading and unloading results for two tests) is 5 to 6% of the strain range, or 0.2 to 0.5% strain. For comparison, the average variation between repeat tests on the same fabrics was 3% of the strain range. The model provides a similar level of accuracy as use of a best fit plane devised specifically for each set of test data, but without the need for biaxial testing. Any set of elastic constants conforming to plane stress theory will provide a worse fit than this.

A novel method has been developed for determining crimp equilibrium for a sinusoidal yarn based on contact forces and geometric constraints, which provides a new approach to realistically modelling coated

woven fabrics. Despite this, the sinusoid model does not provide as good a correlation with test data as the sawtooth model. This may be because other factors such as out-of-plane restraint due to the coating and yarn bending stiffness have not been modelled are inadvertently compensated for by the shorter yarn length in the sawtooth formulation. Inclusion of these additional factors with the sinusoid formulation may provide a more accurate model than the sawtooth.

The model is at least as accurate as a plane stress representation of the fabric test data, and significantly more accurate than use of typical values for elastic constants. The model is therefore suitable for use in structural analysis, and would provide increased accuracy and confidence. Testing for compensation is still required. A database of values from the model could be used to prevent the iterative model calculations from slowing down the FE analysis. Use of the model output would be similar to the interpolation scheme described for the test data (§4.2.3), but would be simpler because:

(i) The data points form a regular array making interpolation between points straightforward,

(ii) Extrapolation is not required as the maximum loads applied to the model can be made high enough to cover any possible stress state in the analysis.

The model will be particularly for useful for the analysis of small or medium size membrane structures for which comprehensive biaxial testing is prohibitively expensive. Another application is for fabric reverse engineering: if certain stress-strain properties are required for a given application, the required yarn properties and/or weave geometry can be calculated. This can inform the choice of fabric, or enable manufacturers to produce fabrics with particular mechanical properties. This may have benefits in other fields, for example for the design of medical textiles which need to replicate the mechanical properties of specific tissues (Gupta, 1998).

Chapter 6

Conclusions & recommendations for future work

Contents

6.1 CONCLUSIONS

Detailed conclusions have been provided at the end of each Chapter, or in the case of Chapter 2 at the end of each main section. This section provides a concise overview of the conclusions of this research.

The design of fabric structures is complicated by the response of coated woven fabrics to biaxial loads in the plane of the fabric. Non-linear material behaviour, large displacements and the use of membrane action to resist loads require a fundamentally different approach to structural design compared to traditional roof structures.

Fabric structures design is hindered by high factors of safety, principally to avoid tear propagation but also because of the over-simplified plane stress representation used to represent the material behaviour. Poor understanding of fabric behaviour results in wrinkling, installation problems, damage during handling, ponding failure and insufficient re-tensioning capabilities. Thorough biaxial testing and a new approach to implementation of the test data in structural analysis may be of significant benefit to the industry.

An extensive literature review has been carried out to determine the current state-of-the-art in:

- non-linear mechanical properties of coated woven fabrics,
- test methods for fabrics,
- methods of representing non-linear test data,
- current practice in representing fabric properties for structural analysis,
- predictive modelling of coated woven fabric biaxial behaviour.

A biaxial test rig with a plane cruciform test piece has been designed and fabricated for this research. The design of the test rig must be appropriate for the particular material properties of the fabrics to be tested. For architectural fabrics this means accommodating large strains (both positive and negative in either axis) and non-orthogonal principal axes. A test rig with a 'floating' frame has been built based on a concept innovated by Architen-Landrell (www); the frame aligns with fabric warp and fill axes (not necessarily orthogonal) to prevent shear during the test. Numerical analysis of the test piece informed the design of the clamp plates and slit cruciform arms. It has also shown that a stress reduction factor must be applied to give the expected stress in the area of interest, which is less than the applied load.

There are no British or European standards on biaxial fabric testing, and little published justification of test regimes used in industry. Test regimes are typically developed to inform a plane stress model rather than fully explore the fabric response. A new biaxial test protocol for architectural fabrics has been developed and used to test a range of PVC coated polyester and PTFE coated glass fibre fabrics.

Application of prestress followed by mechanical conditioning provides repeatable stress-strain data suitable for medium to long term structural design. The test protocol efficiently populates the space of feasible stress states; it is not limited to a few specified stress ratios. A method of removing residual strain from the test data has been developed to prevent skewing of the response surface. Removal of residual strain also enables accurate comparison between repeat tests and with predictive models, without interference from time-dependent, in-elastic creep strain. Test results with residual strain removed are appropriate for elastic analysis which is currently used for membrane structure design.

This research has shown that plane stress theory (i.e. use of elastic constants and Poisson's ratios) is inappropriate for accurately representing the behaviour of coated woven fabrics. Test data can be crudely represented with pseudo-elastic constants, but their values do not comply with plane stress theory. This is because coated woven fabrics are not homogeneous materials, but are better described as a mechanism. A new method of using fabric test data directly in structural analysis has been proposed. This involves linear interpolation between a table of strain and stress values, and is currently being implemented by Arup (www) in their Oasys GSA software. This avoids any simplification of the complex non-linear test data.

Following testing at all feasible stress states, the population of the strain-strain space provides a new tool for quantifying fabric behaviour. For example, PTFE-glass fibre fabrics have small, discrete response envelopes. This limited range of feasible strains is due to the high tensile stiffness of the glass fibre yarns, with virtually all strain a result of crimp interchange.

A predictive model has been developed to determine the biaxial stress-strain response of architectural fabrics, without the need for biaxial testing. Sawtooth and sinusoid models of the fabric unit cell have been formulated, with spring elements between crossovers used to represent the coating. In both models a constant yarn cross-sectional area has been maintained, resulting in a relationship between unit cell length and yarn thickness which eliminates the need to determine the yarn crushing stiffness. All model parameters are determined from standard tests: yarn and coating tensile moduli are inferred from uniaxial strip tests, weave geometry is measured from digital photographs of the fabric cross-section. The model is truly predictive, requiring no calibration against test data for individual fabrics, and as such provides a significant benefit compared with previous work. The model output has been compared with comprehensive biaxial test data for both PTFE-glass fibre and PVC-polyester fabrics. The model provides a more accurate representation of fabric behaviour than current industry best practice (i.e. use of elastic constants based on biaxial test data), but without the need for specialist testing or equipment.

6.2 RECOMMENDATIONS FOR FUTURE WORK

The following sections outline potential solutions to the uncertainties that currently exist in fabric structure design. Much of the research is currently underway in a rapidly expanding research group at the University of Newcastle which has developed from this project. The benefits of the research for fabric structure design and the long-term research aims are emphasised.

6.2.1 Biaxial fabric testing

Additional biaxial testing would enable more detailed analysis of fabric variability, for example across the width and along the length of a roll of fabric and between fabric batches. This would require extensive testing which was not possible in the time scale of this project. However, with the automation of the test rig (§6.2.2) testing will become less time intensive. Statistical distributions of fabric behaviour will be of use for developing a reliability based approach to membrane structure analysis (§6.2.8).

Biaxial failure testing and wide panel tear tests (biaxial and uniaxial) for a wide range of fabrics would enable the validity of the universally adopted minimum factor of safety of four to be assessed. This factor is based on testing of a limited number of fabrics, and any reduction in this factor would be of great benefit to fabric structure design. With multiple tests the upper and lower bounding failure loads (or probabilities of failure at given loads) could be established. This data is necessary for a reliability based analysis of fabric structures (§6.2.8)

Further work is proposed on rapid loading of fabrics to simulate wind gust loading. It is anticipated that fabrics are much stiffer under rapid, short term loading. There is also potential for reduction in strength, in particular with brittle glass fibre yarns shattering under rapid loading. This could lead to a revision of material safety factors based on expected load duration. This is broadly similar to the British Standard for timber design (BS5268-2) which uses widely varying load factors (from 1 to 1.5) dependent on the load duration.

6.2.2 Test rig modifications

The following modifications to the biaxial test rig are proposed to provide increased accuracy and to make future testing less time consuming.

- Servocontrol valves and feedback system to automatically follow any specified load or strain profile. A system based on the Moog (www) M3000 controller will be installed shortly.
- Full use of digital output: the laser extensometer accuracy is compromised by distortion of the analogue output to data logger. Use of digital output direct to a PC would increase accuracy.

- Thermostatically controlled temperature, with the addition of refrigeration for testing at low temperatures.

6.2.3 Test protocol

The test protocol developed for this work provides a general approach to biaxial testing which can be applied to any fabric. The level of detail can easily be varied by changing the number of radial load arms and/or sampling points along the arms. Testing at elevated or lowered temperatures is beyond the scope of this work, but may provide useful information on the variability of the mechanical properties of an in-situ fabric. However, this would not require any profound modifications to the test protocol.

6.2.4 Fabric creep

A major issue in the design and installation of fabric structures is the need to maintain prestress in the membrane for the life of the structure. Currently there is little knowledge of long-term creep behaviour, and after initial re-tensioning most structures will not be monitored or adjusted. This can lead to slack areas, with two main problems:

1. Ponding of rainwater on slack fabric can lead to overloading of the structure and collapse,
2. Excessive movement ('flapping') of under-stressed fabric is noisy and leads to fatigue damage of the fabric and edge details.

The biaxial tests carried out for this work provide a measure of residual strain after testing, which is a good indication of the expected fabric strain after several extreme load events. However, long term creep and recovery testing is necessary to provide a detailed model of fabric creep.

For a given time period (e.g. 6 months, 2 years, long-term) analysis of return periods for environmental loads (wind and snow) will provide expected load intensities and durations. These load intensities will give stress levels in the structure which, combined with load duration and creep data, will determine likely levels of creep strain. These may be used to design sufficient re-tensioning capabilities into the support details to maintain prestress for the life of the structure.

An important consideration when planning long-term re-tensioning is that the fabric may reach a limiting *failure strain* and fail at a stress far below its specified ultimate tensile strength. Tests on strain failure of fabrics and the accompanying reduction in failure stress are proposed.

6.2.5 Shear

It is commonly known that if a fabric structure has high levels of double-curvature then PVC-coated polyester fabric should be used because it has lower shear stiffness than PTFE-coated glass fibre fabric.

The PVC-polyester fabric is more conformable and less likely to wrinkle. A detailed analysis of fabric shear behaviour is often neglected; the shear stiffness is frequently assumed to be low, uncoupled to stress-strain behaviour, and linear elastic (Day, 1986). A thorough treatment of coated woven fabric shear behaviour, however, shows that it is non-linear, hysteretic and discontinuous (Skelton, 1976). For small shear angles the shear stiffness is low, as the yarns are free to rotate at their intersections, with resistance to shearing being provided by the coating and inter-yarn friction. However, at a critical 'lock-up' angle adjacent yarns come into side-by-side contact resulting in a sharp increase in shear stiffness. To form a surface with double curvature from flat panels requires shear deformation of the fabric. Therefore, the level of curvature required can determine the type of fabric used, based on the shear 'lock-up' angle. PTFE-coated glass fibre fabrics, which typically have a tighter weave and a higher level of crimp, have a lower lock-up angle than PVC-polyester.

Future work aims to quantify this shear lock-up angle as a function of warp and weft direct stresses, for a range of fabrics. There is no standard test method or equipment for measuring the shear behaviour of architectural fabrics, and several fundamentally different methods are used. A simple fabric shear tester, frequently used for uncoated textiles in the clothing industry, applies axial load in one direction and shear load in the orthogonal direction (Mörner & Eeg-Olofsson, 1957; Spivak, 1966; Treloar, 1965). The apparatus is designed to measure the maximum shear angle before creasing occurs, with low levels of in-plane stress. For architectural fabrics testing with a higher level of direct stress is required.

Shear testing of fabrics can be carried out by the uniaxial extension of a bias cut strip, i.e. a strip cut at 45° to the yarn directions (Mollaert & Forster, 2004). In this type of test it is difficult to quantify how much of the applied load results in shear stress and how much results in direct stresses:

"It is concluded that it is not possible simply and directly to predict the complete stress-strain properties of a fabric in simple shear from measurements of bias extension" (Spivak & Treloar, 1968).

Culpin (1979) developed a shear tester consisting of a square frame with hinged corners. The frame is clamped on to the fabric and is then loaded diagonally to apply pure shear stress to the test piece. It is proposed that a fabric sample could be mechanically conditioned and loaded to a desired state of direct stress in the biaxial test rig, and then be clamped into a Culpin-type shear rig to test the shear resistance with known direct stresses. This type of shear tester is currently being developed as the University of Newcastle.

Thorough shear testing will quantify the level of shear deformation available in a given fabric before lock-up, and therefore wrinkling, occurs. This will give designers a clearer understanding of which fabrics are suitable for a given structure, or conversely what level of curvature can be attained with a given fabric.

6.2.6 Implementation of test results

The variation between loading and unloading strains varies from zero to 40% of the strain range. This is very significant for the characterisation of the fabric and for understanding the variability of the fabric response. The steep gradient of the strain-strain-stress surfaces increases the importance of including the variability of the test results in the analysis. The proposed method of using the test data (§4.2.3) uses mean values which represent the typical fabric response. A stochastic analysis would enable variability in the test data to be included, with deterministic stress levels being replaced by a combination of stress level and probability. This would enable the design to be based on a probably of failure, as opposed to a simplistic maximum stress criteria.

6.2.7 Simulated installation

A long-term research aim is to develop a model of fabric behaviour that will enable a *simulated installation* to be carried out. This would require biaxial tensile, shear and creep data; all for initial and medium to long-term behaviour. Tests on the tensile and shear properties of welded seams would add to the accuracy of the model.

It is envisaged that the fabric cutting patterns would be assembled in the finite element structural model, to which installation displacements would be applied. The analysis would need to include a time function, allowing the creep of the fabric to be assessed at different stages of the installation. This is a similar concept to the staged construction analysis of, for example, a cable stayed bridge, although the highly non-linear material behaviour is more complex.

Initially, when installation displacements are applied stress concentrations would be found around the jacking points and edges. These would then become distributed around the structure with time, in a process known as 'creep flow'. A temperature factor should be included to modify the rate of creep with ambient temperature. The analysis would provide information for contractors on how long the installation should take. Inclusion of seam and reinforcement elements would enable an assessment of whether the increased fabric stiffness in these areas leads to wrinkling and stress concentrations. An assessment of the quality of the cutting patterns could be made by checking the uniformity of the stress field at prestress after the simulated installation.

The complete model would allow the effect of different erection procedures to be analysed. For example, when a conic is installed either:

1. The edges can be fixed and the central mast can be pushed up into place (as used at Dalton Park),
2. The mast can be fixed and the fabric can be pulled out to the edges,
3. A combination of both.

One technique might lead more easily to an even stress distribution with reduced initial stress concentrations - resulting in a faster installation with reduced risk of fabric damage. The use of accurate biaxial test data could further inform the installation procedure. For example, a rectangular barrel vault can be tensioned by aligning the weft direction of the fabric along the length of the barrel vault, fixing the ends of the warp yarns and tensioning the fabric in the weft direction, using the subsequent negative strain in the warp to induce prestress. This technique is already used, but could be used more effectively if the exact level of negative warp strain (and hence warp stress) was known for all stages of the life of the structure.

The fabric strains measured at prestress for this work were not as expected for some fabrics, for example with negative fill strains (§4.1.3). This was attributed to variations in the order of load application used to achieve prestress (i.e. was the fabric first loaded in the warp or fill direction?). That this could have such a significant effect on the resultant strains at prestress highlights the need for further testing and the importance of the installation method or sequence.

6.2.8 Reliability analysis

The culmination of this research will be a reliability-based structural analysis of fabric structures. The aim is to bring the understanding and analysis of fabric structures in line with more widely used and better understood materials such as steel and concrete.

A comprehensive program of wide panel tear tests (uniaxial and biaxial) is currently underway at the University of Newcastle to assess the affect of damage on fabric strength. This is the dominant factor which currently results in large factors of safety adopted in the design of fabric structures. These results will be combined with data on fabric variability from biaxial tests, structural tolerances and probabilities of load intensity and duration from loading codes (e.g. wind and snow) to give a probability of failure for a structure. This in turn can be represented as a factor of safety to provide a given probability of failure (usually 5%), as used in steel and concrete codes. This would enable designers to move away from the current practice of multiplying together factors of safety for tear propagation, material variability, loading etc. that results in a very large and overly conservative factor of safety.

The reliability based analysis allows a more comprehensive analysis of the stresses in the membrane than the current practice of checking the maximum stress. The probability of failure is based on both the stress levels and the area of membrane subjected to those levels of stress. For example, the probability of failure of a structure may be the same if there is one small but very highly stressed area or if there is a large area at a moderately high stress.

This approach would also generate more accurate loading information for the supporting steelwork and support details. Permissible stress analysis will still be required, however, as the limit state approach is unsuitable for the geometric and material non-linearity inherent in fabric structures.

6.2.9 Predictive unit cell model

The sawtooth formulation of the unit cell model developed for this work provided a good correlation with test data for a range of fabrics, without the need for specialist testing or computer software. Whilst there are many possible developments which can be made to the model, it is important for each to ensure the added model complexity provides a sufficient return in terms of model accuracy, and is not just adding unnecessary complication. Development of the sinusoid model to include out-of-plane restraint due to the coating and/or yarn bending stiffness may enable the expected increase in accuracy of the sinusoidal yarn representation to be realised.

Beyond this, Pargana, Lloyd Smith and Izzuddin (2000) make several recommendations for future developments to the unit cell model. This provides a good starting point for further developments from this work:

1. Use non-linear yarn elements,
2. Non-linear crushing spring,
3. Including frictional effects,
4. Making shear response frictional and non-linear, and include yarn jamming.

Also inclusion of coating Poisson's ratio, particularly for PTFE coating, may improve model accuracy. As with all material properties, the real difficulty is determining this Poisson's ratio. A Poisson's effect could also be included for the yarns, rather than simply maintaining a constant area. Again determining values would be problematic.

Calibration of the model against uniaxial stress-strain curves could provide increased accuracy. Any model parameters that need to be determined (only the compressive coating stiffness in the formulations in this work) could be modified to give the best fit of the model to uniaxial stress-strain curves. This enables model calibration without any additional testing. Whether this provides a good fit at other stress ratios could easily be checked.

The model could be used to assess fabric variability. Rather than using mean values for fabric measurements the model could be run with mean fabric values plus and minus the standard deviation (and/or extreme values). For assessment of fabric variability many more measurements would be required: along a given yarn, from different parts of the fabric roll and from different batches of fabric.

References

Note: internet references marked www in the text are listed separately on the final page.

Ansell, M., Barnes, W. & Williams, C. (1984) *Structural properties tests for coated fabrics*, Proceedings of a Conference on the Design of Air Supported structures, Institute of Structural Engineers, Bristol, 35-45.

Ansell, M., Hill C. & Allgood, C. (1983) *Architectural PTFE-coated glass fabrics – their structure and limitations*, Textile Research Journal, 692-700

Amirbayat, J.; Hearle, J. W. S. (1989) *Anatomy of buckling of textile fabric, drape and conformability*, Journal of the Textile Institute, 80 (1) 51-70

ASCE 17-96, *Air-Supported Structures*, ASCE Standard, American Society of Civil Engineers

ASTM D 4851-97, *Standard Test Methods for Coated and Laminated Fabrics for Architectural Use*, American Society for Testing and Materials

Barnes, M. (1999) *Form finding and analysis of tension structures by dynamic relaxation*, International Journal of Space structures, **14**, n. 2, pp 89-104

Bassett, R., Postle, R. & Pan N. (1999a) *Experimental Methods for Measuring Fabric Mechanical Properties: A Review and Analysis*, Textile Research Journal, 69 (11) 866-875.

Bassett, R., Postle, R. & Pan N. (1999b) *Grip point spacing along the edges of an isotropic fabric sheet in a biaxial tensile test*, Polymer Composites, 20, 305-313.

Behre, B. (1961) *Mechanical properties of textile fabrics, Part I: shearing*, Textile Research Journal, 31, 87-93

Bigaud, D., Hamelin, P. (1997) *Mechanical properties prediction of textile-reinforced composite materials using a multiscale energetic approach*, Composite Structures, 38 (1-4) 361-371

Birkett, D. (2002) *Keeping the thread*, Education in Chemistry, Royal Society of Chemistry website, http://www.rsc.org/lap/educatio/eic/2002/birkett_mar02.htm

Blum, R. (1980), *Mechanics of fabrics in tension structures*, pp 495-512, Mechanics of flexible fibre assemblies, edited by John W.S. Hearle, John J. Thwaites, Jafargholi Amirbayat, Alphen aan den Rijn, Netherlands Germantown, Md. : Sijthoff & Noordhoff

Blum, R. & Bidmon, W. (1987) *Spannungs-Dehnungs-Verhalten von Bautextilien*, SFB 64, Mitteilung 74.

Blum, R. & Bögner, H. (2002) *Evaluation Method for the Elastic Moduli*, Tensinews Newsletter 3, Internet Publication 2002 (www.tensinet.com), p.3.

Boisse, P.; Borr, M.; Buet, K.; Cherouat, A. (1997) *Finite element simulations of textile composite forming including the biaxial fabric behaviour*, Composites Part B:Engineering, v 28B, n 4, p 453-464

Boisse, P.; Gasser, A.; Hivet, G. (2001) *Analyses of fabric tensile behaviour: Determination of the biaxial tension-strain surfaces and their use in forming simulations*, Composites - Part A: Applied Science and Manufacturing, 32 (10) 1395-1414

Brunetti, A. (2000) *Fast and precise genetic algorithm for a non-linear fitting problem*, Computer Physics Communications, 124 (2-3) 204-211

BS 3424-21: 1993, *Testing coated fabrics. Method 24. Method for determination of elongation and tension set*, British Standards Institution

BS 5268-2: 2002, *Structural use of timber – Part 2: Code of practice for permissible stress design, materials and workmanship*, British Standards Institution

BS 6661: 1986, *British Standard Guide for Design, construction and maintenance of single-skin air supported structures*, British Standards Institution

BS EN ISO 1421:1998, *Rubber- or plastics-coated fabrics — Determination of tensile strength and elongation at break*, British Standards Institute

Buckley, C.P. (1980) *Review of the mechanical properties of fibres*, pp 35-49, Mechanics of flexible fibre assemblies, edited by John W.S. Hearle, John J. Thwaites, Jafargholi Amirbayat, Alphen aan den Rijn, Netherlands Germantown, Md. : Sijthoff & Noordhoff

Buet-Gautier, K., Boisse, P. (2001) *Experimental analysis and modelling of biaxial mechanical behaviour of woven composite reinforcements*, Experimental Mechanics, 41, 3.

Chen, S.F., Hu J.L., Teng, J.G. (2001) *A finite-volume method for contact drape simulation of woven fabrics and garments*, Finite Elements in Analysis and Design 37, 513-531

Chen, Y.; Lloyd, D. W.; Harlock, S. C. (1995) *Mechanical characteristics of coated fabrics*, Journal of the Textile Institute, 86 (4) 690-700

Chivate, P. & Jablokow, A. (1995) *Review of surface representations and fitting for reverse engineering*, Computer Integrated Manufacturing Systems, 8 (3) 193-204

Clulow, E.E. and Taylor, H.M. (1963) *An experimental and theoretical investigation of biaxial stress-strain relations in a plain-weave cloth*, Journal of the Textile Institute, 54, T323-T347.

Collier, R.; Collier, B.J.; Toole, G.O.; Sargand, S.M. (1991) *Drape prediction by means of finite element analysis*, Journal of the Textile Institute 82 (1) 96-107

Cook, R., Malkus, D. & Plesha, M. (1989) *Concepts and applications of finite element analysis*, 3rd edition, John Wiley & Sons, 149-152

Cooper, D.N.E. (1960) *A bias extension test* (letters to the editor), Journal of the Textile Institute, 51, 315-317

Culpin, M.F. (1979) *The shearing of fabrics: a novel approach*, Journal of the Textile Institute, 70 (3) 81-88

Cusick, G.E. (1961) *The resistance of fabrics to shearing*, Journal of the Textile Institute, 52 (9) T395-T406

Day, A.S. (1972) *Dilating clay equations*, Arup Journal, 7 (4) 20-23

Day, A.S. (1986) *Stress strain equations for non-linear behaviour of coated woven fabrics*, IASS symposium proceedings: shells, membranes and space frames, Osaka, 1986, vol. 2, Elsevier, Amsterdam

Dimitrov, N.; Schock, H. J. (1986) *Study on the load-extension behaviour of coated fabrics, with special reference to PTFE-coated glass-fibre, using the Meffert model*, LSA 86: Lightweight Structures in Architecture, Proceedings of the First International Conference.

Doering, N. (1993) *Biaxial tensile tests on technical membranes*, Unpublished project report, The University of Essen, December 1993.

Durville, D. (2003) *Numerical simulation of the mechanical behaviour of textile structures at a mesoscopic scale*, Textile composites and inflatable structures, E. Onate & B Kröplin (Eds.), CIMNE, Barcelona, pp 310-315

Eiben, A.E, Schoenauer ,M. (2002) *Evolutionary computing*, Information Processing Letters 82, 1-6

Fontaine, S., Durand, B., Freyburger, J.M. (2002) *Fabric thickness dynamic measurement during a classic uniaxial tensile test*, Experimental mechanics, 42, 1, 84-92

Freeston, W.D.; Platt, M.M.; Schoppee, M.M. (1967) *Stress-strain response of fabrics under two-dimensional loading*, Textile Research Journal, 37, 656-682

Gasser, A., Boisse, Ph., Hanklar, S. (2000) *Mechanical behaviour of dry fabric reinforcements. 3D simulations versus biaxial tests*. Computational Material Science, 17, 7-20

Glaesgen, E.H., Pastore, C.M., Griffin, O.H., Birger, A. (1996) *Geometrical and finite element modelling of textile composites*, Composites - Part B, 27B (1) 43-50

Grosberg, P. and Park, B.J. (1966) *The mechanical properties of woven fabrics, part V: the initial modulus and the frictional restraint in shearing of plain weave fabrics*, Textile Research Journal, 66, 420-431

Grosman, B., Lewin, D.R. (2002) *Automated non-linear model predictive control using genetic programming*, Computers and chemical engineering 26, 631-640

Gupta, B. (1998) *Medical textile structures: an overview*, Medical plastics and biomaterials, Jan. 1998, p.16

Happold, E., Ealey, T., Liddell, W., Pugh, J. & Webster, R. (1987) *Discussion: The design and construction of the Diplomatic Club, Riyadh*, The Structural Engineer, 65A, 1, 377-382.

Hearle, J. W. S.; Sakai, T. (1978) *On the extended theory of mechanics of twisted yarns*, Journal of the Textile Machinery Society of Japan, 25 (3) 68-72

Hearle, J.W.S. (1958) *The mechanics of twisted yarns: the influence of transverse force on tensile behaviour*, The Journal of the Textile Institute, 49, T389-T408

Hearle, J.W.S. (1969) *On the theory of the mechanics of twisted yarns*, Journal of the Textile Institute, 60, T95

Hendry, S. (2005) Arup Research and Development. *Personal correspondence*.

Houtman, R. (2003) *There is no material like membrane material*, Tensinet Symposium – Designing Tensile Architecture, Vrije Universiteit Brussel, p 178-194

Houtman, R. & Orpana, M. (2000) *Materials for Membrane Structures*, Bauen mit Textilien Heft, 4/2000

Javadi, A. A.; Farmani, R.; Toropov, V. V.; Snee, C. P. M. (1999) *Identification of parameters for air permeability of shotcrete tunnel lining using a genetic algorithm*, Computers and Geotechnics, 25 (1) 1-24

Jong, S. de, Postle, R. (1978) *A general analysis of fabric mechanics using optimal control theory*, Textile Research Journal, 48, 127-135

Jüttler, B. & Felis, A. (2002) *Least-squares fitting of algebraic surfaces*, Advances in Computational Mathematics, 17, 135-152

Kageyama, M., Kawabata, S., Niwa, M. (1988) *The validity of a "linearizing method" for predicting the biaxial-extension properties of fabrics*, Journal of the Textile Institute, 79, 543-565

Kato, S., Minami, H., Yoshino, T. and Namita, T., (1997) *Analysis of membrane structures based on fabric lattice model considering viscous characteristics*, Proceedings of the IASS International Symposium 1997 on Shell and Spatial Structures, Singapore, 411-420

Kawabata, S., Niwa, M.., Kawai, H. (1973a) *Finite-deformation theory of plain-weave fabrics. Part I. The biaxial-deformation theory*, Journal of the Textile Institute, 64 (1) 21-46

Kawabata, S., Niwa, M.., Kawai, H. (1973b) *Finite-deformation theory of plain-weave fabrics. Part II. The uniaxial deformation theory*, Journal of the Textile Institute, 64 (1) 47-61

Kawabata, S., Niwa, M.., Kawai, H. (1973c) *Finite-deformation theory of plain-weave fabrics. Part III. The shear deformation theory*, Journal of the Textile Institute, 64 (1) 62-85

Kawabata, S.; Niwa, M.; Matsudaira, M. (1985) *Measurement of yarn thickness change caused by tension and lateral pressure by wire method*, Journal of the Textile Machinery Society of Japan, 31 (1) 7-14

Kelmartin, T. (2003) *A new membrane material for fabric structures*, Tensinet Symposium – Designing Tensile Architecture, Vrije Universiteit Brussel, p 204-211

Kemp, A. (1958) *An extension of Peirce's cloth geometry to the treatment of non-circular threads* (letters to the editor), Journal of the Textile Institute, 49, T44-T48

Kim, H-S., Cho, S-B. (2000) *Application of interactive genetic algorithm to fashion design*, Engineering Applications of artificial intelligence 13, 635-644.

Klein, W. (1959) *Stress-strain response of fabrics under two-dimensional loading, part I, The biaxial tester*, Textile Research Journal, 29, 816-821.

Kostikov, V. (1995) *Fibre science and technology*, London, Chapman & Hall

Koza, J. R. (1992) *Genetic programming: on the programming of computers by means of natural selection*, The MIT Press, Cambridge, Massachusetts, USA

Leaf, G.A.V., Sheta, A.M.F. (1984) *The initial shear modulus of plain-woven fabrics*, Journal of the Textile Institute, 75, 157-163

Lewis, W.J., Gosling, P.D. (1993) *Stable Minimal Surfaces in Form-Finding of Lightweight Tension Structures*, Journal of Space Structures, **8**, n. 3, pp149-166

Lucas, L.J. (1983) *Mathematical fitting of modulus-strain curves of Poly(ethylene Terephthalate) Industrial Yarns*, Textile Research Journal, 53, 771-777

MacRory, B. & McNamara, A. (1977) *Experimental Investigation of the biaxial load-extension properties of plain weft-knitted fabrics*, Textile Research Journal, 47, 233-239.

Masters, T. (1995) *Adanced algorithms for neural networks, a C++ sourcebook*, John Wiley & Sons Inc., USA

Menges, G., Meffert, B., (1976) *Mechanical behaviour of PVC coated polyester fabrics under biaxial stress*, J. Kunststoffe German Plastics, 66 (11) 12-14

Minami, H., Yamamoto, C., Segawa, S., Kono, Y. (1997) *A method for membrane material nonlinear stress analysis using a multi-step linear approximation*, IASS International Symposium on Shell and Spatial Structures, Singapore

Moghe, S. (1980) *From fibres to woven fabrics*, pp 159-173, Mechanics of flexible fibre assemblies, edited by John W.S. Hearle, John J. Thwaites, Jafargholi Amirbayat, Alphen aan den Rijn, Netherlands Germantown, Md. : Sijthoff & Noordhoff

Mollaert & Forster (2004) *European Design Guide for Tensile Surface Structures*, Tensinet

Mörner, B., and Eeg-Olofsson, T. (1957) *Measurement of shearing properties of fabric*, Textile Research Journal, 27, 611

Morris, P.J., Merkin, J.H., Rennell, R.W. (1999) *Modelling of yarn properties from fibre properties*, Journal of the Textile Institute, 90, Part 1 (3), 323-335

Morton, W.E. (1956) *The arrangement of fibres in single yarns*, Textile Research Journal, 26, 325-331

Morton, W.E. and Hearle, J.W.S. (1975) *Physical properties of textile fibres*, 2nd ed, London, Heinemann

Mott, R., Huber, G. & Leewood, A. (1985) *Biaxial test method for characterization of fabric materials used in permanent fabric roof structures*, The American Society for Testing and Materials, Journal of Testing and Evaluation, 9-16.

MSAJ/M-02-1995, *Testing Method for Elastic Constants of Membrane Materials*, Membrane Structures Association of Japan.

Naik, N. K.; Madhavan, V. (2000) *Twisted impregnated yarns: elastic properties*, Journal of Strain Analysis for Engineering Design, 35 (2) 83-91

Nastran, M., Balic, J. (2002) *Prediction of metal wire behaviour using genetic programming*, Journal of materials processing technology 122, 368-373

Nikitas, P., Papageorgiou, A. (2001) *Modifications of the classical genetic algorithm for non-linear fitting to response surface modelling in HPLC*, Computer physics communications 141, 225-229

Olofsson, B. (1964) *A general model of a fabric as a geometric-mechanical structure*, Journal of the Textile Institute, 55, T541-T557

Olofsson, B. (1966) *Deformation properties of stretch fabrics* (letter to the editor), Journal of the Textile Institute, 57, T429-T432

Osswald, T., Menges, G. (1996) *Materials Science of Polymers for Engineers*, Hanser Publishers

Otto, F. (1967) *Tensile Structures*, M. I. T. Press, Cambridge

Pargana, J.B., Lloyd Smith, D., Izzuddin, B.A. (2000) *Advanced material model for the analysis of tensioned fabric structures*, Computational methods for shell and spatial structures, IASS-IACM 2000, Chania-Crete, Greece

Peirce, F.T. (1937) *The Geometry of cloth structure*, Journal of the Textile Institute, 28, 81-88

Postle, R.; Norton, A. H. (1991) *Mechanics of complex fabric deformation and drape*, Journal of Applied Polymer Science: Applied Polymer Symposium, 47, 323-340

Reichardt, C., Woo, H. & Montgomery, D. (1953), *A two-dimensional load-extension tester for woven fabrics*, Textile Research Journal, 23, 424-428

Reinhardt, H. (1976) *On the biaxial testing and strength of coated fabrics*, Experimental Mechanics, 16 (2) 71-74.

Reumann, R.-D. (2000) *Prüverfahren in der Textil- und Bekleidungstechnik* [Testing method in the textile and clothing technology], Berlin Heidelberg, Springer-Verlag. Language: German.

Rice, P. (1994) *An Engineer Imagines*, ••• ellipsis london limited, London

Rossi, R., Lazzari, M., Vitaliani, R. & Oñate, E. (2003) *Convergence of the modified material model for wrinkling simulation of light-weight membrane structures*, Textile Composites and Inflatable Structures, Ed. E.Oñate & B.Kröplin, pp148-153

Sasai, T.; Kawabata, S. (1985) *Biaxial tensile properties of textured yarn fabrics*, Journal of the Textile Machinery Society of Japan, 31 (2) 29-34

Schock, H.J. (1991) *On the structural behaviour and material characteristics of PTFE-coated glass-fibre fabric*, Journal of Coated Fabrics, 20, 277-288

Sette, S., Boullart, L. (2001) *Genetic programming: principles and applications*, Engineering applications of artificial intelligence 14, 727-736

Shanahan, W.J.; Lloyd, D.W.; Hearle, J.W.S. (1978) *Characterising the Elastic Behaviour of Textile Fabrics in Complex deformations*, Textile Research Journal, 48 (9) 495-505

Skelton J. & Freeston, W.D. (1971) *Mechanics of elastic performance of textile materials: Part XIX. The shear behaviour of fabric under biaxial loads*, Textile Research Journal, 41, 871-880

Skelton, J. (1976) *The fundamentals of fabric shear*, Textile Research Journal 46 (12) 862-869

Skelton, J. (1980a) *Mechanical properties of coated fabrics*, pp 461-469, *Mechanics of flexible fibre assemblies*, edited by John W.S. Hearle, John J. Thwaites, Jafargholi Amirbayat, Alphen aan den Rijn, Netherlands Germantown, Md. : Sijthoff & Noordhoff

Skelton, J. (1980b) *Shear of woven fabrics*, pp 211-227, *Mechanics of flexible fibre assemblies*, edited by John W.S. Hearle, John J. Thwaites, Jafargholi Amirbayat, Alphen aan den Rijn, Netherlands Germantown, Md. : Sijthoff & Noordhoff

Soh, C. and Yang, Y. (2000) *Genetic programming-based approach for structural optimization*, Journal of Computing in Civil Engineering, January, 31-37

Spivak, S. (1966) *The behaviour of fabrics in shear, part I, instrumental method and the effect of the test conditions*, Textile Research Journal, 36, 1056

Spivak, S. and Treloar, L. (1968) *The behaviour of fabrics in shear, part III, the relation between bias extension and simple shear*, Textile Research Journal, 38, 963-971

Stroud, K. (1996) *Further engineering mathematics*, 3rd ed., MacMillan

Stubbs, N., Fluss, H. (1980) *A space-truss model for plain weave coated fabrics*, Applied mathematical modelling, 4, 51-58

Tan, K.Y., Barnes, M.R. (1980) *Numerical representation of stress-strain relations for coated fabrics*, IstructE symposium on design of air supported structures, Bristol

Tan, P., Tong, L., Steven, G.P. (1997) *Modelling for predicting the mechanical properties of textile composites – a review*, Composites Part A, 28A, 903-922

Tanov, R.R., Brueggert, M. (2003) *Finite element modelling of non-orthogonal loosely woven fabrics in advanced occupant restraint systems*, Finite Elements in Analysis and Design 39, 357-367

Tarfaoui, M., Drean, J.Y. (2001) *Predicting the stress-strain behaviour of woven fabrics using the finite element method*, Textile Research Journal, 71 (9) 790-795

Tarfaoui, M.; Akesbi, S. (2001) *A finite element model of mechanical properties of plain weave*, Colloids and Surfaces A: Physicochemical and Engineering Aspects, v187-188, 439-448.

Testa, R.B., Stubbs, N., Spillers, W.R. (1978) *Bilinear Model for Coated Square Fabrics*, Journal of Engineering Mechanics, 104, 1027-1042

Testa, R.B.; Yu, L.M. (1989) *Stress-strain relation for coated fabrics*, Journal of engineering mechanics, 113 (11) 1361-1646

Thwaites, J.J. (1980) *A continuum model for yarn mechanics*, pp 87-97, Mechanics of flexible fibre assemblies, edited by John W.S. Hearle, John J. Thwaites, Jafargholi Amirbayat, Alphen aan den Rijn, Netherlands Germantown, Md. : Sijthoff & Noordhoff

Treloar, L. (1965) *The effect of the test-piece dimensions on the behaviour of fabrics in shear*, Journal of the Textile Institute, 56, T533-T550

Uetani, K., Fujiwara, J., Ohsaki, M. *A simple viscoelastic membrane material model for cutting pattern optimisation*, Personal correspondence, submitted for publication 2002

Wang, F. (2002) *Prediction method for tensile property of woven fabrics in lower loads*, Journal of Dong Hua University (English edition), 19 (2) 6-14

Weiss, V., Andor, L., Renner, G. & Várady, T. (2002) *Advanced surface fitting techniques*, Computer Aided Geometric Design, 19, 19-42

Yang, M., Zhang, X., Li, X., Wu, X. (2002) *A hybrid genetic algorithm for the fitting of models to electrochemical impedance data*, Journal of Electroanalytical Chemistry 519, 1-8

Zimliki, D.A., Kennedy, J.M., Hirt, D.E. (2000a) *Determining mechanical properties of yarns and two-ply cords from single-filament data, Part I: Model development and predictions*, Textile Research Journal, 70 (11), 991-1004

Zimliki, D.A., Kennedy, J.M., Hirt, D.E., Reese, G.P. (2000b) *Determining mechanical properties of yarns and two-ply cords from single filament data, part II: comparing model and experimental results for PET*, Textile Research Journal, 70 (12) 1097-1105

Internet references, www:

Addition polymers (accessed 2004):

www.chs.edu.sg/~limth/lessons/2002/Organic%20Chemistry/addition_polymers.htm

Altmann, M. (accessed 2001): www.cs.wpi.edu/~matt/courses/cs563/talks/nurbs.html

Architectural fabrics (accessed 2004): www.architecturalfabrics.com/whitepaper.html

Architen-Landrell (accessed 2005): www.architen.com

Arup (accessed 2005): www.arup.com

Birdair (accessed 2005): www.birdair.com

Ferrari (accessed 2005): www.ferrari-textiles.com

Gore – check (accessed 2005): www.gore.com

Hounsfield (accessed 2005): http://www.hounsfield.com; http://www.tiniusolsen.com/pdf/TD2005.pdf

Laboratorium Blum (accessed 2005): www.labor-blum.de

Lega-musulmana (accessed 2005): http://www.lega-musulmana.it/Information/Immagini/Medina5.htm

LUSAS (accessed 2005): www.lusas.com

Matlab (accessed 2005): www.mathworks.com

Moog (accessed 2005): www.moog.com

Oasys (accessed 2005): www.oasys-software.com

Polymers (accessed 2004): scifun.chem.wisc.edu/chemweek/POLYMERS/Polymers.html

Solver (accessed 2004): www.solver.com

Taconic (accessed 2004): www.4taconic.com/products/architect/documents/productfeatures.html

Tensinet (accessed 2005): www.tensinet.com

Tensys (accessed 2005): www.tensys.com